SYNTHESIS, EVALUATION, AND APPLICATION OF NEW LIGANDS FOR RADIOMETAL BASED RADIOPHARMACEUTICALS

by

ERIC WILLIAM PRICE

Hons. B. Sc, co-op, The University of Victoria, 2009

A THESIS SUBMITTED IN PARTIAL FULFILLMENT OF

THE REQUIREMENTS FOR THE DEGREE OF

DOCTOR OF PHILOSOPHY

in

THE FACULTY OF GRADUATE AND POSTDOCTORAL STUDIES

(Chemistry)

THE UNIVERSITY OF BRITISH COLUMBIA

(Vancouver)

April 2014

© Eric William Price, 2014

Abstract

Radiometals comprise many useful radioactive isotopes of various metallic elements. When properly harnessed, these have valuable emission properties that can be used for diagnostic imaging techniques, such as single photon emission computed tomography (SPECT, e.g. ^{67}Ga, ^{99m}Tc, ^{111}In, ^{177}Lu) and positron emission tomography (PET, e.g. ^{68}Ga, ^{64}Cu, ^{44}Sc, ^{86}Y, ^{89}Zr), as well as therapeutic applications (e.g. ^{47}Sc, ^{114m}In, ^{177}Lu, ^{90}Y, $^{212/213}$Bi, ^{212}Pb, ^{225}Ac, $^{186/188}$Re). A fundamental critical component of a radiometal-based radiopharmaceutical is the ligand that binds the radiometal ion in a tight stable coordination complex so that it can be properly directed to a desirable molecular target *in vivo*. This thesis describes the design, synthesis, and evaluation of novel acyclic ligands based on the versatile picolinic acid moiety. Acyclic ligands have been selected because facile ambient temperature radiolabeling is an important property when working with heat sensitive molecules such as antibodies, as many currently used ligands require high temperatures for optimal radiolabling performance. Previous work in the Orvig group has determined the acyclic ligand H_2dedpa to possess ideal properties for $^{67/68}$Ga radiochemistry. In light of this success, this thesis has been dedicated to expansion of the H_2dedpa molecular scaffold to accommodate larger radiometals with ligand denticities ranging from 8-10. Once synthesized, new ligands are studied by standard chemical characterization, as well as potentiometric titrations to determine thermodynamic stability parameters, and radiolabeling and *in vitro*/*in vivo* stability studies of both "bare" ligands and antibody bioconjugates. The ligand H_4octapa is a highlight of this body of work, and has been found to possess excellent properties with the radiometals ^{111}In and ^{177}Lu, matching or in some cases surpassing the current industry "gold standard" ligand DOTA. A second highlight is the ligand H_6phospa, which is demonstrated to possess enhanced ^{89}Zr radiolabeling properties to H_4octapa, showing the best ^{89}Zr radiolabeling performance of any new ligand in several decades, with only DFO retaining superior properties.

Preface

Chapter 1 is an adaptation of published work, and is reproduced in part, with permission from Price, E. W.; Orvig, C., Matching Chelators to Radiometals for Radiopharmaceuticals. *Chem. Soc. Rev.* **2014,** *43* (1), 260-290, Copyright 2014 The Royal Society of Chemistry. This review article was written by Eric Price, with input and editing from Dr. Chris Orvig.

Chapter 2 is an adaptation of published work, and is reproduced in part, with permission from Price, E. W.; Cawthray, J. F.; Bailey, G. A.; Ferreira, C. L.; Boros, E.; Adam, M. J.; Orvig, C., H_4octapa: An Acyclic Chelator for ^{111}In Radiopharmaceuticals. *J. Am. Chem. Soc.* **2012,** *134* (20), 8670-8683, Copyright 2014 American Chemical Society. Eric Price performed the synthesis, with some assistance from Gwendolyn Bailey during her summer NSERC USRA term. Radiochemistry was performed by Eric Price at TRIUMF/Nordion with assistance from Dr. Cara L. Ferreira. Potentiometric titrations, data fitting, and DFT calculations were performed by Dr. Jacqueline F. Cawthray. Animal experiments were contracted to the BC Cancer Agency, and the protocol used in these animal studies was approved by the Institutional Animal Care Committee (IACC) of the University of British Columbia (protocol # A10-0171) and was performed in accordance with the Canadian Council on Animal Care Guidelines. This project was supervised by Dr. Michael J. Adam and Dr. Chris Orvig. The manuscript was written by Eric Price.

Chapter 3 is an adaptation of published work, and is reproduced in part, with permission from Price, E. W.; Zeglis, B. M.; Cawthray, J. F.; Ramogida, C. F.; Ramos, N.; Lewis, J. S.; Adam, M. J.; Orvig, C., H_4octapa-Trastuzumab: Versatile Acyclic Chelate System for ^{111}In and ^{177}Lu Imaging and Therapy. *J. Am. Chem. Soc.* **2013,** *135* (34), 12707–

12721, Copyright 2014 American Chemical Society. The synthesis work was performed by Eric Price, with some assistance from Caterina F. Ramogida. Eric traveled to Memorial Sloan-Kettering Cancer Center to work with Dr. Brian M. Zeglis and Dr. Jason S. Lewis to perform radiolabeling, SPECT imaging, and animal experiments. Nicholas Ramos assisted with dissection and biodistribution experiments when Dr. Zeglis was unavailable. Dr. Jacqueline F. Cawthray performed potentiometric titrations, data fitting, and DFT calculations. All animal experiments were performed under an Institutional Animal Care and Use Committee-approved protocol at Memorial Sloan-Kettering Cancer Center, and the experiments followed institutional guidelines for the proper and humane use of animals in research. Eric Price wrote the manuscript. Dr. Chris Orvig and Dr. Michael Adam supervised this project.

Chapter 4 is an adaption of published work, and is reproduced in part, with permission from Price, E. W.; Ferreira, C. L.; Adam, M. J.; Orvig, C., High denticity ligands based on picolinic acid for In-111 radiochemistry. *Can. J. Chem.,* doi: 10.1139/cjc-2013-0542, **2014**. Synthesis was performed by Eric Price, and radiochemistry was performed by Eric Price with assistance from Dr. Cara L. Ferreira at TRIUMF/Nordion. The manuscript was written by Eric Price. The project was supervised by Dr. Chris Orivg and Dr. Michael Adam.

Chapter 5 is an adaptation of published work, and is reproduced in part, with permission from Price, E. W.; Cawthray, J. F.; Adam, M. J.; Orvig, C. Modular Syntheses of H_4octapa and H_2dedpa, and Yttrium Coordination Chemistry Relevant to $^{86/90}$Y Radiopharmaceutical. *Dalton Trans.* Doi: 10.1039/C4DT00239C, **2014**. Copyright 2014 The Royal Society of Chemistry. The synthesis work was performed by Eric Price, and the

potentiometry was performed by Eric Price with assistance from Dr. Jacqueline F. Cawthray, with data fitting and DFT calculations done by Dr. Jacqueline F. Cawthray. This project was supervised by Dr. Chris Orvig and Dr. Michael Adam.

Chapter 6 is an adaptation of a manuscript in preparation for publication, Price, E. W.; Zeglis, B. M.; Cawthray, J. F.; Lewis, J. S.; Adam, M. J.; Orvig, C., H_4octapa vs H_4C3octapa for In-111 and Lu-177 Radiochemistry: the Difference of One Carbon. Expected submission date February-March 2014. Synthesis was performed by Eric Price, potentiometry was performed by Eric Price and Dr. Jacqueline F. Cawthray, data fitting and DFT calculations were performed by Dr. Jacqueline F. Cawthray. Ligands were mailed to Dr. Brian M. Zeglis and Dr. Jason S. Lewis at Memorial Sloan-Kettering Cancer Center, and radiolabeling experiments were performed by Dr. Brian M. Zeglis. The manuscript was written by Eric Price. Dr. Chris Orvig and Dr. Michael Adam supervised this project.

Chapter 7 is an adaptation of published work, and is reproduced in part, with permission from Price, E. W.; Zeglis, B. M.; Lewis, J. S.; Adam, M. J.; Orvig, C., H_6phospa-Trastuzumab: Bifunctional Methylenephosphonate-based Chelator with ^{89}Zr, ^{111}In and ^{177}Lu. *Dalton Trans.* **2014,** *43*, 119-131, Copyright 2014 The Royal Society of Chemistry. Synthesis was performed by Eric Price, and radiochemistry experiments and SPECT imaging were performed by Eric Price and Dr. Brian M. Zeglis at Memorial Sloan-Kettering Cancer Center with supervision and funding from Dr. Jason S. Lewis. All animal experiments were performed under an Institutional Animal Care and Use Committee-approved protocol at Memorial Sloan-Kettering Cancer Center, and the experiments followed institutional guidelines for the proper and humane use of animals in research. Eric Price wrote the manuscript, and Dr. Chris Orvig and Dr. Michael Adam supervised the project.

Chapter 8 is an adaptation of published work, and is reproduced in part, with permission from Bailey, G. A.; Price, E. W.; Zeglis, B. M.; Ferreira, C. L.; Boros, E.; Lacasse, M. J.; Patrick, B. O.; Lewis, J. S.; Adam, M. J.; Orvig, C., H_2azapa: a Versatile Acyclic Multifunctional Chelator for ^{67}Ga, ^{64}Cu, ^{111}In, and ^{177}Lu. *Inorg. Chem.* **2012**, *51* (22), 12575-12589, Copyright 2014 The American Chemical Society (*These authors contribued equally to this work). Gwendolyn A. Bailey was an undergraduate honors student supervised by Dr. Orvig and Eric Price, and with supervision and help from Eric Price she completed a majority of the synthesis in this work, assisted with some of the radiochemistry experiments, and co-wrote the manuscript. Eric Price assisted with the synthetic work while supervising, and also performed some early synthetic work for this project prior to Gwendolyn beginning. Eric performed radiochemistry at TRIUMF/Nordion with assistance from Dr. Cara L. Ferreira and Gwendoyln Bailey. Eric performed radiochemistry, PET imaging, and animal experiments at Memorial Sloan-Kettering Cancer Center with Dr. Brian M. Zeglis under the supervision of Dr. Jason S Lewis. Eric co-wrote and co-authored this manuscript with Gwendolyn. No work presented in this chapter was performed by Michael J. Lacasse or Eszter Boros; however, these two had previously attempted synthesis of the H_2azapa ligand using a different synthetic (and unfortunately unsuccessful) methodology, and therefore provided valuable intellectual contributions. Dr. Brian O. Patrick performed X-ray crystallography experiments. All animal experiments were performed under an Institutional Animal Care and Use Committee-approved protocol at Memorial Sloan-Kettering Cancer Center, and the experiments followed institutional guidelines for the proper and humane use of animals in research. Dr. Chris Orvig and Dr. Michael J. Adam supervised all of this work.

All animal experiments performed at Memorial Sloan-Kettering Cancer Center in Chapters 3, 7, and 8 were performed according to a protocol approved by Memorial Sloan-Kettering Cancer Center's Institutional Animal Care and Use Committee (#08-07-013). Animal experiments performed in Chapter 2 used a protocol that was approved by the Institutional Animal Care Committee (IACC) of the University of British Columbia (protocol # A10-0171) and was performed by the BC Cancer Agency in accordance with the Canadian Council on Animal Care Guidelines.

Table of Contents

Abstract ..... **ii**

Preface ..... **iii**

Table of Contents ..... **viii**

List of Tables ..... **xxii**

List of Figures ..... **xxv**

List of Schemes ..... **xxxiii**

List of Symbols and Abbreviations ..... **xxxiv**

Acknowledgements ..... **xxxix**

Dedication ..... **xl**

Chapter 1: Introduction **1**

1.1 Background and aims **1**

1.2 Nuclear imaging and therapy **2**

1.3 Popular radiometal isotopes **4**

1.4 Radiometal-based radiopharmaceutical design **7**

1.4.1 Macrocyclic versus acyclic ligands 10

1.4.2 Matching ligands with radiometals – how are ligands evaluated? 11

1.4.3 Thermodynamic stability 13

1.4.4 Kinetics - Acid dissociation and competitive radiolabeling 15

1.4.5 *In vitro* and *in vivo* stability 16

1.5 A selection of ligands and their most suitable radiometal companions 18

1.5.1 DOTA 19

1.5.2 DOTA Derivatives: CB-DO2A, 3p-C-DEPA, TCMC, and Oxo-DO3A 24

1.5.3 TETA 25

1.5.4 TE2A, CB-TE2A, CB-TE1A1P, CB-TE2P, MM-TE2A, DM-TE2A 27

1.5.5 Diamsar and derivatives 28

1.5.6 NOTA, NETA, and TACN-TM 29

1.5.7 DTPA, 1B4M-DTPA, and CHX-A''-DTPA 33

1.5.8 TRAP (PRP9) and NOPO 37

1.5.9 AAZTA and derivatives (DATA) 39

1.5.10 H_2dedpa, H_4octapa, H_2azapa, and H_5decapa 40

1.5.11 HBED and SHBED 43

1.5.12 BPCA 44

1.5.13 CP256 45

1.5.14 Desferrioxamine (DFO) 46

1.5.15 H_6phospa 49

1.5.16 PCTA 50

1.6 Conclusions 50

Chapter 2: H_4octapa: an acyclic ligand for ^{111}In radiopharmaceutical applications 52

2.1 Introduction 52

2.2 Results and discussion 55

2.2.1 Synthesis and characterization 57

2.2.2 DFT structures and molecular electrostatic potential maps 63

2.2.3 Radiolabeling experiments 65

2.2.4 Thermodynamic stability 67

2.2.5 ^{111}In radiolabeling and stability studies 69

2.3 Conclusions 74

2.4 Experimental methods 76

2.4.1 Materials and methods 76

2.4.2 Methyl 6-(hydroxymethyl)picolinate (2.1) 77

2.4.3 Methyl 6-(bromomethyl)picolinate (2.2) 78

2.4.4 *N,N'*-(Benzyl)ethylenediamine (2.3) 79

2.4.5 *N,N'*-[Benzyl(*tert*-butoxycarbonyl)methyl]aminoethane (2.4) 80

2.4.6 *N,N'*-[(*tert*-Butoxycarbonyl)methyl]aminoethane (2.5) 81

2.4.7 *N,N′* -[[(*tert*-Butoxycarbonyl)methyl]-*N,N′* -[6-(methoxycarbonyl)pyridin-2-yl]methylamino]ethane (2.6) 81

2.4.8 H_4octapa•4HCl•2H_2O, *N,N′* -bis(6-carboxy-2-pyridylmethyl)ethylenediamine-*N,N′* diacetic acid 82

2.4.9 Na[In(octapa)] 83

2.4.10 *N,N''*-[Benzyl]diethylenetriamine (2.7) 83

2.4.11 *N,N''*-[[Benzyl]-*N,N',N''*-[(*tert*-butoxycarbonyl)methyl]]diethylenetriamine (2.8) 84

2.4.12 *N,N',N''*-[[*tert*-Butoxycarbonyl]methyl]diethylenetriamine (2.9) 85

2.4.13 *N,N''*-[[6-(Methoxycarbonyl)pyridin-2-yl]methylamino]-*N,N',N''*-[(*tert*-butoxycarbonyl)methyl]]diethylenetriamine (2.10) 85

2.4.14 H_5decapa•5HCl•2.5H_2O, *N,N′,N′′*-[(triacetic acid]-*N,N′′*-[6-(carboxy)pyridin-2-yl]methylamino]diethylenetriamine 86

2.4.15 Na_2[In(decapa)] 87

2.4.16 H_2dedpa 87

2.4.17 [In(dedpa)]Cl 88

2.4.18 ^{111}In Radiolabeling studies 88

2.4.19 Solution thermodynamics 89

2.4.20 Molecular modeling 90

2.4.21 Mouse serum stability data 91

2.4.22 Biodistribution data 92

Chapter 3: H_4octapa-trastuzumab: the application of a versatile acyclic ligand system for ^{111}In and ^{177}Lu imaging and therapy 93

3.1 Introduction 93

3.2 Results and discussion 96

3.2.1 Synthesis and characterization 96

3.2.2 Thermodynamic stability and density functional theory structure prediction 99

3.2.3 Bioconjugation and *in vitro* characterization 102

3.2.4 Acute biodistribution studies 104

3.2.5 Small animal SPECT/CT imaging and Cerenkov luminescence imaging 108

3.3 Conclusions 110

3.4 Experimental section 112

3.4.1 Materials and methods 112

3.4.2 *N,N*'-(2-Nitrobenzenesulfonamide)-1,2-diaminoethane (3.1) 113

3.4.3 *N,N*'-(2-Nitrobenzenesulfonamide)-*N,N′* -[6-(methoxycarbonyl)pyridin-2-yl]methyl]-1,2-diaminoethane (3.2) 114

3.4.4 *N,N′* -[6-(Methoxycarbonyl)pyridin-2-yl]methyl-1,2-diaminoethane (3.3) 115

3.4.5 *N,N′* -[(*tert*-Butoxycarbonyl)methyl-*N,N′* -[6-(methoxycarbonyl)pyridin-2-yl]methyl]-1,2-diaminoethane (3.4) 116

3.4.6 H_4octapa, *N,N′* -(6-carboxy-2-pyridylmethyl)-*N,N′* -diacetic acid-1,2-diaminoethane (3.5) 116

3.4.7 Na[Lu(octapa)] (3.6) 117

3.4.8 1-(*p*-Nitrobenzyl)ethylenediamine (3.7)..... 118

3.4.9 *N,N'*-(2-Nitrobenzenesulfonamide)-1-(*p*-nitrobenzyl)-1,2-diaminoethane (3.8) 118

3.4.10 *N,N'*-(2-Nitrobenzenesulfonamide)-*N,N'*-[(*tert*-butoxycarbonyl)methyl]-1-(*p*-nitrobenzyl)-1,2-diaminoethane (3.9) 119

3.4.11 *N,N*'-[(*tert*-Butoxycarbonyl)methyl]-1-(*p*-nitrobenzyl)-1,2-diaminoethane (3.10) 120

3.4.12 *N,N'*-[(*tert*-Butoxycarbonyl)methyl]-*N,N'*-[(6-methoxycarbonyl)pyridin-2-yl)methyl]-1-(*p*-nitrobenzyl)-1,2-diaminoethane (3.11) 120

3.4.13 *p*-SCN-Bn-H_4octapa, *N,N'*-[(Carboxylato)methyl]-*N,N'*-[(6-carboxylato)pyridin-2-yl)methyl]-1-(*p*-benzyl-isothiocyanato)-1,2-diaminoethane (3.12) 121

3.4.14 Solution thermodynamics 122

3.4.15 Molecular modeling 123

3.4.16 [^{177}Lu(chelate)] Radiolabeling 123

3.4.17 Trastuzumab antibody modification/thiourea bioconjugation..... 124

3.4.18 ^{111}In- and ^{177}Lu-octapa/DOTA-trastuzumab radiolabeling 124

3.4.19 Chelate number isotopic dilution assay 125

3.4.20 *In vitro* immunoreactivity assay 126

3.4.21 [^{177}Lu(chelate)] Blood serum competition experiments 127

3.4.22 ^{111}In- and ^{177}Lu-octapa/DOTA-trastuzumab blood serum competition experiments 127

3.4.23 Cell culture 128

3.4.24 SKOV-3 xenograft mouse models 128

3.4.25 ^{111}In- and ^{177}Lu-octapa/DOTA-trastuzumab biodistribution studies 129

3.4.26 ^{111}In- and ^{177}Lu-octapa/DOTA-trastuzumab SPECT/CT imaging studies 130

3.4.27 Cerenkov luminescence imaging (CLI) 131

3.4.28 Statistics 131

Chapter 4: High denticity ligands based on picolinic acid for ^{111}In radiochemistry..... 133

4.1 Introduction 133

4.2 Results and discussion 135

4.2.1 Synthesis and characterization 135

4.2.2 Ligand-metal coordination 140

4.2.3 ^{111}In radiolabeling and serum stability 144

4.3 Conclusions 147

4.4 Experimental methods 148

4.4.1 Materials and methods 148

4.4.2 *N,N''*-[Benzyl]diethylenetriamine (4.1) 148

4.4.3 *N,N''*-[(Benzyl)-*N,N',N''*-[(6-methoxycarbonyl)pyridin-2-yl)methyl]-diethylenetriamine (4.2) 149

4.4.4 Bn-H_3nonapa, *N,N''*-[(Benzyl)-*N,N',N''*-[(6-carboxy)pyridin-2-yl)methyl]-diethylenetriamine (4.3) 150

4.4.5 H_3nonapa, *N,N′,N′′*-[(6-carboxy)pyridin-2-yl)methyl]-diethylenetriamine (4.4) 151

4.4.6 *N,N′,N″*-Tris[benzyl]ethylamine (4.5) 151

4.4.7 *N,N′,N′′*-Tris[benzyl]-tris[(6-methoxycarbonyl)pyridin-2-yl)methyl]ethyl-amine (4.6) 152

4.4.8 Bn-H_3trenpa, *N,N′,N′′*-Tris[benzyl]-tris[(6-carboxy)pyridin-2-yl)methyl] ethyl-amine (4.7) 153

4.4.9 *N,N′′*-(*p*-Nitrobenzyl)diethylenetriamine (4.8) 154

4.4.10 *N,N′′*-[(*p*-Nitrobenzyl)-*N,N′,N′′*-[(6-methoxycarbonyl)pyridin-2-yl)methyl]-diethylenetriamine (4.9) 155

4.4.11 *p*-NO_2-Bn-H_3nonapa, *N,N′′*-[(*p*-Nitrobenzyl)-*N,N′,N′′*-[(6-carboxy)pyridin-2-yl)-methyl]diethylenetriamine (4.10) 155

4.4.12 [In(Bn-nonapa)] (4.11) 156

4.4.13 [In(nonapa)] (4.12) 157

4.4.14 [In(Bn-trenpa)] (4.13) 157

4.4.15 ^{111}In radiolabeling studies 158

4.4.16 Mouse serum stability challenge 159

Chapter 5: Modular syntheses of H_4octapa and H_2dedpa, and yttrium coordination chemistry relevant to $^{86/90}$Y radiopharmaceuticals 160

5.1 Introduction 160

5.2 Results and discussion 164

5.2.1 Synthesis and characterization 164

5.2.2 Yttrium coordination chemistry 169

5.2.3 Density functional theory/molecular electrostatic potential structure prediction 177

5.2.4 Thermodynamic stability 179

5.3 Conclusions 180

5.4 Experimental 181

5.4.1 Materials and methods 181

5.4.2 *tert*-Butyl 6-(methyl)picolinate (5.1) 182

5.4.3 *tert*-Butyl 6-(bromomethyl)picolinate (5.2) 183

5.4.4 *N,N*'-(2-Nitrobenzenesulfonamide)-1,2-diaminoethane (5.3) 184

5.4.5 *N,N'*-(2-Nitrobenzenesulfonamide)-*N*,*N*′ -[6-(*tert*-butoxycarbonyl)pyridin-2-yl]methyl]-1,2-diaminoethane (5.4) 185

5.4.6 *N*,*N*′ -[6-(*tert*-Butoxycarbonyl)pyridin-2-yl]methyl-1,2-diaminoethane (5.5) 185

5.4.7 H_2dedpa, *N*,*N*′ -[(6-carboxylato)pyridin-2-yl)methyl]-1,2-diaminoethane (5.6)..... 186

5.4.8 *N*,*N*′ -[(*tert*-Butoxycarbonyl)methyl-*N*,*N*′ -[6-(*tert*-butoxycarbonyl)pyridin-2-yl]methyl]-1,2-diaminoethane (5.7) 187

5.4.9 H_4octapa, *N,N'*-[(6-carboxylato)pyridin-2-yl)methyl]-*N*,*N*′ -diacetic acid-1,2-diaminoethane (5.8) 188

5.4.10 Na[Y(octapa)] (5.9)..... 188

5.4.11 1-(*p*-Nitrobenzyl)ethylenediamine (5.10) 189

5.4.12 *N*,*N*'-(2-Nitrobenzenesulfonamide)-1-(*p*-nitrobenzyl)-1,2-diaminoethane (5.11)..... 190

5.4.13 *N,N'*-(2-Nitrobenzenesulfonamide)-*N,N''*-[6-(methoxycarbonyl)pyridin-2-yl]methyl]-1-(*p*-nitrobenzyl)-1,2-diaminoethane (5.12)..... 190

5.4.14 *N,N'*-[[6-(Methoxycarbonyl)pyridin-2-yl]methyl]-1-(*p*-nitrobenzyl)-1,2-diaminoethane (5.13) 191

5.4.15 *p*-SCN-Bn-H_2dedpa, *N,N'*-[[(6-carboxylato)pyridin-2-yl]methyl]-1-(*p*-benzylisothiocyanato)-1,2-diaminoethane (5.14) 192

5.4.16 *N,N'*-[(*tert*-Butoxycarbonyl)methyl]-*N,N'*-[[(6-*tert*-butoxycarbonyl)pyridin-2-yl]methyl]-1-(*p*-nitrobenzyl)-1,2-diaminoethane (5.15) 193

5.4.17 *p*-SCN-Bn-H_4octapa, *N,N'*-[(Carboxylato)methyl]-*N,N'*-[[(6-carboxylato)pyridin-2-yl]methyl]-1-(*p*-benzylisothiocyanato)-1,2-diaminoethane (5.16) 194

5.4.18 Solution thermodynamics 196

5.4.19 Molecular modeling 196

Chapter 6: H_4octapa vs H_4C3octapa for ^{111}In and ^{177}Lu radiochemistry: the difference of one carbon 198

6.1 Introduction 198

6.2 Results and discussion 202

6.2.1 Synthesis and characterization 202

6.2.2 Variable temperature NMR and 2D NMR spectroscopy of $[In(C3octapa)]^-$ and $[Lu(C3octapa)]^-$ 205

6.2.3 Density functional theory structure calculations 216

6.2.4 Thermodynamic formation constants 219

6.2.5 Trastuzumab antibody conjugation, ^{111}In/^{177}Lu radiolabeling, and *in vitro* serum stability 219

6.3 Conclusions 224

6.4 Experimental section 225

6.4.1 Materials and methods 225

6.4.2 *N,N'*-(2-Nitrobenzenesulfonamide)-1,3-diaminopropane (6.1) 226

6.4.3 *N,N'*-(2-Nitrobenzenesulfonamide)-*N,N'*-[6-(methoxycarbonyl)pyridin-2-yl]methyl]-1,3-diaminopropane (6.2) 226

6.4.4 *N*,*N*′ -[6-(Methoxycarbonyl)pyridin-2-yl]methyl-1,3-diaminopropane (6.3) 227

6.4.5 *N*,*N*′ -[(*tert*-Butoxycarbonyl)methyl-*N*,*N*′ -[6-(methoxycarbonyl)pyridin-2-yl]methyl]-1,3-diaminopropane (6.4) 228

6.4.6 H_4C3octapa, *N*,*N*′ -(6-carboxy-2-pyridylmethyl)-*N*,*N*′ -diacetic acid-1,3-diaminopropane (6.5) 228

6.4.7 Na[In(C3octapa)] (6.6) 229

6.4.8 Na[Lu(C3octapa)] (6.7) 230

6.4.9 Diethyl-2-(4-nitrobenzyl)malonate (6.8) 230

6.4.10 2-(4-Nitrobenzyl)malondiamide (6.9) 231

6.4.11 1,3-Diamino-2-(4-nitrobenzyl)propane dihydrochloride (2-(*p*-nitrobenzyl)-1,3-propylenediamine) (6.10) 232

6.4.12 *N,N'*-(2-Nitrobenzenesulfonamide)-2-(*p*-nitrobenzyl)-1,3-diaminopropane (6.11) ... 233

6.4.13 *N,N'*-(2-Nitrobenzenesulfonamide)-*N,N'*-[(*tert*-butoxycarbonyl)methyl]-2-(*p*-nitrobenzyl)-1,3-diaminopropane (6.12) 233

6.4.14 *N,N'*-[(*tert*-Butoxycarbonyl)methyl]-2-(*p*-nitrobenzyl)-1,3-diaminopropane (6.13) .. 234

6.4.15 *N,N'*-[(*tert*-Butoxycarbonyl)methyl]-*N,N'*-[(6-methoxycarbonyl)pyridin-2-yl)methyl]-2-(*p*-nitrobenzyl)-1,3-diaminopropane (6.14) 235

6.4.16 *p*-SCN-Bn-H_4C3octapa, *N,N'*-[(Carboxylato)methyl]-*N,N'*-[(6-carboxylato)pyridin-2-yl)methyl]-2-(*p*-benzyl-isothiocyanato)-1,3-diaminopropane (6.15) 235

6.4.17 Molecular modeling 237

6.4.18 Trastuzumab antibody modification / thiourea bioconjugation 237

6.4.19 ^{111}In- and ^{177}Lu-C3octapa/octapa-trastuzumab radiolabeling 238

6.4.20 ^{111}In- and ^{177}Lu-C3octapa/octapa-trastuzumab blood serum competition experiments 239

Chapter 7: H_6phospa-Trastuzumab: a bifunctional methylenephosphonate-based ligand with ^{89}Zr, ^{111}In and ^{177}Lu 240

7.1 Introduction 240

7.2 Results and discussion 243

7.2.1 Synthesis and characterization 243

7.2.2 Antibody modification, ^{111}In and ^{177}Lu radiolabeling, and *in vitro* characterization 246

7.2.3 ^{89}Zr Radiolabeling 250

7.2.4 Small animal SPECT/CT imaging 252

7.3 Conclusions 255

7.4 Experimental 257

7.4.1 Materials and methods 257

7.4.2 *N,N′* -[6-(Methoxycarbonyl)pyridin-2-yl]methyl-1,2-diaminoethane (7.1) 257

7.4.3 H_6phospa, (7.2), *N,N′* -(Methylphosphonate)-*N,N′* -[6-(methoxycarbonyl)pyridin-2-yl]methyl]-1,2-diaminoethane 257

7.4.4 Na_3[Lu(phospa)] (7.3) 258

7.4.5 Na_3[In(phospa)] (7.4) 258

7.4.6 1-(*p*-Nitrobenzyl)ethylenediamine (7.5) 259

7.4.7 *N,N′*-(2-Nitrobenzenesulfonamide)-1-(*p*-nitrobenzyl)-1,2-diaminoethane (7.6) 259

7.4.8 *N,N′*-(2-Nitrobenzenesulfonamide)-*N,N″* -[6-(methoxycarbonyl)pyridin-2-yl]methyl]-1-(*p*-nitrobenzyl)-1,2-diaminoethane (7.7) 260

7.4.9 *N,N'*-[6-(Methoxycarbonyl)pyridin-2-yl]methyl]-*p*-nitrobenzyl)-1,2-diaminoethane (7.8) 261

7.4.10 *N,N'*-[Methylphosphonate]-*N,N'*-[(6-carboxylato)pyridin-2-yl)methyl]-1-(*p*-nitrobenzyl)-1,2-diaminoethane (7.9) 261

7.4.11 *p*-SCN-Bn-H_6phospa, *N,N'*-(methylphosphonate)-*N,N'*-[(6-carboxylato)pyridin-2-yl)methyl]-1-(*p*-benzyl-isothiocyanato)-1,2-diaminoethane (7.10) 262

7.4.12 Trastuzumab bioconjugation 263

7.4.13 ^{111}In-, ^{89}Zr-, and ^{177}Lu-phospa-trastuzumab radiolabeling 264

7.4.14 Chelate number – radiometric isotopic dilution assay 265

7.4.15 *In vitro* immunoreactivity assay 265

7.4.16 ^{111}In- and ^{177}Lu-phospa-trastuzumab blood serum competition experiments 265

7.4.17 Cell culture 265

7.4.18 SKOV-3 xenograft mouse models 266

7.4.19 ^{111}In- and ^{177}Lu-phospa-trastuzumab SPECT/CT imaging studies 266

7.4.20 Animal protocol 267

Chapter 8: H_2azapa: a click-based acyclic multifunctional ligand for $^{67/68}$Ga, ^{64}Cu, ^{111}In, and ^{177}Lu 268

8.1 Introduction 268

8.2 Results and discussion 271

8.2.1 Synthesis of H_2azapa 271

8.2.2 NMR Characterization 275

8.2.3 X-ray crystallography 278

8.2.4 Radiolabeling experiments 283

8.2.5 Blood serum stability studies 284

8.2.6 Biodistribution and PET imaging studies 287

8.3 Conclusions 292

8.4 Experimental section 294

8.4.1 Materials and Methods 294

8.4.2 Di-*tert*-butyl ethane-1,2-dicarbamate (8.1) 296

8.4.3 *N,N'*-Propargyl-*N,N'*-*tert*-butoxycarbonyl-1,2-diaminoethane (8.2) 297

8.4.4 *N,N'*-Propargyl-1,2-diaminoethane (8.3) 298

8.4.5 *N,N'*-[6-(Methoxycarbonyl)pyridin-2-yl]methyl-*N,N'*-propargyl-1,2-diaminoethane (8.4) 298

8.4.6 *N,N'*-[1-Benzyl-1,2,3-triazole-4-yl]methyl-*N,N'*-[6-(carboxy)pyridin-2-yl]-1,2-diaminoethane (H_2azapa•2HCl•1.5H_2O) (8.5•2HCl•1.5H_2O) 299

8.4.7 Metal complexation experiments: general procedure 301

8.4.7.1 [Cu(azapa)] 301

8.4.7.2 [Ga(azapa)][ClO_4] 301

8.4.7.3 [In(azapa)(H_2O)][ClO_4] 302

8.4.7.4 [Lu(azapa)][ClO_4] 302

8.4.8 X-Ray crystallography 303

8.4.9 ^{67}Ga/^{111}In Radiolabeling 304

8.4.10 ^{177}Lu/^{64}Cu Radiolabeling 304

8.4.11 ^{67}Ga/^{111}In Mouse serum competition experiments 305

8.4.12 ^{177}Lu/^{64}Cu Blood serum competition experiments 306

8.4.13 ^{64}Cu Biodistribution studies 307

8.4.14 Small-animal ^{64}Cu-PET imaging 308

Chapter 9: Conclusions and future work..... 309

9.1.1 Overview and conclusions for “pa” family of picolinic acid-based ligands 309

9.1.2 General direction for future ligand design 312

Bibliography 314

Appendix 331

Appendix A Supplementary figures and data 331

List of Tables

Table 1.1 Properties of some popular radiometal isotopes, EC = electron capture; some low abundance emissions have been omitted for brevity.[6,13-17] 5

Table 1.2 DOTA and bifunctional derivatives.[a] 22

Table 1.3 DOTA derivatives CB-DO2A, TCMC, 3p-C-DEPA, Oxo-DO3A, and bifunctional derivatives.[a] 23

Table 1.4 TETA, CB-TE2A and derivatives, and bifunctional derivatives. 26

Table 1.5 The copper ligands Diamsar, SarAr, AmBaSar, and BaBaSar.[a] 29

Table 1.6 NOTA, NETA, TACN-TM, and bifunctional derivatives.[a] 31

Table 1.7 DTPA, 1B4M, CHX-A''-DTPA, and bifunctional derivatives. 35

Table 1.8 Promising $^{67/68}$Ga ligands TRAP (PRP9, TRAP-Pr), AAZTA (DATA), and bifunctional derivatives.[a] 38

Table 1.9 H_2dedpa, H_4octapa, H_2azapa, H_5decapa, and bifunctional derivatives. 41

Table 1.10 HBED, SHBED, BPCA, and bifunctional derivatives.[a] 44

Table 1.11 CP256, Desferrioxamine (DFO), PCTA, H_6phospa, and bifunctional derivatives. 48

Table 2.1 Formation constants (log K_{ML}) and pM[a] values for In^{3+} complexes. 68

Table 2.2 Data from mouse serum stability challenges performed at ambient temperature (n=3), evaluated by PD-10 size-exclusion column elution, with stability shown as the percentage of intact ^{111}In complex. 69

Table 2.3 Decay corrected %ID/g values from the biodistribution of ^{111}In-complexes in healthy female ICR mice (6-8 weeks old), n = 4, bold = passed students T-test ($p < 0.05$)... 71

Table 3.1 Chemical and *in vitro* biological characterization data for ^{111}In- and ^{177}Lu-octapa-trastuzumab and ^{111}In- and ^{177}Lu-DOTA-trastuzumab radioimmunoconjugates. 104

Table 3.2 Biodistribution data of ^{111}In/^{177}Lu-octapa-trastuzumab and ^{111}In/^{177}Lu-DOTA-trastuzumab, performed over a 5 day period in mice bearing SKOV-3 ovarian cancer xenografts, tumour size ~2-3 mm diameter (n = 4 for each time point), showing %ID/g values. 105

Table 4.1 Radiolabeling experiments with ^{111}In and the novel acyclic ligands Bn-H_3nonapa (4.3), H_3nonapa (4.4), Bn-H_3trenpa (4.7), and results from the ligands H_2dedpa, H_4octapa, H_5decapa, DOTA, and DTPA (Chapters 2-3).[89] 145

Table 5.1 Formation constants (log K_{ML}) and pM^a values for In^{3+}, Lu^{3+}, and Y^{3+} complexes of relevant chelating ligand. 179

Table 6.1 Relevant bond lengths (Å) and angles (°) comparing the DFT-calculated In^{3+} and Lu^{3+} complexes of H_4octapa and H_4C3octapa. 218

Table 6.2 Human serum stability challenge performed at 37.5 °C (n = 3), with stability shown as the % intact ^{177}Lu complex, deteremined by PD10 size-exclusion column elution. 220

Table 7.1 Chemical and *in vitro* biological characterization data for ^{111}In- and ^{177}Lu-phospa-trastuzumab radioimmunoconjugates. 245

Table 8.1 Selected bond angles and lengths in the X-ray crystal structure of [In(azapa)(H_2O)][ClO_4]. 280

Table 8.2 Selected bond angles and lengths in the X-ray crystal structure of [Cu(azapa)]. Relevant bond angles are compared to the analogous bond angles in the previously reported X-ray crystal structure of $[Ga(dedpa)]^+$ and [Cu(dedpa)].[118,273] 282

Table 8.3 Stability data collected in mouse blood serum at 25 °C for ^{67}Ga and ^{111}In, and in human blood serum with agitation (550 rpm) at 37 °C for ^{64}Cu and ^{177}Lu, with H_2azapa and selected ligand standards. The % stability shown is the percentage of ligand-bound radiometal, and the error is expressed as standard deviation (n = 3). 284

Table 8.4 Biodistribution of [^{64}Cu(azapa)] and [^{64}Cu(DOTA)]$^{2-}$ in healthy nude athymic mice (n=4) showing organ uptake as % ID/g, with the error expressed as standard deviation (SD), at 15 min, 1 h, 4 h, and 24 h time points. 290

List of Figures

Figure 1.1 Examples of bioconjugation reactions: (A) standard peptide coupling reaction between a carboxylic acid and a primary amine with a coupling reagent; (B-C) peptide coupling reactions between activated esters of *N*-hydroxysuccinimide (NHS) or tetrafluorophenyl (TFP) olaand a primary amine; (D) thiourea bond formation between an isothiocyanate and a primary amine; (E) thioether bond formation between a maleimide and thiol; (F) standard Cu(I) catalyzed Huisgen 1,3-dipolar cycloaddition ("click" reaction) between an azide and an alkyne; and (G) strain-promoted Diels-Alder "click" reaction between a tetrazine and transcyclooctene. 7

Figure 1.2 Illustration of an archetypal radiometal-based radiopharmaceutical agent containing a bifunctional chelator (BFC) conjugated to a targeting vector (e.g. antibody, peptide, nanoparticle) using a variety of conjugation methods (e.g. isothiocyanate-amine coupling (shown), peptide coupling, maleimide-thiol coupling, activated ester amide coupling, click-coupling) and then radiolabeled with a radiometal ion (e.g. $^{111}In^{3+}/^{177}Lu^{3+}/^{86/90}Y^{3+}$). 8

Figure 1.3 Cartoon depiction of metal ion coordination kinetics, enhanced off-rate kinetics *in vivo* (extremely dilute conditions), and possible routes of radiometal ion loss *in vivo*. 11

Figure 2.1 Structures of the ^{111}In-coordinating and industry "gold standard" ligands DTPA/CHX-A''-DTPA and DOTA, the ^{68}Ga-coordinating ligand H_2dedpa, and the novel entrants H_4octapa and H_5decapa. 55

Figure 2.2 ^{1}H NMR spectra in D_2O (300 MHz) at ambient temperature of top, H_4octapa and $[In(octapa)]^-$ showing simple diastereotopic splitting due to minimal isomerization and

bottom, H_5decapa and $[In(decapa)]^{2-}$ showing complicated but sharp splitting arising from multiple static isomers. 60

Figure 2.3 DFT structure of $[In(octapa)]^-$ (solvent = water) showing an 8 coordinate structure (left), and the electrostatic potentials of the complex between octapa^{4-} with In^{3+} mapped onto the electron density (right). The MEP represent a maximum potential of 0.03 au, and a minimum of -0.25 au, mapped onto electron density isosurfaces of 0.002 e Å^{-3} (red to blue = negative to positive). DFT calculations performed by Dr. Jacqueline Cawthray. 65

Figure 2.4 DFT structure of $[In(decapa)]^{2-}$ (solvent = water) showing an 8 coordinate structure, and the electrostatic potentials of the complex between decapa^{5-} with In^{3+} mapped onto the electron density (right). The MEP represent a maximum potential of 0.03 au, and a minimum of -0.25 au, mapped onto electron density isosurfaces of 0.002 e Å^{-3} (red to blue = negative to positive). DFT calculations performed by Dr. Jacqueline Cawthray. 65

Figure 2.5 Biodistribution %ID/g values for $[^{111}In(DOTA)]^-$, $[^{111}In(octapa)]^-$, and $[^{111}In(decapa)]^{2-}$, with error bars plotted as standard deviations (note the y-axis set to 2.0 %ID/g, for clarity of the low activity 4 and 24 hour time points). 72

Figure 3.1 Structures of some common bifunctional ligands used for radiometal chemistry, and H_4octapa, the non-bifunctional variant of the ligand *p*-SCN-Bn-H_4octapa used in this work. 94

Figure 3.2 *In silico* DFT structure predictions. a, 8-coordinate structure of $[Lu(octapa)]^-$; b, 9-coordinate structure of $[Lu(octapa)(H_2O)]^-$, as well as the MEP polar-surface area maps (bottom) predicting the charge distribution over the solvent-exposed surface of the metal complexes (red = negative, blue = positive, representing a maximum potential of 0.254 au

and a minimum of -0.254 au, mapped onto electron density isosurfaces of 0.002 $Å^{-3}$). DFT calculations performed by Dr. Jacqueline Cawthray. 101

Figure 3.3 SPECT/CT imaging of the $^{111}In/^{177}Lu$-octapa-trastuzumab and $^{111}In/^{177}Lu$-DOTA-trastuzumab immunoconjugates, in female nude athymic mice with subcutaneous SKOV-3 xenografts (identified by arrow at right shoulder, tumour size ~2-3 mm diameter), showing transverse (top) and coronal (bottom) planar images bisecting the tumour, imaged at 24, 48, 72, 96, and 120 h post injection. 109

Figure 3.4 Cerenkov luminescence image (CLI) of ^{177}Lu-octapa-trastuzumab, obtained 24 h post-injection of a female nude athymic mouse bearing an SKOV-3 ovarian cancer xenograft on the right shoulder, indicated by white arrow (2 minute acquisition time). 110

Figure 4.1 The new chelating ligands Bn-H_3nonapa, H_3nonapa, *p*-NO_2-Bn-H_3nonapa, and Bn-H_3trenpa. 134

Figure 4.2 ^1H NMR spectra of H_3nonapa (4.4) (400 MHz, 25 °C, D_2O, top) and the In^{3+} complex In(nonapa) (4.12) (600 MHz, 25 °C, DMSO-d_6, bottom). 141

Figure 4.3 ^1H NMR spectra of Bn-H_3nonapa (4.3) (300 MHz, 25 °C, MeOD, top) and the In^{3+} complex In(Bn-nonapa) (4.11) (600 MHz, 25 °C, DMSO-d_6, bottom). 142

Figure 4.4 ^1H NMR spectra of Bn-H_3trenpa (4.7) (300 MHz, 25 °C, MeOD, top) and the In^{3+} complex In(Bn-trenpa) (4.13) (400 MHz, 25 °C, DMSO-d_6, bottom)..... 143

Figure 4.5 Mouse serum stability assay of $^{111}In^{3+}$ complexes of ligands from Table 4.1, determined after 1 and 24 h by PD-10 size-exclusion column elution. 146

Figure 5.1 Ligands synthesized in this chapter, including H_2dedpa, H_4octapa, and BFC derivatives *p*-SCN-Bn-H_2dedpa and *p*-SCN-Bn-H_4octapa; and the promising new $^{86/90}Y$ ligand 3p-C-NETA..... 161

Figure 5.2 ^{1}H NMR spectra of [Lu(octapa)]$^{-}$ in D_2O (600 MHz, 25 °C, top, referenced to H-O-D at 4.75 ppm)[87], [Y(octapa)]$^{-}$ in D_2O (400 MHz, 25 °C, bottom). 170

Figure 5.3 Variable temperature (VT) NMR experiments with [Y(octapa)]$^{-}$ (D_2O, 400 MHz), with temperature increased to 85 °C in 20 °C increments, with blue arrows identifying fluxional isomers, and red arrows identifying a static (non-fluxional) isomer. 171

Figure 5.4 ^{1}H-^{1}H COSY NMR (600 MHz, D_2O, 25 °C) expansion of aromatic signals in spectrum of [Y(octapa)]$^{-}$, showing no correlations between broad signals arising from a fluxional species (blue arrows), and sharp signals arising from a single static isomer (see Figure A.6 for full spectrum). 173

Figure 5.5 ^{1}H-^{1}H COSY NMR (600 MHz, D_2O, 25 °C) expansion of alkyl-region signals in spectrum of [Y(octapa)]$^{-}$, showing no correlations between broad signals arising from a fluxional species (blue arrows, identified by VT-NMR, Figure 5.3), and sharp signals arising from a single static isomer (see Figure A.6 for full spectrum). 174

Figure 5.6 ^{1}H-^{13}C HSQC NMR (400/100 MHz, D_2O, 25 °C) expansion of aromatic signals in spectrum of [Y(octapa)]$^{-}$, showing correlations to ~5 unique ^{13}C signals, suggesting the presence of a single static isomer (red arrows), along with a fluxional species (blue arrows) (^{13}C NMR spectra externally referenced to MeOH in D_2O) (see Figure A.7 for full spectrum). 175

Figure 5.7 ^{1}H-^{13}C HSQC NMR (400/100 MHz, D_2O, 25 °C) expansion of alkyl-region signals in spectrum of [Y(octapa)]$^{-}$, showing correlations to ~4 unique and strong ^{13}C signals from a static isomer (red arrows), and several weak correlations arising from a fluxional species (blue arrows) (^{13}C NMR spectra externally referenced to MeOH in D_2O) (see Figure A.7 for full spectrum). 176

Figure 5.8 *In silico* DFT structure predictions: (a) 8-coordinate structure of $[Y(octapa)]^-$ (top, left); (b) 9-coordinate structure of $[Y(octapa)(H_2O)]^-$ (top, right), as well as the MEP polar-surface area maps (bottom) predicting the charge distribution over the solvent-exposed surface of the metal complexes (red = negative, blue = positive, representing a maximum potential of 0.200 au and a minimum of -0.200 au, mapped onto electron density isosurfaces of 0.002 $Å^{-3}$),]. DFT calculations performed by Dr. Jacqueline Cawthray. 178

Figure 6.1 Structures of the new pyridinecarboxylate-based ligand H_4C3octapa (propylene-bridged) and the bifunctional derivative *p*-SCN-Bn-H_4C3octapa, and the popular ^{111}In/^{177}Lu/$^{86/90}$Y bifunctional ligands DO3A-NHS and DO3A-SCN. 199

Figure 6.2 Stacked ^{1}H NMR spectra of the ligand H_4C3octapa (D_2O, 25 °C, 600 MHz), metal complex $[In(C3octapa)]^-$ (D_2O, 25 °C, 400 MHz) showing complicated but sharp signals suggesting multiple static isomers, and $[Lu(C3octapa)]^-$ (D_2O, 25 °C, 300 MHz) showing complicated and broad signals suggesting fluxional isomerization. 205

Figure 6.3 Stacked ^{1}H NMR spectra of the ligand H_4octapa (D_2O, 25 °C, 300 MHz), metal complex $[In(octapa)]^-$ (D_2O, 25 °C, 600 MHz) showing simple and sharp diastereotopic splitting suggesting the presence of one static isomer, and $[Lu(octapa)]^-$ (D_2O, 25 °C, 400 MHz) showing complicated and sharp signals suggesting multiple static isomers. 207

Figure 6.4 ^{1}H COSY NMR (400 MHz, D_2O, 25 °C) spectrum of $[In(C3octapa)]^-$ showing an expansion of the alkyl-region, highlighting two broad signals with red arrows arising from the central $–CH_2-$ of the propylene bridge, showing no ^{1}H-^{1}H correlations to each other. .. 208

Figure 6.5 ^{1}H-^{13}C HSQC NMR (400/100 MHz, D_2O, 25 °C) expansion of aromatic signals in spectrum of $[In(C3octapa)]^-$, showing correlations to 12 unique ^{13}C signals, with an

additional aromatic signal at 125.32 ppm not shown (^{13}C NMR spectra externally referenced to MeOH in D_2O). 210

Figure 6.6 ^{1}H-^{13}C HSQC NMR (600/150 MHz, D_2O, 25 °C) expansion of aromatic signals in spectrum of [Lu(C3octapa)]$^{-}$, showing correlations to 10 unique ^{13}C signals (^{13}C NMR spectra externally referenced to MeOH in D_2O). 211

Figure 6.7 Variable temperature (VT) ^{1}H NMR experiments with [In(C3octapa)]$^{-}$ (D_2O, 400 MHz), with the temperature increased to 85 °C in 20 °C increments. 213

Figure 6.8 Variable temperature (VT) ^{1}H NMR experiments with [Lu(C3octapa)]$^{-}$ (D_2O, 400 MHz), with the temperature increased to 85 °C in 20 °C increments. 214

Figure 6.9 *In silico* DFT structure predictions: (a) 8-coordinate structure of [In(C3octapa)]$^{-}$ (top) from two perspectives; (b) 8-coordinate structure of [Lu(C3octapa)]$^{-}$ (bottom) from two perspectives, with both structures showing overlayed MEP polar-surface area maps predicting the charge distribution over the solvent-exposed surface of the metal complexes (red = negative, blue = positive, representing a maximum potential of 0.254 au and a minimum of -0.254 au, mapped onto electron density isosurfaces of 0.002 Å^{-3}). DFT calculations performed by Dr. Jacqueline Cawthray. 217

Figure 6.10 Stability of the immunoconjugates ^{111}In(octapa)-trastuzumab and ^{111}In(C3octapa)-trastuzumab in both phosphate buffered saline (PBS) and human blood serum, evaluated by spotting ~1 μCi of serum competition mixture on silica-embedded paper iTLC plates and eluting with aqueous EDTA (50 mM, pH 5) mobile phase. 222

Figure 6.11 Stability of the immunoconjugates ^{177}Lu(octapa)-trastuzumab and ^{177}Lu(C3octapa)-trastuzumab in both phosphate buffered saline (PBS) and human blood

serum, evaluated by spotting ~1 μCi of serum competition mixture on silica-embedded paper iTLC plates and eluting with aqueous EDTA (50 mM, pH 5) mobile phase. 223

Figure 7.1 The current "gold standard" ligand for ^{89}Zr, DFO, and the new entrants H_6phospa (7.2) and bifunctional analogue *p*-SCN-Bn-H_6phospa (7.10). 242

Figure 7.2 A) iTLC radiochromatograph of the unpurified radiolabeling mixture of ^{111}In-phospa-trastuzumab (30 minutes, 25 °C, 2.64 mCi/mg); B) iTLC of ^{111}In-phospa-trastuzumab after purification by PD-10 column; C) iTLC trace of the unpurified radiolabeling mixture of ^{177}Lu-phospa-trastuzumab (30 minutes, 25 °C, 2.23 mCi/mg); and D) iTLC trace of ^{177}Lu-phospa-trastuzumab after purification, showing ^{177}Lu transchelated from the weakly-bound ^{177}Lu-phospa-trastuzumab to $EDTA^{4-}$ (~200 μg of antibody conjugate used for each reaction). 248

Figure 7.3 The stability of ^{177}Lu/^{111}In-phospa-trastuzumab in human blood serum over 120 h, agitated at 300 rpm and 37 °C, analyzed via radio-iTLC elution with EDTA mobile phase (50 mM, pH 5), compared to previously obtained values for ^{177}Lu/^{111}In-octapa-trastuzumab as a reference.[87] 249

Figure 7.4 Radiolabeling results of H_6phospa-trastuzumab with ^{89}Zr in phosphate buffered saline (pH 7.4), showing results at both room temperature and 37 °C with H_6phospa-trastuzumab (3.3 ± 0.1 chelates per antibody) (~300 μg of antibody conjugate used for each reaction and ~1 mCi of ^{89}Zr). 251

Figure 7.5 SPECT/CT images of ^{111}In-phospa-trastuzumab in female nude athymic mice bearing SKOV-3 tumour xenografts in the right shoulder (diameter ~2 mm), imaged at 24, 72, and 120 hrs p.i. (~800-810 mCi injected activity, ~150-200 μg antibody per mouse)... 253

Figure 7.6 SPECT/CT images of ^{177}Lu-phospa-trastuzumab in female nude athymic mice bearing SKOV-3 tumour xenografts in the right shoulder (diameter ~2 mm), imaged at 24 and 72 hrs p.i. (~575 mCi injected activity, ~150-200 μg antibody per mouse). 254

Figure 8.1 Structures of selected state-of-the-art "gold standard" ^{64}Cu ligands, and the new ligand H_2azapa. 269

Figure 8.2 ^{1}H NMR spectra (DMSO-d_6, 25 °C) of (top) H_2azapa, 300 MHz; (middle) $[Ga(azapa)]^+$, 600 MHz; (middle) $[In(azapa)]^+$, 400 MHz; and (bottom, 300 MHz, D_2O) $[Lu(azapa)]^+$. 276

Figure 8.3 Variable temperature (VT) ^{1}H NMR spectra of $[In(azapa)]^+$ (400 MHz, DMSO-d_6) with the temperature increasing from 25 °C to 135 °C. 277

Figure 8.4 ORTEP drawing of the solid-state molecular structure of $[In(azapa)(H_2O)][ClO_4]$ obtained by X-ray diffraction. Hydrogen atoms are omitted for clarity. 279

Figure 8.5 ORTEP drawing of the solid-state molecular structure of [Cu(azapa)]. Hydrogen atoms are omitted for clarity. 282

Figure 8.6 Biodistribution of $[^{64}Cu(azapa)]$ and $[^{64}Cu(DOTA)]^{2-}$ showing organ and tissue uptake as percent injected dose per gram (% ID/g) obtained over 24 h in healthy athymic nude mice; Y-axis is normalized at 25% ID/g for clarity. 286

Figure 8.7 PET images of two (A and B) healthy female nude athymic mice injected with $[^{64}Cu(azapa)]$ and imaged at 1, 4, and 24 h post injection, with the scales being different for the left images at 20 %ID/g and for the right images being 8 %ID/g. 287

List of Schemes

Scheme 2.1 Synthesis of compounds 2.1, 2.2, 2.3, 2.4, 2.5, 2.6 and H_4octapa[a] 57

Scheme 2.2 Synthesis of compounds 2.7, 2.8, 2.9, 2.10 and H_5decapa[a] 59

Scheme 3.1 Improved synthesis of picolinic acid-based ligands H_4octapa (3.5) and *p*-SCN-Bn-H_4octapa (3.12).[a] 98

Scheme 4.1 Synthesis of Bn-H_3nonapa (4.3) and H_3nonapa (4.4). [a] 136

Scheme 4.2 Synthesis of Bn-H_3trenpa (4.7). [a] 137

Scheme 4.3 Synthesis of *p*-NO_2-Bn-H_3nonapa (4.10). [a] 138

Scheme 5.1 Syntheses of H_2dedpa (5.6) and H_4octapa (5.8) using *tert*-butyl ester protection chemistry[a] 165

Scheme 5.2 Synthesis of *p*-SCN-Bn-H_2dedpa (5.14), and *p*-SCN-Bn-H_4octapa (5.16) using *tert*-butyl ester protection chemistry[a] 168

Scheme 6.1 Synthesis of H_4C3octapa (6.5) utilizing nosyl protection chemistry.[a] 203

Scheme 6.2 Synthesis of *p*-SCN-Bn-H_4C3octapa (6.15) utilizing nosyl protection chemistry.[a] 204

Scheme 7.1 Synthesis of H_6phospa (7.2) and *p*-SCN-Bn-H_6phospa (7.10) [a] 244

Scheme 8.1 Synthesis of click-based ligand H_2azapa (8.5) [a] 272

List of Symbols and Abbreviations

~	approximate
%ID/g	percentage of injected radioactive dose per gram of tissue
2D	two dimensional
3D	three dimensional
α	alpha particle
Å	Angstrom, $10 \cdot 10^{-10}$ m
β^-	beta particle
β^+	positron
γ	gamma ray
δ	delta or chemical shift in parts per million (NMR)
Δ	heat
μ	micro (10^{-6})
μM	micromolar (10^{-6} M)
AAS	atomic absorption standard
AcOH	acetic acid
Anal.	analytical
ANOVA	analysis of variance
atm	atmosphere
BFC	bifunctional chelate, also means bifunctional ligand
biomolecule	vector, biovector, targeting vector, (e.g. antibody, peptide)
Bn	benzyl
t-Boc	*tert*-butoxycarbonyl
Boc_2O	di-*tert*-butyl-dicarbonate
br	broad (NMR), e.g. br s (broad singlet)
°C	degrees celsius
calcd.	Calculated
MeCN	acetonitrile

Ci	Curie
CLI	Cerenkov luminescence imaging
cm^{-1}	wavenumber
CN	coordination number
COSY	correlation spectroscopy (^{1}H-^{1}H NMR)
CR	Cerenkov radiation
CT	computed tomography
CV	cyclic voltammetry
d	day(s) or doublet (NMR)
DCM	dichloromethane
DFT	density functional theory (*in silico* calculations)
DFO	desferrioxamine B
dien	diethylenetriamine
DMF	dimethylformamide
DMSO	dimethylsulfoxide
DOTA	1,4,7,10-tetraazacyclododecane -*N,N′,N″,N‴*-tetraacetic acid
DTPA	diethylenetetraaminepentaacetic acid
EA	elemental analysis
EDTA	ethylenediaminetetraacetic acid
ESI-MS	electrospray ionization mass spectrometry
EtOAc	ethyl acetate
EtOH	ethanol
en	ethylenediamine
eV	electron volt
equiv.	equivalent(s)
FDA	Food and Drug Administration (USA)
FDG	2-deoxy-2-[^{18}F]fluoro-D-glucose
g	gram
h	hour(s)
Herceptin®	see trastuzumab

HMBC	heteronuclear multiple bond correlation/coherence (^{1}H-^{13}C NMR)
HSQC	heteronuclear single bond correlation/coherence (^{1}H-^{13}C NMR)
HPLC	high performance liquid chromatography
Hz	hertz
iTLC	instant thin layer chromatography (typically radioactive)
in silico	performed on a computer
IR	infrared
ID	injection dose
J	coupling constant (NMR)
k	kilo
K_{ML}	thermodynamic complex stability constant
L	litre or ligand
LET	linear energy transfer
m	milli- or medium or multiplet
M	molar (moles/ litre) or mega
MeOH	methanol
MEP	molecular electrostatic potential
min	minute(s)
mol	mole
MRI	magnetic resonance imaging
MS	mass spectrometry
m/z	mass per unit charge
n	nano (10^{-9}) or number of unit
NBS	*N*-bromosuccinimide
NHE	normal hydrogen electrode
NHS	*N*-hydroxysuccinimide
NMR	nuclear magnetic resonance
nM	nanomolar (10^{-9} M)
Nosyl	2-nitrobenzenesulfonamide (protecting group)
NOTA	1,4,7-triazacyclononane-1,4,7-triacetic acid

NRU	National Research Universal (reactor)
ORTEP	Oak Ridge Thermal Ellipsoid Plot Program
PBS	phosphate buffered saline
Pd/C	palladium on carbon (10% by weight)
PET	positron emission tomography
pH	$-\log[H_3O]^+$
p.i.	post injection
pM	-log[free metal], or picomolar (10^{-12} M)
pn	propylenediamine
ppm	parts per million
q	quartet (NMR)
®	trademark
RCY	radiochemical yield
R_f	retention factor
RIT	radioimmunotherapy
RT	room temperature
R_t	retention time
s	singlet (NMR) or strong (IR)
SD	standard deviation
SPECT	single photon emission computed tomography
t	triplet (NMR) or time
t_R	retention time (HPLC)
$t_{1/2}$	half-life
^{t}BuOH	*tert*-butanol
THF	tetrahydrofuran
TFA	trifluoroacetic acid
TFP	tetrafluorophenyl
TLC	thin layer chromatography
trastuzumab	HER2/*neu* targeting antibody
TREN	tris(2-aminoethyl)amine

UV	ultraviolet
V	volt
VT-NMR	variable temperature NMR
w	weak (IR)

Acknowledgements

There are many people that I want to acknowledge and thank for their important presence in my life during the ~5 year period while I completed the work presented in this thesis. My parents Steve P. and Fiona P., who have offered boundless support and encouragement to me since I was a child, without whom the lofty goals to which I've aspired may never have been achieved. My grandmother Marie Carr, and my brothers Kyle P. and Ryan P., who have remained positive and proud through this process, and Ryan's new family Lindsay P. and their son Wyatt P. The understanding and love of my partner Rhea D. has helped make this process possible. The deep friendships of Brandon L. and David S. have helped keep me grounded, and their generous sponsorship of my inclusion into several of their vacations has been phenomenal. To all of my collaborators and supporters: Eszter B. for helping me get started; Cara F. and Dennis W. for radiochemistry and career inspiration; James I. for mentoring and friendship since my undergraduate days; Kuo-Shyan L. at BC Cancer for peptides and support; and to Brian Z. and Jason L. at Memorial Sloan-Kettering Cancer Center for allowing me to visit and impose on them for 2 months, without whom a huge body of my work would never have been completed. I also want to thank the support staff at UBC for being crucial to solving many of my problems: Maria E. and Paul X. in the NMR labs; Yun L., Marshall L., Derek S., and Marco Y. in the MS labs; and Brian P. and Anita L. in the X-ray labs. I want to thank Gwendolyn B. for being the best undergraduate student anyone could ever hope to work with. I would also like to thank all Orvig group members who have shared the struggles and satisfaction of graduate school with me, for attending countless group meetings and providing a lot of help. I owe a big thank you to Jacqueline C. for being a huge help to me throughout my PhD and playing a very important role in almost every chapter of this thesis. Finally I must thank my supervisors Chris O. and Michael A. for endless support and trust, and for encouraging me and funding me to attend international conferences and collaborations, which I could never have participated in without their help, and at which I met many collaborators and friends. Thank you to my PhD committee Glenn S., Pierre K., and Mike F., because you were available to assist me, and I know you had better things to do than read my verbose 9 chapter thesis. Thank you to NSERC for CGS-M, CGS-D, and now PDF funding. To all of these people I owe sincere thanks and the utmost gratitude.

Dedication

For my family, partner, close friends, collaborators, and mentors, for endless support and encouragement.

Chapter 1: Introduction

This chapter is an adaptation of published work, and is reproduced in part, with permission from Price, E. W.; Orvig, C., Matching Chelators to Radiometals for Radiopharmaceuticals. *Chem. Soc. Rev.* **2014,** *43* (1), 260-290, Copyright 2014 The Royal Society of Chemistry.

1.1 Background and aims

Radiometals are radioactive isotopes that can be harnessed for applications in medical diagnosis, as well as for cancer therapy.[1-9] In order to apply these isotopes to specific biological applications, the "free" radiometal ions must be sequestered from aqueous solution using chelators (ligands) to obviate transchelation and hydrolysis. Ligands used for this application are typically covalently linked to a biologically active targeting molecule (also called vectors or biomolecules), making an active radiopharmaceutical agent. The ligand is used to tightly bind a radiometal ion so that when injected into a patient, the targeting molecule can deliver the isotope without any radiometal loss from the radiopharmaceutical, effectively supplying a site-specific radioactive source *in vivo* for imaging or therapy. Because some of the most popular targeting vectors are sensitive to elevated temperatures, such as antibodies and antibody fragments, ligands that are capable of quantitatively radiolabeling at ambient temperature (25 °C) are of great interest and utility. Acyclic ligands generally possess faster radiolabeling properties than do macrocyclic ligands; however, the stability and inertness of acyclic ligands tends to be inferior to macrocycles *in vivo*. The specific aims of this body of work are to investigate new acyclic ligands with fast

radiolabeling properties with a variety of radiometals, that also possess comparable stability to the currently used macrocyclic ligands.

1.2 Nuclear imaging and therapy

Positron emission tomography (PET) imaging is a very accurate and quantitative imaging technique, which utilizes positron particles (β^+, anti-electrons) that are emitted from a radioactive isotope upon decay. After emission, the β^+ particle travels a short distance before meeting with an electron and annihilating, which results in two gamma rays (511 keV) ejected at 180 degrees to each other. These gamma rays are detected by a fixed circular array of coincidence detectors arranged around the subject, where only gamma rays that strike the detector at the same time are registered. This process allows for 3D images to be constructed that identify the source (radioactive isotope) of β^+ emission within the subject, with this source ideally being targeted to a specific location (e.g. cancer cells). Single photon emission computed tomography (SPECT) operates on a very similar principle to PET. SPECT imaging differs from PET in that emission of single gamma rays from an isotope is detected, rather than two coincident gamma rays ejected from positron annihilation. SPECT has decreased image resolution and sensitivity compared to PET, largely because SPECT machines utilize pinhole collimators, whereas PET utilizes a circular array of coincidence detectors and no collimators. Additionally, gamma ray emission does not occur at the same energy for all isotopes, and many isotopes eject several gamma rays of different energies, which can complicate data collection. To utilize direct gamma ray emissions for SPECT imaging, several detectors physically rotate around the subject, stopping at many different orientations to perform the lengthy process of acquiring many 2D images, which are used to

reconstruct 3D images. The archetypical PET isotope is ^{18}F, which has a very high positron (β^+) abundance of 96%, and a low energy β^+ emission of 640 keV (short mean free path from decay location providing high resolution and accuracy). Many of the more exotic PET radiometal isotopes discussed here have lower positron abundances (low branching ratios, ~20-60% decay by β^+) and higher positron energies, which decreases the accuracy of data collection and requires longer image acquisition times and/or higher activity injected dose.[10] For β^+ annihilation and subsequent detection to occur the β^+ must be sufficiently slowed down after emission for it to meet with an electron and annihilate. The size of the spherical radius that a positron travels from its source is dependent on its energy, and higher energy positrons travel a larger radius and therefore decrease spatial resolution. In general, lower energy β^+ and γ emissions provide better image quality. For example, the nuclides ^{86}Y and ^{89}Zr emit a large amount of γ rays relative to the amount of positrons (poor branching ratios). These additional γ emissions can both complicate PET imaging by interfering with the detection of coincident 511 keV γ rays that originate from β^+ emission/annihilation events, and increase the radioactive dose accumulated by patients.[11,12] Despite these shortcomings, the PET nuclides discussed here have a multitude of chemical and physical properties that make them attractive for imaging purposes.

Radiotherapeutic effects are derived from the damage that ionizing radiation does to living cells, where gamma rays, β^+ particles, and β^- particles (high energy electrons) can strip electrons directly from cells, or can create harmful reactive oxygen species from water and other molecules present in living tissue. Alpha particles (α) are helium nuclei that travel very short distances in living tissue, but that have very high linear energy transfer values (LET), meaning they deposit massive amounts of energy over a very small distance, having

the ability to literally blast cells apart. Radionuclides are typically produced by proton (p,n) or deuteron (d,2n) bombardment via a cyclotron, neutron bombardment via a nuclear reactor (n,xp), or by elution from a generator system (e.g. ^{68}Ge/^{68}Ga, where the parent nuclide in generators must be produced via cyclotron or reactor). The most common production methods of various isotopes are displayed in Table 1.1.

1.3 Popular radiometal isotopes

The availability of a wide range of radiometal ions makes it possible to carefully pick the specific nuclear properties that are needed for a vast number of different applications (Table 1.1).[13-16] Some examples of radiometals that can be used for positron emission tomography (PET) imaging are ^{68}Ga, ^{64}Cu, ^{86}Y, ^{89}Zr, and ^{44}Sc, with PET imaging providing sensitive, quantitative, and non-invasive images of a variety of molecular processes and targets. Single photon emission computed tomography (SPECT) is an older and more ubiquitous imaging modality than PET, and, since its inception in the 1960s, ^{99m}Tc has been the workhorse isotope of SPECT. More recently, the radiometals ^{67}Ga, ^{111}In, and ^{177}Lu have been increasingly used for SPECT imaging in chelator-based radiopharmaceuticals. For therapy applications, particle emitters such as ^{111}In (Auger electron emitter), ^{90}Y and ^{177}Lu (β^-), and ^{225}Ac, ^{212}Pb, and ^{213}Bi (α), are being heavily investigated, typically in conjunction with antibody vectors (immunoconjugates) or peptides. Each radiometal ion has unique aqueous coordination chemistry properties; these must be properly addressed to if these isotopes are to be safely harnessed for medical applications and use *in vivo*.

Table 1.1 Properties of some popular radiometal isotopes, EC = electron capture; some low abundance emissions have been omitted for brevity.[6,13-17]

Isotope	$t_{1/2}$ (h)	Decay mode	E (keV)	Production method
^{60}Cu	0.4	β^+ (93%) EC (7%)	β^+, 3920, 3000, 2000	cyclotron, ^{60}Ni(p,n)^{60}Cu
^{61}Cu	3.3	β^+ (62%) EC (38%)	β^+, 1220, 1150, 940, 560	cyclotron, ^{61}Ni(p,n)^{61}Cu
^{62}Cu	0.16	β^+ (98%) EC (2%)	β^+, 2910	^{62}Zn/^{62}Cu generator
^{64}Cu	12.7	β^+ (19%) EC (41%) β^- (40%)	β^+, 656	cyclotron, ^{64}Ni(p,n)^{64}Cu
^{66}Ga	9.5	β^+ (56%) EC (44%)	β^+, 4150, 935	cyclotron, ^{63}Cu($\alpha,n\gamma$)^{66}Ga
^{67}Ga	78.2	EC (100%)	γ, 93, 184, 300	cyclotron, ^{68}Zn($p,2n$)^{67}Ga
^{68}Ga	1.1	β^+ (90%) EC (10%)	β^+, 1880	^{68}Ge/^{68}Ga generator
^{44}Sc	3.9	β^+ (94%) EC (6%)	γ, 1157 β^+, 1474	^{44}Ti/^{44}Sc generator
^{47}Sc	80.2	β^- (100%)	γ, 159 β^-, 441, 600	^{47}Ti(n,p)^{47}Sc
^{111}In	67.2	EC (100%)	γ, 245, 172	cyclotron, ^{111}Cd(p,n)^{111m,g}In
^{114m}In ^{114}In (daughter)	49.5 d 73 s	EC (100%) β^- (100%)	γ, 190 β^-, 1989	cyclotron, ^{114}Cd(p,n)^{114m}In or ^{116}Cd($p,3n$)^{114m}In
^{177}Lu	159.4	β^- (100%)	γ, 112, 208 β^-, 177, 385, 498	^{176}Lu(n,γ)^{177}Lu
^{86}Y	14.7	β^+ (33%) EC (66%)	β^+, 1221	cyclotron, ^{86}Sr(p,n)^{86}Y
^{90}Y	64.1	β^- (100%)	β^-, 2280	^{90}Zr(n,p)^{90}Y
^{89}Zr	78.5	β^+ (23%) EC (77%)	β^+, 897	cyclotron, ^{89}Y(p,n)^{89}Zr
^{212}Bi	1.1	α (36%) β^- (64%)	α, 6050 β^-, 6089	^{228}Pb/^{212}Pb generator
^{213}Bi	0.76	α (2.2%) β^- (97.8%)	α, 5549 β^-, 5869	^{228}Th/^{212}Pb generator
^{212}Pb (daughter is ^{212}Bi)	10.6	β^- (100%)	α, 570	^{224}Ra/^{212}Pb generator
^{225}Ac	240	α (100%)	α, 5600-5830 (6)	^{226}Ra($p,2n$)^{225}Ac n-Capture of ^{232}Th ➔ ^{233}U ➔ ^{225}Ac

The major difference between radioactive ("hot") and non-radioactive ("cold") metal ion chemistry is that radiochemistry is typically performed under extremely dilute conditions, with radiometal ions typically being utilized at nmol to pmol quantities.[18] It is also important to note that several of the elements being discussed have multiple radioactive isotopes that are useful for diagnostic or therapeutic purposes (e.g. $^{86/90}$Y, $^{67/68}$Ga, $^{44/47}$Sc, $^{60/61/62/64}$Cu), and all isotopes of a given element have identical chemistry.[19-24] This means that a single radiopharmaceutical agent can be radiolabeled with different isotopes of the same element (e.g. $^{86/90}$Y), and provide the same charge and physical properties, and therefore the same biological behavior and distribution *in vivo*.[19-24] This class of radiopharmaceutical that utilizes two isotopes of the same element, such as ^{86}Y for PET imaging and ^{90}Y for therapy, has been referred to as a theranostic agent.[25,26] Alternatively, ^{90}Y is unique and in some circumstances can be used directly for PET imaging because it emits a very low abundance of positrons (0.003%), which can be used to collect imaging data superior to that obtained by ^{90}Y Bremsstrahlung imaging.[27]

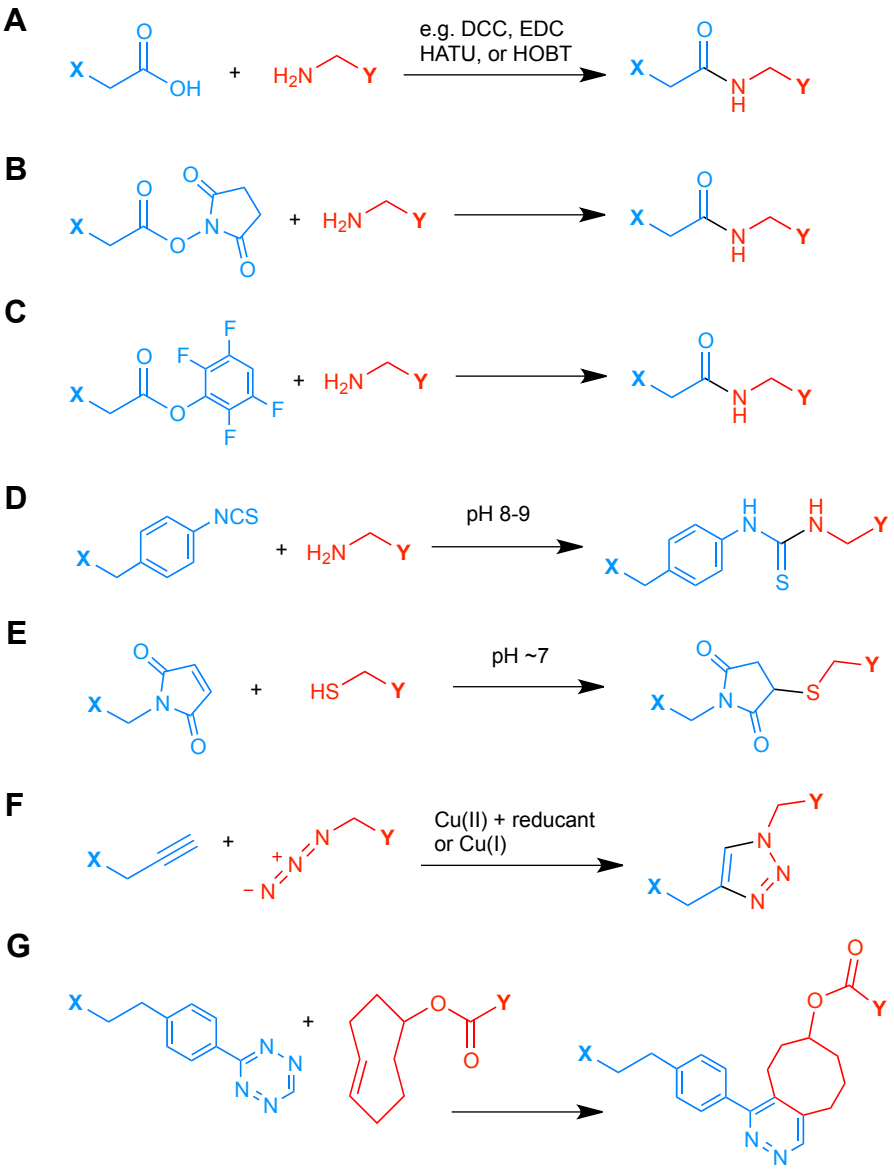

Figure 1.1 Examples of bioconjugation reactions: (A) standard peptide coupling reaction between a carboxylic acid and a primary amine with a coupling reagent; (B-C) peptide coupling reactions between activated esters of *N*-hydroxysuccinimide (NHS) or tetrafluorophenyl (TFP) olaand a primary amine; (D) thiourea bond formation between an isothiocyanate and a primary amine; (E) thioether bond formation between a maleimide and thiol; (F) standard Cu(I) catalyzed Huisgen 1,3-dipolar cycloaddition ("click" reaction) between an azide and an alkyne; and (G) strain-promoted Diels-Alder "click" reaction between a tetrazine and transcyclooctene.

1.4 Radiometal-based radiopharmaceutical design

Ligands that are typically used to construct radiometal-based radiopharmaceuticals (not always with ^{99m}Tc) are bifunctional chelators (BFCs), which are simply ligands with

reactive functional groups that can be covalently coupled (conjugated) to targeting vectors (e.g. peptides, nucleotides, antibodies, nanoparticles). Common bioconjugation techniques utilize functional groups such as carboxylic acids or activated esters (e.g. *N*-hydroxysuccinimide NHS-ester, tetrafluorophenyl TFP-ester) for amide couplings, isothiocyanates for thiourea couplings, and maleimides for thiol couplings (Figure 1.1).[2,28] Click chemistry is gaining popularity in bioconjugate chemistry, with both the traditional copper(I) catalyzed azide-alkyne Huisgen 1,3-dipolar cycloaddition "click" reaction (forming a 1,2,3-triazole-ring linkage), or newer copper-free reactions such as strain-promoted azide-alkyne cycloadditions (e.g. dibenzocyclooctyne/azide reaction) and Diels-Alder click reactions (e.g. transcyclooctene/1,2,4,5-tetrazine) (Figure 1.1).[29] It is interesting to note that the transcyclooctene/1,2,4,5-tetrazine copper-free click coupling displays remarkably fast reaction kinetics, allowing for novel applications such as *in vivo* pre-targeting, where the click reaction can occur *in vivo* at very dilute concentrations.[30-34] The modular design of BFC systems allows for a theoretically limitless number of different vectors to be conjugated, providing molecular targeting to a constantly increasing number of biological targets.

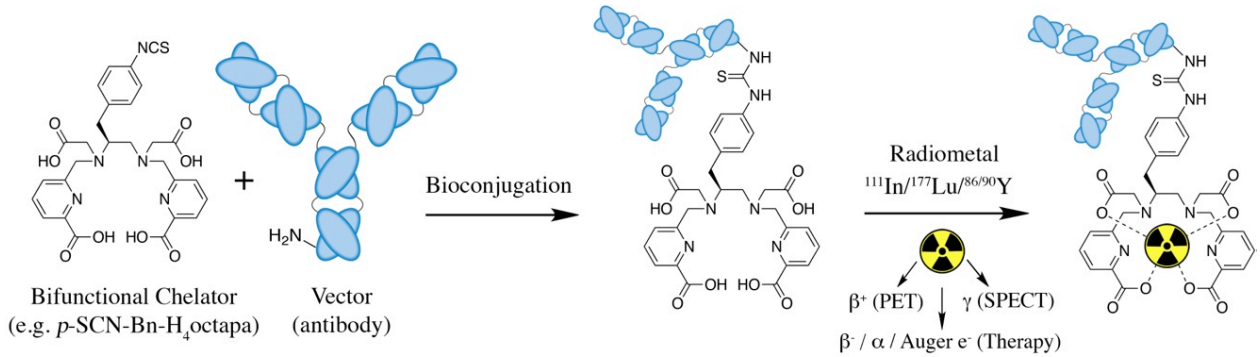

Figure 1.2 Illustration of an archetypal radiometal-based radiopharmaceutical agent containing a bifunctional chelator (BFC) conjugated to a targeting vector (e.g. antibody, peptide, nanoparticle) using a variety of conjugation methods (e.g. isothiocyanate-amine coupling (shown), peptide coupling, maleimide-thiol coupling, activated ester amide coupling, click-coupling) and then radiolabeled with a radiometal ion (e.g. $^{111}In^{3+}/^{177}Lu^{3+}/^{86/90}Y^{3+}$).

The structure and physical properties of the radiometal-chelate complex have a large impact on the overall pharmacokinetic properties of a radiopharmaceutical, with many radiometal complexes being very hydrophilic and subsequently leading to rapid renal excretion when attached to small vectors such as peptides and nucleotides (less prominent with large ~150 kDa antibodies).[19-24] It has been observed in peptide-conjugates that keeping the radiometal ion and peptide constant, and changing only the ligand can have drastic effects on biodistributions.[35] Radiometal-based radiopharmaceuticals contain many synthetically exchangeable components, which can be separated into different modules: the radiometal, which changes the radioactive emission properties and half life (γ for SPECT, β^+ for PET, and β^-/α particles or Auger electrons for therapy); the ligand, which must be carefully matched with the radiometal for optimal stability; the BFC-vector conjugation method, for different types of bioconjugation reactions and linkages; and the vector/targeting moiety, which allows for the selection of any known molecular target for site-specific delivery of the radioactive "payload" (Figure 1.2).

Each radiometal ion has different chemical demands, including ligand donor atom preferences (e.g. N, O, S, hard/soft), coordination number, and coordination geometry; however, there are many key design considerations that can be applied universally.[7] Ligand synthesis should be relatively simple and avoid stereoisomers, and the ligand should ideally be synthesized with modular synthons so that bioconjugation handles and donor atoms can be easily changed. There is much utility in being able to tune the denticity and physical properties/polarity/charge of the ligand (the degree of polarity can be assessed by octanol-water partition coefficients (log P)), so that biodistribution properties can be adjusted.

Before creating new ligands for radiochemistry, it should be understood how to properly evaluate them. The methods by which ligands are evaluated with different radiometals will be discussed, and the current "gold standard" ligands for each relevant radiometal ion will be identified. A substantial amount of work has been done in the field of radiometal chelation, and it is prudent to properly introduce the material relevant to the work done in this thesis.[2,4-9,15,26,28,36-56]

1.4.1 Macrocyclic versus acyclic ligands

When designing new ligands, a historical glance at previous work reveals that macrocycles are generally more kinetically inert than acyclic chelators, even if their thermodynamic stabilities have been determined to be very similar.[57-61] Macrocyclic chelators require minimal physical manipulation during metal ion coordination, as they possess inherently constrained geometries and partially pre-organized metal ion binding sites, thereby decreasing the entropic loss experienced upon metal ion coordination.[62] To contrast this, acyclic chelators must undergo a more drastic change in physical orientation and geometry in solution in order to arrange donor atoms to coordinate with a metal ion, and subsequently they suffer a more significant decrease in entropy than do macrocycles (thermodynamically unfavorable). The thermodynamic driving force towards complex formation is therefore greater for macrocycles in general, a phenomenon referred to as the macrocycle effect.[62] A crucial property where most acyclic chelators excel and most macrocycles suffer is in the coordination kinetics and radiolabeling efficiency. The ability to quantitatively radiolabel/coordinate with a radiometal in less than 15 minutes at room temperature is a common property of acyclic chelators, whereas macrocycles often require

heating to 60-95 °C for extended times (30-90 minutes).[63-65] Fast room temperature radiolabeling becomes a crucial property when working with BFC-conjugates of heat sensitive molecules such as antibodies and their derivatives, or when working with short half-life isotopes such as ^{68}Ga, $^{212/213}$Bi, ^{44}Sc, and ^{62}Cu.

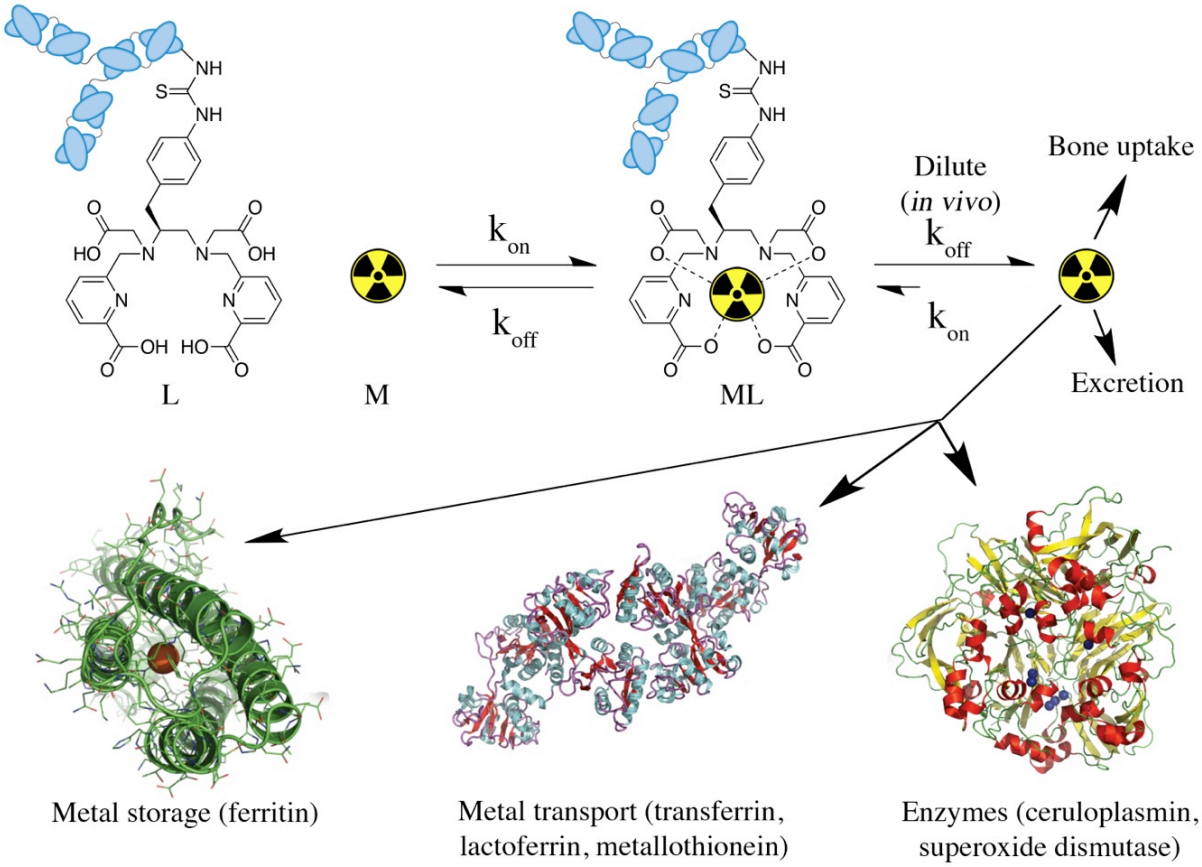

Figure 1.3 Cartoon depiction of metal ion coordination kinetics, enhanced off-rate kinetics *in vivo* (extremely dilute conditions), and possible routes of radiometal ion loss *in vivo*.

1.4.2 Matching ligands with radiometals – how are ligands evaluated?

When a new ligand is synthesized for the purpose of radiometal ion sequestration, or an old ligand is repurposed for use with a new radiometal ion, initial screening experiments

are usually done by simple radiolabeling to determine a number of factors: whether the ligand can bind the radiometal ion and effectively radiolabel in high yields (quantitative is best), what temperature is required (ambient temperature is best), and what reaction time is required (faster is better). Short half-life isotopes such as ^{68}Ga are ideally matched with ligands that can radiolabel rapidly (fast radiolabeling kinetics). Longer half-life isotopes such as ^{111}In and ^{177}Lu allow for extended reaction times, but even if the half-life allows for long reaction times, completing the radiolabeling portion of radiopharmaceutical preparation is most convenient if finished in less than 10 or 15 minutes. As previously mentioned, room temperature radiolabeling is crucial for sensitive antibody vectors, which are degraded at elevated temperatures. DOTA inconveniently requires elevated temperatures for radiolabeling with essentially all radiometals (e.g. ^{44}Sc, ^{111}In, ^{177}Lu, $^{86/90}$Y, ^{225}Ac) but its abundant application in radiochemistry for decades, its exceptional *in vivo* stability, and the commercial availability of many different bifunctional DOTA derivatives and vector conjugates are consistent with it being the most commonly used ligand to this day. Moving forward to the design and testing of new ligands, fast room temperature radiolabeling kinetics should be a priority; however, fast kinetics of radiometal incorporation (on-rate) and consequently low energetic barriers to radiometal-chelate complexation can also mean fast radiometal decorporation (off-rates) and low energetic barriers to radiometal release (Figure 1.3, solid-state structures of ferritin H-chain homopolymer PDB file 1FHA, ceruloplasmin PDB file 2J5W, and *apo*-transferrin PDB file 2HAV shown). An arduous balancing act is required to obtain the best set of ligand properties for each application and radiometal ion, requiring the study and availability of a broad selection of different ligands with a variety of properties from which to choose.

When a ligand is identified through early screening to possess radiolabeling properties that are suitable for use with a particular radiometal ion, it must then be experimentally determined to be highly thermodynamically stable and kinetically inert. Further experiments are performed with the specific radiometal-chelate complex under conditions relevant to *in vivo* translation to judge its potential as the core component of a radiometal-based radiopharmaceutical. The result of radiometal loss from a radiopharmaceutical *in vivo* is the non-targeted distribution of the "free" radiometal ion in the body, and its exact fate and distribution in the body depends on the properties and biological behavior of the specific radiometal ion in question (Figure 1.3). For example, ^{89}Zr and ^{68}Ga are known to accumulate in the bone when released from a BFC, where ^{64}Cu is known to accumulate in the liver. The fate of these radiometal ions can be tracked using PET/SPECT imaging in the living animal, and/or biodistribution experiments where animals are euthanized at predetermined time points, their organs harvested, and the distribution of radioactivity measured and calculated for the percentage of injected dose of radioactivity per gram of tissue (%ID/g). Each metal ion has its own unique properties that must be considered when constructing a radiometal-based imaging/therapeutic agent, such as its aqueous hydrolysis chemistry, redox chemistry, and affinity for native biological chelators.

1.4.3 Thermodynamic stability

When evaluating and selecting a ligand to match with a specific radiometal ion for use in a radiopharmaceutical, kinetic inertness *in vivo* is ultimately the most crucial consideration, even beyond that of the absolute thermodynamic stability of the metal-chelate complex. Thermodynamic stability/formation constants (K_{ML} = [ML] / [M][L]) are usually

experimentally determined by potentiometric and/or spectrophotometric titrations, but evaluating kinetic inertness under conditions relevant to *in vivo* applications can be much more problematic. Thermodynamic stability constants can be a useful metric for preliminary comparisons of various ligand with a particular metal ion, but they do not predict *in vivo* stability with any level of competence.[66,67] A thermodynamic parameter that provides more biologically relevant information than K_{ML} values is the pM value ($-\log[M]_{Free}$).[68-71] The pM value is the negative log of the concentration of free metal ion uncomplexed by a given ligand under specific conditions, and is essentially the metal scavenging ability of the ligand; the higher the pM value, the lower the concentration of free metal ion. The pM value is a condition-dependent value that is calculated from the standard thermodynamic stability constant ($\log K_{ML}$), accounting for variables and conditions such as ligand basicity, metal ion hydrolysis, (physiological) pH, and ligand:metal ratio.

Stability constants and pM values provide a number for the direction and magnitude of the equilibrium in a metal-chelate coordination reaction under specific conditions, but give no kinetic information (e.g. off-rates for dissociation).[72,73] This is a very important factor because the rate of dissociation *in vivo* is what governs the kinetic inertness of a radiometal complex, regardless of thermodynamic stability, and these off-rates are greatly influenced by the high dilution encountered *in vivo* when a tiny quantity of radiopharmaceutical (micro- or nano-grams) is diluted into the blood pool (Figure 1.3). Even more complicating is the abundant presence in the body of many strong native biological chelators and competing ions that can transchelate radiometals from BFC-conjugates. These are often present in higher concentrations than is the radiopharmaceutical, and include transport proteins such as transferrin, ceruloplasmin, and metallothionein, storage proteins such as ferritin, and metal

containing enzymes such as superoxide dismutase (Figure 1.3). This wide range of complicating factors means that a single *in vitro* assay is typically not accurate in predicting *in vivo* stability.

1.4.4 Kinetics - Acid dissociation and competitive radiolabeling

Acid dissociation experiments can be used to measure and assess the relative kinetic inertness of a metal complex to acidic conditions. Most complexes are found to de-ligate fairly quickly below pH 2.0,[74] and experiments evaluating the rate of dissociation at a constant pH (e.g. 2.0) have been performed to compare and evaluate ligands with a particular metal/radiometal ion.[59,74,75] In these acid dissociation experiments, decomplexation can be observed over time with techniques such as high-performance liquid chromatography (HPLC), thin-layer chromatography (TLC), and nuclear magnetic resonance (NMR) for diamagnetic metal complexes. With the exception of copper chelates,[72,76] acid dissociation experiments are not commonly performed as they do not provide an accurate prediction of *in vivo* kinetic inertness, because low pH is not encountered in the blood or most organs (except the stomach) and radiometal dissociation typically occurs via transchelation to serum proteins and enzymes, and is not acid-mediated.[73,77-81]

Competitive radiolabeling experiments can be performed by adding to a radiolabeling mixture an excess of non-radioactive ions, such as Na^{+}, K^{+}, Ca^{2+}, Mg^{2+}, Cu^{2+}, Zn^{2+}, or Fe^{3+}, followed by addition of a ligand to evaluate the impact of these competing ions on radiolabeling yields.[59,82-85] These experiments can reveal the radiolabeling selectivity of a ligand for a specific radiometal ion in the presence of other biologically relevant competing ions. Alternatively, if the radiometal complex is preformed under standard metal-free

radiolabeling conditions, and is then added to a mixture containing these competing ions, stability to transchelation can be assessed. Because ligand-based radiopharmaceuticals are typically radiolabeled in strictly metal-free conditions (deionized ultrapure water, often passed through a metal-scavenging chelex resin), these experiments may not appear completely relevant for predicting *in vivo* stability and utility. Depending on the method of radiometal production and purification, the specific activity of radiometal ions can vary greatly, as can the concentrations of impurity metals ions.[18] Radiometals are used in very small quantities and under extremely dilute conditions; therefore, any impurity metal ions present (even if only a few nanomoles) may actually be in excess of the radiometal ion concentration, and competitive binding could be problematic.[18,86] The presence and quantity of metal ion impurities in radiometal mixtures depends on the source of the radiometal ion, method of production, and purification.[18,86]

1.4.5 *In vitro* and *in vivo* stability

Experiments that are more pertinent to *in vivo* translation are metal-exchange competitions with biologically relevant mixtures, including blood serum, *apo*-transferrin, superoxide dismutase, and hydroxyapatite (bone).[28,87-92] By incubating radiometallated ligands with these different competition mixtures, the quantity of radiometal that is transchelated from ligand to serum proteins/enzymes can be evaluated over time using size exclusion HPLC, iTLC, or disposable PD10 size exclusion columns.[28,87-92] These experiments provide a directly relevant measure of stability and kinetic inertness by competition with the most likely transchelation culprits *in vivo*; additionally, in these *in vitro*

assays the concentrations of these biological reagents can often be elevated above normal physiological levels to provide a more stringent challenge.

Ultimately the most relevant and practical test of radiopharmaceutical stability is *in vivo*. Biodistribution studies in healthy mice can be performed on "naked" radiometal-ligand complexes (no conjugated vectors) to assess clearance and uptake profiles and ensure no abnormal organ distribution or critical instability occurs. If a radiometal-ligand complex is very stable *in vivo*, the complex is typically cleared quickly from the animal through the kidneys/bladder/urine or digestive system/liver/feces depending on polarity and metabolism.[93] Unstable complexes often demonstrate persistent uptake in organs and tissues where the non-bound radiometal is known to associate (e.g. Zr^{4+} and lanthanides in the bone, Cu^{2+} in the liver).[93] The major drawback to this type of experiment with "naked" ligand complexes is that highly polar and charged radiometal-ligand complexes are typically cleared very quickly from the body, and therefore do not persist *in vivo* for long enough to encounter any significant challenge to their structural integrity.[88,89] Conversely, highly lipophilic complexes tend to accumulate in the liver and digestive tract, regardless of stability.[88,89]

To evaluate properly the stability and kinetic inertness of a ligand *in vivo*, a suitable vector must be attached (e.g. peptide, antibody, nanoparticle) so that the radiometal-ligand complex is made to persist in blood circulation for a substantial period of time, and can be monitored over several hours or days (depending on isotope half-life and the subsequent imaging/therapy window).[94] An additional concern with *in vivo* experiments is the significant normal variance between animals that introduces error; for example, 10 mice of the same sex and breed, procured from the same supplier, will often show significant differences in biodistribution of the same radiopharmaceutical. Additionally, the specific

experimental techniques and methods (e.g. radiopharmaceutical preparation, injection, animal dissection, organ counting) used for these biodistribution experiments can cause large variability between data sets. Variables such as specific activity of the source radiometal, specific activity of the radiolabeled agent, radiolabeling temperature, purity of the final radiopharmaceutical preparation, injected mass of radiopharmaceutical, and injected volume can make large differences in biodistribution profiles. The same radiopharmaceutical used at different institutions may offer drastically different tumour uptake and organ distribution values, if the above variables are not tightly controlled, and even then differences between animals and between experimental techniques can introduce large variances. For these reasons it is crucial to include internal control experiments for every study; for example, evaluation of a new ligand *in vivo* should be done in parallel with an existing and established "gold standard" ligand so that a direct comparison can be made, because comparison to previously performed studies (even in the exact same animal model and/or cell line) is often not reliable due to the above mentioned complications.[83,87,89,95]

1.5 A selection of ligands and their most suitable radiometal companions

In order to properly design and prioritize experiments towards the discovery and elaboration of new acyclic ligands for radiopharmaceutical applications, a survey of previous work and existing ligands must be executed. A review of radiometal ligands has been undertaken, with the most relevant and promising examples being discussed. The most suitable ligand-radiometal matches have been identified, and detailed tables included, with the aim of providing a quick reference for finding the optimal match between ligand and radiometal. A color-coding scheme has been used, and justification for the assignment of

good (green), fair (orange), and poor (red) matches between ligands and radiometals can be found in the text and the provided references. The color code indicates the general suitability of a ligand for use with a specific radiometal, accounting for factors such as radiolabeling conditions and *in vitro*/*in vivo* stability. An assignment of green may suggest that either a ligand is currently the "gold standard" for use with a given radiometal, or that early work with a new ligand looks very promising and *in vivo* studies have shown that it works comparably to the current "gold standards". Assignment of orange to a ligand-radiometal pair may be made if the combination has been used *in vivo* successfully, but perhaps in recent years has been surpassed by a new and superior ligand and is no longer the best choice. Also, an assignment of orange could mean that a new chelator-radiometal ion pair looks very promising, but perhaps a bifunctional derivative has yet to be synthesized, or only preliminary *in vivo* work has been done and more study is required (e.g. no study of bioconjugates, or no direct comparisons to existing "gold standards" for internal reference). An assignment of red indicates that the highlighted chelator-radiometal ion pair is an unsuitable match, and generally should not be used due to severe instability or radiolabeling problems. These color "ratings" were made using the referenced studies and reflect the current trends in radiochemistry and nuclear medicine.

1.5.1 DOTA

DOTA is one of the primary workhorse ligands for radiometal chemistry, and is one of the current "gold standards" for a number of isotopes, including ^{111}In, ^{177}Lu, $^{86/90}$Y, ^{225}Ac, and $^{44/47}$Sc. DOTA has been extensively used with $^{67/68}$Ga, but is widely accepted to be less stable than its more petite macrocyclic counterpart NOTA (Table 1.2). ^{68}Ga-DOTATOC has

been shown to exhibit superior *in vivo* properties to ^{111}In-DOTATOC (Octreoscan) despite non-optimal stability.[96] Even though a chelator may be more stable and inert with a given radiometal (e.g. NOTA vs. DOTA for ^{68}Ga), it may not be the optimal choice for a certain application (e.g. a specific peptide vector). For example, NOTA is widely accepted to form a more stable complex with ^{68}Ga than does DOTA, but due to differences in charge and physical properties (e.g. neutral vs. charged complex), DOTA may provide superior *in vivo* properties with certain vectors.[35,83] This example highlights the complex set of variables one must consider when constructing radiometal-based radiopharmaceuticals.

When designing new BFCs or modifying existing ligands to make BFC derivatives, care should be taken not to disrupt the original coordination sphere of the chelator. Some common bifunctional DOTA derivatives utilize one of the carboxylic acid arms for the site of vector conjugation, effectively blocking one of the coordinating carboxylate arms (amide carbonyl groups may still coordinate, albeit weakly) (e.g. DOTA-NHS, Table 1.2).[63] DOTAGA, DOTASA, and various isothiocyanate derivatives of DOTA have been synthesized and solve this problem by conjugating to vectors through the carbon backbone and side-arm functionalization (Table 1.2).[63,97-99] These bifunctional DOTA derivatives retain their maximum potential denticity (octadentate) as well as the same thermodynamic stability and kinetic inertness as unadulterated DOTA.[63,97,98]

Despite its slow radiolabeling kinetics and required heating, DOTA is currently the "gold standard" ligand for use with ^{111}In, ^{177}Lu, and $^{86/90}$Y (Table 1.2). The coordination chemistry and properties of Y^{3+} and Lu^{3+} are very similar; they both preferentially form 8-9 coordinate complexes in square antiprismatic or monocapped square antiprismatic geometries, and are hard metal ions with a preference for hard ligand donors such as

carboxylate-oxygens and amine-nitrogens. In^{3+} has similar properties to Y^{3+} and Lu^{3+}, but being smaller forms 7-8 coordinate complexes, typically with square antiprismatic geometry. According to acid dissociation experiments performed at pH 2.0 with the ^{90}Y complexes of DOTA, DTPA (*vide infra*), and CHX-A''DTPA, DOTA is the most kinetically inert to acid dissociation by a significant margin, with CHX-A''-DTPA showing moderate stability, and DTPA decomposing almost immediately.[59] The validity of acid dissociation experiments is questionable, as conditions such as these are never encountered *in vivo* (except for the gastrointestinal tract), but they are a quantifiable metric for measuring off-rate kinetics and further substantiates the place of DOTA as the current "gold standard" ligand for ^{111}In, ^{177}Lu, and $^{86/90}Y$.[59]

Although very little investigation of this isotope has been performed, DOTA is also the current ligand of choice for ^{44}Sc, but the requisite high temperature (90 °C) radiolabeling conditions are not optimal.[100-102] As ^{44}Sc has only recently become more popular in the literature, little *in vivo* work has been performed, and new ligands (preferably with ambient temperature radiolabeling properties) are of strong interest. Another isotope of recent interest for use with DOTA is the α-emitter ^{225}Ac, a large actinide isotope that possesses no non-radioactive isotopologue, making study of its coordination chemistry difficult. The large macrocycles HEHA and PEPA had previously been used most extensively with ^{225}Ac, but recently DOTA has been shown to have superior *in vivo* properties.[103] The long half-life of ^{225}Ac (10.0 days) lends well to radioimmunotherapy (RIT), and so the high temperatures required for ^{225}Ac radiolabeling with DOTA are very unfavorable for sensitive antibodies.

Table 1.2 DOTA and bifunctional derivatives.[a]

Chelator and Common Bifunctional Derivatives	Radiometal Ion	[a]	Radiolabeling Conditions	Log K_{ML}	Proposed Geometry	Ref.
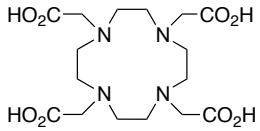 **DOTA**, 1,4,7,10-tetraazacyclododecane-1,4,7,10-tetraacetic acid, maximum CN = 8, donor set N_4O_4	$^{64}Cu^{2+}$	~	25-90 °C, 30-60 min, pH 5.5-6.5	22.2, 22.7	distorted octahedron	88,91,94,104-110
	$^{67/68}Ga^{3+}$	~	37-90 °C, 10-30 min, pH 4.0-5.5	21.3 (pM 15.2, 18.5)	distorted octahedron	68,96,110-118
	$^{44/47}Sc^{3+}$	✓	95 °C, 20-30 min, pH 4.0	27.0 (pM 26.5)	square antiprism	100-102
	$^{111}In^{3+}$	✓	37-100 °C, 15-60 min, pH 4.0-6.0	23.9 (pM 17.8-18.8)	square antiprism?	68,89,97,114,117,119-124
	$^{177}Lu^{3+}$	✓	25-100 °C, 15-90 min, pH 4.0-6.0	23.5, 21.6 (pM 17.1)	square antiprism	124-130
	$^{86/90}Y^{3+}$	✓	25-100 °C, 15-90 min, pH 4.0-6.0	24.3-24.9	square antiprism	59,74,97,124,127,130-132
	$^{213}Bi^{3+}$	~	95-100[133] °C, 5 min, pH 6.0-8.7	-	square antiprism	134,135
	$^{212}Pb^{2+}$	~	25-75 °C, 30-60 min, pH 4.0-5.5	-	square antiprism	127,136-138
	$^{225}Ac^{3+}$	✓	37-60 °C, 30-120 min, pH 6.0	-	square antiprism?	139,140

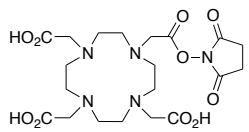
DOTA-NHS-ester[141]

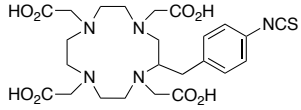
p-SCN-Bn-DOTA (C-DOTA)[99,142,143]

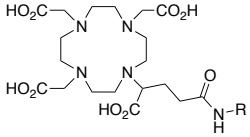
DOTAGA, R = amide, NHS ester[144]

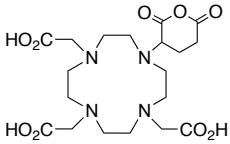
DOTAGA-anhydride[145]

[a] highlighting relevant radiometal ions, radiolabeling conditions, thermodynamic stability constants (Log K_{ML}), coordination geometry, and color-coded ranking ([a] green "✓" = good/best match, orange "~" = suitable match, or requires more evaluation but shows potential, red "✗" = poor/unstable match).

The current method used for synthesizing ^{225}Ac-DOTA-antibody conjugates is to radiolabel the BFC *p*-SCN-Bn-DOTA at 60 °C with ^{225}Ac first, followed by antibody conjugation (thiourea coupling) and purification.[139,140] It is important to realize that the isothiocyanate functionality in the BFC *p*-SCN-Bn-DOTA is very sensitive and degrades rapidly under these conditions. A study comparing the therapeutic effects of ^{225}Ac, ^{213}Bi, and ^{90}Y using an antibody vector demonstrated ^{225}Ac to be the most effective, with renal toxicity from the daughters ^{221}Fr and ^{213}Bi being the most significant concern.[146] A recent clinical trial in humans with ^{225}Ac-DOTA-HuM195 (humanized anti-CD33 monoclonal antibody) has shown promise, with DOTA being the current "gold standard" for ^{225}Ac.[140,147] A high

denticity acyclic ligand (CN = 8-10) that could match the *in vivo* stability of DOTA and radiolabel at room temperature would be of great utility and would offer a more streamlined radiopharmaceutical preparation than the one outlined above for *p*-SCN-Bn-DOTA.

Table 1.3 DOTA derivatives CB-DO2A, TCMC, 3p-C-DEPA, Oxo-DO3A, and bifunctional derivatives.[a]

Chelator and Common Bifunctional Derivatives	Radiometal Ion	[a]	Radiolabeling Conditions	Log K_{ML}	Proposed Geometry	Ref.
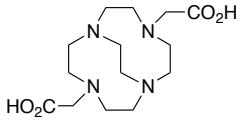 **CB-DO2A**, 4,10-bis (carboxymethyl)-1,4,7,10-tetraazabicyclo[5.5.2] tetradecane, N_4O_2, CN = 6	$^{64}Cu^{2+}$	~	80 °C, 30-60 min, pH 5-7	-	distorted octahedron	72,148
	$^{67/68}Ga^{3+}$	~	-	-	distorted octahedron	149
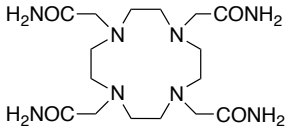 **TCMC**, 1,4,7,1O-tetrakis (carbamoylmethyl)-l,4,7,1O-tetraaza cyclododecane, N_4O_4, CN = 8	$^{212}Pb^{2+}$	✓	37 °C, 30-60 min, pH 5-6.5	>19	Square antiprismatic	138,150-154
	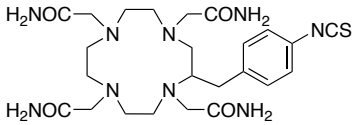 *p*-SCN-Bn-TCMC[153]					
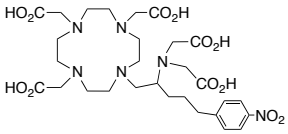 **3p-C-DEPA**, N_5O_5, CN = 10	$^{212/213}Bi$	✓	25 °C, 5-10 min, pH 5.5	-	Square antiprismatic	155
	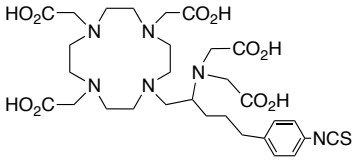 3p-C-DEPA-NCS[155]			**3p-C-DEPA** = 2-[(carboxymethyl)][5-(4-nitrophenyl-1-[4,7,10-tris-(carboxymethyl)-1,4,7,10-tetraazacyclododecan-1-yl]pentan-2-yl)-amino]acetic acid		
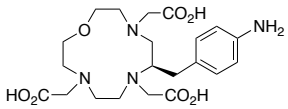 ***p*-NH$_2$-Bn-Oxo-DO3A**, N_3O_4, CN = 7	$^{64}Cu^{2+}$	~	25 °C, 10 min, pH 5.5	-	distorted octahedron?	90,91,156,157
	$^{67/68}Ga^{3+}$	~	25 °C, 10 min, pH 4-5	-	distorted octahedron?	90,158,159

[a] highlighting relevant radiometal ions, radiolabeling conditions, thermodynamic stability constants (Log K_{ML}), coordination geometry, and color-coded ranking ([a] green "✓" = good/best match, orange "~" = suitable match, or requires more evaluation but shows potential, red "✗" = poor/unstable match).

1.5.2 DOTA Derivatives: CB-DO2A, 3p-C-DEPA, TCMC, and Oxo-DO3A

CB-DO2A has only been investigated with the radiometal ^{64}Cu for radiochemical use (Table 1.3).[72,148] An X-ray crystal structure of CB-DO2A with Ga^{3+} is available and shows a distorted octahedral coordination geometry, and acid stability experiments have been performed with Ga^{3+}, revealing impressive acid inertness.[149] Although very little work has been done with CB-DO2A, studies with the non-bifunctional ^{64}Cu(CB-DO2A) have suggested that it had superior *in vivo* stability to DOTA and TETA, but inferior stability to CB-TE2A.[139]

Further comparision of CB-DO2A to CB-TE2A, DOTA, and TETA revealed that CB-TE2A possessed superior acid and electrochemical inertness, which explains why DOTA and its cross-bridged derivative CB-DO2A have been replaced by CB-TE2A and are no longer a prominent subject of current research with ^{64}Cu.[56] Another interesting DOTA derivative is Oxo-DO3A, which is a heptadentate N_3O_4 macrocycle that has shown improved radiolabeling kinetics and stability with ^{64}Cu and $^{67/68}Ga$ compared to DOTA (Table 1.3). The *p*-NH_2-Bn-Oxo-DO3A derivative is shown in Table 1.3; it can be directly coupled to a peptide via standard peptide coupling reactions, or transformed to a benzyl-isothiocyanate.

Although DOTA has been used successfully with ^{212}Pb, its slow radiolabeling kinetics and stability properties were not ideal.[160] Replacement of the carboxylic acid donor arms of DOTA with amide arms has produced the ligand TCMC (Table 1.3), which to date is the best ligand available for ^{212}Pb.[151,152,161] Chappel *et al.* have shown TCMC to be superior to C-DOTA (Table 1.2) with ^{212}Pb due to improved radiolabeling kinetics and *in vivo* stability.[153,162] Although not optimal for ^{212}Pb, 3p-C-DEPA (Table 1.3) has been shown to be an excellent ligand for $^{212/213}Bi$, with superior properties to C-DOTA.[155] The DOTA

derivative 3p-C-DEPA has demonstrated greatly improved radiolabeling kinetics with $^{212/213}$Bi compared to DOTA, with comparable *in vivo* stability.[155] 3p-C-DEPA can be considered to be one of the current "gold standards" for $^{212/213}$Bi; however, the NOTA analogue 3p-C-NETA (*vide infra*) also looks very promising and has not been directly compared with 3p-C-DEPA, and so the superior of the two has yet to be identified.

1.5.3 TETA

TETA is an octadentate N_4O_4 macrocyclic ligand that has only been investigated with ^{64}Cu for radiopharmaceutical applications (Table 1.4). TETA is generally not used anymore, and has been superseded by newer generation ligands such as NOTA, CB-TE2A, and CB-TE1A1P/CB-TE2P (Table 1.4) that are more stable and kinetically inert *in vivo*. Copper is a difficult metal ion to harness, as it is quite labile, has active redox chemistry between Cu^{1+}/Cu^{2+} *in vivo*, and Cu^{2+} has a fast aqua ligand exchange rate of 2×10^8 s^{-1}.[44,163] Copper is a first row transition metal with a d^9 electron configuration, is best used with hexadentate ligands that saturate its coordination sphere, and has a preference for borderline soft ligand donor atoms such as amines, imines, and thiols.[6,44] Despite being made obsolete in recent years, TETA has previously been used successfully for ^{64}Cu imaging with vectors such as octreotide.[164,165] TETA can radiolabel with ^{64}Cu at room temperature, but it lacks kinetic inertness and overall stability *in vivo*. Surprisingly, the TETA derivative TE2A (Table 1.4) shows enhanced kinetic inertness, despite the fact that TE2A is merely a hexadentate derivative of TETA that is missing two carboxylic acid arms.[166] This effect is enhanced even further when the two secondary amines of TE2A are methylated or cross-bridged by an ethylene unit (Table 1.4).[148,167] Unlike DOTA (cyclen-based), TETA (cyclam-based) has not

been heavily investigated with any radiometals other than ^{64}Cu; however, some structural and physical data is available with other metal ions (Table 1.4).

Table 1.4 TETA, CB-TE2A and derivatives, and bifunctional derivatives.

Chelator and Common Bifunctional Derivatives	Radiometal Ion	[a]	Radiolabeling Conditions	Log K_{ML}	Proposed Geometry	Ref.
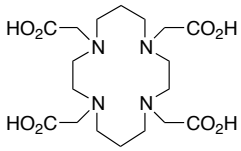 **TETA**, 1,4,8,11-tetraazacyclotetradecane-1,4,8,-11-tetraacetic acid, N_4O_4 CN = 8	$^{64}Cu^{2+}$	~	25 °C, 60 min, pH 5-7.	21.9, 21.6.	Distorted octahedron	[164,168]
	$^{67/68}Ga^{3+}$	✗	-	19.74 (pM 14.1)	Distorted octahedron	[68]
	$^{111}In^{3+}$	✗	-	21.9 (pM 16.3)	Distorted octahedron?	[68]
	$^{177}Lu^{3+}$	✗	-	15.3	Distorted dodecahedron?	[169]
	$^{86/90}Y^{3+}$	✗	-	14.8	Distorted dodecahedron?	[169]
	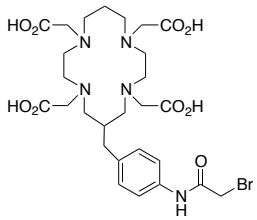 BAT (C-TETA derivative)[170]					
	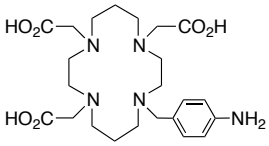 *p*-H_2NBn-TE3A[171]					
	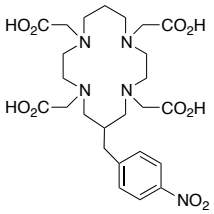 C-TETA (*p*-NO2-Bn-TETA)[172]					
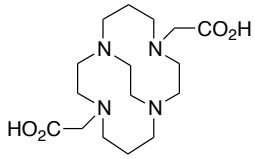 **CB-TE2A**, 4,11-bis(carboxymethyl)-1,4,8,11-tetraazabicyclo[6.6.2]hexadecane, N_4O_2 CN = 6	$^{64}Cu^{2+}$	✓	95 °C, 60 min, pH 6-7	-	Distorted octahedron	[72,94,106,108,173-178]
	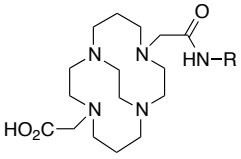					
	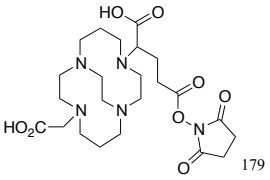 [179]					
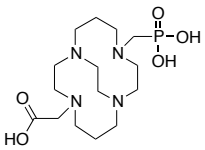 CB-TE1A1P[174,180]						
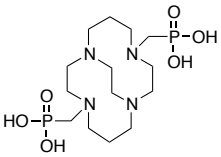 CB-TE2P[174,180]						
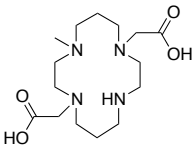 MM-TE2A[167]						
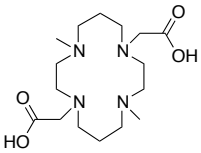 DM-TE2A[167]						
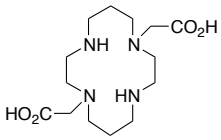 TE2A[166]						

1.5.4 TE2A, CB-TE2A, CB-TE1A1P, CB-TE2P, MM-TE2A, DM-TE2A

The cyclam-based macrocycle TETA has spawned a large number of successful derivatives (Table 1.4). Despite the requisite harsh radiolabeling conditions (95 °C), CB-TE2A has become one of the premier ^{64}Cu ligands, having superior *in vivo* stability to TETA, TE2A, DOTA, NOTA, and CB-DO2A.[148] The stability gains from adding an ethylene cross bridge to TETA/TE2A are significant, despite the removal of two coordinating carboxylic acid arms, and a subsequent decrease in denticity from 8 to 6. In order to surmount the harsh radiolabeling conditions required for CB-TE2A, several derivatives of CB-TE2A have been synthesized. Improved radiolabeling kinetics have been achieved by replacement of one (CB-TE1A1P) or both (CB-TE2P) carboxylic acid arms with methylenephosphonate groups, with *in vitro* and *in vivo* stability being retained or enhanced compared to the native CB-TE2A (Table 1.4).[148,174-177,181] Most importantly, the methylenephosphonate derivatives CB-TE1A1P and CB-TE2P can be radiolabeled with ^{64}Cu at room temperature, although relatively slowly. Another noteworthy set of derivatives were made by methylating one (MM-TE2A) or two (DM-TE2A) nitrogen atoms of TETA/TE2A, instead of linking them together with an ethylene bridge (Table 1.4).[167] Surprisingly, these methylated TE2A derivatives possessed similar radiolabeling kinetics and stability to CB-TE2A.[167] This observation suggests that the high stability of CB-TE2A is not a result of steric protection by the cage-like structure created by the cross-bridged ethylene unit, but instead by changing the electronic properties of the nitrogen atoms (secondary to tertiary amines) and their donor properties. Although CB-TE2A has been the most heavily investigated ligand of the above mentioned TETA derivatives, the new methylenephosphonate derivatives CB-TE1A1P and

CB-TE2P show the most promise, as they appear to retain the stability of CB-TE2A, while having greatly enhanced radiolabeling kinetics.

1.5.5 Diamsar and derivatives

The radiometal ion $^{64}Cu^{2+}$, similar to $^{68}Ga^{3+}$, has been extremely popular in recent years due to its favorable positron emission (β^+) properties for PET imaging and its intermediate half-life (12.7 hours), which is suitable for use with peptides, antibody fragments, and even whole antibodies. Unlike ^{68}Ga, ^{64}Cu also undergoes β^- emission, making it useful for therapy in addition to PET imaging. It follows, therefore, that there has been a strong interest in developing new and improved bifunctional chelators to optimize radiolabeling procedures and *in vivo* performance with isotopes of copper. In addition to the ubiquitous ligand NOTA (*vide infra*), new entrants such as CB-TE2A, CB-TE1A1P, CB-TE2P, MM-TE2A, and DM-TE2A have recently been determined to be excellent ^{64}Cu ligands (*vide supra*). The Sar family of ligands (hexamine sarcophagines) are hexaazamacrobicyclic cage type ligands, and include the ligands SarAr, SarAr-NCS, diamSar, AmBaSar, and BaBaSar (Table 1.5). One of the major benefits of these nitrogen rich ligands is that they can radiolabel with ^{64}Cu in only a few minutes (5-10 min) at room temperature, which is faster even than the recently devised ligands CB-TE1A1P and CB-TE2P (Table 1.4).[44,182-184] Of all the ligands discussed for ^{64}Cu, Sar derivatives have the fastest room temperature radiolabeling kinetics. In addition to fast kinetics, they demonstrate excellent *in vivo* stability, and strong resistance to acid dissociation *in vitro*.[182-185] One drawback to nitrogen rich N_6 ligands such as the Sar family is lipophilicity, as they contain little or no acid functionality to add negative charge, and as a result form cationic or neutral

complexes with ^{64}Cu (depending on the Sar derivative). Because the half-life of ^{64}Cu (~12 h) pairs exceptionally well with the distrubtion and localization times for peptides, a lipophilic radiometal-ligand complex can have deleterious affects on biodistribution and tumour targeting properties by directing activity to the liver and digestive tract (depending on hydrophilicity of the selected peptide). The Sar derivative BaBaSar adds two carboxylic acid functional groups to the Sar scaffold, thereby augmenting hydrophilicity. Animal studies have been promising with the Sar family of ligands, but more work is required for further validation; furthermore, limited commercial availability and challenging synthesis may be a reason why widespread adoption has yet to occur.[44,182-185]

Table 1.5 The copper ligands Diamsar, SarAr, AmBaSar, and BaBaSar.[a]

Chelator and Common Bifunctional Derivatives	Radiometal Ion	[a]	Radiolabeling Conditions	Log K_{ML}	Proposed Geometry	Ref.
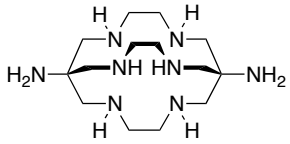 **Diamsar**, N_6, CN = 6	$^{64}Cu^{2+}$	✓	25 °C, 5-30 min, pH 5.5		Distorted octahedron or trigonal prism	182-185
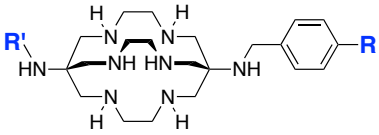	1-*N*-(4-aminobenzyl)-3,6,10,13,16,19-hexaazabicyclo[6.6.6]-eicosane-1,8-diamine (SarAr)[182-186] SarAr **R** = NH_2, **R'** = H SarAr-NCS **R** = NCS, **R'** = H AmBaSar **R** = COOH, **R'** = H BaBaSar **R** = -COOH, **R'** = $-CH_2$-Ph-COOH					

[a] highlighting relevant radiometal ions, radiolabeling conditions, thermodynamic stability constants (Log K_{ML}), coordination geometry, and color-coded ranking ([a] green "✓" = good/best match, orange "~" = suitable match, or requires more evaluation but shows potential, red "✗" = poor/unstable match).

1.5.6 NOTA, NETA, and TACN-TM

NOTA is a hexadentate N_3O_3 ligand, and is one of the oldest and most successful ligands for use with $^{67/68}$Ga and ^{64}Cu (Table 1.6). NOTA is generally considered to be the

"gold standard" for Ga^{3+} chelation, possessing favorable radiolabeling conditions (RT, 30-60 minutes) and excellent *in vivo* stability.[110,117,187,188] Of all the isotopes discussed in this chapter, ^{68}Ga is probably the most popular in recent years. ^{68}Ga has a very favorable positron emission (1880 keV, 90%) for PET imaging, and a short half-life (68 min) suitably matched for imaging with peptide vectors. The recent development of several $^{68}Ge/^{68}Ga$-generator systems with shelf-lives of ~9-12 months has propelled this radiometal into the spotlight of the international research scene.[189] Ga^{3+} is a hard acidic metal ion (pK_a 2.6) with an ionic radius of 62 pm (CN = 6), a preference for amine and oxygen donor atoms, and is ultimately a challenging metal ion to chelate because it has a strong affinity for hydroxide anions causing precipitation of gallium hydroxide ($Ga(OH)_3$) between pH 3-7.[66,163,190]

Because of gallium's potential clinical utility, many new gallium ligands have been published in the last ~5 years; however, most have not yet amassed the same amount of *in vivo* data as NOTA. NOTA has been shown to have superior radiolabeling properties and stability with ^{64}Cu when compared to common ligands such as DOTA, EDTA, DTPA, and TETA.[191, 155] NOTA can radiolabel with ^{64}Cu at room temperature in 30-60 minutes, making it compatible with heat sensitive antibody vectors.[192] Although many new ligands such as TRAP, AAZTA (DATA), H_2dedpa, CP256, and PCTA (*vide infra*) show great promise for use with $^{67/68}Ga$ in early experiments, due to commerical availability of BFC derivatives and widespread acceptance, NOTA is still currently the "gold standard" for $^{67/68}Ga$. A similar story can be told for ^{64}Cu, where a plethora of new ligands, including the Sar family (e.g. SarAr, DiamSar), CB-TE2A, and various CB-TE2A derivatives (e.g. CB-TE1A1P, CB-TE2P, MM/DM-TE2A) appear to possess many superior properties, but NOTA is still the practical "gold standard" for ^{64}Cu.

Table 1.6 NOTA, NETA, TACN-TM, and bifunctional derivatives.[a]

Chelator and Common Bifunctional Derivatives	Radiometal Ion	[a]	Radiolabeling Conditions	Log K_{ML}	Proposed Geometry	Ref.
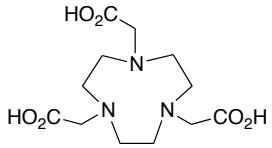 **NOTA**, 1,4,7-triazacyclononane-1,4,7-triacetic acid, CN = 6, N_3O_3	$^{64}Cu^{2+}$	✓	25 °C, 30-60 min, pH 5.5-6.5	21.6	distorted trigonal prism	[191,193]
	$^{67/68}Ga^{3+}$	✓	25 °C, 30-60 min, pH 4.0-5.5	31.0 (pM 26.4, 27.9)	distorted octahedron	[110,117,118,187,188,194,195]
	$^{44/47}Sc^{3+}$	~	95 °C, 20-30 min, pH 4.0	16.5 (pM 19.2)	distorted octahedron	[102]
	$^{111}In^{3+}$	~	60-95 °C, 20-30 min, pH 4.0-5.0	26.2 (pM 21.6)	distorted octahedron	[74,117,188,196-198]
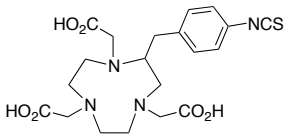 *p*-SCN-Bn-NOTA(C-NOTA)[143,196] amide[197]						
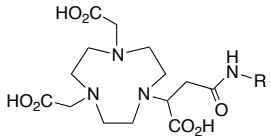 NODASA, R = NHS ester, amide[199]						
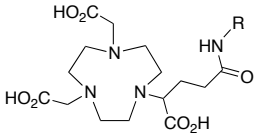 NODAGA, R = NHS ester,						
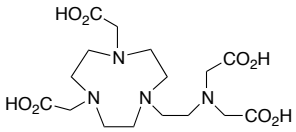 **NETA**, [2-(4,7-Biscarboxymethyl[1,4,7]triazacyclononan-1-ylethyl)carbonylmethyl-amino]acetic acid, N_4O_4, CN = 8	$^{177}Lu^{3+}$	✓	25 °C, 5 min, pH 4.5	-	Square antiprism?	[127,161,200,201]
	$^{86/90}Y^{3+}$	✓	25 °C, 5 min, pH 4.0	-	Square antiprism?	[127,201,202]
	$^{212/213}Bi^{3+}$	✓	25 °C, 5 min, pH 4.0	-	Square antiprism?	[161,200,201,203]
	$^{212}Pb^{2+}$	✗	25 °C, 5 min, pH 4.0	-	Square antiprism?	[201]
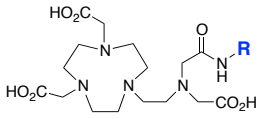 NETA-monoamide[202]						
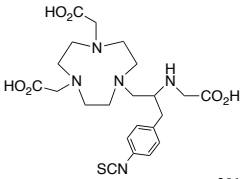 C-NE3TA-NCS[201]						
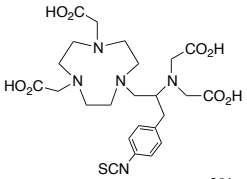 C-NETA-NCS[201]						
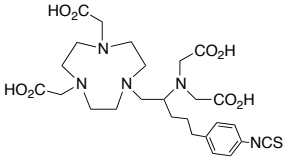 3p-C-NETA[127,203,204]						
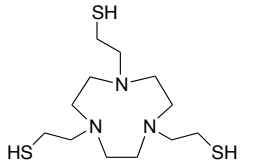 **TACN-TM,** N,N',N'', tris(2-mercaptoethyl)l,4,7-triazacyclononane, N_3S_3 CN6	$^{67/68}Ga^{3+}$	✗	25 °C, 10 min, degassed ethanol	34.2	distorted octahedron	[110,205-207]
	$^{111}In^{3+}$	✗	25 °C, 10 min, degassed ethanol	36.1	distorted octahedron	[99, 176, 177, 183]

[a] highlighting relevant radiometal ions, radiolabeling conditions, thermodynamic stability constants (Log K_{ML}), coordination geometry, and color-coded ranking ([a] green "✓" = good/best match, orange "~" = suitable match, or requires more evaluation but shows potential, red "✗" = poor/unstable match).

The modified NOTA ligand NETA (Table 1.6) is an interesting derivative that shows promise with $^{86/90}Y$, possessing fast radiolabeling kinetics similar to those of acyclic ligands (5-10 minutes, RT), as well as a high degree of stability and rigidity imparted by the macrocyclic framework.[202] A direct comparison between NETA and DOTA has demonstrated greatly enhanced radiolabeling kinetics for NETA with Y^{3+}.[202] Biodistribution experiments performed with the ^{86}Y complexes of the non-bifunctional chelators NETA and DOTA have suggested that NETA had comparable clearance and stability properties to DOTA, even showing lower bone accumulation than DOTA.[202] NETA has been evaluated with other therapeutic isotopes for radioimmunotherapy (RIT), including $^{203/212}Pb$, $^{212/213}Bi$, and ^{177}Lu.[161,200,201] NETA and bifunctional derivatives C-NETA and C-NE3TA (Table 1.6) were found to be unstable with $^{203/212}Pb$ isotopes, but looked very stable with $^{212/213}Bi$, ^{90}Y, and ^{177}Lu during a period of 11 days in blood serum.[201,204,208] Biodistribution studies of C-NETA complexes in healthy mice demonstrated excellent clearance and stability of the $^{212/213}Bi$, ^{90}Y, and ^{177}Lu complexes, with the exception of high kidney uptake with the $^{212/213}Bi$-C-NETA complex.[201]

Recent experiments with an isothiocyanate bearing derivative of C-NETA, 3p-C-NETA (Table 1.6) have demonstrated that ^{90}Y and ^{177}Lu radiolabeled immunoconjugates (trastuzumab) had very rapid room temperature radiolabeling kinetics, and excellent *in vivo* performance, with the potential to surpass DOTA and also DTPA analogues such as CHX-A''-DTPA.[127] 3p-C-NETA has been further evaluated with $^{212/213}Bi$ for RIT applications, and trastuzumab immunoconjugates have been shown to exhibit rapid radiolabeling kinetics and excellent *in vitro* and *in vivo* stability, suggesting improved stability over C-NETA, which showed high kidney accumulation of $^{212/213}Bi$.[203, 201] It is interesting to note that these

studies were actually performed with $^{205/206}$Bi, as the longer half-lives (15.3/6.2 days, respectively) of these $^{212/213}$Bi isotopologues are more amenable to extensive *in vitro* and *in vivo* study than are the short half-lives of $^{212/213}$Bi (0.76-1.1 hrs).[203] Currently it is not clear if 3p-C-DEPA (Table 1.3) is superior to 3p-C-NETA (Table 1.6) for use with $^{212/213}$Bi, and a direct comparison would be timely.

TACN-TM (Table 1.6) is an interesting thiol-based ligand, and shows extremely high thermodynamic stability constants (log K_{ML}) with Ga^{3+} and In^{3+} of 34.2 and 36.1, respectively.[99, 176, 177, 183] Another interesting thiol TACN derivative is TACN-HSB, which substitutes alkyl-thiols for thiophenol groups.[206] Despite the high thermodynamic stabilities, radiolabeling experiments required the use of degassed ethanol due to instability of the thiol groups of TACN-TM/TACN-HSB to air, and ultimately these ligands could not be used for *in vivo* applications.[206] For these reasons, no bifunctional derivatives have been synthesized of these thiol-based TACN/NOTA derivatives, and further study has not been pursued.

1.5.7 DTPA, 1B4M-DTPA, and CHX-A''-DTPA

DTPA is one of the oldest and most pervasive acyclic ligands used in radiochemistry, and like most acyclic ligands it can be radiolabeled with many radiometal ions at room temperature in a matter of minutes (Table 1.7). As a first generation radiometal ligand, it suffers from stability issues *in vivo* with many radiometal ions, is universally not as stable as the macrocycles DOTA and NOTA, and has become obsolete in recent years.[60] DTPA has been successfully used as the BFC in the FDA-approved SPECT agent OctreoScan™ (^{111}In-DTPA-octreotide), a somatostatin-targeting peptide-conjugate used for imaging neuroendocrine tumours.[209,210] DTPA has also been successfully used with radiometals such

as ^{64}Cu, ^{111}In, ^{177}Lu, and $^{86/90}$Y, but has been made redundant by more stable new ligands such as DOTA, NOTA, and CHX-A''-DTPA (Table 1.7).[60,165] The shortcomings of DTPA have been improved through design of novel derivatives, such as the DTPA derivatives 1B4M-DTPA (Tiuxetan) and CHX-A"-DTPA.[60,211] 1B4M-DTPA is a bifunctional DTPA derivative that contains a single methyl group on one of its ethylene backbones, and has been successfully incorporated into the FDA-approved ^{90}Y therapeutic immunoconjugate Zevalin (Table 1.7).[211-213, 214]

Although DTPA and DOTA are the most commonly investigated chelate systems for Y^{3+}, the ligand CHX-A"-DTPA (Table 1.7) shows significantly improved stability over DTPA; however, it is still generally considered to be less stable than DOTA.[60] The cyclohexyl backbone of CHX-A"-DTPA makes the ligand more rigid and imposes a degree of preorganization on the metal ion binding site, enhancing kinetic inertness, but retarding radiolabeling kinetics compared to those of DTPA.[60,215] Due to the success of antibody vectors, developing acyclic ligands with fast radiometal ion coordination kinetics, as well as high stability and kinetic inertness comparable to that of macrocycles such as DOTA is an important goal. The work done towards developing CHX-A"-DTPA was particularly interesting because of the 4 possible isomers of this ligand. The CHX-B"-DTPA isomer was found to be much less stable than the CHX-A''-DTPA isomer *in vivo* with ^{90}Y, despite *in vitro* stability assays suggesting they were very similar.[60,216] If CHX-DTPA were to be used as a racemic mixture it would result in significant decomposition of the less stable isomers and would lead to radiodemetallation *in vivo*, highlighting the importance of enantiopurity.[60,216] Different isomers of a BFC-radiometal complex can have different

stabilities and off-rates (kinetic inertness), potentially leading to differential biodistributions.[49,63]

Table 1.7 DTPA, 1B4M, CHX-A''-DTPA, and bifunctional derivatives.

Chelator and Common Bifunctional Derivatives	Radiometal Ion	[a]	Radiolabeling Conditions	Log K_{ML}	Proposed Geometry	Ref.
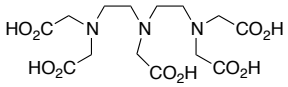 **DTPA**, Diethylenetriamine pentaacetic acid, N_3O_5, CN = 8	$^{64}Cu^{2+}$	✗	40 °C, 60 min, pH 6.5	21.4	Distorted octahedron?	[119,217]
	$^{67/68}Ga^{3+}$	✗	25 °C, 30 min, pH 3.5	24.3, 25.5 (pM 20.2)	Distorted octahedron?	[117,119,218]
	$^{44/47}Sc^{3+}$	~	25 °C, 10 min, pH 6.0	-	Square antiprism?	[17]
	$^{111}In^{3+}$	~	25 °C, 5-10 min, pH 4.5-5.5	29.0 (pM 24.9)	Pentagonal bipyramid or square antiprism	[117,119,219-221]
	$^{177}Lu^{3+}$	~	25 °C, 10-20 min, pH 5.5	22.6	Square antiprism?	[119,131,222]
	$^{86/90}Y^{3+}$	~	25 °C, 10-20 min, pH 5.5	21.2, 22.0, 22.5	Monocapped square antiprism	[59,131,132,222]
	^{89}Zr	✗	25 °C, 60 min, pH 7 (<0.1 % yield)	35.8-36.9	Distorted dodecahedron	[119,223]
	$^{212/213}Bi^{3+}$	✗	25 °C, 10-20 min, pH 5	35.6	Square antiprism	[119,224-226]
	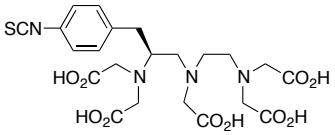 *p*-SCN-Bn-1B-DTPA[215,227]					
	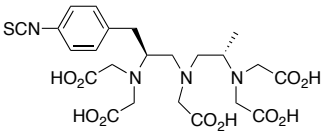 *p*-SCN-Bn-1B4M-DTPA[228-230]					
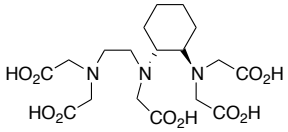 **CHX-A''-DTPA**, 2-(*p*-isothiocyanatobenzyl)-cyclohexyldiethylenetriamine pentaacetic acid, N_3O_5, CN = 8	$^{67/68}Ga^{3+}$	✗	85 °C, 20 min, pH 5.5	-	Distorted octahedron?	[231]
	$^{111}In^{3+}$	✓	25-60 °C, 30-60 min, pH 5.5	-	Square antiprism	[228,231-237]
	$^{177}Lu^{3+}$	✓	37-75 °C, 30-60 min, pH 5-5.5	-	Square antiprism	[58,126,128]
	$^{86/90}Y^{3+}$	✓	37-75 °C, 30-60 min, pH 5-5.5	-	Square antiprism	[19,20,59,60,216,231,232,238-243]
	$^{213}Bi^{3+}$	~	25 °C, 10-20 min, pH 5	-	Square antiprism	[244, 201 245,246]
	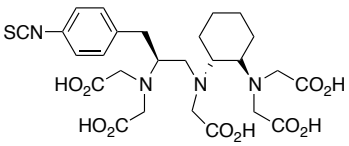 *p*-SCN-Bn-CHX-A''-DTPA[60,216,247]					

Although CHX-A''-DTPA has enhanced radiolabeling kinetics when compared to DOTA, both are still much slower than typical acyclic ligands such as DTPA and H_4octapa

(Table 1.9), and often require mild heating (~37-60 °C) and reaction times of 30-60 minutes to achieve reasonable yields. CHX-A''-DTPA has been heavily investigated for use with many radiometals, including $^{86/90}$Y,[19,20,59,60,216,231,232,238-243] ^{177}Lu,[58,126,128] and $^{212/213}$Bi,[244, 201 245,246] but work with ^{111}In has comparatively been limited.[228,231-237] Studies that have been performed with ^{111}In(CHX-A''-DTPA) conjugates have shown good *in vivo* results, but to our knowledge little work has been done comparing it with the "gold standard" ^{111}In ligand DOTA.[236]

A study comparing the *in vivo* behavior of the affibody conjugate ^{114m}In-CHX-A''-DTPA-ABD-$(Z_{HER2:342})_2$ to ^{111}In-DOTA-ABD-$(Z_{HER2:342})_2$ suggests that both ligands have comparable stability and performance, with CHX-A''-DTPA exhibiting slightly higher tumour uptake, but also slightly higher non-target organ uptake (e.g. kidneys, liver, bone).[236] ^{114m}In is a notable γ-emitting isotope because it has identical chemistry to ^{111}In, but a longer 49.5-day half-life and interesting decay scheme (Table 1.1).[236] When ^{114m}In decays it emits a γ-ray for SPECT imaging, but the daughter nuclide ^{114}In has a half-life of 72 seconds and emits high-energy (1989 keV) β^- particles useful for therapy.[236] When the parent ^{114m}In radiolabeled affibody internalizes into cells, it acts as an *in vivo* generator of ^{114}In for intracellular delivery of therapeutic radioactivity (β^- particles) to cancer cells.[236]

Investigations with $^{212/213}$Bi have found DTPA to possess fast radiolabeling kinetics, but poor *in vivo* stability, ultimately rendering the complex unusable.[119,224-226] CHX-A''-DTPA has been shown to possess enhanced stability with $^{212/213}$Bi when compared to DTPA and 1B4M-DTPA, and even comparable stability to DOTA, while additionally possessing greatly enhanced radiolabeling kinetics (important for the short half-life of $^{212/213}$Bi).[225,244,248, 201 245,246] The solid-state structure of the $[Bi(CHX\text{-}A''\text{-}DTPA)]^{2-}$ complex suggests that the

partially pre-organized binding site offered by the rigid cyclohexyl backbone may contribute to the enhanced stability of the complex (also suggested as the cause for enhanced stability with other isotopes such as $^{86/90}$Y and ^{177}Lu).[244] Although comparable to DOTA, CHX-A''-DTPA is still considered to be inferior to 3p-C-NETA and 3p-C-DEPA for use with $^{212/213}$Bi.

1.5.8 TRAP (PRP9) and NOPO

TRAP (PRP9) is a derivative of the macrocycle NOTA, wherein the traditional carboxylic acid arms have been replaced with phosphinic acid groups (Table 1.8).[83-85,249-253] The most successful TRAP derivative, TRAP-Pr, contains an additional ethyl-carboxylate moiety extending distally from the phosphinic acid groups (Table 1.8).[83-85,249-253] The most interesting property of the TRAP-Pr ligand is its improved apparent specificity for Ga^{3+} when compared to NOTA.[82,85] This phenomenon is expressed by the difference in thermodynamic stability constants (log K_{ML}) of TRAP and NOTA for competing metal ions such as Mg^{2+}, Ca^{2+}, Cu^{2+}, and Zn^{2+},[85] and by competitive radiolabeling experiments done in the presence of an excess of these other ions.[82] As a general rule, radiolabeling experiments are performed in strictly metal-free water and so the selectivity of TRAP-Pr for Ga^{3+} may not appear to be totally relevant, but it does suggest that transchelation by these competing metal ions *in vivo* should occur to a lesser extent than with NOTA. Additionally, the enhanced specificity of TRAP-Pr for ^{68}Ga over NOTA may be of benefit if trace-impurities are present in the stock radiometal solution (e.g. ^{68}Ge/^{68}Ga generator eluent, or commercially supplied ^{64}Cu). A similar derivative to TRAP is NOPO, which is a triazacyclononane-triphospinate ligand that has a similar structure to TRAP-Pr, but with two terminal alcohol groups in place of

carboxylic acids.[78, 248, 250] Like TRAP, NOPO has shown promising properties for ^{64}Cu and ^{68}Ga radiolabeling.[78, 248, 250]

Table 1.8 Promising $^{67/68}$Ga ligands TRAP (PRP9, TRAP-Pr), AAZTA (DATA), and bifunctional derivatives.[a]

Chelator and Common Bifunctional Derivatives	Radiometal Ion	[a]	Radiolabeling Conditions	Log K_{ML}	Proposed Geometry	Ref.
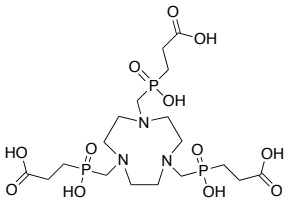 **TRAP (PRP9, TRAP-Pr)**, 1,4,7-triazacyclononane-1,4,7-tris[methyl(2-carboxyethyl)phosphinic acid], N_3O_3 CN = 6 (+ distal carboxylates CN = 9?)	$^{67/68}$Ga^{3+}	✓	95 °C, 5 min, pH 3.2	26.24	Distorted octahedron	83-85,95,249-253
	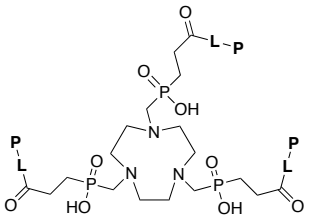		L = Linker, e.g. PEG8, PEG4, Glu, AHX, N3AHX. P = Peptide, e.g. RGD, DRG. 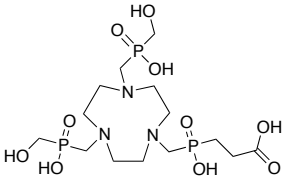 **NOPO**[82,252,254]			
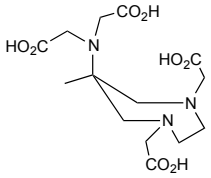 **AAZTA, and novel DATA derivatives**, 1,4-bis (hydroxycarbonyl methyl)-6-[bis (hydroxylcarbonyl methyl)] amino-6-methyl perhydro-1,4-diazepine, N_2O_4 or N_3O_3, CN = 6	$^{67/68}$Ga^{3+}	~	25 °C, 1-5 min, pH 4-6.8	-	Distorted octahedron	255-258
	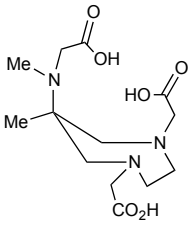 H_3L^1			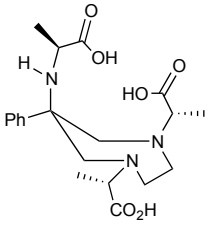 H_3L^4		

The peptide conjugate TRAP(RGD)$_3$ was radiolabeled with ^{68}Ga in 5 minutes at 95 °C (HEPES, pH 3.2), and despite the high reaction temperature was able to radiolabel at lower ligand concentrations than the corresponding DOTA or NOTA conjugates.[14,15] RGD (arginine-glycine-aspartic acid tripeptide) is a popular cyclic peptide vector that targets overexpression of integrin $\alpha_v\beta_3$ receptors on various types of cancer, and is commonly used

as a proof-of-principle vector for studying new isotopes and new BFC.[38,95,259,260, 14,15] ^{68}Ga-TRAP(RGD)$_3$ demonstrated good *in vivo* tumour targeting properties, showing great promise for use in ^{68}Ga-based PET imaging agents;[14,15] however, a recent comparative biodistribution study between ^{68}Ga-TRAP(RGD)$_3$ and ^{68}Ga-NODAGA-RGD revealed higher uptake in several non-target organs for the TRAP-based agent.[83,95,250] Despite these apparent shortcomings, TRAP-Pr is a very promising ^{68}Ga ligand, which is a claim substantiated by the work of Dr. Richard P. Baum at Zentralklinik Bad Berka in Germany, who has performed imaging experiments in human patients using ^{68}Ga-TRAP-peptide conjugates.[261]

1.5.9 AAZTA and derivatives (DATA)

The novel AAZTA derivatives H_3L^1 and H_3L^4 are new $^{67/68}$Ga-ligands that have shown improved radiolabeling and serum stability properties over the parent AAZTA ligand (Table 1.8). The parent AAZTA ligand was found to form multiple isomers with Ga^{3+}, and so the derivatives H_3L^1 and H_3L^4 were crafted such that one major isomer of the Ga^{3+} complex was kinetically trapped by attachment of bulky alkyl/aryl groups.[255-258] These AAZTA derivatives (now called DATA) are promising new Ga^{3+} ligands with extremely fast radiolabeling kinetics (1-5 minutes at RT) and good preliminary *in vitro* and *in vivo* stability results (as non-bifunctional ligands). These ligands are very recent, as most of this work has just been published in 2013, and so more extensive *in vitro* and *in vivo* experimentation will likely follow in the coming years. Additionally, no bifunctional derivatives (e.g. peptide conjugates) have been published to date, which will be required for proper evaluation and comparison *in vivo* to existing "gold standards" such as NOTA.

1.5.10 H_2dedpa, H_4octapa, H_2azapa, and H_5decapa

This family of ligands has only been published over the previous 4 years and has been referred to as the "pa family", as they are all crafted around central picolinic acid ("pa") binding moieties (Table 1.9). The body of this thesis discusses the work performed with many of these picolinic acid-based ligands (e.g. H_4octapa, H_5decapa, H_6phospa, H_2azapa), and so those that were published at the time of writing have been included in this introduction to provide a broad perspective of where they fit into the current canon of radiometal ligands. This work originated in ligands made by Rodriguez-Blas and coworkers, originally purposed as contrast agents for magnetic resonance imaging (MRI) and luminescence.[262-271] H_2dedpa was the first ligand in this family to be investigated, with its acyclic hexadentate scaffold being ideal for $^{67/68}$Ga, radiolabeling in less than 10 minutes at room temperature and forming a very symmetrical hexedentate coordination geometry (determined by solid-state X-ray structure).[118,266,268,269,271] *In vitro* analysis of the $[^{67/68}Ga(dedpa)]^+$ complex demonstrated excellent stability and resistance to transchelation by *apo*-transferrin and blood serum.[118] The bifunctional derivative *p*-SCN-Bn-H_2dedpa has been synthesized and conjugated to the cyclic peptide RGD, radiolabeled with ^{68}Ga and ^{64}Cu, and has shown promising results for *in vivo* tumour targeting and PET imaging.[272,273] The H_2dedpa ligand has also been functionalized with lipophilic moieties, and the resulting cationic ^{68}Ga complexes have been investigated for cardiac perfusions imaging.[274] Although preliminary work looks very promising for H_2dedpa, especially towards the production of kit-formulations with its very fast room temperature radiolabeling kinetics, more *in vivo* validation is required.

Table 1.9 H_2dedpa, H_4octapa, H_2azapa, H_5decapa, and bifunctional derivatives.

Chelator and Common Bifunctional Derivatives	Radiometal Ion	[a]	Radiolabeling Conditions	Log K_{ML}	Proposed Geometry	Ref.
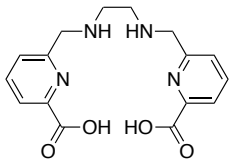 **H_2dedpa**, 1,2-[[6-(carboxy)-pyridin- 2-yl]methylamino]ethane, N_4O_2 CN = 6	$^{64}Cu^{2+}$	~	25 °C, 5-10 min, pH 5.5	19.2 (pM = 18.5)	Distorted octahedron	[273]
	$^{67/68}Ga^{3+}$	✓	25 °C, 5-10 min, pH 4.5	28.1 (pM = 27.4)	Distorted octahedron	[118,272,274]
	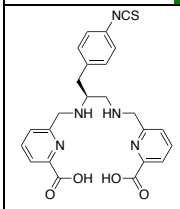 *p*-SCN-Bn-H_2dedpa[118,272]					
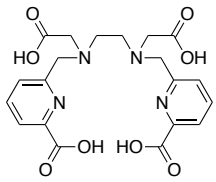 **H_4octapa**, *N,N′*-bis(6-carboxy-2-pyridylmethyl)ethylenediamine-*N,N′*-di-acetic acid, N_4O_4 CN = 8	$^{111}In^{3+}$	✓	25 °C, 5-10 min, pH 4.5	26.8 (pM = 26.5)	Square antiprism	[87,89]
	$^{177}Lu^{3+}$	✓	25 °C, 5-10 min, pH 4.5	20.1 (pM = 19.8)	Square antiprism	[87]
	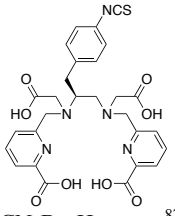 *p*-SCN-Bn-H_4octapa[87]					
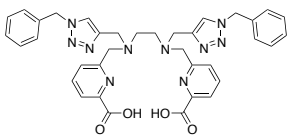 **H_2azapa**, *N,N′-[*1-Benzyl-1,2,3-triazole-4-yl]methyl-*N,N′*-[6-(carboxy)- pyridin-2-yl]-1,2-diaminoethane, N_6O_2 CN = 8	$^{64}Cu^{2+}$	~	25 °C, 5-10 min, pH 5.5	-	Distorted octahedron?	[88]
	$^{67/68}Ga^{3+}$	✗	25 °C, 5-10 min, pH 4-4.5	-	Distorted octahedron?	[88]
	$^{111}In^{3+}$	✗	25 °C, 5-10 min, pH 4.5	-	Square antiprism?	[88]
	$^{177}Lu^{3+}$	✗	25 °C, 5-10 min, pH 4.5	-	Square antiprism?	[88]
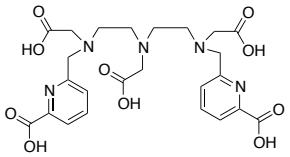 **H_5decapa**, *N,N″*-[[6-(Carboxy)pyridin-2-yl]-methyl]diethylenetriamine-*N,N′,N″*-triacetic Acid, N_5O_5 CN = 10	$^{111}In^{3+}$	✗	25 °C, 5-10 min, pH 4.5	27.56 (pM = 23.1)	Square antiprism	[87,89]

H_2azapa (Chapter 8) was built on a variation of the click-to-chelate approach, where the peptide vector is conjugated to the ligand by click-chemistry, and the resultant triazole-

rings are uniquely positioned so that they are capable of coordinating to radiometal ions in the inner-coordination sphere.[40,88,275] The triazole-containing H_2dedpa/H_4octapa derivative, H_2azapa, has been synthesized and evaluated with ^{64}Cu, ^{68}Ga, ^{111}In, and ^{177}Lu (Table 1.9).[88] Preliminary results were promising with ^{64}Cu, but *in vitro* stability assays suggest that complexes with ^{68}Ga, ^{111}In, and ^{177}Lu were unstable.[88] Due to the very lipophilic character of the neutral [Cu(azapa)] complex, *in vivo* evaluation revealed high liver and digestive tract uptake as expected, therefore more hydrophilic conjugates (e.g. peptide conjugates) must be synthesized and evaluated in the future.[88] The large decadentate derivative of H_4octapa, H_5decapa (Chapter 2), was evaluated with ^{111}In *in vitro* and *in vivo*, and was found to be significantly less stable than were H_4octapa and DOTA (Table 1.9).[87,89]

H_4octapa (Chapters 2-3 and 5-6) is a derivative of H_2dedpa, with an additional two carboxylic acid arms increasing the maximum denticity from 6 to 8 (Table 1.9).[87,89,266,271] H_4octapa has recently been found to exhibit ideal properties for ^{111}In and ^{177}Lu radiochemistry, radiolabeling in quantitative yields at room temperature in less than 10-15 minutes.[87,89] Direct comparisons between H_4octapa and DOTA with both ^{111}In and ^{177}Lu have demonstrated similar *in vivo* properties and stability, with H_4octapa having greatly enhanced radiolabeling kinetics (significantly faster even than CHX-A''-DTPA), suggesting that it may be a suitable alternative and improvement to DOTA.[87,89] Based on its excellent properties with ^{177}Lu, H_4octapa may also be a suitable match for the similar isotopes $^{86/90}$Y, although no results have been published towards this goal thus far. Further preclinical work must be performed to validate H_4octapa as a suitable alternative to DOTA, although a direct comparison has been made with ^{111}In and ^{177}Lu *in vitro* and *in vivo*.[87,89]

It appears that CHX-A''-DTPA, C-NETA/3p-C-NETA, and H_4octapa are the best current alternatives to DOTA for fast radiolabeling kinetics and excellent *in vivo* stability with ^{111}In for SPECT imaging and dosimetry, and ^{177}Lu and $^{86/90}$Y for therapeutic applications.[87,89,127] It is currently not clear how C-NETA/3p-C-NETA perform with ^{111}In because, to our knowledge, no studies have been published, and work with ^{111}In and CHX-A''-DTPA is limited. If a SPECT imaging surrogate isotope such as ^{111}In is required for pre-therapy imaging and dosimetry, it appears that currently CHX-A''-DTPA and H_4octapa are the most promising alternatives to DOTA.[87,89] A direct comparison between all of these ligands with ^{111}In, ^{177}Lu, and $^{86/90}$Y in the same animal model at the same time would be of significant value.

1.5.11 HBED and SHBED

HBED and its derivative SHBED present an interesting example of ligand development, as the addition of an aromatic para-sulfonate group in SHBED to the phenol functionality of HBED serves to decrease the pK_a of the phenolic protons and alter their hard/soft metal-donor properties (Table 1.10). The original purpose of adding this aryl-sulfonate group to HBED was to increase its negative charge and hydrophilicity/solubility (fully deprotonated SHBED has a 6^- charge vs 4^- for HBED), but the effect of changing the donor properties of the attached phenolic oxygen highlights an interesting option for tuning other ligands that contain aromatic donor groups.[276] Decreasing the pK_a of acidic functional groups in ligands can also help to improve radiolabeling efficiency: in this example by making the phenolic protons of SHBED more acidic and easier to deprotonate, and subsequently making SHBED a more effective ligand at lower pH.

Table 1.10 HBED, SHBED, BPCA, and bifunctional derivatives.[a]

Chelator and Common Bifunctional Derivatives	Radiometal Ion	[a]	Radiolabeling Conditions	Log K_{ML}	Proposed Geometry	Ref.
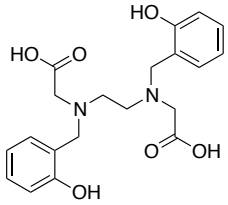 **HBED**, *N,N′*-bis(2-hydroxybenzyl)ethylenediamine-*N,N′*-diacetic acid, N_2O_4, CN = 6	$^{67/68}Ga^{3+}$	~	25 °C, 10-20 min, pH 4-4.5	38.5 (pM 28.6)	Distorted octahedron?	117,277-280
	$^{44/47}Sc^{3+}$	✗	25 °C, 10 min, pH 6.0	-	Square antiprism?	17
	$^{111}In^{3+}$	✗	25 °C, 10-20 min, pH 4-7	27.9 (pM 17.9)	Distorted octahedron?	117,277,280
	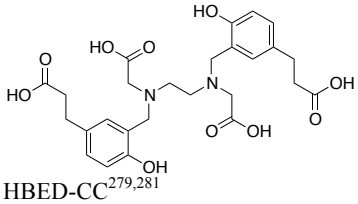 HBED-CC[279,281]			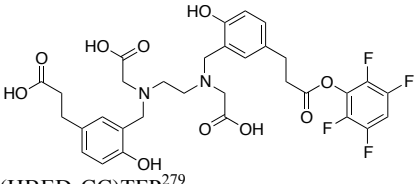 (HBED-CC)TFP[279]		
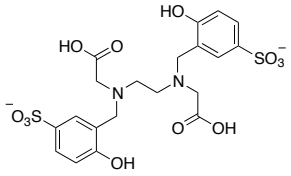 **SHBED**, *N,N′*-bis(2-hydroxy-5-sulfobenzyl ethylenediamine-*N,N′*-diacetic acid, N_2O_4, CN = 6	$^{67/68}Ga^{3+}$	~	25 °C, 10-20 min, pH 4-4.5	37.5 (pM 28.3)	Distorted octahedron?	117,276,280
	$^{111}In^{3+}$	~	25 °C, 10-20 min, pH 4-7	29.4 (pM 20.6)	Distorted octahedron?	117,276,280
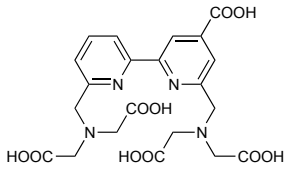 **BPCA**, N_4O_4, CN = 8	$^{111}In^{3+}$	~	25 °C, 60 min, pH 5	-	Square antiprism?	282,283

[a] highlighting relevant radiometal ions, radiolabeling conditions, thermodynamic stability constants (Log K_{ML}), coordination geometry, and color-coded ranking ([a] green "✓" = good/best match, orange "~" = suitable match, or requires more evaluation but shows potential, red "✗" = poor/unstable match).

1.5.12 BPCA

BPCA is an interesting ligand that was published in 2010, which is based on a 2,2'-bipyridine backbone, and provides an octadentate N_4O_4 donor set (Table 1.10).[282,283] BPCA was conjugated to a novel cholecystokinin C-terminal tetrapeptide (CCK4), which targets tumours expressing the cholecystokinin receptor subtype 2 (CCK2R), and radiolabeled with

^{111}In in high RCY after 1 hour at room temperature. The novel peptide-conjugate BPCA-$(Ahx)_2$-CCK4 was evaluated *in vitro* by serum stability transchelation assays, and *in vivo* by biodistrubtion and planar scintigraphy experiments. The same $(Ahx)_2$-CCK4 conjugate was made with CHX-A''-DTPA as an internal reference, and it was demonstrated that BPCA possessed superior stability to CHX-A''-DTPA in serum (89% vs 45% stable after 2.5 hours, respectively). Biodistribution and planar scintigraphic imaging studies showed that BPCA-based conjugates had higher tumour uptake, lower background organ uptake, and higher tumour/muscle ratios than CHX-A''-DTPA, suggesting that BPCA is a very promising new ligand for ^{111}In. A study evaluating BPCA with the ^{177}Lu and $^{86/90}$Y would be of great interest.

1.5.13 CP256

CP256 and its bifunctional derivative YM103 are acyclic tripodal tris(hydroxypyridinone) ligands that can rapidly radiolabel with ^{68}Ga in 5 minutes at room temperature (Table 1.11).[284] The maleimide derivative YM103 was conjugated to cysteine residues of the protein C2Ac, and *in vivo* experiments in normal healthy mice (no tumour models) showed rapid clearance through the kidneys with no observable decomposition after 1.5 hours.[284] This new ligand was published in 2011, and further studies in tumour bearing mice will help to establish its potential utility. CP256 has an interesting acyclic tripodal design, similar to L3 (hydroxamate-based), and most interestingly both ligands are oxygen-rich with O_6 donor sets, suggesting a potential untapped application as ^{89}Zr ligands (yet to be investigated, to our knowledge).

1.5.14 Desferrioxamine (DFO)

Desferrioxiamine B (DFO) is a bacterial siderophore that natively binds Fe^{3+}, and has also been used extensively with isotopes of gallium and zirconium (Table 1.11). DFO is the only competent ^{89}Zr ligand available for radiolabeling and *in vivo* applications.[285] Zr^{4+} is a highly charged, very hard metal ion with a relatively small ionic radius (84 and 89 pm for CN = 8 and 9, respectively),[190] that is prone to forming insoluble polynuclear hydroxide species in aqueous solution under non-acidic conditions, and subsequently is difficult to radiolabel effectively. DFO is thought to bind ^{89}Zr with its three hydroxamate groups in a hexadentate fashion, although no crystal structures have been obtained.[286] For many years the next best ligand for ^{89}Zr has been DTPA, which forms a thermodynamically stable complex with Zr^{4+} (log K_{ML} = 35.8-36.9), but studies have shown that radiolabeling with ^{89}Zr is inefficient and *in vivo* stability is exceptionally poor.[119] A DTPA-antibody conjugate of Zevalin was radiolabeled with ^{89}Zr, and radiochemical yields obtained were < 0.1% after 1 hour at room temperature;[223] in contrast, DFO can radiolabel with ^{89}Zr in quantitative yields (> 99%) after 1 hour. The new ligand H_6phospa has recently been studied with ^{89}Zr, and has shown greatly improved radiolabeling performance relative to DTPA, but still inferior to DFO (*vide infra).*

No FDA-approved radiopharmaceuticals currently utilize ^{89}Zr, although a number of ^{89}Zr-DFO-antibody conjugates are in clinical trials.[212] ^{89}Zr has a long half life (78.5 hours), making it ideally paired with antibody vectors, as the biological half-life of an antibody is on the order of 2-3 weeks.[45] ^{89}Zr-DFO-Zevalin was the first ^{89}Zr antibody conjugate imaged in humans, and was shown to be a suitable PET surrogate for ^{90}Y-Zevalin dosimetry.[223] A number of other studies have been performed using ^{89}Zr-DFO-antibody conjugates with success, such as ^{89}Zr-DFO-U36 (anti-CD446 chimeric mAb),[212,287] ^{89}Zr-DFO-

bevacizumab,[212,288] ^{89}Zr-DFO-J591,[285] ^{89}Zr-DFO-TRC105,[289] and ^{89}Zr-DFO-trastuzumab.[212,290,291]

The high 4+ charge makes ^{89}Zr challenging to incorporate into BFC systems while still retaining bioequivalence with other common 3+ cationic metal ions (e.g. In^{3+}, Ga^{3+}, Y^{3+}, Lu^{3+}), because the chelate-radiometal charge and polarity is different. Evaluating the stability of potential BFC for ^{89}Zr can be done *in vivo*, because ^{89}Zr that is lost from a BFC typically localizes in bone, as demonstrated by the highly unstable ^{89}Zr-DOTA- and ^{89}Zr-DTPA-based antibody conjugates with cetuximab that showed significant ^{89}Zr accretion in the thighbone 72 hours post injection.[130] ^{89}Zr-chloride and ^{89}Zr-oxalate have also been injected directly into mice, with ^{89}Zr-chloride forming colloids and accumulating in the liver, and the weakly chelated ^{89}Zr-oxalate demonstrating rapid bone uptake.[285] Although DFO is an excellent ^{89}Zr ligand, some decomposition can be observed over time *in vivo* as ^{89}Zr slowly accumulates in bone.[36,56] The design of novel ligands for ^{89}Zr with improved solubility, *in vivo* stability, and chelation properties would be timely, considering there is currently only one option (DFO). Based on the success of DFO, it would appear that oxygen-rich donors are most suitable for ^{89}Zr chelation, with O_6-O_8 coordination being preferred, and donor groups including hydroxamates, carboxylates, carbonyls, catechols, and hydroxypyridinones being logical choices.

Table 1.11 CP256, Desferrioxamine (DFO), PCTA, H_6phospa, and bifunctional derivatives.

Chelator and Common Bifunctional Derivatives	Radiometal Ion [a]		Radiolabeling Conditions	Log K_{ML}	Proposed Geometry	Ref.
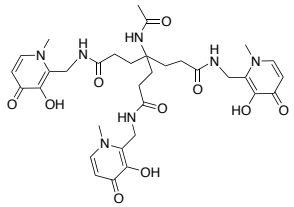 **CP256**, O_6 CN = 6	$^{67/68}Ga^{3+}$	✓	25 °C, 5 min, pH 6.5	-	Distorted octahedron	284
	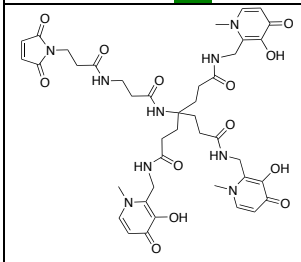 Bifunctional derivative YM103[284]			**CP256** = 4-Acetylamino-4-[2-[(3-hydroxy-1,6-dimethyl-4-oxo-1,4-dihydro-pyridin-2-ylmethyl)-carbamoyl]-ethyl]-heptanedioic acid bis-[(3-hydroxy-1,6-dimethyl-4-oxo-1,4-dihydro-pyridin-2-ylmethyl)-amide]		
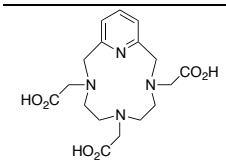 **PCTA**, 3,6,9,15-tetraazabicyclo[9.3.1]pentadeca-1(15),11,13-triene-3,6,9,-triacetic acid, N_4O_3 CN = 7	$^{64}Cu^{2+}$	~	25 °C, 5 min, pH 5.5	19.1	Distorted octahedron	91,94, 214,292
	$^{67/68}Ga^{3+}$	✓	25 °C, 5-10 min, pH 4-5	-	Distorted octahedron	90,292-294
	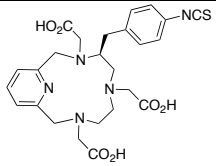 *p*-SCN-Bn-PCTA[214]					
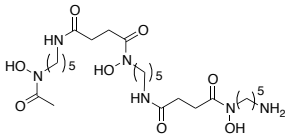 **DFO,** Desferrioxamine B, O_6, CN = 6	$^{67/68}Ga^{3+}$	~	25 °C, 30 min, pH 3.5	28.6	Distorted octahedron?	218,295
	$^{89}Zr^{4+}$	✓	25 °C, 60 min, pH 7-7.3.	-	Distorted octahedron?	56,130,223,285,287-291,296-302
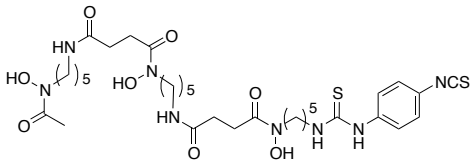 *p*-SCN-Bn-DFO[298]	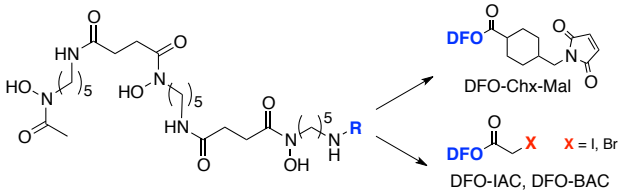 Bifunctional DFO derivatives[299,303]					
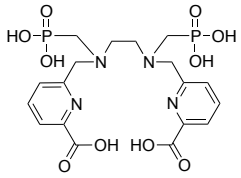 **H_6phospa**, *N*,*N*'-(methylenephosphonate)-*N*,*N*'-[6-(methoxycarbonyl) pyridin-2-yl]methyl]-1,2-diaminoethane, N_4O_4 CN = 8	$^{89}Zr^{4+}$	~	25 °C, 60 min, pH 7.4	-	Square antiprism?	304
	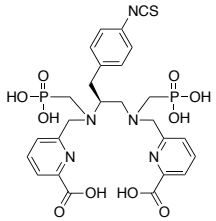 Bifunctional derivative *p*-SCN-Bn-H_6phospa					

1.5.15 H_6phospa

Developing new chelating agents for ^{89}Zr is currently of great interest, as the only ligand available that can radiolabel with ^{89}Zr with any level of proficiency is DFO. The best alternative ligand to DFO for ^{89}Zr radiolabeling is DTPA; however, with meager radiochemical yields of < 0.1% after 1 hour at room temperature and poor *in vivo* stability, DTPA is not a viable alternative to DFO.[223] DFO can radiolabel with ^{89}Zr in quantitative yields (> 99%) after 1 hour at room temperature, and demonstrates imperfect but acceptable stability *in vivo*, and no acceptable alternatives have been published to date. The acyclic ligand H_6phospa (Chapter 7, Table 1.11),[268,269] and the bifunctional derivative *p*-SCN-Bn-H_6phospa are methylenephosphonate derivatives of H_4octapa (Table 1.9) that have been recently studied with ^{89}Zr.[304] The antibody conjugate H_6phospa-trastuzumab was able to achieve radiochemical yields of ~8% with ^{89}Zr after 1 hour at room temperature (PBS, pH 7.4).[304] This work was compared to previous attempts to radiolabel H_4octapa-trastuzumab with ^{89}Zr, which performed similarly to DTPA and exhibited essentially no radiolabeling after 1 hour.[304] These results demonstrate that replacing the carboxylic acid arms of H_4octapa with methylenephosphonate arms in H_6phospa improved radiolabeling kinetics with ^{89}Zr, suggesting that methylenephosphonate groups are more suitable than carboxylic acid groups for chelating ^{89}Zr.[304] Although a RCY of ~8% is insufficient to supplant DFO as the "gold standard" ligand for radiolabeling with ^{89}Zr, it is a significant improvement over DTPA and H_4octapa, and to our knowledge is the highest ^{89}Zr radiolabeling yield behind DFO to be published.

1.5.16 PCTA

The heptadentate macrocyclic ligand PCTA was originally synthesized by Sherry and coworkers as a potential MRI contrast agent (Table 1.11).[292] PCTA has been recently re-purposed and evaluated with ^{68}Ga and ^{64}Cu, and has been shown to possess much faster radiolabeling kinetics than DOTA (5-10 min, RT).[90] The serum stability of the $^{67/68}$Ga-PCTA complex was found to be superior to DOTA, and comparable to NOTA.[90] Additionally, the biodistribution profile of the non-bifunctional ^{68}Ga-PCTA revealed lower kidney retention than ^{68}Ga-NOTA, showing potential improvement over NOTA for use in peptide conjugates.[90] Comparisons of RGD conjugates of the bifunctional derivatives of both PCTA and NOTA have demonstrated excellent *in vivo* stability and comparable biodistribution profiles, with the PCTA-based agent having lower kidney uptake than its NOTA counterpart.[294] PCTA has also been investigated with ^{64}Cu, showing greater radiolabeling kinetics and yields to DOTA, and superior *in vitro* and *in vivo* stability.[75] PCTA has only recently been investigated, but further work may show it to be an excellent ligand for copper and gallium-based radiopharmaceuticals.

1.6 Conclusions

With the methods for evaluating ligands with radiometals explained, and the plethora of existing ligands reviewed, we now set out to study novel acyclic ligands for radiochemistry applications. While synthesizing and evaluating a number of new ligands, factors such as the charge, polarity, denticity, donor atom type (e.g. N, O, S), and kinetics (e.g. macrocyclic vs. acyclic) will be studied and optimized with the goal of achieving maximum *in vivo* stability. The following 8 chapters will discuss work on 8 new ligands (as

well as bifunctional derivatives) for radiochemistry, covering radiometals such as ^{64}Cu, ^{68}Ga, ^{111}In, ^{177}Lu, and ^{89}Zr. The synthesis of these oxygen- and nitrogen-rich ligands has been challenging, and much work has been directed towards applying new synthetic methods and protecting group chemistry towards their production. Once synthesized, ligands and many of their non-radioactive metal complexes were evaluated by standard analytical techniques, such as nuclear magnetic resonance (NMR), mass spectrometry (MS), infrared spectroscopy (IR), elemental analysis (EA), and high-performance liquid chromatography (HPLC). These ligands, and where possible their bifunctional derivatives, were radiolabeled with a variety of radiometals, and their efficiency and stability were studied using *in vitro* (e.g. serum stability) and *in vivo* (e.g. PET/SPECT/Cerenkov imaging, biodistribution) experiments. A number of the new ligands discussed in this thesis were summarized in the tables presented in Chapter 1 and compared to the entire field, and now their study and elaboration will be discussed in detail.

Chapter 2: H_4octapa: an acyclic ligand for ^{111}In radiopharmaceutical applications

This chapter is an adaptation of published work, and is reproduced in part, with permission from Price, E. W.; Cawthray, J. F.; Bailey, G. A.; Ferreira, C. L.; Boros, E.; Adam, M. J.; Orvig, C., H_4octapa: An Acyclic Chelator for ^{111}In Radiopharmaceuticals. *J. Am. Chem. Soc.* **2012,** *134* (20), 8670-8683, Copyright 2014 American Chemical Society.

2.1 Introduction

^{111}In is an important isotope in nuclear medicine for SPECT imaging and performing dosimetry for therapeutic chelate-based radiopharmaceuticals. ^{111}In is a cyclotron produced isotope (^{111}Cd(p,n)^{111}In) that decays with a half-life of ~2.8 days via electron capture (100% EC); it emits γ rays (245 and 172 keV) that can be used for imaging, and Auger electrons that can be used for therapy.[15] One of the most promising radiotherapeutic isotopes, ^{90}Y ($t_{1/2}$ = ~2.67 days), is essentially radiographically silent as it only emits β^- particles, and therefore must be used in combination with an imaging isotope such as ^{111}In, ^{89}Zr, ^{86}Y, ^{64}Cu, or $^{67/68}$Ga to study its organ uptake and perform dosimetry.[25,56,305] The generator produced indium isotope ^{110m}In ($t_{1/2}$ = 69 min) is a very attractive PET (positron emission tomography) imaging surrogate for ^{111}In, and the two isotopes can be seamlessly interchanged in bifunctional-chelate (BFC) based radiopharmaceuticals because they share identical chemical properties.[306] When used with the OctreoScan kit (BFC-peptide conjugate), ^{110m}In has been shown to significantly improve spatial resolution, dosimetry, and tumour identification when

compared to ^{111}In;[306] however, the generator parent isotope ^{110}Sn has a half-life of ~4.1 hours, which makes the generator life very short.[307] Also, commercial availability of ^{110m}In is limited, which restricts usage.

There are currently several ^{111}In/^{90}Y-based radiopharmaceuticals FDA-approved for clinical use and many more in clinical trials, demonstrating the importance of these isotopes in nuclear medicine.[28,211,214,308-311] The combination of ^{111}In for imaging and dosimetry and ^{90}Y/^{177}Lu for therapy is very effective, but is dependent on having a solid ligand foundation that can bind both isotopes with exceptionally high stability (thermodynamic and kinetic) and that has very similar biological behavior with both isotopes (biologically equivalent).[19-24,213,312] The macrocycle DOTA (1,4,7,10-tetraazacyclododecane-1,4,7,10-tetraacetic acid) is the industry "gold standard" for chelation of ^{111}In, ^{90}Y, and ^{177}Lu (Figure 2.1); however, biovector conjugates suffer from the need for elevated temperatures and extended reaction times to achieve quantitative radiolabeling yields (typically 60-95 °C, for 30-120 minutes), which is not optimal for use with heat-sensitive biomolecules such as antibodies.[106,177,232,240] Peptide biovectors can often be labeled at elevated temperatures without suffering deleterious effects to their binding integrity, and have also shown excellent tumour targeting and uptake; however, with the current ligand offerings they sometimes demonstrate high and persistent kidney uptake that can disrupt the predictive power of dosimetry calculations and cause unwanted radiation exposure.[312,313]

Since the properties of the radiometal-chelate complex can strongly influence the biodistribution profile of its biomolecule conjugate, a new ligand with an improved clearance profile and decreased persistent kidney uptake would be a welcome improvement. Although the influence of ligand properties on the biodistribution of BFC-conjugates is less significant

for large biovectors such as antibodies (~150 kDa for an intact antibody) than it is for smaller peptides, the difference can still be significant.[213,305,312] Antibody biovectors show exceptionally high tumour uptake and have long biological half-lives (2-3 weeks[45]), and so are well matched with the long half-lives of ^{90}Y (~2.67 days) and ^{177}Lu (~6.6 days).[15] The acyclic ligand DTPA (diethylenetriaminepentaacetic acid) will successfully radiolabel with these isotopes in 10-15 minutes at ambient temperature (Figure 2.1); however, the *in vivo* stability is less than optimal, showing a greater extent of decomposition and non-target organ uptake than DOTA.[60,215,216,312] The DTPA derivative CHX-A''-DTPA has an improved stability profile with $^{86/90}$Y when compared to DTPA, while retaining its low temperature labeling abilities (30-60 minutes); however, the stability and *in vivo* kinetic inertness are still not as good as DOTA, and its In^{3+} complexes have been less studied.[59,60,215,216,244] Despite the poor *in vivo* stability, DTPA is the ligand used in the currently available FDA approved ^{111}In-based radiopharmaceuticals.

Our group has recently investigated a series of acyclic ligands based on picolinic acid, resulting in identification of the promising $^{67/68}$Ga ligand H_2dedpa (Figure 2.1).[118,266,272,273] Initial radiolabeling experiments, *in vitro apo*-transferrin stability experiments, and biodistribution studies in mice have demonstrated H_2dedpa to be an ideal ligand for $^{67/68}$Ga-based radiopharmaceuticals.[274] This success has prompted the investigation of larger acyclic frameworks based on a similar picolinic acid scaffold, supporting higher denticities for accommodating larger radiometal ions such as ^{111}In, ^{90}Y, ^{177}Lu, ^{89}Zr, and ^{225}Ac. Herein we report the synthesis, characterization, coordination chemistry, thermodynamic stability, radiolabeling, *in vitro* mouse serum stability, and *in vivo* biodistribution studies of the ^{111}In complexes of the octadentate ligand *N,N'*-bis(6-carboxy-2-pyridylmethyl)ethylenediamine-

N,N'-diacetic acid (referred to herein as H_4octapa) (Figure 2.1),[271] and the decadentate analogue H_5decapa. DOTA and DTPA were used as benchmarks of the industry "gold standards" for ^{111}In chelation. The ligands H_2dedpa and H_4octapa had previously been published for applications as MRI contrast agents, and later as Pb(II), Cd(II), and Zn(II) sequestration agents.[266,269-271]

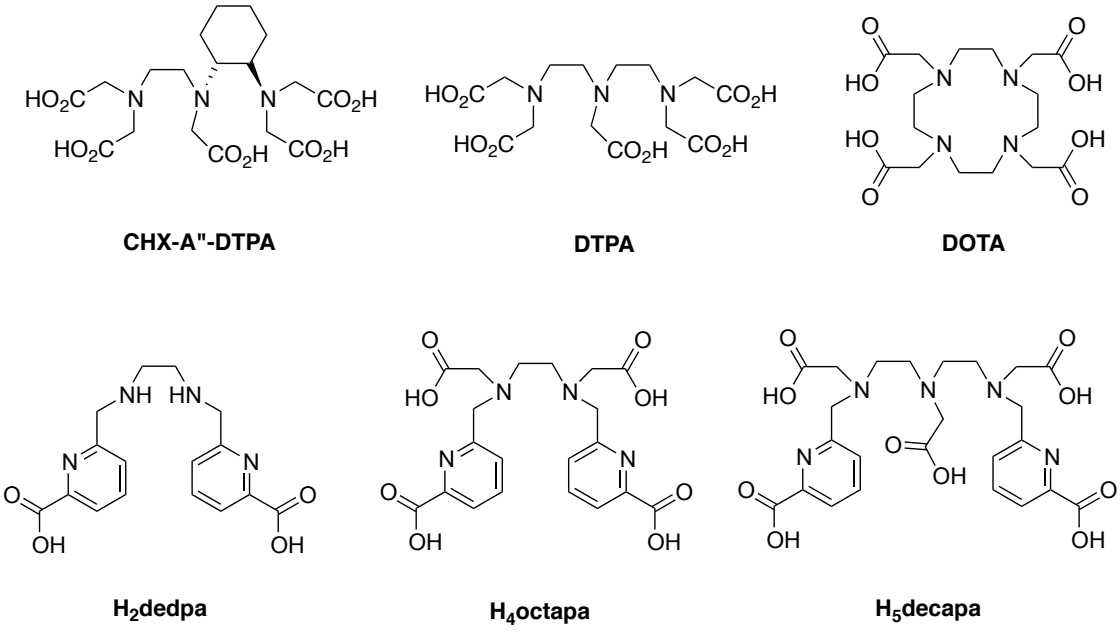

Figure 2.1 Structures of the ^{111}In-coordinating and industry "gold standard" ligands DTPA/CHX-A''-DTPA and DOTA, the ^{68}Ga-coordinating ligand H_2dedpa, and the novel entrants H_4octapa and H_5decapa.

2.2 Results and discussion

Although the macrocycle DOTA is regarded as the most stable ligand for ^{111}In, it is not best suited for use with antibodies due to its optimal high-temperature radiolabeling, and the excellent match of antibodies with long-lived therapeutic isotopes makes this mismatch especially unfortunate. DOTA radiolabels with many radiometals at the moderate and antibody-compatible temperature of 37 °C; however, reaction times of 60-180 h are required

and radiochemical yields are inconsistent (~50-90%).[58-65,94,97,119,127-129,142] This suggests an important and high priority need for new, highly stable acyclic ligands for use with isotopes such as ^{111}In, ^{90}Y, and ^{177}Lu, especially when conjugated to antibodies. There is a need for ligands that combine the exceptional *in vivo* stability and kinetic inertness of DOTA with the fast ambient temperature labeling kinetics of DTPA. These observations suggest that the target for an ideal ^{111}In/^{90}Y/^{177}Lu ligand would have the following properties. It should 1) be acyclic, or if macrocyclic, be constructed with free-moving appendages to emulate ambient temperature acyclic radiolabeling kinetics, such as the NOTA derivative NETA.[202] The coordination complex should 2) be very stable; both thermodynamically and kinetically, but with top priority placed on exceptional *in vivo* kinetic inertness, particularly to demetallation and/or transchelation. The ligand should 3) be isomerically pure with preferably only one stable isomer being formed and administered, or such as CHX-A''-DTPA, the superior isomer of the ligand isolated and administered pure.[60,215,216] Finally, it should 4) ideally have similar properties in its ligand/bifunctional-chelate complexes with both of the radiometal ions to be used in an imaging/therapy pair (i.e. ^{111}In/^{90}Y), so that biological clearance and organ uptake are sufficiently similar and that accurate dosimetry information can be obtained (bio-equivalence). Not every one of these four points must be met for a ligand to be useful as a BFC for radiometal ions, and especially point number four may be hard to achieve, considering the different coordination numbers and geometries preferred by different metal ions such as ^{111}In (6-8 coordinate) and ^{90}Y (8-9 coordinate).[6]

Scheme 2.1 Synthesis of compounds **2.1, 2.2, 2.3, 2.4, 2.5, 2.6** and **H_4octapa**[a]

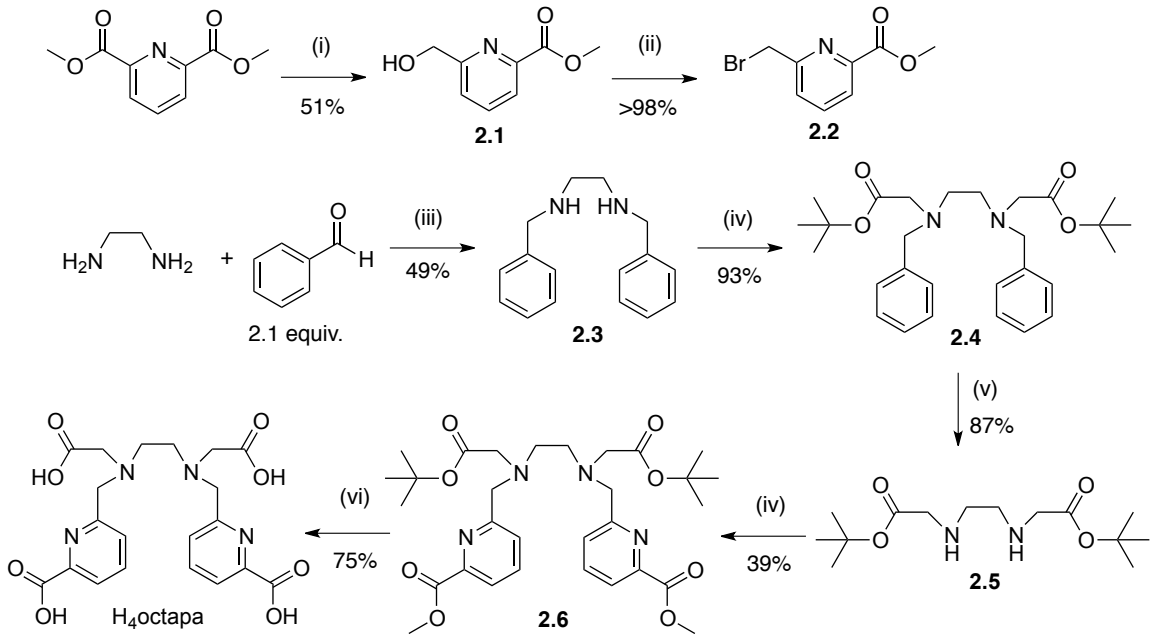

[a] Reagents and conditions: i) $NaBH_4$ (2.4 eq.), CH_3OH, 4 h, 0 °C; ii) PBr_3 (1.1 eq.), $CHCl_3$, 0 °C, 3.5 h; iii) CH_3OH, $NaBH_4$ (4.3 eq.), 8 h; iv) CH_3CN, Na_2CO_3 (excess), 60 °C, Ar (g), 12-16 h, **2.4** = alkylation with *tert*-butyl bromoacetate, **2.6** = alkylation with **2.2**; v) AcOH, Pd/C (10 wt%), H_2 (g), 12 h; vi) HCl (6 M), 8 h.

2.2.1 Synthesis and characterization

We have studied a number of novel acyclic ligands, and herein we report our two most promising candidates for use with ^{111}In. The octadentate ligand *N,N'*-bis(6-carboxy-2-pyridylmethyl)ethylenediamine-*N,N'*-diacetic acid (H_4octapa) was previously used with various paramagnetic lanthanides to assess their abilities as MRI contrast agents.[271] As an expansion of this scaffold, the novel decadentate derivative H_5decapa has also been synthesized and evaluated. The ligands H_4octapa and H_5decapa were synthesized with a general reaction scheme that follows *N*-benzyl protection, *N*-alkylation with an alkyl halide, benzyl deprotection via hydrogenation, a second alkyl halide *N*-alkylation, and finally deprotection in boiling HCl (6 M) (Schemes 2.1 and 2.2). Previous methods to synthesize

the similar acyclic ligand H_2dedpa utilized reductive amination reactions;[118,271] however, this method resulted not only in reduction of the imines, but also hydrolysis/reduction of the picolinic acid methyl ester groups to carboxylates and alcohols, which were very difficult to separate in subsequent steps, resulting in arduous purifications and low yields. The synthetic scheme presented here circumvents this problem by avoiding the use of sodium borohydride in the presence of the picolinic acid moiety (Schemes 2.1 and 2.2). The only significant problem encountered with these syntheses is the lability of the picolinate groups to hydrogenation. Benzylated intermediates that contain picolinate groups undergo unwanted cleavage during hydrogenation, and to minimize this undesirable pathway the reaction order was optimized to perform the debenzylation step only in the presence of the *tert*-butylacetate groups (Schemes 2.1 and 2.2). The obvious drawback to this method is that after hydrogenation, the *tert*-butylacetate-alkylated ethylenediamine/diethylenetriamine compounds (**2.5/2.9**) are not UV active and must be stained with iodine to be visualized. Hydrogenation of the diethylenetriamine scaffold during the synthesis of H_5decapa resulted in substantial cleavage of the diethylenetriamine backbone, resulting in lower yields than the equivalent hydrogenation of the ethylenediamine scaffold in the H_4octapa synthesis. Decreasing the Pd/C catalyst loading appeared to slow down reaction kinetics but did not improve selectivity for debenzylation over the unwanted side reactions.

The presented synthetic schemes are a substantial improvement over previous attempts, allowing for improved yields and the purification of all intermediates despite the large number of polar functional groups; however, the problem of non-selective debenzylation and ethylene backbone cleavage of diethylenetriamine (H_5decapa) is problematic, and with larger scaffolds such as tris(2-aminoethyl)amine (TREN) this problem becomes more severe (see

Chapter 4). These challenges suggest that new protecting group chemistry must be employed to further improve the synthesis of these picolinic acid-based ligands and facilitate the elaboration of larger scaffolds and novel bifunctional derivatives (see Chapter 3). The relatively simple 5-step synthesis of H_4octapa is achieved with a cumulative yield of ~12%, and the 5-step synthesis of H_5decapa was completed with a cumulative yield of ~2.5% (yields for both compounds using previous reductive aminations methods were under 1%). The incorporation of multiple synthons in the synthesis of these ligands will allow for more straightforward synthesis of bifunctional derivatives via (4-nitrobenzyl)ethylenediamine/diethylenetriamine backbone derivatives, which should be an improvement over the difficult and tedious synthesis of bifunctional macrocycles such as *p*-isothiocyanatobenzyl-DOTA.[143]

Scheme 2.2 Synthesis of compounds **2.7, 2.8, 2.9, 2.10** and **H_5decapa**[a]

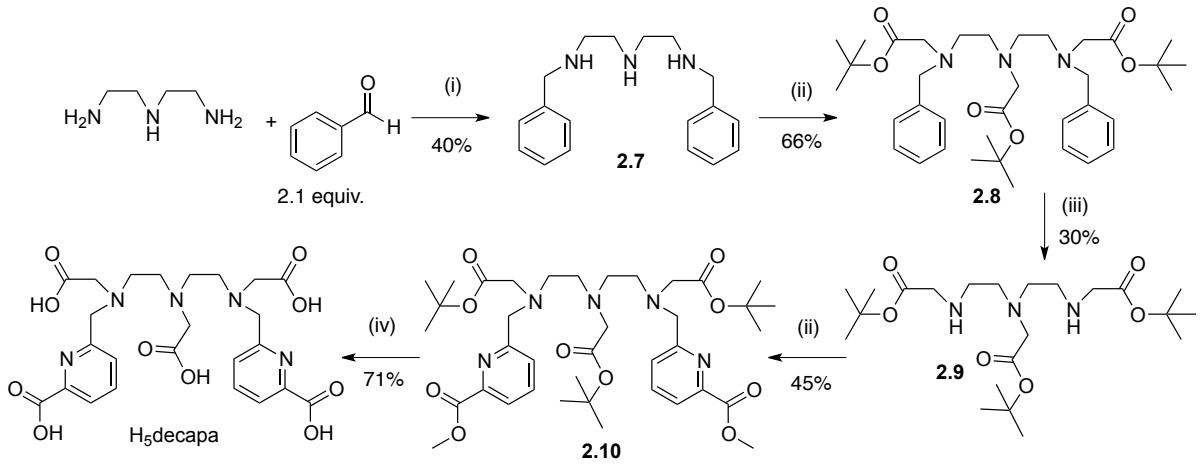

[a] Reagents and conditions: (i) CH_3OH, $NaBH_4$ (7 eq.), 8 h; (ii) CH_3CN, Na_2CO_3 (excess), 60 °C, Ar (g), 12-16 h, **8** = alkylation with *tert*-butyl bromoacetate, **2.10** = alkylation with **2.2**; (iii) AcOH, Pd/C (5 wt%), H_2 (g), 12 h; (iv) HCl (6 M), 8 h.

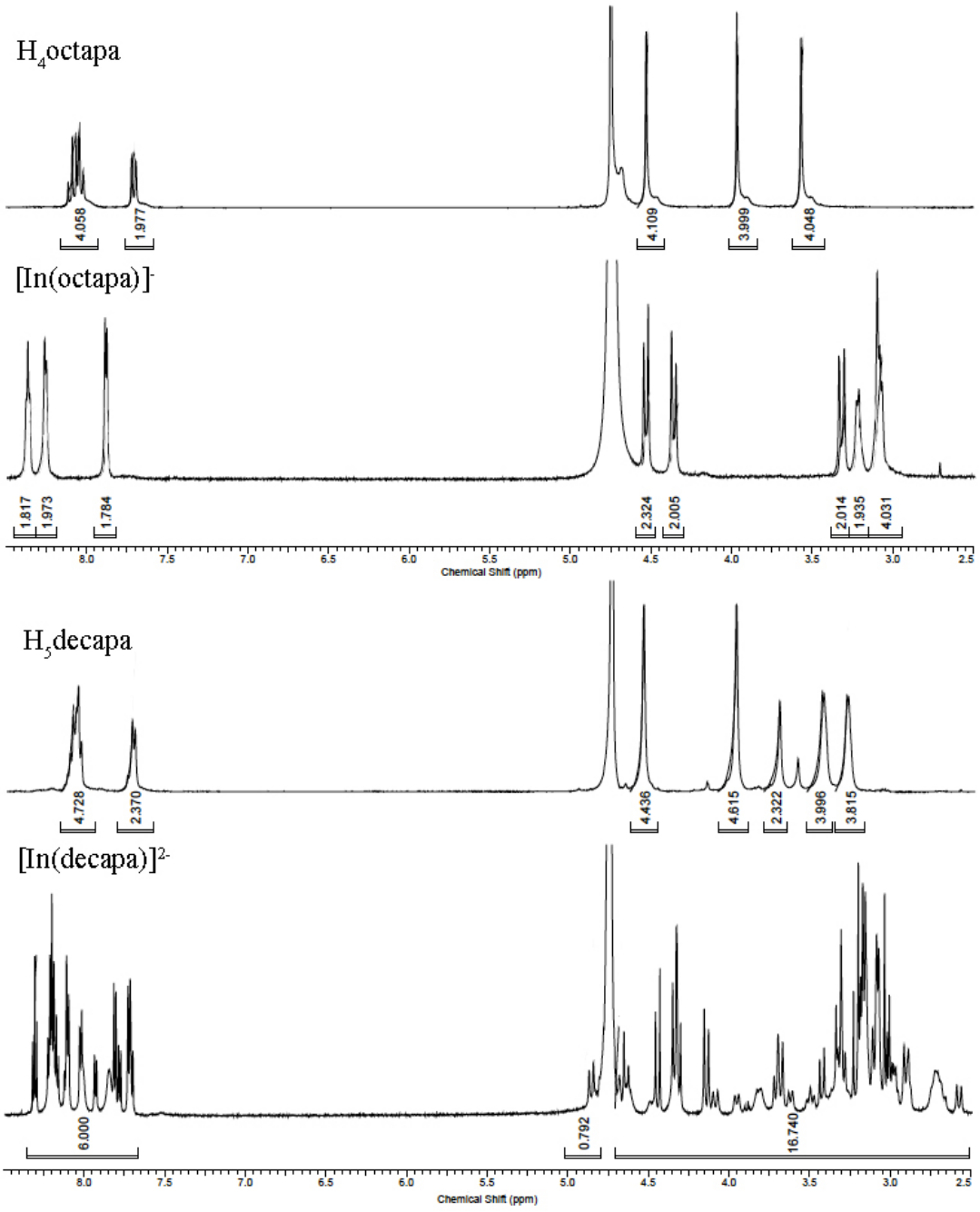

Figure 2.2 ^{1}H NMR spectra in D_2O (300 MHz) at ambient temperature of top, H_4octapa and $[In(octapa)]^-$ showing simple diastereotopic splitting due to minimal isomerization and bottom, H_5decapa and $[In(decapa)]^{2-}$ showing complicated but sharp splitting arising from multiple static isomers.

In general, ligands/BFC that exhibit minimal isomerization are preferred, although no definitive trend has been identified for this phenomenon.[49,63,97] The ^{1}H NMR spectrum of

[In(octapa)]$^-$ reveals clear and sharply resolved diastereotopic splitting of the protons associated with both picolinic acid moieties (methylene-*H*, 4.49 ppm, ^{2}J = 16.1 Hz, and 4.34 ppm, ^{2}J = 16.1 Hz), as well as one of the acetic acid arms (3.27 ppm, ^{2}J = 19.3 Hz), suggesting a 7-coordinate solution structure (Figure 2.2). The coupling constants observed for these metal-bound appendages were ^{2}J = 16.1 Hz for the two picolinic acid methylene groups, and ^{2}J = 19.3 Hz for the acetic acid arm. The second acetic acid arm appeared as a broad doublet (3.19 ppm) with a much smaller coupling constant of ^{2}J = 8.4 Hz, showing diasterotopic splitting, but suggesting that it is not metal-bound and does not form a 5-membered metallocycle as do the other metal-bound appendages.

The sharp and clear diasterotopic splitting seen for [In(octapa)]$^-$ suggests the presence of a single static isomer with no observable fluxional interconversion at ambient temperature (on the NMR timescale). No change in the number of peaks in the ^{13}C NMR spectrum of the ligand H_4octapa was observed upon In^{3+} coordination, suggesting no chemically distinct isomers were formed (different coordination number/polarity). The HPLC radiotrace of [In(octapa)]$^-$ showed a single sharp peak, affirming that the radiometal-complex exists as a single isomer (Figure A.1). This analysis depicts a very stable and inert coordination structure present as a single isomer, unlike the [In(DOTA)]$^-$ complex which shows multiple isomers with rapid fluxional isomerization at ambient temperature.[62,97]

The In^{3+} complex formed with the potentially decadentate ligand H_5decapa, [In(decapa)]$^{2-}$, displayed a more complex ^{1}H NMR splitting (Figure 2.2) and a large number of additional ^{13}C NMR peaks that were not observed for the free ligand H_5decapa. This observation, along with the presence of two peaks in the HPLC radiotrace (t_R = 5.4 min (5%), 7.7 min (95%), Figure A.1) suggests that multiple isomers of [In(decapa)]$^{2-}$ are present in

solution at ambient temperature. Considering that In^{3+} typically forms 7-8 coordinate complexes, the decadentate ligand H_5decapa may have several unbound carboxylates, which could give rise to different protonation species in solution and could explain the two peaks observed in the radio-HPLC trace. Additionally, NMR experiments (D_2O) and HPLC experiments were performed at different pH (0.1% TFA as HPLC buffer, pH ~2), which could influence the protonation species present in solution. $[In(DTPA)]^{2-}$ displays a complicated splitting of the ^1H NMR peaks in a similar fashion to $[In(decapa)]^{2-}$, and also yields sharp splitting patterns suggesting that little or no fluxional behavior between multiple static isomers/diastereomers occurs in solution at ambient temperature (Figure 2.2).[314,315] Unlike $[In(decapa)]^{2-}$, $[In(DTPA)]^{2-}$ retains a simple ^{13}C NMR spectrum, with the same number of ^{13}C signals being observed as with unbound DTPA.[314] These observations for $[^{111}In(DTPA)]^{2-}$ suggest that little or no fluxional behavior between isomers/diastereomers occurs in solution at ambient temperature (on the NMR timescale), although multiple isomers are indeed formed.[97,314,315] If minimal isomerization and fluxional behaviour are preferred for stability,[49,63,97] then the NMR solution structures of the currently investigated In^{3+} ligand complexes would have them ranked as $[In(octapa)]^-$ > $[^{111}In(DTPA)]^{2-}$ > $[In(DOTA)]^-$ > $[In(decapa)]^{2-}$. As previously discussed, DTPA has been shown to be inferior to DOTA in terms of *in vivo* stability with In^{3+} and so does not fit with this trend; however, this work largely follows the trend with the *in vivo* stability of H_4octapa being superior to that of DOTA (*vide infra*), and H_5decapa being inferior to both. It may be the case that acyclic and macrocyclic ligands cannot be compared in this manner, as a fluxional macrocyclic complex is likely to remain more stable than an analogous fluxional acyclic complex, because the metal remains encapsulated inside of the protective macrocyclic framework and is less likely

to be released.

The ^{1}H NMR spectrum of the hexadentate $[In(dedpa)]^{+}$ complex in D_2O was very similar to that of $[In(octapa)]^{-}$, revealing a sharp doublet for each set of methylene protons (4.58 ppm, ^{2}J = 17.3 Hz, and 4.13 ppm, ^{2}J = 17.4 Hz) associated with the picolinic acid moiety (Figure A.2). The ^{1}H NMR spectrum of the hexadentate $[In(dedpa)]^{+}$ complex in DMSO-d_6 revealed two sharp doublets for each set of methylene protons (4.27 ppm, ^{2}J = 16.6 Hz, 4.26 ppm, ^{2}J = 16.3 Hz, 3.90 ppm, ^{2}J = 16.6 Hz. 3.89 ppm, ^{2}J = 16.6 Hz) attached to the picolinic acid moieties, suggesting clean diastereotopic splitting arising from two separate isomers, most likely from DMSO binding to the open coordination sites of In^{3+} (Figure A.2). The sharp peaks observed for $[In(dedpa)]^{+}$ in D_2O and DMSO-d_6 suggest no observable fluxional behavior at ambient temperature, and the presence of only one set of peaks in the ^{13}C NMR spectrum (same as unbound H_2dedpa) and one peak in the radio-HPLC trace (*vide infra*) suggest the formation of only one isomer. In consideration of these results, the very simple and sharp diastereotopic proton splitting observed in the ^{1}H NMR spectrum of $[In(octapa)]^{-}$, coupled with the single sharp peak observed in the HPLC-radiotrace suggest that this complex displays the least amount of isomerization and fluxional behaviour in solution at ambient temperature out of the currently investigated novel ligands and the industry "gold standards" DTPA and DOTA.

2.2.2 DFT structures and molecular electrostatic potential maps

Although solid-state structures of metal-ligand complexes obtained from X-ray crystallography are useful, they are often not representative of the solution phase structures, and so DFT calculations (modeled in water) and NMR studies in D_2O of solution structures

are most relevant to a discussion of potential *in vivo* applications.[6,9,97] The DFT structure of $[In(octapa)]^-$ (Figure 2.3, left) reveals an 8-coordinate complex with approximately C_{2v} symmetry, showing tight binding of In^{3+} with slight puckering of the picolinic acid moieties. The solution structure of $[In(octapa)]^-$ as deduced by NMR spectroscopy suggests a 7-coordinate structure with one acetic acid arm unbound; however, it is not certain from the broad doublet (3.22 ppm) and smaller coupling constant (8.4 Hz) of the unbound acetic acid arm whether or not there is transient metal binding. The DFT structure of $[In(decapa)]^{2-}$ (Figure 2.4, left) shows an 8-coordinate structure, with one picolinic acid group and all 3 acetic acid arms bound to indium (as well as the 3 tertiary backbone nitrogen atoms), and one picolinic acid group unbound and extended away from the metal center into solution. This unsymmetric coordination sphere has a large impact on the molecular electrostatic potential (MEP) of the complex (Figure 2.4, right), with the MEP distribution revealing the entire molecular surface to be more electronegative than for $[In(octapa)]^-$ (Figure 2.3, right). $[In(decapa)]^{2-}$ shows areas of very high electronegative potential around the unbound picolinic acid group, most likely from the unbound deprotonated carboxylate group (Figure 2.4, right). The unsymmetric high density of electronegative potential shown on the MEP map of $[In(decapa)]^{2-}$, in contrast to the symmetric and less electronegative charge distribution of $[In(octapa)]^-$, may result in a higher propensity towards protonation and protein binding *in vivo*, and may be partially responsible for the poor stability *in vivo* (*vide infra*).

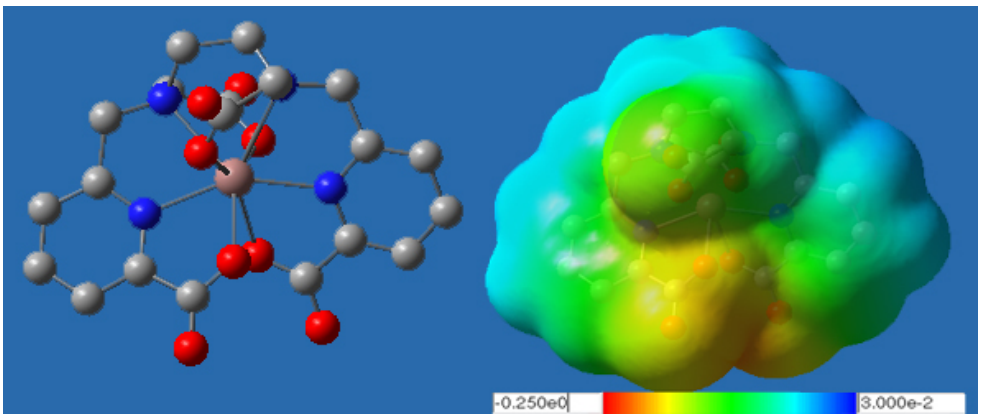

Figure 2.3 DFT structure of $[In(octapa)]^-$ (solvent = water) showing an 8 coordinate structure (left), and the electrostatic potentials of the complex between $octapa^{4-}$ with In^{3+} mapped onto the electron density (right). The MEP represent a maximum potential of 0.03 au, and a minimum of -0.25 au, mapped onto electron density isosurfaces of 0.002 e $Å^{-3}$ (red to blue = negative to positive). DFT calculations performed by Dr. Jacqueline Cawthray.

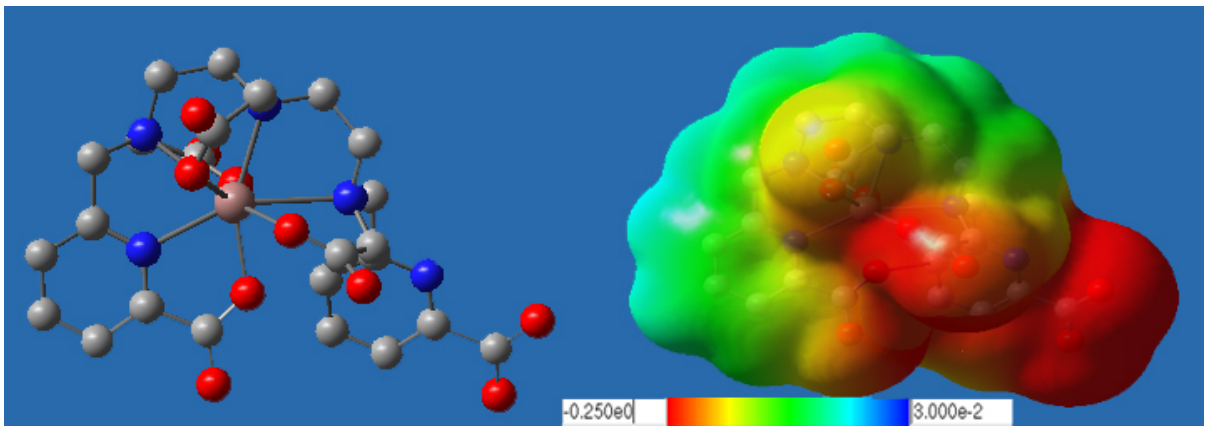

Figure 2.4 DFT structure of $[In(decapa)]^{2-}$ (solvent = water) showing an 8 coordinate structure, and the electrostatic potentials of the complex between $decapa^{5-}$ with In^{3+} mapped onto the electron density (right). The MEP represent a maximum potential of 0.03 au, and a minimum of -0.25 au, mapped onto electron density isosurfaces of 0.002 e $Å^{-3}$ (red to blue = negative to positive). DFT calculations performed by Dr. Jacqueline Cawthray.

2.2.3 Radiolabeling experiments

Initial radiolabeling experiments demonstrated the ability of H_4octapa to radiolabel quantitatively with ^{111}In at ambient temperature in 10 minutes, showing a single sharp peak

in the HPLC radiotrace at t_R = 4.7 min (Figure A.1). Radiolabeling to produce [In(octapa)]$^-$ yields specific activities as high as 2.3 mCi/nmol (~5 mCi/μg, 2300 mCi/μmol) in 10 minutes at ambient temperature. DOTA was radiolabeled with the same activity of ^{111}In (~1 mCi) at the same ligand concentration (10^{-7} M) used to obtain the specific activity listed above for [In(octapa)]$^-$, and after 10 minutes at ambient temperature less than 40% ^{111}In was radiometallated. This demonstrates the ability of H_4octapa to radiolabel with ^{111}In quantitatively and rapidly in high specific activities at ambient temperature, which is in sharp contrast to the "gold standard" DOTA. The theoretical maximum ^{111}In specific activity has been calculated to be ~46 mCi/nmol, and specific activities as high as 22 mCi/nmol have been reported for ^{111}In-labeled DOTA-peptide conjugates under ideal conditions; however, temperatures of 100 °C for 30 minutes were required and specific activities that high are not typical with DOTA-conjugates.[124] To compare recently reported examples, a ^{111}In-CHX-A''-DTPA-Re(Arg11)CCMSH peptide conjugate yielded a specific activity of ~0.29 mCi/nmol,[231] DTPA-(gp100:154–162mod) (HLA-A.1 binding peptide conjugate) showed a maximum specific activity of ~0.35 mCi/nmol,[316] and a DOTA-RGD conjugate obtained a specific activity as high as ~0.050 mCi/nmol;[122] these are more typical values and are much lower than the ~2.3 mCi/nmol specific activity obtained for [In(octapa)]$^-$ during this study. It must be considered, however, that the examples listed above are for ligand-peptide conjugates, and the values obtained in this study were for non-conjugated [In(octapa)]$^-$. DOTA-biovector conjugates typically offer lower specific activities when compared to acyclic ligands such as DTPA and CHX-A''-DTPA.[231] The HPLC radiotrace of [In(decapa)]$^{2-}$ was less promising and revealed two peaks (t_R = 5.4 min (5%), 7.7 min (95%)), possibly due to multiple chemically distinct isomers being formed, with specific activities

being low at ~0.030 mCi/nmol. As previously discussed, DOTA required temperatures of 80 °C in a microwave reactor for ~20 minutes to optimally radiolabel with ^{111}In.

2.2.4 Thermodynamic stability

Formation/stability constants (log K_{ML}) are well-established measurements of thermodynamic stability for metal-ligand complexes and are typically reported in the literature; however, pM (-log[M^{n+}_{free}]) values are much more accurate figures for predicting *in vivo* thermodynamic stability under physiologically relevant conditions. Values of pM are calculated (at specific conditions, here pH 7.4, [M^{n+}] = 1 μM, [L^{x-}] = 10 μM) to take into account all of ligand basicity (ligand pK_a values), free metal concentration, ligand-to-metal ratios, pH, and metal hydroxide formation. The thermodynamic stability of [In(octapa)]$^-$ was determined by potentiometric titrations to be log K_{ML} = 26.8(1) (pM = 26.5), which is significantly higher than that for DOTA (log K_{ML} = 23.9(1), pM = 18.8) and similar to DTPA (log K_{ML} = 29.0, pM = 25.7), but possesses the highest pM value of all three In^{3+} complexes (Table 2.1). Although CHX-A''-DTPA has been evaluated with Lu^{3+}/Y^{3+} to be very stable,[238] it has not been thoroughly studied with In^{3+} and to our knowledge formation constants have not yet been reported for any metal ions. Despite [In(DOTA)]$^-$ being significantly more stable *in vivo* than is [In(DTPA)]$^{2-}$ [60,215,216,312] the log K_{ML} and pM values are much lower for DOTA than DTPA with In^{3+}. It is interesting to note that the trend of stability constants (log K_{ML}) and pM values in Table 2.1 do not correlate well with *in vivo* stability, which emphasizes that these thermodynamic parameters are not the only factors involved in determining biological stability. The kinetic parameters of ligand-metal on/off rates are the most important factor, and an example of this is observed by [In(DOTA)]$^-$

having one of the lowest pM values but very high stability/kinetic inertness *in vivo*, and with $In(oxine)_3$ having the highest log K_{ML} and pM values (log K_{ML} = 35.3, pM = 34.1) shown here, but dissociating very quickly *in vivo*.[311] These values reinforce the concept that *in vitro* competition experiments such as mouse serum and *apo*-transferrin assays, and *in vivo* biodistribution and stability studies are essential to evaluate the practical *in vivo* kinetic inertness and metabolism of radiometal complexes. Because the thermodynamic formation constants of the H_4octapa, H_5decapa, and H_2dedpa ligands with In^{3+} are all very similar, the large differences in pM values must be a result of ligand basicity. Despite these complications and the lack of predictive power of log K_{ML}/pM values for *in vivo* stability, it is encouraging that $[In(octapa)]^-$ has an exceptionally high pM value of 26.9, which is higher than the values determined previously for DOTA (18.8) and DTPA (25.7) with In^{3+}.[68,119,317]

Table 2.1 Formation constants (log K_{ML}) and pM[a] values for In^{3+} complexes.

Ligand	log K_{ML}	pM[a]
dedpa^{2-}	26.60(4)	25.9
octapa^{4-}	26.8(1)	26.5
decapa^{5-}	27.56(5)	23.1
Oxine (tris) [119]	35.4	34.1
DTPA [119,317]	29.0	25.7
DOTA [68,119]	23.9(1)	18.8
transferrin [318]	18.3	18.7

[a] Calculated for 10 μM total ligand and 1 μM total metal at pH 7.4 and 25 °C.

2.2.5 ^{111}In radiolabeling and stability studies

In consideration of the fact that *in vivo* kinetic inertness plays a crucial role in determining stability, competition experiments using native biological ligands such as those contained in blood serum (e.g. *apo*-transferrin, albumin) are useful *in vitro* assays for predicting the *in vivo* stability and kinetic inertness of radiometal ion complexes. During preliminary experiments, mouse serum stability assays were found to transchelate In^{3+} from ligands more aggressively than were *apo*-transferrin assays. These mouse serum competition experiments (incubated at ambient temperature) have demonstrated $[In(octapa)]^-$ to have marginally higher stability than $[In(DOTA)]^-$ and $[In(DTPA)]^{2-}$ after 24 hours, within error (92.3 ± 0.04%, 89.4 ± 2.2%, 88.3 ± 2.2%, respectively) (Table 2.2). $[In(decapa)]^{2-}$ also demonstrated exceptional stability against mouse serum transchelation with a stability of 89.1 ± 1.7% at 24 hours.

Table 2.2 Data from mouse serum stability challenges performed at ambient temperature (n=3), evaluated by PD-10 size-exclusion column elution, with stability shown as the percentage of intact ^{111}In complex.

Complex	1 hour stability	24 hour stability
$[^{111}In(dedpa)]^+$	96.1 ± 0.1%	19.7 ± 1.5%
$[^{111}In(octapa)]^-$	93.8 ± 3.6%	92.3 ± 0.04%
$[^{111}In(decapa)]^{2-}$	89.7 ± 1.6%	89.1 ± 1.7%
$[^{111}In(DOTA)]^-$	89.6 ± 2.1%	89.4 ± 2.2%
$[^{111}In(DTPA)]^{2-}$	86.5 ± 2.2%	88.3 ± 2.2%

To provide a more definitive answer to which of these ligands is most suitable for *in vivo* radiopharmaceutical applications, mouse biodistribution studies were performed with $[^{111}In(octapa)]^-$, $[^{111}In(DOTA)]^-$, and $[^{111}In(decapa)]^{2-}$. The data summarized in Figure 2.5

(y-axis adjusted to 2 %ID/g for visualization of 4 and 24 hour time points) show rapid clearance through the kidneys for $[^{111}In(octapa)]^-$ and $[^{111}In(DOTA)]^-$, with radioactivity clearing quickly from all organs. The clearance of $[^{111}In(decapa)]^{2-}$ was found to be slower, with ^{111}In levels slowly increasing over 24 hours in the liver, spleen, and bone (Table 2.3). These results are typical of a metal-ligand complex that shows instability *in vivo* and undergoes demetallation/transchelation, which is surprising because of the high degree of stability of $[^{111}In(decapa)]^{2-}$ in mouse serum competition experiments (Table 2.3). The most promising result from these animal experiments is that the radiometal complex $[^{111}In(octapa)]^-$ has exceptional *in vivo* stability over 24 hours, with improved clearance compared to $[^{111}In(DOTA)]^-$ (Figure 2.5), most notably from the kidneys (0.189 ± 0.019 %ID/g vs 0.664 ± 0.108 %ID/g, respectively), liver (0.0248 ± 0.0030 %ID/g vs 0.0605 ± 0.0022 %ID/g, respectively), and spleen (0.0202 ± 0.0083 %ID/g vs 0.0426 ± 0.0067 %ID/g, respectively) at 24 hours ($p < 0.05$).

These findings are significant because *in vivo* instability resulting in demetallation or transchelation via serum proteins typically results in high uptake of "free" $^{111}In^{3+}$ metal ion in the liver, spleen, bone, and kidneys (typical of transferrin-bound 3+ metals), with accumulation of radioactivity increasing over time.[93] Surprisingly, despite the exceptional mouse serum stability of $[In(decapa)]^{2-}$, the *in vivo* stability in mice was found to be sub-optimal, with slower clearance from the blood pool and most notably high persistent kidney uptake (3.68 ± 0.54 %ID/g) and increasing bone uptake (1.95 ± 0.12 %ID/g) after 24 hours; however, all other organs contained less than 1 %ID/g after 24 hours (Figure 2.5, Table 2.3). Although these values for H_5decapa are inadequate when compared to the *in vivo* stability and clearance of exceptionally stable ligands such as $[^{111}In(DOTA)]^-$ and $[In(octapa)]^-$, it is

still fair when compared to the very labile ^{111}In-citrate complex, which has shown values of 18.7 ± 3.7 %ID/g in the kidneys after 24 hours.[319]

Table 2.3 Decay corrected %ID/g values from the biodistribution of ^{111}In-complexes in healthy female ICR mice (6-8 weeks old), n = 4, bold = passed students T-test ($p < 0.05$).

Chelate	Organ	15 min	SD	1 hour	SD	4 hours	SD	24 hours	SD
$[^{111}In(DOTA)]^-$	SPLEEN	0.564	0.140	0.074	0.030	**0.054**	0.013	**0.043**	0.007
	KIDNEY	6.275	3.652	1.175	0.631	0.935	0.259	**0.664**	0.108
	INTESTINE	0.638	0.173	0.088	0.047	0.055	0.019	0.047	0.008
	LIVER	0.518	0.172	0.093	0.033	0.064	0.025	**0.061**	0.002
	HEART	0.967	0.228	0.077	0.042	**0.034**	0.005	0.017	0.004
	LUNG	2.218	0.776	0.134	0.095	0.053	0.007	0.018	0.009
	BRAIN	0.090	0.013	0.015	0.010	**0.010**	0.001	0.001	0.0005
	MUSCLE	0.527	0.152	0.040	0.025	0.028	0.005	0.010	0.004
	FEMUR	0.826	0.119	0.095	0.063	0.077	0.023	0.044	0.011
	BLOOD	2.768	0.536	0.177	0.116	0.038	0.008	0.008	0.002
	URINE	306.197	120.471	523.638	542.402	3.726	3.643	0.131	0.069
$[^{111}In(octapa)]^-$	SPLEEN	0.462	0.113	0.072	0.024	**0.072**	0.004	**0.020**	0.008
	KIDNEY	5.738	1.027	1.327	0.907	0.654	0.078	**0.189**	0.019
	INTESTINE	0.619	0.085	0.109	0.080	0.064	0.020	0.041	0.007
	LIVER	0.811	0.235	0.182	0.051	0.053	0.009	**0.025**	0.003
	HEART	0.775	0.259	0.066	0.033	**0.045**	0.006	0.014	0.002
	LUNG	2.003	0.175	0.111	0.088	0.047	0.003	0.014	0.007
	BRAIN	0.073	0.008	0.019	0.004	**0.014**	0.001	0.003	0.002
	MUSCLE	0.435	0.248	0.028	0.019	0.034	0.003	0.007	0.002
	FEMUR	0.785	0.154	0.079	0.035	0.064	0.009	0.047	0.012
	BLOOD	2.422	0.523	0.132	0.068	0.035	0.005	0.010	0.002
	URINE	506.246	146.573	229.086	200.871	5.961	5.761	0.124	0.045
$[^{111}In(decapa)]^{2-}$	SPLEEN	0.567	0.049	0.455	0.170	0.525	0.187	0.661	0.085
	KIDNEY	10.380	2.095	10.210	2.835	7.554	0.928	3.681	0.539
	INTESTINE	0.843	0.107	0.513	0.172	0.541	0.136	0.647	0.113
	LIVER	0.790	0.040	0.457	0.255	0.838	0.149	0.934	0.175
	HEART	1.123	0.170	0.671	0.272	0.691	0.188	0.376	0.093
	LUNG	2.375	0.082	1.146	0.691	1.347	0.373	0.566	0.117
	BRAIN	0.071	0.007	0.055	0.033	0.065	0.014	0.036	0.004
	MUSCLE	0.692	0.126	0.378	0.203	0.396	0.070	0.256	0.045
	FEMUR	1.453	0.124	1.410	0.790	1.772	0.193	1.950	0.121
	BLOOD	2.456	0.980	2.207	0.795	1.999	0.463	0.518	0.115
	URINE	318.209	91.598	53.949	13.363	60.685	66.949	0.666	0.513

Often $^{111}InCl_3$ and ^{111}In-citrate are used to emulate the conditions of an unstable ligand that would undergo complete and rapid decomposition/transchelation *in vivo*. One commonly cited study (Ando *et al.*) has shown $^{111}InCl_3$ to have higher liver, spleen, and kidney uptake than ^{111}In-citrate;[93] however, another study has shown the kidney uptake of $^{111}InCl_3$ at 24 hours in healthy rats to be 2.58 ± 0.83 %ID/g,[320] which is significantly less than the value for ^{111}In-citrate (cited above) of 18.7 ± 3.7 %ID/g,[319] and contradicts the observations from Ando *et al.*[93]

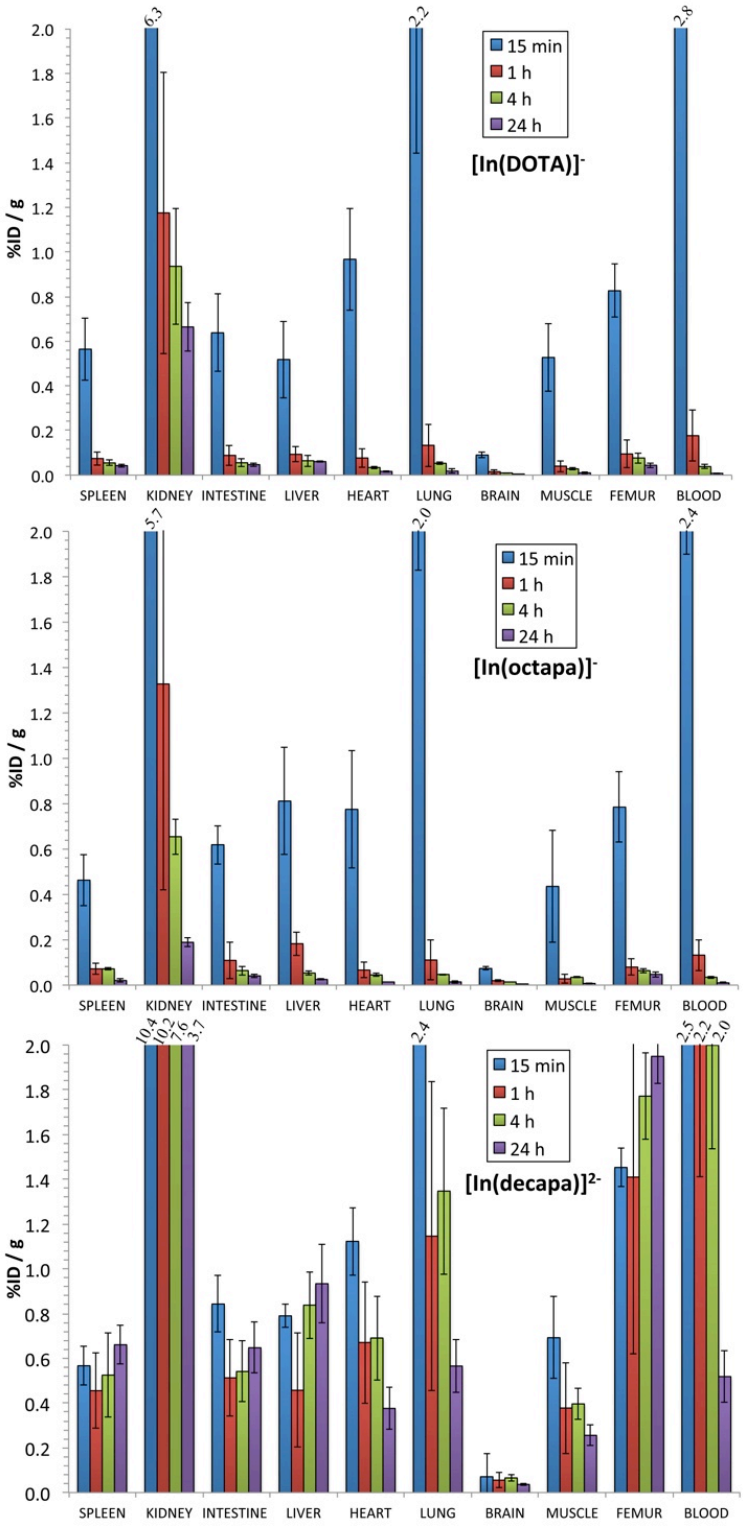

Figure 2.5 Biodistribution %ID/g values for $[^{111}In(DOTA)]^-$, $[^{111}In(octapa)]^-$, and $[^{111}In(decapa)]^{2-}$, with error bars plotted as standard deviations (note the y-axis set to 2.0 %ID/g, for clarity of the low activity 4 and 24 hour time points).

Additionally, the highly anionic ^{111}In-citrate clears much more quickly through the kidneys than $^{111}InCl_3$, demonstrating that the hypothesis of rapid and complete dissociation upon introduction of these radiometal species into an animal is not accurate.[93] Considering these inconsistencies, it is important to utilize internal standards (such as $[^{111}In(DOTA)]^-$ in this study), and additionally there is a need for more clear and reliable baseline data for the biodistribution of ^{111}In in its most commonly used forms.[93,321,322]

In biological systems, transchelated indium(III) is nearly all bound to transferrin, with a maximum stability constant of log K_{ML} = 18.3.[318] Demetallation and hydroxide formation is a significant concern for acidic metal ions such as Ga^{3+} and In^{3+}, and a conditional stability constant for transferrin that takes hydrolysis into account has been calculated as being ~10.0 for In^{3+}, which is higher even than Ga^{3+} at 6.9 and close to Fe^{3+} at 11.4.[318] This demonstrates the strong competition that transferrin holds for In^{3+} *in vivo*; however, the ligand exchange kinetics of In^{3+} are quite slow and it forms a more inert complex with transferrin than do Ga^{3+} and Fe^{3+}.[79,318] It is most likely that due to the high stability and inertness of complexes such as $[In(DOTA)]^-$, and the slow exchange kinetics with transferrin, only gradual *in vivo* decomplexation is observed over long periods such as > 24 hours. The higher levels of ^{111}In in the kidneys, liver, and spleen observed for $[In(DOTA)]^-$ after 24 hours is most likely a result of this gradual exchange process, and the improved inertness and clearance observed for $[^{111}In(octapa)]^-$ correlates well with its lower isomerization and higher pM value of 26.8(1) ($[In(DOTA)]^-$ pM = 18.8) (Table 2.1), and suggests superior kinetic inertness. Additionally, the lower levels of ^{111}In in the kidneys at 24 hours seen for $[In(octapa)]^-$, being roughly a third of that for $[In(DOTA)]^-$, are very promising because persistent kidney uptake is observed with many peptide conjugates of DOTA, CHX-A''-DTPA, and especially

DTPA.[60,213,215,216,231,305,312] High residual activity in the kidneys can decrease image quality, obstruct the delineation of tumours for surrounding tissue, decrease the accuracy of dosimetry, and deliver harmful doses of radiation to the healthy and non-targeted kidneys when used with therapeutic isotopes such as ^{90}Y and ^{177}Lu.

2.3 Conclusions

Preliminary investigations of the octadentate acyclic ligand H_4octapa (N_4O_4) with $^{111}In/In^{3+}$ have demonstrated it to be a significant improvement on the shortcomings of the current industry gold standards DOTA (N_4O_4) and DTPA (N_3O_5). Four major points were identified in the discussion as guidelines to be used in selecting an ideal chelating agent for radiometal ions, and $[In(octapa)]^-$ has been shown to be superior to $[In(DOTA)]^-$ and $[In(DTPA)]^{2-}$ for a majority of these points. We have demonstrated the ability of H_4octapa to quantitatively radiolabel with ^{111}In at ambient temperature, which, in contrast to DOTA, allows it to be effectively used with sensitive biovectors such as antibodies. H_4octapa has been radiolabeled with ^{111}In in 10 minutes at ambient temperature with specific activities as high as 2.3 mCi/nmol (97.5% radiochemical yield). *In vitro* mouse serum stability assays have demonstrated H_4octapa to have slightly improved stability with ^{111}In compared to DOTA and DTPA over 24 hours, within error. Mouse biodistribution studies have shown that the radiometal complex $[^{111}In(octapa)]^-$ has exceptionally high *in vivo* stability and kinetic inertness, and compared to $[^{111}In(DOTA)]^-$, $[^{111}In(octapa)]^-$ has improved stability and improved clearance from the kidneys, liver, and spleen at 24 hours. $^1H/^{13}C$ NMR studies of the $[In(octapa)]^-$ complex have revealed a 7-coordinate solution structure, which forms a single isomer and exhibits no observable fluxional behavior at ambient temperature on the

NMR timescale and is an improvement on the multiple static isomers observed for $[In(DTPA)]^{2-}$ and the fluxional isomerization of $[In(DOTA)]^{-}$.[49,63,97] Potentiometric titrations have determined the thermodynamic formation constant of the $[In(octapa)]^{-}$ complex to be log K_{ML} = 26.8(1) (pM = 26.5), which reveals a higher pM value than those determined for $[In(DOTA)]^{-}$ and $[In(DTPA)]^{2-}$ (18.8 and 25.7, respectively). The same set of experiments and analyses was performed with the potentially decadentate ligand H_5decapa (N_5O_5) and its $[In(decapa)]^{2-}$ complex; however, the formation of multiple isomers observed via radio-HPLC and NMR studies was not optimal, and unfavorable organ uptake and clearance were observed in biodistribution studies performed in mice. These results for H_5decapa suggest that it is not a suitable candidate for ^{111}In radiopharmaceutical elaboration; however, it may be a suitable candidate for coordinating lanthanide and actinide radiometal ions that can accommodate higher denticities, such as ^{90}Y, ^{177}Lu, and ^{225}Ac. The relatively simple 5-step synthesis of H_4octapa is achieved with a cumulative yield of ~12%, and the 5-step synthesis of H_5decapa was completed with a cumulative yield of ~2.5%. Optimization of reaction conditions and/or exploration of alternative protecting groups may improve these yields.

Our initial investigations have revealed the acyclic ligand H_4octapa to be a valuable alternative to the macrocycle DOTA and the acyclic ligand DTPA by showing improved stability and kinetic inertness, as well as fast ambient temperature radiolabeling kinetics. Pending the results of investigations with ^{90}Y and ^{177}Lu, H_4octapa could present a very strong alternative to DOTA as an ideal ligand for incorporation into radiometal-based radiopharmaceuticals. The next step in the evaluation and study of the ligand H_4octapa will be the synthesis of a bifunctional derivative that can be conjugated to targeting vectors, such as peptides and antibodies (Chapter 3). The major shortcoming of *in vivo* experiments with

"bare" and non-bifunctional ligands such as those described in this chapter, is that the highly hydrophilic and charged radiometal complexes are very quickly excreted. This means that the residency time in blood and tissue is very small, and the time period over which stability can be evaluated is very short (a few hours). Conjugating a bifunctional derivative of H_4octapa to a large biovector such as an antibody will increase the biological half-life from a few hours to a few weeks, allowing for longer experiments to be carried out under conditions that are more realistic for imaging and therapy applications *in vivo*.

2.4 Experimental methods

2.4.1 Materials and methods

All solvents and reagents were purchased from commercial suppliers (TCI America, Sigma Aldrich, Fisher Scientific) and were used as received. Mouse serum was purchased frozen from Sigma Aldrich. DOTA was purchased from Macrocyclics. The acyclic ligand H_2dedpa was synthesized according to the literature.[118,271] The analytical thin-layer chromatography (TLC) plates used were aluminum-backed ultrapure silica gel 60 Å, 250 μm thickness; the flash column silica gel (standard grade, 60 Å, 32–63 mm) was provided by Silicycle. ^{1}H and ^{13}C NMR spectra were recorded at ambient temperature on Bruker AV300, AV400, or AV600 instruments; the NMR spectra are expressed on the δ scale and were referenced to residual solvent peaks and/or internal tetramethylsilane. ^{13}C NMR experiments run in D_2O were externally referenced to a sample of CH_3OD/D_2O. Low-resolution mass spectrometry was performed using a Waters ZG spectrometer with an ESCI electrospray/chemical-ionization source, and high-resolution electrospray-ionization mass spectrometry (ESI-MS) was performed on a Micromass LCT time-of-flight instrument at the

Department of Chemistry, University of British Columbia. Microanalysis for C, H, and N was performed by UBC MS staff on a Carlo Erba Elemental Analyzer EA 1108. IR spectra were collected neat in the solid state on a Thermo Nicolet 6700 FT-IR spectrometer. ^{111}In(chelate) mouse serum stability experiments were analyzed using GE Healthcare Life Sciences PD-10 desalting columns (size exclusion for MW < 5000 Da) and counted with a Capintec CRC 15R well counter. Radiolabeling of DOTA with ^{111}In was performed using a Biotage® Initiator microwave reactor (μW). The HPLC system used for analysis and purification of cold compounds consisted of a Waters 600 controller, Waters 2487 dual wavelength absorbance detector, and a Waters delta 600 pump. Phenomenex synergi hydro-RP 80 Å columns (250 x 4.6 mm analytical and 250 x 21.2 mm semi-preparative) were used for purification of several of the deprotected ligands. Analysis of radiolabeled complexes was carried out using a Waters xbridge BEH130 C18 reverse phase (150 x 6 mm) analytical column using a Waters Alliance HT 2795 separation module equipped with a Raytest Gabi Star NaI (Tl) detector and a Waters 996 photodiode array (PDA) detector. $^{111}InCl_3$ was cyclotron produced and provided by Nordion as a ~0.05 M HCl solution.

2.4.2 Methyl 6-(hydroxymethyl)picolinate (2.1)

Compound **2.1** was synthesized according to a modified literature protocol.[323] A suspension of dimethylpyridine-2,6-dicarboxylate (10.0 g, 51.2 mmol) in methanol (400 mL) in a round bottom flask (1000 mL) was cooled in a salted ice bath. Sodium borohydride (5.56 g, 146.9 mmol, 2.4 eq.) was then added slowly over a period of 1 hour, where the reaction mixture turned pink upon the addition of sodium borohydride. The reaction mixture was stirred and kept on ice for 4 hours. After 4 hours, TLC analysis revealed that the

reaction mixture contained starting material (*Rf* : 0.45, TLC in 100% EtOAc), product (*Rf* : 0.33), and doubly-reduced product (*Rf* : 0.24). The reaction mixture was quenched regardless of the remaining starting material in order to prevent over-reduction. The solution was diluted using dichloromethane (200 mL) and then quenched using saturated $NaHCO_3$ (~200 mL). The aqueous and organic layers were separated, and much of the methanol from the aqueous phase was evaporated *in vacuo*. The aqueous layer was then extracted with chloroform (2 x 100 mL) and ethyl acetate (3 x 100 mL). The combined organic layers were dried ($MgSO_4$), filtered, and concentrated *in vacuo* to dryness. The resulting white solid was purified by column chromatography (column 10"L x 2"W; eluted with a gradient of 3:1 ethyl acetate/petroleum ether to 100% ethyl acetate) to afford the product as a white solid (4.35 g, 51%, *Rf*: 0.33 in 100% EtOAc). ^{1}H NMR (300 MHz, $CDCl_3$): δ = 7.95 (d, 1H, pyr-*H*), 7.79 (t, 1H, pyr-*H*), 7.55 (d, 1H, pyr-*H*), 4.83 (s, 2H, methylene-*H*), 4.31 (s, 1H, -O*H*), 3.92 (s, 3H, methyl-*H*). ^{13}C NMR (75 MHz, $CDCl_3$): 165.4, 160.6, 146.7, 137.6, 123.9, 123.5, 64.6, 52.7. HR-ESI-MS calcd. for $[C_8H_9NO_3 + H]^+$: 168.0661; found $[M + H]^+$ 168.0658.

2.4.3 Methyl 6-(bromomethyl)picolinate (2.2)

Compound **2.2** was synthesized according to a modified literature protocol.[323] To a solution of **2.1** (4.00 g, 23.9 mmol) in chloroform (100 mL) under argon at 0 °C, phosphorus tribromide (2.50 mL, 26.3 mmol, 1.1 eq.) in chloroform (10 mL) was added dropwise over 15 minutes via dropping funnel. A white precipitate formed, and then the solution turned bright yellow. The dropping funnel was rinsed using chloroform (15 mL) and the reaction mixture was stirred at 0 °C and monitored by TLC. A mini-workup using sodium carbonate

in water and ethyl acetate was required to see reaction progress by TLC. At 3.5 hours TLC indicated the quantitative conversion of alcohol to alkyl halide. The reaction mixture was quenched using sodium carbonate in water (75 mL) and was extracted with chloroform (4 x 25 mL). The combined organic layers were dried over $MgSO_4$, filtered, and concentrated *in vacuo* to dryness to afford an off-white solid. The crude product was purified through a short silica plug (2"L x 2"W, 25% EtOAc in petroleum ether) to afford **2.2** as an off-white solid (5.55 g, >99%, *Rf* : 0.64 in 30% petroleum ether in EtOAc). ^{1}H NMR (400 MHz, $CDCl_3$) δ: 8.01 (d, 1H, pyr-*H*), 7.84 (t, 1H, pyr-*H*), 7.65 (d, 1H, pyr-*H*), 4.61 (s, 2H, methylene-*H*), 3.96 (s, 3H, methyl-*H*). ^{13}C NMR (100 MHz, $CDCl_3$) δ: 165.1, 157.2, 147.3, 138.1, 127.0, 124.3, 53.9, 32.9. HR-ESI-MS calcd. for $[C_8H_8NO_2{}^{79}Br + H]^+$: 229.9817; found $[M + H]^+$: 229.9812.

2.4.4 *N,N'*-(Benzyl)ethylenediamine (2.3)

To a solution of ethylenediamine (2.78 mL, 41.6 mmol) in dry methanol (distilled over CaH_2, 100 mL) was added benzaldehyde (8.48 mL, 83.2 mmol, 2 eq.). The solution was heated to reflux for 4 hours and then cooled via ice bath. Addition of $NaBH_4$ (6.77 g, 179 mmol, 4.3 eq.) was performed slowly and in small portions to prevent boiling, and the reaction mixture was stirred for 4 hours until completion. The solvent was evaporated *in vacuo* and then saturated $NaHCO_3$ (~50 mL), water (~50 mL), and chloroform (200 mL) were added. The aqueous layer was extracted twice more with chloroform (100 mL). The combined organic layers were dried over $MgSO_4$, filtered, and concentrated *in vacuo* to afford a waxy yellow solid. Product was purified by silica column chromatography (column 10"L x 2"W; eluted with a gradient of 100% dichloromethane to 25% CH_3OH in

dichloromethane) to afford **2.3** as yellow oil (4.90 g, 49%, *Rf* : 0.33 in 20% CH_3OH in dichloromethane). ^1H NMR (400 MHz, $CDCl_3$) δ: 7.42 (d, 8H, Bn-*H*), 7.34 (m, 2H, Bn-*H*), 3.86 (s, 4H, Bn-C*H*$_2$-N), 2.83 (s, 4H, ethylene-*H*), 1.72 (s, 2H, amine-*H*). ^{13}C NMR (100 MHz, $CDCl_3$) δ: 140.2, 127.9, 127.7, 126.4, 53.5, 48.4. HR-ESI-MS calcd. for $[C_{16}H_{20}N_2 + H]^+$: 241.1705; found $[M + H]^+$: 241.1703.

2.4.5 *N,N'*-[Benzyl(*tert*-butoxycarbonyl)methyl]aminoethane (2.4)

To a solution of **2.3** (1.0 g, 4.2 mmol) and sodium carbonate (1.76 g, 16.6 mmol, 3.9 eq.) in dry acetonitrile (distilled over CaH_2, 80 mL) was added dropwise a solution of *tert*-butyl bromoacetate (1.31 mL, 8.88 mmol, 2.1 eq.). The reaction mixture was stirred at 60 °C for 16 hours. TLC (5% CH_3OH in dichloromethane) showed quantitative conversion of **2.3** to the tertiary diamine. Sodium carbonate was removed by suction filtration, and the filtrate was concentrated *in vacuo* to dryness. The resulting yellow oil was purified by column chromatography (column 2"L x 2"W; eluted with a gradient of 100% petroleum ether to 10% ethyl acetate in petroleum ether) to afford **2.4** as a yellow solid (1.85 g, 93%, *Rf* : 0.59 in 5% CH_3OH in dichloromethane). ^1H NMR (400 MHz, $CDCl_3$) δ: 7.40-7.29 (m, 10H, Bn-*H*), 3.85 (s, 4H, Bn-C*H*$_2$-N), 3.30 (s, 4H, $(CH_3)_3CO$-C(O)-C*H*$_2$-N), 2.88 (s, 4H, ethylene-*H*), 1.52 (s, 18H, $(CH_3)_3CO$-C(O)-CH_2-N). ^{13}C NMR (100 MHz, $CDCl_3$) δ: 170.8, 139.1, 128.8, 128.1, 126.8, 80.5, 58.3, 55.0, 51.6, 28.1. HR-ESI-MS calcd. for $[C_{28}H_{40}N_2O_4 + H]^+$: 469.3066; found $[M + H]^+$: 469.3055.

2.4.6 *N,N'*-[(*tert*-Butoxycarbonyl)methyl]aminoethane (2.5)

To a solution of **2.4** (776.3 mg, 1.656 mmol) in glacial acetic acid (7 mL) was added Pd/C (78 mg, ~10 wt%). Hydrogen gas was bubbled through the solution for 3 minutes and then the reaction mixture was stirred under a sealed hydrogen atmosphere (balloon) for 16 hours. The Pd/C was removed by filtration over Celite, rinsing well with methanol, and the filtrate was evaporated to dryness *in vacuo*. The crude product was purified by silica gel column chromatography (eluted with a gradient of 100% dichloromethane to 5% methanol in dichloromethane) and identified by TLC using an I_2 chamber to stain. Product fractions were combined and concentrated *in vacuo* to afford the product **2.5** as a waxy yellow solid (0.51 g, 87%, *Rf* : 0.20 in 10% CH_3OH in dichloromethane). ^{1}H NMR (300 MHz, $CDCl_3$) δ: 3.37 (s, 4H, $(CH_3)_3CO$-C(O)-C*H*$_2$-N), 2.68 (s, 4H, ethylene-*H*), 2.03 (s, 2H, -N*H*-), and 1.43 (s, 18H, $(CH_3)_3$CO-C(O)-CH_2-N). ^{13}C NMR (75 MHz, $CDCl_3$) δ: 171.7, 80.9, 51.4, 48.7, 28.0. HR-ESI-MS calcd. for $[C_{14}H_{28}N_2O_4 + H]^+$: 289.2127; found $[M + H]^+$: 289.2126.

2.4.7 *N,N'*-[[(*tert*-Butoxycarbonyl)methyl]-*N,N'*-[6-(methoxycarbonyl)pyridin-2-yl]methylamino]ethane (2.6)

To a solution of **2.5** (431.5 mg, 1.496 mmol) and **2.2** (725 mg, 3.142 mmol, 2.1 eq.) in dry acetonitrile (distilled over CaH_2, 20 mL) was added sodium carbonate (~300 mg). The solution was heated for 16 hours at 60 °C under argon. Sodium carbonate was removed by filtration and rinsed with acetonitrile. The filtrate was concentrated *in vacuo* to dryness and the resulting yellow oil was purified by column chromatography (eluted with a gradient of 100% dichloromethane to 5% methanol in dichloromethane) to afford **2.6** as colorless oil (342 mg, 39%, *Rf* : 0.40 in 10% CH_3OH in dichloromethane). ^{1}H NMR (300 MHz, CDCl3)

δ: 7.85-7.82 (m, 2H, pyr-H), 7.65-7.63 (m, 4H, pyr-H), 3.85 (s, 4H, Pyr-CH_2-), 3.83 (s, 6H, -O-CH_3), 3.16 (s, 4H, $(CH_3)_3$CO-CO-C*H*$_2$-N), 2.67 (s, 4H, ethylene-H), 1.28 (s, 18H, (C*H*$_3$)$_3$CO-C(O)-CH_2-N). ^{13}C NMR (75 MHz, $CDCl_3$) δ: 170.1, 165.4, 160.3, 146.7, 137.1, 125.8, 123.2, 80.6, 60.2, 55.9, 52.4, 52.1, 27.7. HR-ESI-MS calcd. for $[C_{30}H_{42}N_4O_8 + H]^+$: 587.3081; found $[M + H]^+$: 587.3091.

2.4.8 H$_4$octapa•4HCl•2H$_2$O, *N,N′*-bis(6-carboxy-2-pyridylmethyl)ethylenediamine-*N,N′*diacetic acid

A portion of **2.6** (277.4 mg, 0.4728 mmol) was dissolved in HCl (6 M) and heated to reflux for 8 hours. White solid was observed to precipitate from hot HCl (aq) below ~60 °C. The solution was then cooled in the freezer for 1 hour. The product was filtered and washed with cold ethanol and diethyl ether to afford the HCl salt H$_4$octapa as a white solid (265 mg, 75% yield using the molecular weight of the HCl salt from elemental analysis). ^{1}H NMR (300 MHz, D_2O) δ: 8.12-8.02 (m, 4H, pyr-*H*), 7.72-7.69 (d, 2H, pyr-*H*), 4.53 (s, 4H, Pyr-C*H*$_2$-N), 3.97 (s, 4H, HOOC-C*H*$_2$-N), 3.57 (s, 4H, ethylene-*H*). ^{13}C NMR (75 MHz, D_2O) δ: 170.6, 165.6, 151.4, 145.4, 142.9, 128.8, 126.3, 58.1, 55.2, 51.5. IR (neat, ATR-IR): ν = 1720.9 cm^{-1} (C=O), 1635.9/1618.2 cm^{-1} (C=C py). HR-ESI-MS calcd. for $[C_{20}H_{20}N_4O_8 + H]^+$: 445.1359; found $[M + H]^+$: 445.1368. Elemental analysis: calcd % for H$_4$octapa•4HCl•2H$_2$O ($C_{20}H_{20}N_4O_8$•4HCl•2H$_2$O = 628.283): C 38.23, H 4.81, N 8.92; found: C 38.34, H 4.81, N 8.93.

2.4.9 Na[In(octapa)]

A portion of H_4octapa•4HCl•$2H_2O$ (9.9 mg, 0.019 mmol) and $In(ClO_4)_3$•$8H_2O$ (11.7 mg, 0.021 mmol, 1.1 eq.) were dissolved in HCl (aq) (1 mL, 0.1 M) in a 1 dram screw cap vial. The pH was adjusted to ~4.5 with NaOH (aq) (0.1 M) while stirring. The reaction mixture was stirred at 60 °C for 4 h, then evaporated to dryness to afford Na[In(octapa)] as a white solid. ^{1}H NMR (600 MHz, D_2O) δ: 8.34-8.32 (m, 2H, pyr-*H*), 8.23 (d, 2H, pyr-*H*), 7.85 (d, 2H, Pyr-*H*), 4.49 (d, 2H, Pyr-C*H*$_2$-N, ^{2}J = 16.1 Hz), 4.34 (d, 2H, Pyr-C*H*$_2$-N, ^{2}J = 16.1 Hz), 3.27 (d, 2H, HOOC-C*H*$_2$-N, ^{2}J = 19.3 Hz), 3.19-3.18 (broad d, 2H, HOOC-C*H*$_2$-N, ^{2}J = 8.4 Hz), 3.07-3.04 (m, 4H, ethylene-*H*). ^{13}C NMR (150 MHz, D_2O) δ: 177.2, 167.8, 153.7, 148.2, 144.2, 128.3, 124.6, 59.4, 58.3, 55.2. HR-ESI-MS calcd. for $[C_{20}H_{18}{}^{115}InN_4O_8$ + 2•Na]$^+$: 602.9959; found [M + 2•Na]$^+$: 602.9942.

2.4.10 *N,N''*-[Benzyl]diethylenetriamine (2.7)

To a solution of diethylenetriamine (5 mL, 46.2 mmol) in dry methanol (distilled over CaH_2, 100 mL) was added benzaldehyde (9.43 mL, 96.56 mmol, 2 eq.). The solution was heated to reflux for 4 hours, and then cooled (0 °C) via ice bath. Addition of $NaBH_4$ (12.26 g, 323 mmol, 7 eq.) was performed slowly and in small portions to prevent solvent boiling. The reaction solution was stirred for 4 hours until completion. The solvent was evaporated *in vacuo* and then saturated $NaHCO_3$ (~100 mL) and chloroform (200 mL) were added. The aqueous layer was extracted twice more with dichloromethane (100 mL). The combined organic layers were dried over $MgSO_4$, filtered, and concentrated *in vacuo* to afford a yellow solid. The crude product was purified by silica gel column chromatography (column 16"L x 3"W; eluted with a gradient of 2 to 10% CH_3OH and 2% triethylamine in

dichloromethane) to afford **2.7** as yellow oil (5.23 g, 40%, *Rf* : 0.30 in 20% CH_3OH in dichloromethane). ^1H NMR (300 MHz, $CDCl_3$) δ: 7.34-7.26 (m, 10H, Bn-*H*), 3.80 (s, 4H, Bn-C*H*$_2$-N), 2.75 (s, 8H, ethylene-*H*), 1.94 (s, 3H, -N*H*-). ^{13}C NMR (75 MHz, $CDCl_3$) δ: 140.5, 128.6, 128.3, 127.1, 54.1, 49.4, 48.9. HR-ESI-MS calcd. for $[C_{18}H_{25}N_3 + H]^+$: 284.2127; found $[M + H]^+$: 284.2124.

2.4.11 *N,N''*-[[Benzyl]-*N,N',N''*-[(*tert*-butoxycarbonyl)methyl]]diethylenetriamine (2.8)

To a solution of **2.7** (673.3 mg, 2.37 mmol) and sodium carbonate (excess, 450 mg) in dry acetonitrile (distilled over CaH_2, 20 mL) was added dropwise *tert*-butyl bromoacetate (1.071 mL, 7.25 mmol, 3.05 eq.) under argon. The solution was stirred at 60 °C for 20 hours. Sodium carbonate was removed by suction filtration and the filtrate was concentrated *in vacuo* to dryness. The resulting yellow oil was purified by column chromatography (column 10"L x 2"W; eluted with a gradient of 1 CH_3OH to 10% CH_3OH in dichloromethane) to afford **2.8** as light yellow oil (974.4 mg, 66%, *Rf* : 0.36 in 10% CH_3OH in dichloromethane). ^1H NMR (400 MHz, $CDCl_3$) δ: 7.41-7.29 (m, 10H, Bn-*H*), 3.86 (s, 4H, Bn-C*H*$_2$-N), 3.39 (s, 2H, $(CH_3)_3$CO-CO-C*H*$_2$-N'), 3.31 (s, 4H, $(CH_3)_3$CO-CO-C*H*$_2$-N/N''), 2.84 (s, 8H, ethylene-*H*), 1.54 (s, 18H, $(CH_3)_3$CO-CO-CH_2-N/N''), 1.50 (s, 9H, $(CH_3)_3$CO-CO-CH_2-N'). ^{13}C NMR (100 MHz, $CDCl_3$) δ: 170.8, 170.7, 139.0, 128.8, 128.0, 126.8, 80.4, 80.4, 58.2, 55.9, 55.0, 52.4, 51.9, 28.1, 28.0. HR-ESI-MS calcd. for $[C_{36}H_{55}N_3O_6 + H]^+$: 626.4169; found $[M + H]^+$: 626.4166.

2.4.12 *N,N',N''*-[[*tert*-Butoxycarbonyl]methyl]diethylenetriamine (2.9)

To a solution of **2.8** (702.6 mg, 1.12 mmol) in glacial acetic acid (10 mL) was added Pd/C (35 mg, ~5 wt%). Hydrogen gas was bubbled through the solution for 3 minutes and then the reaction mixture was stirred under a sealed hydrogen atmosphere (balloon) for 16 hours. The Pd/C was filtered over celite, rinsing with methanol, and then the filtrate was evaporated to dryness *in vacuo*. The crude product was purified by silica gel column chromatography (0 to 10% methanol in dichloromethane) and identified by TLC using an I_2/silica chamber to stain. Product fractions were combined and concentrated *in vacuo* to dryness to afford the product **2.9** as colorless oil (150 mg, 30%, *Rf* : 0.26 in 2.5% CH_3OH and 2.5% triethylamine in dichloromethane). Cleavage of the ethylene bridges was observed during hydrogenation and produced large amounts of byproduct. ^{1}H NMR (300 MHz, $CDCl_3$) δ: 3.28 (s, 2H, $(CH_3)_3CO$-CO-C*H*$_2$-N'), 3.25 (s, 4H, $(CH_3)_3CO$-CO-C*H*$_2$-N/N''), 2.77-2.73 (m, 4H, ethylene-*H*), 2.62-2.59 (m, 4H, ethylene-*H*), 2.14 (s, 2H, -N*H*-), 1.40 (s, 18H, $(CH_3)_3CO$-CO-CH_2-N/N''), 1.39 (s, 9H, $(CH_3)_3CO$-CO-CH_2-N'). ^{13}C NMR (75 MHz, $CDCl_3$) δ: 170.4, 170.8, 80.7, 80.7, 55.5, 54.0, 51.5, 47.2, 28.0, 27.9. HR-ESI-MS calcd. for $[C_{22}H_{43}N_3O_6 + H]^+$: 446.3230; found $[M + H]^+$: 446.3239.

2.4.13 *N,N''*-[[6-(Methoxycarbonyl)pyridin-2-yl]methylamino]-*N,N',N''*-[(*tert*-butoxycarbonyl)methyl]]diethylenetriamine (2.10)

To a solution of **2.9** (101.8 mg, 0.228 mmol) and **2.2** (110.4 mg, 0.479 mmol, 2.1 eq.) in dry acetonitrile (distilled over CaH_2, 10 mL) was added sodium carbonate (~100 mg). The solution was heated for 16 hours at 60 °C under argon. Sodium carbonate was removed by filtration and rinsed with acetonitrile. The filtrate was concentrated *in vacuo* to dryness

and the resulting yellow oil was purified by column chromatography (100% dichloromethane to 5% CH_3OH in dichloromethane) to afford **2.10** as colorless oil (75.7 mg, 45%, *Rf* : 0.27 in 2.5% CH_3OH and 2.5% triethylamine in dichloromethane). ^{1}H NMR (300 MHz, $CDCl_3$) δ: 7.96-7.94 (m, 2H, Pyr-*H*), 7.82-7.70 (m, 4H, Pyr-*H*), 3.97 (s, 4H, Pyr-C*H*$_2$-N), 3.96 (s, 6H, -O-C*H*$_3$), 3.28 (s, 4H, $(CH_3)_3$CO-CO-C*H*$_2$-N/N''), 3.23 (s, 2H, $(CH_3)_3$CO-CO-C*H*$_2$-N'), 2.72 (s, 8H, ethylene-*H*), 1.41 (s, 18H, (C*H*$_3$)$_3$CO-CO-CH_2-N/N''), 1.37 (s, 9H, (C*H*$_3$)$_3$CO-CO-CH_2-N'). ^{13}C NMR (75 MHz, $CDCl_3$) δ: 170.6, 170.4, 170.4, 165.8, 160.9, 147.0, 137.3, 126.0, 123.4, 80.9, 80.8, 80.6, 60.5, 56.3, 56.3, 55.8, 52.7, 56.7, 55.7, 52.7, 52.7, 52.6, 52.4, 28.1. HR-ESI-MS calcd. for $[C_{38}H_{57}N_5O_{10} + H]^+$: 744.4184; found $[M + H]^+$: 744.4199.

2.4.14 H_5decapa•5HCl•2.5H_2O, *N,N′,N′′*-[(triacetic acid]-*N,N′′*-[6-(carboxy)pyridin-2-yl]methylamino]diethylenetriamine

A portion of **2.10** (76.7 mg, 0.1031 mmol) was dissolved in HCl (6 M) and heated to reflux for 8 hours. The reaction mixture was concentrated *in vacuo* to an off-white powder, which was then purified by reverse-phase HPLC (gradient: A: 0.1% TFA (trifluoroacetic acid), B: CH_3CN. 0 to 100% B linear gradient 25 min. t_R = broad, 13.2-15 min). The HPLC fractions were combined, 2 mL of HCl (6 M) was added, and the solvent was removed *in vacuo* to drive off residual trifluoroacetic acid. Another 2 mL of HCl (6 M) was added, then concentrated *in vacuo* to afford the HCl salt of H_5decapa as a white solid (56 mg, 71% using molecular weight from elemental analysis). ^{1}H NMR (400 MHz, D_2O) δ: 8.11-8.04 (m, 4H, Pyr-*H*), 7.72-7.71 (m, 2H, Pyr-*H*), 4.55 (s, 4H, Pyr-C*H*$_2$-N), 3.98 (s, 4H, HOOC-C*H*$_2$-N/N''), 3.71 (s, 2H, HOOC-C*H*$_2$-N'), 3.44 (s, 4H, ethylene-*H*), 3.28 (s, 4H, ethylene-*H*). ^{13}C NMR

(100 MHz, D_2O) δ: 172.5, 170.2, 168.2, 151.1, 145.9, 142.3, 128.8, 126.3, 57.9, 54.9, 54.3, 51.9, 50.8. IR (neat, ATR-IR): ν = 1727.2 cm^{-1} (C=O), 1642.7 cm^{-1} (C=C py). HR-ESI-MS calcd. for $[C_{24}H_{29}N_5O_{10} + H]^+$: 548.1993; found $[M + H]^+$: 548.1987. Elemental analysis: calcd % for H_5decapa•5HCl•2.5H_2O ($C_{24}H_{29}N_5O_{10}$•5HCl•2.5H_2O = 774.856): C 37.20, H 5.07, N 9.04; found: C 37.28, H 4.91, N 8.72.

2.4.15 Na_2[In(decapa)]

A portion of H_5decapa (8.6 mg, 0.0112 mmol) and $In(ClO_4)_3$•8H_2O (6.9 mg, 0.0124mmol, 1.1 eq.) was dissolved in HCl (aq) (1 mL, 0.1 M) in a 1 dram screw cap vial. The pH was adjusted to ~4.5 with NaOH (aq) (0.1 M) while stirring. The reaction mixture was stirred at 60 °C for 16 hours, then evaporated to dryness to afford Na_2[In(decapa)]. ^{1}H NMR (600 MHz, D_2O) δ: 8.33-7.71 (m, 6H, Pyr-*H*), 4.87-2.57 (m, 18H, complex diastereotopic splitting). ^{13}C NMR (150 MHz, D_2O) δ: 178.5, 178.3, 178.0, 177.4, 176.6, 168.4, 167.8, 154.0, 153.6, 148.5, 146.6, 145.4, 145.0, 144.2, 143.2, 142.8, 142.5, 128.8, 128.2, 128.1, 128.0, 124.4, 123.6, 123.5, 123.1, 61.3, 59.5, 59.3, 59.1, 58.3, 57.8, 55.7, 55.3, 53.9, 52.5, 52.4, 51.0. HR-ESI-MS calcd. for $[C_{24}H_{24}{}^{115}InN_5O_{10} + H + 2Na]^+$: 704.0436; found $[M + H + 2Na]^+$: 704.0430.

2.4.16 H_2dedpa

The hexadentate ligand H_2dedpa was synthesized according to a literature procedure,[118,271,274] with a modified purification step performed by reverse-phase HPLC (gradient: A: 0.1% TFA, B: CH_3CN. 0 to 100% B linear gradient 25 min. t_R = broad, 9.7-11

min), followed by a second HPLC purification with a modified gradient (A: distilled deionized water, B: CH_3CN. 0 to 100% B linear gradient 25 min. t_R = broad, 8.5-10 min).

2.4.17 [In(dedpa)]Cl

A portion of H_2dedpa (10 mg, 0.020 mmol) and $In(ClO_4)_3 \cdot 8H_2O$ (13 mg, 0.023 mmol, 1.2 eq.) was dissolved in HCl (aq) (1 mL, 0.1 M) in a 1 dram screw cap vial. The pH was adjusted to ~4-4.5 with NaOH (aq) (0.1 M) while stirring. The reaction solution was stirred at 60 °C for 16 hours, then evaporated to dryness to afford [In(dedpa)]Cl as a white solid. ^{1}H NMR (600 MHz, DMSO-d_6) δ: 8.19 (t, 2H, pyr-*H*), 8.07 (d, 2H, pyr-*H*), 7.71 (d, 2H, pyr-*H*), 4.40 (s, 2H, -N*H*-), 4.27/4.26 (two overlapping d, 2H, Pyr-C*H*$_2$-N, ^{2}J = 16.6/16.3 Hz), 3.90/3.89 (two overlapping d, 2H, Pyr-C*H*$_2$-N, ^{2}J = 16.6 Hz), 2.63-2.56 (m, 4H, ethylene-*H*). ^{1}H NMR (400 MHz, D_2O) δ: 8.28 (t, 2H, pyr-*H*), 8.20 (d, 2H, pyr-*H*), 7.79 (d, 2H, pyr-*H*), 4.58 (d, 2H, Pyr-C*H*$_2$-N, ^{2}J = 17.3 Hz), 4.13 (d, 2H, Pyr-C*H*$_2$-N, ^{2}J = 17.4 Hz), 2.96-2.81 (m, 4H, ethylene-*H*). ^{13}C NMR (300 MHz, DMSO-d_6) δ: 163.7, 151.9, 146.9, 141.3, 124.6, 121.8, 49.5, 44.9. HR-ESI-MS calcd. for $[C16H16^{115}InN4O4]^+$: 443.0210; found $[M]^+$: 443.0216.

2.4.18 ^{111}In Radiolabeling studies

The ligands H_4octapa, H_5decapa, H_2dedpa, DTPA, and DOTA were made up as stock solutions (1 mg/mL, ~10^{-3} M) in deionized water. An aliquot of each ligand stock solution was transferred to screw cap mass spectrometry vials and made up to 1 mL with pH 5.5 NaOAc (10 mM) buffer, to a final ligand concentration of ~365 μM for each sample. A ~10 μL aliquot of the $^{111}InCl_3$ stock solution (~1 mCi for labeling studies and ~5-7 mCi for

mouse serum competitions) was transferred into the vials containing each ligand, allowed to radiolabel at ambient temperature for 10 minutes, and then analyzed by RP-HPLC to confirm radiolabeling and calculate yields. $[^{111}In(DOTA)]^-$ was heated at 80 °C for 20 minutes in a microwave reactor to achieve quantitative radiolabeling yields. Areas under the peaks observed in the radioactive HPLC trace were integrated to determine radiolabeling yields. The highest specific activity of 2.3 mCi/nmol obtained for H_4octapa was the result of labeling a 990 μL solution of 3.65 x 10^{-7} M chelate in NaOAc buffer (pH 5.3, 10 mM) with 10 μL of $^{111}In^{3+}$ in a 0.05 M HCl solution (1.02 mCi) for 10 minutes at ambient temperature in 97.5% radiolabeling yield. Elution conditions used for RP-HPLC analysis were gradient: A: 10 mM NaOAc buffer pH 4.5, B: CH_3CN. 0 to 100% B linear gradient 20 minutes. The radiometal complex $[^{111}In(dedpa)]^+$ used a modified HPLC gradient of A: 10 mM NaOAc buffer pH 4.5, B: CH_3CN. 0 to 5% B linear gradient 20 min. $[^{111}In(dedpa)]^+$ (t_R = 5.9 min), $[^{111}In(octapa)]^-$ (t_R = 4.7 min), $[^{111}In(decapa)]^{2-}$ [t_R = 5.4 min (5%), 7.7 min (95%)], $[^{111}In(DTPA)]^{2-}$ (t_R = 6.5 min), and $[^{111}In(DOTA)]^-$ (t_R = 3.5 min) were all formed in >99% radiochemical yields. Overlayed HPLC radiotraces are shown in Figure A.1.

2.4.19 Solution thermodynamics

The experimental procedures and details of the apparatus closely followed those of a previous study for H_2dedpa with Ga^{3+}.[118] As a result of the strength of the binding of the In^{3+} complex $[^{111}In(octapa)]^-$, the complex formation constant with this ligand could not be determined directly and the ligand-ligand competition method using the known competitor Na_2H_2EDTA was used. For H_5decapa, the ligand-ligand competition method was not required owing to the presence of a stable MHL species, and instead it was titrated directly

with In^{3+}. Potentiometric titrations were performed by Dr. Jacqueline Cawthray using a Metrohm Titrando 809 equipped with a Ross combination pH electrode and a Metrohm Dosino 800. Data were collected in triplicate using PC Control (Version 6.0.91, Metrohm). The titration apparatus consisted of a water-jacketed glass vessel maintained at 25.0 (± 0.1 °C, Julabo water bath). Prior to and during the course of the titration, a blanket of nitrogen, passed through 10% NaOH to exclude any CO_2, was maintained over the sample solution. Indium ion solutions were prepared by dilution of the appropriate atomic absorption standard (AAS) solution. The exact amount of acid present in the indium standard was determined by titration of an equimolar solution of In^{3+} and Na_2H_2EDTA. The amount of acid present was determined by Gran's method.[324] Calibration of the electrode was performed prior to each measurement by titrating a known amount of HCl with 0.1 M NaOH. Calibration data were analyzed by standard computer treatment provided within the program MacCalib[325] to obtain the calibration parameters E_0. Equilibration times for titrations were 10 minutes pK_a titrations and 15 minutes for metal complex titrations. Ligand and metal concentrations were in the range of 0.75-1.0 mM for potentiometric titrations. The data were treated by the program Hyperquad2008.[326] The four successive proton dissociation constants corresponding to hydrolysis of In^{3+}_{aq} ion and the indium-chloride stability constants included in the calculations were taken from Baes and Mesmer.[163] All values and errors represent the average of at least three independent experiments.

2.4.20 Molecular modeling

Calculations were performed by Dr. Jacqueline Cawthray using the Gaussian 09[327] and GaussView packages. Molecular geometries and electron densities were obtained from

density functional theory calculations, with the B3LYP functional employing the 6-31+G(d,p) basis set for 1st and 2nd row elements and the ECP basis set, LANL2DZ, was employed for indium.[328,329] Solvent (water) effects were described through a continuum approach by means of the IEF PCM as implemented in G09. The electrostatic potential was mapped onto the calculated electron density surface. The corresponding harmonic vibration frequencies were computed at the same level to characterize the geometry as a minima.

2.4.21 Mouse serum stability data

The compounds $[^{111}In(octapa)]^-$, $[^{111}In(decapa)]^{2-}$, $[^{111}In(DOTA)]^-$, $[^{111}In(DTPA)]^{2-}$, and $[^{111}In(dedpa)]^+$ were prepared with the radiolabeling protocol as described above. Mouse serum was removed from the freezer and allowed to thaw at ambient temperature for 30 minutes. In triplicate for each ^{111}In complex listed above, solutions were made in sterile vials with 750 μL mouse serum, 500 μL of ^{111}In-complex (10 mM NaOAc buffer, pH 5.5), 250 μL phosphate buffered saline (PBS), and were left to sit at ambient temperature. After 1 hour, half of the mouse serum competition mixture (750 μL) was removed from each vial, diluted to a total volume of 2.5 mL with phosphate buffered saline, and then counted in a Capintec CRC 15R well counter to obtain a value for the total activity to be loaded on the PD-10 column. The 2.5 mL of diluted mouse serum competition mixture was then loaded onto a PD-10 column that had previously been conditioned via elution with 20 mL of PBS. The 2.5 mL of loading volume was allowed to elute into a ^{111}In waste container, and then the PD-10 column was eluted with 3.5 mL PBS and collected into another sterile vial. The eluent which contained ^{111}In bound/associated with serum-proteins (size-exclusion for MW < 5000 Da) was counted in a well counter, and then compared to the total amount of activity that was

loaded on the PD-10 column to obtain the percentage of ^{111}In that was bound to serum proteins and therefore no longer chelate-bound. The percent stability values shown in Table 2.2 represent the percentage of ^{111}In that was retained on the PD-10 column and therefore still chelate-bound.

2.4.22 Biodistribution data

The protocol used in these animal studies was approved by the Institutional Animal Care Committee (IACC) of the University of British Columbia (protocol # A10-0171) and was performed by the BC Cancer Agency in accordance with the Canadian Council on Animal Care Guidelines. A total of 16 female ICR mice (20-25 g, 6-8 weeks) were used for the biodistribution study of three radiometal complexes. $[^{111}In(octapa)]^-$, $[^{111}In(DOTA)]^-$, and $[^{111}In(decapa)]^{2-}$ were prepared as described above, and then diluted in phosphate-buffered saline to a concentration of 100 μCi/mL. Each mouse was intravenously injected through the tail vein with ~10 μCi (100 μL) of the ^{111}In complex and then sacrificed by CO_2 inhalation 15 min, 1 h, 4 h, or 24 h after injection (n = 4 at each time point). Blood (500-700 μL) was collected by cardiac puncture with a 25 G needle and placed into an appropriate microtainer tube for scintillation counting. Urine was collected from the bladder after sacrifice and counted. Tissues collected included spleen, kidney, intestine, liver, heart, lung, brain, muscle, and femur. Tissues were weighed and counted with a Capintec CRC 15R well counter, and the counts were decay corrected from the first 15 minute time point and then converted to the percentage of injected dose (%ID) per gram of organ tissue (%ID/g).

Chapter 3: H_4octapa-trastuzumab: the application of a versatile acyclic ligand system for ^{111}In and ^{177}Lu imaging and therapy

This chapter is an adaptation of published work, and is reproduced in part, with permission from Price, E. W.; Zeglis, B. M.; Cawthray, J. F.; Ramogida, C. F.; Ramos, N.; Lewis, J. S.; Adam, M. J.; Orvig, C., H_4octapa-Trastuzumab: Versatile Acyclic Chelate System for ^{111}In and ^{177}Lu Imaging and Therapy. *J. Am. Chem. Soc.* **2013,** *135* (34), 12707–12721, Copyright 2014 American Chemical Society.

3.1 Introduction

Radiometallated bioconjugates possess an inherent modularity that can prove extremely useful in the design and construction of agents for nuclear imaging and therapy. Indeed, they contain a set of four distinct chemical components that can be swapped systematically to tune the properties and functions of the whole: the *radiometal* can be exchanged to harness isotopes with different decay characteristics; the *ligand* can be altered to accommodate different radiometals; the nature of the *covalent linkage* between the ligand and the biomolecule can be changed to take advantage of different types of conjugation chemistry; and, of course, the *biomolecule* itself can be replaced in order to change the targeting properties or pharmacokinetics of the construct.[2,6,7,25,28,36,56] In clinical practice, the use of different isotopes with a single targeting vector becomes especially important in pre-therapy imaging and dosimetry studies, procedures in which an agent bearing an imaging radioisotope is used for scouting scans prior to radiotherapy using the same vector labeled

with a therapeutic nuclide. Two isotopes that are ideally suited for this purpose are ^{111}In, a cyclotron produced radiometal (^{111}Cd(p,n)^{111}In) for SPECT imaging ($t_{1/2}$ ~2.8 days), and ^{177}Lu, a reactor produced therapeutic radiometal (^{176}Lu(n, γ)^{177}Lu) that emits β^- particles as well as γ-rays ($t_{1/2}$ ~6.6 days).[15]

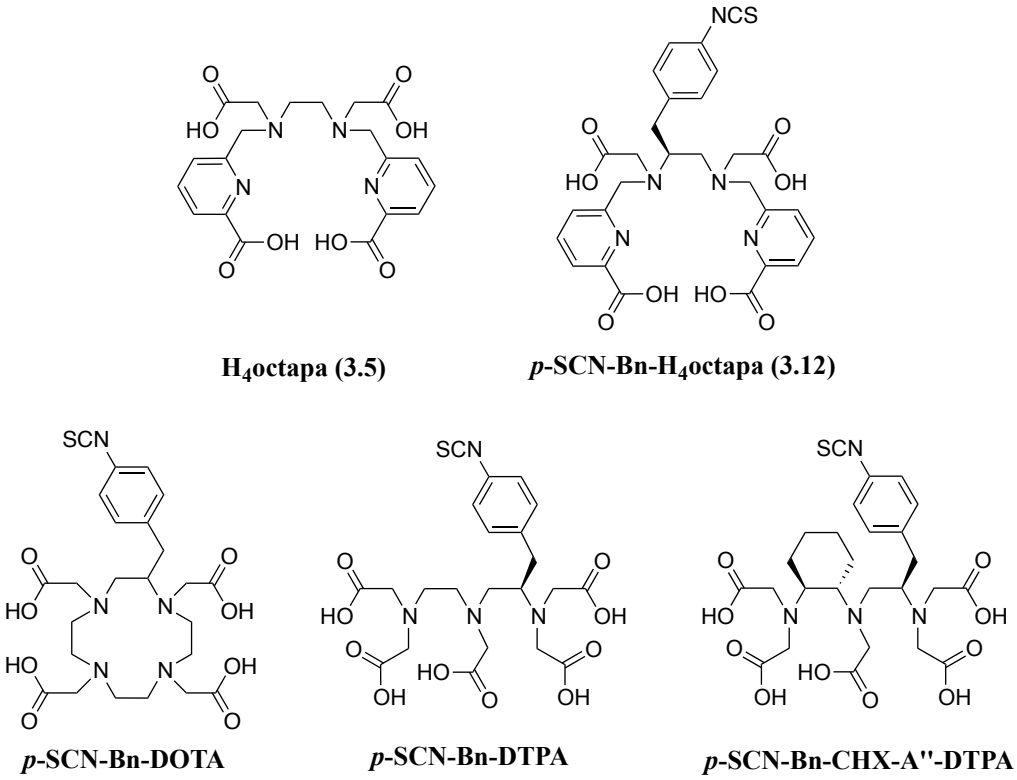

Figure 3.1 Structures of some common bifunctional ligands used for radiometal chemistry, and H_4octapa, the non-bifunctional variant of the ligand *p*-SCN-Bn-H_4octapa used in this work.

As discussed in Chapter 1, antibodies have emerged as extremely promising biomolecules for the delivery of radioactive payloads to cancerous tissues.[285,45] However, antibodies are not without their limitations as radiopharmaceutical vectors. For example, while they are generally considered robust *in vivo*, antibodies can become damaged or break

down when subjected to the elevated temperatures required by many radiometal chelation reactions.[330] Because macrocycles such as DOTA (Chapter 1 and 2) must be used with elevated temperatures (40-90 °C) and extended reaction times (30-180 min) to achieve quantitative radiolabeling, conditions that can be incompatible with antibodies and other biomolecules, to search for suitable acyclic ligands is important (Figure 3.1).[58-65,94,97,119,127-129,142] Acyclic ligands offer improvements in this regard, but not without cost. The acyclic ligand diethylenetriaminepentaacetic acid (DTPA), for example, exhibits much faster reaction kinetics than DOTA and can radiolabel with a variety of radiometals quantitatively in a matter of minutes at ambient temperature; however, it is not nearly as stable *in vivo* as its macrocyclic counterparts.[60,61,215,216,312]

Thus, choosing a radiometal ligand for an antibody conjugate requires a delicate balancing act. An immunoconjugate bearing a macrocyclic ligand such as DOTA can require extended incubations at elevated temperatures, often at the expense of antibody stability or immunoreactivity, in order to achieve suitable radiochemical yields; however, a radioimmunoconjugate bearing an acyclic ligand such as DTPA risks the unintentional release of the radiometal *in vivo*, an especially pressing problem considering the long pharmacokinetic half-life of many antibodies.[8,10,19-22,26-28] It thus becomes clear that a versatile ligand that combines the thermodynamic stability and kinetic inertness of macrocyclic ligands with the facile radiolabeling of acyclic ligand could prove tremendously valuable in the synthesis and development of novel radioimmunoconjugates.

Our efforts towards these goals have led us to the discovery of H_4octapa (Chapter 2). In this chapter is reported the synthesis, characterization, and *in vivo* validation of *p*-SCN-Bn-H_4octapa, a bifunctional, versatile, acyclic ligand that can be radiolabeled rapidly at room

temperature and exhibits significant thermodynamic stability and kinetic inertness with ^{111}In and ^{177}Lu (Figure 3.1). Members of the versatile "pa family" of ligands — including H_4octapa, H_2dedpa, H_5decapa, and H_2azapa (Chapter 8) — cover nearly all of the current medicinally relevant radiometals.[88,89,118,266,271-274,331] H_4octapa specifically has demonstrated high *in vitro* and *in vivo* stability and rapid radiolabeling kinetics with ^{111}In. Further, comparisons with ^{111}In-DOTA have revealed that H_4octapa possesses much more facile radiolabeling kinetics, can be labeled in higher specific activity, undergoes less fluxional isomerization in solution, and exhibits comparable stability *in vitro* and *in vivo*.[89] A major hurdle during this work, however, has been the cumbersome syntheses of the ligands.[88,89,118,272-274,331] As a result, in this chapter we report the synthesis of the bifunctional chelate *p*-SCN-Bn-H_4octapa via a vastly improved synthetic protocol. More importantly, we have employed the HER2/*neu*-targeted antibody trastuzumab as a model system for the *in vitro* and *in vivo* validation of ^{111}In-octapa- and ^{177}Lu-octapa-based radioimmunoconjugates in a murine model of ovarian cancer, as well as the comparative evaluation of these radioimmunoconjugates to those employing the more traditional macrocyclic ligand DOTA.

3.2 Results and discussion

3.2.1 Synthesis and characterization

In order to properly evaluate the potential of H_4octapa for use in biomolecular radiopharmaceuticals, we first sought to develop a highly efficient synthesis of a novel bifunctional variant, *p*-SCN-Bn-H_4octapa (Scheme 3.1), which had never been reported before. As for other bifunctional chelators (BFC), we have utilized the versatile and enantiopure starting material L-4-nitrophenylalanine.[118,215,89] While the *N*-benzyl-based

protecting group chemistry used in Chapter 2 for the synthesis of non-bifunctional H_4octapa proved adequate for the construction of the bare ligand, the requisite vigorous hydrogenation conditions resulted in poor yields and were completely incompatible with the synthesis of bifunctional derivatives based on 4-nitrophenylalanine.[118,89] Consequently, we revamped the synthesis to utilize the 2-nitrobenzenesulfonamide (nosyl) protecting group, a change that has significantly improved the synthesis of H_4octapa (**3.5**) and has made the synthesis of *p*-SCN-Bn-H_4octapa (**3.12**) feasible.[88,89,118,332-334]

Specifically, the switch to the nosyl protecting group has dramatically increased the cumulative yield of H_4octapa (**3.5**) from ~10-12% to ~45-50% over five synthetic steps.[89] Further, using this strategy, the bifunctional variant *p*-SCN-Bn-H_4octapa, which was previously inaccessible using *N*-benzyl protection chemistry (Chapter 2), can now be routinely produced with cumulative yields in 7 steps of ~25-30 %. The 2-nitrobenzenesulfonamide (nosyl) amine-protecting group has been crucial for the synthesis of these chelating ligands.[332-336] Compared to the challenging syntheses of bifunctional macrocycles such as *p*-SCN-Bn-DOTA, this streamlined route to *p*-SCN-Bn-H_4octapa should be of significant utility. The use of nosyl protecting groups results in a reduced number of purification steps (compounds **3.1**, **3.2**, and **3.8** can be purified via crystallization), greater yields, and, most relevantly, the accessibility of *p*-SCN-Bn-H_4octapa. The final 3 steps in the synthesis of *p*-SCN-Bn-H_4octapa are performed sequentially without purification due to the high polarity and difficult separation of the intermediates, and the final molecule is purified via reverse-phase HPLC chromatography.

Scheme 3.1 Improved synthesis of picolinic acid-based ligands H_4octapa (**3.5**) and *p*-SCN-Bn-H_4octapa (**3.12**).[a]

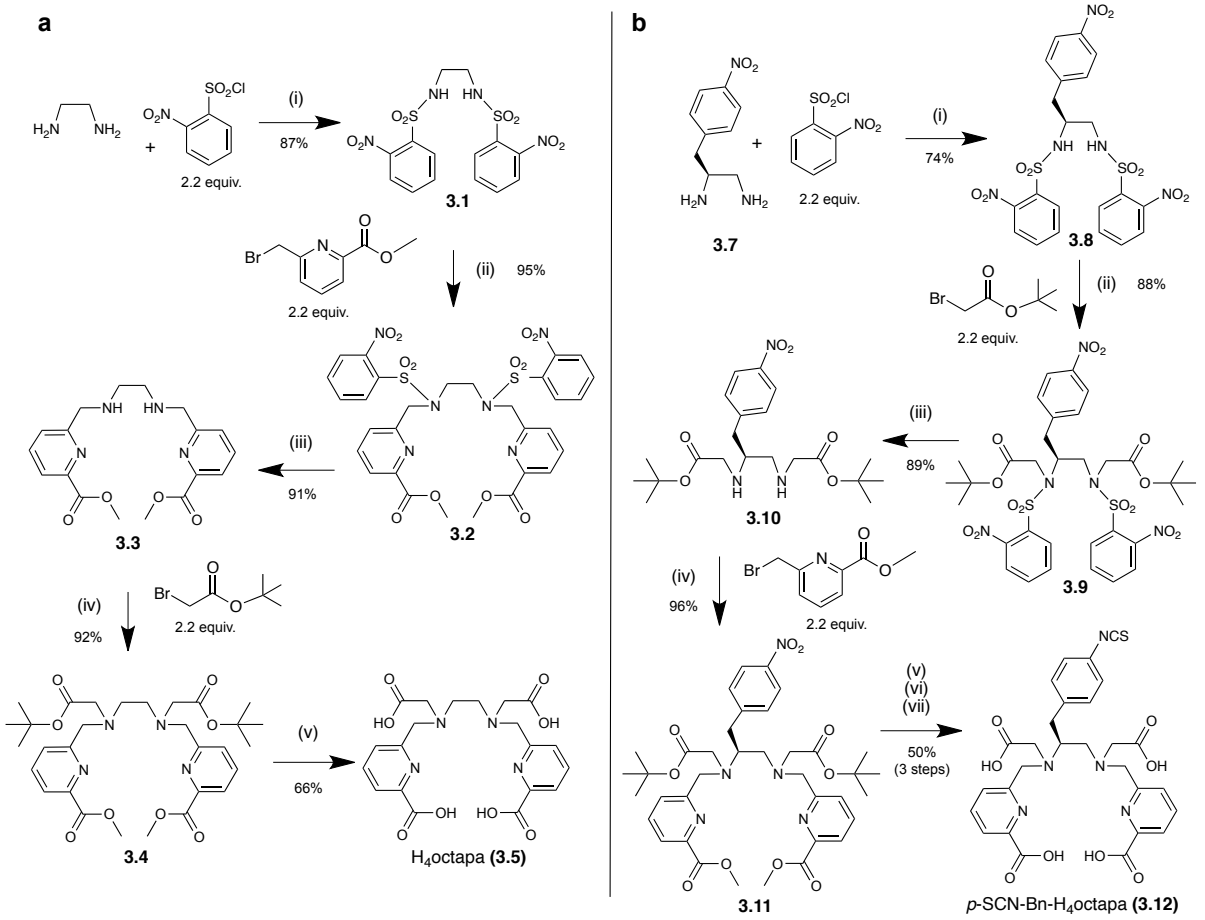

[a] (i) THF, $NaHCO_3$, RT, 24 h (ii) DMF, Na_2CO_3, methyl-6-bromomethylpicolinate (2.2 equiv), 50 °C, 24 h (iii) THF, thiophenol (2.2 equiv), K_2CO_3, RT, 72 h; (iv) MeCN, Na_2CO_3, 50 °C, 24 h; (v) 6 M HCl, reflux, 24 h. **b**) (i) THF, $NaHCO_3$, 50 °C, 24 h; (ii) DMF, Na_2CO_3, 50 °C, 24 h; (iii) THF, thiophenol (2.2 equiv), K_2CO_3, RT, 72 h; (iv) CH_3CN, Na_2CO_3, 50 °C, 24 h; (v) 5 mL of (1:1) glacial acetic acid:3 M HCl, Pd/C (20 wt%), H_2 (g), RT, 1 h; (vi) 6 M HCl, reflux, 24 h; (vii) thiophosgene in DCM (15 equiv), 3 M HCl, RT, 24 h.

Following synthesis, the HCl salt of pure H_4octapa was successfully metallated via reaction with indium perchlorate[89] [$In(ClO_4)_3$] and lutetium chloride [$LuCl_3$] to form quantitatively coordinated complexes. Further, all of the new ligands and their metal complexes were characterized using ^{1}H NMR, ^{13}C NMR, HR-ESI-MS, and ATR-IR where

appropriate. Particularly interesting, however, were the ^{1}H NMR spectra of the metallated H$_4$octapa ligand. Variable temperature NMR experiments with In^{3+} complexes of DOTA have demonstrated fluxional isomerization in solution, despite the macrocyclic nature of the ligand.[89,97,337] In this case, however, the ^{1}H NMR spectra obtained for $[In(octapa)]^-$ and $[Lu(octapa)]^-$ (**3.6**) reveal sharp and distinct coupling patterns, indicating little fluxional isomerization in solution at ambient temperature (Figure A.3).[89]

3.2.2 Thermodynamic stability and density functional theory structure prediction

The thermodynamic stability constants (log K_{ML}) for DOTA with Lu^{3+} have previously been determined by spectrophotometric methods (UV) to be 23.5 and ~25,[125,338] and by a competitive potentiometric titration with oxalate to be 29.2 ± 0.2.[339] In these studies the only species for which log K_{ML} has been documented is for the ML species (no metal hydroxide), and titrations were not done in the presence of NaCl, which is known to lower formation constants values (our titrations are done in 0.15 M NaCl for physiologically relevant conditions).[340] These factors, combined with the inconsistencies in the reported log K_{ML} values and the methods used, prompted us to perform competitive potentiometric titration experiments of DOTA with EDTA and Lu^{3+} in order to provide a formation constant that was determined under identical experimental conditions to our own system. Using potentiometric titrations, we have experimentally determined the thermodynamic stability constant (log K_{ML}) for Lu^{3+} with H$_4$octapa to be 20.08 ± 0.09 (pM = 19.8) and with DOTA to be 21.62 ± 0.10 (pM = 17.1). In addition, the log K_{ML} value for Lu^{3+} with DTPA has been reported in the literature to be 22.4, and we have calculated a pM value of 19.1.[119] Although the presence of sodium in our experiments can be expected to lower the stability constant of

DOTA with Lu^{3+} from previously reported values, and the different experimental methods used are expected to vary in their results, the low log K_{ML} value we have obtained could be inaccurate as a result of the slow complex formation kinetics of DOTA. During the potentiometric titrations, up to 15 minutes was allowed for stabilization of the electrode reading between each addition of base, which may have been too brief for a proper equilibrium to be established with DOTA. Previous work has waited over 2 weeks for equilibrium to be reached in this system, which highlights the sluggish formation kinetics.[125] Because of this uncertainty, our experimentally determined log K_{ML} value for DOTA with Lu^{3+} cannot be relied on solely or be considered to be more accurate than previously determined values, and therefore all reported formation constants must be considered. The thermodynamic stability constants of the In^{3+} complexes of H_4octapa, DOTA, and DTPA have been determined to be 26.6 (pM = 26.5), 23.9 (pM = 18.8), and 29.0 (pM = 25.7), respectively.[89] It is important to note that thermodynamic stability is generally regarded as an unreliable predictor of *in vivo* stability on its own,[94] and the kinetic inertness of a radiometal-complex is a much more valuable factor. For example, the $[^{111}In(DOTA)]^-$ complex is widely established as being significantly more stable than $[^{111}In(DTPA)]^{2-}$ both *in vivo* and *in vitro*, yet the thermodynamic stability constant for In^{3+} with DTPA is ~5 orders of magnitude higher than with DOTA (29.0 and 23.9, respectively). In fact, pM values, which are calculated from log K_{ML} values while taking into account ligand pK_a and metal ion hydroxide formation under specific and physiologically relevant conditions (here pH 7.4, $[M^{n+}]$ = 1 μM, $[L^{x-}]$ = 10 μM), are generally considered more useful in predicting *in vivo* stability than log K_{ML} values. H_4octapa has been shown to have high pM values with both

In^{3+} (26.5) and Lu^{3+} (19.8), further substantiating its promising properties with these metals and their radioactive isotopologues.

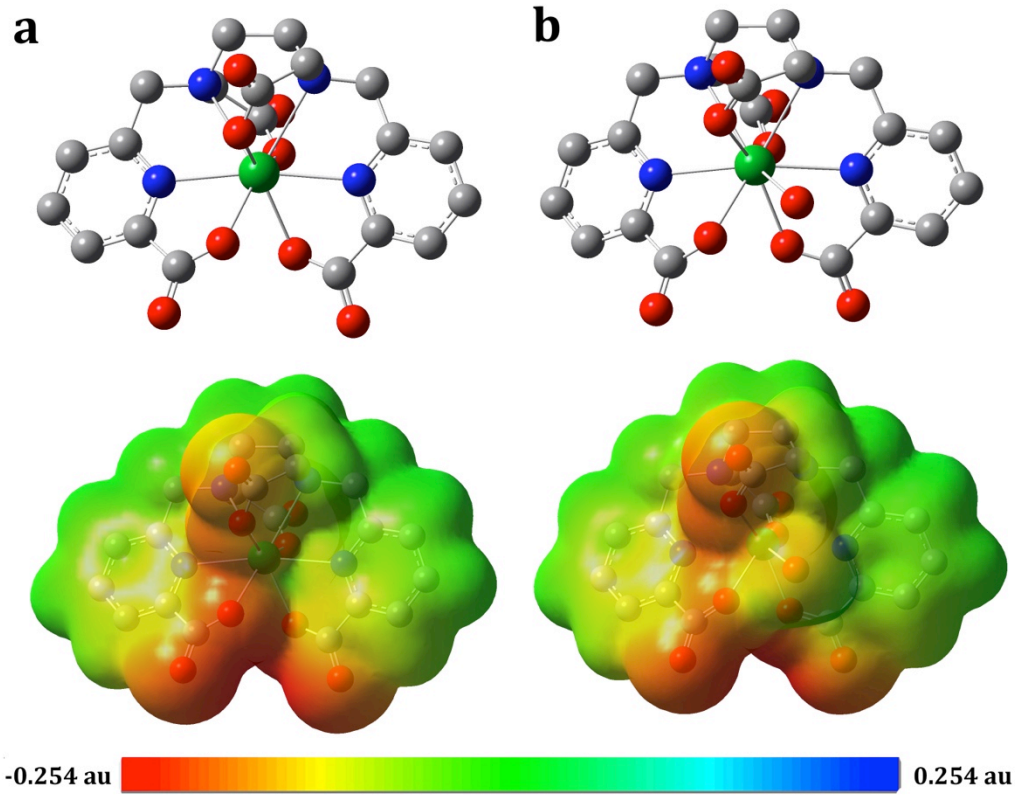

Figure 3.2 *In silico* DFT structure predictions. a, 8-coordinate structure of $[Lu(octapa)]^-$; b, 9-coordinate structure of $[Lu(octapa)(H_2O)]^-$, as well as the MEP polar-surface area maps (bottom) predicting the charge distribution over the solvent-exposed surface of the metal complexes (red = negative, blue = positive, representing a maximum potential of 0.254 au and a minimum of -0.254 au, mapped onto electron density isosurfaces of 0.002 $Å^{-3}$). DFT calculations performed by Dr. Jacqueline Cawthray.

The coordination geometries of both the 8- and 9-coordinate $[Lu(octapa)]^-$ and $[Lu(octapa)(H_2O)]^-$ complexes were estimated *in silico* using density functional theory (DFT) calculations, and MEP polar surface area maps were superimposed onto the structures (Figure 3.2). Both Lu^{3+} complexes were found to be highly symmetrical and very similar to

one another; indeed, that the addition of an H_2O ligand results in very little change in metal-ligand bond lengths and angles suggests that water binding bears little influence on the coordination of the ligand. Importantly, the $[Lu(octapa)]^-$ and $[Lu(octapa)(H_2O)]^-$ DFT structures shown here are quite similar to the DFT structure of the 8-coordinate $[In(octapa)]^-$ complex.[89] Taken together, the high log K_{ML} and pM values, the absence of fluxional behavior in solution, and the structural similarity between the $[Lu(octapa)]^-$ and $[In(octapa)]^-$ complexes strongly suggest that these two complexes should exhibit similar behavior *in vitro* and *in vivo.* This is especially important when considering ^{111}In as a SPECT imaging surrogate isotope for ^{177}Lu-based radiotherapies, where seamless interchangeability is imperative.

3.2.3 Bioconjugation and *in vitro* characterization

Synthesis and characterization data aside, the true value of any radiometal ligand ultimately lies in its behavior *in vitro* and *in vivo.* As a result, the next step in our investigation was to assess the *in vitro* and *in vivo* performance of H_4octapa in a model system based on the HER2/*neu*-targeting antibody trastuzumab and HER2-expressing SKOV-3 ovarian cancer cells. In order to provide a basis for comparison, radioimmunoconjugates bearing the ubiquitous ligand DOTA were also constructed and employed in parallel in all *in vitro* and *in vivo* experiments. As mentioned in Chapter 2, the antibody will act as a physiological anchor, imparting a long biological half-life to the conjugated radiometal-ligand complex, and allowing for extensive stability evaluation that was not possible with "bare" H_4octapa.

To begin, purified trastuzumab was incubated under slightly basic conditions (pH 8.5-9.0) with 4 equivalents of *p*-SCN-Bn-H_4octapa or *p*-SCN-Bn-DOTA and purified via size

exclusion chromatography (PD-10, GE Healthcare, UK). Subsequent radiometric isotopic dilution experiments indicated that these modifications yielded 3.03 ± 0.1 chelates per antibody in the case of *p*-SCN-Bn-H_4octapa and 3.40 ± 0.1 chelates per antibody in the case of *p*-SCN-Bn-DOTA. H_4octapa-trastuzumab was then radiolabeled with either ^{111}In or ^{177}Lu in NH_4OAc buffer (pH 5.5, 200 mM) for 15 min at room temperature, rapidly producing quantitatively labeled radioimmunoconjugates (>95% radiochemical yield) in high radiochemical purity (>99% in each case) and specific activity (4.0 ± 0.3 and 3.5 ± 0.4 mCi/mg, respectively) (Table 3.1). It is important to note that these labile kinetics offer a significant improvement over DOTA-trastuzumab, which required the less favorable reaction conditions of 1 h at 37 °C to achieve highly variable radiochemical yields of ~50-88% and to produce ^{111}In- and ^{177}Lu-labeled radioimmunoconjugates with slightly lower specific activities of 2.0 ± 0.2 and 3.4 ± 0.3 mCi/mg, respectively (Table 3.1). These results are of practical significance because antibodies and radiometals are very expensive, and so the inconsistent yields provided when radiolabeling DOTA-trastuzumab could waste as much as 50% of the antibody construct and radiometal, greatly increasing cost and making translation to a clinical radiopharmacy setting more challenging where routine and reliable production is require.

The mild radiolabeling conditions afforded by H_4octapa-trastuzumab likely contributed to the extremely high immunoreactivity of the immunoconjugates as determined by *in vitro* cellular assays using SKOV-3 cancer cells: 99.9 ± 0.02% for ^{111}In-octapa-trastuzumab and 98.7 ± 0.8% for ^{177}Lu-octapa-trastuzumab. These values compared favorably to the slightly lower but statistically different values determined for ^{111}In- and ^{177}Lu-DOTA-trastuzumab: 93.2 ± 0.5 % and 95.2 ± 0.2 %, respectively (p-values of 0.003

and 0.02, respectively) (Table 3.1). In order to assay the stability of the radioimmunoconjugates under biological conditions, all four constructs were incubated in human serum at 37 °C for a period of 5 days. Over the course of this experiment, the stability of the ^{111}In-octapa- and ^{111}In-DOTA-trastuzumab were both determined to be excellent at 94.9 ± 0.6% and 91.1 ± 0.6%, respectively, and that of the ^{177}Lu-octapa- and ^{177}Lu-DOTA-based conjugates was found to be 92.4 ± 0.6% and 98.6 ± 0.6%, respectively (Table 3.1). In the future, acid dissociation experiments, and studies probing the ability of H_4octapa to radiolabel with ^{111}In and ^{177}Lu in the presence of an excess of other metal ions such as Ca^{2+}, Mg^{2+}, Cu^{2+}, Zn^{2+}, and Fe^{3+} are of interest.[82,85]

Table 3.1 Chemical and *in vitro* biological characterization data for ^{111}In- and ^{177}Lu-octapa-trastuzumab and ^{111}In- and ^{177}Lu-DOTA-trastuzumab radioimmunoconjugates.

Immunoconjugate	Isotope	Radiolabeling conditions and yield	Chelates / mAb[a]	Specific activity (mCi/mg)	Immunoreactive fraction (%)[b]	Serum stability 120 h (%)[c]
H_4octapa-trastuzumab	^{111}In	15 min, 25 °C, 94%	3.0 ± 0.1	4.0 ± 0.3	99.9 ± 0.02	94.9 ± 0.6
	^{177}Lu	15 min, 25 °C, 95%	3.0 ± 0.1	3.5 ± 0.4	99.2 ± 0.8	92.4 ± 0.6
DOTA-trastuzumab	^{111}In	60 min, 37 °C, 50-85%	3.4 ± 0.1	2.0 ± 0.2	93.2 ± 0.5	91.1 ± 0.6
	^{177}Lu	60 min, 37 °C, 50-88%	3.4 ± 0.1	3.4 ± 0.3	95.2 ± 0.2	98.6 ± 0.6

[a] Isotopic dilution assays, n = 3. [b] Determined immediately prior to *in vivo* experimentation, n = 6. [c] Calculated for incubation in human serum at 37 °C for 120 h, n = 3.

3.2.4 Acute biodistribution studies

Biodistribution experiments were performed in order to directly compare the *in vivo* behavior and pharmacokinetics of the ^{111}In- and ^{177}Lu-based trastuzumab radioimmunoconjugates. To this end, each of the four radiolabeled antibodies — ^{111}In-octapa-trastuzumab, ^{177}Lu-octapa-trastuzumab, ^{111}In-DOTA-trastuzumab, and ^{177}Lu-DOTA-trastuzumab — were injected via tail vein into female nude athymic mice bearing

subcutaneous SKOV-3 ovarian cancer xenografts in the right shoulder (~30 μCi, ~8-15 μg, in 200 μL of sterile saline; tumour size ~ 2-3 mm diameter). After 24, 48, 72, 96, or 120 h (n = 4 per time point) the mice were euthanized via CO_2 (g) asphyxiation, and 13 organs, including the SKOV-3 tumours, were removed, weighed, and assayed for radioactivity content on a γ-counter.

Table 3.2 Biodistribution data of ^{111}In/^{177}Lu-octapa-trastuzumab and ^{111}In/^{177}Lu-DOTA-trastuzumab, performed over a 5 day period in mice bearing SKOV-3 ovarian cancer xenografts, tumour size ~2-3 mm diameter (n = 4 for each time point), showing %ID/g values.

^{111}In-octapa-trastuzumab						**^{111}In-DOTA-trastuzumab**					
Organ	**24 h**	**48 h**	**72 h**	**96 h**	**120 h**	**Organ**	**24 h**	**48 h**	**72 h**	**96 h**	**120 h**
Blood	6.9 ± 5.1	7.6 ± 6.5	10.5 ± 7.1	6.9 ± 6.6	11.4 ± 6	Blood	18 ± 1.7	17.3 ± 2.6	16.8 ± 2.2	15 ± 3.6	14.3 ± 1.6
Tumor	57.4 ± 22	58.3 ± 17.2	57.8 ± 14.6	68.7 ± 20.5	72.4 ± 21.3	Tumor	22.3 ± 6.4	28.4 ± 5.2	30.6 ± 9.1	32.8 ± 7.3	31.5 ± 3.8
Heart	2.6 ± 0.5	2.5 ± 1.5	2.7 ± 1.4	1.9 ± 1.4	3.6 ± 1.6	Heart	6.1 ± 0.9	6.6 ± 2	5.6 ± 1.3	5.2 ± 1.8	5.2 ± 0.9
Lungs	4.4 ± 2.1	3.9 ± 2.3	5 ± 2.8	3.8 ± 3.3	6.3 ± 3	Lungs	7.2 ± 1.6	6.8 ± 3.3	5.2 ± 1.4	6.3 ± 1.2	5.7 ± 2.2
Liver	12 ± 2.4	10.6 ± 1.2	9.1 ± 0.8	8.5 ± 2	6.6 ± 0.6	Liver	6.2 ± 0.4	5.5 ± 1.4	4.8 ± 1.3	4.4 ± 1.7	5.2 ± 1.2
Spleen	8.9 ± 2.4	7.6 ± 1	8.1 ± 0.8	7.4 ± 1.1	6.5 ± 1.6	Spleen	3.6 ± 0.8	3.7 ± 1.6	3 ± 0.7	2.7 ± 0.7	3.4 ± 1.4
Stomach	1.4 ± 0.2	0.8 ± 0.2	1.2 ± 0.1	0.7 ± 0.3	0.7 ± 0.2	Stomach	0.7 ± 0.1	0.7 ± 0.4	0.8 ± 0.2	0.3 ± 0.2	0.6 ± 0.3
Lg Intestine	3.7 ± 0.4	2.5 ± 0.7	2 ± 0.9	1.7 ± 0.4	1.2 ± 0.1	Lg Intestine	0.5 ± 0.1	0.6 ± 0.1	0.7 ± 0.1	0.5 ± 0.1	0.5 ± 0.1
Sm Intestine	3.8 ± 0.7	2.1 ± 0.4	2.5 ± 0.6	2.1 ± 0.4	1.5 ± 0.1	Sm Intestine	1.9 ± 0.1	1.6 ± 0.5	1.7 ± 0.1	1.1 ± 0.2	1.3 ± 0.1
Kidney	3.6 ± 1.2	4.2 ± 2.1	4.3 ± 2.1	3.5 ± 2	4.3 ± 1.6	Kidney	5.3 ± 0.5	6.3 ± 0.9	5.1 ± 1.7	5.8 ± 1.7	4.9 ± 0.4
Muscle	1.3 ± 0.5	0.9 ± 0.5	1 ± 0.5	0.8 ± 0.5	0.9 ± 0.5	Muscle	0.7 ± 0.2	0.8 ± 0.3	0.5 ± 0.1	0.4 ± 0.1	0.3 ± 0.1
Bone	4.1 ± 2	3.5 ± 0.4	2.8 ± 1	3.3 ± 0.5	1.4 ± 0.3	Bone	1 ± 0.3	0.9 ± 0.1	1.1 ± 0.4	0.9 ± 0.4	0.6 ± 0.2
Skin	10.8 ± 1.4	9.3 ± 1.4	7.2 ± 2.1	5.4 ± 1.2	3 ± 1.1	Skin	1.8 ± 0.4	2.1 ± 0.7	2.6 ± 0.1	1.7 ± 0.8	2.2 ± 0.8
^{177}Lu-octapa-trastuzumab						**^{177}Lu-DOTA-trastuzumab**					
Organ	**24 h**	**48 h**	**72 h**	**96 h**	**120 h**	**Organ**	**24 h**	**48 h**	**72 h**	**96 h**	**120 h**
Blood	19.1 ± 1.5	9.1 ± 9.5	9.7 ± 5.2	8.9 ± 6.9	7.6 ± 5.7	Blood	20.4 ± 1.7	17.4 ± 1	18.1 ± 2.8	15 ± 0.8	14.7 ± 0.7
Tumor	50 ± 5.4	63.5 ± 15	62.4 ± 20	70.4 ± 25.8	56.6 ± 12.7	Tumor	18.3 ± 4.8	31.6 ± 2.9	32.1 ± 7.4	37 ± 9.5	37.4 ± 10.3
Heart	4.2 ± 0.7	3.2 ± 1.9	2.5 ± 0.9	2.3 ± 0.7	2.6 ± 1.4	Heart	7.2 ± 1	4.9 ± 3.3	5.8 ± 1.6	4.6 ± 1.1	5.4 ± 0.6
Lung	7.8 ± 3.6	3.9 ± 3.1	5 ± 2.3	4.4 ± 2.5	2.7 ± 1.8	Lungs	10 ± 1.5	6.7 ± 4.6	7.1 ± 2.3	6.3 ± 0.6	6 ± 2.1
Liver	10.1 ± 1.3	13.2 ± 4	9.5 ± 3.5	9.8 ± 1.7	8 ± 2.6	Liver	4.5 ± 2	5.7 ± 3.6	5.7 ± 2.5	2.8 ± 0.9	3.7 ± 1.9
Spleen	8.8 ± 2.3	11.5 ± 2.5	7.4 ± 2.8	9.2 ± 1.2	6.7 ± 2.4	Spleen	3.8 ± 0.5	3.1 ± 2.9	3.2 ± 1	3.5 ± 0.4	3.8 ± 1
Stomach	1.4 ± 0.3	1 ± 0.5	0.9 ± 0.4	1.1 ± 0.3	0.6 ± 0.2	Stomach	0.7 ± 0.2	1.3 ± 1.9	0.9 ± 0.2	0.8 ± 0.2	0.7 ± 0.2
Lg Intestine	1.3 ± 0.3	1 ± 0.3	1.1 ± 0.5	1.1 ± 0.2	0.8 ± 0.2	Lg Intestine	0.6 ± 0.1	0.5 ± 0.3	0.8 ± 0.2	0.5 ± 0.1	0.6 ± 0.2
Sm Intestine	1.9 ± 0.5	2.5 ± 1.1	2 ± 0.9	2.3 ± 0.4	1.6 ± 0.4	Sm Intestine	1.7 ± 0.2	1.5 ± 1	1.5 ± 0.4	1.4 ± 0.3	1.2 ± 0.1
Kidney	4.9 ± 0.9	3.8 ± 2	3.7 ± 1.2	3.8 ± 1.8	2.8 ± 1.2	Kidney	5.5 ± 1.7	7.3 ± 0.7	5.1 ± 0.8	4.4 ± 0.2	7.1 ± 5
Muscle	0.9 ± 0.2	0.7 ± 0.5	0.8 ± 0.5	0.5 ± 0.2	0.4 ± 0.2	Muscle	0.7 ± 0.2	0.5 ± 0.4	0.4 ± 0.1	0.5 ± 0.2	0.5 ± 0.1
Bone	3.2 ± 0.5	4 ± 0.6	3.1 ± 0.7	4.2 ± 1.5	3.6 ± 1.7	Bone	1.2 ± 0	1.3 ± 0.8	1.3 ± 0.3	0.9 ± 0.2	1.4 ± 0.3
Skin	8.4 ± 2	6.8 ± 2.9	6.9 ± 0.5	5.6 ± 1.2	4.1 ± 2.2	Skin	1.9 ± 0.9	2.4 ± 1.7	2.1 ± 0.2	2.1 ± 0.7	3.1 ± 1.3

In all four cases, the biodistribution results showed all the hallmarks of tumour-targeted radioimmunoconjugates, specifically high levels of uptake in the blood pool at early

time points giving way over time to increasing levels of uptake in the tumour and, ultimately, very high tumour-to-background organ activity ratios. In all four cases, the level of uptake in non-target organs is roughly similar, with the highest levels of background uptake in the liver, spleen, and kidneys (Tables 3.2). However, past 24 h, the amount of activity in non-target organs rarely exceeds 5-10 %ID/g; for example, at 96 h post-injection, ^{177}Lu-octapa-trastuzumab displays uptakes of 9.8 ± 1.7 %ID/g, 9.2 ± 1.1 %ID/g, and 3.8 ± 1.8 %ID/g in the liver, spleen, and kidneys, respectively. A close inspection of Table 3.2 reveals slightly higher uptake of ^{111}In/^{177}Lu-octapa-trastuzumab in the bone when compared to the DOTA-trastuzumab conjugates, but also slightly lower uptake of ^{111}In/^{177}Lu-octapa-trastuzumab in the kidneys.

Far more interesting are the levels of tumour uptake, which are markedly higher with the ^{111}In-octapa- and ^{177}Lu-octapa-based variants compared to their ^{111}In-DOTA- and ^{177}Lu-DOTA-based analogs. For example, at 96 h post-injection the tumour uptake for ^{111}In-octapa-trastuzumab and ^{177}Lu-octapa-trastuzumab was found to be 68.7 ± 20.5 %ID/g and 70.4 ± 25.8 %ID/g, respectively, compared to 32.8 ± 7.3 %ID/g and 37.0 ± 9.5 %ID/g for the ^{111}In-DOTA-trastuzumab and ^{177}Lu-DOTA-trastuzumab constructs. Notably, despite the large range in errors, the p-values for these differences are 0.04 for the ^{111}In data sets and 0.05 for ^{177}Lu data sets, indicating statistically significant differences (two-tailed students t-test). Statistical analysis of tumour uptake by one-way ANOVA provided p-values of 0.02 for the ^{111}In data sets and 0.05 for ^{177}Lu data sets, also indicating statistical significance. In imaging, tumour-to-tissue activity ratios are arguably even more important measures than absolute uptake values, as these ratios provide quantitative information regarding the contrast that will be observed during imaging. As a result of the excellent tumour uptake of the

H_4octapa-based radioimmunoconjugates, the tumour-to-background activity ratios were higher than the corresponding DOTA-based agents for almost all organs. For example, the tumour-to-blood ratios for ^{111}In-octapa- and ^{111}In-DOTA-trastuzumab at 120 h were found to be 6.4 ± 3.8 and 2.2 ± 0.4, respectively, while for ^{177}Lu-octapa- and ^{177}Lu-DOTA-trastuzumab they were 7.5 ± 5.8 and 2.5 ± 0.7, respectively.

The origin of the elevated tumour uptake values observed for the H_4octapa-trastuzumab agents could lie in the enhanced immunoreactivity conferred by the fast and mild radiolabeling conditions. However, the difference in immunoreactivity was only about 5%, a discrepancy that would not be expected to cause such a change *in vivo*. Alternatively, it could be postulated that while the antigen-binding region of the antibody was only slightly adversely affected by temperature in the DOTA-trastuzumab conjugate, a separate region of the immunoglobulin may have suffered bond cleavage or protein structure disruption during radiolabeling, which in turn affected tumour uptake and retention. Finally, the differences in pharmacokinetic properties from attaching three to four relatively small chelating moieties (H_4octapa vs DOTA) to a 150 kD antibody is almost certainly insignificant, but it is not inconceivable that this modification could somehow affect the distribution of the radioimmunoconjugates *in vivo*. Because the difference in uptake between the H_4octapa- and DOTA-trastuzumab radioimmunoconjugates was not expected and is not easily explained, further experiments in a different cell line (e.g. SkBr3) should be performed in the future. Ultimately, regardless of the causation, the superior tumour uptake and tumour-to-tissue activity ratios plainly show that ^{111}In-octapa-trastuzumab and ^{177}Lu-octapa-trastuzumab are highly effective and versatile radioimmunoconjugates and, more generally, that H_4octapa is a very promising ligand for the construction of biomolecular radiopharmaceuticals.

3.2.5 Small animal SPECT/CT imaging and Cerenkov luminescence imaging

Single photon emission computed tomography (SPECT) was used in conjunction with standard helical X-ray CT for *in vivo* imaging of all ^{111}In and ^{177}Lu labeled immunoconjugates over 5 days, visually demonstrating high uptake and clear delineation of the SKOV-3 ovarian cancer xenografts by ^{111}In- and ^{177}Lu-octapa-trastuzumab as well as ^{111}In- and ^{177}Lu-DOTA-trastuzumab (Figure 3.3). Images taken at early time points show residual activity in the blood pool at 24 h, as expected; however, at later time points, the background activity in the blood clears and is accompanied by a concomitant increase in the amount of activity in the tumour, culminating at a point at which the tumour is by far the most prominent feature in the image (Figure 3.3). Overall, the image quality, tumour uptake, and tumour contrast observed are very similar between the H_4octapa- and DOTA-based constructs. In all four cases, high levels of tumour uptake and excellent tumour-to-background contrast are observed at later time points, data which correlate well with the high tumour uptake and tumour-to-tissue ratios revealed in the biodistribution experiments (Tables 3.2). It is important to note that while the ^{111}In- and ^{177}Lu-octapa-trastuzumab images do not appear qualitatively superior to those produced by the ^{111}In-DOTA- and ^{177}Lu-DOTA variants, the enhanced tumour-to-background activity ratios of the ^{111}In- and ^{177}Lu-octapa-based constructs could potentially be of value in identifying small lesions or metastases in which absolute uptake of radioactivity is limited and for which contrast is crucial. The use of Cerenkov radiation (CR) for Cerenkov luminescence imaging (CLI) has been emerging as a promising new imaging modality, with applications such as intraoperative radionuclide-guided surgery for the resection of cancers.[341] In order to probe the potential of our ^{177}Lu-labeled immunoconjugate, we have successfully imaged ^{177}Lu-octapa-trastuzumab via

external optical imaging through the skin 24 h post injection via CLI (Figure 3.4). To our knowledge, this was the first published example of *in vivo* CLI imaging of ^{177}Lu (Figure 3.4).[87] The bright spots on the head of the mouse in Figure 3.4 are from fluorescence molecules present in the animal's food.

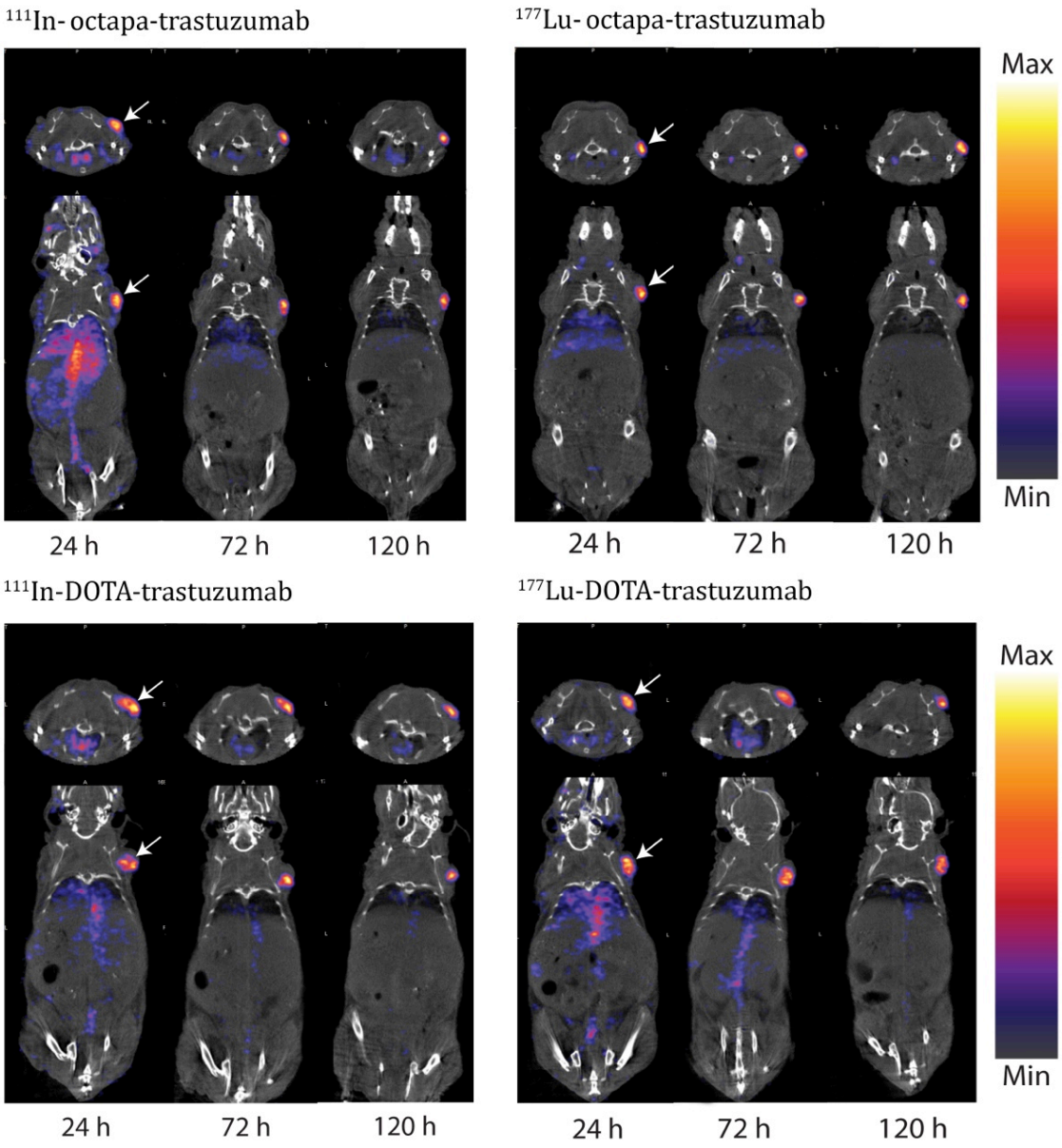

Figure 3.3 SPECT/CT imaging of the ^{111}In/^{177}Lu-octapa-trastuzumab and ^{111}In/^{177}Lu-DOTA-trastuzumab immunoconjugates, in female nude athymic mice with subcutaneous SKOV-3 xenografts (identified by arrow at right shoulder, tumour size ~2-3 mm diameter), showing transverse (top) and coronal (bottom) planar images bisecting the tumour, imaged at 24, 48, 72, 96, and 120 h post injection.

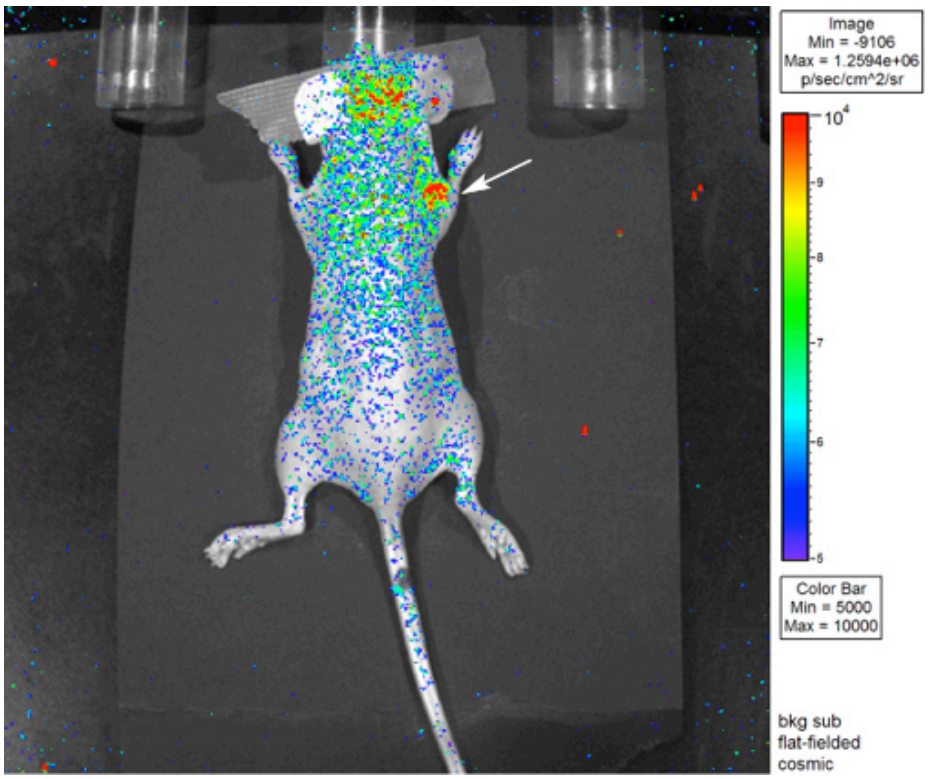

Figure 3.4 Cerenkov luminescence image (CLI) of ^{177}Lu-octapa-trastuzumab, obtained 24 h post-injection of a female nude athymic mouse bearing an SKOV-3 ovarian cancer xenograft on the right shoulder, indicated by white arrow (2 minute acquisition time).

3.3 Conclusions

Ultimately, the major benefit of the acyclic H_4octapa ligand system over macrocyclic ligands such as DOTA lies in the ability to radiolabel with rapid kinetics at room temperature, a trait which has the potential to shorten radiolabeling times (< 15 min), streamline radiopharmaceutical production, and aid in the retention of antibody integrity and immunoreactivity during radiolabeling. Trastuzumab is a robust antibody and can generally withstand the radiolabeling conditions required by DOTA. Although H_4octapa provides significant and tangible benefits over DOTA as outlined in this chapter, its use is not strictly required; however, when working with antibodies that are more sensitive than trastuzumab and are less forgiving of elevated temperatures and extended reaction times, a ligand with

more facile reaction kinetics such as *p*-SCN-Bn-H_4octapa may become crucial. The high and reproducible radiochemical yield that H_4octapa provides (>95%) is additionally important because antibodies are the most expensive component of these radiolabeled immunoconjugate systems. The inconsistent yields obtained with DOTA (50-90%) can waste as much as 50% of these expensive biomolecules and radiometals, and could make it difficult to reliably produce specific doses in a clinical radiopharmacy setting. Yet the advantages provided by H_4octapa do not end with facile radiolabeling protocols. Potentiometric titrations, spectroscopic measurements, and prolonged serum stability assays indicate that this broadly versatile ligand forms highly thermodynamically stable and kinetically inert coordination complexes with isotopes of both Lu^{3+} and In^{3+}. Finally, and most importantly, acute biodistribution studies have shown that ^{111}In- and ^{177}Lu-octapa-trastuzumab specifically and selectively accumulate in SKOV-3 ovarian cancer xenografts *in vivo* to a degree unmatched by analogous ^{111}In-DOTA- and ^{177}Lu-DOTA-trastuzumab radioimmunoconjugates. Further, SPECT/CT imaging reveals that both ^{111}In- and ^{177}Lu-octapa-trastuzumab are capable of delineating HER2-positive tumours *in vivo* with excellent contrast and high tumour-to-background activity ratios, producing images that are comparable to those created using ^{111}In- and ^{177}Lu-DOTA-trastuzumab. Taken together, these data clearly indicate that *p*-SCN-Bn-H_4octapa is a versatile and promising bifunctional ligand for the construction of highly potent and effective ^{111}In- and ^{177}Lu-labeled radiopharmaceuticals. The last major hurdle for evaluation of H_4octapa is experiments with $^{86/90}$Y, which will compare radiolabeling and stability properties of H_4octapa with DOTA. Preliminary experiments with non-radioactive Y^{3+} have been performed (Chapter 5).

3.4 Experimental section

3.4.1 Materials and methods

The general materials and methods for this chapter are the same as outlined in Chapter 2, with the following additions. DMSO used for ligand stock solutions was of molecular biology grade (>99.9%: Sigma, D8418). 1,4,7,10-Tetraazacyclododecane-1,4,7,10-tetraacetic acid *para*-benzylisothiocyanate (*p*-SCN-Bn-DOTA) was purchased from Macrocyclics, Inc. (Dallas, TX). Methyl-6-bromomethylpicolinate was synthesized according to a literature protocol, as performed in Chapter 2.[89] ^{177}Lu(chelate) analysis was performed using an HPLC system comprised of a Shimadzu SPD-20A prominence UV/Vis, LC-20AB prominence LC, a Bioscan flow-count radiation detector, and a C18 reverse phase column (Phenomenex Luna Analytical 250 x 4.6 mm). UV/Vis measurements for determining antibody stock solution concentrations were taken on a Thermo Scientific Nanodrop 2000 spectrophotometer (Wilmington, DE).

^{111}In was cyclotron produced (Advanced Cyclotron Systems, Model TR30) by proton bombardment through the reaction ^{111}Cd(*p,n*)^{111}In and was provided by Nordion as $^{111}InCl_3$ in 0.05 M HCl. ^{177}Lu was procured from Perkin Elmer (Perkin Elmer Life and Analytical Sciences, Wellesley, MA, effective specific activity of 29.27 Ci/mg) as $^{177}LuCl_3$ in 0.05 M HCl. Radiolabeling reactions were monitored using silica-gel impregnated glass-microfiber instant thin layer chromatography paper (iTLC-SG, Varian, Lake Forest, CA) and analyzed on a Bioscan AR-2000 radio-TLC plate reader using Winscan Radio-TLC software (Bioscan Inc., Washington, DC). All radiolabeling chemistry was performed with ultrapure water (>18.2 MΩ cm^{-1} at 25 °C, Milli-Q, Millipore, Billerica, MA) that had been passed through a 10 cm column of Chelex resin (BioRad Laboratories, Hercules, CA). Human blood serum

(Sigma, Sera, human, aseptically filled, S7023-100 mL) competition solutions were agitated at 550 rpm and held at 37 °C using an Eppendorf Thermomixer and then ^{177}Lu(chelate) mixtures were analyzed using GE Healthcare Life Sciences PD-10 desalting columns (GE Healthcare, United Kingdom, MW < 5000 Da filter) that were conditioned by elution of 25 mL phosphate-buffered saline (PBS) before use. ^{177}Lu/^{111}In-immunoconjugates were analyzed using iTLC as described above, and purified using PD-10 desalting columns and Corning 50k MW Amicon® Ultra centrifugation filters. Radioactivity in samples was measured using a Capintec CRC-15R dose calibrator (Capintec, Ramsey, NJ), and for biodistribution studies a Perkin-Elmer (Waltham, MA) Automated Wizard Gamma Counter was used for counting organ activities and creating calibration curves. SPECT/CT imaging was performed using a four-headed NanoSPECT/CT®PLUS camera (Bioscan Inc., Washington DC, USA) with a multi-pinhole focused collimator and a temperature controlled animal bed (Minerve equipment veterinaire). Imaging of Cerenkov radiation (CR) was performed using a IVIS 200 (Caliper Life Sciences) optical imager. Human breast cancer cell line SKOV-3 was obtained from the American Type Culture Collection (ATCC, Manassas, VA) and was grown by serial passage. All animals used were female nude athymic mice (Taconic Farms, Inc., Hudson, NY).

3.4.2 *N,N*'-(2-Nitrobenzenesulfonamide)-1,2-diaminoethane (3.1)

Ethylenediamine (548 μL, 8.2 mmol) was dissolved in THF (10 mL) and the round bottom flask (25 mL) was placed in an ice bath. Sodium bicarbonate (~2 g) was then added, followed by slow addition of 2-nitrobenzenesulfonyl chloride (4.00 g, 18.1 mmol). The reaction mixture was allowed to warm to ambient temperature and stirred overnight. The

yellow mixture was filtered to remove sodium bicarbonate, rotary evaporated to a red oil, and then dissolved in a minimum volume of dichloromethane and placed in the freezer overnight. Product precipitated, was isolated by suction filteration, and then washed with cold dichloromethane (3 x 10 mL), and this process was repeated with the filtrate once more to recover more material. The faint yellow powder (**3.1**) was dried *in vacuo* for a yield of 87% (~3.07 g). ^{1}H NMR (300 MHz, DMSO-d_6, 25 °C) δ: 8.16 (br s, 2H), 8.00-7.94 (m, 4H), 7.90-7.83 (m, 4H), 3.00 (s, 4H). ^{13}C NMR (75 MHz, DMSO-d_6, 25 °C) δ: 147.6, 134.2, 132.76, 132.4, 129.4, 124.5, 42.4. HR-ESI-MS calcd. for $[C_{14}H_{14}N_4O_8S_2+Na]^+$: 453.0151; found: 453.0154 $[M+Na]^+$, PPM = 0.7.

3.4.3 *N,N*'-(2-Nitrobenzenesulfonamide)-*N,N'*-[6-(methoxycarbonyl)pyridin-2-yl]methyl]-1,2-diaminoethane (3.2)

To a solution of **3.1** (1.17 g, 2.72 mmol) in dimethylformamide (10 mL, dried over molecular sieves 4 Å) was added methyl-6-bromomethyl picolinate[89] (1.38 g, 5.98 mmol) and sodium carbonate (~2 g). The faint yellow reaction mixture was stirred at 50 °C overnight, filtered to remove sodium carbonate, and concentrated *in vacuo*. The crude product was purified by silica chromatography (CombiFlash R_f automated column system; 40 g HP silica; A: dichloromethane, B: methanol, 100% A to 20% B gradient) to yield the product **3.2** as white fluffy solid (95%, ~1.88 g) (R_f: 0.9, TLC in dichloromethane). ^{1}H NMR (300 MHz, $CDCl_3$, 25 °C) δ: 8.10-8.08 (m, 2H), 7.93 (dd, J = 7.8, 0.9 Hz, 2H), 7.75 (t, J = 7.8 Hz, 2H), 7.66-7.62 (m, 4H), 7.60-7.57 (m, 2H), 7.51 (dd, J = 7.8, 0.9 Hz, 2H), 4.71 (s, 4H), 3.91 (s, 6H), 3.51 (s, 4H). ^{13}C NMR (75 MHz, $CDCl_3$, 25 °C) δ: 165.1, 156.2, 147.8,

147.4, 137.9, 133.6, 132.3, 131.9, 131.2, 125.6, 124.1, 124.0, 53.5, 52.6, 46.7. HR-ESI-MS calcd. for $[C_{30}H_{28}N_6O_{12}S_2+H]^+$: 729.1285; found: 729.1263, $[M+H]^+$, PPM = -3.0.

3.4.4 *N,N′*-[6-(Methoxycarbonyl)pyridin-2-yl]methyl-1,2-diaminoethane (3.3)

To a solution of **3.2** (1.48 g, 2.03 mmol) in tetrahydrofuran (10 mL) was added thiophenol (457 μL, 4.47 mmol) and potassium carbonate (excess, ~1 g). The reaction mixture was stirred at ambient temperature for 72 hours, where a slow color change from colorless to dark yellow occurred. The reaction mixture was split into two 20 mL falcon tubes, diluted with additional tetrahydrofuran, centrifuged for 5 minutes at 4000 rpm, and then the solvent was decanted. The potassium carbonate in the falcon tubes was rinsed/centrifuged/decanted with tetrahydrofuran 3 times, pooled, and the organic fractions were concentrated to dryness *in vacuo*. Please note that the potassium carbonate can be very sticky (varies between supplier) and can clog gravity and vacuum filters, and so to prevent product loss the method of centrifugation is recommended if a sticky texture is observed after reaction. The resulting crude yellow oil was purified by silica chromatography (CombiFlash R_f automated column system; 24 g neutral alumina; A: dichloromethane, B: methanol, 100% A to 30% B gradient) to yield **3.3** as clear colorless oil (91%, ~0.66 g). Compound **3.3** was purified using neutral alumina, as it demonstrates an abnormally high affinity for silica and requires the use of ammonium hydroxide and >20% methanol to be eluted, resulting in partial methyl-ester deprotection and dissolving of some silica. ^{1}H NMR (300 MHz, MeOD, 25 °C) δ: 8.02 (d, J = 7.5 Hz, 2H), 7.94 (t, J = 7.6 Hz, 2H), 7.66 (d, J = 7.5 Hz, 2H), 3.96 (s, 6H), 2.79 (s, 4H). ^{13}C NMR (75 MHz, MeOD, 25 °C) δ: 167.0, 161.4, 148.5, 139.5, 127.6,

124.8, 54.9, 53.4, 50.0, 49.3. HR-ESI-MS calcd. for $[C_{18}H_{22}N_4O_4+H]^+$: 359.1719; found: 359.1720, $[M+H]^+$, PPM = 0.2.

3.4.5 *N,N′*-[(*tert*-Butoxycarbonyl)methyl-*N,N′*-[6-(methoxycarbonyl)pyridin-2-yl]methyl]-1,2-diaminoethane (3.4)

To a solution of **3.3** (212 mg, 0.593 mmol) in dry acetonitrile (10 mL, distilled over CaH_2) was added *tert*-butylbromoacetate (202 μL, 1.36 mmol) and sodium carbonate (~300 mg). The reaction was stirred at 60 °C overnight. Sodium carbonate was removed by filtration and the crude reaction mixture was concentrated *in vacuo*. The crude oil was purified by column chromatography (CombiFlash R_f automated column system; 24 g HP silica; A: dichloromethane, B: methanol, 100% A to 20% B gradient) to afford the product **3.4** as light yellow oil (92%, ~0.32 g). ^{1}H NMR (300 MHz, $CDCl_3$, 25 °C) δ: 7.95 (dd, J = 7.2, 1.4 Hz, 2H), 7.80-7.70 (m, 4H), 3.97 (s, 4H), 3.95 (s, 6H), 3.28 (s, 4H), 2.78 (s, 4H), 1.40 (s, 18H). ^{13}C NMR (75 MHz, $CDCl_3$, 25 °C) δ: 170.4, 165.8, 160.8, 147.1, 137.3, 126.0, 123.5, 80.9, 60.5, 56.3, 52.7, 52.4, 28.0. HR-ESI-MS calcd. for $[C_{30}H_{42}N_4O_8+H]^+$: 587.3081; found: 587.3085, $[M+H]^+$, PPM = 0.7.

3.4.6 H_4octapa, *N,N′*-(6-carboxy-2-pyridylmethyl)-*N,N′*-diacetic acid-1,2-diaminoethane (3.5)

Compound **3.4** (138 mg, 0.235 mmol) was dissolved in HCl (10 mL, 6 M) and heated to reflux for 12 hours at 140 °C. The reaction mixture was concentrated *in vacuo* and then purified via semi-prep reverse-phase HPLC (10 mL/min, gradient: A: 0.1% TFA (trifluoroacetic acid) in deionized water, B: 0.1% TFA in CH_3CN. 0 to 70% B linear gradient

30 min. t_R = 12.6 min, broad). Product fractions were pooled, concentrated *in vacuo,* dissolved in 6M HCl, and then concentrated *in vacuo* again to remove trifluoroacetic acid. The HCl salt H_4octapa•4HCl•2H_2O **(3.5)** was obtained as a white solid (66% yield, ~0.097 g, using the molecular weight of the HCl salt as determined by elemental analysis). ^{1}H NMR (300 MHz, D_2O) δ: 8.11-8.01 (m, 4H, pyr-*H*), 7.72-7.69 (m, 2H, pyr-*H*), 4.53 (s, 4H, Pyr-C*H*$_2$-N), 3.97 (s, 4H, HOOC-C*H*$_2$-N), 3.57 (s, 4H, ethylene-*H*). ^{13}C NMR (75 MHz, D_2O) δ: 170.3, 165.3, 151.2, 145.1, 142.6, 128.6, 126.1, 57.8, 54.9, 51.2. IR (neat, ATR-IR): n = 1721 cm^{-1} (C=O), 1636/1618 cm^{-1} (C=C py). HR-ESI-MS calcd. for $[C_{20}H_{22}N_4O_8 + H]^+$: 447.1515; found $[M + H]^+$: 447.1526, PPM = 0.7. Elemental analysis: calcd % for H_4octapa•4HCl•2H_2O ($C_{20}H_{22}N_4O_8$•4HCl•2H_2O = 628.2839): C 38.23, H 4.81, N 8.92; found: C 37.94, H 4.66, N 8.59.

3.4.7 Na[Lu(octapa)] (3.6)

H_4octapa•4HCl•2H_2O **(3.5)** (9.8 mg, 0.013 mmol) was suspended in 0.1 M HCl (1.5 mL) and $LuCl_3$•6H_2O (6.1 mg, 0.015 mmol) was added. The pH was adjusted to 4-5 using 0.1 M NaOH and then the solution was stirred at room temperature. After 1 hour the product was confirmed via mass spectrometry and the solvent was removed *in vacuo* to yield Na**[Lu(octapa)] (3.6)**. ^{1}H NMR (600 MHz, D_2O, 25 °C) δ: 8.28-8.12 (m, 3H), 8.06 (d, *J* = 8.2 Hz, 2H), 7.81-7.67 (m, 2H), 4.56-4.48 (m, 1.5H), 4.33-4.05 (m, 2H), 3.81-3.74 (m, 1H), 3.51-3.43 (m, 2H) 3.26-3.16 (m, 4H), 3.00-2.98 (m, 0.5H), 2.57-2.55 (m, 0.5H), 2.12 (br s, 0.5H). ^{13}C NMR (150 MHz, D_2O, 25 °C) δ: 180.7, 177.1, 173.3, 172.8, 171.7, 158.2, 157.2, 155.6, 154.3, 150.6, 149.9, 149.5, 143.8, 142.9, 142.5, 141.4, 126.8, 126.4, 124.6, 124.5, 123.9, 65.7, 64.2, 62.3, 61.0, 60.5, 59.1, 57.6, 55.9. HR-ESI-MS calcd. for

$[C_{20}H_{18}{}^{175}LuN_4O_8 + 2Na]^+$: 663.0328; found: 663.0318, $[M + 2Na]^+$, PPM = -1.5.

3.4.8 1-(*p*-Nitrobenzyl)ethylenediamine (3.7)

Compound **3.7** was prepared according to a literature preparation.[342] Product was purified with a modified procedure using column chromatography (CombiFlash R_f automated column system; 40 g HP silica;, A: 95% dichloromethane 5% ammonium hydroxide, B: 95% methanol 5% ammonium hydroxide, 100% A to 30% B gradient) to afford **3.7** as brown/amber oil in a cumulative yield of 40% over 3 steps (~3 g). ^{1}H NMR (300 MHz, $CDCl_3$, 25 °C) δ: 7.91 (d, J = 8.9 Hz, 2H), 7.18 (d, J = 8.5 Hz, 2H), 2.80-2.57 (m, 3H), 2.45-2.31 (m, 2H). ^{13}C NMR (75 MHz, $CDCl_3$, 25 °C) δ: 147.1, 147.7, 129.4, 122.8, 54.3, 47.5, 41.4. HR-ESI-MS calcd. for $[C_9H_{13}N_3O_2+H]^+$: 196.1086; found: 196.1084 [M + H], PPM = -1.0.

3.4.9 *N,N'*-(2-Nitrobenzenesulfonamide)-1-(*p*-nitrobenzyl)-1,2-diaminoethane (3.8)

Compound **3.7** (578 mg, 2.96 mmol) was dissolved in THF (10 mL) and placed in an ice bath, then sodium bicarbonate (~2 g) was added, followed by slow addition of 2-nitrobenzenesulfonyl chloride (1.58 g, 7.1 mmol). The reaction mixture was heated to 50 °C and stirred overnight. The yellow/orange mixture was filtered to remove sodium bicarbonate, rotary evaporated to an orange oil, and then dissolved in a minimum volume of dichloromethane and placed in the freezer. Product precipitated and was isolated by suction filtration, then washed with cold dichloromethane (3 x 10 mL), and this process was repeated with the filtrate twice more to recover more product. The faint yellow powder (**3.8**) was dried *in vacuo* for a yield of 74% (~1.24 g) (R_f : 0.90, TLC in 10% methanol in

dichloromethane). ^{1}H NMR (300 MHz, acetone-d_6, 25 °C) δ: 8.18-8.15 (m, 1H), 7.99-7.94 (m, 2H), 7.79-7.57 (m, 5H), 7.33 (d, *J* = 8.5 Hz, 2H), 7.04-6.98 (m, 2H), 4.01 (br s, 1H), 3.41-3.38 (m, 2H), 3.26 (dd, *J* = 3.4, 13.7 Hz, 1H), 2.98 (m, 1H). ^{13}C NMR (75 MHz, acetone-d_6, 25 °C) δ: 206.3, 149.2, 148.1, 147.6, 146.7, 135.2, 134.8, 134.3, 133.9, 133.8, 133.6, 131.7, 131.4, 130.9, 126.0, 125.7, 123.9, 57.7, 49.4, 38.2. HR-ESI-MS calcd. for $[C_{21}H_{19}N_5O_{10}S_2+Na]^+$: 588.0471; found: 588.0465 $[M+Na]^+$, PPM = -1.0.

3.4.10 *N,N'*-(2-Nitrobenzenesulfonamide)-*N,N'*-[(*tert*-butoxycarbonyl)methyl]-1-(*p*-nitrobenzyl)-1,2-diaminoethane (3.9)

To a solution of **3.8** (224 mg, 0.390 mmol) in dimethylformamide (5 mL, dried over molecular sieves 4 Å) was added *tert*-butylbromoacetate (169.7 mg, 0.87 mmol) and sodium carbonate (~400 mg). The yellow reaction mixture was stirred at 50 °C overnight, filtered to remove sodium carbonate, and concentrated *in vacuo*. The crude product was purified by silica chromatography (CombiFlash R_f automated column system; 40 g HP silica; A: ethyl acetate, B: petroleum ether, 100% A to 100% B gradient) to yield **3.9** as white fluffy solid (88%, ~0.27 g). ^{1}H NMR (300 MHz, $CDCl_3$, 25 °C) δ: 7.98 (d, *J* = Hz, 2H), 7.84-7.39 (m, 8H), 7.25 (d, *J* = Hz, 2H), 4.46 (Br s, 1H), 4.33-3.85 (m, 6 H), 3.53 (m, 1H), 3.39 (m, 1H), 2.91 (m, 1H), 1.40 (s, 18H). ^{13}C NMR (75 MHz, $CDCl_3$, 25 °C) δ: 168.3, 167.6, 148.0, 147.1, 146.3, 144.8, 133.9, 133.6, 132.5, 131.8, 131.7, 131.6, 131.5, 130.6, 129.8, 124.0, 123.0, 82.7, 82.5, 58.5, 52.5, 50.7, 45.4, 35.0, 27.7. HR-ESI-MS calcd. for $[C_{33}H_{39}N_5O_{14}S_2+Na]^+$: 816.1833; found: 816.1838, $[M+Na]^+$, PPM = 0.6.

3.4.11 *N,N'*-[(*tert*-Butoxycarbonyl)methyl]-1-(*p*-nitrobenzyl)-1,2-diaminoethane (3.10)

To a solution of **3.9** (151 mg, 0.189 mmol) in tetrahydrofuran (5 mL) was added thiophenol (41 μL, 0.398 mmol) and potassium carbonate. The reaction mixture was stirred at ambient temperature for 72 hours, where a slow color change from colorless to dark yellow occurred. The reaction mixture was split into two 20 mL centrifuge tubes, diluted with additional tetrahydrofuran, centrifuged for 5 minutes at 4000 rpm, and then the solvent was decanted. The potassium carbonate in the falcon tubes was rinsed with tetrahydrofuran and centrifuged 3 times, pooled, and then concentrated to dryness *in vacuo*. The resulting crude yellow oil was purified by silica chromatography (CombiFlash R_f automated column system; 24 g HP silica; A: dichloromethane, B: methanol, 100% A to 20% B gradient) to yield **3.10** as clear colorless oil (89%, ~0.071 g). ^{1}H NMR (300 MHz, $CDCl_3$, 25 °C) δ: 8.12 (d, J = 8.2 Hz, 2H), 7.35 (d, J = 8.2 Hz, 2H), 3.30 (s, 2H), 3.23-3.22 (m, 2H), 2.87-2.84 (m, 3H), 2.62 (m, 1H), 2.40 (m, 1H), 2.12 (Br s, 2H, -N*H*), 1.41 (s, 18H). ^{13}C NMR (75 MHz, $CDCl_3$, 25 °C) δ: 171.7, 171.5, 147.1, 146.5, 130.1, 123.5, 81.2, 81.0, 58.3, 51.6, 49.3, 39.2, 28.0. HR-ESI-MS calcd. for $[C_{21}H_{33}N_3O_6+H]^+$: 424.2448; found: 424.2451, $[M+H]^+$, PPM = 0.7.

3.4.12 *N,N'*-[(*tert*-Butoxycarbonyl)methyl]-*N,N'*-[(6-methoxycarbonyl)pyridin-2-yl)methyl]-1-(*p*-nitrobenzyl)-1,2-diaminoethane (3.11)

To a solution of **3.10** (71.7 mg, 0.169 mmol) in dry acetonitrile (5 mL, distilled over CaH_2) was added methyl 6-(bromomethyl)picolinate[89] (85.7 mg, 0.372 mmol) and sodium carbonate (~200 mg). The reaction was stirred at 60 °C overnight. Sodium carbonate was removed by filtration and the crude reaction mixture was concentrated *in vacuo*. The crude

oil was purified by column chromatography (CombiFlash R_f automated column system; 24 g HP silica; A: dichloromethane, B: methanol, 100% A to 20% B gradient) to afford the product **3.11** as light yellow oil (96%, ~0.117 g). ^{1}H NMR (300 MHz, MeOD, 25 °C) δ: 8.18 (d, J = 8.7 Hz, 2H), 8.11-8.02 (m, 3H), 7.95 (t, J = 7.8 Hz, 1H), 7.73-7.72 (m, 1H), 7.48-7.45 (m, 3H), 4.05 (s, 3H, methyl ester), 3.98 (s, 3H, methyl ester), 3.76 (m, 2H), 3.51 (d, J = 17.4 Hz, 1H), 3.38-3.31 (m, 2H), 3.25-3.20 (m, 2H), 3.16-3.01 (m, 2H), 2.89-2.82 (m, 2H), 2.71-2.64 (m, 1H), 2.55-2.51 (m, 1H), 1.39 (s, 18H). ^{13}C NMR (75 MHz, MeOD, 25 °C) δ: 174.4, 173.4, 167.1, 166.8, 160.2, 160.1, 149.3, 148.7, 148.5, 148.1, 140.3, 140.1, 131.6, 129.0, 128.6, 125.1, 125.0, 124.8, 83.4, 83.3, 63.8, 61.8, 58.4, 57.0, 53.8, 53.6, 34.1, 28.4. HR-ESI-MS calcd. for $[C_{36}H_{48}N_5O_{10}+H]^+$: 722.3401; found: 722.3390, $[M+H]^+$, PPM = -1.5.

3.4.13 *p*-SCN-Bn-H$_4$octapa, *N,N'*-[(Carboxylato)methyl]-*N,N'*-[(6-carboxylato)pyridin-2-yl)methyl]-1-(*p*-benzyl-isothiocyanato)-1,2-diaminoethane (3.12)

Compound **3.11** (118 mg, 0.16 mmol) was dissolved in glacial acetic acid (2.5 mL) with hydrochloric acid (2.5 mL, 3 M), palladium on carbon (20 wt%), and hydrogen gas (balloon). The reaction was stirred vigorously at RT for 1 hour, then filtered to remove Pd/C and washed *ad libitum* with methanol and hydrochloric acid (3 M). The crude reaction mixture was concentrated *in vacuo*, dissolved in 15 mL of hydrochloric acid (6 M), and heated to reflux overnight to facilitate deprotection of the methyl and *tert*-butyl esters. HR-ESI-MS calcd. for $[C_{27}H_{29}N_5O_8+H]^+$: 552.2094; found: 552.2098, $[M+H]^+$, PPM = 0.7. Without purification, the crude reaction mixture was dissolved in hydrochloric acid (1 mL, 3 M) and then mixed with thiophosgene (purchased suspended in chloroform) in ~0.2 mL of additional chloroform (15 eq, 2.45 mmol) to react overnight at ambient temperature with

vigorous stirring. The reaction mixture was washed with chloroform (5 x 1 mL) by vigorous biphasic stirring followed by decanting of the organic phase with a pipette to remove excess thiophosgene, diluted to a volume of 4.5 mL with deionized water, and injected directly onto a semi-prep HPLC column for purification (A: 0.1% TFA in deionized water, B: 0.1% TFA in CH_3CN, 100% A to 60% B gradient over 40 minutes). ***p*-SCN-Bn-H$_4$octapa (3.12)** was found in the largest peak at R_t = 34 minutes, lyophilized overnight, and was isolated as a fluffy white solid (50% over 3 steps from **3.11**, ~0.047 g). ^{1}H NMR (400 MHz, MeOD, 25 °C) δ: 8.00-7.87 (m, 4H), 7.59-7.54 (m, 2H), 7.14 (dd, *J* = 7.7 Hz, 35.4 Hz, 4H), 5.03 (Br m, 1H), 4.66 (Br m, 2H), 4.49-4.45 (Br m, 1H), 4.11 (Br m, 1H), 3.92 (Br m, 2H), 3.66-3.59 (m, 2H), 3.35-3.18 (Br m, 3H), 2.66-2.60 (m, 1H). ^{13}C NMR (100 MHz, MeOD, 25 °C) δ: 173.1, 167.9, 166.0, 165.8, 161.3, 160.9, 159.4, 151.4, 147.7, 147.2, 138.6, 138.5, 137.6, 135.7, 130.3, 129.7, 127.5, 126.6, 125.6, 124.7, 123.9, 60.3, 59.7, 54.2, 54.1, 33.3. HR-ESI-MS calcd. for $[C_{28}H_{27}N_5O_8S+H]^+$: 594.1659; found: 594.1661, $[M+H]^+$, PPM = 0.3.

3.4.14 Solution thermodynamics

The experimental procedures and details of the apparatus closely followed those of a previous study for H$_2$dedpa with Ga^{3+} and work in Chapter 2 with H$_4$octapa for In^{3+}.[89,118] As a result of the strength of the binding of the Lu^{3+} complexes, [^{177}Lu(octapa)]$^-$and [Lu(DOTA)], the complex formation constants with these ligands could not be determined directly and the ligand-ligand competition method using the known competitor Na_2H_2EDTA was used. Potentiometric titrations were performed by Dr. Jacqueline Cawthray using a Metrohm Titrando 809 equipped with a Ross combination pH electrode and a Metrohm Dosino 800. Experimental procedures and data fitting were performed as in Chapter 2

(**2.4.19**), with the following modifications. The proton dissociation constant corresponding to hydrolysis of $Lu^{3+}_{(aq)}$ ion included in the calculations were taken from Baes and Mesmer.[163] The acid dissociation constants for DOTA and the K_{ML} value for the lutetium-edta complex were taken from Martell.[119] pM values were calculated at physiologically relevant conditions of pH 7.4, 100 μM ligand, and 10 μM metal. All values and errors represent the average of at least three independent experiments.

3.4.15 Molecular modeling

Calculations were performed by Dr. Jacqueline Cawthray using the Gaussian 09[327] and GaussView packages. Molecular geometries and electron densities were obtained from density functional theory calculations, with the B3LYP functional employing the 6-31+G(d,p) basis set for 1st and 2nd row elements and the Stuttgart−Dresden effective core potential, SDD for lutetium.[328,329,343] Solvent (water) effects were described through a continuum approach by means of the IEF PCM as implemented in G09. The electrostatic potential was mapped onto the calculated electron density surface. The corresponding harmonic vibration frequencies were computed at the same level to characterize the geometry as a minima.

3.4.16 [^{177}Lu(chelate)] Radiolabeling

For ^{177}Lu experiments, the ligands H_4octapa, DTPA, and DOTA were used. Aliquots of each ligand stock solution (1 mg / mL) were transferred to Corning® 2.0 mL self-standing micro-centrifuge tubes containing ~1.2 mCi of ^{177}Lu to a ligand concentration of ~180 μM, and made up to 1 mL with NaOAc buffer (10 mM, pH 5.0). H_4octapa and DTPA were each

allowed to react at ambient temperature for 10 minutes and DOTA was left for 1 hour at 90 °C to react. Radiometal complexes were then evaluated using radio-HPLC (linear gradient A: 0.1% TFA in H_2O, B: CH_3CN, 0 - 80% B over 30 minutes): $[^{177}Lu(octapa)]^-$ t_R = 5 min, >99%; $[^{177}Lu(DOTA)]^-$ t_R = 6.8 min, >99%, $[^{177}Lu(DTPA)]^{2-}$ t_R = 5.2 min, >99%. Radiolabeled ligands were then used for blood serum stability assays.

3.4.17 Trastuzumab antibody modification/thiourea bioconjugation

Trastuzumab (purchased commercially as Herceptin, Genentech, San Francisco, CA) was purified using centrifugal filter units with a 50000 molecular weight cutoff (Amicon® ultra centrifuge filters, Ultracel®-50: regenerated cellulose, Millipore Corp., Billerica, MA) and phosphate buffered saline (PBS, pH 7.4) to remove α-α-trehalose dihydrate, L-histidine, and polysorbate 20 additives. After purification, the antibody was taken up in PBS pH 7.4. Subsequently, 300 μL of antibody solution (150-250 μM) was combined with 100 μL PBS (pH 8.0), the pH of the resulting solution was adjusted to 8.8-9.0 with 0.1 M Na_2CO_3, and 4 equiv of the *p*-SCN-Bn-H_4octapa or *p*-SCN-Bn-DOTA were added in 10 μL DMSO. The reactions were incubated at 37 °C for 1 h, followed by centrifugal filtration to purify the resultant antibody conjugate. The final modified antibody stock solutions were stored in PBS (pH 7.4) at 4 °C.

3.4.18 ^{111}In- and ^{177}Lu-octapa/DOTA-trastuzumab radiolabeling

Aliquots of H_4octapa/DOTA-trastuzumab immunoconjugates were transferred to 2 mL microcentrifuge tubes and made up to 1 mL of ammonium acetate buffer (pH 5.5, 200 mM), and then aliquots of ^{177}Lu or ^{111}In were added (~2-3 mCi). The H_4octapa-trastuzumab

mixtures were allowed to react at room temperature for 15 minutes and then analyzed via iTLC, with an eluent of 50 mM EDTA (pH 5), confirming reproducible values >95% RCY. The DOTA-trastuzumab mixtures were heated to 37 ± 0.1 °C for 1 hour and then analyzed via iTLC with RCY ranging from ~50-90%. 30 μL of EDTA solution (50 mM, pH 5) was then added to the reaction mixture, and the resultant radiolabeled immunoconjugates were then purified using size-exclusion chromatography (Sephadex G-25 M, PD-10 column, 30 kDa, GE Healthcare; dead volume = 2.5 mL, eluted with 1 mL fractions of PBS, pH 7.4) and centrifugal column filtration (Amicon® ultra 50k). The radiochemical purity of the final radiolabeled bioconjugate was assayed by radio-iTLC and was found to be >99% in all preparations. In the iTLC experiments, ^{111}In- and ^{177}Lu-octapa/DOTA-trastuzumab remained at the baseline, while $^{177}Lu^{3+}/^{111}In^{3+}$ ions complexed as [^{111}In/^{177}Lu]-EDTA eluted with or near the solvent front.

3.4.19 Chelate number isotopic dilution assay

The number of accessible H_4octapa chelates conjugated to trastuzumab was measured by radiometric isotopic dilution assays following methods similar to those described by Anderson et al. and Holland et al.[285,290,344,345] The experimental procedure was modified to use ^{111}In and SKOV-3 ovarian cancer cells.[87] All experiments were performed in triplicate. Conjugating 4 equivalents of *p*-SCN-Bn-H_4octapa was found to yield 3.3 ± 0.1 accessible chelates per antibody. Aliquots of [^{111}In]$InCl_3$ (10 μL, <5 kBq [0.1 μCi]) were added to 12 solutions containing 1:2 serial dilutions of non-radioactive $In(NO_3)_3$ (aq.) (100 μL fractions; 100 – 0.05 nmol, pH 7.5 – 8.5). The mixture was vortexed for 30 s before adding aliquots of H_4octapa -trastuzumab (20 μL, 5.0 mg/mL, [100 μg of mAb, 0.7 nmol], in 0.9% sterile

saline). The reactions were incubated at room temperature for 1 h before quenching with EDTA (20 μL, 50 mM pH 7). The extent of complexation was assessed developing iTLC strips (EDTA, 50 mM) and counting the activity at the baseline and solvent front. The fraction of ^{111}In-radiolabeled mAb (Ab) was plotted versus the inverse of the number of nano-moles of In^{3+} and the number of chelates was calculated from the gradient by Equation 1, where *c* is the number of accessible chelates, *n*(mAb) is the amount of mAb (nmol), and *n*(In^{3+}) is the total number of In^{3+} added (nmol).[346]

$$c = A_b \cdot \frac{n(\mathrm{In})}{n(\mathrm{mAb})} \qquad \text{(equation 3.1)}$$

3.4.20 *In vitro* immunoreactivity assay

The immunoreactivity of the ^{111}In/^{177}Lu-octapa-trastuzumab and ^{111}In/^{177}Lu-DOTA-trastuzumab bioconjugates was determined using specific radioactive cellular-binding assays following procedures derived from Lindmo et al.[347,348] To this end, SKOV-3 cells were suspended in microcentrifuge tubes at concentrations of 5.0, 4.0, 3.0, 2.5, 2.0, 1.5, and 1.0 × 10^6 cells/mL in 500 μL PBS (pH 7.4). Aliquots of either ^{111}In/^{177}Lu-octapa-trastuzumab or ^{111}In/^{177}Lu-DOTA-trastuzumab (50 μL of a stock solution of 10 μCi in 10 mL of 1% bovine serum albumin in PBS pH 7.4) were added to each tube (n = 6; final volume: 550 μL), and the samples were incubated on a mixer for 60 min at room temperature. The treated cells were then pelleted via centrifugation (3000 rpm for 5 min), resuspended, and washed twice with cold PBS before removing the supernatant and counting the activity associated with the cell pellet. The activity data were background-corrected and compared with the total number

of counts in appropriate control samples. Immunoreactive fractions were determined by linear regression analysis of a plot of (total/bound) activity against (1/[normalized cell concentration]). No weighting was applied to the data, and data were obtained as n = 6.

3.4.21 [^{177}Lu(chelate)] Blood serum competition experiments

Frozen human blood serum was thawed for 30 minutes, and 750 μL aliquots were transferred to 2.0 mL Corning centrifuge vials. 300 μL of each ^{177}Lu(chelate) was transferred to 750 μL of blood serum, along with 450 μL of PBS to a total volume of 1.5 mL (n = 3 for each ligand). The final ^{177}Lu(chelate) concentration present in serum was ~36 μM. Serum competition samples were then incubated at 37 ± 0.1 °C with constant agitation (550 rpm) and analyzed via PD-10 size-exclusion column elution (filters MW < 5000 Da) at 1.5 hr and 24 hr time points and counted using a Capintec CRC-15R dose calibrator. 500 μL of each serum/^{177}Lu(chelate) competition solution (n = 3) was removed from the competition vial, diluted to 2.5 mL with PBS, and counted. The diluted aliquot of serum competition mixture was loaded onto a conditioned PD-10 column. The loading volume (2.5 mL) was eluted into radioactive waste, and then an additional 3.5 mL of PBS was loaded, collected, and counted in the dose calibrator as the serum-bound ^{177}Lu (non-chelate bound). Percent stability was reported as a percentage of ^{177}Lu still chelate-bound and not associated with serum proteins (MW < 5000 Da).

3.4.22 ^{111}In- and ^{177}Lu-octapa/DOTA-trastuzumab blood serum competition experiments

Frozen human blood serum was thawed for 30 minutes, and 300 μL aliquots were

transferred to 2.0 mL Corning centrifuge vials. A portion of radiolabeled immunoconjugate (~300 μCi) was transferred to the blood serum (n = 3 for each ligand). Serum competition samples were then incubated at 37 ± 0.1 °C with gentle agitation (300 rpm) and analyzed via iTLC with an EDTA eluent (50 mM, pH 5.0) (Bioscan AR-2000) at time points of 0, 24, 48, 72, 96, and 120 hours.

3.4.23 Cell culture

Human ovarian cancer cell line SKOV-3 was obtained from the American Tissue Culture Collection (ATCC, Bethesda, MD) and maintained in a 1:1 mixture of Dulbecco's Modified Eagle medium: F-12 medium, supplemented with 10% heat- inactivated fetal calf serum (Omega Scientific, Tarzana, Ca), 2.0 mM glutamine, nonessential amino acids, 100 units/mL penicillin, and 100 units/mL streptomycin in a 37 °C environment containing 5% CO_2. Cell lines were harvested and passaged weekly using a formulation of 0.25% trypsin/0.53 mM EDTA in Hank's Buffered Salt Solution without calcium and magnesium.

3.4.24 SKOV-3 xenograft mouse models

All experiments were performed under an Institutional Animal Care and Use Committee-approved protocol, and the experiments followed institutional guidelines for the proper and humane use of animals in research. Six- to eight-week-old athymic nu/nu female mice (NCRNU-M) were obtained from Taconic Farms Incorporated (Hudson, NY). Animals were housed in ventilated cages, were given food and water *ad libitum*, and were allowed to acclimatize for approximately 1 week prior to treatment. After several days, SKOV-3 tumours were induced on the right shoulder by a subcutaneous injection of 1.0×10^6 cells in

a 100 μL cell suspension of a 1:1 mixture of fresh media/BD Matrigel (BD Biosciences, Bedford, Ma).

3.4.25 ^{111}In- and ^{177}Lu-octapa/DOTA-trastuzumab biodistribution studies

Biodistribution studies were used to evaluate the 5-day stability and tumour uptake of the ^{111}In- and ^{177}Lu-octapa-trastuzumab preparations and were compared to the same system using the "gold standard" ^{111}In- and ^{177}Lu-DOTA-Trastuzumab. DOTA- and H_4octapa-trastuzumab constructs were radiolabeled with ^{111}In- and ^{177}Lu under the same conditions as described above and prepared for biodistribution and SPECT/CT imaging studies in nude athymic mice (female, 6-8 weeks old) bearing subcutaneous SKOV-3 ovarian cancer xenografts (HER2-positive, small with tumour size ~2-3 mm diameter). The radiolabeled immunoconjugates were purified via PD-10 size exclusion columns, followed by further purification and concentration via centrifuge filtration (Amicon® Ultra centrifuge filters, Ultracel®-50: regenerated cellulose, Millipore Corp., Billerica, MA). The purified immunoconjugates were suspended in sterile saline (0.9% NaCl) to a concentration and dose of ~30 μCi (1.1 MBq) in 200 μL per mouse. The specific activity of ^{111}In-octapa-trastuzumab was ~3.7 μCi/μg, and for ^{177}Lu-octapa-trastuzumab it was 3.3 μCi/μg. The specific activity of ^{111}In-DOTA-trastuzumab was ~ 2.0 μCi/μg, and for ^{177}Lu-DOTA-trastuzumab it was 3.4 μCi/μg. The amount of immunoconjugate injected per mouse was ~ 10-15 μg. Each mouse was intravenously injected through the tail vein and euthanized by CO_2 (g) asphyxiation at time points of 24, 48, 72, 96, and 120 hours (n = 4 per time point). Organs collected after sacrifice included blood, tumour, heart, lungs, liver, spleen, kidneys, large intestine, small intestine, muscle, bone (femur), and skin (ear). All organs were rinsed

in water after removal and air-dried for 5 minutes. Tissues were weighed and counted (calibrated for ^{111}In or ^{177}Lu), the counts were background- and decay-corrected from the time of injection and then converted to the percentage of injected dose (%ID) per gram of organ tissue (%ID/g). The radioactivity counts measured in each organ were converted to activity (μCi) using a calibration curve created from known standards of ^{111}In or ^{177}Lu.

3.4.26 ^{111}In- and ^{177}Lu-octapa/DOTA-trastuzumab SPECT/CT imaging studies

Mice with SKOV-3 ovarian cancer xenografts were imaged with ^{111}In (n = 2) and ^{177}Lu (n = 2) labeled immunoconjugates, using a four-headed NanoSPECT/CT®PLUS camera (Bioscan Inc., Washington DC, USA) with a multi-pinhole focused collimator and a temperature control animal bed unit (Minerve Equipment Veterinaire). Nine pinhole apertures with a diameter of 2.5 mm were used on each head, with a field of view (FOV) of 24 mm. Settings of the ^{111}In energy peaks were 245 and 171 keV, and the ^{177}Lu peaks were 208, 112, and 56 keV. A CT at 45 kVp was acquired (180 projections, pitch of 1). Based on the helical CT topogram, SPECT images were obtained over a range of 85 mm. For the octapa-based radioimmunoconjugates, the mice were administered with either ~550 μCi of ^{111}In-octapa-trasuzumab (specific activity ~3.7 μCi/μg) or ~450 μCi of ^{177}Lu-octapa-trastuzumab (3.3 μCi/μg) in 200 μL of sterile saline (0.9% NaCl) via intravenous tail vein injection. For the DOTA-based radioimmunoconjugates, the mice were administered with either ~400 μCi of ^{111}In-DOTA-trasuzumab (specific activity ~2.0 μCi/μg) or ~550 μCi of ^{177}Lu-octapa-trastuzumab (3.4 μCi/μg) in 200 μL of sterile saline (0.9% NaCl) via intravenous tail vein injection. The amount of immunoconjugate injected per mouse was ~ 150-200 μg. Approximately 5 minutes prior to SPECT/CT image acquisition, mice were

anesthetized via inhalation of 2% isoflurane/oxygen gas mixture (Baxter Healthcare, Deerfield, IL) and placed on the scanner bed. Anesthesia was maintained during imaging using a reduced 1.5% isoflurane/oxygen mixture. Animals were imaged at 24, 48, 72, 96, and 120 h p.i. Mice injected with ^{177}Lu-labeled immunoconjugates were imaged for 1.5-2 hours each, and mice injected with ^{111}In-labeled immunoconjugates were imaged for 40 min (24 and 48 h time points), 50 min (72 h), and 60 min (96 and 120 h). Image collection was performed using Nucline software (V1.02 build 009), and images were processed and reconstructed using InVivoScope (2.00 patch3, 64 bit) and HiSPECT (v 1.4.3049) software. To derive the isotope-specific calibration factors, a mouse-sized phantom filled with 1.5-2 mCi of $^{111}InCl_3$ or $^{177}LuCl_3$ was scanned.

3.4.27 Cerenkov luminescence imaging (CLI)

Optical images of Cerenkov radiation (CR) were obtained using an IVIS 200 (Caliper Life Sciences) optical imaging machine. This system uses a cryo-cooled charge-coupled device for high-sensitivity detection of low-intensity sources. Two-minute exposures were obtained of isoflurane anesthetized mice (n = 2) 24 hours post injection of ~450 μCi of ^{177}Lu-octapa-trastuzumab (3.3 μCi/μg) in 200 μL of sterile saline (0.9% NaCl) via intravenous tail vein injection. These experiments were performed with assistance from Dr. Daniel L. J. Thorek.

3.4.28 Statistics

All data used was obtained in at least triplicate (n = 3), and all values were expressed as mean ± S.D. A student's two-tailed t-test was used to compare all biodistribution data

sets. A p-value ≤ 0.05 was considered statistically significant. A one-way ANOVA analysis was also performed on select data points; a p-value ≤ 0.05 was considered statistically significant.

Chapter 4: High denticity ligands based on picolinic acid for ^{111}In radiochemistry

This chapter is an adaption of published work, and is reproduced in part, with permission from Price, E. W.; Ferreira, C. L.; Adam, M. J.; Orvig, C., High denticity ligands based on picolinic acid for In-111 radiochemistry. *Can. J. Chem.,* doi: 10.1139/cjc-2013-0542, **2014**.

4.1 Introduction

There are a number of ligands that perform adequately for radiolabeling with ^{111}In, such as DOTA,[68,97,114,117,119-124] CHX-A''-DTPA,[117,119,219-221] and the recent discovery H_4octapa.[87-89,118,304] A newly published acyclic ligand BPCA has also shown promise for fast ambient temperature radiolabeling with ^{111}In and strong *in vivo* stability.[1,282,283] Other than H_4octapa and BPCA, not many new ligands have been published for use with ^{111}In in recent years, with most efforts being focused on newer positron emission computed tomography (PET) isotopes such as ^{68}Ga.[1,2,4,6,7,9,28] As mentioned in previous chapters, macrocycles have traditionally been favored over acyclic ligands because they are generally more kinetically inert than acyclic ligands, largely as a result of their constrained geometries and partially pre-organized binding cavities.[58-62,94,97,119] The major drawbacks with macrocycles such as DOTA are the requisite heating (40-90 °C) and extended reaction times (30-180 min) needed for quantitative radiolabeling; these conditions are unsuitable for sensitive vectors such as antibodies.[58-65,94,97,119,127-129,142] The acyclic ligand diethylenetriaminepentaacetic acid (DTPA) (as with most acyclic ligands) exhibits much faster reaction kinetics than DOTA and

can radiolabel quantitatively in a matter of minutes at ambient temperature, but the resulting complexes are not nearly as stable *in vivo* as those of DOTA (Chapter 1).[60,61,215,216,312] New acyclic ligands with rapid ambient temperature radiolabeling kinetics, robust *in vivo* stability and inertness (compared to macrocycles such as DOTA), and a variety of physical properties (e.g. charge, denticity, donor atoms) are especially important for antibody vectors; these highly successful vectors are used for targeting a variety of cancers and cannot withstand the elevated reaction temperatures required for macrocycles such as DOTA.[60,61,215,216,312]

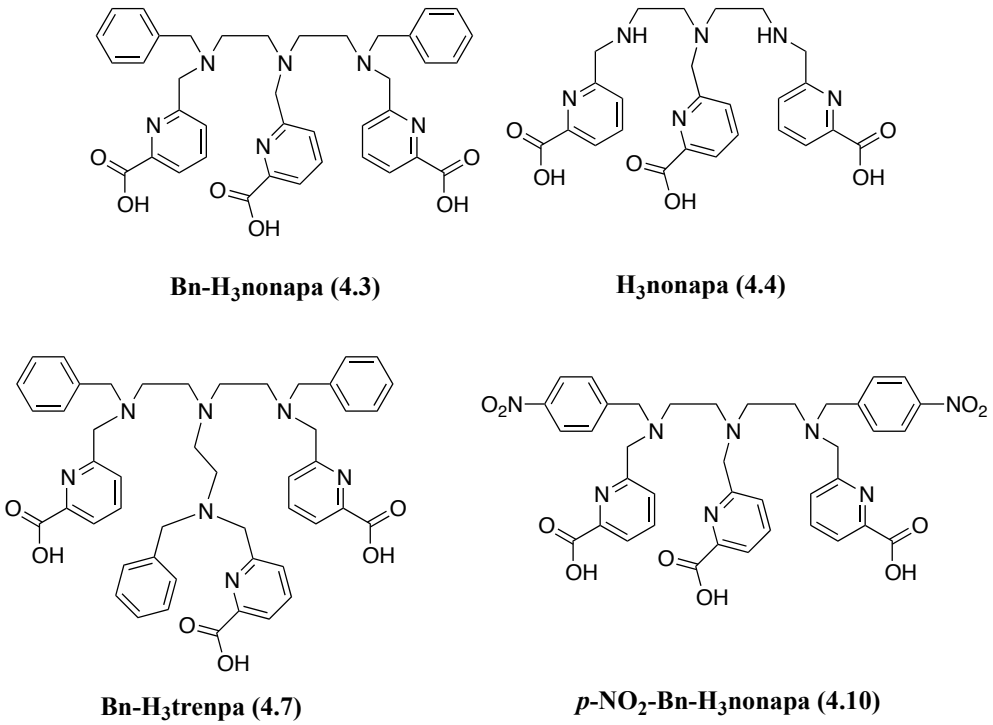

Bn-H_3nonapa (4.3)

H_3nonapa (4.4)

Bn-H_3trenpa (4.7)

***p*-NO_2-Bn-H_3nonapa (4.10)**

Figure 4.1 The new chelating ligands Bn-H_3nonapa, H_3nonapa, *p*-NO_2-Bn-H_3nonapa, and Bn-H_3trenpa.

In this Chapter are reported the synthesis of four new acyclic ligands based on picolinic acid. These ligands have denticities ranging from 9-10, and are based on either a

diethylenetriamine (dien) or tris(2-aminoethyl)amine (tren) backbone. The ligands Bn-H_3nonapa (**4.3**), H_3nonapa (**4.4**), *p*-NO_2-Bn-H_3nonapa (**4.10**), and Bn-H_3trenpa (**4.7**) have been synthesized and characterized for the first time (Figure 4.1). The non-radioactive In^{3+} complexes of ligands **4.3**, **4.4**, and **4.10** were synthesized and characterized. These ligands were also studied with the radiometal ion $^{111}In^{3+}$, and assessed by radiolabeling experiments and mouse serum stability assays.

4.2 Results and discussion

4.2.1 Synthesis and characterization

The four novel ligands Bn-H_3nonapa (**4.3**), H_3nonapa (**4.4**), *p*-NO_2-Bn-H_3nonapa (**4.10**), and Bn-H_3trenpa (**4.7**) were synthesized using the same general methods used for the original synthesis of the ligand H_2depda.[118,268,269,271] The amine-backbones diethylenetriamine (dien) and tris(2-aminoethyl)amine (tren) were chosen as platforms for assembling high-denticity derivatives of H_2dedpa and H_4octapa, although any permutation of these backbones could theoretically be used. Dien and tren were benzyl-protected via reductive amination with benzaldehyde to allow for controlled alkylation of bromopicolinic acid in subsequent steps (Schemes 4.1-4.3). After alkylation of bromopicolinc acid, benzyl groups could be removed via hydrogenation in glacial acetic acid, or benzyl groups could be retained by bypassing this step (Schemes 4.1-4.3). For the ligand H_3nonapa (**4.4**, Scheme 4.1), hydrogenation was performed to remove benzyl protecting groups, followed by deprotection by heating in HCl (12 M) or stirring with LiOH at ambient temperature.

Scheme 4.1 Synthesis of Bn-H_3nonapa (**4.3**) and H_3nonapa (**4.4**). [a]

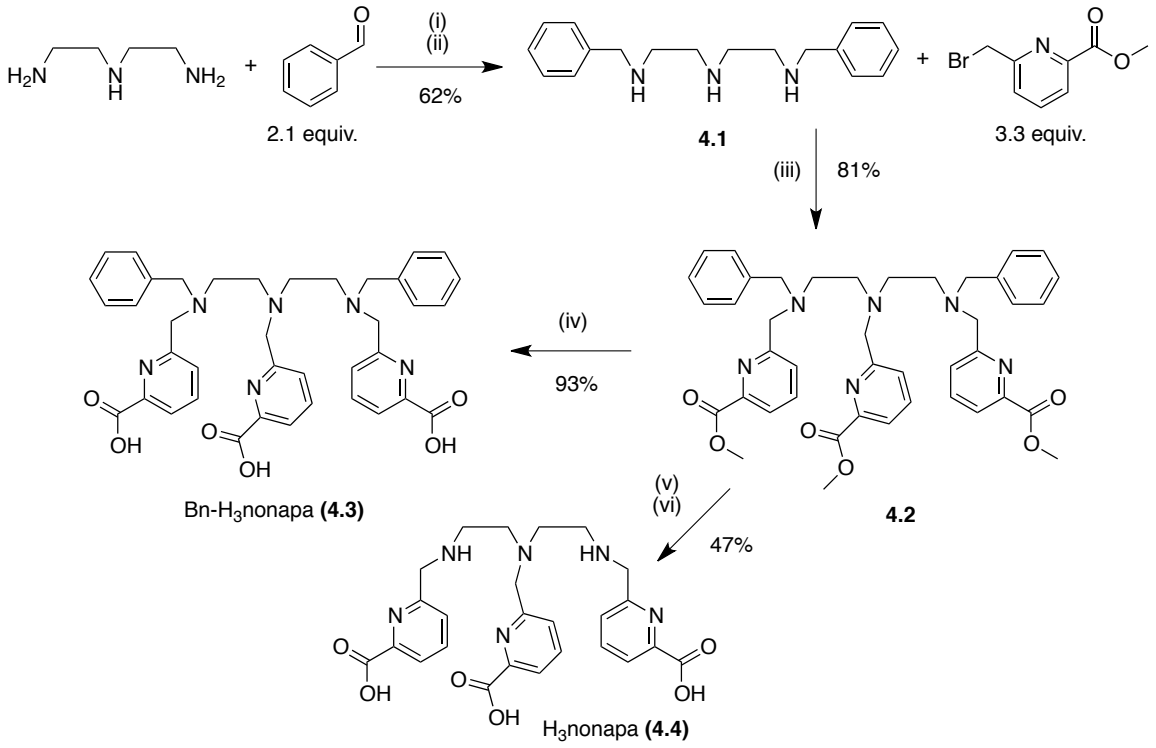

[a](i) MeOH, Ar (g), Δ, 2 h; (ii) MeOH, 0 °C, $NaBH_4$, 16 h; (iii) methyl-6-bromomethylpicolinate, CH_3CN, 60 °C, 20 h; (iv) THF:H_2O (3:1), LiOH, RT, 2 h; (v) AcOH, Pd/C (10 wt%), H_2 (g), RT, 16 h; (vi) HCl (12 M), Δ, 16 h.

Benzyl groups were used as placeholders for *p*-NO_2-benzyl groups (e.g. *p*-NO_2-Bn-H_3nonapa (**4.10**), Scheme 4.3), which have the potential to be transformed into *p*-SCN-benzyl groups to yield active bifunctional derivatives. Benzyl-isothiocyanate groups are commonly used for facile conjugation reactions to free primary amine groups (e.g. antibodies, peptides), forming stable thiourea bioconjugates. Although excess benzyl groups can result in undesirably high lipophilicity, this is only an issue for peptide conjugates, and will not be an issue when conjugated to large targeting vectors such as antibodies and nanoparticles. The cumulative yield obtained for H_3nonapa (**4.4**) was ~24% in 4 steps, which

was significantly lower than that for Bn-H_3nonapa which was synthesized in a cumulative yield of ~47% in 3 steps. This decreased yield is largely a result of a problem discussed in Chapter 2 for the synthesis of H_4octapa, where it was determined that hydrogenation conditions resulted in the cleavage of both benzyl and picolinic acid moieties, producing significant quantities of byproduct and substantially decreasing yields and complicating purification of final products.[89] This inefficiency was largely obviated in the synthesis of H_4octapa by not performing the hydrogenation reaction in the presence of the picolinic acid moiety; however, for the synthesis of the currently discussed ligands this was not possible.[89]

Scheme 4.2 Synthesis of Bn-H_3trenpa (**4.7**). [a]

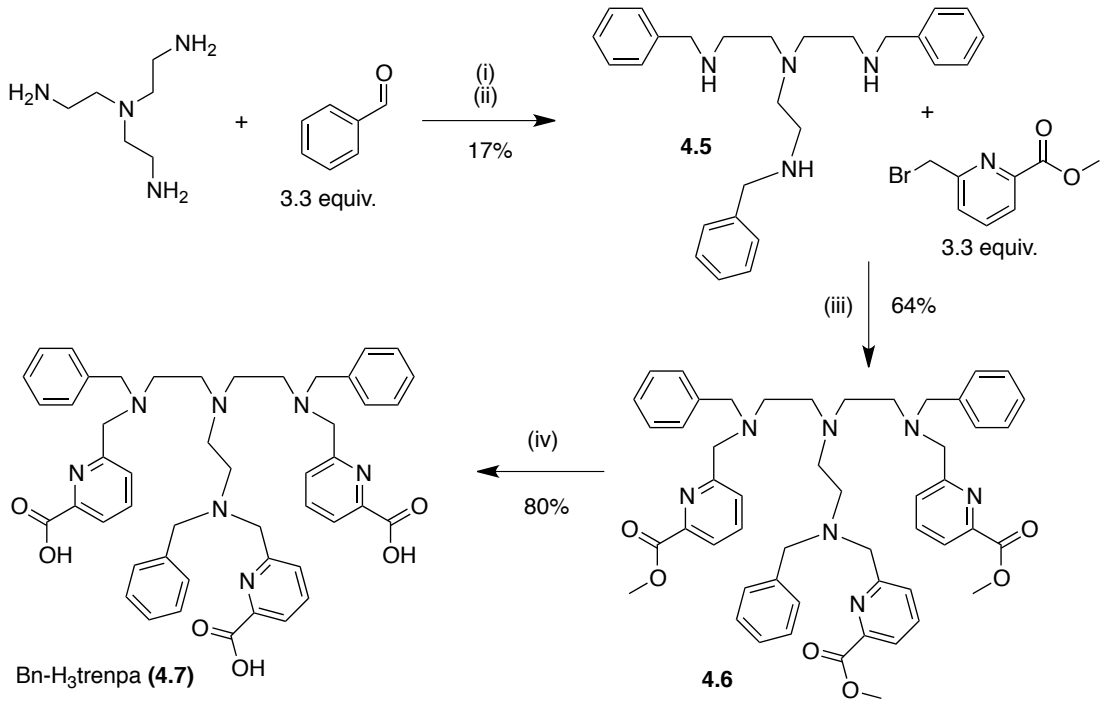

[a](i) MeOH, Ar (g), Δ, 2 h; (ii) MeOH, 0 °C, $NaBH_4$, 16 h; (iii) CH_3CN, 60 °C, 20 h; (iv) THF:H_2O (3:1), LiOH, RT, 2 h.

The synthesis of Bn-H_3trenpa (**4.7**) was more challenging than that of H_3nonapa (**4.4**)/Bn-H_3nonapa (**4.3**). During synthesis of Bn-H_3trenpa (**4.7**), the hydrogenation reaction was found to completely decompose the Bn-$(Me)_3$trenpa precursor (compound **4.6**, Scheme 4.2). In addition to cleaving benzyl and picolinic acid moieties from the tren backbone, it was also observed by mass spectrometry that hydrogenation conditions cleaved the ethylene bridges of tren. For this reason, the tren-based ligand, H_3trenpa, analogous to the dien-based ligand, H_3nonapa, could not be produced. Additionally, *p*-NO_2-Bn-H_3trenpa could not be synthesized, as the target ligand was found to be unstable and decomposed during synthesis. In light of the synthetic issues plaguing Bn-H_3trenpa (**4.7**), it was determined to be the least robust ligand of those presented in this work, and synthesis of a *p*-NO_2-Bn bearing bifunctional precursor was attempted but could not be completed, suggesting little potential of this TREN-based ligand system for use in ^{111}In radiopharmaceuticals.

Scheme 4.3 Synthesis of *p*-NO_2-Bn-H_3nonapa (**4.10**). [a]

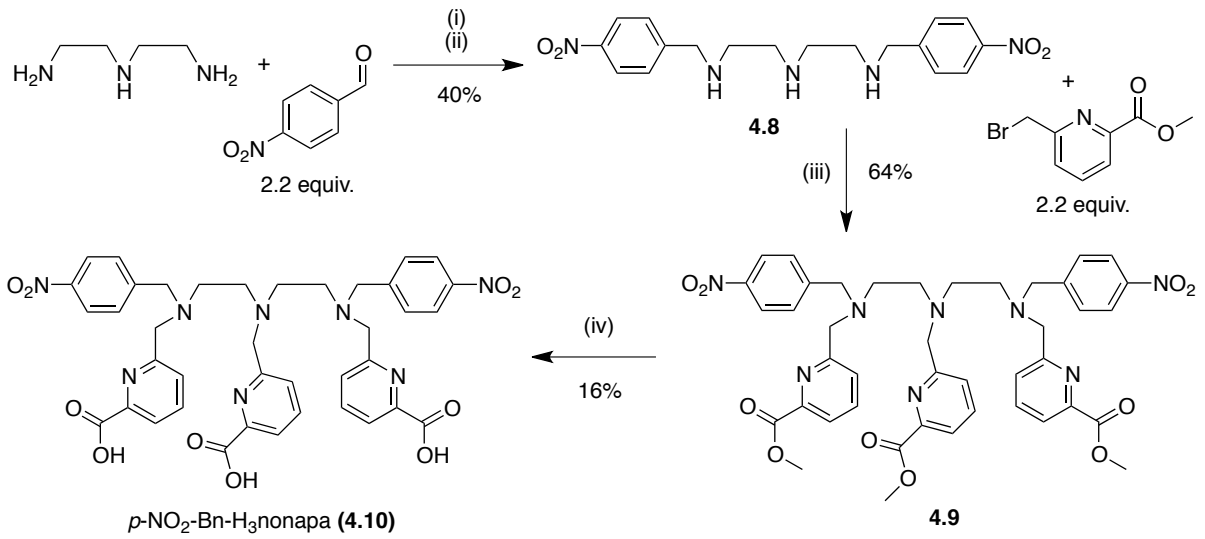

[a](i) MeOH, Ar (g), Δ, 2 h; (ii) MeOH, 0 °C, $NaBH_4$, 16 h; (iii) CH_3CN, 60 °C, 20 h; (iv) THF:H_2O (3:1), LiOH, RT, 2 h.

Ligand **4.10** (*p*-NO_2-Bn-H_3nonapa) was synthesized in the same manner as was Bn-H_3nonapa, with the only modification to the procedure being the substitution of *p*-NO_2-benzaldehyde for benzaldehyde in the initial reductive amination reaction. The *p*-NO_2-Bn functionality appeared to be more labile and sensitive to decomposition than the regular benzyl groups, decreasing yields and complicating purifications, to an extent that made synthesis unfeasible. Ligand **4.10** was produced in 3 synthetic steps with a low cumulative yield of ~4%, demonstrating the poor stability of the *p*-NO_2-Bn functionality, because the analogous synthesis of Bn-H_3nonapa (**4.3**) was also completed in 3 steps, albeit in yields of ~47%. The bifunctional precursor *p*-NO_2-Bn-H_3nonapa (**4.10**) was not transformed into the active isothiocyanate, although it can be expected that the requisite hydrogenation conditions would effect further decomposition and decreased yields. A synthetic methodology to circumvent the destructive effects of hydrogenation reactions on this system was previously determined, where instead of the *p*-NO_2-Bn groups, *tert*-butyl ester protected *p*-NH_2-Bn functionality was used successfully.[272] Should the radiolabeling efficiency and blood serum stability of these ligands with ^{111}In have been promising enough (*vide infra*), this synthetic revision could be applied to the presented ligands to produce more efficiently bifunctional derivatives.[272] If these ligands were to find purpose in the future with other radiometals (e.g. ^{177}Lu, $^{86/90}$Y, or ^{225}Ac), a combination of this *tert*-butyl ester protected *p*-NH_2-Bn functionality and the recently devised nosyl-protection strategy (Chapter 3) should provide reasonable synthetic access to fully bifunctional derivatives.[87,272,304]

4.2.2 Ligand-metal coordination

The ligands Bn-H_3nonapa (**4.3**), H_3nonapa (**4.4**), and Bn-H_3trenpa (**4.7**) were synthesized and obtained as their HCl salts, and mixed with indium perchlorate ($In(ClO_4)_3 \bullet 6H_2O$) to react under aqueous conditions (pH 4-5). The coordination complexes were confirmed via high-resolution mass spectrometry and nuclear magnetic resonance (NMR) spectroscopy. Coordination to In^{3+} was confirmed by significant changes in chemical shifts and coupling patterns in their NMR spectra (Figures 4.2-4.4). The NMR spectra of the indium complexes were obtained in DMSO-d_6, as the solubility of these neutral indium complexes was very poor in water and methanol. Because these ligands are designed with *in vivo* radiopharmaceutical applications in mind, their partial insolubility in water is not ideal; however, under the extremely dilute conditions used in radiochemistry, and when coupled to highly soluble targeting vectors such as peptides and antibodies, such insolubility can be overcome.[272] Additionally, highly stable but lipophilic compounds can sometimes be applied to cardiac perfusion imaging or passing the blood-brain-barrier, and so investigation into their stability is still warranted.[274]

The complex In(nonapa) (**4.12**) was the most soluble in water and provided the highest radiochemical yields with ^{111}In, and additionally demonstrated the highest stability in mouse serum (*vide infra*). It can be observed that the NMR spectra of the free ligands displayed sharp and well-resolved peaks, but upon coordination to In^{3+}, the ^1H NMR spectra became much more complicated and broad (Figures 4.2-4.4). In(Bn-nonapa) (**4.11**) displayed the most significant broadening of peaks, suggesting rapid fluxional isomerization in solution (Figure 4.3). The NMR spectrum of In(nonapa) (**4.12**) (Figure 4.2) became much more complicated with many new signals being observed compared to the free ligand, but the

NMR peaks still appeared sharp and well resolved, suggesting little fluxional isomerization, and a decrease in symmetry and/or the presence of multiple static isomers giving rise to a more complex spectrum.

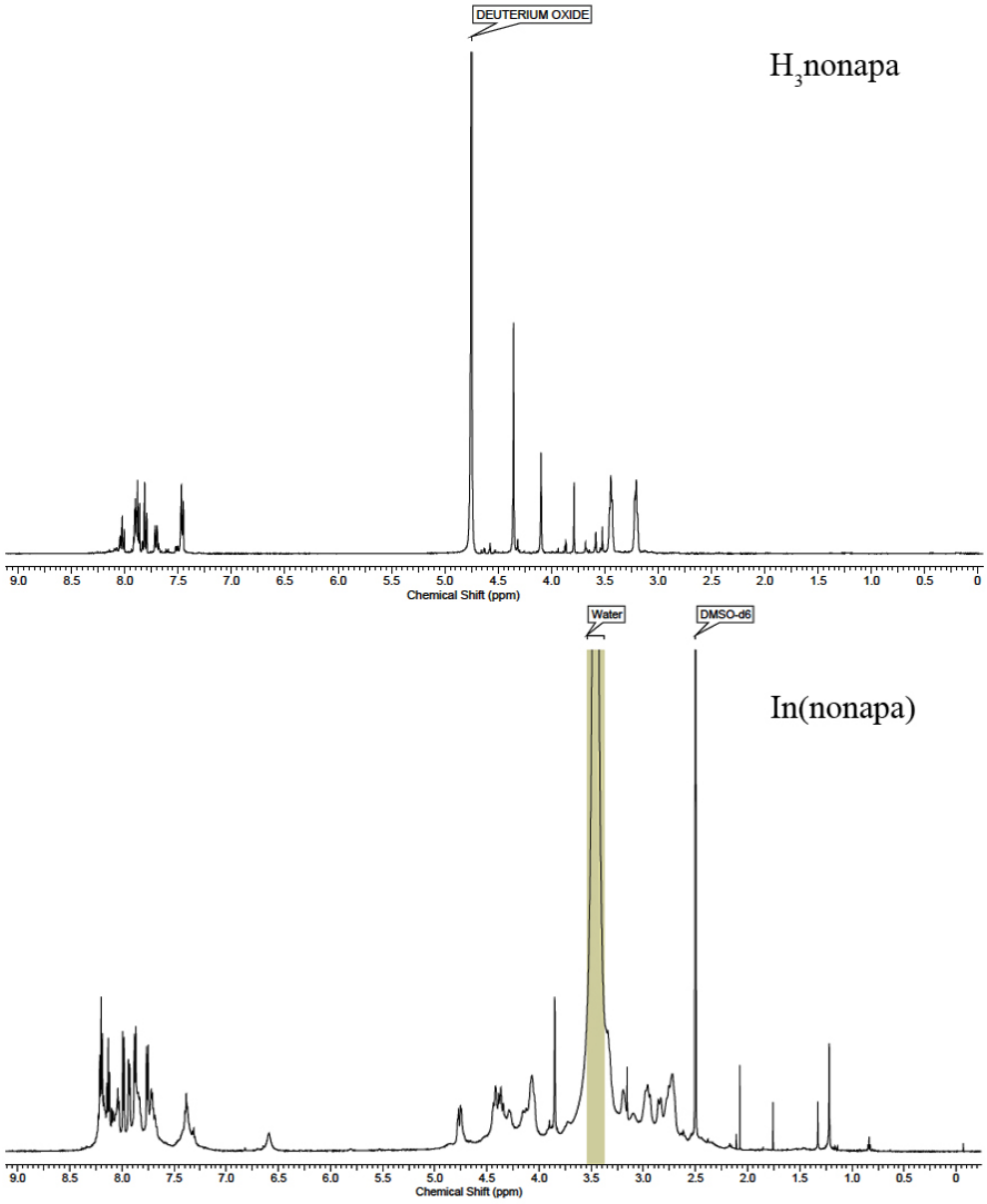

Figure 4.2 ^{1}H NMR spectra of H_3nonapa (**4.4**) (400 MHz, 25 °C, D_2O, top) and the In^{3+} complex In(nonapa) (**4.12**) (600 MHz, 25 °C, DMSO-d_6, bottom).

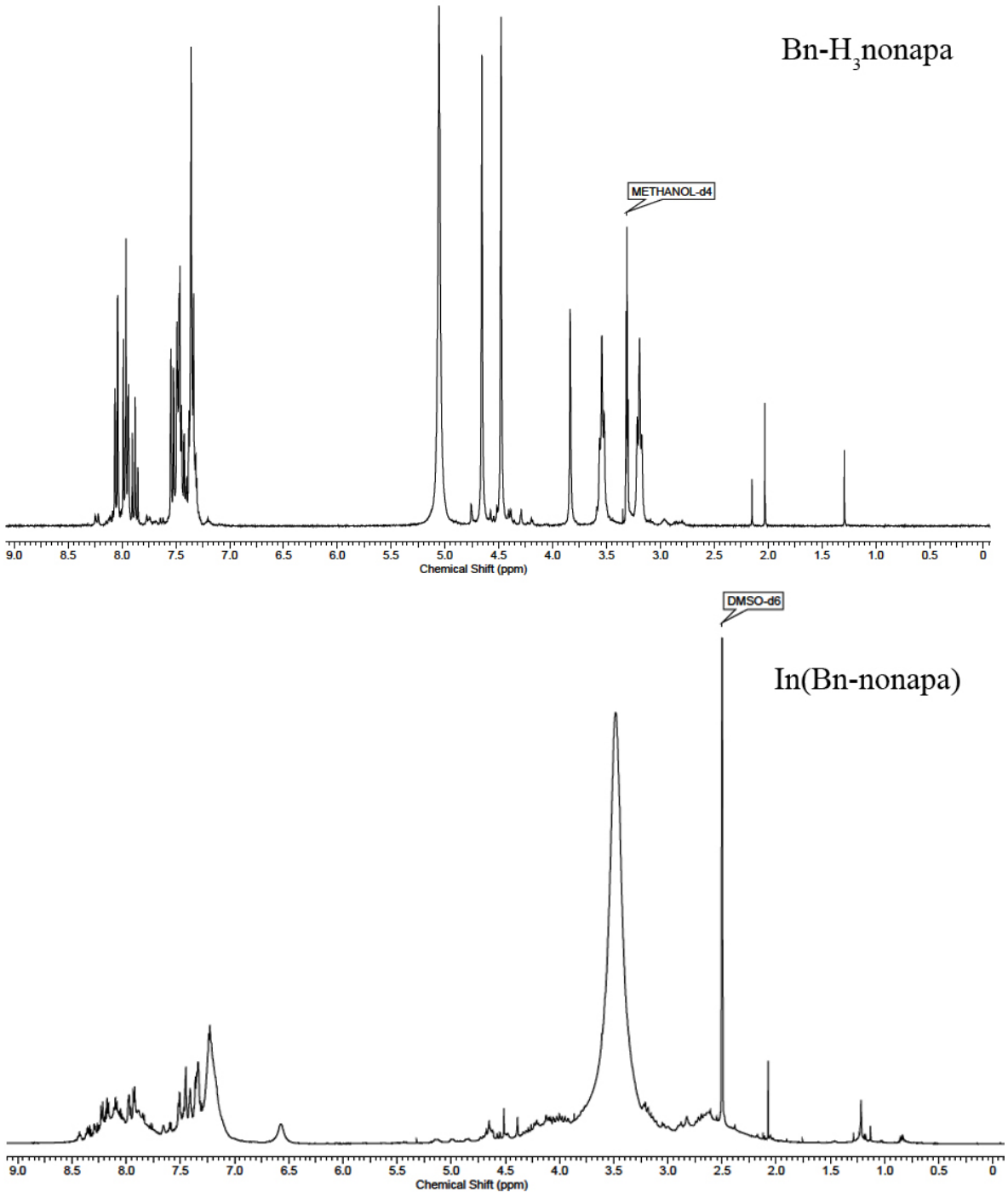

Figure 4.3 ^{1}H NMR spectra of Bn-H_3nonapa (**4.3**) (300 MHz, 25 °C, MeOD, top) and the In^{3+} complex In(Bn-nonapa) (**4.11**) (600 MHz, 25 °C, DMSO-d_6, bottom).

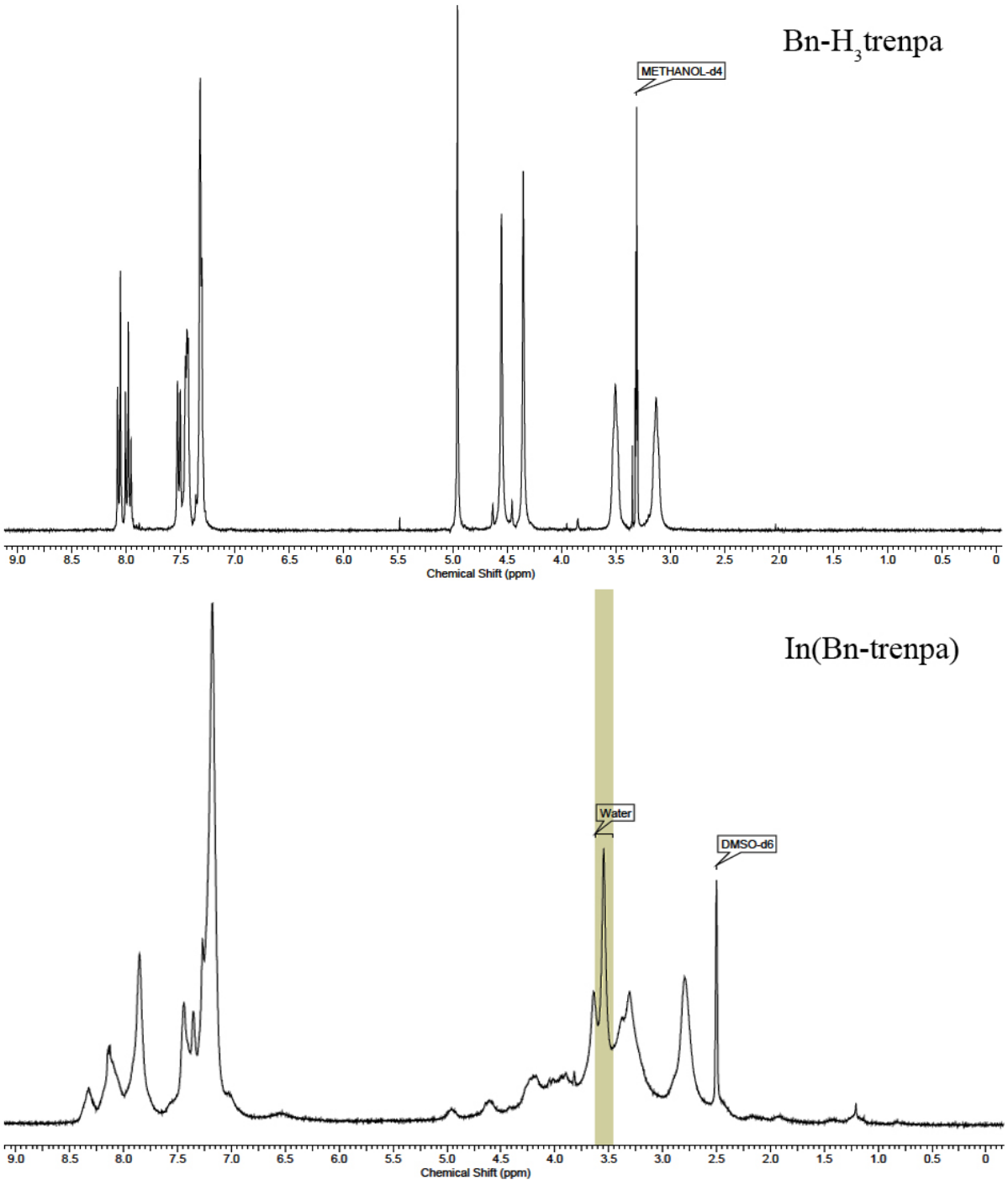

Figure 4.4 ^{1}H NMR spectra of Bn-H_3trenpa (**4.7**) (300 MHz, 25 °C, MeOD, top) and the In^{3+} complex In(Bn-trenpa) (**4.13**) (400 MHz, 25 °C, DMSO-d_6, bottom).

In(Bn-trenpa) (**4.13**, Figure 4.4) showed an NMR spectrum somewhere between those of In(nonapa) (**4.12**) and In(Bn-nonapa) (**4.11**), displaying many new signals, and broadening of signals to a lesser degree than that observed for In(Bn-nonapa) (**4.11**). Metal-ligand complexes that form highly symmetric complexes with no fluxional isomerization typically show much more simple NMR spectra than those observed here, as in the spectra obtained previously for $[Ga(dedpa)]^+$ and $[In(octapa)]^-$.[89,118] Although it is interesting to obtain a general idea of the behavior and isomerization of these complexes in solution, to assess properly their potential *in vivo* as radiopharmaceuticals they must be studied using radiolabeling and serum stability experiments.

4.2.3 ^{111}In radiolabeling and serum stability

The new acyclic ligands H_3nonapa (**4.4**), Bn-H_3nonapa (**4.3**), and Bn-H_3trenpa (**4.7**) were radiolabeled with ^{111}In under conditions similar to those used in Chapter 2 with the acyclic chelating ligand H_4octapa (NaOAc buffer, pH 4.5, RT).[89] It was found that the potentially nonadentate ligand H_3nonapa efficiently radiolabeled with ^{111}In, providing a radiochemical yield of ~97% after 10 minutes at ambient temperature (Table 4.1, Figure A.4). The benzylated derivative of H_3nonapa (Bn-H_3nonapa) achieved less optimal radiolabeling kinetics, with a still respectable yield of ~93% after 45 minutes at ambient temperature. The potentially decadentate, TREN-based ligand, Bn-H_3trenpa, displayed poor radiolabeling performance, with a radiochemical yield of only ~15% after 45 minutes at room temperature. Elevated temperatures may have increased the radiochemical yield of Bn-H_3trenpa beyond ~15%; however, the purpose of these acyclic ligands is to provide facile room temperature radiolabeling kinetics and so this eventuality was not explored.

Table 4.1 Radiolabeling experiments with ^{111}In and the novel acyclic ligands Bn-H_3nonapa (**4.3**), H_3nonapa (**4.4**), Bn-H_3trenpa (**4.7**), and results from the ligands H_2dedpa, H_4octapa, H_5decapa, DOTA, and DTPA (Chapters 2-3).[89]

Complex	Radiolabeling conditions	RCY [a] (%)	HPLC t_R (min)	Serum stability 1 h (%) [b]	Serum stability 24 h (%) [b]
[^{111}In(nonapa)]	pH 4.5, 10 min, RT	97	5.0	93.5 ± 0.4	44.5 ± 25.9
[^{111}In(Bn-nonapa)]	pH 4.5, 45 min, RT	93	8.9	27.0 ± 0.9	16.6 ± 0.4
[^{111}In(Bn-trenpa)]	pH 4.5, 45 min, RT	15	10.5	n/a	n/a
[^{111}In(dedpa)]$^{+}$	pH 4.5, 10 min, RT	99	5.9	96.1 ± 0.1	19.7 ± 1.5
[^{111}In(octapa)]$^{-}$	pH 4.5, 10 min, RT	99	4.7	93.8 ± 3.6	92.3 ± 0.1
[^{111}In(decapa)]$^{2-}$	pH 4.5, 10 min, RT	95	5.4	89.7 ± 1.6	89.1 ± 1.7
[^{111}In(DOTA)]$^{-}$	pH 4.5, 30 min, 90 °C	97	3.5	89.6 ± 2.1	89.4 ± 2.2
[^{111}In(DTPA)]$^{2-}$	pH 4.5, 10 min, RT	99	6.5	86.5 ± 2.2	88.3 ± 2.2

[a] Radiochemical yield.
[b] Blood serum stability results evaluated by PD-10 size-exclusion column elution.

Once radiolabeled with ^{111}In, the radiometal complexes were incubated with mouse blood serum as a transchelation challenge (e.g. to transferrin in serum) to estimate their *in vivo* inertness. ^{111}In(nonapa) demonstrated excellent stability in mouse serum after 1 hour of 93.5 ± 0.4%, but after 24 hours had undergone significant transchelation with only 44.5 ± 25.9% remaining intact (Figure 4.5). Of the three new ligands investigated, H_3nonapa was the most promising, with ^{111}In(Bn-nonapa) remaining only 16.6 ± 0.4% intact after 24 hours in mouse serum, and ^{111}In(Bn-trenpa) providing insufficient radiolabeling yields (~15%) to warrant evaluation by serum stability challenge. It was observed that the serum stability and radiolabeling efficiency were decreased for the ^{111}In complex of Bn-H_3nonapa compared to that of H_3nonapa (Table 4.1, Figure 4.5), suggesting that benzylating the secondary amines of H_3nonapa to tertiary amines with Bn-H_3nonapa may have resulted in weaker coordination to indium, which was therefore more easily transchelated by serum proteins. This is a trend that was observed for the gallium complex of H_2dedpa, where alkylating the secondary amines to

tertiary amines generally resulted in decreased stability and inertness to transchelation in *apo*-transferrin and serum stability challenges.[118,272,274] It is important to note that macro-scale synthesis of non-radioactive In(Bn-nonapa)] produced a water insoluble complex, and although poor solubility is expected to be less of a problem at the extremely dilute conditions used for radiolabeling with ^{111}In, it may have contributed to the inferior stability with ^{111}In by means of precipitation or non-specific association with serum proteins. In consideration of the superior radiolabeling and serum stability properties of the ligands studied in Chapters 2-3, H_4octapa, H_5decapa, DOTA, and DTPA, the three new ligands H_3nonapa (**4.4**), Bn-H_3nonapa (**4.3**), and Bn-H_3trenpa (**4.7**), were not investigated for *in vivo* applications with ^{111}In.[87,89] These new ligands may prove useful in the future for larger radiometals that could benefit from their high denticities, such as ^{177}Lu, $^{86/90}$Y, and ^{225}Ac.

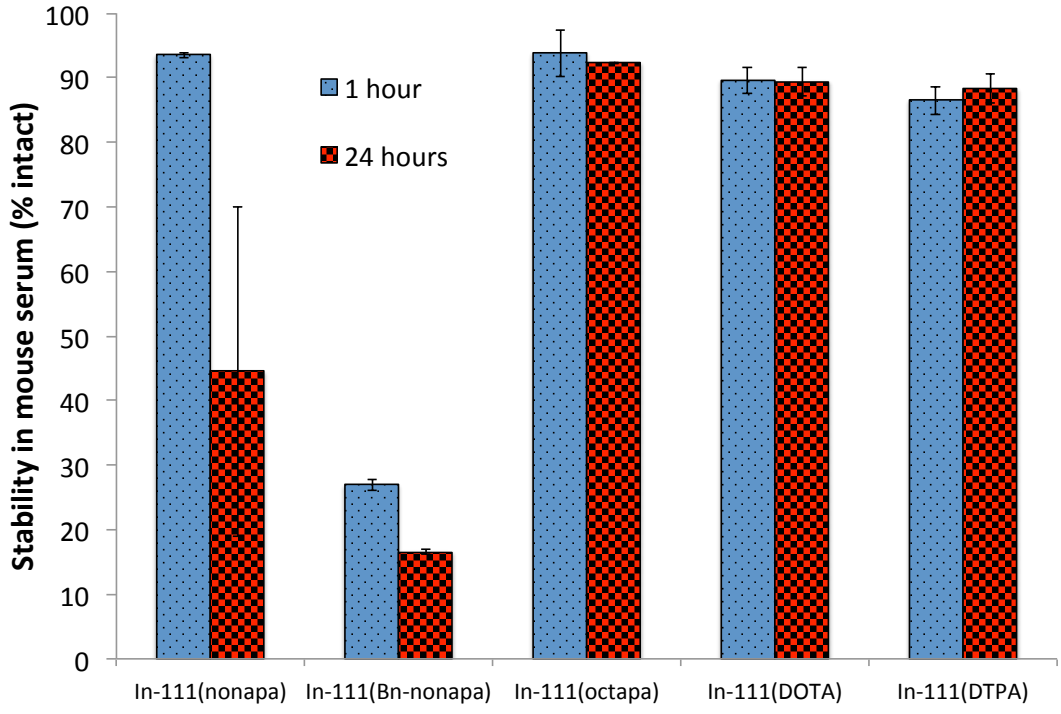

Figure 4.5 Mouse serum stability assay of $^{111}In^{3+}$ complexes of ligands from Table 4.1, determined after 1 and 24 h by PD-10 size-exclusion column elution.

4.3 Conclusions

The four new acyclic ligands Bn-H_3nonapa (**4.3**), H_3nonapa (**4.4**), *p*-NO_2-Bn-H_3nonapa (**4.10**), and Bn-H_3trenpa (**4.7**) were synthesized and studied with non-radioactive In^{3+}, and with radioactive $^{111}In^{3+}$. The coordination of these ligands to In^{3+} was confirmed by high-resolution mass spectrometry and nuclear magnetic resonance spectrometry. The ^{1}H NMR spectra of the complexes In(nonapa) (**4.12**), In(Bn-nonapa) (**4.11**), and In(Bn-trenpa) (**4.13**), revealed broad and complicated splitting patterns, suggesting low symmetry and/or fluxional isomerization, or the presence of multiple isomers in solution. The poor solubility of the In(Bn-nonapa) and In(Bn-trenpa) complexes in aqueous conditions was not promising for potential *in vivo* applications. Radiolabeling experiments were performed with $^{111}In^{3+}$, which demonstrated H_3nonapa (**4.4**) to be the most proficient ligand studied herein, achieving radiochemical yields of ~97% in 10 minutes at ambient temperature, and possessing stability to transchelation by mouse serum of 44.5 ± 25.9 % after 24 hours. Although the radiolabeling kinetics of H_3nonapa (**4.4**) were excellent, serum stability results were inferior to the previously studied ligands DOTA, DTPA, and H_4octapa, suggesting that these ligands are not robust enough for ^{111}In radiopharmaceutical applications. The ligand Bn-H_3nonapa (**4.3**) possessed poor radiolabeling properties with ^{111}In, requiring 45 minutes at ambient temperature to achieve radiochemical yields of ~93%, and demonstrated poor serum stability (16.6 ± 0.4 % after 24 hours). The ligand Bn-H_3trenpa (**4.7**) only achieved radiochemical yields of ~15% after 45 minutes at ambient temperature, which was deemed unacceptable for further study. Owing to the high denticity of these ligands (potentially 9-10 coordinate), they may hold value for study with large isotopes such as ^{177}Lu, $^{86/90}Y$, and ^{225}Ac.

4.4 Experimental methods

4.4.1 Materials and methods

Materials and methods follow those listed in Chapter 2 and 3, with the following changes. ^{111}In(chelate) mouse serum stability experiments were analyzed using GE Healthcare Life Sciences PD-10 desalting columns (size exclusion for MW < 5000 Da) and counted with a Capintec CRC 15R well counter. Radiolabeling of DOTA with ^{111}In was performed using a Biotage® Initiator microwave reactor (μW). Analyses of radiolabeled complexes were carried out using a Waters xbridge BEH130 C18 reverse phase (150 x 6 mm) analytical column on a Waters Alliance HT 2795 separation module equipped with a Raytest Gabi Star NaI (Tl) detector and a Waters 996 photodiode array (PDA) detector. ^{111}In was cyclotron produced (Advanced Cyclotron Systems, Model TR30) by proton bombardment through the reaction ^{111}Cd(*p,n*)^{111}In and was provided by Nordion as $^{111}InCl_3$ in 0.05 M HCl.

4.4.2 *N,N''*-[Benzyl]diethylenetriamine (4.1)

Diethylenetriamine (5.0 mL, 46.3 mmol) was added to dry methanol (distilled over CaH_2, 100 mL), followed by benzaldehyde (9.43 mL, 96.6 mmol), and the mixture heated to reflux for 2 hours under Ar. The reaction mixture was cooled (0 °C) in an ice bath, and $NaBH_4$ (12.2 g, 323 mmol) was added slowly and in small portions to control heat release. The reaction mixture was stirred overnight for ~16 hours at ambient temperature. The reaction mixture was concentrated *in vacuo* and then a saturated aqueous solution of $NaHCO_3$ (~100 mL) and chloroform (200 mL) was added. The aqueous layer was extracted twice more with dichloromethane (100 mL); the combined organic layers were dried over $MgSO_4$, filtered, and concentrated *in vacuo* to afford a yellow oil. The crude product was

purified by silica chromatography (CombiFlash R_f automated column system; 120 g HP silica; A: dichloromethane, B: methanol, A: gradient 100% to 40%) to afford **4.1** as yellow oil (8.15 g, 28.8 mmol, 62%). ^{1}H NMR (300 MHz, $CDCl_3$) δ: 7.33-7.24 (m, 10H, Bn-*H*), 3.80 (s, 4H, Bn-C*H*$_2$-N), 2.75 (m, 8H, ethylene-*H*), 1.44 (s, 3H, -N*H*-). ^{13}C NMR (75 MHz, $CDCl_3$) δ: 140.2, 129.7, 129.1, 128.6, 128.3, 127.3, 55.1, 53.7, 44.7. HR-ESI-MS calcd. for $[C_{18}H_{25}N_3 + H]^+$: 284.2127; found $[M + H]^+$: 284.2133, PPM = 2.1.

4.4.3 *N,N''*-[(Benzyl)-*N,N',N''*-[(6-methoxycarbonyl)pyridin-2-yl)methyl]-diethylenetriamine (4.2)

To a solution of **4.1** (260 mg, 0.917 mmol) and sodium carbonate (excess, ~500 mg) in dry acetonitrile (distilled over CaH_2, 10 mL) was added methyl-6-bromomethylpicolinate (synthesized according to a literature procedure)[89] (654 mg, 2.84 mmol). The resulting solution was stirred at 60 °C for 20 hours under Ar. Sodium carbonate was removed by filtration and the solvent was removed *in vacuo*. The crude product was purified by silica chromatography (CombiFlash R_f automated column system; 40 g HP silica; A: dichloromethane, B: methanol, A: gradient 100% to 20%) to afford **4.2** as yellow oil (541 mg, 0.741 mmol, 81%). ^{1}H NMR (300 MHz, $CDCl_3$) δ: 7.90-7.88 (m, 3H), 7.67-7.65 (m, 4H), 7.20-7.13 (m, 10H, Bn), 3.91 (s, 9H), 3.75 (s, 4H, Pic-C*H*$_2$-N), 3.71 (s, 2H, (Pic-C*H*$_2$-N), 3.50 (s, 4H, Bn-C*H*$_2$-N), 2.54 (m, 8H, dien-*H*). ^{13}C NMR (75 MHz, $CDCl_3$) δ: 165.5, 160.8, 146.7, 138.6, 136.9, 128.3, 127.9, 126.7, 126.5, 123.2, 60.8, 60.2, 58.9, 52.5, 51.8. HR-ESI-MS calcd. for $[C_{42}H_{46}N_6O_6 + H]^+$: 731.3557; found $[M + H]^+$: 731.3549, PPM = -1.1.

4.4.4 Bn-H_3nonapa, *N,N''*-[(Benzyl)-*N,N',N''*-[(6-carboxy)pyridin-2-yl)methyl]-diethylenetriamine (4.3)

To a solution of **4.2** (375 mg, 0.513 mmol) in a mixture of tetrahydrofuran and deionized water (3:1, 5 mL) was added LiOH (300 mg). The reaction mixture was stirred at ambient temperature for 2 hours. A portion of HCl was added (5 mL, 6 M), and then the mixture was reduced to dryness *in vacuo*. The mixture was dissolved in deionized water (4 mL) and purified via semi-preparative reverse-phase HPLC (10 mL/min, gradient: A: 0.1% TFA (trifluoroacetic acid) in deionized water, B: CH_3CN 5 to 100% B linear gradient in 25 min. t_R = 16 min, broad). Product fractions were pooled, concentrated *in vacuo,* dissolved in HCl (5 mL, 6 M), and then concentrated *in vacuo* again to remove trifluoroacetic acid. The HCl salt Bn-H_3nonapa•4HCl•H_2O **(4.3)** was obtained as a light yellow solid (330.3 mg, 93%, using the molecular weight of the HCl salt as determined by elemental analysis). ^{1}H NMR (300 MHz, MeOD) δ: 8.05 (d, *J* = 7.8 Hz, 2H), 7.99-7.94 (m, 3H), 7.88 (t, *J* = 7.7 Hz, 1H) 7.54-7.42 (m, 3H), 7.38-7.30 (m, 10H), 4.66 (s, 4H), 4.48 (s, 4H), 3.84 (s, 2H), 3.54 (m, 4H, dien-*H*), 3.19 (m, 4H, dien-*H*). ^{13}C NMR (75 MHz, $CDCl_3$) δ: 165.8, 164.6, 151.7, 150.7, 146.9, 146.2, 145.7, 141.9, 139.8, 131.7, 130.3, 129.2, 129.1, 128.8, 128.4, 127.7, 125.8, 125.2, 59.7, 56.8, 56.3, 49.6, 49.5. HR-ESI-MS calcd. for $[C_{39}H_{40}N_6O_6 + H]^+$: 689.3088; found $[M + H]^+$: 689.3077, PPM = -1.5. Elemental analysis: calcd % for Bn-H_3nonapa•4HCl•H_2O ($C_{39}H_{40}N_6O_6$•4HCl•H_2O = 852.562): C 54.94, H 5.44, N 9.86; found: C 55.21 (Δ = 0.27), H 5.65 (Δ = 0.21), N 9.54 (Δ = 0.32).

4.4.5 H_3nonapa, *N,N',N''*-[(6-carboxy)pyridin-2-yl)methyl]-diethylenetriamine (4.4)

To a solution of **4.2** (60.0 mg, 0.0822 mmol) in glacial acetic acid (10 mL) was added Pd/C (6 mg, ~10 wt%). Hydrogen gas was purged and vented for 3 minutes through the reaction mixture, which was then stirred under a hydrogen atmosphere (balloon) for 16 hours. The Pd/C was filtered out on a fine fritted glass filter and rinsed with HCl (3 M) and acetonitrile; the filtrate was then evaporated to dryness *in vacuo*. The crude product was deprotected without further purification by adding HCl (10 mL, 12 M) and heating for 16 hours. The reaction mixture was concentrated *in vacuo*, dissolved in deionized water (4 mL) and purified via semi-preparative reverse-phase HPLC (10 mL/min, gradient: A: 0.1% TFA (trifluoroacetic acid) in deionized water, B: CH_3CN. 5 to 100% B linear gradient in 25 min. t_R = 8.1 min, broad). Product fractions were pooled, concentrated *in vacuo,* dissolved in HCl (5 mL, 6 M), and then concentrated *in vacuo* again to remove trifluoroacetic acid. The HCl salt of H_3nonapa **(4.4)** was obtained as a light yellow solid (17.3 mg, 47%). ^{1}H NMR (400 MHz, D_2O) δ: 8.05-8.01 (m, 1H), 7.91-7.86 (m, 3H), 7.84-7.80 (m, 2H), 7.72-7.70 (m, 1H), 7.47-7.45 (m, 2H), 4.36 (s, 4H), 4.10 (s, 2H), 3.44 (m, 4H), 3.21 (m, 4H). ^{13}C NMR (100 MHz, D_2O) δ: 168.0, 166.6, 163.3, 162.9, 157.8, 151.1, 147.7, 147.5, 146.9, 141.0, 139.6, 129.9, 129.5, 127.4, 126.7, 125.5, 125.1, 124.7, 57.1, 52.0, 50.6, 45.6. HR-ESI-MS calcd. for $[C_{25}H_{28}N_6O_6 + H]^+$: 509.2149; found $[M + H]^+$: 509.2144, PPM = -0.9.

4.4.6 *N,N',N''*-Tris[benzyl]ethylamine (4.5)

Tris(2-aminoethyl)amine (tren) (2.0 mL, 13.4 mmol) was added to dry methanol (distilled over CaH_2, 25 mL), followed by benzaldehyde (3.92 mL, 44.1 mmol), and the mixture heated to reflux for 2 hours under Ar. The reaction mixture was cooled (0 °C) in an

ice bath, and $NaBH_4$ (4.10 g, 107 mmol) was added slowly and in small portions to prevent boiling. The reaction mixture was stirred overnight for ~16 hours at ambient temperature. The reaction mixture was concentrated *in vacuo* and then a saturated aqueous solution of $NaHCO_3$ (~100 mL) and chloroform (100 mL) was added. The aqueous layer was extracted twice more with dichloromethane (100 mL), the combined organic layers were dried over $MgSO_4$, filtered, and concentrated *in vacuo* to afford a yellow solid. The crude product was purified by silica chromatography (CombiFlash R_f automated column system; 120 g HP silica; A: dichloromethane with 0.5% triethylamine, B: methanol, A: gradient 100% to 50%) to afford **4.5** as orange oil (938 mg, 2.25 mmol, 17%). The product streaked very badly on the column, and significant yield was lost. ^{1}H NMR (300 MHz, $CDCl_3$) δ: 7.25 (m, 15H, Bn-*H*), 3.71 (s, 6H, Bn-C*H*$_2$-N), 3.24 (s, 3H, -N*H*), 2.64-2.56 (m, 12H, dien-*H*). ^{13}C NMR (75 MHz, $CDCl_3$) δ: 139.1, 127.9, 127.8, 126.6, 53.5, 53.1, 46.4. HR-ESI-MS calcd. for $[C_{27}H_{36}N_4 + H]^+$: 417.3018; found $[M + H]^+$: 417.3018, PPM = 0.

4.4.7 *N,N',N''*-Tris[benzyl]-tris[(6-methoxycarbonyl)pyridin-2-yl)methyl]ethyl-amine (4.6)

To a solution of **4.5** (299 mg, 0.717 mmol) and sodium carbonate (excess, ~1 g) in dry acetonitrile (distilled over CaH_2, 10 mL) was added methyl-6-bromomethylpicolinate (synthesized according to a literature procedure)[89] (495 mg, 2.15 mmol). The solution was stirred at 60 °C for 20 hours under Ar. Sodium carbonate was removed by filtration and the solvent was removed *in vacuo*. The crude product was purified by silica chromatography (CombiFlash R_f automated column system; 80 g HP silica; A: hexanes, B: ethyl acetate, A: gradient 100% to 0%) to afford **4.6** as orange oil (394 mg, 0.456 mmol, 64%). ^{1}H NMR

(300 MHz, $CDCl_3$) δ: 7.96-7.93 (m, 3H), 7.72-7.70 (m, 6H), 7.28-7.18 (m, 15H), 3.97 (s, 9H, methyl ester), 3.78 (s, 6H), 3.51 (s, 6H), 2.46 (m, 12H). ^{13}C NMR (75 MHz, $CDCl_3$) δ: 165.7, 161.1, 146.9, 138.9, 137.1, 128.5, 128.1, 126.9, 125.6, 123.3, 60.4, 59.0, 52.9, 52.7, 51.9. HR-ESI-MS calcd. for $[C_{51}H_{57}N_7O_6 + H]^+$: 864.4449; found $[M + H]^+$: 864.4466, PPM = 2.0.

4.4.8 Bn-H_3trenpa, *N,N',N''*-Tris[benzyl]-tris[(6-carboxy)pyridin-2-yl)methyl] ethyl-amine (4.7)

To a solution of **4.6** (237 mg, 0.274 mmol) in a mixture of tetrahydrofuran : deionized water (3:1, 5 mL) was added LiOH (170 mg). The reaction mixture was stirred at ambient temperature for 2 hours. A portion of HCl was added (5 mL, 6 M), and then the mixture was reduced to dryness *in vacuo*. The solid was dissolved in deionized water (4 mL) and purified via semi-preparative reverse-phase HPLC (10 mL/min, gradient: A: 0.1% TFA (trifluoroacetic acid) in deionized water, B: CH_3CN. 5 to 100% B linear gradient in 25 min. t_R = 17.7 min, broad). Product fractions were pooled, concentrated *in vacuo,* dissolved in HCl (5 mL, 6 M), and then concentrated *in vacuo* again to remove trifluoroacetic acid. The HCl salt Bn-H_3trenpa•6HCl **(4.7)** was obtained as a yellow solid (229 mg, 0.220 mmol, 80%, using the molecular weight of the HCl salt as determined by elemental analysis). ^{1}H NMR (300 MHz, MeOD) δ: 8.08-7.96 (m, 6H), 7.53-7.43 (m, 9H), 7.36-7.31 (m, 9H), 4.55 (s, 6H), 4.35 (s, 6H), 3.51 (m, 6H, ethylene-*H*), 3.13 (m, 6H, ethylene-*H*). ^{13}C NMR (75 MHz, MeOD) δ: 167.1, 151.9, 151.8, 148.3, 148.2, 140.9, 140.8, 132.8, 132.7, 131.4, 131.4, 130.5, 130.4, 130.3, 128.7, 126.6, 126.4, 60.8, 60.3, 57.1, 56.9, 51.7. HR-ESI-MS calcd. for $[C_{48}H_{51}N_7O_6 + H]^+$: 822.3979; found $[M + H]^+$: 822.3977, PPM = -0.3. Elemental analysis:

calcd % for Bn-H_3trenpa•6HCl ($C_{16}H_{18}N_4O_4$•6HCl = 1040.097): C 55.4, H 5.52, N 9.42; found: C 55.50 (Δ = 0.10), H 5.83 (Δ = 0.31), N 9.64 (Δ = 0.22).

4.4.9 *N,N''*-(*p*-Nitrobenzyl)diethylenetriamine (4.8)

Diethylenetriamine (0.775 mL, 7.18 mmol) was added to dry methanol (distilled over CaH_2, 15 mL), followed by *p*-4-nitrobenzaldehyde (2.17 mg, 14.4 mmol), and the mixture heated to reflux for 2 hours. The reaction mixture was cooled (0 °C) in an ice bath, and $NaBH_4$ (2.72 g, 71.8 mmol) was added slowly and in small portions to prevent boiling. The reaction mixture was stirred overnight for ~16 hours at ambient temperature. The reaction mixture was concentrated *in vacuo* and then a saturated aqueous solution of $NaHCO_3$ (~50 mL) and chloroform (50 mL) was added. The aqueous layer was extracted twice more with dichloromethane (50 mL), the combined organic layers were dried over $MgSO_4$, filtered, and concentrated *in vacuo* to afford an orange oil. The crude product was purified by silica chromatography (CombiFlash R_f automated column system; 80 g HP silica; A: dichloromethane, B: methanol, A: gradient 100% to 40%) to afford **4.8** as a yellow oil (1.07 g, 2.87 mmol, 40%). ^{1}H NMR (300 MHz, $CDCl_3$) δ: 8.14-8.11 (m, 4H, NO_2-Bn-*H*), 7.49-7.47 (m, 4H, NO_2-Bn-*H*), 3.88 (s, 4H), 2.73 (s, 8H), 1.71 (s, 3H, -N*H*-). ^{13}C NMR (75 MHz, $CDCl_3$) δ: 148.3, 146.8, 128.4, 123.4, 53.0, 49.5, 48.8. HR-ESI-MS calcd. for $[C_{18}H_{23}N_5O_4 + H]^+$: 374.1828; found $[M + H]^+$: 374.1829, PPM = 0.2.

4.4.10 *N,N''*-[(*p*-Nitrobenzyl)-*N,N',N''*-[(6-methoxycarbonyl)pyridin-2-yl)methyl]-diethylenetriamine (4.9)

To a solution of **4.8** (92.1 mg, 0.246 mmol) and sodium carbonate (excess, ~300 mg) in dry acetonitrile (distilled over CaH_2, 10 mL) was added methyl-6-bromomethyl picolinate (synthesized according to a literature procedure)[89] (170.2 mg, 0.739 mmol). The solution was stirred at 60 °C for 20 hours under Ar. Sodium carbonate was removed by filtration and the solvent was removed *in vacuo*. The crude product was purified by silica gel chromatography (CombiFlash R_f automated column system; 40 g HP silica; A: dichloromethane, B: methanol, A: gradient 100% to 20%) to afford **4.9** as orange oil (130 mg, 0.158 mmol, 64%). ^{1}H NMR (300 MHz, $CDCl_3$) δ: 8.08-8.04 (m, 4H), 7.95-7.91 (m, 3H), 7.76-7.71 (m, 2H), 7.65-7.57 (m, 3H), 7.44-7.40 (m, 5H), 3.95 (s, 6H, methyl ester), 3.94 (s, 3H, methyl ester), 3.78 (s, 4H), 3.75 (s, 2H), 3.63 (s, 4H), 2.62-2.58 (m, 8H, dien-*H*). ^{13}C NMR (75 MHz, $CDCl_3$) δ: 165.5, 160.4, 159.9, 147.2, 146.9, 146.9, 137.4, 137.1, 129.0, 125.6, 123.6, 123.6, 123.5, 123.4, 123.3, 60.8, 60.3, 58.3, 52.8, 52.3. HR-ESI-MS calcd. for $[C_{42}H_{44}N_8O_{10} + H]^+$: 821.3259; found $[M + H]^+$: 821.3268, PPM = 1.1.

4.4.11 *p*-NO_2-Bn-H_3nonapa, *N,N''*-[(*p*-Nitrobenzyl)-*N,N',N''*-[(6-carboxy)pyridin-2-yl)-methyl]diethylenetriamine (4.10)

To a solution of **4.9** (130 mg, 0.158 mmol) in a mixture of tetrahydrofuran : deionized water (3:1, 5 mL) was added LiOH (150 mg). The reaction mixture was stirred at ambient temperature for 2 hours. A portion of HCl was added (5 mL, 6 M), and then the mixture was reduced to dryness *in vacuo*. The mixture was dissolved in deionized water (4 mL) and purified via semi-preparative reverse-phase HPLC (10 mL/min, gradient: A: 0.1%

TFA (trifluoroacetic acid) in deionized water, B: CH_3CN. 5 to 100% B linear gradient in 25 min. t_R = 18 min, broad). Product fractions were pooled, concentrated *in vacuo,* dissolved in HCl (5 mL, 6 M), and then concentrated *in vacuo* again to remove trifluoroacetic acid. The product *p*-NO_2-Bn-H_3nonapa **(4.10)** was obtained as a light/orange solid (20 mg, 16%). Due to instability and decomposition, elemental analysis and ^{13}C NMR were not obtained. Further work with this scaffold has not been undertaken due to instability. ^1H NMR (300 MHz, D_2O) δ: 8.03-7.79 (m, 10H), 7.55-7.45 (m, 7H), 4.56 (s, 4H), 4.41 (s, 4H), 3.81 (s, 2H), 3.48-3.44 (m, 4H, dien-*H*), 3.15-3.10 (m, 4H, dien-*H*).

4.4.12 [In(Bn-nonapa)] (4.11)

Bn-H_3nonapa•4HCl•1H_2O (**4.3**) (10.0 mg, 0.0117 mmol) and $In(ClO_4)_3$•6H_2O (8.00 mg, 0.0153 mmol) were dissolved in HCl (aq) (1 mL, 0.1 M) in a 20 mL screw cap vial. The pH was adjusted to ~4.5 with NaOH (aq) (0.1 M) with stirring. The reaction mixture was stirred at 60 °C for 1 h, then evaporated to dryness to afford [In(Bn-nonapa)] **(4.11)** as a white solid in quantitative yield. The reaction mixture turned cloudy white during the reaction, as the insoluble and neutrally charged metal complex formed. ^1H NMR (600 MHz, DMSO-d_6) δ: 8.45-8.7.6 (broad m, 9H, pyr-*H*), 7.52-7.23 (broad m, 10H, benzyl-*H*), 4.65-3.70 (broad m, 8H), 3.30-2.55 (broad m, 8H), 2.45-2.10 (broad m, 2H). ^{13}C NMR (150 MHz, DMSO-d_6) δ: 166.2, 164.2, 153.8, 153.2, 153.1, 148.0, 147.8, 147.7, 147.6, 147.5, 142.1, 139.2, 138.4, 138.0, 133.5, 132.2, 131.9, 131.7, 128.8, 128.7, 128.6, 128.4, 128.3, 128.2, 127.8, 127.1, 126.3, 126.0, 123.4, 123.0, 122.9, 122.7, 118.2, 64.1, 59.7, 57.9, 53.3, 52.2, 49.6, 49.5, 49.1, 48.9, 44.1. HR-ESI-MS calcd. for $[C_{39}H_{37}{}^{115}InN_6O_6 + H]^+$: 801.1892; found $[M + H]^+$: 801.1888, PPM = -0.5.

4.4.13 [In(nonapa)] (4.12)

H_3nonapa (**4.4**) (14.9 mg, 0.0222 mmol) and $In(ClO_4)_3$•$6H_2O$ (15.0 mg, 0.0288 mmol) were dissolved in HCl (aq) (1 mL, 0.1 M) in a 20 mL screw cap vial. The pH was adjusted to ~4.5 with NaOH (aq) (0.1 M) with stirring. The reaction mixture was stirred at 60 °C for 1 h, then evaporated to dryness to afford [In(nonapa)] **(4.12)** as a white solid in quantitative yield. No product was observed to precipitate from the yellow reaction mixture. ^{1}H NMR (600 MHz, DMSO-d_6) δ: 8.21-7.75 (m, 8H, pyr-*H*), 7.38-7.31 (m, 1H, pyr-*H*), 4.77-4.75 (m, 1H), 4.44-3.70 (m, 7H), 3.34-2.70 (m, 8H). ^{13}C NMR (150 MHz, DMSO-d_6) δ: 164.5, 163.6, 153.2, 152.4, 152.0, 146.5, 146.3, 141.7, 141.6, 141.1, 137.8, 129.0, 128.7, 127.5, 126.5, 125.2, 125.1, 123.9, 122.0, 121.9, 52.6, 51.8, 51.8, 51.0, 50.1, 49.9, 49.1, 44.3, 43.1, 29.9, 29.1. HR-ESI-MS calcd. for $[C_{25}H_{25}{}^{115}InN_6O_6 + H]^+$: 621.0953; found $[M + H]^+$: 621.0958, PPM = 0.8.

4.4.14 [In(Bn-trenpa)] (4.13)

Bn-H_3trenpa•6HCl (**4.7**) (41.5 mg, 0.0399 mmol) and $In(ClO_4)_3$•$6H_2O$ (27.0 mg, 0.0519 mmol) were dissolved in HCl (aq) (1 mL, 0.1 M) in a 20 mL screw cap vial. The pH was adjusted to ~4.5 with NaOH (aq) (0.1 M) with stirring. The reaction mixture was stirred at 60 °C for 1 h, then evaporated to dryness to afford [In(Bn-trenpa)] **(4.13)** as a white solid in quantitative yield. The reaction mixture turned cloudy white during the reaction, as the insoluble and neutrally charged metal complex formed. ^{1}H NMR (400 MHz, DMSO-d_6) δ: 8.33-7.85 (m, 8H), 7.44-7.18 (m, 16H), 4.93-4.64 (broad m, 2H), 4.18-3.64 (broad m, 8H), 3.40-3.00 (broad m, 8H), 3.00-2.52 (broad m, 6H). ^{13}C NMR (100 MHz, DMSO-d_6) δ:

166.1, 164.6, 163.8, 163.1, 158.9, 158.2, 153.8, 153.1, 147.8, 147.7, 147.5, 144.9, 144.4, 138.2, 137.6, 137.6, 131.7, 131.1, 129.1, 128.8, 128.7, 128.5, 128.3, 127.8, 127.3, 127.1, 127.1, 126.7, 126.2, 125.9, 125.8, 123.6, 123.4, 123.1, 122.6, 59.9, 58.6, 58.5, 58.3, 58.2, 57.9, 57.4, 57.4, 57.2, 50.4, 50.3, 48.0, 47.7. HR-ESI-MS calcd. for $[C_{48}H_{48}{}^{115}InN_7O_6 + H]^+$: 934.2783; found $[M + H]^+$: 934.2775, PPM = -0.9.

4.4.15 ^{111}In radiolabeling studies

The chelating ligands Bn-H_3nonapa (**4.3**), H_3nonapa (**4.4**), and Bn-H_3trenpa (**4.7**) were made up as stock solutions (1 mg/mL, ~10^{-3} M) in deionized water. An aliquot of each ligand stock solution was transferred to screw cap mass spectrometry vials and made up to 1 mL with pH 5.0 NaOAc (10 mM) buffer, to a final concentration of ~365 μM for each sample. A ~10 μL aliquot of the $^{111}InCl_3$ stock solution (~1 mCi for labeling studies and ~3-5 mCi for mouse serum competitions) was transferred into each vial, allowed to react at ambient temperature for 10 minutes, and then analyzed by RP-HPLC to confirm radiolabeling and calculate yields. If the reaction was not complete, it was left for 45 minutes total reaction time and then checked again by RP-HPLC. Previously obtained radiolabeling yields and serum stability results for the ligands DTPA, DOTA, H_2dedpa, H_4octapa, and H_5decapa (Chapters 2-3) are also presented, and were performed under identical experimental protocols at the same facilities (TRIUMF/Nordion).[89] Areas under the peaks observed in the radioactive HPLC trace were integrated to determine radiolabeling yields. Elution conditions used for RP-HPLC analysis were gradient: A: 10 mM NaOAc buffer pH 4.5, B: CH_3CN. 0 to 100% B linear gradient 20 minutes. The radiometal complex $[^{111}In(dedpa)]^+$ used a modified HPLC gradient of A: 10 mM NaOAc buffer pH 4.5, B:

CH_3CN. 0 to 5% B linear gradient 20 min. [^{111}In(Bn-nonapa)] (t_R = 8.9 min), [^{111}In(nonapa)] (t_R = 5.0 min), [^{111}In(Bn-trenpa)] (t_R = 10.5 min).

4.4.16 Mouse serum stability challenge

The compounds [^{111}In(Bn-nonapa)], [^{111}In(nonapa)], and [^{111}In(Bn-trenpa)] were prepared with the radiolabeling protocol as described above. Mouse serum was removed from the freezer and allowed to thaw at ambient temperature for 30 minutes. In triplicate for each ^{111}In complex listed above, solutions were made in sterile vials with 750 μL mouse serum, 500 μL of ^{111}In-complex (10 mM NaOAc buffer, pH 5.5), 250 μL phosphate buffered saline (PBS), and were left to sit at ambient temperature. After 1 hour, half of the mouse serum competition mixture (750 μL) was removed from each vial, diluted to a total volume of 2.5 mL with phosphate buffered saline, and then counted in a Capintec CRC 15R well counter to obtain a value for the total activity to be loaded on the PD-10 column. The 2.5 mL of diluted mouse serum competition mixture was then loaded onto a PD-10 column that had previously been conditioned via elution with 20 mL of PBS. The 2.5 mL of loading volume was allowed to elute into a ^{111}In waste container, and then the PD-10 column was eluted with 3.5 mL PBS and collected into another sterile vial. This 3.5 mL of collected eluent which contained ^{111}In bound/associated with serum-proteins (size-exclusion for MW < 5000 Da) was counted in a well counter, and then compared to the total amount of activity that was loaded on the PD-10 column to obtain the percentage of ^{111}In that was bound to serum proteins and therefore no longer chelate-bound. The percent stability values shown in Table 4.1 represent the percentage of ^{111}In that was retained on the PD-10 column and therefore still chelate-bound.

Chapter 5: Modular syntheses of H_4octapa and H_2dedpa, and yttrium coordination chemistry relevant to $^{86/90}$Y radiopharmaceuticals

This chapter is an adaptation of published work, and is reproduced in part, with permission from Price, E. W.; Cawthray, J. F.; Adam, M. J.; Orvig, C. Modular Syntheses of H_4octapa and H_2dedpa, and Yttrium Coordination Chemistry Relevant to $^{86/90}$Y Radiopharmaceutical. *Dalton Trans.* **2014.** doi: 10.1039/C4DT00239C. Copyright 2014 The Royal Society of Chemistry.

5.1 Introduction

The modular aspect of BFC-based radiopharmaceuticals has been discussed throughout Chapters 1-4. By changing the radiometal, the same molecular construct can be used for different types of imaging and therapy, with a variety of half-lives and emission energies.[1] The acyclic chelating ligand H_4octapa has demonstrated its facile radiolabeling kinetics and excellent *in vitro*/*in vivo* stability with the single photon emission computed tomography (SPECT) radiometal ^{111}In ($t_{1/2}$ ~2.8 days), and the β^- therapeutic radiometal ^{177}Lu ($t_{1/2}$ ~6.6 days).[15,87-89,304] Another attractive isotope is the β^- emitting ^{90}Y, with a shorter half-life ($t_{1/2}$ ~2.7 days) and higher β^- emission energy (2288 keV vs 498 keV) than ^{177}Lu, allowing ^{90}Y to treat much larger and more poorly vascularized tumours (maximum *in vivo* β^- range of ~12 mm for ^{90}Y vs ~2 mm ^{177}Lu).[2,6,15,349-351] The increased range of β^- particles emitted by ^{90}Y can provide therapeutic effects to neighboring tumours up to ~550 cell diameters away via the "crossfire effect".[2,6,15,349-351] The yttrium isotopologue ^{86}Y emits β^+

particles for positron emission tomography (PET), ideal for pre-therapy imaging and dosimetry. The substitution of ^{86}Y (PET) for ^{90}Y (therapy) is seamless, with the aqueous chemistry and radiolabeling properties of both isotopes of yttrium being identical.[19-24]

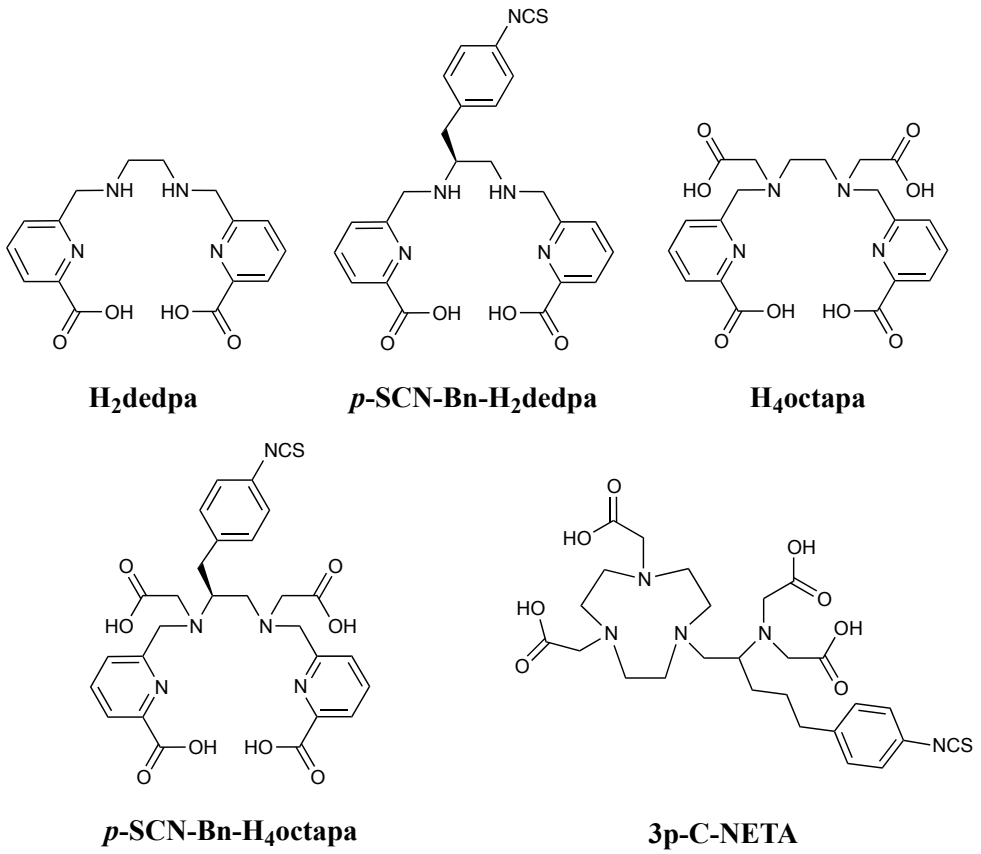

Figure 5.1 Ligands synthesized in this chapter, including H_2dedpa, H_4octapa, and BFC derivatives *p*-SCN-Bn-H_2dedpa and *p*-SCN-Bn-H_4octapa; and the promising new $^{86/90}$Y ligand 3p-C-NETA.

Although seemingly more attractive than ^{111}In due to its β^+ emission for PET and its identical chemistry to ^{90}Y for exchange, the limitations of ^{86}Y include a shorter half-life (14.7 h) than the common therapeutic radiometals ^{177}Lu and ^{90}Y, high energy β^+ emission (2019, 2335 keV) that decreases image quality, and a number of high energy γ emissions (1077,

1153, 1854, 1921 keV) that present radiation dose concerns and require substantial radioactive shielding for handling and transport.[15] For these reasons, BFCs such as DOTA and CHX-A''-DTPA, which can effectively bind multiple radiometals such as ^{111}In, ^{177}Lu, and $^{86/90}$Y, are valued (Figure 5.1). 3p-C-NETA is a new NOTA derivative that has shown excellent properties with ^{177}Lu and $^{86/90}$Y, radiolabeling in only 5 minutes at room temperature, but its radiolabeling properties with ^{111}In are uncertain (Figure 5.1).[127,201,202]

Although excellent thermodynamic stability and kinetic inertness are crucial properties for BFCs, fast radiolabeling at ambient temperature is also a very attractive property, because these radiometals are often used with antibody-based radiopharmaceuticals, which are heat sensitive. H_4octapa has been shown in Chapters 2 and 3 to radiolabel with ^{111}In and ^{177}Lu in under 15 minutes at room temperature, where DOTA requires temperatures of 37-90 °C over a period of 30-60 minutes, and CHX-A''-DTPA typically requires conditions of 37-75 °C over a period of 30-60 minutes.[60,61,89,215,216,312] Although the optimal radiolabeling temperatures for DOTA and CHX-A''-DTPA are high (60-100 °C), antibody-conjugates can be effectively radiolabeled at 37 °C, albeit with longer reaction times, lower yields, and typically inconsistent yields.[87] Because of its proficiency with ^{111}In and ^{177}Lu, H_4octapa should demonstrate similarly fast radiolabeling kinetics and robust stability with $^{86/90}$Y. Towards this end, we have performed potentiometric titrations with H_4octapa and Y^{3+} to determine the thermodynamic formation constants (log K_{ML}) and pM value, and have prepared the coordination complex of H_4octapa with non-radioactive Y^{3+} to compare its properties to the complexes with In^{3+} and Lu^{3+}, which were studied in Chapters 2-3.[87,89] Future studies with radioactive $^{86/90}$Y will assess radiolabeling performance and *in vitro*/*in vivo* stability with H_4octapa. The current challenges facing

yttrium radiochemistry are the scarce availability of ^{86}Y in North America, and the lack of concomitant β^+/γ emissions of ^{90}Y that make detection and handling more challenging.

In order to facilitate the inclusion of H_2dedpa and H_4octapa into peptide conjugates, we have developed new protection chemistry to allow them to conjugate to peptides synthesized on-resin (e.g. Wang resin), and deprotect under standard conditions (e.g. mixture of trifluoroacetic acid:dichloromethane:triisopropylsilane). Standard peptide coupling reactions of these fully deprotected ligands with peptides is not possible, as the presence of two (H_2dedpa) or four (H_4octapa) free carboxylic acid groups can also form amide linkages. Previously published synthetic routes for H_2dedpa[118] and H_4octapa (Chapters 2-4) have relied on methyl ester protection of the picolinic acid moiety, requiring harsh deprotection conditions of LiOH or heating HCl (6-12 M). By utilizing nosyl protection chemistry, we have incorporated *tert*-butyl ester protection of the picolinic acid moiety, allowing for room temperature deprotection in trifluoroacetic acid. This new synthetic route is reported for H_2dedpa, H_4octapa, *p*-SCN-Bn-H_2dedpa, and *p*-SCN-Bn-H_4octapa. The potential of the ligand H_4octapa for use with $^{86/90}$Y is also investigated, through formation and study of the non-radioactive $[Y(octapa)]^-$ complex, DFT calculations of the $[Y(octapa)]^-$ coordination structure and molecular electrostatic potential (MEP), and potentiometric titrations of H_4octapa with Y^{3+} to determine its solution thermodynamic stability parameters (pM, log K_{ML}).

5.2 Results and discussion

5.2.1 Synthesis and characterization

Previously (Chapters 2-4), only methyl-ester protection chemistry was compatible with the picolinic acid moiety of the "pa" family of ligands (Figure 5.1), and attempts to utilize *tert*-butyl esters had failed due to incompatibility with reductive amination methods.[118] This new protection chemistry allows the final *tert*-butyl ester protected pro-ligands to be deprotected under less harsh conditions that previously required, using trifluoroacetic acid in dichloromethane at room temperature. Trifluoracetic acid is typically used in the final deprotection step of on-resin peptide synthesis, and the previously used conditions of heating HCl (6-12 M) or LiOH were not compatible with peptides. Using standard peptide coupling conditions with the fully deprotected ligands is not possible, as the carboxylic acid arms of H_4octapa and H_2dedpa could participate in the coupling reaction, and so labile protection chemistry to mask carboxylic acid functionality is required for this application.

The commercially available starting material 6-methylpicolinic acid was *tert*-butyl ester protected following a modified literature procedure that utilized *tert*-butyl-2,2,2-trichloroacetimidate (Scheme 5.1).[352] The *tert*-butyl protected product (**5.1**) was synthesized here for the first time, and then transformed to the alkyl-bromide derivative (**5.2**) using a modified literature procedure with *N*-bromosuccinimide and benzoyl peroxide as radical initiator.[353] The general synthetic scheme relies heavily on the nosyl protection group, and follows the same general pathway as the nosyl-based synthesis of *p*-SCN-Bn-H_4octapa (Chapter 3).[87,304]

Scheme 5.1 Syntheses of H_2dedpa (**5.6**) and H_4octapa (**5.8**) using *tert*-butyl ester protection chemistry[a]

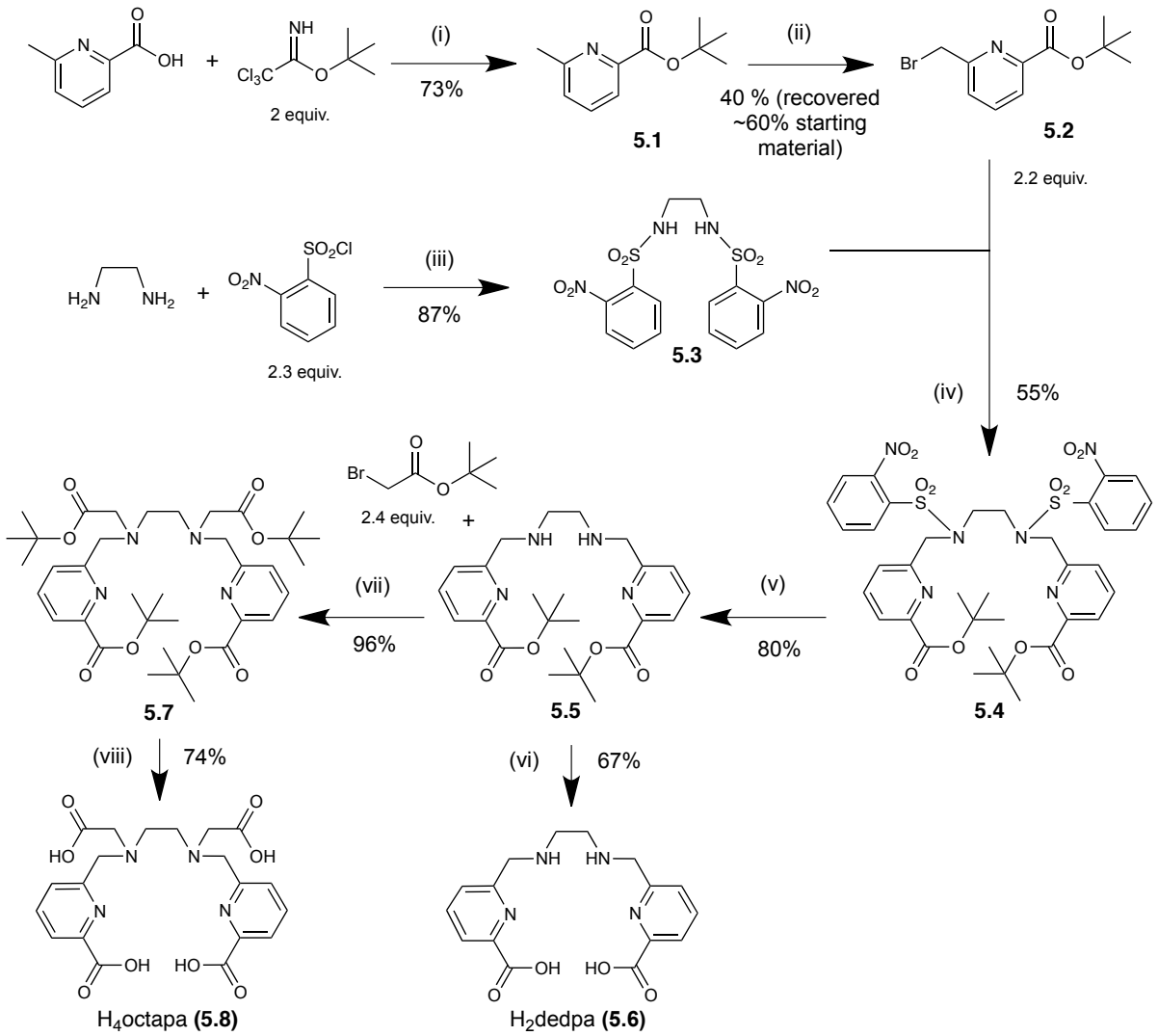

[a](i) CH_2Cl_2, BF_3•etherate (20 μL per mmol starting material), RT, 20 h; (ii) CCl_4, Bz_2O_2, *N*-bromosuccinimide (NBS, 0.7 equiv), 70 °C, 4 h; (iii) THF, $NaHCO_3$, RT, 24 h; (iv) DMF, Na_2CO_3, 80 °C, 48 h; (v) THF, thiophenol (2.3 equiv), K_2CO_3, 50 °C, 48 h; (vi) trifluoroacetic acid (TFA) (1 mL) and CH_2Cl_2 (1 mL), RT, 16 h, (cumulative yield of ~26% over 4 steps); (vii) MeCN, Na_2CO_3, 60 °C, 48 h; (viii) trifluoroacetic acid (TFA) (1 mL) and CH_2Cl_2 (1 mL), RT, 16 h, (cumulative yield of ~27% over 5 steps).

The enhanced lability of the *tert*-butyl ester protecting group resulted in some decomposition during synthesis, which was partially responsible for decreased yields relative to the analogous methyl ester-based synthetic route.[87-89] Additionally, the solvent methanol

was problematic, as during silica column chromatography some methyl ester product was formed from the *tert*-butyl ester, creating byproducts and decreasing yields. Because the combination of methanol and dichloromethane was most effective for separating intermediates via column chromatography, it was still used; however, methanol was avoided whenever possible, such as when rinsing, filtering, rotary evaporating, and heating. The previously used synthetic protocols for H_2dedpa relied upon a reductive amination reaction, which utilized $NaBH_4$ to reduce the Schiff-base (imine) to a secondary amine.[118,266,268,271-273] This method produced byproducts at the methyl ester protected picolinic acid moiety by transforming them to a mixture of carboxylic acids and primary alcohols, but for the more labile *tert*-butyl ester protection group complete ester cleavage and reduction to primary alcohols was observed, and no product could be isolated.[89] It has not been until our recent implementation of nosyl protection chemistry for the synthesis of these ligands that application of *tert*-butyl ester protection chemistry could be realized.[87]

An important deviation of the synthetic pathway reported here from the nosyl-based synthesis of *p*-SCN-Bn-H_4octapa (Chapter 3) is the enhanced modularity, with the *tert*-butyl ester protected precursors (tBu)$_2$dedpa (**5.5**) and *p*-NO_2-Bn-(tBu)$_2$dedpa (**5.13**) being arranged as precursors to (tBu)$_4$octapa (**5.7**) and *p*-NO_2-Bn-(tBu)$_4$octapa (**5.15**) (Schemes 5.1 and 5.2). Using this layout, common synthetic precursors are used for both H_2dedpa and H_4octapa, rendering the reaction schemes nearly identical for each. The utility of this approach is that the ^{64}Cu and $^{67/68}$Ga ligand H_2dedpa can be made in the same procedure as the ^{111}In, ^{177}Lu, and $^{86/90}$Y ligand H_4octapa, sharing common precursors and resulting in broad radiometal application from one synthetic scheme. Previously, in order to optimize purification and yields, *p*-SCN-Bn-H_4octapa was synthesized using a different reaction

ordering that did not allow for this overlap (Chapter 3).[87] Despite this alternate approach, the same reaction pathways (Schemes 5.1 and 5.2) can be performed using the methyl ester protected picolinic acid group instead of its *tert*-butyl protected analogue, as shown in Chapter 3.

The drawback to the methyl ester protected picolinic acid moiety lies in the purification of the $(Me)_2$dedpa intermediate, which is more challenging than the more lipophilic $(t\text{Bu})_2$dedpa derivative; however, the enhanced stability of the methyl ester protection group affords higher yields, at the price of harsh deprotection conditions.[87,89,118] H_2dedpa and H_4octapa have previously been synthesized as HCl salts (Chapters 2-4), but for this new synthesis they were lyophilized after final high-performance liquid chromatography (HPLC) purification as their trifluoroacetate salts. The final trifluoroacetate salts (formulae determined from elemental analysis results) H_2dedpa•2trifluoroacetic acid•1.5H_2O and H_4octapa•2trifluoroacetic acid were more soluble in water than their HCl counterparts, and were now soluble in methanol.

During the syntheses of the bifunctional derivatives *p*-SCN-Bn-H_2dedpa (**5.14**) and *p*-SCN-Bn-H_4octapa (**5.16**), it was observed that the hydrogenation reaction conditions used with the precursors *p*-NO_2-Bn-$(t\text{Bu})_2$dedpa (**5.13**) and *p*-NO_2-Bn-$(t\text{Bu})_4$octapa (**5.15**) surprisingly did not effect full *tert*-butyl ester deprotection. The hydrogenation was performed using 1:1 glacial acetic acid and hydrochloric acid (3 M) as solvent at room temperature for 1 hour, and mass spectrometry confirmed that *p*-NH_2-Bn-$(t\text{Bu})_2$dedpa (not isolated, used without further purification) was formed without *tert*-butyl ester cleavage. Curiously, mass spectrometry revealed that using the same reaction conditions *p*-NH_2-Bn-$(t\text{Bu})_2H_2$octapa was formed, with two *tert*-butyl ester groups being cleaved and two

remaining attached, suggesting that the *tert*-butylacetate arms are more easily cleaved than are the *tert*-butylpicolinate counterparts.

Scheme 5.2 Synthesis of *p*-SCN-Bn-H_2dedpa (**5.14**), and *p*-SCN-Bn-H_4octapa (**5.16**) using *tert*-butyl ester protection chemistry[a]

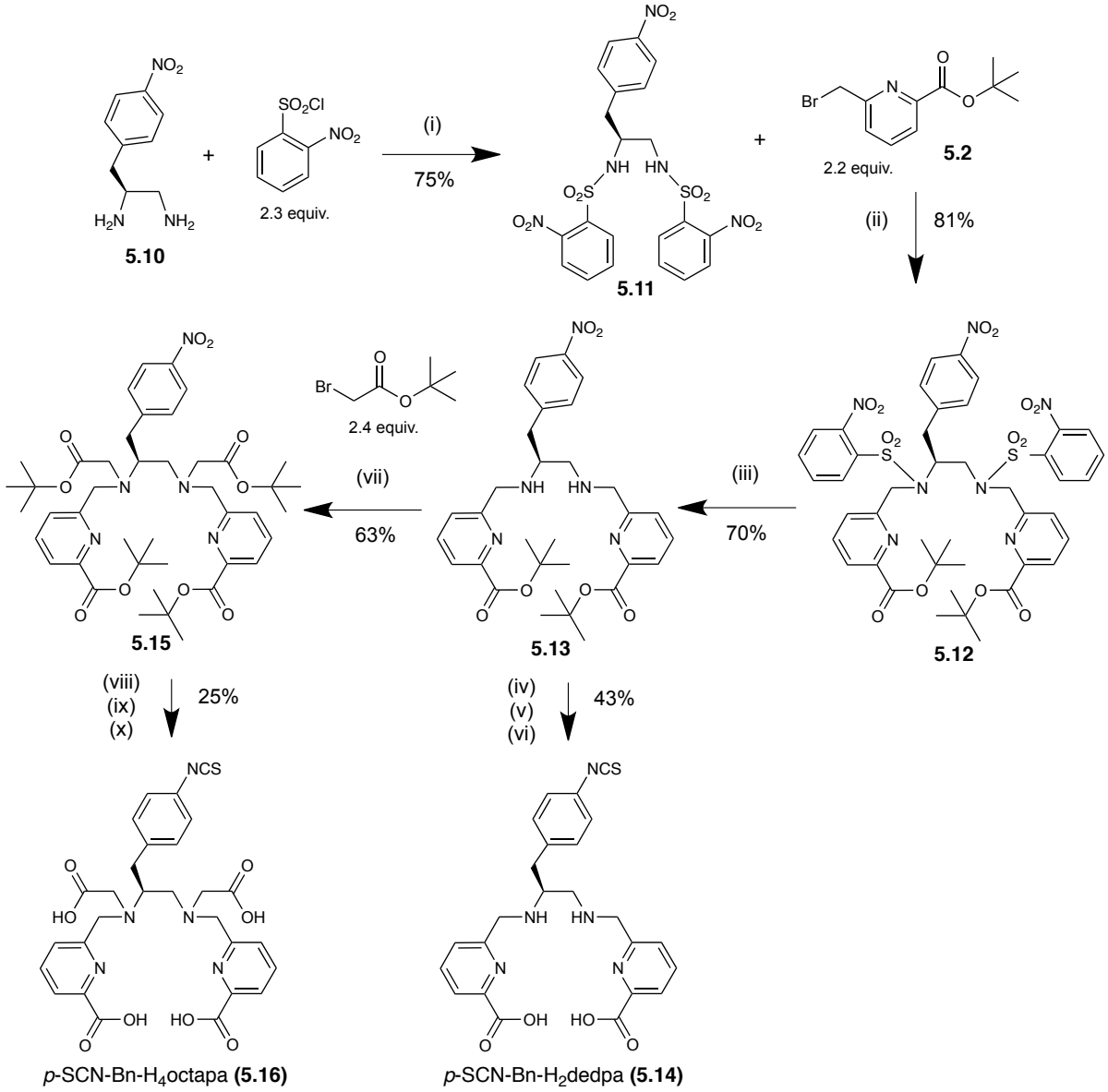

[a](i) THF, $NaHCO_3$, 50 °C, 24 h; (ii) DMF, Na_2CO_3, 80 °C, 48 h; (iii) THF, thiophenol (2.3 equiv), K_2CO_3, 60 °C, 48 h; (iv) 5 mL of (1:1) glacial acetic acid:3 M HCl, Pd/C (20 wt%), H_2 (g), RT, 1 h; (v) 3 M HCl, heat to reflux for 1 minute; (vi) thiophosgene in DCM (15 equiv), 3 M HCl, RT, 24 h, (cumulative yield of ~18% in 6 steps); (vii) MeCN, K_2CO_3, 80 °C, 48 h; (viii) 5 mL of (1:1) glacial acetic acid:3 M HCl, Pd/C (30 wt%), H_2 (g), RT, 1 h; (ix) 3 M HCl, heat to reflux for 1 minute; (x) thiophosgene in DCM (15 equiv), 3 M HCl, RT, 24 h, (cumulative yield of ~7% in 7 steps).

H_2dedpa (**6**) was synthesized in 4 synthetic steps and H_4octapa (**8**) in 5 steps, with cumulative yields of ~26% and ~27%, respectively. The more challenging bifunctional derivative *p*-SCN-Bn-H_2dedpa (**14**) was synthesized in 6 steps and *p*-SCN-Bn-H_4octapa (**16**) in 7 steps, with cumulative yields of ~18% and ~7%, respectively. The nosyl-based synthesis of H_4octapa and *p*-SCN-Bn-H_4octapa discussed in Chapter 3, which utilized methyl ester protection chemistry of the picolinic acid moieties, provided higher cumulative yields of ~45-50% and ~25-30%, respectively.[87] H_2dedpa (**6**) and *p*-SCN-Bn-H_2dedpa (**14**) have not been previously synthesized using nosyl protection chemistry. Largely due to the enhanced lability of the *tert*-butyl ester protected picolinic acid, a penalty in cumulative yield was paid for access to less harsh room temperature deprotection in trifluoroacetic acid. As ^{68}Ga is often used with peptide vectors, synthesis of *p*-SCN-Bn-(*t*Bu)$_2$dedpa or *p*-NH_2-Bn-(*t*Bu)$_2$dedpa for direct conjugation to on-resin peptides should afford easy purification and high yields, which was not previously possible using the methyl ester protected derivative.

5.2.2 Yttrium coordination chemistry

The Y^{3+} complex of H_4octapa, $[Y(octapa)]^-$ (**9**), was synthesized by mixing **8** (H_4octapa•2trifluoroacetic acid) with YCl_3•$6H_2O$ in deionized water, adjusting the pH to ~4-5 with NaOH (0.1M), and stirring at room temperature for 1 hour. After confirming formation of the coordination complex by mass spectrometry, the product was studied by NMR in both D_2O and DMSO-d_6 (Figure 5.2, Figure A.5). A comparison of the ^{1}H NMR spectra of $[Lu(octapa)]^-$ (Figure 5.2, top) and $[Y(octapa)]^-$ (Figure 5.2, bottom) in D_2O reveals similarly sharp signals and coupling patterns, but slightly different chemical shift values, suggesting similar solution structures.[87] Different absolute chemical shift values are

expected, as Y^{3+} and Lu^{3+} have different electronic properties, but these two metal ions are known to form coordination structures with similar geometries (CN = 8-9), as they both have similar ionic radii (CN = 8, 101.9 pm vs 97.7 pm, and CN = 9, 107.4 pm vs 103.2 pm, respectively).[190]

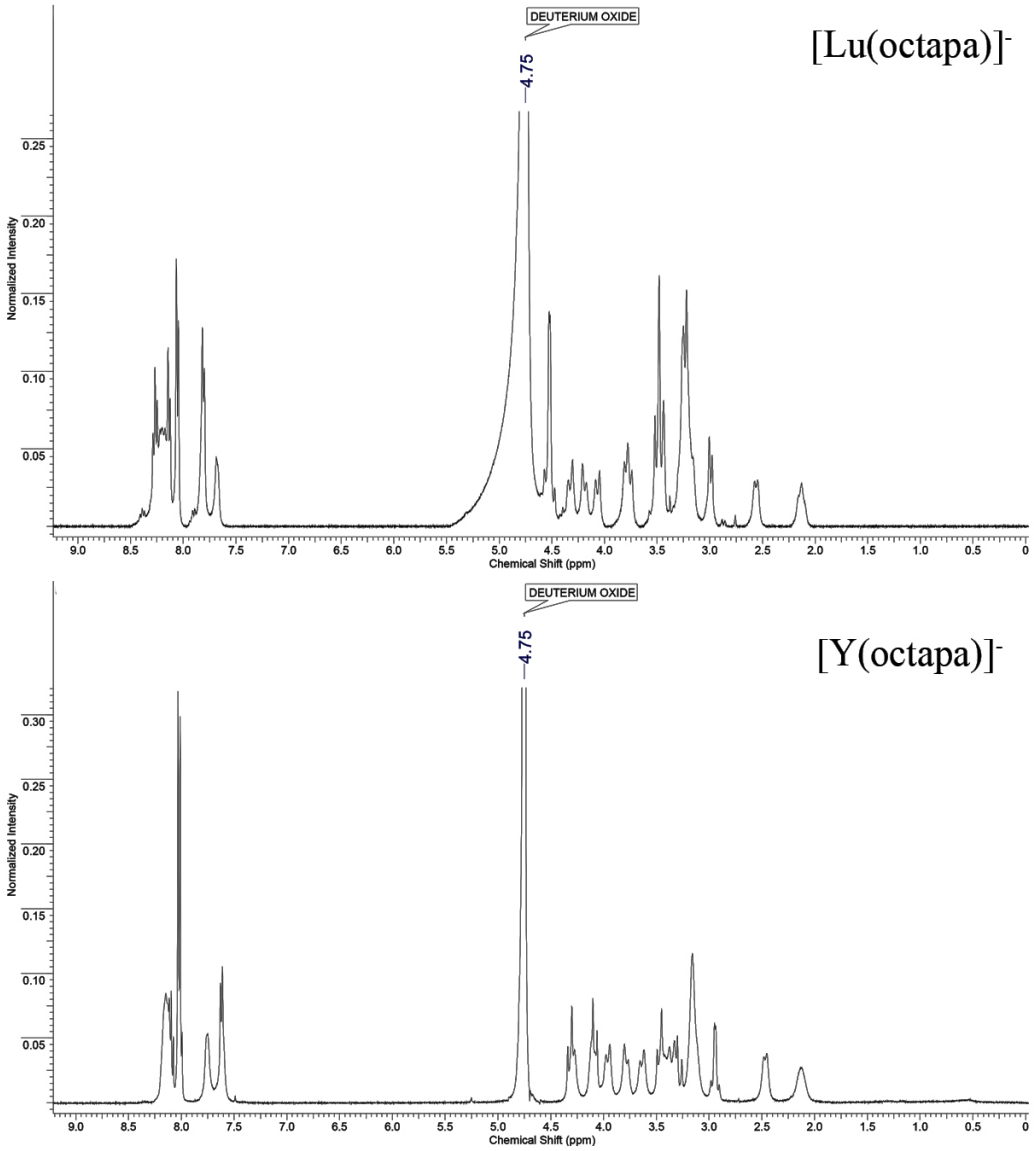

Figure 5.2 ^{1}H NMR spectra of $[Lu(octapa)]^-$ in D_2O (600 MHz, 25 °C, top, referenced to H-O-D at 4.75 ppm)[87], $[Y(octapa)]^-$ in D_2O (400 MHz, 25 °C, bottom).

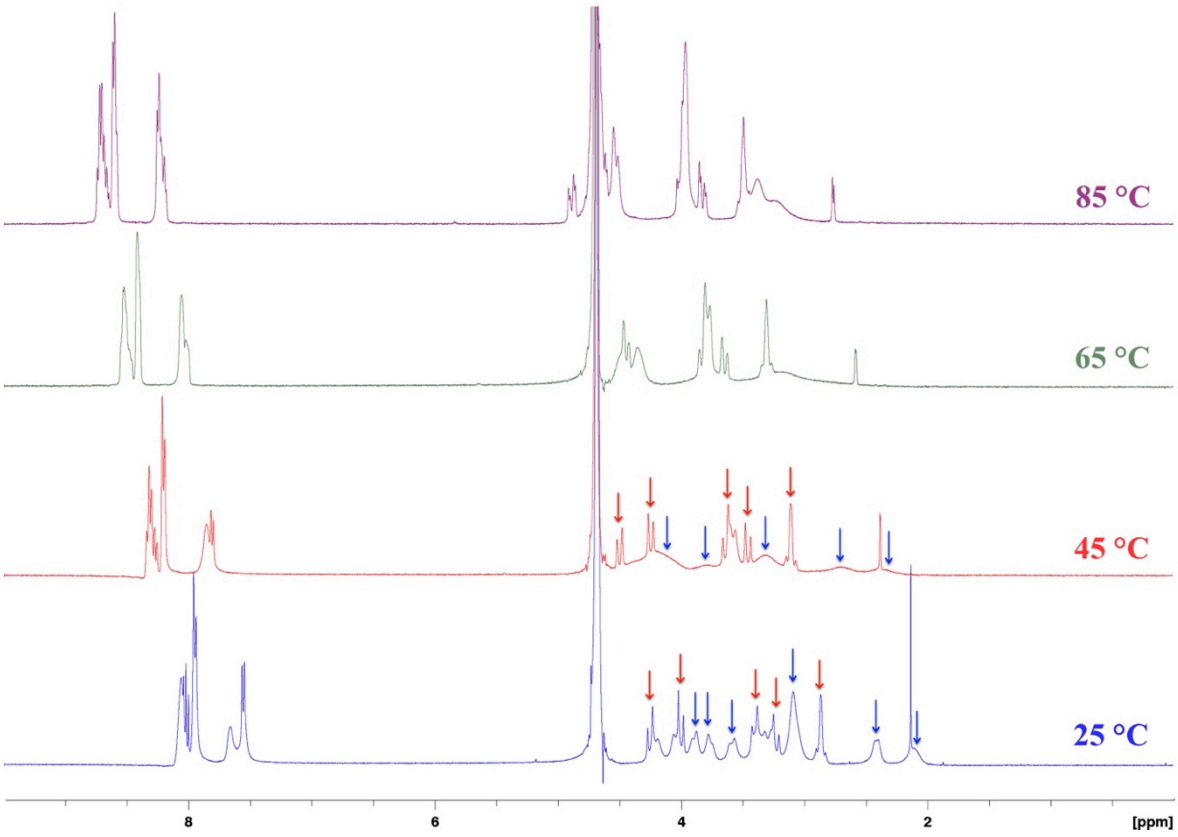

Figure 5.3 Variable temperature (VT) NMR experiments with $[Y(octapa)]^-$ (D_2O, 400 MHz), with temperature increased to 85 °C in 20 °C increments, with blue arrows identifying fluxional isomers, and red arrows identifying a static (non-fluxional) isomer.

At first glance, the sharp and well-resolved peaks and couplings observed for both the Y^{3+} and Lu^{3+} complexes of $octapa^{4-}$ suggest little fluxional behavior in solution at 25 °C, but the large number of signals and complicated coupling patterns relative to the simple ^1H NMR spectra of $[In(octapa)]^-$ and the unbound ligand H_4octapa suggest the presence of multiple static isomers.[89] In addition to multiple geometric isomers, it is possible that upon coordination of a single water molecule to the $[Y(octapa)]^-$ complex, the 9-coordinate $[Y(octapa)(H_2O)]^-$geometry is lower symmetry giving a greater number of non-equivalent protons and a more complicated spectrum. The NMR spectrum of $[Y(octapa)]^-$ in DMSO-d_6

was significantly different than in D_2O, potentially as a result of coordination of DMSO to Y^{3+} (Figure A.5). The increased broadening of NMR signals (Figure A.5) in DMSO-d_6 also suggests an increased rate of fluxional isomerization.

To further probe the coordination structure and isomerization of $[Y(octapa)]^-$, variable temperature-NMR (VT-NMR) and 2D-COSY/HSQC experiments were performed. Upon increasing the NMR sample (D_2O) temperature from 25 °C to 85 °C, the multiple sharp peaks observed in the 25 °C spectrum did not change drastically, which suggests the presence of a stable static isomer (red arrows, Figure 5.3). For the broad signals observed at 25 °C (blue arrows, Figure 5.3), substantial change in the ^1H NMR spectrum was observed from the small change in temperature between 25 °C and 45 °C, with some signals broadening to such an extent that they nearly disappeared from the spectrum. This trend of broadening and coalescing of signals continued up to 85 °C; however, even at 85 °C some signals remained sharp. It can be seen in Figure 5.3 that some sharp signals remain the same between 25 °C and 45 °C (red arrows), where other more broad signals that overlap these sharp signals are observed to rapidly broaden and coalesce (blue arrows). This observation suggests that a single major static isomer is present in solution (red arrows, sharp peaks that remain as temperature is increased), with at least one fluxional isomer existing at the same time (blue arrows). The signals highlighted by red arrows (Figure 5.3) resemble the more simple spectra obtained for $[In(octapa)]^-$ in Chapter 2, where only a single static isomer was present, with several doublets and simple multiplets arising from neighboring protons becoming diastereotopic and coupling to each other upon metal coordination.[89] Because yttrium can form 9-coordinate complexes, the coordination of an aqua ligand could be involved in the fluxional isomerization of $[Y(octapa)]^-$. These VT-NMR experiments suggest that one static

isomer and at least one set of fluxional isomers are present under aqueous conditions at ambient temperature.

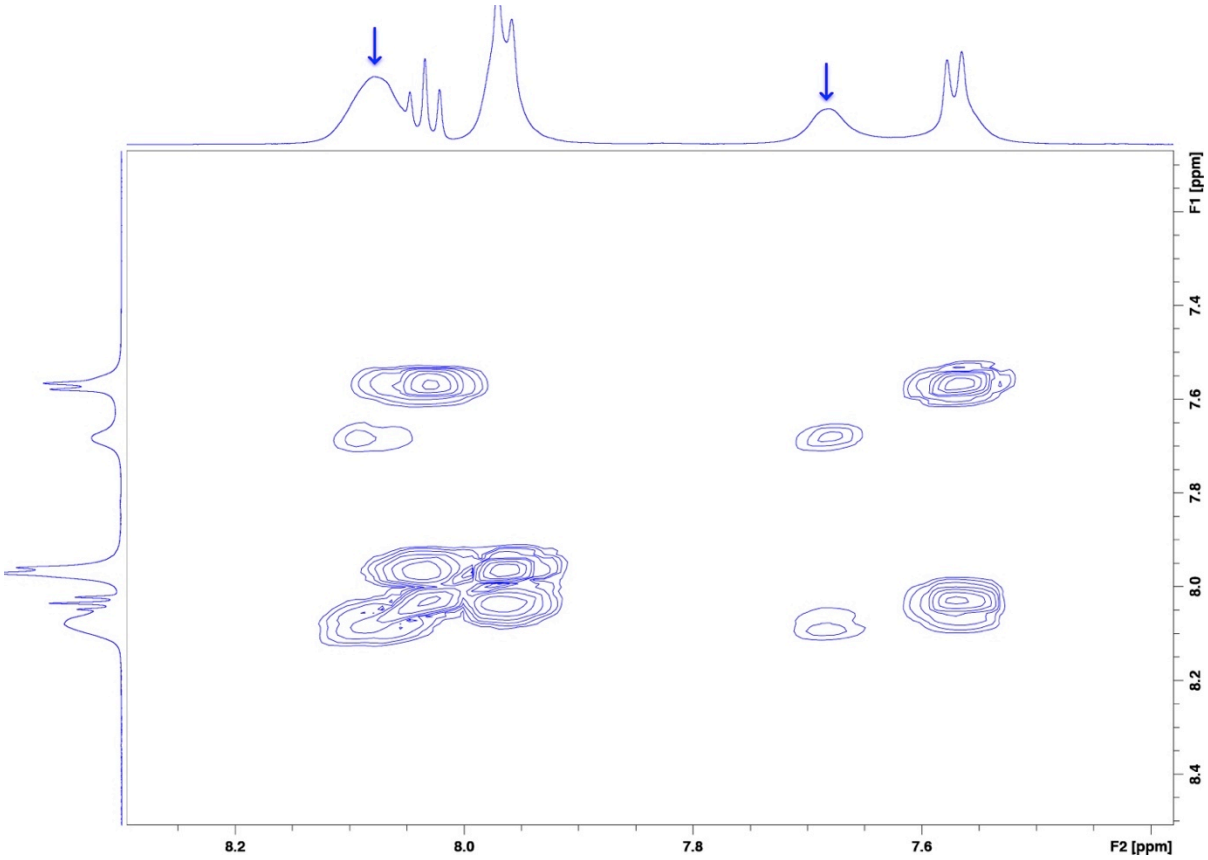

Figure 5.4 ^{1}H-^{1}H COSY NMR (600 MHz, D_2O, 25 °C) expansion of aromatic signals in spectrum of [Y(octapa)]$^{-}$, showing no correlations between broad signals arising from a fluxional species (blue arrows), and sharp signals arising from a single static isomer (see Figure A.6 for full spectrum).

The 2D-COSY experiment was used to probe ^{1}H-^{1}H correlations, to see if distinct static isomers could be observed at ambient temperature and confirm VT NMR results (Figures 5.4 and 5.5). An expansion of the aromatic region of the 2D-COSY spectrum revealed strongly correlated cross-peaks between the sharp signals, which were attributed to a single major static isomer in solution. Additionally, weak cross-peaks between the broad signals that were assigned as a fluxional isomer in VT NMR experiments (blue arrows, Figure 5.4) were observed, and showed no correlation to the sharp signals. The same

conclusion can be drawn from the COSY alkyl-region expansion (blue arrows, Figure 5.5), where the broad signals that were observed to rapidly disappear after the temperature was increased during VT-NMR experiments (Figure 5.3), can now be seen to weakly correlate with each other, and further to show no correlation with the sharp signals assigned as the major static isomer. These 2D NMR experiments confirm the results of the VT-NMR experiments, suggesting one major static isomer in solution, along with at least one fluxional species. Fluxional species typically produce very weak NMR signals, observed in weak cross peaks correlating to a fluxional species in the 2D COSY experiments discussed above, and strong cross peaks correlating to the major static isomer.

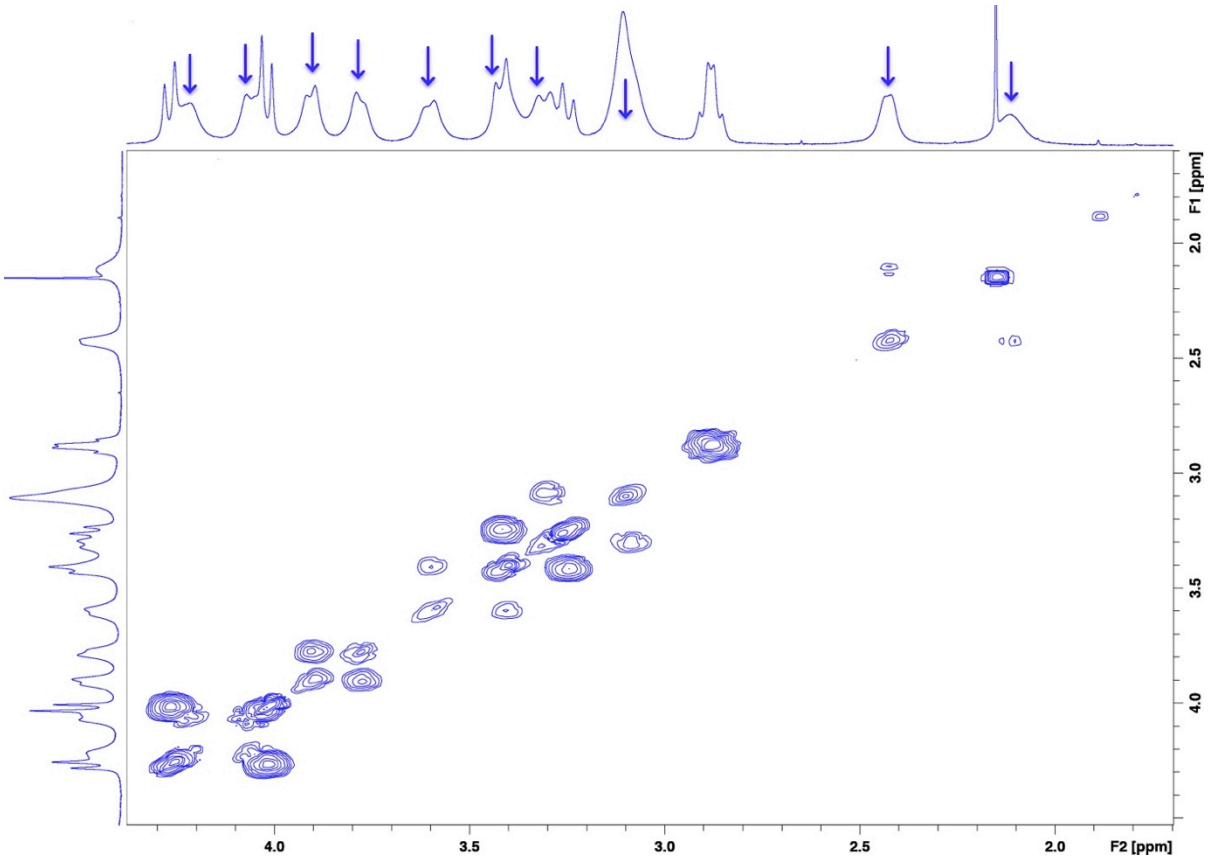

Figure 5.5 ^{1}H-^{1}H COSY NMR (600 MHz, D_2O, 25 °C) expansion of alkyl-region signals in spectrum of $[Y(octapa)]^-$, showing no correlations between broad signals arising from a fluxional species (blue arrows, identified by VT-NMR, Figure 5.3), and sharp signals arising from a single static isomer (see Figure A.6 for full spectrum).

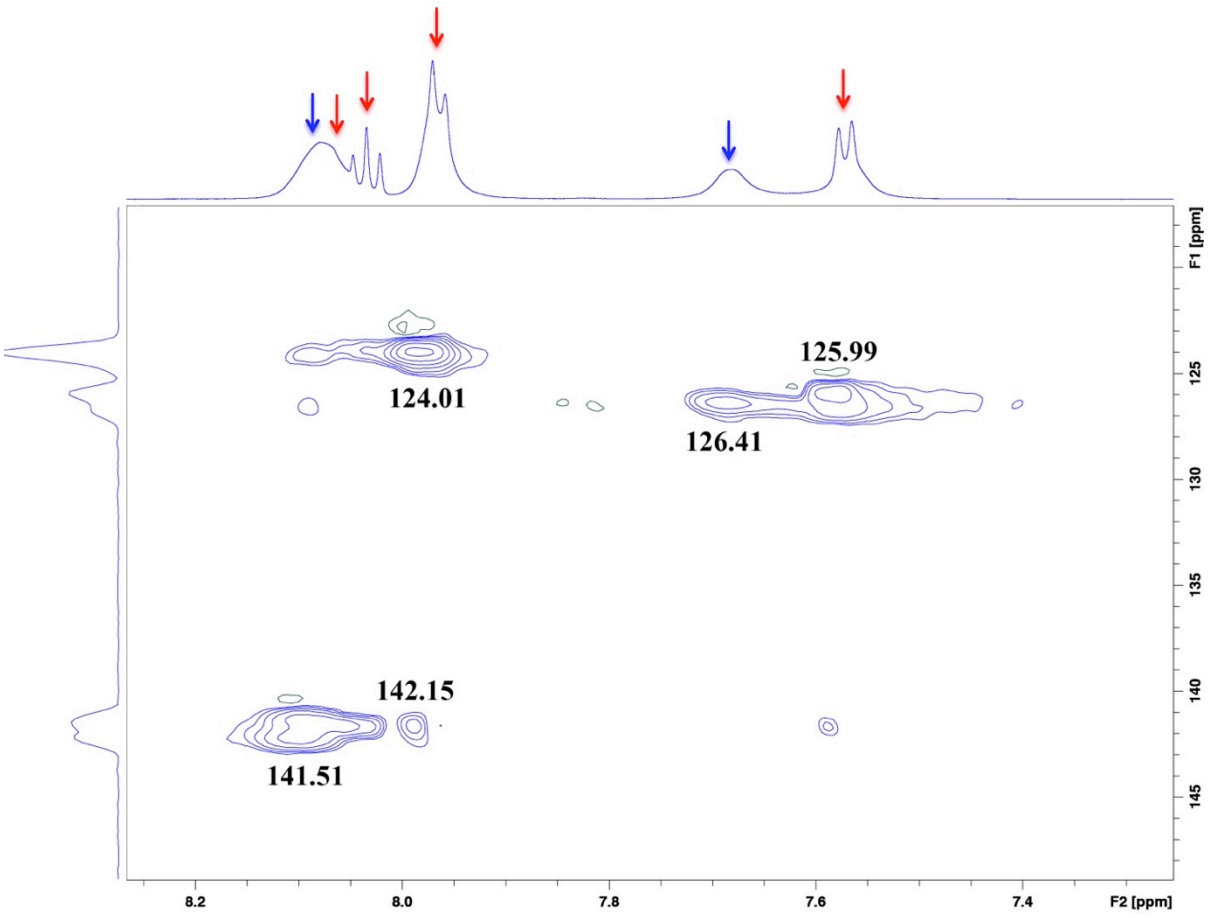

Figure 5.6 ^{1}H-^{13}C HSQC NMR (400/100 MHz, D_2O, 25 °C) expansion of aromatic signals in spectrum of $[Y(octapa)]^-$, showing correlations to ~5 unique ^{13}C signals, suggesting the presence of a single static isomer (red arrows), along with a fluxional species (blue arrows) (^{13}C NMR spectra externally referenced to MeOH in D_2O) (see Figure A.7 for full spectrum).

Because 2D-HSQC experiments utilize ^{1}H-^{13}C heteronuclear correlations, the signals obtained for fluxional species are even weaker than those for the COSY spectra, as they rely on ^{13}C NMR data as well as ^{1}H NMR. The 2D-HSQC ^{1}H-^{13}C single-bond heteronuclear correlation experiment revealed a strong set of cross-peaks arising from a single static isomer (red arrows, Figure 5.6), with only weak signals and cross-peaks arising from the observed fluxional species (blue arrows, Figure 5.6). For the unbound and symmetric ligand H_4octapa,

one would expect to see 3 distinct aromatic ^{13}C signals arising from the three distinct C-H pyridines (~C_{2v} symmetry), and for a single static isomer of $[Y(octapa)]^-$ there would be 3-6 signals (depending on symmetry). It was observed that the aromatic region of the $[Y(octapa)]^-$ HSQC NMR spectrum displayed ~5 unique and strong ^{13}C correlation signals, supporting the hypothesis of a single major static isomer (Figure 5.6).

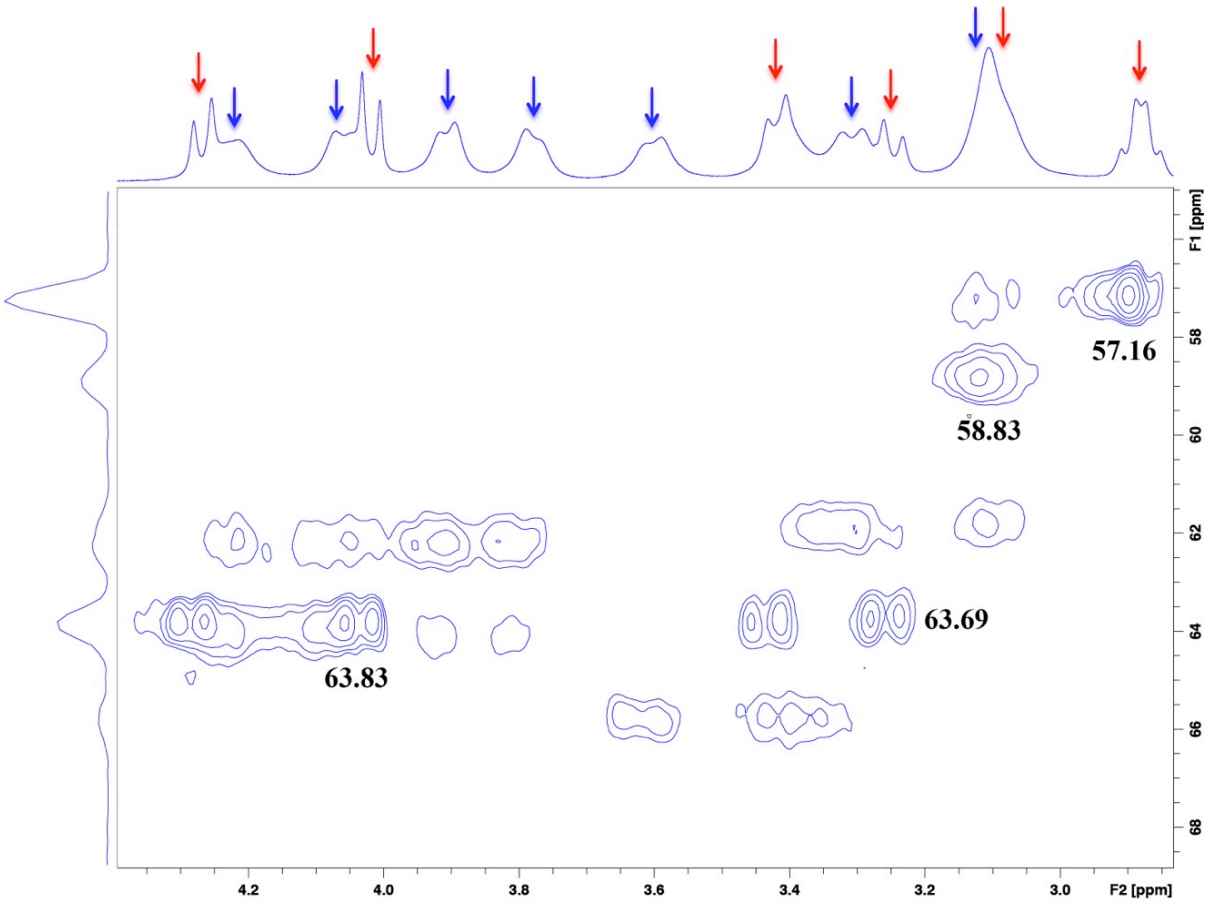

Figure 5.7 ^{1}H-^{13}C HSQC NMR (400/100 MHz, D_2O, 25 °C) expansion of alkyl-region signals in spectrum of $[Y(octapa)]^-$, showing correlations to ~4 unique and strong ^{13}C signals from a static isomer (red arrows), and several weak correlations arising from a fluxional species (blue arrows) (^{13}C NMR spectra externally referenced to MeOH in D_2O) (see Figure A.7 for full spectrum).

There are 6 unique alkyl-carbon atoms present in H_4octapa/[Y(octapa)]$^-$, which manifest as 3 signals for the free H_4octapa ligand. Expansion of the alkyl region of the HSQC NMR spectrum revealed strong correlations to ~4 unique carbon atoms (red arrows, Figure 5.7), with many weaker signals likely corresponding to the fluxional species (blue arrows, Figure 5.7), again suggesting the presence of a single major static isomer of [Y(octapa)]$^-$, along with a fluxional species. Because yttrium typically forms 8-9 coordinate complexes, there is potentially a mixture of [Y(octapa)]$^-$ and [Y(octapa)(H_2O)]$^-$, with the single aqua ligand exchanging in solution and producing the observed fluxional species. It is unclear if these two isomers are a mixture of [Y(octapa)]$^-$ and [Y(octapa)(H_2O)]$^-$, or of different geometric isomers. RP-HPLC purification of [Y(octapa)]$^-$ revealed a single broad peak, as observed for all H_2dedpa/H_4octapa free ligand and metal complexes to date, suggesting that the two isomers have similar or identical physical properties (e.g. polarity). These VT-NMR and 2D NMR studies have not been performed on the [Lu(octapa)]$^-$ complex, but the similarities between their basic ^{1}H NMR spectra (Figure 5.2) would suggest that [Lu(octapa)]$^-$ also exists in solution as a mixture of a single static isomer and a fluxional species.

5.2.3 Density functional theory/molecular electrostatic potential structure prediction

Coordination geometries were calculated by density functional theory (DFT) calculations for both the binary 8-coordinate [Y(octapa)]$^-$ (Figure 5.8, a) complex and the 9-coordinate monohydrate [Y(octapa)(H_2O)]$^-$ (Figure 5.8, b), as yttrium can form either 8- or 9-coordinate complexes in solution. The DFT structures of the complexes [Lu(octapa)]$^-$, [Lu(octapa)(H_2O)]$^-$, and [In(octapa)]$^-$ have been calculated and studied previously in

Chapters 2-3.[87,89] The molecular electrostatic potential (MEP) surfaces shown in Figure 5.8 (bottom) show very similar charge distributions between the 8- or 9-coordinate complexes of octapa^{4-} with Y^{3+}, and are very similar to those calculated for the Lu^{3+} and In^{3+} complexes.[87,89] These observations suggest that the solution behavior of the coordination complexes of octapa^{4-} with Lu^{3+} and Y^{3+} may be very similar, with both metal complexes having the same overall 1- charge and nearly identical charge distributions as predicted by DFT/MEP calculations, foreshadowing both metal complexes to share *in vivo* properties.

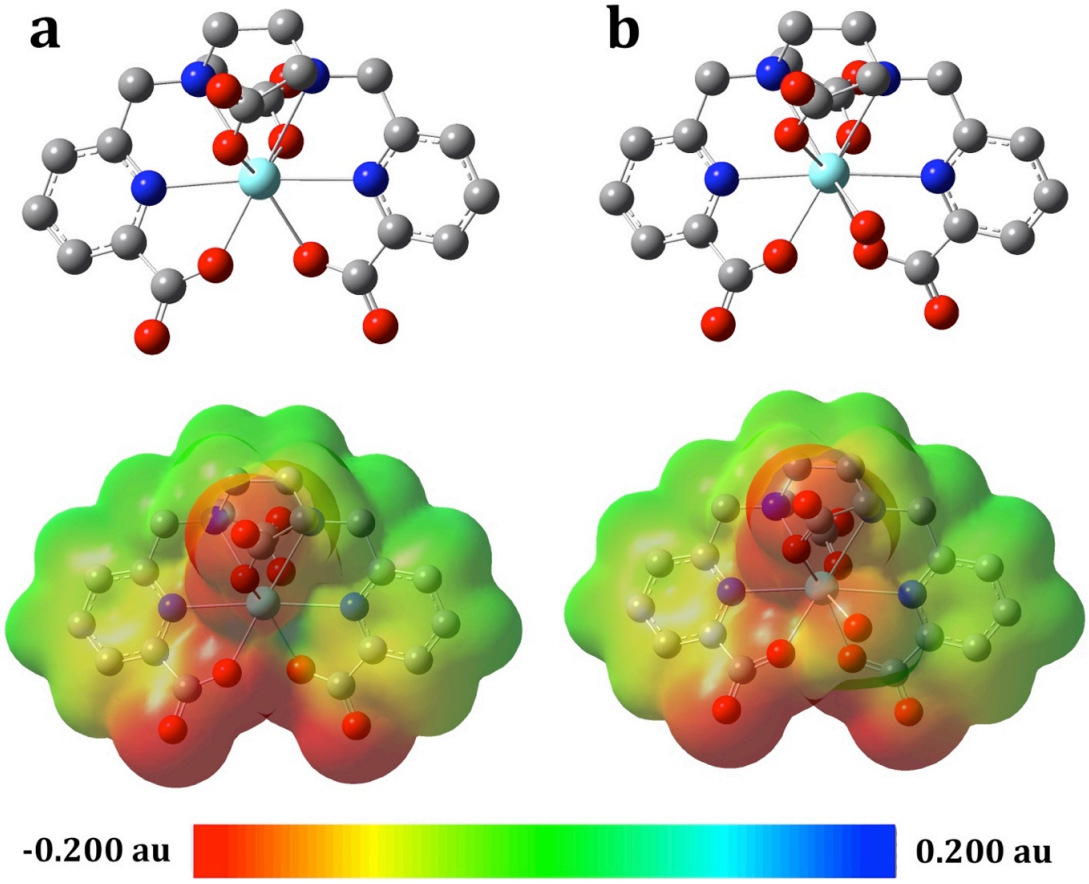

Figure 5.8 *In silico* DFT structure predictions: (a) 8-coordinate structure of $[Y(octapa)]^-$ (top, left); (b) 9-coordinate structure of $[Y(octapa)(H_2O)]^-$ (top, right), as well as the MEP polar-surface area maps (bottom) predicting the charge distribution over the solvent-exposed surface of the metal complexes (red = negative, blue = positive, representing a maximum potential of 0.200 au and a minimum of -0.200 au, mapped onto electron density isosurfaces of 0.002 $Å^{-3}$),]. DFT calculations performed by Dr. Jacqueline Cawthray.

5.2.4 Thermodynamic stability

The ligands H_2dedpa and H_4octapa have previously been evaluated with a number of metal ions, including Cu^{2+}, Ga^{3+}, In^{3+}, and Lu^{3+} (Chapters 2-3).[87,89,118,272,273] Recently, H_4octapa has been found to have exceptional radiolabeling properties with ^{111}In and ^{177}Lu, and has shown very promising *in vivo* behavior when compared to the industry "gold standards" DTPA and DOTA.[87,89] Thermodynamic stability constants for the ligands H_2dedpa, H_4octapa, DTPA, and DOTA, with the metal ions In^{3+}, Lu^{3+}, and Y^{3+} are shown in Table 5.1. The formation constant (log K_{ML}) and pM value for H_4octapa with Y^{3+} have been experimentally determined for the first time using EDTA competition potentiometric titrations. The pM (-log[M]) value was defined in Chapters 2-3.[68-71]

Table 5.1 Formation constants (log K_{ML}) and pM[a] values for In^{3+}, Lu^{3+}, and Y^{3+} complexes of relevant chelating ligand.

Ligand	M^{3+}	log K_{ML}	pM[a]	Ref.
$dedpa^{2-}$	In^{3+}	26.60(4)	25.9	89
$octapa^{4-}$	In^{3+}	26.8(1)	26.5	89
	Lu^{3+}	20.08(9)	19.8	87
	Y^{3+}	18.3(1)	18.1	
$DTPA^{4-}$	In^{3+}	29.0	25.7	119,317
	Lu^{3+}	22.6	19.1	87,119
	Y^{3+}	21.2, 21.9, 22.5	17.6-18.3[b]	131,132
$DOTA^{4-}$	In^{3+}	23.9(1)	18.8	68,119
	Lu^{3+}	21.6(1), 23.6, 25, 29.2	17.1	87,125,338,339
	Y^{3+}	24.3, 24.4, 24.9	19.3-19.8[b]	74,131,132
transferrin	In^{3+}	18.3	18.7	318
	Lu^{3+}	11.08	-	354
	Y^{3+}	-	-	-

[a] Calculated for 10 μM total ligand and 1 μM total [M^{3+}] at pH 7.4 and 25 °C.
[b] pM values for DTPA and DOTA with Y^{3+} were calculated for this work, based upon previously determined log K_{ML},[132] ligand pK_a,[119,131] and metal ion pK_a values.[163]

As determined in Chapters 2-3, H_4octapa has been shown to possess exceptionally high log K_{ML} and pM values with In^{3+} and Lu^{3+}, with pM values exceeding those of the ligands DTPA and DOTA (Table 5.1). The log K_{ML} for H_4octapa with Y^{3+} was determined to be 18.3 ± 0.1 (pM = 18.1) (Table 5.1). A comparison of the thermodynamic stability constant of H_4octapa to other ligands with Y^{3+} show the numbers being similar to DTPA, but lower than the current "gold standard" DOTA (Table 5.1). Values of pM were not available for DTPA and DOTA from the literature, and so values were calculated based on previously determined log K_{ML},[132] ligand pK_a,[119,131] and metal pK_a values.[163] From a range of log K_{ML} values that have been published for DTPA (21.2, 21.9) and DOTA (24.4, 24.9), pM values were calculated to be 17.6-18.3 (DTPA) and 19.3-19.8 (DOTA) (Table 5.1). Although thermodynamic parameters are very valuable, the *in vivo* stability is the most important factor for determining the usefulness of radiometal complexes, as thermodynamic stability may not correlate to *in vivo* stability. To this end, serum stability assays and studies in mice must be performed in the future with the $^{86/90}$Y complexes of H_4octapa to properly assess the potential utility for radiopharmaceutical applications.

5.3 Conclusions

The ligands H_2dedpa, H_4octapa, *p*-SCN-Bn-H_2dedpa, and *p*-SCN-Bn-H_4octapa were synthesized using a new *tert*-butyl ester protection group scheme, allowing for deprotection at room temperature in TFA, which compares favorably to the harsh conditions of heating HCl (6-12 M) or LiOH that were previously required for methyl ester cleavage. Additionally, the ligands H_2dedpa and *p*-SCN-Bn-H_2dedpa were synthesized using nosyl protection chemistry for the first time. Lyophilizing the final HPLC purified ligands yielded

trifluoroacetic acid salts, which were more soluble in water than their previously synthesized HCl counterparts, and were now soluble in methanol. The less harsh deprotection conditions afforded by the *tert*-butyl ester groups may allow these ligands to be incorporated into sensitive molecular scaffolds in the future, such as peptides synthesized on-resin (e.g. Wang resin), accommodating the standard deprotection conditions of a mixture of trifluoroacetic acid, dichloromethane, and triisopropylsilane. H_4octapa has been recently shown to be a very promising ligand for ^{111}In and ^{177}Lu in radiopharmaceutical applications, and density functional theory (DFT) calculations of the predicted structures of H_4octapa with Y^{3+}, In^{3+} and Lu^{3+} look similar. Potentiometric titrations have determined H_4octapa to have a formation constant (log K_{ML}) with Y^{3+} of 18.3 ± 0.1 (pM = 18.1), revealing high thermodynamic stability. Due to the excellent radiochemistry of H_4octapa with ^{111}In and ^{177}Lu, and the similarities in aqueous coordination chemistry between these metal ions and Y^{3+}, this suggests that H_4octapa may be a competent ligand for $^{86/90}$Y radiopharmaceutical applications.

5.4 Experimental

5.4.1 Materials and methods

All solvents and reagents were purchased from commercial suppliers (Sigma Aldrich, St. Louis, MO; TCI America, Portland, OR; Fisher Scientific, Waltham, MA) and were used as received unless otherwise indicated. Methyl-6-bromomethylpicolinate was synthesized according to a literature protocol.[89] Water used was ultra-pure (18.2 MΩ cm^{-1} at 25 °C, Milli-Q, Millipore, Billerica, MA). The analytical thin-layer chromatography (TLC) plates were aluminum-backed ultrapure silica gel (Siliaplate^{TM}, 60 Å pore size, 250 μM plate

thickness, Silicycle, Quebec, QC). Flash column silica gel was purchased from Silicycle (Siliaflash® Irregular Silica Gels F60, 60 Å pore size, 40-63 mm particle size, Silicycle, Quebec, QC). Automated column chromatography was performed using a Teledyne Isco (Lincoln, NE) CombiFlash® R_f automated system with solid load cartridges packed with flash column silica gel and RediSep R_f Gold® reusable normal-phase silica columns and neutral alumina columns (Teledyne Isco, Lincoln, NE). ^{1}H and ^{13}C NMR spectra were recorded on Bruker AV300, AV400, or AV600 instruments; all spectra were internally referenced to residual solvent peaks except for ^{13}C NMR spectra in D_2O, which were externally referenced to a sample of CH_3OH/D_2O. Low-resolution mass spectrometry was performed using a Waters liquid chromatography-mass spectrometer (LC-MS) consisting of a Waters ZQ quadrupole spectrometer equipped with an ESCI electrospray/ chemical ionization ion source and a Waters 2695 HPLC system (Waters, Milford, MA). High-resolution electrospray-ionization mass spectrometry (EI-MS) was performed by UBC MS staff on a Waters Micromass LCT time of flight instrument. Microanalyses for C, H, N were performed by UBC MS staff on a Carlo Erba EA 1108 elemental analyzer. The HPLC system used for purification of compounds consisted of a semi-preparative reverse phase C18 Phenomenex Synergi hydro-RP (80 Å pore size, 250 x 21.2 mm, Phenomenex, Torrance, CA) column connected to a Waters 600 controller, a Waters 2487 dual wavelength absorbance detector, and a Waters delta 600 pump.

5.4.2 *tert*-Butyl 6-(methyl)picolinate (5.1)

Commercially available 6-methylpicolinic acid (15.00 g, 109.38 mmol) was suspended in CH_2Cl_2 (500 mL). To the reaction mixture was added *tert*-butyl-2,2,2-

trichloroacetimidate (47.80 g, 218.8 mmol), followed by BF_3•etherate (20 μL per mmol of starting material, ~2.19 mL), and the mixture was stirred overnight at ambient temperature. The reaction mixture volume was reduced *in vacuo* to ~100 mL; the resulting white solid was isolated by filtration through a fritted glass filter and discarded, and the filtrate reduced to dryness *in vacuo*. The crude product was then resuspended in hexanes (~50 mL) and filtered again to remove additional white precipitate (unreacted *tert*-butyl-2,2,2-trichloroacetimidate, visualized by ninhydrin staining of TLC plates). The crude product was purified by silica chromatography (CombiFlash R_f automated column system; 80 g HP silica; A: CH_2Cl_2, B: MeOH, 100% A to 95% A gradient) to yield product **5.1** as a clear colourless oil, which later solidified into a, off-white wax (73%, ~15.4 g) (R_f: 0.6, TLC in 95% CH_2Cl_2: 5% MeOH). ^{1}H NMR (400 MHz, $CDCl_3$, 25 °C) δ: 7.75 (d, J = 7.8 Hz, 1H), 7.60 (t, J = 7.7 Hz, 1H), 7.21 (d, J = 7.9 Hz, 1H), 2.56 (s, 3H), 1.55 (s, 9H). ^{13}C NMR (100 MHz, $CDCl_3$, 25 °C) δ: 163.9, 158.7, 148.5, 136.7, 126.0, 121.6, 81.8, 27.8, 24.3. HR-ESI-MS calcd. for $[C_{11}H_{15}NO_2+H]^+$: 194.1181; found: 194.1183, $[M+H]^+$, PPM = 1.0.

5.4.3 *tert*-Butyl 6-(bromomethyl)picolinate (5.2)

Compound **5.1** (1.82 g, 9.45 mmol) was dissolved in CCl_4 (15 mL), followed by addition of *N*-bromosuccinimide (NBS, 1.18 g, 6.62 mmol) and benzoyl peroxide (Bz_2O_2, 0.2 g, ~10 wt %). The reaction mixture was brought to reflux for 4 h, removed from heat and allowed to cool to room temperature, filtered through a fritted glass filter, reduced to dryness *in vacuo*, resuspended in CH_2Cl_2, again filtered through a fritted glass filter and reduced to dryness. The crude product was purified by silica chromatography (CombiFlash R_f automated column system; 80 g HP silica; A: hexanes, B: ethyl acetate, 100% A to 75% A

gradient) to yield the product **5.2** as a waxy faint-yellow solid (40%, ~1.04 g) (R_f: 0.4, TLC in 75% hexanes: 25% ethyl acetate). In addition, ~1.15 g of starting material was recovered (R_f: 0.3, TLC in 75% hexanes: 25% ethyl acetate). The major byproduct observed was the dibrominated product (R_f: 0.5, TLC in 75% hexanes: 25% ethyl acetate). ^{1}H NMR (300 MHz, $CDCl_3$, 25 °C) δ: 7.86 (d, J = 7.1 Hz, 1H), 7.75 (t, J = 7.6 Hz, 1H), 7.57 (d, J = 7.1 Hz, 1H), 4.56 (s, 2H), 1.54 (s, 9H). ^{13}C NMR (75 MHz, $CDCl_3$, 25 °C) δ: 163.2, 157.0, 148.5, 137.8, 126.3, 123.7, 82.1, 33.1, 27.8. HR-ESI-MS calcd. for $[C_{11}H_{14}NO_2Br+H]^+$: 272.0286; found: 272.0289, $[M+H]^+$, PPM = 1.1.

5.4.4 *N,N*'-(2-Nitrobenzenesulfonamide)-1,2-diaminoethane (5.3)

Compound **5.3** was prepared according to a literature procedure:[87] ethylenediamine (548 μL, 8.2 mmol) was dissolved in THF (10 mL) and the solution vessel placed in an ice bath. Sodium bicarbonate (~2 g) was then added, followed by slow addition of 2-nitrobenzenesulfonyl chloride (4.00 g, 18.1 mmol). The reaction mixture was allowed to warm to ambient temperature and stirred overnight. The yellow mixture was filtered to remove sodium bicarbonate, reduced to dryness *in vacuo* to yield a red oil, and then dissolved in a minimum volume of dichloromethane and placed in the freezer overnight. The precipitated product was filtered and then washed with cold dichloromethane (3 x 10 mL). This process was repeated with the filtrate once more to recover more material. The faint yellow powder (**5.3**) was dried *in vacuo* for a yield of 87% (~3.07 g). ^{1}H NMR (300 MHz, DMSO-d_6, 25 °C) δ: 8.16 (br s, 2H), 8.00-7.94 (m, 4H), 7.90-7.83 (m, 4H), 3.00 (s, 4H). ^{13}C NMR (75 MHz, DMSO-d_6, 25 °C) δ: 147.6, 134.2, 132.8, 132.4, 129.4, 124.5, 42.4. HR-ESI-MS calcd. for $[C_{14}H_{14}N_4O_8S_2+Na]^+$: 453.0151; found: 453.0154 $[M+Na]^+$, PPM = 0.7.

5.4.5 *N,N'*-(2-Nitrobenzenesulfonamide)-*N,N'*-[6-(*tert*-butoxycarbonyl)pyridin-2-yl]methyl]-1,2-diaminoethane (5.4)

To a solution of **5.3** (0.206 g, 0.479 mmol) in dimethylformamide (10 mL, dried over molecular sieves, 4 Å) was added **5.2** (0.391 g, 1.44 mmol) and sodium carbonate (~1 g). The faint yellow reaction mixture was stirred at 80 °C for 48 h, filtered to remove sodium carbonate, and concentrated *in vacuo*. The separation of the mono- and di-alkylated products was very difficult, and so the reaction was left until as complete as possible. The crude product was purified by silica chromatography (CombiFlash R_f automated column system; 40 g HP silica; A: hexanes, B: ethyl acetate, 100% A to 50% A slow gradient) to yield the product **5.4** as light yellow fluffy solid (55%, ~0.213 g) (R_f : 0.9, TLC in 95% dichloromethane: 5% MeOH). ^{1}H NMR (400 MHz, $CDCl_3$, 25 °C) δ: 8.18-8.16 (m, 2H), 7.86 (d, J = 7.6 Hz, 2H), 7.73 (t, J = 7.6 Hz, 2H), 7.69-7.62 (m, 4H), 7.60-7.56 (m, 2H), 7.50 (d, J = 7.6 Hz, 2H), 4.73 (s, 4H), 3.56 (s, 4H), 1.58 (s, 18H). ^{13}C NMR (100 MHz, $CDCl_3$, 25 °C) δ: 163.4, 156.1, 148.9, 147.9, 137.7, 133.5, 132.6, 132.1, 131.4, 125.3, 123.9, 123.7, 82.0, 53.3, 46.5, 28.0. HR-ESI-MS calcd. for $[C_{36}H_{40}N_6O_{12}S_2+Na]^+$: 835.2043; found: 835.2042, $[M+Na]^+$, PPM = -0.1.

5.4.6 *N,N'*-[6-(*tert*-Butoxycarbonyl)pyridin-2-yl]methyl-1,2-diaminoethane (5.5)

To a solution of **5.4** (0.234 g, 0.288 mmol) in tetrahydrofuran (5 mL) was added thiophenol (68 μL, 0.662 mmol) and potassium carbonate (excess, ~0.5 g). The reaction mixture was stirred at 50 °C for 48 h, during which time a colour change from colourless to dark yellow occurred. In Chapter 3, the potassium carbonate had become sticky during the

course of the reaction, and would clog fritted glass filters, and so it was removed via centrifugation in 20 mL centrifuge tubes.[87,304] Here the crude reaction mixture was less sticky than previously found, and was filtered with a large fritted glass filter, rinsed liberally with THF and CH_3CN, and then concentrated to dryness *in vacuo*. The resulting crude yellow oil was purified by silica chromatography (CombiFlash R_f automated column system; 24 g neutral alumina; A: dichloromethane, B: methanol, 100% A to 75% A gradient) to yield **5.5** as clear colourless oil (80%, ~0.102 g). Compound **5.5** was purified using column chromatography on neutral alumina; silica should be avoided as **5.5** has a high affinity for silica and requires the use of ammonium hydroxide and >20% methanol for elution, giving partial *tert*-butyl ester deprotection and dissolution of some silica. ^{1}H NMR (400 MHz, $CDCl_3$, 25 °C) δ: 7.87 (d, J = 7.6 Hz, 2H), 7.74 (t, J = 7.6 Hz, 2H), 7.52 (d, J = 7.6 Hz, 2H), 4.00 (s, 4H), 2.81 (s, 4H), 2.26 (s, -N*H*-, 2H), 1.61 (s, 18H). ^{13}C NMR (100 MHz, $CDCl_3$, 25 °C) δ: 164.1, 160.5, 148.8, 137.1, 125.0, 122.9, 99.9, 81.9, 55.0, 49.0, 28.0. HR-ESI-MS calcd. for $[C_{24}H_{34}N_4O_4+K]^+$: 481.2217; found: 481.2213, $[M+K]^+$, PPM = -0.8.

5.4.7 H_2dedpa, *N*,*N*′-[(6-carboxylato)pyridin-2-yl)methyl]-1,2-diaminoethane (5.6)

Compound **5.5** (49.3 mg, 0.114 mmol) was dissolved in a mixture of trifluoroacetic acid (TFA) (1 mL) and CH_2Cl_2 (1 mL) and stirred overnight at room temperature. The reaction mixture was concentrated *in vacuo* and then purified via semi-preparative reverse-phase HPLC (10 mL/min, gradient: A: 0.1% TFA in deionized water, B: 0.1% TFA in CH_3CN. 5% to 50% B linear gradient 30 min. t_R = 14.8 min, broad). Product fractions were pooled and lyophilized to a white powder overnight. The trifluoroacetate salt H_2dedpa•2trifluoroacetate •1.5H_2O **(5.6)** was obtained as a white solid (~45 mg, 67% yield,

using the molecular weight of the trifluoroacetate salt as determined by elemental analysis), with a cumulative yield of 26% over 4 steps. ^{1}H NMR (300 MHz, MeOD, 25 °C) δ: 8.19 (d, *J* = 7.7 Hz, 2H, pyr-*H*), 8.11 (t, *J* = 7.7 Hz, 2H, pyr-*H*), 7.76 (d, *J* = 7.8 Hz, 2H, pyr-*H*), 4.78 (s, 4H, Pyr-C*H*$_2$-N), 3.72 (s, 4H, ethylene-*H*). ^{13}C NMR (75 MHz, MeOD, 25 °C) δ: 167.8, 153.3, 148.6, 140.8, 127.7, 126.5, 50.9, 45.6. IR (neat, ATR-IR): ν = 1719 cm^{-1} (C=O), 1679/1591 cm^{-1} (C=C py). HR-ESI-MS calcd. for $[C_{16}H_{18}N_4O_4 + H]^+$: 331.1406; found $[M + H]^+$: 331.1409, PPM = 0.9. Elemental analysis: calcd % for H_2dedpa•2CF_3COOH•1.5H_2O ($C_{16}H_{18}N_4O_4$•2CF_3COOH•1.5H_2O = 585.408): C 41.03, H 3.96, N 9.57; found: C 40.92 (Δ = 0.11), H 3.97 (Δ = 0.01), N 9.32 (Δ = 0.25).

5.4.8 *N*,*N*′-[(*tert*-Butoxycarbonyl)methyl-*N*,*N*′-[6-(*tert*-butoxycarbonyl)pyridin-2-yl]methyl]-1,2-diaminoethane (5.7)

To a solution of **5.5** (22.8 mg, 0.0515 mmol) in acetonitrile (5 mL) was added *tert*-butylbromoacetate (18.3 μL, 0.124 mmol) and sodium carbonate (~300 mg). The reaction mixture was stirred at 60 °C for 48 h. Sodium carbonate was removed by filtration and the crude reaction mixture was concentrated *in vacuo*. The crude oil was purified by column chromatography (CombiFlash R_f automated column system; 40 g HP silica; A: dichloromethane, B: methanol, 100% A to 80% A gradient) to afford the product **5.7** as light yellow oil (96%, ~33.2 mg) (R_f: 0.65, TLC in 80% dichloromethane: 20% MeOH). ^{1}H NMR (400 MHz, $CDCl_3$, 25 °C) δ: 7.90-7.89 (m, 4H), 7.55-7.53 (m, 2H), 3.86 (s, 4H), 3.05 (s, 4H), 2.68 (s, 4H), 1.50 (s, 18H), 1.33 (s, 18H). ^{13}C NMR (100 MHz, $CDCl_3$, 25 °C) δ: 171.6, 163.8, 158.1, 148.1, 138.7, 126.7, 123.5, 82.9, 82.0, 60.5, 56.1, 53.3, 27.8. HR-ESI-MS calcd. for $[C_{36}H_{54}N_4O_8+H]^+$: 671.4020; found: 671.4019, $[M+H]^+$, PPM = -0.1.

5.4.9 H_4octapa, *N,N'*-[(6-carboxylato)pyridin-2-yl)methyl]-*N,N'*-diacetic acid-1,2-diaminoethane (5.8)

Compound **5.7** (33.2 mg, 0.0495 mmol) was dissolved in a mixture of trifluoroacetic acid (TFA) (1 mL) and CH_2Cl_2 (1 mL) and stirred overnight at room temperature. The reaction mixture was concentrated *in vacuo* and then purified via semi-preparative reverse-phase HPLC (10 mL/min, gradient: A: 0.1% TFA in deionized water, B: 0.1% TFA in CH_3CN. 5% to 50% B linear gradient 30 min. t_R = 14.8 min, broad). Product fractions were pooled and lyophilized to a white powder overnight. The trifluoroacetate salt H_4octapa•2trifluoroacetate **(5.8)** was obtained as white solid (~45 mg, 74% yield, using the molecular weight of the trifluoroacetate salt as determined by elemental analysis), with a cumulative yield of ~27% over 5 steps. ^{1}H NMR (300 MHz, MeOD, 25 °C) δ: 8.04 (d, *J* = 7.6, 2H, pyr-*H*), 7.95 (t, *J* = 7.7, 2H, pyr-*H*), 7.63 (d, *J* = 7.5, 2H, pyr-*H*), 4.59 (s, 4H, Pyr-C*H*$_2$-N), 4.07 (s, 4H, HOOC-C*H*$_2$-N), 3.63 (s, 4H, ethylene-*H*). ^{13}C NMR (75 MHz, MeOD, 25 °C) δ: 171.8, 167.4, 156.7, 148.9, 140.0, 128.6, 125.8, 58.9, 56.0, 52.3. IR (neat, ATR-IR): ν = 1687/1672 cm^{-1} (C=O), 1618/1594 cm^{-1} (C=C py). HR-ESI-MS calcd. for $[C_{20}H_{22}N_4O_8 + H]^+$: 447.1516; found $[M + H]^+$: 447.1515, PPM = -0.2. Elemental analysis: calcd % for H_4octapa•2CF_3COOH ($C_{20}H_{22}N_4O_8$•2CF_3COOH = 674.457): C 42.74, H 3.59, N 8.31; found: C 42.51 (Δ = 0.23), H 3.69 (Δ = 0.10), N 8.38 (Δ = 0.07).

5.4.10 Na[Y(octapa)] (5.9)

H_4octapa **(5.8)** (10 mg, 0.015 mmol) was suspended in 0.1 M HCl (1.0 mL) and YCl_3•$6H_2O$ (5.5 mg, 0.018 mmol) was added. The pH was adjusted to ~4.0-4.5 using 0.1 M

NaOH and then the solution was stirred at room temperature. After 1 hour the product was confirmed via mass spectrometry and the solvent was removed *in vacuo* to yield Na[Y(octapa)] **(5.9)**. ^{1}H NMR (400 MHz, D_2O, 25 °C) δ: 8.11-7.99 (m, 4H), 7.75-7.61 (m, 2H), 4.34-4.30 (m, 1H), 4.10-4.06 (m, 1H), 3.94 (m, 1H), 3.80-3.77 (m, 1H) 3.62 (m, 1H), 3.49-3.26 (m, 2H), 3.16 (m, 2H), 2.95-2.94 (m, 1H), 2.48-2.45 (m, 1H), 2.14-2.13 (m, 1H). ^{1}H NMR (300 MHz, DMSO-d_6, 25 °C) δ: 8.12-7.48 (m, 4H), 7.60-7.28 (m, 2H), 4.50-3.80 (m, 6H), 3.25-2.50 (m, 6H). ^{13}C NMR (150 MHz, DMSO-d_6, 25 °C) δ: 176.2, 168.8, 168.5, 168.2, 158.7, 157.5, 156.3, 155.7, 152.9, 152.8, 152.3, 141.5, 140.8, 140.4, 131.2, 130.5, 129.2, 124.7, 124.3, 124.1, 123.7, 122.9, 122.7, 122.6, 122.6, 122.4, 82.4, 62.9, 62.5, 62.1, 58.2, 56.9, 55.0, 53.7, 47.9, 40.0. HR-ESI-MS calcd. for $[C_{20}H_{18}{}^{89}YN_4O_8 + 2Na]^+$: 576.9979; found: 576.9966, $[M + 2Na]^+$, PPM = -2.2.

5.4.11 1-(*p*-Nitrobenzyl)ethylenediamine (5.10)

Compound **5.10** was prepared according to a literature procedure,[342] and was purified with a modified procedure using column chromatography (CombiFlash R_f automated column system; 40 g HP silica;, A: 95% dichloromethane 5% ammonium hydroxide, B: 95% methanol 5% ammonium hydroxide, 100% A to 30% B gradient) to afford a **5.10** as brown/amber oil in a cumulative yield of 40% over 3 steps. ^{1}H NMR (300 MHz, $CDCl_3$, 25 °C) δ: 7.91 (d, J = 8.9 Hz, 2H), 7.18 (d, J = 8.5 Hz, 2H), 2.80-2.57 (m, 3H), 2.45-2.31 (m, 2H). ^{13}C NMR (75 MHz, $CDCl_3$, 25 °C) δ: 147.1, 147.7, 129.4, 122.8, 54.2, 47.5, 41.4. HR-ESI-MS calcd. for $[C_9H_{13}N_3O_2+H]^+$: 196.1086; found: 196.1084 [M + H], PPM = -1.0.

5.4.12 *N,N'*-(2-Nitrobenzenesulfonamide)-1-(*p*-nitrobenzyl)-1,2-diaminoethane (5.11)

Compound **5.11** was prepared according to a literature procedure.[87] Briefly, **5.10** (578 mg, 2.96 mmol) was dissolved in THF (10 mL) in a round bottom flask and placed in an ice bath, then sodium bicarbonate (~2 g) was added, followed by slow addition of 2-nitrobenzenesulfonyl chloride (1.58 g, 7.1 mmol). The reaction mixture was heated to 50 °C and stirred overnight. The yellow/orange mixture was filtered to remove sodium bicarbonate, rotary evaporated to an orange oil, dissolved in a minimum volume of dichloromethane and then placed in the freezer. The precipitated product was filtered and then washed with cold dichloromethane (3 x 10 mL); this process was repeated with the filtrate twice more to recover more product. The faint yellow powder (**5.11**) was dried *in vacuo* for a yield of 74% (~1.24 g) (R_f: 0.90, TLC in 10% methanol in dichloromethane). ^{1}H NMR (300 MHz, acetone-d_6, 25 °C) δ: 8.18-8.15 (m, 1H), 7.99-7.94 (m, 2H), 7.79-7.57 (m, 5H), 7.33 (d, J = 8.5 Hz, 2H), 7.04-6.98 (m, 2H), 4.01 (br s, 1H), 3.41-3.38 (m, 2H), 3.26 (dd, J = 3.4, 13.7 Hz, 1H), 2.98 (m, 1H). ^{13}C NMR (75 MHz, acetone-d_6, 25 °C) δ: 206.3, 149.2, 148.1, 147.6, 146.7, 135.2, 134.8, 134.2, 133.9, 133.8, 133.6, 131.7, 131.4, 130.9, 126.0, 125.7, 123.9, 57.7, 49.3, 38.2. HR-ESI-MS calcd. for $[C_{21}H_{19}N_5O_{10}S_2+Na]^+$: 588.0471; found: 588.0465 $[M+Na]^+$, PPM = -1.0.

5.4.13 *N,N'*-(2-Nitrobenzenesulfonamide)-*N,N''*-[6-(methoxycarbonyl)pyridin-2-yl]methyl]-1-(*p*-nitrobenzyl)-1,2-diaminoethane (5.12)

To a solution of **5.11** (188 mg, 0.332 mmol) in dimethylformamide (5 mL, dried over molecular sieves, 4 Å) was added **5.2** (225.8 mg, 0.830 mmol) and sodium carbonate (~0.5 g). The yellow reaction mixture was stirred at 80 °C for 48 h, over which time the colour

slowly changed to red. The reaction mixture was filtered to remove sodium carbonate and concentrated *in vacuo*. As with the analogous compound **5.4**, chromatographic separation of the mono- and di-alkylated product was very difficult, with the Rf difference being ~ 0.1 in 50:50 hexanes:ethyl acetate. The crude product was purified by silica chromatography (CombiFlash R_f automated column system; 40 g HP silica; A: hexanes, B: ethyl acetate, 100% A to 50% A gradient) to yield **5.12** as faint yellow solid (81%, ~255 mg) (Rf = 0.65 in 50:50 EtOAc:Hex). ^{1}H NMR (300 MHz, $CDCl_3$, 25 °C) δ: 8.00-7.83 (m, 4H), 7.78-7.60 (m, 7H), 7.59-7.7.42 (m, 4H), 7.38-7.21 (m, 1H), 7.01 (d, J = 9 Hz, 2H), 4.97-4.65 (m, 4H), 4.36-4.29 (m, 1 H), 3.40-3.24 (m, 2H), 3.20-3.11 (m, 1H), 3.00-2.93 (m, 1H), 1.58 (s, 9H), 1.56 (s, 9H). ^{13}C NMR (75 MHz, $CDCl_3$, 25 °C) δ: 163.5, 163.2, 157.5, 155.9, 148.7, 148.6, 147.7, 146.9, 146.1, 144.7, 137.9, 137.7, 133.7, 133.3, 132.5, 132.3, 132.1, 132.0, 131.4, 129.6, 126.5, 125.3, 124.0, 123.9, 123.8, 123.8, 122.9, 82.2, 82.1, 57.8, 53.0, 51.4, 49.8, 34.4, 27.9. HR-ESI-MS calcd. for $[C_{43}H_{45}N_7O_{14}S_2+Na]^+$: 970.2364; found: 970.2355, $[M+Na]^+$, PPM = -0.9.

5.4.14 *N,N'*-[[6-(Methoxycarbonyl)pyridin-2-yl]methyl]-1-(*p*-nitrobenzyl)-1,2-diaminoethane (5.13)

To a solution of **5.12** (125 mg, 0.132 mmol) in tetrahydrofuran (5 mL) was added thiophenol (31 μL, 0.304 mmol) and potassium carbonate (excess, ~300 mg). The reaction mixture was stirred at 60 °C for 48 h, over which time the colour slowly changed from colourless to dark yellow. The crude reaction mixture was filtered with a fritted glass filter, rinsed *ad libitum* with THF and CH_3CN, and then concentrated to dryness *in vacuo*. The resulting crude yellow oil was purified by silica chromatography (CombiFlash R_f automated

column system; 24 g neutral alumina; A: dichloromethane, B: methanol, 100% A to 75% A gradient) to yield **5.13** as light yellow oil (70%, ~76 mg). ^{1}H NMR (400 MHz, $CDCl_3$, 25 °C) δ: 8.09 (d, *J* = 8.9 Hz, 2H), 7.86 (d, *J* = 7.9 Hz, 2H), 7.74-7.69 (m, 2H), 7.46 (t, *J* = 8.6 Hz, 2H), 7.34 (d, *J* = 8.5 Hz, 2H), 4.06-3.88 (m, 4H), 3.01-2.96 (m, 2H), 2.88-2.82 (m, 1H), 2.69-2.66 (m, 1H), 2.56-2.52 (m, 1H), 1.60 (s, 18H). ^{13}C NMR (100 MHz, $CDCl_3$, 25 °C) δ: 163.9, 163.9, 160.4, 148.7, 148.6, 147.3, 146.4, 137.2, 137.1, 130.1, 125.1, 125.0, 123.4, 122.9, 81.9, 58.3, 54.9, 52.4, 51.7, 39.2. HR-ESI-MS calcd. for $[C_{31}H_{39}N_5O_6+H]^+$: 578.2979; found: 578.2984, $[M+H]^+$, PPM = 0.9.

5.4.15 *p*-SCN-Bn-H_2dedpa, *N,N'*-[[(6-carboxylato)pyridin-2-yl]methyl]-1-(*p*-benzylisothiocyanato)-1,2-diaminoethane (5.14)

Compound **5.13** (43.1 mg, 0.0746 mmol) was dissolved in glacial acetic acid (2.5 mL) with hydrochloric acid (2.5 mL, 3 M), palladium on carbon (20 wt%), and hydrogen gas (balloon). The reaction mixture was stirred vigorously at rt for 1 hour, then filtered to remove Pd/C and washed *ad libitum* with acetonitrile and hydrochloric acid (3 M). The product was confirmed by low-resolution mass spectrometry (LRMS), and revealed that the *tert*-butyl ester protecting groups remained intact. The crude product was dissolved in HCl (2-3 mL, 3M), and heated to reflux for 1 minute. Following this heating step, quantitative removal of the *tert*-butyl ester protecting groups was confirmed by LRMS. Without purification, the crude reaction mixture (in 2-3 mL of 3M HCl) was mixed with thiophosgene (suspension in chloroform) in ~0.2 mL of additional chloroform (~86 μL, 1.12 mmol) to react overnight at ambient temperature with vigorous stirring. The reaction mixture was washed with chloroform (5 x 1 mL) by vigorous biphasic stirring, followed by decanting of

the organic phase with a pipette to remove excess thiophosgene, diluted to a volume of 4.5 mL with deionized water, and injected directly onto a semi-preparative HPLC column for purification (A: 0.1% TFA in deionized water, B: 0.1% TFA in CH_3CN, 95% A to 60% B gradient over 40 min). *p*-SCN-Bn-H_2dedpa•2trifluoroacetate•H_2O **(5.14)** was found in the largest peak at R_t = 29 min, lyophilized overnight, and was isolated as a white solid (~23 mg, 43% over 3 steps from **5.13**, using the molecular weight of the trifluoroacetate salt as determined by elemental analysis). ^{1}H NMR (400 MHz, MeOD, 25 °C) δ: 8.18-8.08 (m, 4H), 7.77-7.72 (m, 2H), 7.36 (d, *J* = 8.5 Hz, 2H), 7.23 (m, *J* = 8.5 Hz, 2H), 4.95-4.84 (m, 3H), 4.68 (d, *J* = 16.7 Hz, 1H), 4.03-3.97 (m, 1H), 3.71-3.65 (m, 1H), 3.52-3.47 (m, 2H), 3.01-2.95 (m, 1H). ^{13}C NMR (100 MHz, MeOD, 25 °C) δ: 167.7, 167.6, 153.9, 153.5, 153.3, 148.4, 140.9, 140.3, 137.7, 135.5, 132.3, 132.2, 132.0, 130.6, 127.7, 127.4, 127.3, 126.6, 126.5, 59.8, 59.5, 50.7, 35.8. IR (neat, ATR-IR): ν = 2097 cm^{-1} (S=C=N-), 1665 cm^{-1} (C=O), 1594 cm^{-1} (C=C py). HR-ESI-MS calcd. for $[C_{24}H_{23}N_5O_4S + H]^+$: 478.1549; found $[M + H]^+$: 478.1548, PPM = -0.2. Elemental analysis: calcd % for *p*-SCN-Bn-H_2dedpa•2CF_3COOH•1H_2O ($C_{24}H_{23}N_5O_4S$•2CF_3COOH•1H_2O = 723.597): C 46.48, H 3.76, N 9.68; found: C 46.68 (Δ = 0.20), H 3.73 (Δ = 0.03), N 9.60 (Δ = 0.08).

5.4.16 *N,N'*-[(*tert*-Butoxycarbonyl)methyl]-*N,N'*-[[(6-*tert*-butoxycarbonyl)pyridin-2-yl]methyl]-1-(*p*-nitrobenzyl)-1,2-diaminoethane (5.15)

To a solution of **5.13** (78.1 mg, 0.135 mmol) in acetonitrile (15 mL) was added *tert*-butylbromoacetate (~48 μL, 0.324 mmol) and potassium carbonate (~500 mg). The reaction mixture was stirred at 80 °C for 48 h. Potassium carbonate was removed by filtration and the crude reaction mixture was concentrated *in vacuo*. The crude oil was purified by column

chromatography (CombiFlash R_f automated column system; 24 g HP silica; A: dichloromethane, B: methanol, 100% A to 80% A gradient) to afford the product **5.15** as light yellow oil (63%, ~69 mg) (R_f = 0.61 in 80:20 CH_2Cl_2:MeOH). ^{1}H NMR (400 MHz, $CDCl_3$, 25 °C) δ: 8.02-7.97 (m, 3H), 7.89-7.73 (m, 3H), 7.64-7.60 (m, 1H), 7.56-7.46 (m, 3H), 4.03-3.93 (m, 4H), 3.43-3.21 (m, 4H), 3.03-2.95 (m, 2H), 2.86-2.81 (m, 2H), 2.50-2.45 (m, 1H), 1.62 (m, 18H), 1.46 (m, 18H). ^{13}C NMR (100 MHz, $CDCl_3$, 25 °C) δ: 170.6, 170.5, 163.9, 160.2, 160.1, 148.7, 148.6, 148.2, 146.2, 136.9, 136.9, 130.2, 126.1, 125.6, 123.4, 123.2, 123.1, 82.0, 81.9, 81.1, 80.9, 61.4, 60.8, 56.9, 56.6, 54.1, 52.4, 35.7, 29.6, 28.1, 28.1, 28.0. HR-ESI-MS calcd. for $[C_{43}H_{59}N_5O_{10}+H]^+$: 806.4340; found: 806.4339, $[M+H]^+$, PPM = -0.1.

5.4.17 *p*-SCN-Bn-H$_4$octapa, *N,N'*-[(Carboxylato)methyl]-*N,N'*-[[(6-carboxylato)pyridin-2-yl]methyl]-1-(*p*-benzylisothiocyanato)-1,2-diaminoethane (5.16)

Compound **5.15** (59.6 mg, 0.0739 mmol) was dissolved in glacial acetic acid (2.5 mL) with hydrochloric acid (2.5 mL, 3 M), palladium on carbon (30 wt%), and hydrogen gas (balloon). The reaction mixture was stirred vigorously at rt for 1 hour, filtered to remove Pd/C and washed *ad libitum* with acetonitrile and hydrochloric acid (3 M). The product was confirmed by low-resolution mass spectrometry (LRMS), and revealed that two of the *tert*-butyl ester protecting groups remained intact and two had been removed. Based on the results from compound **5.14**, the *tert*-butyl esters protecting the picolinic acid moiety were probably the two left intact. The crude product was dissolved in HCl (2-3 mL, 3M), and heated to reflux for 1 minute to effect full ester deprotection. Following heating, quantitative removal of the *tert*-butyl ester protecting groups was confirmed by LRMS. Without

purification, the crude reaction mixture (in 2-3 mL of 3M HCl) was mixed with thiophosgene (suspension in chloroform) in ~0.2 mL of additional chloroform (~85 μL, 1.11 mmol) to react overnight at ambient temperature with vigorous stirring. The reaction mixture was washed with chloroform (5 x 1 mL) by vigorous biphasic stirring followed by decanting of the organic phase with a pipette to remove excess thiophosgene, diluted to a volume of 4.5 mL with deionized water, and injected directly onto a semi-preparative HPLC column for purification (A: 0.1% TFA in deionized water, B: 0.1% TFA in CH_3CN, 100% A to 40% A gradient over 40 min). *p*-SCN-Bn-H_4octapa•2trifluoroacetate •0.5H_2O•0.5CH_3CN **(5.16)** was found in the largest peak at R_t = 34.5 min, lyophilized overnight, and was isolated as a white solid (~11 mg, 25% over 3 steps from **5.15**, using the molecular weight of the trifluoroacetate salt as determined by elemental analysis). ^{1}H NMR (400 MHz, MeOD, 25 °C) δ: 8.03-7.90 (m, 4H), 7.61-7.56 (m, 2H), 7.21-7.11 (m, 4H), 5.07 (m, 2H), 4.70 (m, 2H), 4.52-4.48 (m, 2H), 4.16-4.13 (m, 1H), 4.00-3.94 (m, 2H), 3.68-3.57 (m, 2H), 3.25-3.20 (m, 1H), 2.68-2.62 (m, 1H). ^{13}C NMR (150 MHz, MeOD, 25 °C) δ: 174.5, 169.3, 167.8, 167.4, 167.2, 160.8, 152.7, 149.1, 148.6, 140.0, 139.9, 138.9, 131.8, 131.7, 131.1, 129.2, 128.0, 127.0, 126.1, 125.3, 125.1, 61.1, 55.5, 52.1, 50.7, 38.1, 34.7. IR (neat, ATR-IR): ν = 2096 cm^{-1} (S=C=N-), 1703/1660 cm^{-1} (C=O), 1593 cm^{-1} (C=C py). HR-ESI-MS calcd. for $[C_{28}H_{27}N_5O_8S + H]^+$: 594.1659; found $[M + H]^+$: 594.1650, PPM = -1.5. Elemental analysis: calcd % for *p*-SCN-Bn-H_4octapa •2CF_3COOH •0.5H_2O •0.5CH_3CN ($C_{28}H_{27}N_5O_8S$ •2CF_3COOH •0.5H_2O •0.5CH_3CN = 851.188): C 46.57, H 3.73, N 9.05; found: C 46.92 (Δ = 0.35), H 4.00 (Δ = 0.27), N 8.67 (Δ = 0.38).

5.4.18 Solution thermodynamics

The experimental procedures and details of the apparatus closely followed our reported studies of H_2dedpa/Ga^{3+}, and those outlined in Chapters 2 and 3, with the following changes.[87,89,118] As a result of the strength of the binding of the Y^{3+} complex $[Y(octapa)]^-$, the complex formation constant with this ligand could not be determined directly and ligand-ligand competition using Na_2H_2EDTA was used. Potentiometric titrations were performed with great assistance from Dr. Jacqueline Cawthray using a Metrohm Titrando 809 equipped with a Ross combination pH electrode and a Metrohm Dosino 800. Equilibration times for titrations were up to 10 min for pK_a titrations and up to 3 h for metal complex titrations. The proton dissociation constants corresponding to hydrolysis of $Y^{3+}_{(aq)}$ ion included in the calculations were taken from Baes and Mesmer.[163] The K_{ML} value for the yttrium-EDTA complex was taken from Martell.[119] It was necessary to include a ML(OH) species in the equilibrium model used for fitting where log $K_{ML(OH)}$ = 10.6(1). This is consistent with a 9-coordinate structure and only becomes relevant above pH 9.5. Values of pM were calculated at physiologically relevant conditions of pH 7.4, 10 μM ligand, and 1 μM metal. All values and errors represent the average of at least three independent experiments.

5.4.19 Molecular modeling

Calculations were performed by Dr. Jacqueline Cawthray using the Gaussian 09[327] and GaussView packages. Molecular geometries and electron densities were obtained from density functional theory calculations, with the B3LYP functional employing the 6-31+G(d,p) basis set for 1st and 2nd row elements and the Stuttgart−Dresden effective core potential, SDD for yttrium.[328,329,343] Solvent (water) effects were described through a

continuum approach by means of the IEF PCM as implemented in G09. The electrostatic potential was mapped onto the calculated electron density surface. The corresponding harmonic vibration frequencies were computed at the same level to characterize the geometry as a minima.

Chapter 6: H_4octapa vs H_4C3octapa for ^{111}In and ^{177}Lu radiochemistry: the difference of one carbon

This chapter is an adaptation of a manuscript in preparation for publication, Price, E. W.; Zeglis, B. M.; Cawthray, J. F.; Lewis, J. S.; Adam, M. J.; Orvig, C., H_4octapa vs H_4C3octapa for In-111 and Lu-177 Radiochemistry: the Difference of One Carbon. Expected submission date April-May **2014**.

6.1 Introduction

In recent years, radiometal-based radiopharmaceuticals have been increasingly recognized for their utility in diagnostic and therapeutic medicine.[1-3,6,7,25,28,36,56] The modular and versatile nature of these systems has been continually espoused throughout this thesis, and allows for a continually increasing number of routinely produced radiometals to be harnessed for single photon emission computed tomography (SPECT), positron emission tomography (PET), and therapy (e.g. Auger electron, β^-, α).[1-3,6,7,25,28,36,56] It has become increasing evident that the bifunctional chelator (bifunctional ligand) is perhaps the most crucial piece of these intricate radiopharmaceuticals, with the bifunctional chelator needing to be carefully matched to each radiometal so that maximum stability and radiolabeling efficiency can be achieved.[1-3,6,7,25,28,36,56] The process of carefully matching a wide-selection of ligands and radiometals to each other is complicated, and it has become apparent that even subtle changes to the structure, site of conjugation, and donor arms of ligands can cause drastic changes. It can be difficult to properly assess the stability of a selection of ligands

with various radiometals, and proper comparisons require extensive *in vitro* and *in vivo* experiments. Whether ligands are modified to add functional groups to allow conjugation with targeting vectors (e.g. peptides, antibodies, nanoparticles), or small changes to ligand donor arms to change the denticity are made, or donor types are modified (e.g. changing primary amines to secondary amines), the effects can be significant.

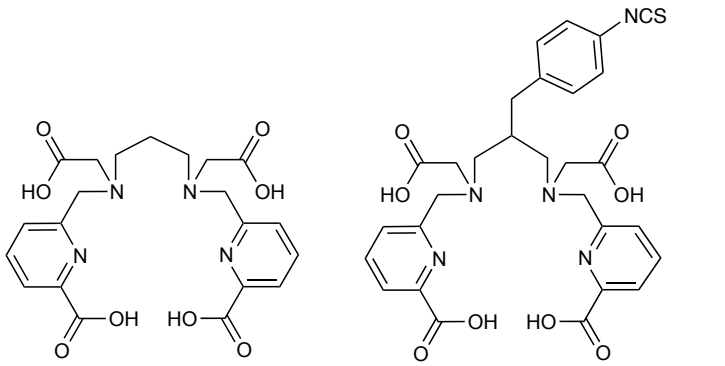

H_4C3octapa (6.5) **p-SCN-Bn-H_4C3octapa (6.15)**

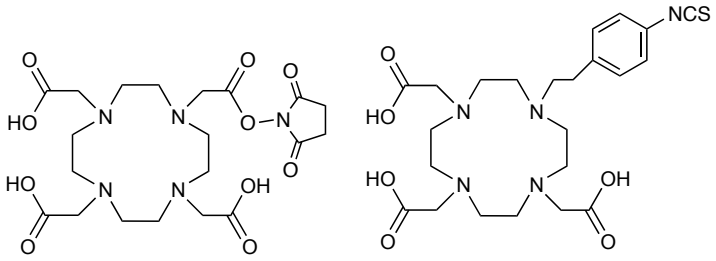

DO3A-NHS **DO3A-SCN**

Figure 6.1 Structures of the new pyridinecarboxylate-based ligand H_4C3octapa (propylene-bridged) and the bifunctional derivative *p*-SCN-Bn-H_4C3octapa, and the popular ^{111}In/^{177}Lu/$^{86/90}$Y bifunctional ligands DO3A-NHS and DO3A-SCN.

An example of the impact that optimal matching of ligands to radiometals can have is the case of DOTA vs NOTA for ^{64}Cu, where the denticity and cavity size of the macrocycle NOTA is smaller than that of DOTA (CN = 6 vs 8) and a better fit for ^{64}Cu, resulting in

increased stability and inertness.[191,193] DOTA is an example of a previously studied ligand system where small changes in structure, denticity, and donor type has had significant effects on stability. A common site of bifunctional derivatization of DOTA is one of its 4 carboxylic acid arms, which masks one of the carboxylic acid chelating arms, effectively reducing the denticity from 8 to 7 (although the carbonyl can still coordinate to metal ions weakly), resulting in a noted decrease in *in vitro/in vivo* stability, as found with DO3A-NHS (Figure 6.1).[63] Another example is the ligand CHX-A''-DTPA, where 4 possible ligand isomers can be synthesized, with CHX-A''-DTPA being the most stable isomer by a substantial margin (Chapter 1).[60,216]

There are several new TE2A derivatives (Chapter 1) that have shown an interesting trend: by simply alkylating the two secondary amine groups of TE2A to form tertiary amines, either with methyl groups (MM/DM-TE2A) or an ethylene bridge (CB-TE2A), the results are a large improvement in their *in vitro*/*in vivo* stability with ^{64}Cu, relative to TE2A.[148,167] An illustration from our work on picolinic acid-based ligands is the ligand H_6phospa (Chapter 7), which is nearly structurally identical to the ligand H_4octapa (Chapters 2-3), with the exception of the two acetic acid chelating arms being swapped with methylenephosphonate arms.[304] It was demonstrated that this modification made H_6phospa very unstable *in vitro*/*in vivo* with ^{111}In/^{177}Lu relative to H_4octapa, but substantially increased its radiolabeling yields with ^{89}Zr compared to H_4octapa.[304] These examples illustrate the delicacy and overall impact of ligand design and radiometal matching on the performance of radiometal-based radiopharmaceuticals.

In Chapters 2-3 was discussed the acyclic ligand H_4octapa and the bifunctional derivative *p*-SCN-Bn-H_4octapa, which showed very promising ambient temperature

radiolabeling performance and *in vitro*/*in vivo* stability with ^{111}In and ^{177}Lu, using an antibody (trastuzumab) conjugate as a proof-of-principle vector.[87,89] These two isotopes are widely used in both research and clinical settings, and have been discussed throughout Chapters 1-5.[15] To evaluate further the impact of ligand structure changes on radiolabeling efficiency and stability, we have synthesized the novel derivative of H_4octapa, H_4C3octapa, modified with only a single additional carbon atom (propylene vs ethylene backbone) (Chapters 2-3, Figure 6.1). Herein we report the synthesis, characterization, In^{3+}/Lu^{3+} metal complexation, density functional theory (DFT) structure prediction, potentiometric titrations (thermodynamic stability constants), and ^{111}In/^{177}Lu radiolabeling/*in vitro* stability of the new ligand H_4C3octapa and its bifunctional derivative *p*-SCN-Bn-H_4C3octapa (Figure 6.1). In this study we have conjugated both the new *p*-SCN-Bn-H_4C3octapa, and the known *p*-SCN-Bn-H_4octapa to the HER2/*neu*-targeted antibody trastuzumab, and directly compared their properties to determine the extent to which a small structural change that does not affect denticity or metal coordinating groups may affect radiometal/metal complex stability. The most obvious effect that the structural modification of H_4C3octapa has is that upon metal coordination, a 6-membered chelate ring is now formed with the *N,N'*-propylene backbone instead of the 5-membered chelate ring formed with the *N,N'*-ethylene backbone of H_4octapa. Our laboratory has been studying new acyclic ligands based on the pyridinecarboxylate scaffold for several years now, and this chapter aims to broaden our understanding of ligand design and radiometal-ligand matching (Figure 6.1).[88,89,118,266,271-274,331]

6.2 Results and discussion

6.2.1 Synthesis and characterization

The ligand H_4C3octapa and its bifunctional derivative *p*-SCN-Bn-H_4C3octapa were synthesized for the first time using a synthetic route similar to that for H_4octapa in Chapter 3 (Scheme 6.1).[87] Although the synthesis of *p*-SCN-Bn-H_4octapa utilizes the enantiopure starting material L-4-nitrophenylalanine, for *p*-SCN-Bn-H_4C3octapa a different synthesis was used in order to insert a single additional carbon atom and obtain a symmetric propylene bridged backbone, starting from diethylmalonate and 4-nitrobenzylbromide (Scheme 6.2).[118,215,89,355] The 2-nitrobenzenesulfonamide (nosyl) amine-protecting group, first discussed in Chapter 3, has made the synthesis of these picolinic acid-based ligands higher yielding and more efficient.[87,304,332-336] Synthesis of H_4C3octapa was completed in 5 steps with a cumulative yield of ~44 %, and *p*-SCN-Bn-H_4C3octapa in 7 steps with a cumulative yield of ~29 %.

Following ligand synthesis and purification, the HCl salt of pure H_4C3octapa was mixed with indium nitrate [$In(NO_3)_3 \bullet 6H_2O$] and lutetium nitrate [$Lu(NO_3)_3 \bullet 6H_2O$] to react and form coordinated complexes (quantitative). These metal ion complexes were characterized using standard ^{1}H NMR and HR-ESI-MS techniques, and additionally with 2D ^{1}H-^{1}H COSY and ^{1}H-^{13}C HSQC, and variable temperature (VT) NMR spectroscopy (*vide infra*). Due to the presence of multiple isomers in aqueous conditions for $[In(C3octapa)]^-$ and $[Lu(C3octapa)]^-$, and fluxional isomerization for $[Lu(C3octapa)]^-$, clear ^{13}C NMR spectra could not be obtained in a reasonable time (e.g. ^{13}C NMR, 150 MHz, 20 h). 2D-HSQC heteronuclear single bond correlation experiments provide more sensitive acquisition of ^{13}C signals than do standard ^{13}C NMR experiments, and so HSQC spectra were obtained. It is important to note that the different isomers of these metal complexes could not be separated

during purification by semi-preparative reverse-phase high-performance liquid chromatography.

Scheme 6.1 Synthesis of H_4C3octapa (**6.5**) utilizing nosyl protection chemistry.[a]

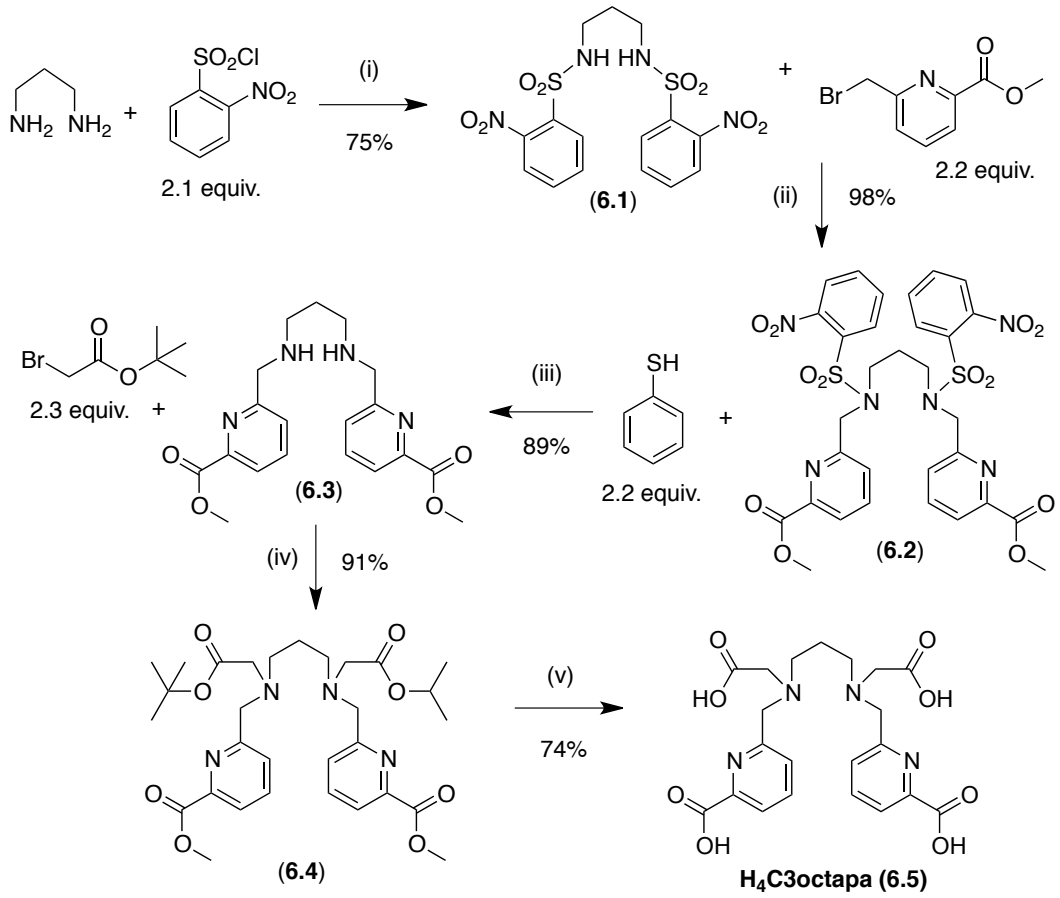

[a] (i) THF, $NaHCO_3$ (excess), 2-nitrobenzenesulfonyl chloride (2.1 equiv), 0 °C -> RT, 20 h, 75% (**6.1**); (ii) DMF, Na_2CO_3 (excess), methyl-6-bromomethylpicolinate (2.2 equiv), 50 °C, 20 h, 98% (**6.2**); (iii) THF, thiophenol (2.2 equiv), K_2CO_3 (excess), RT, 72 h, 89% (**6.3**); (iv) MeCN, Na_2CO_3 (excess), *tert*-butylbromoacetate (2.3 equiv), 60 °C, 20 h, 91% (**6.4**); (v) THF:H_2O (3:1), LiOH, RT, 4 h, 74% (H_4C3octapa, **6.5**). Cumulative yield of ~44% in 5 steps.

Scheme 6.2 Synthesis of *p*-SCN-Bn-H_4C3octapa (**6.15**) utilizing nosyl protection chemistry.[a]

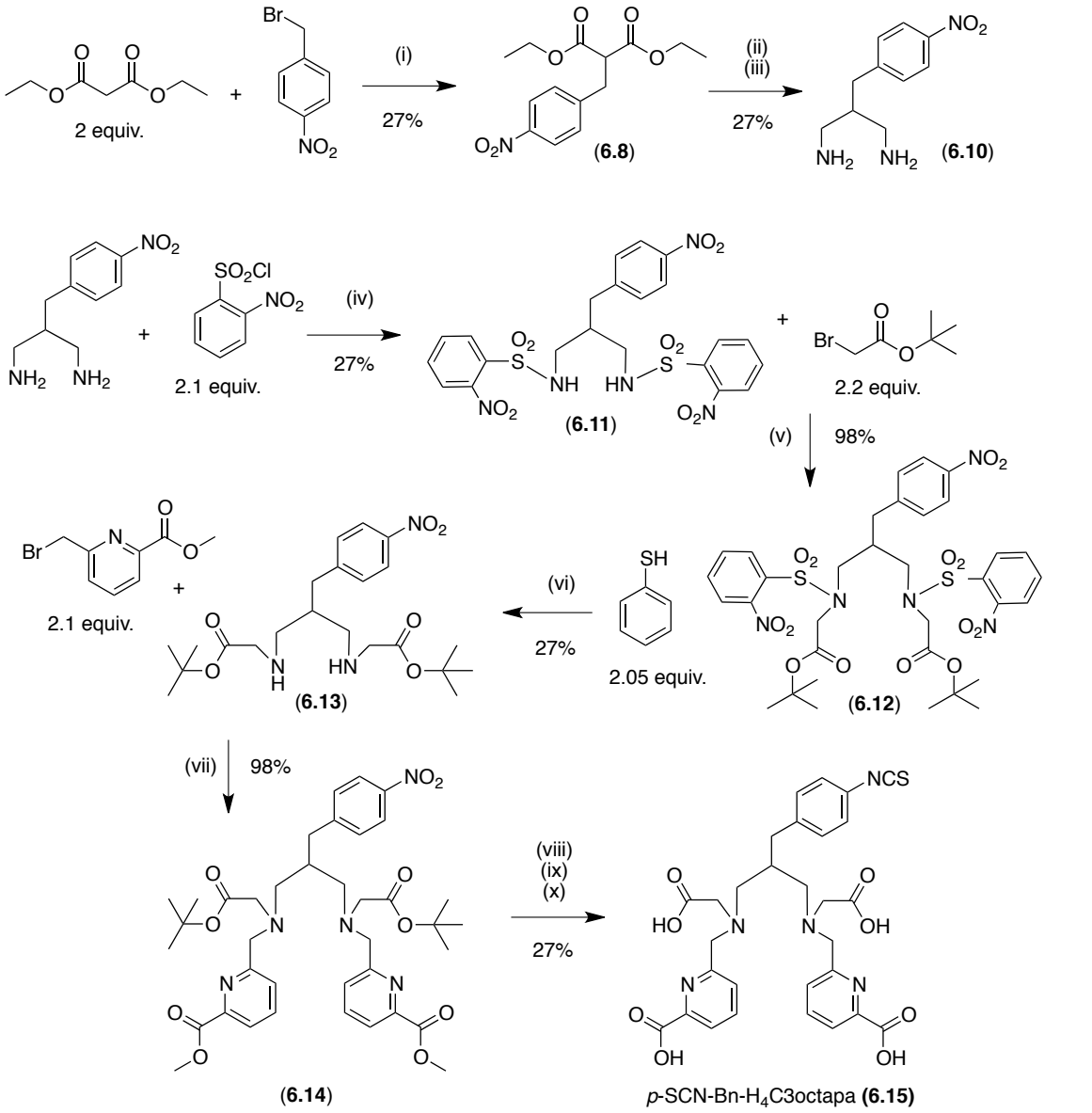

[a] (i) EtOH, NaOEt, Δ, 20 h; (ii) MeOH, NH_3 (g), 0 °C -> RT, 36 h; (iii) BH_3•THF, Δ, Ar (g), 20 h; (iv) THF, $NaHCO_3$ (excess), 0 °C -> RT, 20 h; (v) DMF, Na_2CO_3 (excess), 50 °C, 20 h; (vi) THF, K_2CO_3 (excess), RT, 72 h; (vii) MeCN, Na_2CO_3 (excess), 60 °C, 20 h; (viii) 5 mL of (1:1) AcOH (glacial):HCl (3 M), Pd/C (10 wt%), H_2 (g), RT, 1 h; (ix) THF:H_2O (3:1), LiOH, RT, 4 h, 74%; (x) thiophosgene in $CHCl_3$ (15 equiv), HCl (3 M), RT, 20 h, (cumulative yield of ~29% in 7 steps).

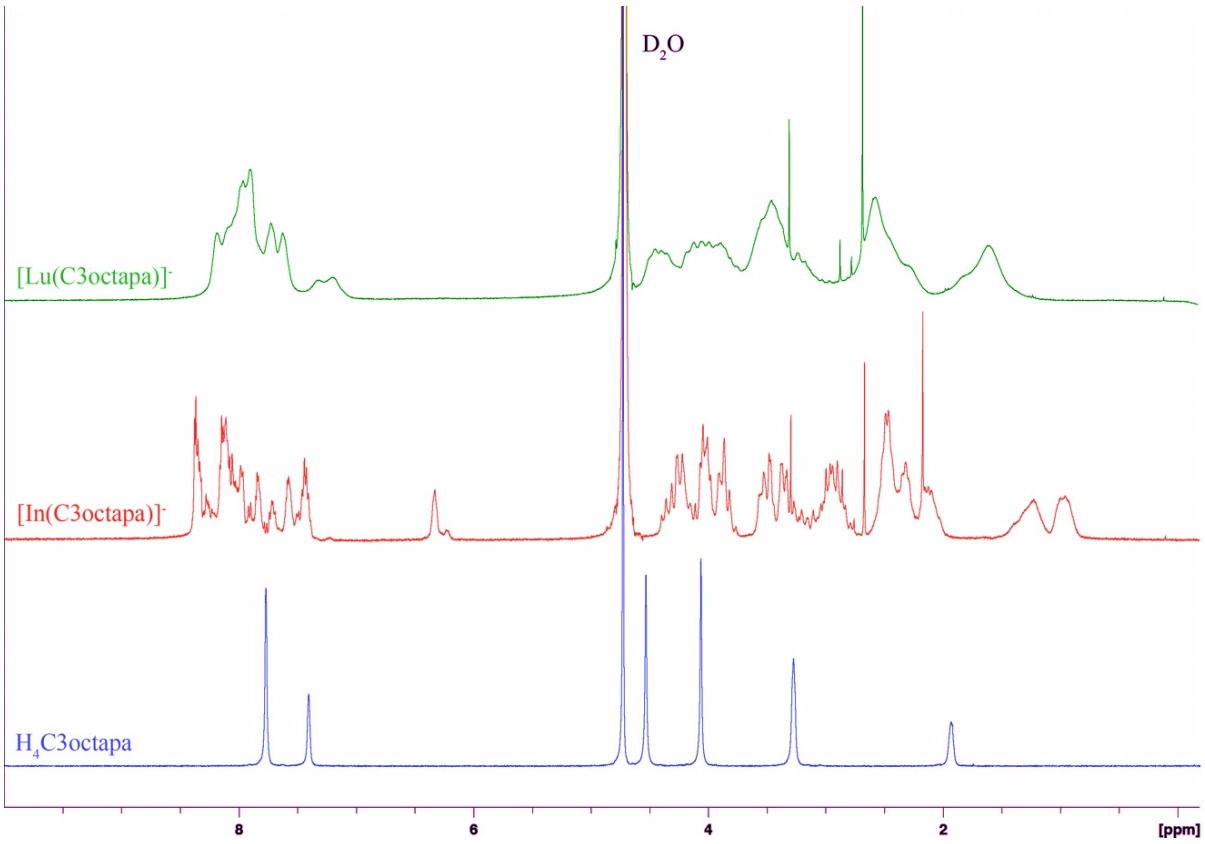

Figure 6.2 Stacked ^{1}H NMR spectra of the ligand H_4C3octapa (D_2O, 25 °C, 600 MHz), metal complex $[In(C3octapa)]^-$ (D_2O, 25 °C, 400 MHz) showing complicated but sharp signals suggesting multiple static isomers, and $[Lu(C3octapa)]^-$ (D_2O, 25 °C, 300 MHz) showing complicated and broad signals suggesting fluxional isomerization.

6.2.2 Variable temperature NMR and 2D NMR spectroscopy of $[In(C3octapa)]^-$ and $[Lu(C3octapa)]^-$

The compound *p*-SCN-Bn-H_4octapa contains a single stereocenter, which results in weak nuclear magnetic resonance (NMR) spectra with complicated coupling patterns, making NMR characterization challenging. In contrast, *p*-SCN-Bn-H_4C3octapa contains no stereocenters, which results in more simple coupling patterns, easier interpretation of NMR spectra, and faster spectral acquisition. The $[C3octapa]^{4-}$ metal ion complexes with In^{3+} and Lu^{3+} were compared to the analogous $[octapa]^{4-}$ (Chapters 2-3) complexes to compare the

differences between the coordination chemistry of these two slightly different ligands. A comparison of Figures 6.2 and 6.3 highlights a large difference in the NMR spectra of the In^{3+} and Lu^{3+} metal complexes of $[octapa]^{4-}$ and $[C3octapa]^{4-}$, despite these ligands only having one carbon different (ethylene vs propylene bridge, respectively). H_4octapa forms a 5-membered chelate ring when coordinated to metal ions, where H_4C3octapa forms 6-membered chelate rings. It is established that 5-membered chelate rings are generally more thermodynamically favorable than 6-membered rings for large metal ions, so this small structure difference between ligands (ethylene vs propylene bridge) may have a large impact on stability and isomerization.[62] The metal ion complexes of H_4octapa (Figure 6.3) display less isomerization and fluxionality than those of H_4C3octapa (Figure 6.2), with the $[In(octapa)]^-$ complex showing only 1 static isomer at ambient temperature, where the ^1H NMR spectrum of $[In(C3octapa)]^-$ shows a complicated set of sharp peaks, suggesting multiple static isomers at ambient temperature. The contrast between Lu^{3+} complexes is similar, with the sharp and well resolved ^1H NMR spectrum of $[Lu(octapa)]^-$ suggesting the presence of multiple static isomers at ambient temperature, where $[Lu(C3octapa)]^-$ shows broad signals suggesting fluxional isomerization between multiple isomers at ambient temperature (slow on the NMR time scale).

The ethylene protons of H_4octapa originally appear as a single multiplet at ~3.0 ppm (Figure 6.3), but these signals in the $[Lu(octapa)]^-$ complex appear as two broad multiplets at ~2.0-2.5 ppm, suggesting the presence of multiple isomers. Based on these observations, H_4octapa appears to form In^{3+} and Lu^{3+} complexes with less fluxionality and fewer isomers than the analogous H_4C3octapa ligands, suggesting that the extra carbon present in H_4C3octapa results in a more flexible backbone and a lower energetic barrier to

interconversion between isomers. Because these ligands are studied with applications as radiopharmaceutical agents, it would be logical that more inert and static complexes such as those formed by H_4octapa would be favorable, in order to maximize stability and inertness *in vivo*.

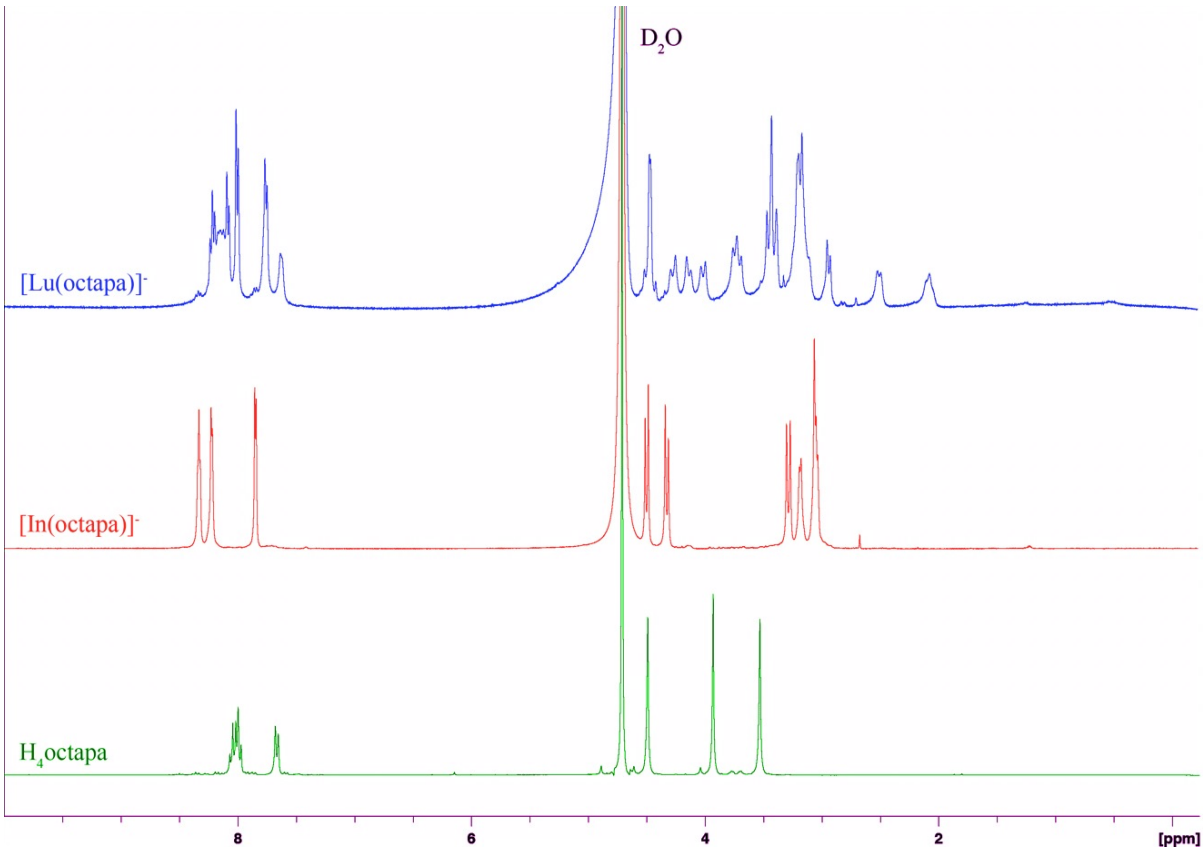

Figure 6.3 Stacked ^{1}H NMR spectra of the ligand H_4octapa (D_2O, 25 °C, 300 MHz), metal complex $[In(octapa)]^-$ (D_2O, 25 °C, 600 MHz) showing simple and sharp diastereotopic splitting suggesting the presence of one static isomer, and $[Lu(octapa)]^-$ (D_2O, 25 °C, 400 MHz) showing complicated and sharp signals suggesting multiple static isomers.

The ^{1}H NMR spectra of $[In(C3octapa)]^-$ and $[Lu(C3octapa)]^-$ revealed substantially more complicated splitting patterns than the analogous H_4octapa spectra, and required 2D NMR techniques ^{1}H-^{1}H COSY and ^{1}H-^{13}C HSQC to provide information on the number of

isomers present. Due to the manifestation of fluxional isomerization and/or multiple isomers for these metal complexes, ^{13}C NMR spectra were not obtained, as the sensitivity was very poor (e.g. no usable ^{13}C spectrum after 20 h at 150 MHz). In order to gain more insight into the type of isomerization occurring with these metal complexes, 2D-COSY NMR experiments were performed to assess the ^{1}H-^{1}H correlations.

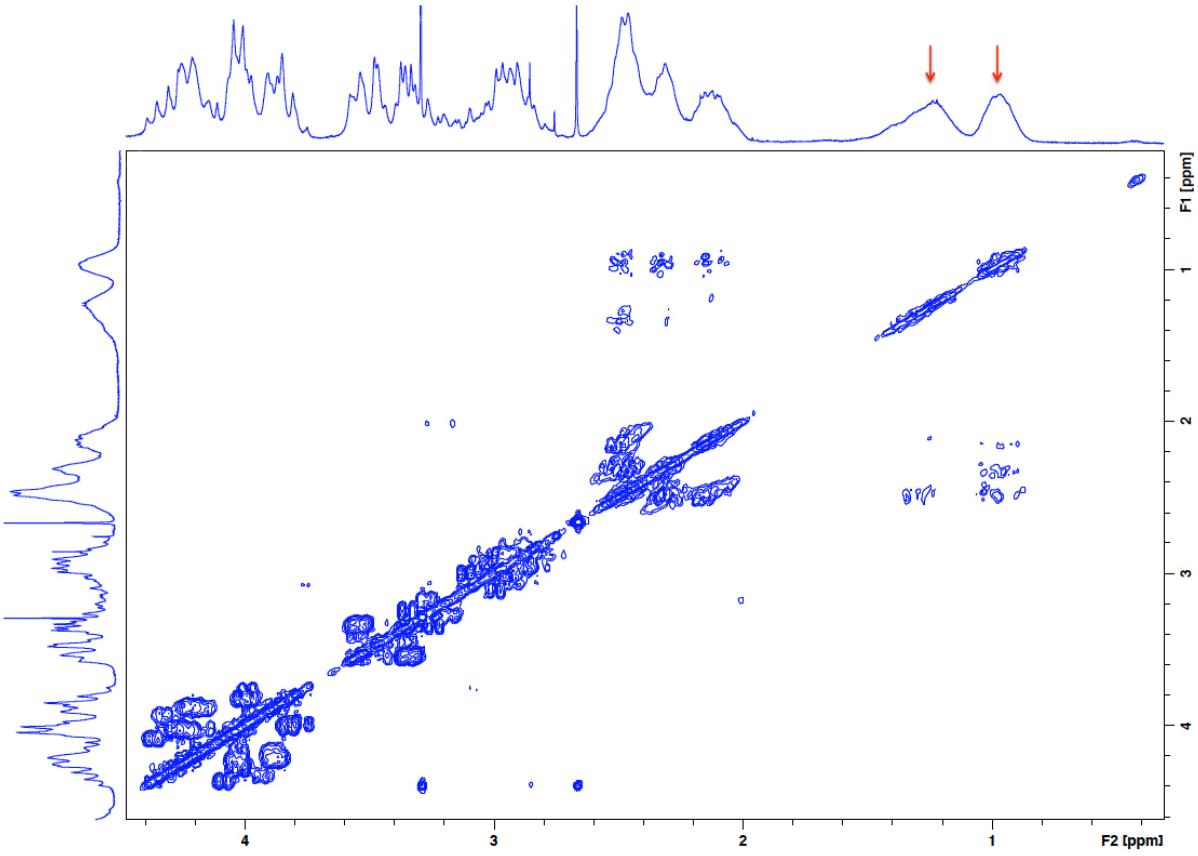

Figure 6.4 ^{1}H COSY NMR (400 MHz, D_2O, 25 °C) spectrum of $[In(C3octapa)]^-$ showing an expansion of the alkyl-region, highlighting two broad signals with red arrows arising from the central $–CH_2-$ of the propylene bridge, showing no ^{1}H-^{1}H correlations to each other.

It can be observed in the ^{1}H NMR spectrum of $[In(C3octapa)]^-$ (Figure 6.2) that the signal arising from the central propylene-bridge CH_2 changed from a singlet in the free

ligand at ~1.9 ppm, to two broad signals at ~0.9 ppm and ~1.3 ppm, which show no correlation to each other in the COSY spectra (see red arrows, Figure 6.4). The splitting of this ^{1}H NMR singlet into two broad peaks upon In^{3+} coordination suggest that at least two major isomers are formed, and the lack of correlation between these two peaks in the COSY NMR suggests that they arise from chemically distinct isomers in solution (Figure 6.4). The ^{1}H NMR signal arising from the central propylene-bridge CH_2 of $[Lu(C3octapa)]^-$ was a single broad signal, rather than two broad signals as observed for $[In(C3octapa)]^-$ (Figure 6.2), most likely due to signal averaging due to fluxional isomerization.

In addition to COSY experiments, 2D-HSQC heteronuclear single bond correlation (^{1}H-^{13}C) NMR were obtained, which provided an interesting diagnostic handle to assess isomerization via the ^{1}J C-H correlations of the pyridine rings. As previously mentioned, the 2D-HSQC experiments were more sensitive than standard ^{13}C experiments, allowing for detection of ^{13}C signals via ^{1}H-^{13}C cross peaks. The 2D-HSQC ^{1}H-^{13}C single-bond heteronuclear correlation experiments revealed a complicated set of cross-peaks arising from multiple static isomers, with the aromatic C-H pyridine signals being the most diagnostic and simple to evaluate. In the case of the free ligand or a single metal coordination isomer, 6 carbon signals (3 if C_{2v} symmetric) should be observed in the HSQC spectra arising from the ^{1}J C-H pyridine ring correlations.

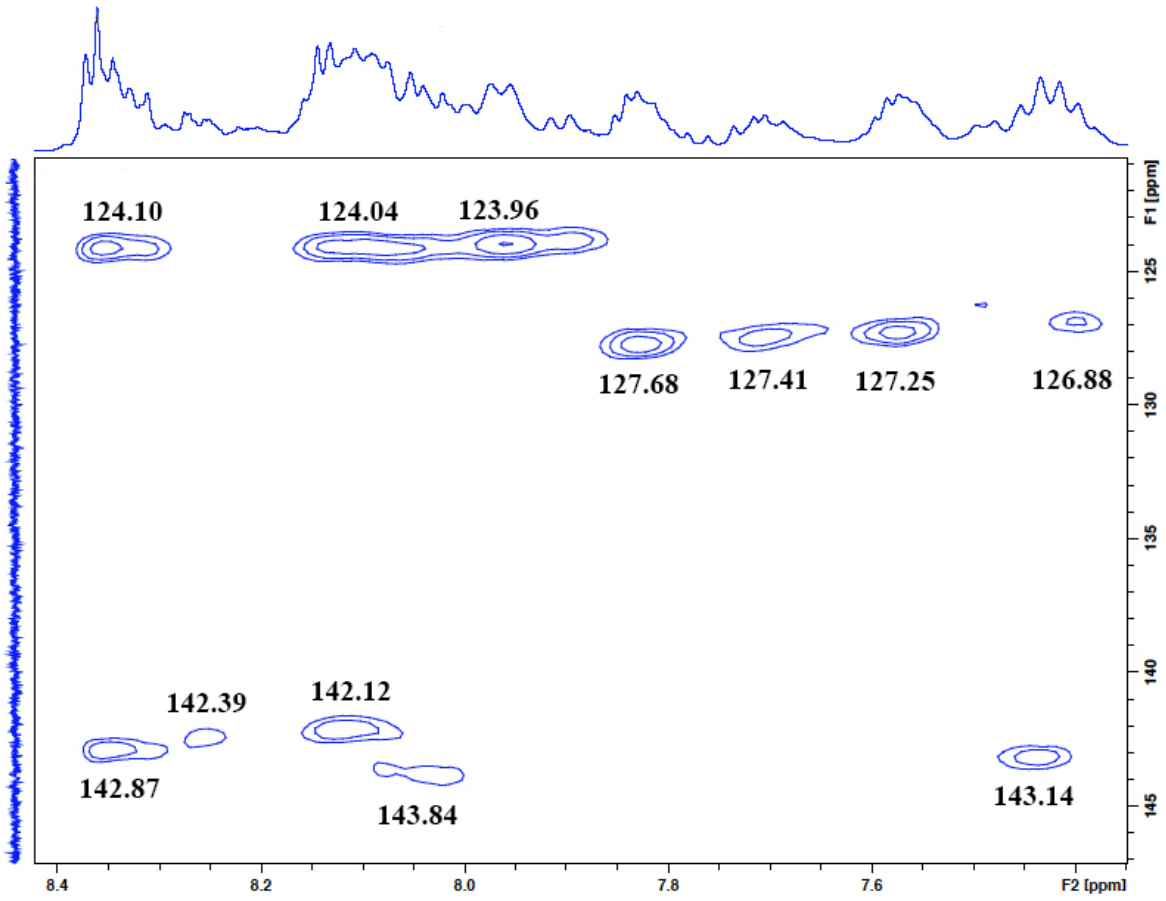

Figure 6.5 ^{1}H-^{13}C HSQC NMR (400/100 MHz, D_2O, 25 °C) expansion of aromatic signals in spectrum of $[In(C3octapa)]^-$, showing correlations to 12 unique ^{13}C signals, with an additional aromatic signal at 125.32 ppm not shown (^{13}C NMR spectra externally referenced to MeOH in D_2O).

It was observed in the HSQC spectra of $[In(C3octapa)]^-$ that 12 unique ^{13}C signals were detected, suggesting that at least 2 major isomers were present (Figure 6.5). If minor isomers were present, the signals may have been too weak to observe. The number of alkyl-region C-H correlations in the HSCQ spectrum of $[In(C3octapa)]^-$ reveals correlations to at least 17 unique carbon atoms, with each single molecule possessing only 7 alkyl-region carbon atoms (Figure A.8). Because 14 unique carbon atoms would be expected to arise from two unique isomers, this observation suggests that there are more than 2 static isomers

present in aqueous solution, with the most likely explanation being two major isomers and one or more minor isomers.

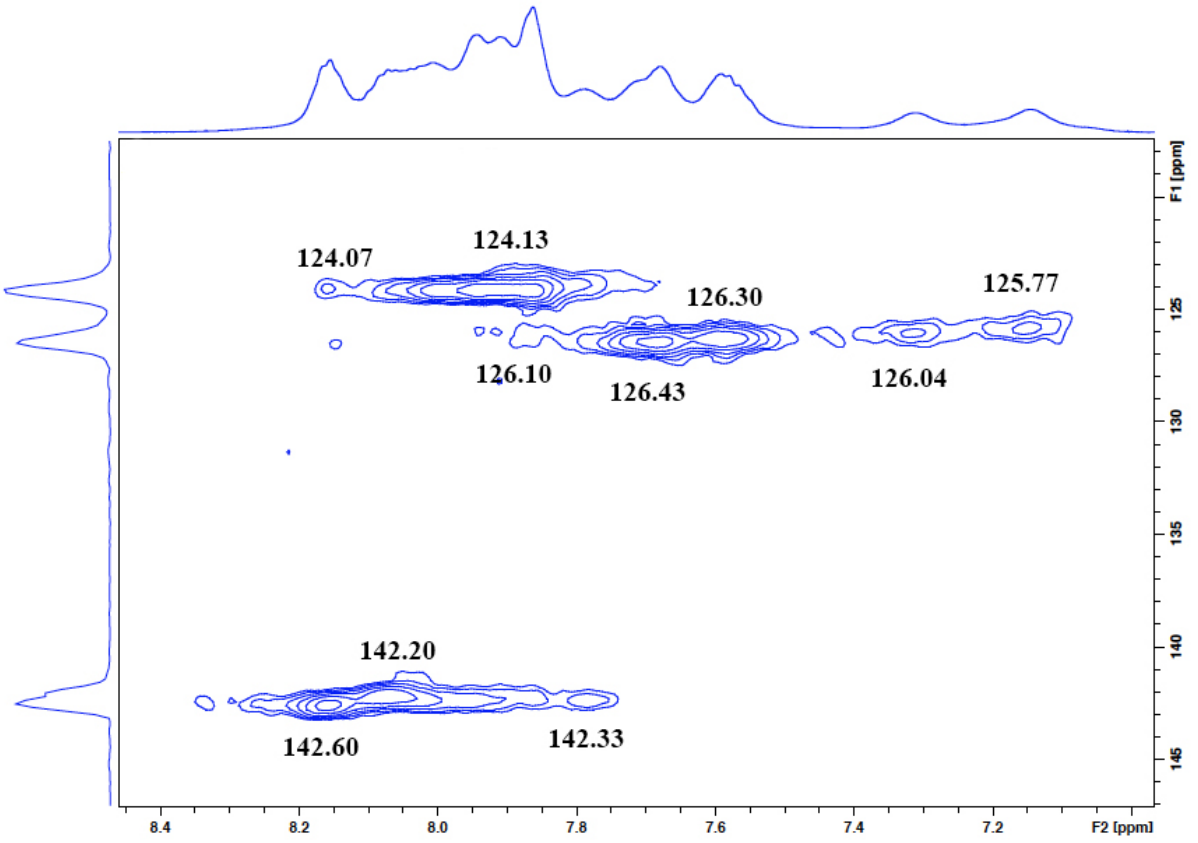

Figure 6.6 ^{1}H-^{13}C HSQC NMR (600/150 MHz, D_2O, 25 °C) expansion of aromatic signals in spectrum of [Lu(C3octapa)]$^{-}$, showing correlations to 10 unique ^{13}C signals (^{13}C NMR spectra externally referenced to MeOH in D_2O).

The COSY and HSQC spectral signals of [Lu(C3octapa)]$^{-}$ were substantially weaker than those of [In(C3octapa)]$^{-}$, as would be expected due to the increased fluxional behavior of the Lu^{3+} complex, demonstrated by the broad ^{1}H spectrum at 25 °C (Figure 6.6). The HSQC spectrum of [Lu(C3octapa)]$^{-}$ was poorly resolved as expected for a fluxional metal-ligand complex, with 9 unique carbons being observed in the aromatic region corresponding

to pyridine C-H carbons, supporting the presence of more than 1 isomer in solution (Figure 6.6). The higher rate of fluxional isomerization and coalescence of NMR signals observed for [Lu(C3octapa)]$^-$ explains why fewer ^{13}C NMR signals are detected relative to [In(C3octapa)]$^-$ (Figure 6.5 vs 6.6). 2D-HMBC heteronuclear multiple bond correlation NMR experiments were also performed; however, after 10-12 hours of acquisition time the spectral signals obtained were too weak to evaluate (~15 mg of compound in ~300 μL of D_2O).

In order to gain more insight into the solution chemistry of these metal complexes, VT ^{1}H NMR experiments were carried out with [In(C3octapa)]$^-$ and [Lu(C3octapa)]$^-$. At 85 °C (maximum for D_2O) full coalescence could not be achieved with either complex, but significant broadening from fluxional isomerization could be clearly observed in both samples. [Lu(C3octapa)]$^-$ demonstrated broad signals at ambient temperature, suggesting fluxional isomerization (slow on the NMR time scale), and as the temperature was increased to 85 °C, the peaks were observed to coalesce, merging towards 4 broad peaks (Figure 6.8) as the rate of fluxional interconversion increased, correlating to the 4 unique ^{1}H NMR signals observed as singlets in the spectra of the free ligand H_4C3octapa (Figure 6.2). [In(C3octapa)]$^-$ showed sharp but complicated splitting patterns at ambient temperature, suggesting multiple static isomers, with peaks broadening and beginning to coalesce as the temperature was increased to 85 °C (Figure 6.7).

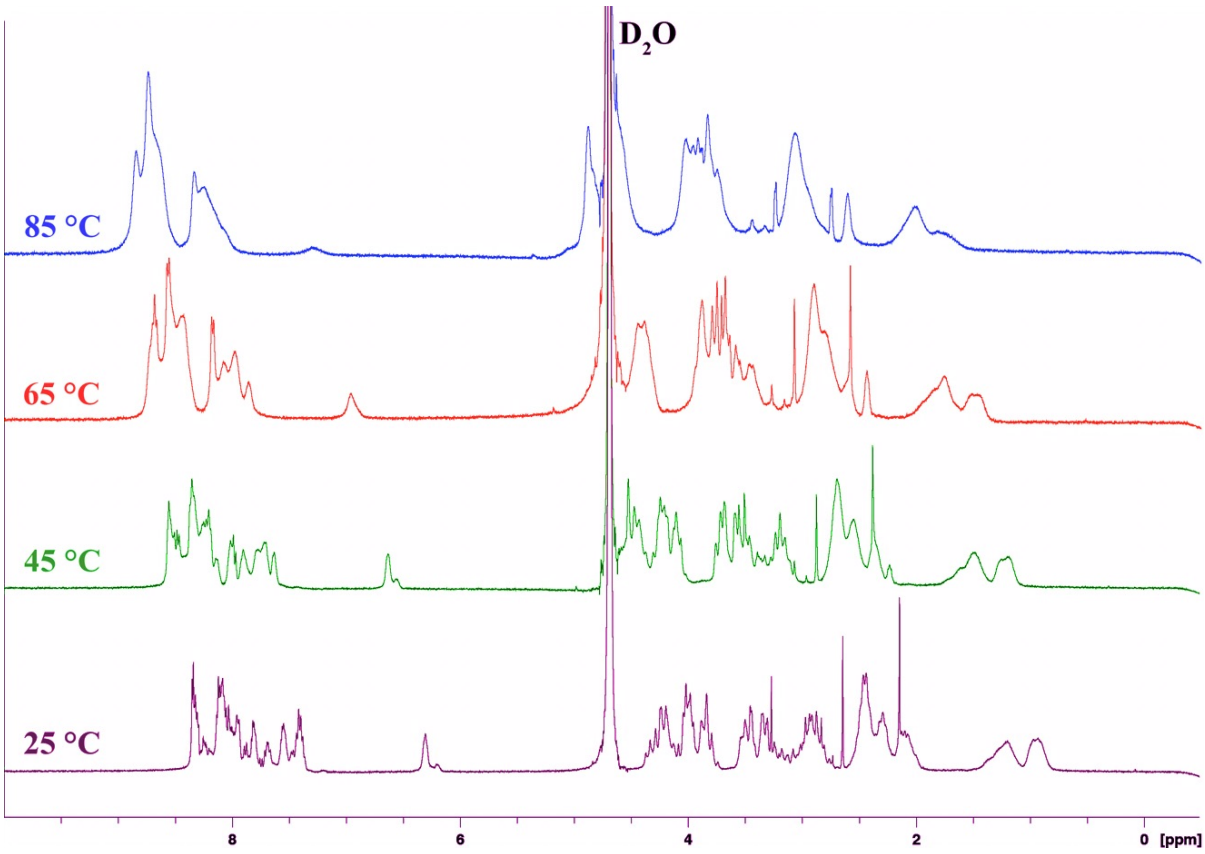

Figure 6.7 Variable temperature (VT) ^{1}H NMR experiments with [In(C3octapa)]$^{-}$ (D_2O, 400 MHz), with the temperature increased to 85 °C in 20 °C increments.

At 85 °C, the ^{1}H NMR signals of [In(C3octapa)]$^{-}$ were also coalescing towards 4 broad signals in a manner similar to that observed with [Lu(C3octapa)]$^{-}$; however, the signals from [Lu(C3octapa)]$^{-}$ remained substantially broader than those in the In^{3+} complex, suggesting a higher energetic barrier to fluxional interconversion for [In(C3octapa)]$^{-}$. It can also be observed that the signals arising from the central propylene bridge –CH_2- group of [In(C3octapa)]$^{-}$ (red arrow, Figure 6.4) were observed to merge at elevated temperatures (Figure 6.7), further supporting their assignment as arising from different isomers. If higher temperatures could be achieved (e.g. 135 °C in DMSO-d_6), increased coalescence may be observed for both samples; however, D_2O was chosen as solvent for its biological relevance.

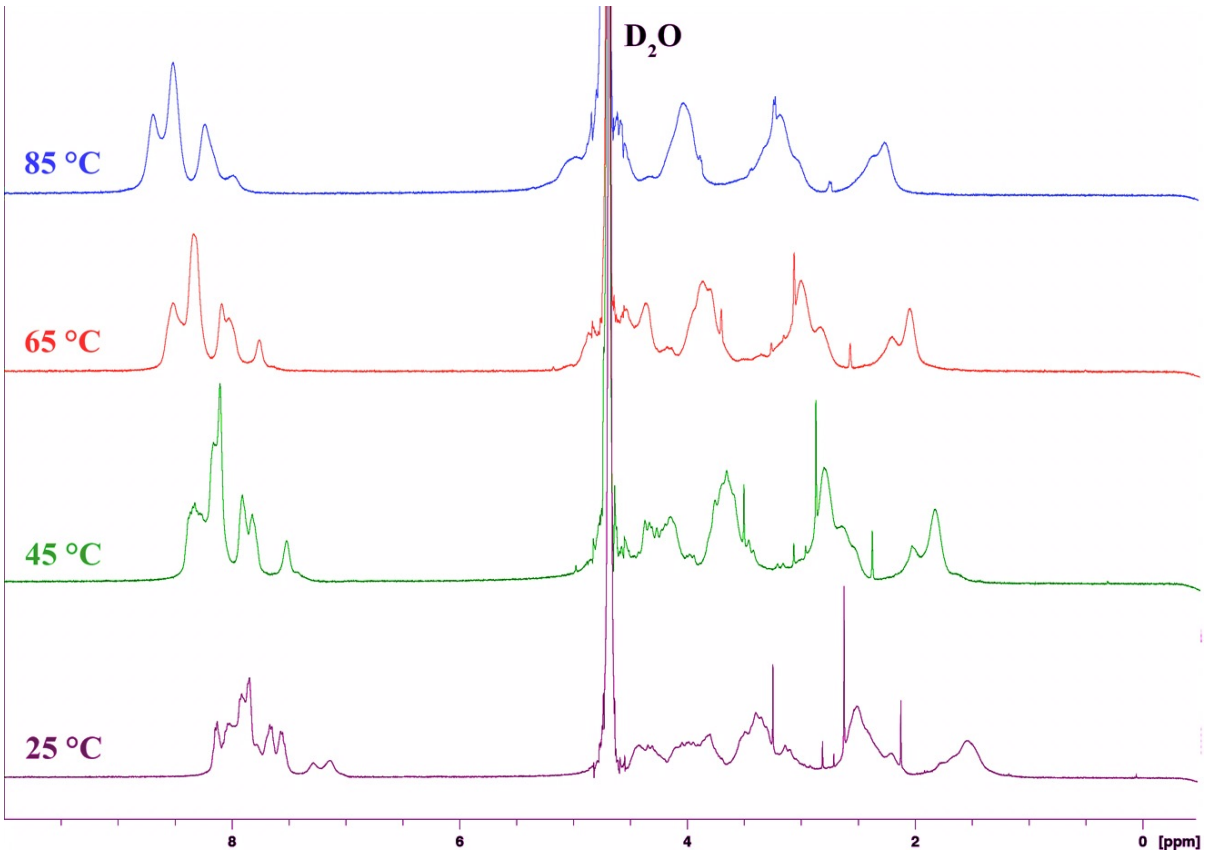

Figure 6.8 Variable temperature (VT) ^{1}H NMR experiments with [Lu(C3octapa)]$^{-}$ (D_2O, 400 MHz), with the temperature increased to 85 °C in 20 °C increments.

Fluxional radiometal complexes may be unfavorable, as the rapid process of deligation-ligation of ligand donor arms that occurs as the fluxional complex constantly rearranges could open temporary "holes" in the coordination sphere, which *in vivo* may give competing ligands such as aqua, phosphate, and serum proteins (e.g. transferrin) opportunities to bind to the metal ion and transchelate. Further to this point, the presence of a single static isomer (as in [In(octapa)]$^{-}$) of an acyclic metal complex would be ideal, because it is possible that different static isomers, although not interconverting, but because of their different structures, may exhibit different susceptibilities to external ligand attack, and may effectively exhibit different kinetic "off-rates" and therefore different *in vivo*

stability and inertness. This undeveloped idea may not translate to macrocyclic complexes; for example $[In(DOTA)]^-$ has been observed to be fluxional at ambient temperature through ^1H NMR experiments, although remarkably stable and inert *in vivo*.[97,120] Applying to macrocycles the same conceptual model as described above for fluxional acyclic metal complexes, the rapid interconversion between isomers of a macrocyclic complex like DOTA may not provide the same "holes" in the coordination sphere for competing ligands to access the metal center, as the metal ion remains enshrouded and protected within the macrocyclic framework during this process, making transchelation slower and less likely to occur.

It is important to note that this discussion pertains to isomers formed during metal coordination by a ligand and not isomers of the ligand itself. The case of ligand isomerization is demonstrated by CHX-DTPA (Figure 6.1), which has 4 enantiomers (CHX-A'-DTPA, CHX-A''-DTPA, CHX-B'-DTPA, CHX-B''-DTPA), and it was demonstrated that the single CHX-A''-DTPA isomer was substantially more stable than the other 3 isomers.[59,60,165,216] In order to indirectly test the above hypothesis that decreased or absent fluxional isomerization may correlate to increased stability *in vivo*, we are in the process of evaluating the stability of the In^{3+} and Lu^{3+} metal complexes of both H_4C3octapa and H_4octapa using potentiometric titrations to determine their formation constants (thermodynamic stability); however, these experiments were incomplete at the time of writing. To gain further insight into their differences in stability (thermodynamic and kinetic), we also conjugated the bifunctional chelate derivatives *p*-SCN-Bn-H_4C3octapa and *p*-SCN-Bn-H_4octapa to the antibody trastuzumab, radiolabeled the resulting ligand-antibody immunoconjugate with ^{111}In and ^{177}Lu, and evaluated their stability and inertness to transchelation by serum proteins over a period of 5 days (*vide infra*).

6.2.3 Density functional theory structure calculations

The coordination geometry of both the 8-coordinate $[In(octapa)]^-$ and $[Lu(octapa)]^-$ complexes were calculated *in silico* using density functional theory (DFT) in Chapters 2-3, and MEP polar surface area maps were superimposed onto the structures.[87,89] These same DFT calculations were performed for $[In(C3octapa)]^-$ and $[Lu(C3octapa)]^-$, to compare their geometries, polar surface areas, and bond lengths/angles (Figure 6.9). A visual inspection of In^{3+} and Lu^{3+} complexes of both ligands suggests they are very similar to one another, with similar charge distributions determined by the overlayed molecular electrostatic potential (MEP) polar surface area maps (Figures 6.9, 3.2, and 2.3).

Upon qualitative visual comparison, the structures and charge distributions are very similar between these $[C3octapa]^-$ complexes and the previously determined $[In(octapa)]^-$ and $[Lu(octapa)]^-$ DFT structures.[87,89] It has been noted in the literature that the ideal L-M-L bond angle and length for a 6-member M-L chelate ring (e.g. *N,N'*-propylene) is 109.5° and 1.6 Å, and for a 5-member chelate ring (e.g. *N,N'*-ethylene) is 69° and 2.5 Å, with 5-member chelate rings being ideal for larger metal ions.[62] A selection of bond lengths and angles from DFT calculated ML complexes are shown in Table 6.1, with the H_4octapa ethylene N1-M-N2 bond angle being very close to 69°, with values of 74.8° and 67.8° for In^{3+} and Lu^{3+}, respectively.

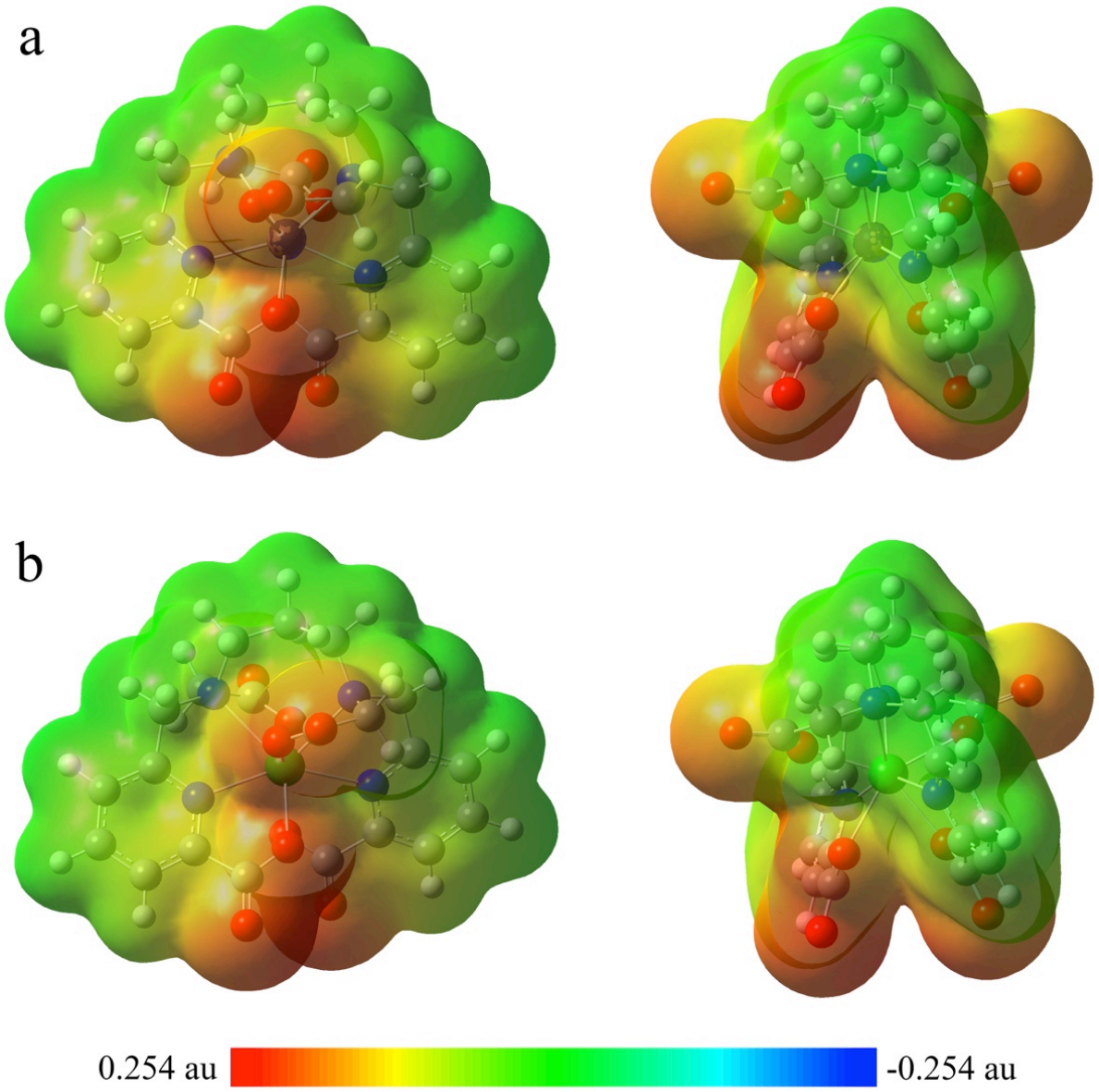

Figure 6.9 *In silico* DFT structure predictions: (a) 8-coordinate structure of $[In(C3octapa)]^-$ (top) from two perspectives; (b) 8-coordinate structure of $[Lu(C3octapa)]^-$ (bottom) from two perspectives, with both structures showing overlayed MEP polar-surface area maps predicting the charge distribution over the solvent-exposed surface of the metal complexes (red = negative, blue = positive, representing a maximum potential of 0.254 au and a minimum of -0.254 au, mapped onto electron density isosurfaces of 0.002 $Å^{-3}$). DFT calculations performed by Dr. Jacqueline Cawthray.

The ethylene N-M bond lengths are also very close to the reported ideal lengths of 2.5 Å, with values being calculated to be 2.538/2.538 Å for the In^{3+} complex and 2.756/2.756 Å

for the Lu^{3+} complex. For the H_4C3octapa complexes, the numbers obtained are much further from the optimal N1-M-N2 angle of 109.5°, with values of 93.0° and 90.8° for In^{3+} and Lu^{3+}, respectively. Following this trend, the bond lengths for the H_4C3octapa complexes diverge from the reported optimum en-N-en value of 1.6 Å for a 6-member chelate ring, with bond lengths of 2.494/2.486 Å for the In^{3+} complex and 2.593/2.576 Å for the Lu^{3+} complex. An inspection of the bond lengths presented in Table 6.1 highlight the very symmetric nature of M-L bonds in the H_4octapa complexes (~C_2 symmetry), and the comparatively unsymmetric bonds for the H_4C3octapa complexes. The NMR spectra of the H_4C3octapa complexes revealed lower symmetry and more fluxional species than the H_4octapa complexes, which supports the conclusions drawn from these DFT calculated structures. These results suggest that the H_4octapa complexes should be more stable and inert than the analogous H_4C3octapa complexes.

Table 6.1 Relevant bond lengths (Å) and angles (°) comparing the DFT-calculated In^{3+} and Lu^{3+} complexes of H_4octapa and H_4C3octapa.

Bond lengths (Å)	**[In(octapa)]$^-$**	**[In(C3octapa)]$^-$**	**[Lu(octapa)]$^-$**	**[(Lu(C3octapa)]$^-$**
(Ac-COO) O1-M	2.200	2.213	2.218	2.296
(Ac-COO) O2-M	2.201	2.250	2.218	2.280
(pyr-COO) O3-M	2.295	2.263	2.315	2.326
(pyr-COO) O4-M	2.294	2.280	2.315	2.325
(en-N) N1-M	2.538	2.494	2.756	2.593
(en-N) N2-M	2.538	2.486	2.756	2.576
(pyr-N) N3-M	2.241	2.256	2.501	2.451
(pyr-N) N4-M	2.241	2.280	2.501	2.399
N1-M-N2 angle	74.8	93.0	67.8	90.8

6.2.4 Thermodynamic formation constants

At the time of writing, potentiometric titration experiments, as discussed in Chapters 2-3 and 5, were being performed to determine the thermodynamic stability/formation constants of H_4C3octapa with the metal ions In^{3+} and Lu^{3+}. Based on the results of other experiments in this chapter, it is expected that the formation constants for H_4C3octapa complexes will be lower than the analogous H_4octapa complexes, but the experiments are currently incomplete.

6.2.5 Trastuzumab antibody conjugation, ^{111}In/^{177}Lu radiolabeling, and *in vitro* serum stability

NMR studies and DFT structure analysis suggest that H_4octapa is a superior ligand to H_4C3octapa for the metal ions In^{3+} and Lu^{3+}, and that the addition of a single carbon to the structure of H_4C3octapa was detrimental. Ultimately, the stability and inertness of these metal ion complexes must be evaluated *in vitro* and *in vivo*. To evaluate and compare the stability of these ligands in biologically relevant media, the non-bifunctional ligands H_4octapa and H_4C3octapa, along with standards DOTA and DTPA were radiolabeled with ^{177}Lu and incubated in human blood serum as a transchelation challenge. The amount of transchelated ^{177}Lu from ligands to serum proteins was measured at 1.5 h and 24 h using PD10 size-exclusion columns. The results summarized in Table 6.2 reveal that the stability of H_4octapa, H_4C3octapa, and DOTA in human serum were nearly identical during a 24 hour period, with DTPA having inferior stability. These results are observed to diverge from the serum stability values obtained for the same ligands, but as bifunctional derivatives conjugated to the antibody trastuzumab (*vide infra*).

Table 6.2 Human serum stability challenge performed at 37.5 °C (n = 3), with stability shown as the % intact ^{177}Lu complex, deteremined by PD10 size-exclusion column elution.

Complex	1.5 h stability (%)	24 h stability (%)
[^{177}Lu(octapa)]$^{-}$	88.1 ± 1.2	87.7 ± 0.7
[^{177}Lu(C3octapa)]$^{-}$	90.3 ± 1.8	86.2 ± 1.0
[^{177}Lu(DOTA)]$^{-}$	87.7 ± 0.7	87.4 ± 2.1
[^{177}Lu(DTPA)]$^{2-}$	77.4 ± 1.2	81.6 ± 2.3

To further compare the stability of these ligands, the next step evaluates a model system by conjugating these ligands to the HER2/*neu*-targeting antibody trastuzumab. In order to provide a basis for comparison, immunoconjugates bearing both *p*-SCN-Bn-H$_4$octapa (Chapter 3) and *p*-SCN-Bn-H$_4$C3octapa were synthesized, radiolabeled, and serum stability experiments were performed. Although the results summarized in Table 6.2 suggest that the ^{177}Lu complexes of H$_4$octapa and H$_4$C3octapa possess identical stability against serum transchelation, a much more relevant experiment is to evaluate their stability when attached to a biovector like trastuzumab. To begin, trastuzumab was purified by centrifuge filtration to remove additives present in the antibody kit (e.g. L-histidine HCl), and then under basic conditions (pH 8.5-9.0) mixed with 4 equivalents of *p*-SCN-Bn-H$_4$octapa or *p*-SCN-Bn-H$_4$C3octapa to react, and finally purified via size exclusion chromatography (PD-10, GE Healthcare, UK). H$_4$octapa-trastuzumab and H$_4$C3octapa-trastuzumab were then radiolabeled with either ^{111}In or ^{177}Lu in NH$_4$OAc buffer (pH 5.5, 200 mM) for 60 min at room temperature to ensure maximum radiolabel incorporation. H$_4$octapa-trastuzumab has been previously determined in Chapter 3 to radiolabel quantitatively with ^{111}In and ^{177}Lu in 15 minutes at ambient temperature;[87] results which were reproduced here with >95% radiochemical yields for both ^{111}In and ^{177}Lu with high radiochemical purity (>99% in each

case) and specific activity (~2.2 and ~2.5 mCi/mg, respectively, iTLC traces in Figures A.9-A.12). H_4C3octapa-trastuzumab radiolabeled with ^{111}In and ^{177}Lu in radiochemical yields and specific activities of ~95 % (~2.3 mCi/mg) and ~8 % (~0.3 mCi/mg), respectively (iTLC traces in Figures A.9-A.12), foretelling poor performance and stability with ^{177}Lu.

In order to assay the stability of these radioimmunoconjugates under biological conditions, all four constructs were incubated in human serum and PBS (control) at 37 °C for a period of 5 days (Figures 6.10 and 6.11). At the end of 5 days the stability of the ^{111}In-octapa- and ^{111}In-C3octapa-trastuzumab immunoconjugates were determined to be ~91% and ~24%, respectively, revealing a significant decrease in stability of H_4C3octapa compared to H_4octapa (Figure 6.10). The stability of the ^{177}Lu-octapa- and ^{177}Lu-C3octapa-trastuzumab conjugates were found to be ~89 % and ~4% stable after 5 days, respectively, showing a more drastic decrease in stability than observed for the analogous ^{111}In complexes (Figure 6.11). Although it was known that 6-membered ligand-metal chelate rings (as with H_4C3octapa) are less favorable than 5-membered chelate rings (as with H_4octapa),[62] these serum stability results prove this point more drastically than expected. These experiments were monitored by spotting ~1 μCi (~0.5-1 μL) of serum challenge mixture onto iTLC radiochromatography strips, and then eluting with a mobile phase of aqueous EDTA (50 mM, pH 5).

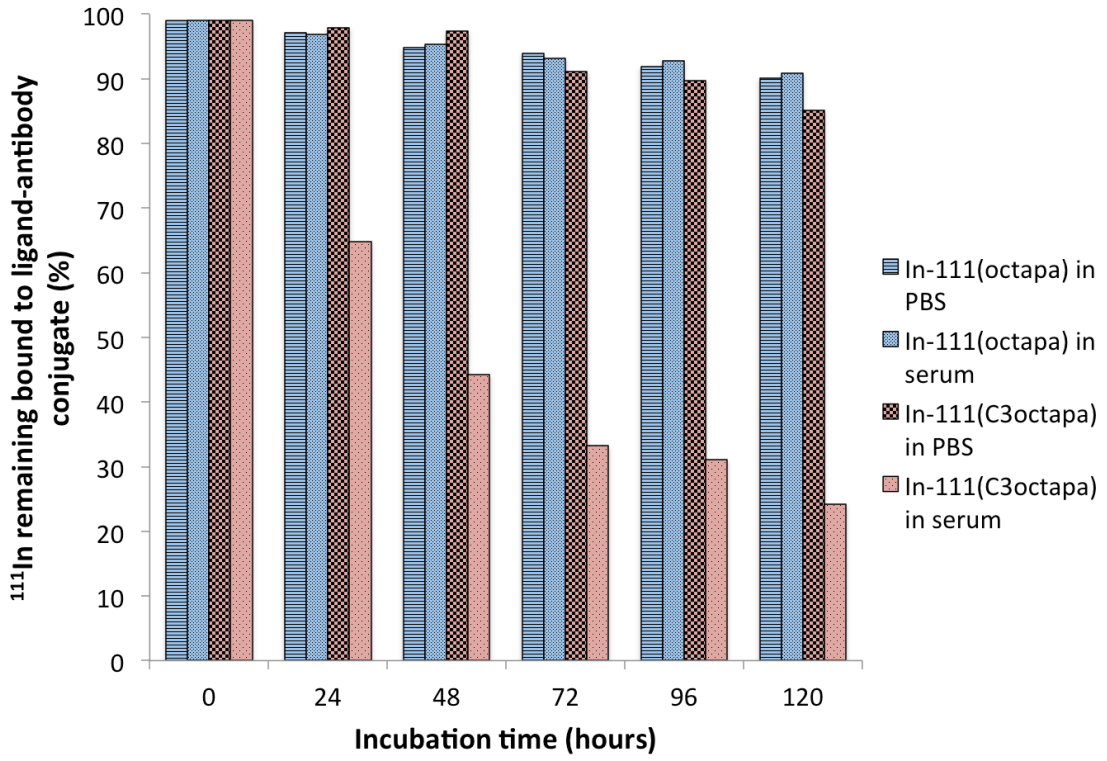

Figure 6.10 Stability of the immunoconjugates ^{111}In(octapa)-trastuzumab and ^{111}In(C3octapa)-trastuzumab in both phosphate buffered saline (PBS) and human blood serum, evaluated by spotting ~1 μCi of serum competition mixture on silica-embedded paper iTLC plates and eluting with aqueous EDTA (50 mM, pH 5) mobile phase.

Because EDTA is a ligand present in great excess over the small amount of radioimmunoconjugate spotted onto the iTLC strips, transchelation during elution is possible. The 4 serum stability challenges were therefore run in both human serum and phosphate buffered saline (PBS) as a control, to determine if transchelation and radiometal leaching was occurring as a result of serum proteins or because of the excess of EDTA present in the iTLC mobile phase (Figures 6.10 and 6.11). For the ^{111}In/^{177}Lu-octapa-trastuzumab samples, there was <1 % difference in stability between serum and PBS solutions. The H_4C3octapa samples demonstrated more interesting results, with the stability of ^{111}In-C3octapa-trastuzumab after 120 h in serum being ~24 %, but much higher at ~85 % in PBS (Figure 6.10). This result

shows that in a solution of PBS the ^{111}In-C3octapa-trastuzumab immunoconjugate remains stable, and very little ^{111}In is transchelated by EDTA during iTLC elution, but when placed in a solution of blood serum, a substantial amount of ^{111}In was transchelated by serum proteins.

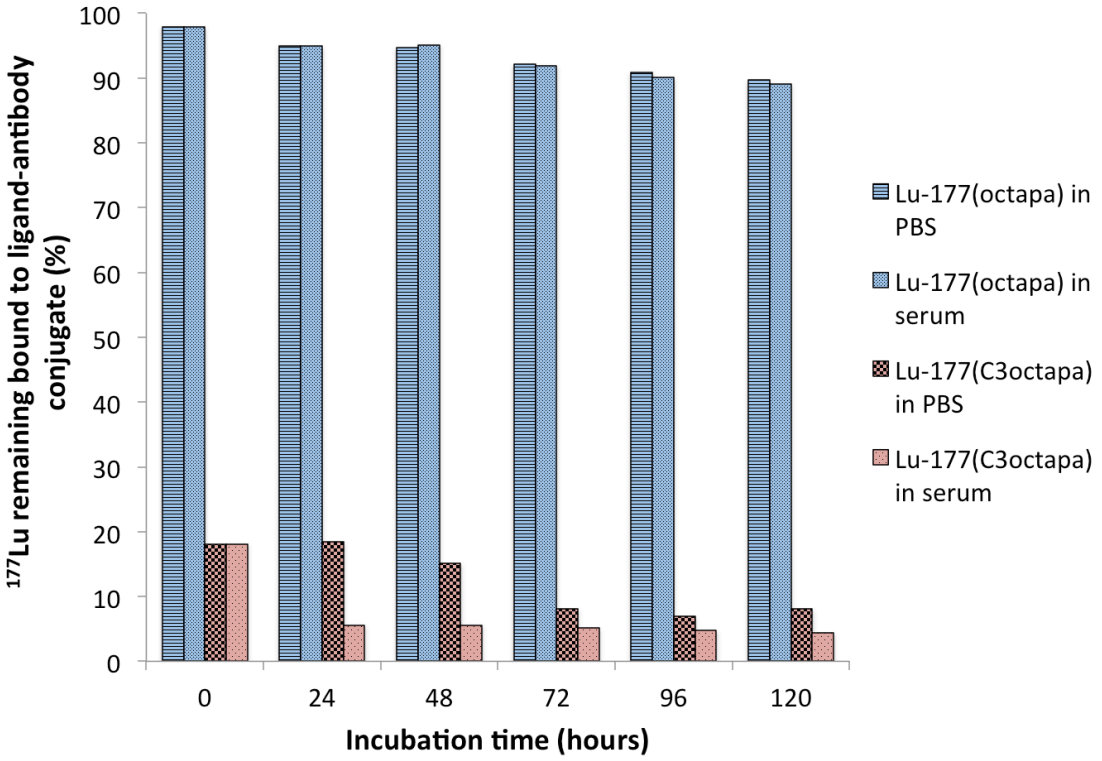

Figure 6.11 Stability of the immunoconjugates ^{177}Lu(octapa)-trastuzumab and ^{177}Lu(C3octapa)-trastuzumab in both phosphate buffered saline (PBS) and human blood serum, evaluated by spotting ~1 μCi of serum competition mixture on silica-embedded paper iTLC plates and eluting with aqueous EDTA (50 mM, pH 5) mobile phase.

The stabilities of ^{177}Lu-C3octapa-trastuzumab after 5 days in PBS and serum were ~8 % and ~4 %, respectively, suggesting that the ^{177}Lu-C3octapa complex is very unstable, being easily transchelated by PBS and/or the EDTA present in the iTLC mobile phase (Figure 6.11). One of the reasons for the poor radiolabeling yield and specific activity of

H_4C3octapa-trastuzumab with ^{177}Lu was that the complex formed was very weak, with initial iTLC analysis after radiolabeling showing substantial leaching of ^{177}Lu from the immunconjugate to the EDTA mobile phase (Figures A.9-A.12). These results are intriguing, as a difference of a single carbon in the backbone of this ligand scaffold resulted in such a substantial decrease in stability. Even more surprising is that the denticity and binding groups were not changed between H_4octapa and H_4C3octapa, demonstrating the crucial importance of chelate ring size and ligand-metal bite size/angle, reinforcing the importance of carefully matching ligands with radiometals for imaging and therapeutic applications.[1] These results also suggest that evaluating the stability of non-bifunctional ligands using serum transchelation experiments (using PD10 size-exclusion elution) may not be a reliable method, and that bifunctional ligands attached to a relevant biovector must be studied.

6.3 Conclusions

The ligands H_4C3octapa and *p*-SCN-Bn-H_4C3octapa were synthesized for the first time, using nosyl protection chemistry. These new ligands were compared with H_4octapa and *p*-SCN-Bn-H_4octapa (Chapters 2-3), to determine whether addition of a single carbon atom to the backbone of these ligand scaffolds would effect metal/radiometal chelation and stability. The In^{3+} and Lu^{3+} complexes of H_4C3octapa were synthesized, studied by NMR spectroscopy, and DFT structure analysis, and compared to the analogous H_4octapa complexes. It was found that the ^{1}H NMR spectra of $[In(C3octapa)]^-$ and $[Lu(C3octapa)]^-$ were substantially different from the analogous H_4octapa complexes, with fluxional isomerization and a higher number of isomers being observed by VT-NMR and 2D

COSY/HSQC-NMR experiments. Evaluation of DFT structures revealed very symmetric [In(octapa)]$^-$ and [Lu(octapa)]$^-$ complexes (Chapters 2-3), with the 5-member chelate ring being formed between the *N,N'*-ethylene backbone and the metal centers possessing close to ideal bond lengths and angles. In contrast, the [In(C3octapa)]$^-$ and [Lu(C3octapa)]$^-$ complexes were much less symmetric, with the 6-membered chelate ring being formed between the *N,N'*-propylene backbone and the metal centers having far from optimal bond lengths and angles, supporting the NMR spectral analysis that these complexes are less symmetric and rigid than the analogous H_4octapa complexes. The bifunctional ligands *p*-SCN-Bn-H_4C3octapa and *p*-SCN-Bn-H_4octapa were conjugated to the HER2/*neu* targeting antibody trastuzumab, radiolabeled with ^{111}In and ^{177}Lu, and their radiochemical yields and serum stability were directly compared. It was observed that the H_4C3octapa-trastuzumab conjugates displayed inferior radiochemistry properties to H_4octapa-trastuzumab, with radiochemical yields and serum stability being substantially worse. Over a 5 day stability challenge experiment in blood serum, ^{111}In-octapa- and ^{111}In-C3octapa-trastuzumab immunoconjugates were determined to be ~91% and ~24% stable, respectively, and ^{177}Lu-octapa- and ^{177}Lu-C3octapa-trastuzumab to be ~89 % and ~4% stable, respectively. Although only a single carbon atom was added to H_4C3octapa, and the metal donor atoms were not changed, the solution chemistry and radiochemistry properties were drastically altered, highlighting the importance of careful ligand design and radiometal-ligand matching.

6.4 Experimental section

6.4.1 Materials and methods

General materials and methods are the same as those listed in Chapter 3.

6.4.2 *N,N'*-(2-Nitrobenzenesulfonamide)-1,3-diaminopropane (6.1)

Propylenediamine (173 μL, 2.05 mmol) was dissolved in THF (10 mL) and placed in an ice bath, then sodium bicarbonate (~1 g) was added, followed by slow addition of 2-nitrobenzenesulfonyl chloride (0.954 g, 4.31 mmol). The reaction mixture was allowed to warm to ambient temperature and stirred overnight. The yellow mixture was filtered to remove sodium bicarbonate, rotary evaporated to a red oil, purified by silica chromatography (CombiFlash R_f automated column system; 120 g HP silica; A: dichloromethane, isocratic elution), and dried *in vacuo* to yield the product (**6.1**) as yellow solid (75%, ~0.684 g). ^{1}H NMR (300 MHz, $CDCl_3$, 25 °C) δ: 8.13-8.06 (m, 2H), 7.97-7.84 (m, 6H), 6.65 (br s, 2H, -NH-), 3.19 (m, 4H), 1.81 (quin, J = 6.9 Hz, 2H). ^{13}C NMR (75 MHz, DMSO-d_6, 25 °C) δ: 149.5, 135.2, 134.6, 133.9, 131.7, 126.2, 41.9, 31.2. HR-ESI-MS calcd. for $[C_{15}H_{16}N_4O_8S_2+H]^+$: 445.0488; found: 445.0481 $[M+H]^+$, PPM = -1.5.

6.4.3 *N,N'*-(2-Nitrobenzenesulfonamide)-*N,N'*-[6-(methoxycarbonyl)pyridin-2-yl]methyl]-1,3-diaminopropane (6.2)

To a solution of **6.1** (0.418 g, 0.941 mmol) in dimethylformamide (10 mL, dried over molecular sieves 4 Å) was added methyl-6-bromomethyl picolinate[89] (0.476 g, 2.07 mmol) and sodium carbonate (~1 g). The faint yellow reaction mixture was stirred at 50 °C overnight, filtered to remove sodium carbonate, and concentrated *in vacuo*. The crude product was purified by silica chromatography (CombiFlash R_f automated column system; 80 g HP silica; A: chloroform, B: methanol, 100% A to 25% B gradient) to yield the product **6.2** as yellow solid (98%, ~0.685 g). ^{1}H NMR (300 MHz, $CDCl_3$, 25 °C) δ: 8.03-7.93 (m, 4H), 7.78-7.73 (m, 2H), 7.68-7.52 (m, 8H), 4.60 (s, 4H), 3.93 (s, 6H), 3.25 (t, J = 7.0 Hz, 4H),

1.64-1.57 (m, 2H). ^{13}C NMR (75 MHz, $CDCl_3$, 25 °C) δ: 165.1, 156.6, 147.8, 147.3, 137.9, 133.7, 132.5, 131.9, 130.7, 125.4, 124.1, 124.0, 52.8, 52.7, 45.9, 26.3. HR-ESI-MS calcd. for $[C_{31}H_{30}N_6O_{12}S_2+H]^+$: 743.1441; found: 743.1440, $[M+H]^+$, PPM = -0.1.

6.4.4 *N,N′*-[6-(Methoxycarbonyl)pyridin-2-yl]methyl-1,3-diaminopropane (6.3)

To a solution of **6.2** (0.685 g, 0.922 mmol) in tetrahydrofuran (10 mL) was added thiophenol (223 μL, 2.03 mmol) and potassium carbonate (excess, ~0.4 g). The reaction mixture was stirred at 60 °C for 48 hours, during which time the color changed from light yellow to dark yellow. The reaction mixture was filtered with a large fritted glass filter to remove K_2CO_3, rinsed liberally with THF and CH_3CN, and then concentrated to dryness *in vacuo*. The resulting crude yellow oil was purified by alumina chromatography (CombiFlash R_f automated column system; 24 g neutral alumina; A: dichloromethane, B: methanol, 100% A to 30% B gradient) to yield **3** as yellow oil (89%, ~0.306 g). Compound **6.3** was purified using neutral alumina, as it demonstrates an abnormally high affinity for silica and requires the use of ammonium hydroxide and >20% methanol to be eluted, resulting in partial methyl-ester deprotection and dissolving of some silica. ^{1}H NMR (300 MHz, $CDCl_3$, 25 °C) δ: 7.95-7.93 (m, 2H), 7.77-7.74 (m, 2H), 7.54-7.52 (m, 2H), 4.01 (s, 4H), 3.92 (s, 6H), 3.61 (br s, -NH-, 2H), 2.81 (s, 4H), 1.78 (s, 2H). ^{13}C NMR (75 MHz, $CDCl_3$, 25 °C) δ: 165.5, 159.5, 147.3, 137.4, 125.7, 123.5, 54.3, 52.7, 48.0, 28.6. HR-ESI-MS calcd. for $[C_{19}H_{24}N_4O_4+H]^+$: 373.1876; found: 373.1881, $[M+H]^+$, PPM = 1.3.

6.4.5 *N*,*N*′-[(*tert*-Butoxycarbonyl)methyl-*N*,*N*′-[6-(methoxycarbonyl)pyridin-2-yl]methyl]-1,3-diaminopropane (6.4)

To a solution of **6.3** (188.3 mg, 0.506 mmol) in acetonitrile (10 mL) was added *tert*-butylbromoacetate (172 μL, 1.16 mmol) and sodium carbonate (~200 mg). The reaction mixture was stirred at 60 °C overnight. Sodium carbonate was removed by filtration and the crude reaction mixture was concentrated *in vacuo*. The crude oil was purified by column chromatography (CombiFlash R_f automated column system; 40 g HP silica; A: dichloromethane, B: methanol, 100% A to 20% B gradient) to afford the product **6.4** as yellow oil (91%, ~0.276 g). ^{1}H NMR (300 MHz, $CDCl_3$, 25 °C) δ: 7.94-7.91 (m, 2H), 7.72-7.71 (m, 4H), 3.94 (s, 6H), 3.92 (s, 4H), 3.20 (s, 4H), 2.64-2.60 (m, 4H), 1.62-1.58 (m, 2H), 1.39 (s, 18H). ^{13}C NMR (75 MHz, $CDCl_3$, 25 °C) δ: 170.3, 165.8, 160.8, 147.1, 137.3, 126.0, 123.5, 80.9, 60.5, 56.3, 52.7, 52.4, 28.0. HR-ESI-MS calcd. for $[C_{31}H_{44}N_4O_8+H]^+$: 601.3237; found: 601.3244, $[M+H]^+$, PPM = 1.2.

6.4.6 H_4C3octapa, *N*,*N*′-(6-carboxy-2-pyridylmethyl)-*N*,*N*′-diacetic acid-1,3-diaminopropane (6.5)

To a solution of **6.4** (248 mg, 0.413 mmol) in a mixture of tetrahydrofuran : deionized water (3:1, 5 mL) was added LiOH (150 mg). The reaction mixture was stirred at ambient temperature for 4 hours. A portion of HCl was added (5 mL, 6 M), and then the mixture was reduced to dryness *in vacuo*. The mixture was dissolved in deionized water (4 mL) and purified via semi-preparative reverse-phase HPLC (10 mL/min, gradient: A: 0.1% TFA (trifluoroacetic acid) in deionized water, B: CH_3CN. 5 to 100% B linear gradient in 30 min. t_R = 11.5-13.3 min, broad). Product fractions were pooled, concentrated *in vacuo,* dissolved

in HCl (5 mL, 6 M), and then concentrated *in vacuo* again to remove trifluoroacetic acid. This processes was repeated three times to remove traces of TFA. The HCl salt H_4C3octapa•4HCl•2H_2O **(6.5)** was obtained as a yellow solid (74% yield, ~0.195 g, using the molecular weight of the HCl salt as determined by elemental analysis). ^{1}H NMR (600 MHz, D_2O) δ: 7.79 (br s, 4H, pyr-*H*), 7.43 (br s, 2H, pyr-*H*), 4.56 (s, 4H, Pyr-C*H*$_2$-N), 4.09 (s, 4H, HOOC-C*H*$_2$-N), 3.30 (br s, 4H, propylene-1,3-*H*), 1.95 (m, 2H, propylene-2-*H*). ^{13}C NMR (150 MHz, D_2O) δ: 167.2, 166.1, 148.9, 145.2, 139.5, 126.7, 126.5, 125.1, 57.4, 54.6, 52.7, 19.4. IR (neat, ATR-IR): n = 1732 cm^{-1} (C=O), 1629/1614 cm^{-1} (C=C py). HR-ESI-MS calcd. for $[C_{21}H_{24}N_4O_8 + H]^+$: 461.1672; found $[M + H]^+$: 461.1665, PPM = -1.5. Elemental analysis: calcd % for H_4C3octapa•4HCl•2H_2O ($C_{21}H_{24}N_4O_8$•4HCl•2H_2O = 642.312 g/mol): C 40.40, H 4.84, N 8.97; found: C 40.14 (Δ = 0.26), H 4.74 (Δ = 0.10), N 8.84 (Δ = 0.13).

6.4.7 Na[In(C3octapa)] (6.6)

H_4C3octapa• 4HCl• 2H_2O (6.5) (15.54 mg, 0.024 mmol) was suspended in 0.1 M HCl (1.5 mL) and In$(NO_3)_3$•6H_2O (12.9 mg, 0.031 mmol) was added. The pH was adjusted to 4-5 using 0.1 M NaOH and then the solution was stirred at room temperature. After 1 hour the product was confirmed via mass spectrometry and the solvent was removed *in vacuo* to yield Na[In(C3octapa)] **(6.6)**. ^{1}H NMR (400 MHz, D_2O, 25 °C) δ: 8.42-7.88 (m, 4H), 7.76-7.47 (m, 2H), 4.45-3.85 (m, 4H), 3.64-3.33 (m, 2H), 3.15-2.73 (m, 2H), 2.53-2.19 (m, 4H), 1.30 (m, 1H), 1.04 (m, 1H). HR-ESI-MS calcd. for $[C_{21}H_{18}{}^{115}InN_4O_8 + 2H]^+$: 571.0320; found: 571.0317, $[M + 2H]^+$, PPM = -0.5.

6.4.8 Na[Lu(C3octapa)] (6.7)

H_4C3octapa •4HCl•2H_2O **(6.5)** (15.9 mg, 0.025 mmol) was suspended in 0.1 M HCl (1.5 mL) and $Lu(NO_3)_3$•6H_2O (15.1 mg, 0.032 mmol) was added. The pH was adjusted to 4-5 using 0.1 M NaOH and then the solution was stirred at room temperature. After 1 hour the product was confirmed via mass spectrometry and the solvent was removed *in vacuo* to yield Na[Lu(C3octapa)] **(6.6)**. ^{1}H NMR (300 MHz, D_2O, 25 °C) δ: 8.22-7.66 (m, 5H), 7.36-7.22 (m, 1H), 4.54-4.38 (m, 1H), 4.22-3.85 (m, 3H), 3.58-3.21 (m, 4H), 2.81-2.32 (m, 4H), 1.87-1.64 (m, 2H). HR-ESI-MS calcd. for $[C_{21}H_{18}{}^{175}LuN_4O_8 + 2H]^+$: 631.0689; found: 631.0680, $[M + 2H]^+$, PPM = -1.4.

6.4.9 Diethyl-2-(4-nitrobenzyl)malonate (6.8)

This synthesis was adapted from a literature preparation.[355] Sodium ethoxide (3.47 g, 50.9 mmol) was added to ethanol (100 mL), followed by slow addition of diethyl malonate (14.1 mL, 14.8 g, 92.6 mmol), and then 4-nitrobenzylbromide (10.0 g, 46.3 mmol). The dark orange reaction mixture was heated to reflux overnight, and it was observed that a fine white precipitate formed. The volume of the reaction mixture was reduced to 20 mL, it was placed in the freezer for several hours to encourage maximum precipitation, and then the shiny white solid was isolated via suction filtration. This processed was repeated, this time reducing the volume to ~5-10 mL and then placing in the freezer to recover more product. The white solid was filtered and rinsed with cold ethanol to isolate pure **6.8** (3.76 g, 12.7 mmol, ~27%). ^{1}H NMR (300 MHz, $CDCl_3$) δ: 8.16 (m, 2H, NO_2-Ph-H), 7.40 (m, 2H, NO_2-Ph-H), 4.18 (m, 4H, -O-CH_2-), 2.91 (t, 1H, -CO-CH-CO, ^{3}J = 7.8 Hz), 3.32 (d, 2H, -CH_2-Ph-NO_2, ^{3}J = 7.8 Hz), 1.23 (t, 6H, -O-CH_2-**CH_3**-, ^{3}J = 7.1 Hz). ^{13}C NMR (100 MHz, CDCl3) δ:

168.2, 146.9, 145.6, 129.8, 123.7, 61.8, 53.1, 34.3, 13.9. HR-ESI-MS calcd. for $[C_{14}H_{17}NO_6+H]^+$: 296.1134; found $[M + H^+]^+$ 296.1133, PPM = -0.4.

6.4.10 2-(4-Nitrobenzyl)malondiamide (6.9)

Compound **6.8** (3.52 g, 11.9 mmol) was dissolved in methanol (125 mL) to form a clear and colourless mixture, and was then placed in an ice/salt bath. After cooling, ammonia gas was purged through the reaction vessel for ~10 minutes with vigorous stirring to allowed for NH_3 (g) saturation. After NH_3 (g) saturation, the reaction mixture turned clear yellow. The ammonia gas flow was ceased and the reaction vessel was sealed with a rubber septum, and then allowed to stir in the ice bath overnight. While stirring overnight, the ice bath melted and the reaction was allowed to warm to ambient temperature. After stirring overnight, a precipitate was observed to have formed and the reaction mixture was a yellow/orange suspension. The reaction mixture was allowed to stir at ambient temperature for a second night (~36 h total). The precipitate was filtered out and washed with methanol, followed by boiling acetonitrile, and then dried *in vacuo*. The product (**6.9**) was isolated as yellow solid (2.34 g, 9.86 mmol, ~83%). ^{1}H NMR (300 MHz, DMSO-d_6) δ: 8.15-8.12 (m, 2H, NO_2-Ph-H), 7.49-7.46 (m, 2H, NO_2-Ph-H), 7.30 (s, 2H, -NH_2), 7.08 (s, 2H, -NH_2), 3.39 (t, 1H, ^{3}J = 7.8 Hz, -CO-CH-CO-), 3.10 (d, 2H, ^{3}J = 7.6 Hz, -CH_2-Ph-NO_2-). ^{13}C NMR (75 MHz, DMSO-d_6) δ: 170.1, 148.0, 146.0, 130.1, 123.2, 54.0, 34.5. HR-ESI-MS calcd. for $[C_{10}H_{11}N_3O_4+Na]^+$: 260.0647; found $[M + Na^+]^+$ 260.0654, PPM = 2.6. Elemental analysis: calcd % for $C_{10}H_{11}N_3O_4$•0.1CH_3OH = 240.424 g/mol: C 50.46, H 4.78, N 17.71; found: C 50.61 (Δ = 0.15), H 4.60 (Δ = 0.18), N 17.26 (Δ = 0.22).

6.4.11 1,3-Diamino-2-(4-nitrobenzyl)propane dihydrochloride (2-(*p*-nitrobenzyl)-1,3-propylenediamine) (6.10)

Compound **6.9** (1.99 g, 8.40 mmol) was added to a two-neck round bottom flask under argon gas, and an addition funnel was attached. Borane stabilized in THF (BH_3•THF, 1 M, 15 mL) was added, and the reaction mixture was heated to reflux under argon gas for 20 hours. The reaction mixture was clear yellow with solid precipitate on the sides of the flask. The reaction mixture was removed from heat, ~30 mL of concentrated HCl (12 M) was added slowly, and the mixture heated to reflux for ~1 hour. The reaction mixture was reduced to dryness in vacuo, and then ~40 mL of NaOH (6 M) was added. The aqueous phase was extracted with dichloromethane (5 x 30 mL); the light yellow organic extractions were pooled and dried over magnesium sulfate, filtered, and reduced to dryness *in vacuo*. The product as then suspended in ~20 mL of ethanol, concentrated HCl was added (~3 mL, 12 M), and the flask placed in the freezer to crystallize. A light yellow precipitate formed, which was filtered out, washed with dichloromethane, and dried *in vacuo* to isolate pure **6.10** (0.544 g, 2.39 mmol, ~28 %). ^{1}H NMR (400 MHz, D_2O) δ: 8.18 (m, 2H, NO_2-Ph-H (meta to NO_2)), 7.51 (m, 2H, NO_2-Ph-H (ortho to NO_2)), 3.19 (dd, 2H, H_2N-CH_2-), ^3J = 6.7 Hz, ^2J = 13.6 Hz), 3.06 (dd, 2H, H_2N-CH_2-), ^3J = 6.7 Hz, ^2J = 13.5 Hz), 2.97 (2, 2H, NO_2-Ph-CH_2-, ^3J = 7.6 Hz), 2.56 (septet, 1H, -CH-, ^3J = 6.9 Hz). ^{13}C NMR (100 MHz, D_2O) δ: 146.6, 145.6, 130.4, 124.2, 40.22, 36.7, 34.9. HR-ESI-MS calcd. for $[C_{10}H_{15}N_3O_2+H]^+$: 210.1214; found $[M + H^+]^+$ 210.1240, PPM = -1.2.

6.4.12 *N,N'*-(2-Nitrobenzenesulfonamide)-2-(*p*-nitrobenzyl)-1,3-diaminopropane (6.11)

Compound **6.10** (205 mg, 0.979 mmol) was dissolved in THF (10 mL) and the reaction mixture placed in an ice bath. Sodium bicarbonate (~1 g) was added, followed by slow addition of 2-nitrobenzenesulfonyl chloride (445 mg, 2.01 mmol). The reaction mixture was stirred overnight at ambient temperature. The yellow/orange mixture was filtered to remove sodium bicarbonate, rotary evaporated to a red oil, and purified by silica chromatography (CombiFlash R_f automated column system; 40 g HP silica; A: hexanes, B: ethyl acetate, 100% A to 100% B gradient) and dried *in vacuo* to yield **6.11** as off-white solid (77%, ~439 mg). ^{1}H NMR (300 MHz, acetone-d_6, 25 °C) δ: 8.14-8.11 (m, 2H), 8.04-8.01 (m, 2H), 7.97-7.82 (m, 6H), 7.50 (d, J = 9.0 Hz, 2H), 6.76 (t, J = 8.0 Hz, 2H), 3.29-3.12 (m, 4H), 2.91 (d, J = 9.0 Hz, 2H), 2.34 (sept, J = 8.0 Hz, 1H). ^{13}C NMR (75 MHz, acetone-d_6, 25 °C) δ: 149.0, 148.8, 147.5, 135.0, 133.8, 133.6, 131.4, 131.1, 125.9, 124.3, 45.0, 41.8, 35.9. HR-ESI-MS calcd. for $[C_{22}H_{21}N_5O_{10}S_2+H]^+$: 580.0808; found: 580.0812 $[M+H]^+$, PPM = 0.7.

6.4.13 *N,N'*-(2-Nitrobenzenesulfonamide)-*N,N'*-[(*tert*-butoxycarbonyl)methyl]-2-(*p*-nitrobenzyl)-1,3-diaminopropane (6.12)

To a solution of **6.11** (195 mg, 0.336 mmol) in dimethylformamide (5 mL, dried over molecular sieves 4 Å) was added *tert*-butylbromoacetate (109 μL, 0.740 mmol) and sodium carbonate (~400 mg). The yellow reaction mixture was stirred at 50 °C overnight, filtered to remove sodium carbonate, and concentrated *in vacuo*. The crude product was purified by silica chromatography (CombiFlash R_f automated column system; 40 g HP silica; A: ethyl acetate, B: petroleum ether, 100% A to 100% B gradient) to yield **6.12** as light yellow fluffy

solid (83%, ~224 mg). ^{1}H NMR (300 MHz, $CDCl_3$, 25 °C) δ: 8.11 (d, *J* = 8.0 Hz, 2H), 7.92-7.90 (m, 2H), 7.67 (m, 4H), 7.58-7.55 (m, 2H), 7.38 (d, *J* = 9.0 Hz, 2H), 4.08-3.93 (m, 4H), 3.55 (dd, *J* = 13.5 Hz, *J* = 9.0 Hz, 2H), 3.23 (dd, *J* = 13.5 Hz, *J* = 9.0 Hz, 2H), 2.89 (d, *J* = 9.0 Hz, 2H), 2.46 (sept, *J* = 8.0 Hz, 1H), 1.26 (s, 18H). ^{13}C NMR (75 MHz, $CDCl_3$, 25 °C) δ: 167.1, 147.9, 147.4, 146.5, 133.7, 132.7, 132.2, 131.7, 130.8, 129.7, 123.9, 123.6, 82.5, 50.9, 49.6, 38.0, 36.4, 27.6. HR-ESI-MS calcd. for $[C_{34}H_{41}N_5O_{14}S_2+Na]^+$: 830.1989; found: 830.1996, $[M+Na]^+$, PPM = 0.8.

6.4.14 *N,N'*-[(*tert*-Butoxycarbonyl)methyl]-2-(*p*-nitrobenzyl)-1,3-diaminopropane (6.13)

To a solution of **6.12** (224.4 mg, 0.278 mmol) in tetrahydrofuran (5 mL) was added thiophenol (58.2 μL, 0.569 mmol) and potassium carbonate (excess, ~0.4 g). The reaction mixture was stirred at ambient temperature for 72 hours, as a slow color change from light yellow to dark yellow occurred. The crude reaction mixture was filtered out with a large fritted glass filter, rinsed liberally with THF and CH_3CN, and then concentrated to dryness *in vacuo*. The resulting crude yellow oil was purified by silica chromatography (CombiFlash R_f automated column system; 24 g HP silica; A: dichloromethane, B: methanol, 100% A to 30% B gradient) to yield **6.13** as clear yellow oil (90%, ~109 mg). ^{1}H NMR (300 MHz, $CDCl_3$, 25 °C) δ: 8.08 (d, *J* = 9.0 Hz, 2H), 7.32 (d, *J* = 9.0 Hz, 2H), 3.20 (s, 4H), 2.74 (d, *J* = 8.0 Hz, 2H), 2.53 (d, *J* = 8.0 Hz, 4H), 1.93 (m, 1H), 1.85 (s, 2H), 1.39 (s, 18H). ^{13}C NMR (75 MHz, $CDCl_3$, 25 °C) δ: 171.6, 148.6, 146.2, 129.8, 123.3, 80.9, 51.8, 51.5, 40.8, 36.8, 27.9. HR-ESI-MS calcd. for $[C_{22}H_{35}N_3O_6+H]^+$: 438.2604; found: 438.2593, $[M+H]^+$, PPM = -2.5.

6.4.15 *N,N'*-[(*tert*-Butoxycarbonyl)methyl]-*N,N'*-[(6-methoxycarbonyl)pyridin-2-yl)methyl]-2-(*p*-nitrobenzyl)-1,3-diaminopropane (6.14)

To a solution of **6.13** (52.2 mg, 0.119 mmol) in acetonitrile (5 mL) was added methyl 6-(bromomethyl)picolinate[89] (57.6 mg, 0.251 mmol) and sodium carbonate (~200 mg). The reaction mixture was stirred at 60 °C overnight. Sodium carbonate was removed by filtration and the crude mixture was concentrated *in vacuo*. The crude oil was purified by column chromatography (CombiFlash R_f automated column system; 24 g HP silica; A: dichloromethane, B: methanol, 100% A to 20% B gradient) to afford **6.14** as light yellow oil (95%, ~83.6 mg). ^{1}H NMR (300 MHz, $CDCl_3$, 25 °C) δ: 8.00 (dd, J = 8.5 Hz, J = 19.5 Hz, 4H), 7.70-7.70 (m, 4H), 7.21 (d, J = 9 Hz, 2H), 3.95 (s, 6H, methyl ester), 3.90 (s, 4H), 3.16 (s, 4H), 2.74-2.66 (m, 4H), 2.45-2.38 (m, 2H), 1.95 (m, 1H), 1.38 (s, 18H). ^{13}C NMR (75 MHz, $CDCl_3$, 25 °C) δ: 170.1, 165.6, 160.4, 149.2, 147.2, 146.1, 137.3, 129.7, 126.0, 123.6, 123.3, 81.0, 60.8, 57.5, 56.7, 52.8, 37.9, 37.3, 28.0. HR-ESI-MS calcd. for $[C_{38}H_{49}N_5O_{10}+H]^+$: 736.3558; found: 736.3575, $[M+H]^+$, PPM = 2.3.

6.4.16 *p*-SCN-Bn-H_4C3octapa, *N,N'*-[(Carboxylato)methyl]-*N,N'*-[(6-carboxylato)pyridin-2-yl)methyl]-2-(*p*-benzyl-isothiocyanato)-1,3-diaminopropane (6.15)

Compound **6.14** (92.4 mg, 0.126 mmol) was dissolved in glacial acetic acid (2.5 mL) with hydrochloric acid (2.5 mL, 3 M); palladium on carbon (10 wt%) was added and hydrogen gas (balloon) was purged through the reaction vessel which was then sealed with a rubber septum. The reaction mixture was stirred vigorously at ambient temperature for 1 hour, then filtered to remove Pd/C and washed *ad libitum* with methanol and hydrochloric

acid (3 M). The crude reaction mixture was concentrated *in vacuo*, dissolved in a mixture of tetrahydrofuran : deionized water (3:1, 5 mL) and LiOH (150 mg) was added and stirred at ambient temperature for 1 hour. The crude reaction mixture was dissolved in hydrochloric acid (~2 mL, 3 M), heated to near boiling with a heat gun to affect full *tert*-butyl ester deprotection, and then allowed to cool to ambient temperature. The crude reaction mixture was then mixed with thiophosgene (purchased suspended in chloroform) in ~0.2 mL of additional chloroform (15 eq, 144 μL, 1.88 mmol) to react overnight at ambient temperature with vigorous stirring. The reaction mixture was washed with chloroform (5 x 1 mL) by vigorous biphasic stirring, followed by removal of the organic phase using a pipette, to extract excess thiophosgene. The aqueous phase was then diluted to a volume of 4.5 mL with deionized water, and injected directly onto a semi-prep HPLC column for purification (A: 0.1% TFA in deionized water, B: 0.1% TFA in CH_3CN, 100% A to 60% B gradient over 40 minutes). *p*-SCN-Bn-H_4C3octapa **(6.15)** was found in the largest peak at R_t = 35 minutes (broad), lyophilized overnight, and was isolated as a fluffy off-white solid (53% over 3 steps from **6.15**, ~40 mg). ^{1}H NMR (400 MHz, MeOD, 25 °C) δ: 8.06-8.03 (m, 2H), 7.91 (t, *J* = 7.9 Hz, 2H), 7.55-7.53 (m, 2H), 7.27 (d, *J* = 8.6 Hz, 2H), 7.16 (d, *J* = 8.2 Hz, 2H), 4.70 (d, *J* = 7.3 Hz, 2H), 4.48 (d, *J* = 14.3 Hz, 2H), 4.19 (d, *J* = 17.7 Hz, 2H), 3.84 (d, *J* = 17.7 Hz, 2H), 3.44 (d, *J* = 12.0 Hz, 2H), 3.28 (d, *J* = 12.6 Hz, 2H), 2.94 (m, 1H), 2.61 (d, *J* = 7.2 Hz, 2H). ^{13}C NMR (100 MHz, MeOD, 25 °C) δ: 171.7, 167.4, 155.0, 149.7, 139.9, 139.5, 137.1, 131.8, 139.5, 129.4, 126.9, 126.1, 61.2, 58.7, 55.3, 37.2, 33.3. IR (neat, ATR-IR): ν = 2097 cm^{-1} (S=C=N-), 1718/1661 cm^{-1} (C=O), 1594 cm^{-1} (C=C py). HR-ESI-MS calcd. for $[C_{29}H_{29}N_5O_8S+H]^+$: 608.1815; found: 608.1822, $[M+H]^+$, PPM = 1.2.

6.4.17 Molecular modeling

Calculations were performed by Dr. Jacqueline Cawthray using the Gaussian 09[327] and GaussView packages. Molecular geometries and electron densities were obtained from density functional theory calculations, with the B3LYP functional employing the 6-31+G(d,p) basis set for 1st and 2nd row elements, and the ECP basis set, LANL2DZ, was employed for indium, and the Stuttgart−Dresden effective core potential, SDD for lutetium.[328,329,343] Solvent (water) effects were described through a continuum approach by means of the IEF PCM as implemented in G09. The electrostatic potential was mapped onto the calculated electron density surface. The corresponding harmonic vibration frequencies were computed at the same level to characterize the geometry as a minima.

6.4.18 Trastuzumab antibody modification / thiourea bioconjugation

Trastuzumab (purchased commercially as Herceptin, Genentech, San Francisco, CA) was purified using centrifugal filter units with a 50000 molecular weight cutoff (Amicon® ultra centrifuge filters, Ultracel®-50: regenerated cellulose, Millipore Corp., Billerica, MA) and phosphate buffered saline (PBS, pH 7.4) to remove α-α-trehalose dihydrate, L-histidine, and polysorbate 20 additives. After purification, the antibody was taken up in PBS pH 7.4. Subsequently, 300 μL of antibody solution (150-250 μM) was combined with 100 μL PBS (pH 8.0); the pH of the resulting solution was adjusted to 8.8-9.0 with 0.1 M Na_2CO_3, and 4 equiv of the *p*-SCN-Bn-H_4C3octapa or *p*-SCN-Bn-H_4octapa were added in 10 μL DMSO. The reactions were incubated at 37 °C for 1 h, followed by centrifugal filtration to purify the resultant antibody conjugate. The final modified antibody stock solutions were stored in PBS (pH 7.4) at 4 °C.

6.4.19 ^{111}In- and ^{177}Lu-C3octapa/octapa-trastuzumab radiolabeling

Aliquots of H_4C3octapa/H_4octapa-trastuzumab immunoconjugates were transferred to 2 mL microcentrifuge tubes and made up to 1 mL of ammonium acetate buffer (pH 5.5, 200 mM), and then aliquots of ^{177}Lu or ^{111}In were added (~2-3 mCi). The H_4octapa-trastuzumab mixtures were allowed to radiolabel at room temperature for 30 minutes and then analyzed via iTLC with an eluent of 50 mM EDTA (pH 5) and confirmed reproducible values >95% RCY, with ^{111}In being ~94-95% (~2.23 mCi/mg) and ^{177}Lu being ~97-98% (~2.52 mCi/mg). The H_4C3octapa-trastuzumab mixtures were allowed to radiolabel at room temperature for 60 minutes and then analyzed via iTLC with RCY for ^{111}In of ~95-96% (~2.25 mCi/mg), and RCY of ^{177}Lu of ~8-9% (~0.3 mCi/mg). EDTA solution (30 μL, 50 mM, pH 5) was then added to the reaction mixture; the resultant radiolabeled immunoconjugates were then purified using size-exclusion chromatography (Sephadex G-25 M, PD-10 column, 30 kDa, GE Healthcare; dead volume = 2.5 mL, eluted with 1 mL fractions of PBS, pH 7.4) and centrifugal column filtration (Amicon® ultra 50k). The radiochemical purity of the final radiolabeled bioconjugate was assayed by radio-iTLC and was found to be >99% for both H_4octapa-trastuzumab samples (Figures A.9-A.12), but for ^{111}In-C3octapa-trastuzumab a small amount of ^{111}In was transchelated by the EDTA mobile phase after purification (Figures A.9-A.12), and for ^{177}Lu-C3octapa-trastuzumab a very substantial amount of ^{177}Lu was leached out of the ligand and transchelated by the EDTA mobile phase (Figures A.9-A.12). In the iTLC experiments, ^{111}In- and ^{177}Lu-octapa/DOTA-trastuzumab remained at the baseline, while $^{177}Lu^{3+}$/$^{111}In^{3+}$ ions complexed as [^{111}In/^{177}Lu]-EDTA eluted with or near the solvent front.

6.4.20 ^{111}In- and ^{177}Lu-C3octapa/octapa-trastuzumab blood serum competition experiments

Frozen human blood serum was thawed for 30 minutes, and 300 μL aliquots were transferred to 2.0 mL Corning centrifuge vials. A portion of radiolabeled immunoconjugate (~300 μCi) was transferred to the blood serum. Serum competition samples were then incubated at 37 ± 0.1 °C with gentle agitation (300 rpm) and analyzed via iTLC with an EDTA eluent (50 mM, pH 5.0) (Bioscan AR-2000) at time points of 0, 24, 48, 72, 96, and 120 hours.

Chapter 7: H_6phospa-Trastuzumab: a bifunctional methylenephosphonate-based ligand with ^{89}Zr, ^{111}In and ^{177}Lu

This chapter is an adaptation of published work, and is reproduced in part, with permission from Price, E. W.; Zeglis, B. M.; Lewis, J. S.; Adam, M. J.; Orvig, C., H_6phospa-Trastuzumab: Bifunctional Methylenephosphonate-based Chelator with ^{89}Zr, ^{111}In and ^{177}Lu. *Dalton Trans.* **2014,** *43*, 119-131, Copyright 2014 The Royal Society of Chemistry.

7.1 Introduction

Recent years have witnessed a surge in interest in the development and application of ^{89}Zr-based radiopharmaceuticals for positron emission tomography (PET) imaging.[15,28,36,130,285,287,291,296,356-359] A large part of this attention can be attributed to the intermediate half-life ($t_{1/2}$ = ~3.3 days) of ^{89}Zr, a property that makes the isotope nearly ideal for use with biological vectors that have long circulation times, such as antibodies and nanoparticles.[15,28,36,56,285,291,356] Very few isotopes combine the nuclear properties of an intermediate half-life (2-7 days) with a suitable positron emission for PET imaging, making ^{89}Zr uniquely situated amongst its radiometal peers.[15] To date, the only ligand proven competent enough for use with ^{89}Zr is the acyclic hydroxamate-based desferrioxamine (DFO), which can quantitatively radiolabel with ^{89}Zr in less than one hour at room temperature; most ligands, it is important to note, cannot adequately complex ^{89}Zr under any conditions in aqueous media (Figure 7.1).[28,36,56,291] DTPA is currently the best alternative ligand to DFO for ^{89}Zr radiolabeling, but can only achieve radiolabeling yields of < 0.1%

after 1 hour at room temperature.[223] Despite the excellent radiolabeling properties and sufficient *in vitro* and *in vivo* stability of DFO, over prolonged periods of time *in vivo*, some ^{89}Zr can be observed to decomplex, leach out of the DFO chelate, and ultimately accumulate in the skeletal system.[28,36,56,291] Because of this mild shortcoming of DFO, the goal of discovering a new ligand that can quickly and completely radiolabel with ^{89}Zr under mild conditions, while concomitantly improving on the thermodynamic stability and kinetic inertness of DFO would be of great interest and utility towards the translation of ^{89}Zr from the bench to the clinic. Due to the propensity of Zr(IV) to quickly precipitate, aggregate, and form polynuclear oxo/hydroxo species at typical radiolabeling pH (2-8), an acyclic ligand with very rapid radiolabeling kinetics is required.[36] Additionally, due to the ideal pairing of ^{89}Zr with heat-sensitive antibodies, the room-temperature radiolabeling properties that most acyclic ligands provide are likewise crucial.

A number of recent works have illustrated that the use of methylenephosphonate groups in ligands can provide improved radiolabeling properties with a variety of radiometals, most notably accelerated reaction kinetics that allow for faster and lower temperature radiolabel incorporation.[84,148,174-177,181,253] In particular, the replacement of carboxylic acid groups with methylenephosphonates has yielded both improved reaction kinetics, and enhanced chelate stability. Most notable is the example of CB-TE2A, in which the replacement of one (CB-TE1A1P) or both (CB-TE2P) carboxylic acid arms with methylenephosphonate groups resulted in improved radiolabeling kinetics, with *in vitro* and *in vivo* stability being retained or enhanced compared to the CB-TE2A parent ligand (see Chapter 1).[148,174-177,181] The use of methylenephosphonate groups with our existing "pa"

family of acyclic ligands (Figure 7.1), such as H_2dedpa, H_4octapa, H_2azapa, and H_5decapa is enticing, as it could potentially provide improved radiochemical properties.[88,89,118,272]

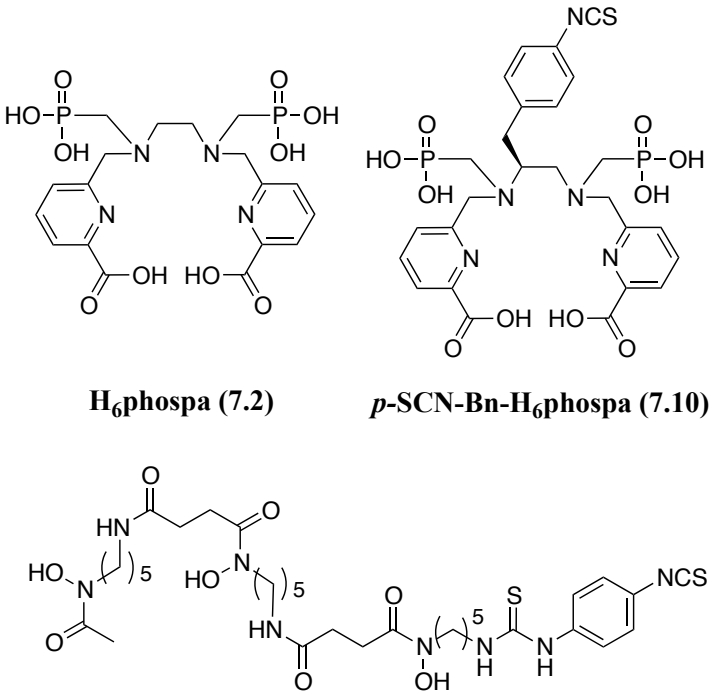

H_6phospa (7.2) **_p_-SCN-Bn-H_6phospa (7.10)**

***p*-SCN-Bn-Desferrioxamine (DFO)**

Figure 7.1 The current "gold standard" ligand for ^{89}Zr, DFO, and the new entrants H_6phospa (**7.2**) and bifunctional analogue *p*-SCN-Bn-H_6phospa (**7.10**).

The idea of improving radiolabeling kinetics by replacing carboxylic acid chelating arms with methylenephosphonate groups led us to the synthesis of H_6phospa (Figure 7.1). H_6phospa is a methylenephosphonate derivative of the acyclic ligand H_4octapa (Chapters 2-3), with 8 potential donors in an N_4O_4 set (octadentate).[89] Previous attempts to radiolabel the H_4octapa-trastuzumab immunoconjugate with ^{89}Zr in a variety of buffers (including HEPES, ammonium acetate, phosphate buffered saline) during the experiments performed for Chapter

3 resulted in no radiometal incorporation as evaluated by radio-iTLC. It was hypothesized that replacement of the acetic acid arms of H_4octapa with methylenephosphonate arms might improve radiochemical yields and reaction kinetics. Fortuitously, the methylenephosphonate derivative of H_4octapa had been previously published by Rodriguez-Blas and co-workers, and so the synthesis of the octadentate ligand H_6L^2 (which we have now called H_6phospa) was performed using a modified literature procedure in one step from the Me_2dedpa precursor,[268,269] and the new and unpublished bifunctional derivative *p*-SCN-Bn-H_6phospa was synthesized in six steps. Subsequently, *p*-SCN-Bn-H_6phospa was conjugated to the antibody trastuzumab, and radiolabeling experiments were performed with ^{89}Zr, ^{111}In, and ^{177}Lu, in order to assess the potential of H_6phospa-based conjugates for application with these three radiometals for molecular imaging agents (SPECT/PET) and therapeutics.

7.2 Results and discussion

7.2.1 Synthesis and characterization

An important modification of our literature procedure (Chapter 3) was used to synthesize the acyclic ligand H_6phospa.[87,89,268,269] The precursor Me_2dedpa (**7.1**) was synthesized in Chapter 3 in 3 steps utilizing unique 2-nitrobenzenesulfonamide (nosyl) protection chemistry in a cumulative yield of 70-75% (Scheme 7.1).[87] Purification of the Me_2dedpa precursor was performed using neutral alumina, due to the high affinity of this molecule to silica. To afford H_6phospa, a one-pot procedure was used. Me_2dedpa and phosphorous acid were first heated to reflux together in HCl (6 M) for a short period of time (~1 h), followed by the slow addition of paraformaldehyde to form a transient imine, which could then react with phosphorous acid to yield the methylenephosphonate product. If the

paraformaldehyde reagent were added first or added too quickly, the *N*-methylated product would form as a major product, which would greatly reduce yields and complicate purification. The product H_6phospa (**7.2**) formed an insoluble HCl salt after reducing the crude reaction mixture to dryness *in vacuo*, resuspending in HCl (6 M), and filtering.

Scheme 7.1 Synthesis of H_6phospa (**7.2**) and *p*-SCN-Bn-H_6phospa (**7.10**) [a]

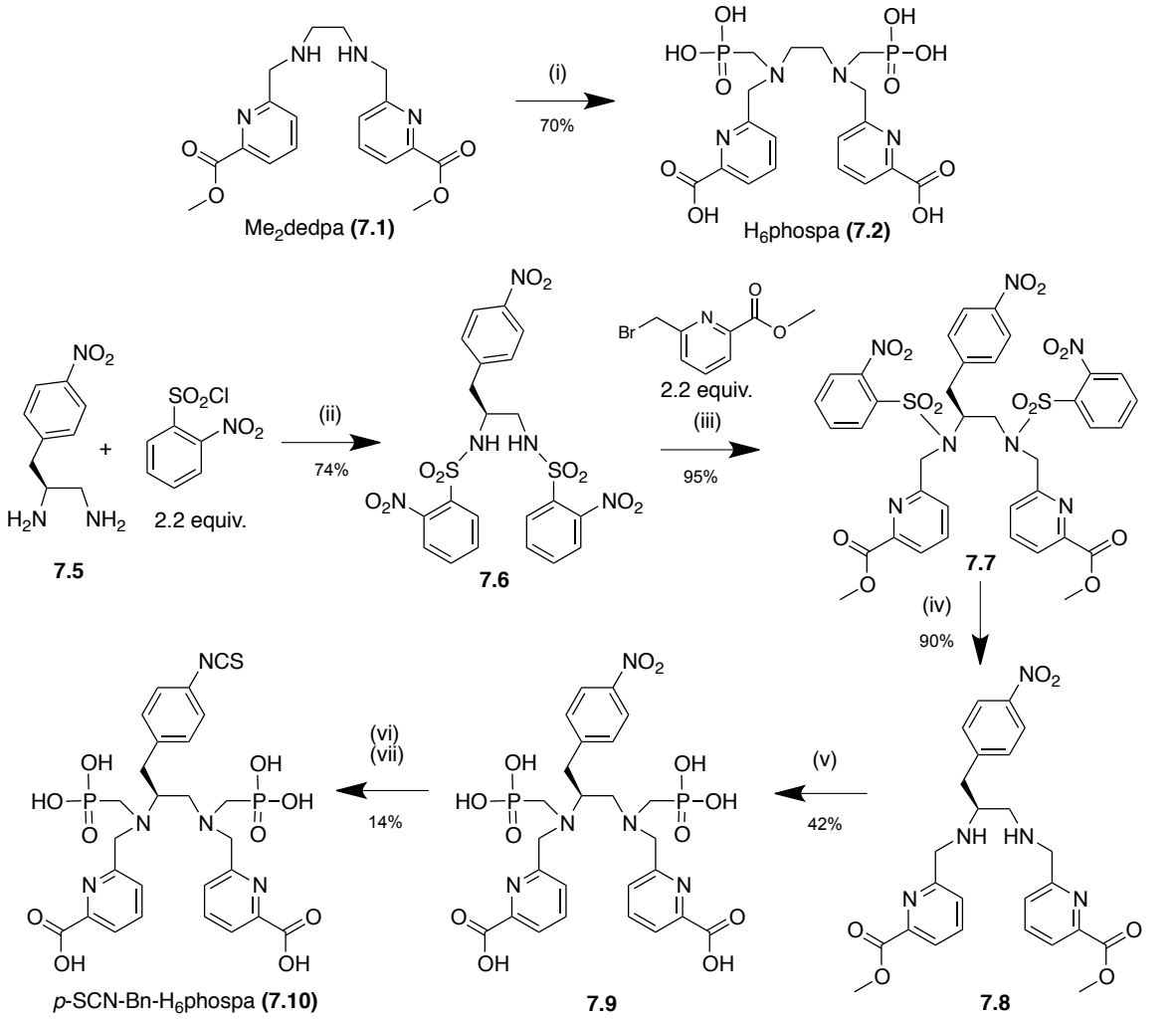

[a] (i) paraformaldehyde (12 eq.), phosphorous acid (20 eq.), HCl (5 mL, 6 M), reflux, 48 h; (ii) THF, $NaHCO_3$, RT, 24 h; (iii) DMF, Na_2CO_3, 60 °C, 48 h; (iv) THF, thiophenol (2.2 equiv), K_2CO_3, RT, 72 h; (v) paraformaldehyde (16 eq.), phosphorous acid (40 eq.), HCl (5 mL, 6 M), reflux, 48 h; (vi) 3 mL of (1:1) glacial acetic acid:3 M HCl, Pd/C (20 wt%), H_2 (g), RT, 1 h, used without further purification (vii) thiophosgene in DCM (15 equiv), HCl (2 mL, 3M), RT, 24 h, (~4% cumulative yield in 6 steps).

Nosyl protection chemistry was crucial for the synthesis of *p*-SCN-Bn-H_6phospa, as it allowed for deprotection under mild conditions (no strong acid/base or hydrogenation) with thiophenol and potassium carbonate in tetrahydrofuran at room temperature. The use of benzyl protection chemistry was not feasible for this synthesis, as deprotection would require hydrogenation (Scheme 7.1, step iv), which would transform the *p*-NO_2-benzyl functionality to *p*-aniline. The aniline primary amine would then react (Scheme 7.1, step v) with paraformaldehyde and phosphorous acid creating unwanted *N*-methyl/methylenephosphonate products, and prevent later isothiocyanate formation. The bifunctional derivative *p*-SCN-Bn-H_6phospa (**7.10**) was synthesized for the first time in 6 steps with a low cumulative yield of ~4%. Briefly, the isothiocyanate precursor *p*-NO_2-Bn-H_6phospa (**7.9**) was synthesized through a pathway analogous to that for H_6phospa, with the *p*-NO_2-Bn-Me_2dedpa precursor made first, followed by a very similar methylenephosphonate formation in HCl (6 M) with paraformaldehyde and phosphorous acid. The *p*-NO_2-Bn-H_6phospa product was purified via semi-preparative reverse-phase (RP) HPLC, hydrogenated to form *p*-NH_2-Bn-H_6phospa, and finally mixed with thiophosgene in chloroform and HCl (3 M) to react and yield *p*-SCN-Bn-H_6phospa (**7.10**), which was lyophilized after RP-HPLC purification to yield an off-white powder.

Table 7.1 Chemical and *in vitro* biological characterization data for ^{111}In- and ^{177}Lu-phospa-trastuzumab radioimmunoconjugates.

Immunoconjugate	Isotope	Radiolabeling conditions and yield	Chelates / mAb[a]	Specific activity (mCi/mg)	Immunoreactive fraction (%)[b]	Serum stability 120 h (%)[c]
H_6phospa-trastuzumab	^{111}In	30 min, 25 °C, 70-90%	3.3 ± 0.1	2.9 ± 0.7	97.9 ± 2.6	52.0 ± 5.3
	^{177}Lu	30 min, 25 °C, 40-80%	3.3 ± 0.1	2.8 ± 0.8	n/a	2.0 ± 0.3

[a] Isotopic dilution assays, n = 3. [b] Determined immediately prior to *in vivo* experimentation, n = 9. [c]Determined in human serum at 37 °C for 120 h, n = 3.

Once synthesized, H_6phospa was mixed with $ZrCl_4$, $In(ClO_4)_3$, and $LuCl_3$ in three attempts to react and make non-radioactive metal complexes. The In^{3+} complex was identified by low-resolution and high-resolution mass spectrometry, but was too insoluble to perform other characterization techniques, and no crystals were obtained for X-ray solid-state structure determination. The Lu^{3+} complex was also very insoluble, could not be detected by mass spectrometry, and, like the In^{3+} complex, could not be characterized by other techniques (for example, they were not soluble in MeOD, D_2O or DMSO-d_6 for NMR spectroscopic analysis). The Zr^{4+} complex also could not be detected by mass spectrometry or characterized by other techniques, though it was observed that a fine white precipitate formed shortly after addition of the zirconium salt to an aqueous solution of H_6phospa. Although synthesis of these metal complexes was attempted, none could be confirmed. Radiolabeling experiments (*vide infra*) with ^{111}In and ^{177}Lu confirmed that coordination of these metal ions does indeed occur, while radiolabeling experiments with ^{89}Zr have demonstrated that the H_6phospa complex of this radiometal does indeed form, albeit inefficiently in low yields.

7.2.2 Antibody modification, ^{111}In and ^{177}Lu radiolabeling, and *in vitro* characterization

Moving beyond radiolabeling efficiency and chemical characterization, the *in vitro* and *in vivo* stability of a ligand will determine its ultimate value for use in radiopharmaceuticals. To this end, a model system based on the HER2/*neu*-targeting antibody trastuzumab and HER2-expressing SKOV-3 ovarian cancer cells was used. After modification of the purified antibody trastuzumab with *p*-SCN-Bn-H_6phospa and subsequent radiolabeling experiments, the resulting radioimmunoconjugates were characterized by radio-iTLC, radiometric isotopic dilution assays, cellular binding assays, serum stability

challenges, and *in vivo* SPECT/CT imaging using female nude athymic mice bearing subcutaneous SKOV-3 xenografts (Table 7.1).

The bifunctional chelate derivative *p*-SCN-Bn-H_6phospa was conjugated to purified trastuzumab via incubation under mildly basic conditions (pH 8.5-9.0) with 4 equivalents of *p*-SCN-Bn-H_6phospa, and the resulting conjugates were purified via size exclusion chromatography (PD-10, GE Healthcare). Subsequent radiometric isotopic dilution experiments revealed that 3.3 ± 0.1 accessible chelates per antibody had been successfully conjugated (Table 7.1). H_6phospa-trastuzumab was then radiolabeled with either ^{111}In or ^{177}Lu in NH_4OAc buffer (pH 5.5, 200 mM) for 30 min at room temperature, producing ^{111}In-labeled radioimmunoconjugates with acceptable yields (70-90% radiochemical yield) and high specific activities (2.9 ± 0.7 mCi/mg) (Table 7.1). Radiolabeling experiments with ^{177}Lu resulted in inconsistent yields (40-80% radiochemical yield) but high specific activities (2.8 ± 0.8 mCi/mg). The radiochemical purity of ^{111}In-phospa-trastuzumab was excellent after purification (>99%), but iTLC evaluation of ^{177}Lu-phospa-trastuzumab showed impurities that eluted at the solvent front, even after purification. This was most likely a result of weakly-bound ^{177}Lu undergoing ligand exchange between the ^{177}Lu-phospa-trastuzumab immunoconjugate and $EDTA^{4-}$ (50 mM, pH 5) in the aqueous mobile phase (Figure 7.2).

The ^{111}In-phospa-trastuzumab conjugate was produced quickly under mild room temperature conditions, but the radiolabeling properties of H_6phospa are admittedly inferior to H_4octapa with both ^{111}In and ^{177}Lu (Chapter 3, H_4octapa providing quantitative RCY in < 15 min at RT). However, *in vitro* assays with HER2-expressing SKOV-3 cancer cells designed to calculate the immunoreactive fraction of an antibody at infinite antigen levels

revealed an immunoreactivty of 97.9 ± 2.6% for ^{111}In-phospa-trastuzumab (n=9, Table 7.1). This represents a negligible decrease from the theoretical maximum of 100% assumed for unmodified trastuzumab. Cellular immunoreactivity assays were not performed with ^{177}Lu-phospa-trastuzumab due to limited stability. The stabilities of the ^{111}In/^{177}Lu-phospa-trastuzumab radioimmunoconjugates were assessed using a human serum transchelation challenge at 37 °C over a period of 5 days (gentle agitation, 300 rpm, Eppendorf Thermomixer) (Table 7.1).

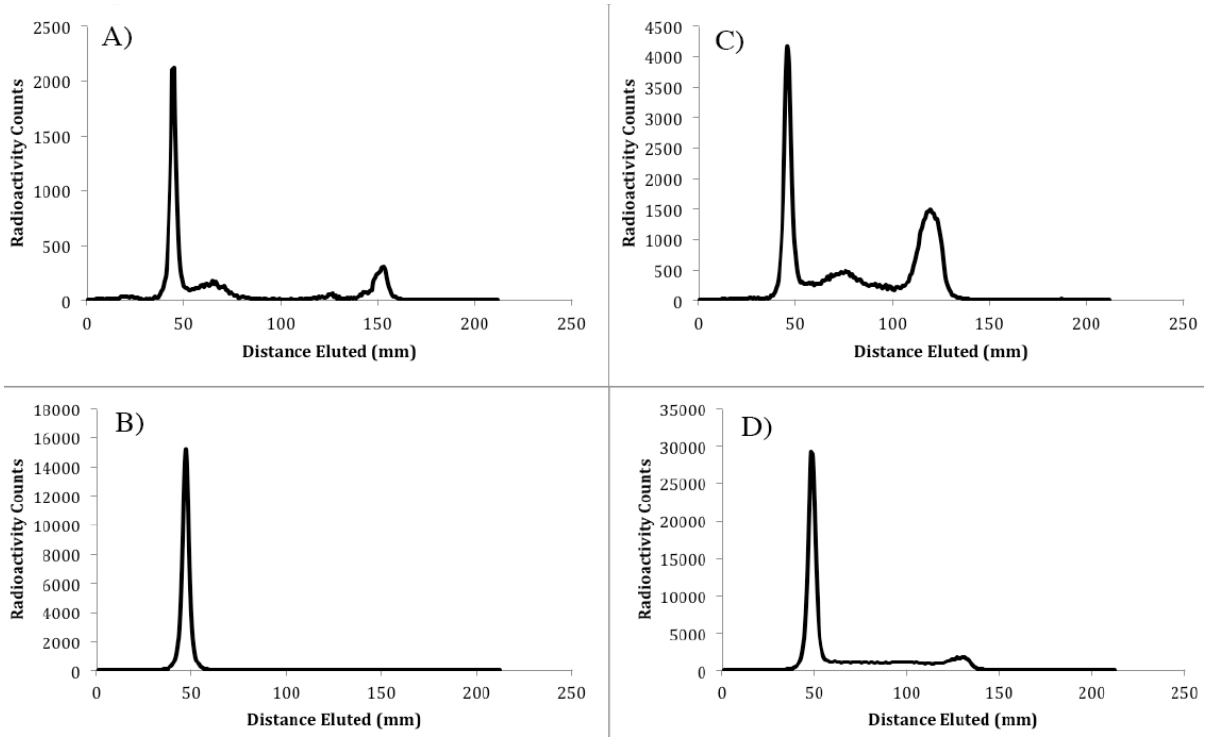

Figure 7.2 A) iTLC radiochromatograph of the unpurified radiolabeling mixture of ^{111}In-phospa-trastuzumab (30 minutes, 25 °C, 2.64 mCi/mg); B) iTLC of ^{111}In-phospa-trastuzumab after purification by PD-10 column; C) iTLC trace of the unpurified radiolabeling mixture of ^{177}Lu-phospa-trastuzumab (30 minutes, 25 °C, 2.23 mCi/mg); and D) iTLC trace of ^{177}Lu-phospa-trastuzumab after purification, showing ^{177}Lu transchelated from the weakly-bound ^{177}Lu-phospa-trastuzumab to EDTA^{4-} (~200 μg of antibody conjugate used for each reaction).

The amount of radiometal that remained bound to the H_6phospa-trastuzumab immunoconjugate was determined using radio-iTLC at various time points. ^{177}Lu-phospa-

trastuzumab proved to be very unstable; the ^{177}Lu was quickly transchelated by serum proteins (e.g. transferrin), with only 8% of the ^{177}Lu remaining chelate-bound after 24 hours, and only 2% still intact after 5 days (Figure 7.3). The ^{111}In-phospa-trastuzumab construct fared better, with 67% of the ^{111}In remaining intact after 24 hours and 53% after 5 days. Included for comparison in Figure 7.3 are human serum stability data of the H_4octapa-based constructs ^{111}In/^{177}Lu-octapa-trastuzumab from Chapter 3, both of which quantitatively and rapidly radiolabeled at room temperature in less than 15 minutes, remained > 90% intact throughout an entire 5 day transchelation challenge, and demonstrated excellent *in vivo* stability.[87]

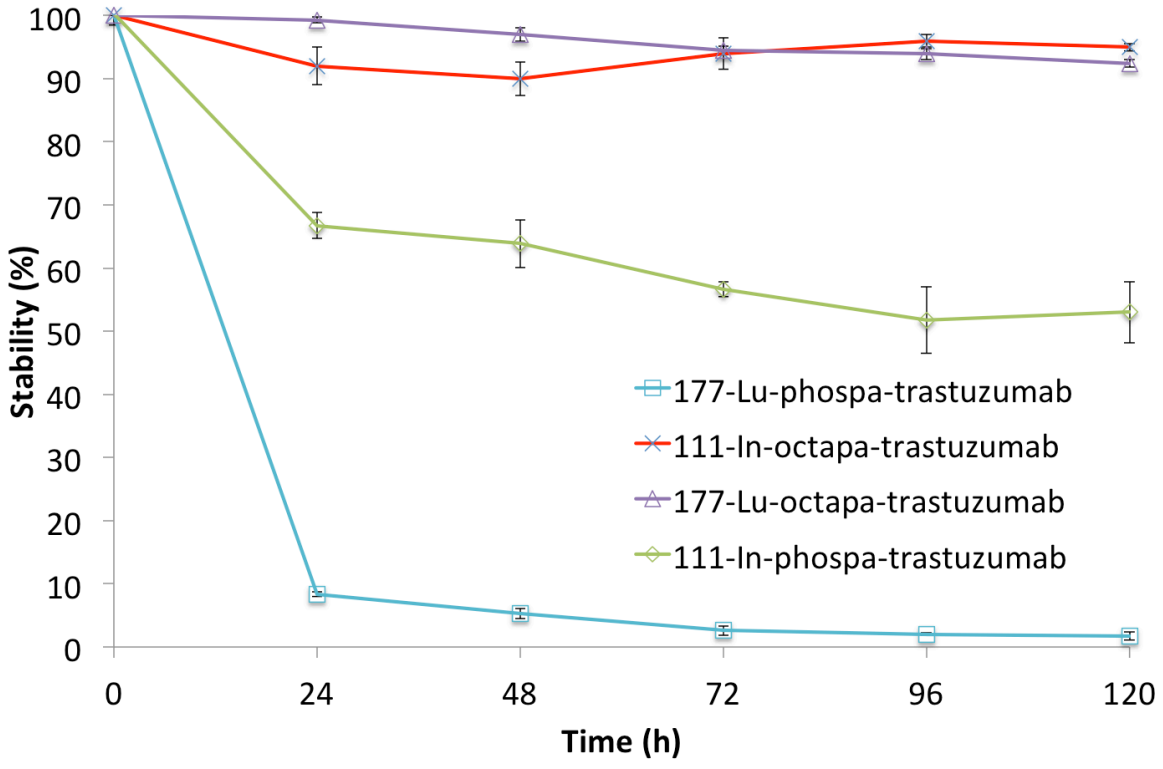

Figure 7.3 The stability of ^{177}Lu/^{111}In-phospa-trastuzumab in human blood serum over 120 h, agitated at 300 rpm and 37 °C, analyzed via radio-iTLC elution with EDTA mobile phase (50 mM, pH 5), compared to previously obtained values for ^{177}Lu/^{111}In-octapa-trastuzumab as a reference.[87]

7.2.3 ^{89}Zr Radiolabeling

DFO has been used as the ligand of choice for ^{89}Zr for over 20 years.[36] During this time, no challengers have emerged that improve upon it, or, for that matter, display comparable radiochemical properties.[36] The challenges faced when trying to improve upon DFO are significant, and these difficulties are only amplified by the problematic aqueous chemistry of ^{89}Zr.[36] Although the acyclic ligand H$_4$octapa has been shown to have great potential for use with the radiometals ^{111}In and ^{177}Lu in Chapters 2-3, experiments that were not discussed in Chapter 3 (also unpublished) have revealed its incompetence for radiolabeling with ^{89}Zr. Using a variety of buffers (NH$_4$OAc, HEPES, PBS, pH 5.5-7.4) and temperatures (RT to 90 °C) no measureable quantity of ^{89}Zr could be incorporated into the H$_4$octapa-trastuzumab immunoconjugate. Our hypothesis from these observations was that by using methylenephosphonate donor arms in place of the carboxylic acid arms in H$_4$octapa, we could potentially enhance radiolabeling kinetics and improve radiometal-complex stability with ^{89}Zr. From these observations, we modified the design of H$_4$octapa by taking advantage of its inherent modularity and replaced its pendant acetic acid chelating arms with methylenephosphonate groups to synthesize H$_6$phospa.

Radiolabeling experiments with the H$_6$phospa-trastuzumab construct have proven our original hypothesis correct in a rather anticlimactic way, with the methylenephosphonate groups providing increased ^{89}Zr incorporation up to a maximum yield of 12% (3.3 ± 0.1 chelates per antibody, PBS pH 7.4, 37 °C, 18 hr) (Figure 7.4). Under the more realistic radiolabeling conditions typically used for ^{89}Zr-DFO - RT, pH 7.0-7.5, 1 hr - radiochemical yields of 7-8% were achieved. Despite the improved ^{89}Zr radiolabeling yields of H$_6$phospa-trastuzumab (8-12%) compared to H$_4$octapa-trastuzumab (~0-1%), it was not sufficient for

H_6phospa to be used as a ligand for ^{89}Zr-based radiopharmaceutical preparations. Although PBS buffer is commonly used for ^{89}Zr radiolabeling, HEPES buffer is a good alternative.[56,285,297,298,301] ^{89}Zr Radiolabeling experiments with H_6phospa-trastuzumab in HEPES buffer (500 mM, pH 7.1) were attempted, but after 1 hour at room temperature, radiochemical yields of only ~2% were achieved. These results compare poorly to the current "gold standard" ligand desferrioxamine (DFO, Figure 7.1), that can achieve quantitative radiochemical yields (>95%) at room temperature in less than 1 hour. It is important to note that although H_6phospa has been found to be inferior to DFO, to our knowledge it is the best alternative ligand published to date (see Chapter 1.5.14-1.5.15). Previously, the best alternative ligand to DFO was DTPA, with a DTPA-antibody conjugate of Zevalin demonstrating ^{89}Zr radiochemical yields of < 0.1% after 1 hour at room temperature.[223]

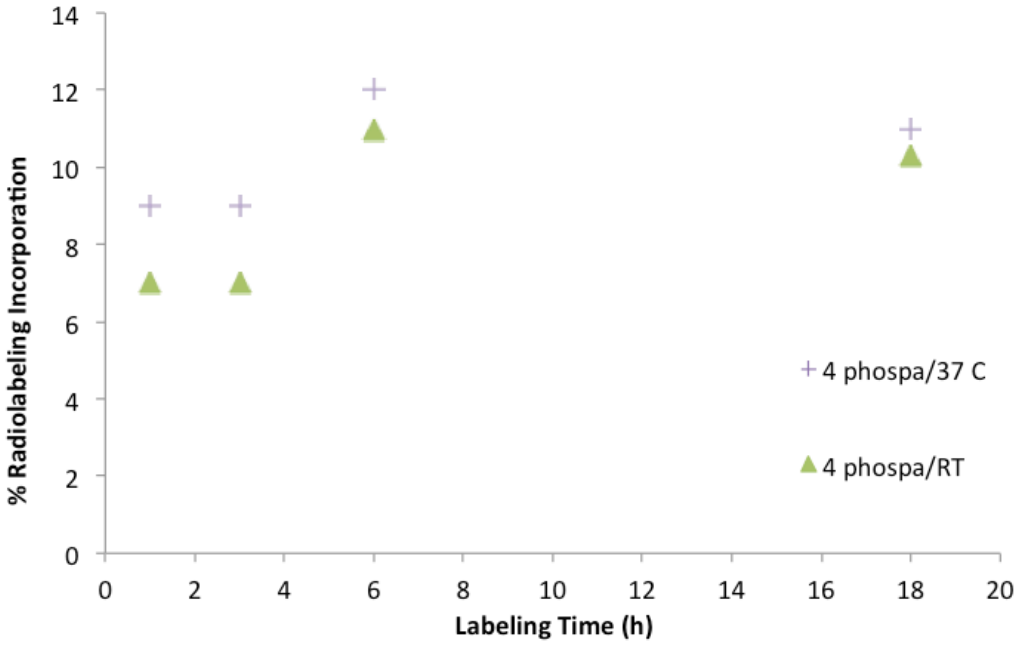

Figure 7.4 Radiolabeling results of H_6phospa-trastuzumab with ^{89}Zr in phosphate buffered saline (pH 7.4), showing results at both room temperature and 37 °C with H_6phospa-trastuzumab (3.3 ± 0.1 chelates per antibody) (~300 μg of antibody conjugate used for each reaction and ~1 mCi of ^{89}Zr).

Although the hypothesis that replacing the carboxylic acid pendant arms of H_4octapa with the methylenephosphonate arms of H_6phospa would improve radiolabeling kinetics and radiochemical yields was proven correct, the improvement was modest. However, these results do provide compelling evidence that methylenephosphonate-O donor groups may be superior to traditional carboxylate-O donor groups for ^{89}Zr coordination. The N_4O_4 donor set of the picolinate-based ligands H_4octapa and H_6phospa may be too nitrogen rich, and future ligands should take advantage of the oxophilic nature of Zr(IV). Taking a lesson from the only suitable ^{89}Zr ligand, DFO (Figure 7.1), acyclic ligands with O_8 donor sets and binding groups such as hydroxamates, carboxylates, carbonyls, catechols, and hydroxypyridinones are likely the most suitable. This valuable insight suggests that H_6phospa is a good starting point for further design modifications towards new ^{89}Zr ligands.

7.2.4 Small animal SPECT/CT imaging

Despite the modest radiolabeling performance of H_6phospa-trastuzumab with ^{89}Zr, and the non-optimal radiochemical yields and serum stability results with ^{111}In and ^{177}Lu, *in vivo* imaging was performed to determine the biological behaviour of these radioimmunoconjugates. SPECT imaging was used in conjunction with standard helical X-ray CT for *in vivo* imaging of the ^{111}In and ^{177}Lu radiolabeled H_6phospa-trastuzumab immunoconjugates over a 5-day period. The poor *in vitro* serum stability of ^{177}Lu-phospa-trastuzumab foretold poor *in vivo* stability; however, our laboratory has had a long-standing interest in the delivery of therapeutic doses of lanthanide ions to bone for the treatment of osteoporosis.[360,361] Towards this goal, SPECT/CT imaging was performed with the purified ^{177}Lu-phospa-trastuzumab immunoconjugate in order to visualize biodistribution and confirm

bone-localization of ^{177}Lu for the potential application of H_6phospa to transiently bind lanthanide ions for bone delivery.[360,361]

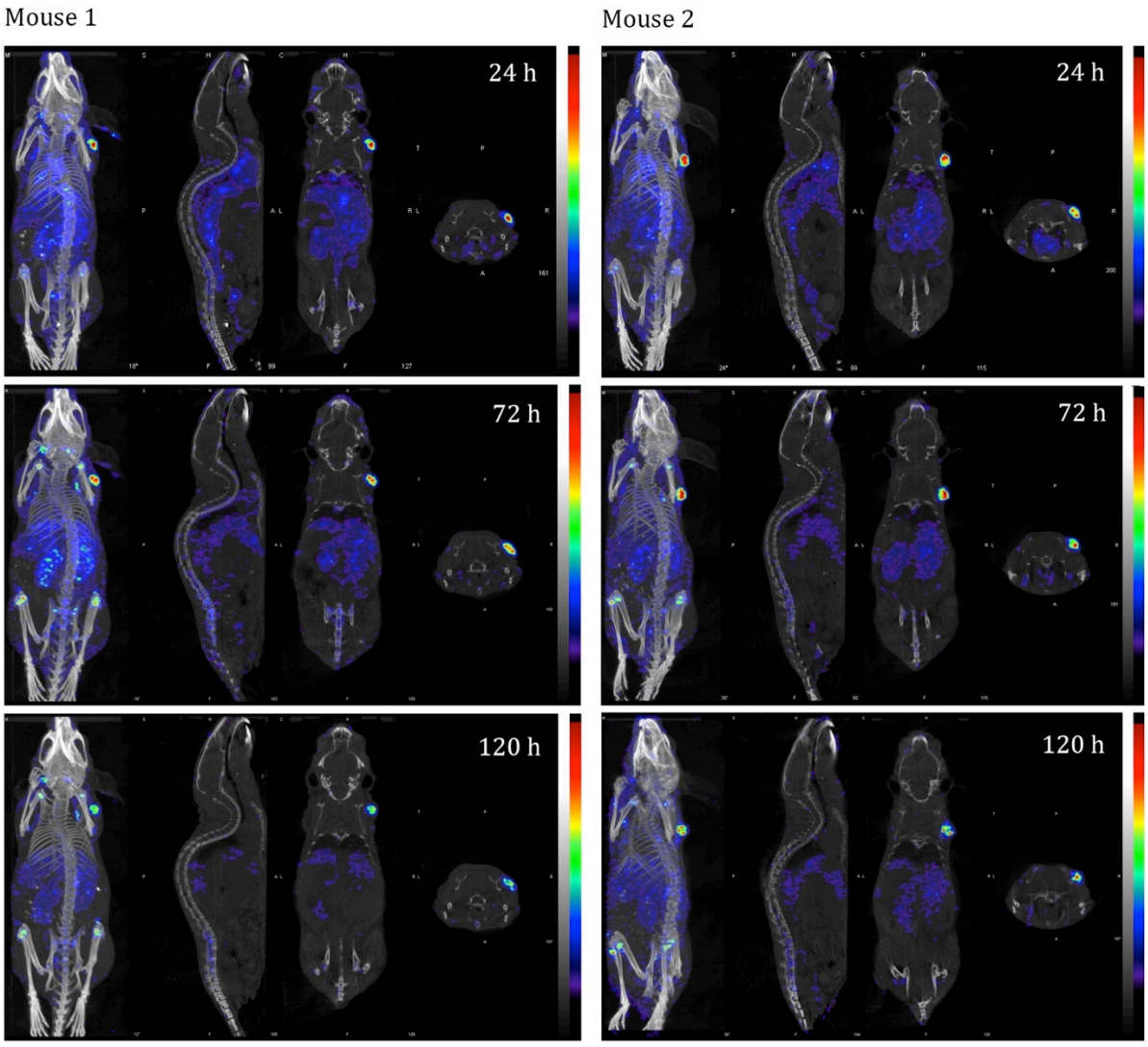

Figure 7.5 SPECT/CT images of ^{111}In-phospa-trastuzumab in female nude athymic mice bearing SKOV-3 tumour xenografts in the right shoulder (diameter ~2 mm), imaged at 24, 72, and 120 hrs p.i. (~800-810 mCi injected activity, ~150-200 μg antibody per mouse).

^{111}In-phospa-trastuzumab SPECT/CT images showed significant tumour uptake 24 hours post injection (p.i.), with residual activity remaining in blood circulation, as is typical

for antibody constructs (Figure 7.5). Unlike highly stable ^{111}In and ^{177}Lu radiometal ligands such as DOTA (and most recently, H_4octapa), some instability and radiometal dissociation can be visualized by moderate uptake in the kidneys and bones/joints (Figure 7.5). Despite these shortcomings, the SKOV-3 tumours were the most prominent tissue in the SPECT images. As expected from the poor stability results in serum, images of the ^{177}Lu-phospa-trastuzumab construct showed complete decomplexation of the radiometal after 24 hours, with free ^{177}Lu metal ions accumulating almost entirely in the bone (e.g. joints, spine, Figure 7.6).

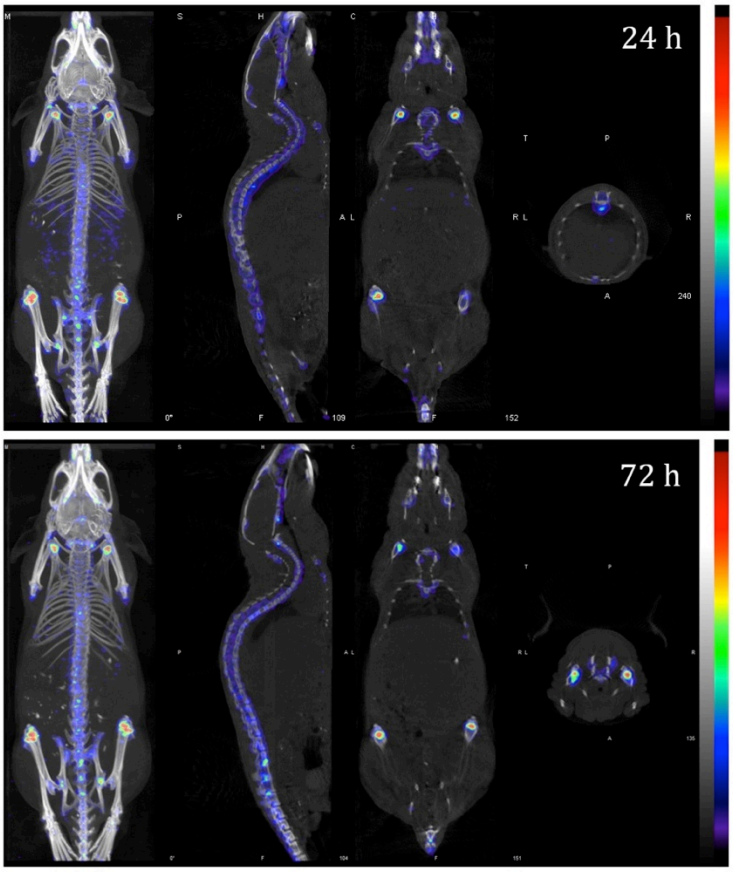

Figure 7.6 SPECT/CT images of ^{177}Lu-phospa-trastuzumab in female nude athymic mice bearing SKOV-3 tumour xenografts in the right shoulder (diameter ~2 mm), imaged at 24 and 72 hrs p.i. (~575 mCi injected activity, ~150-200 μg antibody per mouse).

At 72 hours p.i. the ^{177}Lu-phospa-trastuzumab images looked nearly identical to 24 hours p.i., with no residual activity remaining in blood circulation and no tumour uptake apparent. The ^{177}Lu-phospa-trastuzumab images also serve as negative control experiments, demonstrating the true effects of poor radiometal-chelate stability *in vivo*. Since antibody vectors such as trastuzumab have very long biological half-lives, persistent blood uptake is generally a positive sign of stability; not surprisingly, this was not observed for ^{177}Lu-phospa-trastuzumab (Figure 7.5 vs Figure 7.6). An interesting aspect of the ^{177}Lu-phospa-trastuzumab SPECT/CT images (Figure 7.6) is the lack of uptake in the liver, spleen, and the lungs, with radioactivity almost entirely localizing in the skeletal system. This suggests that there may be a silver lining for H_6phospa with respect to ^{177}Lu, as its failure as a stable ligand for immunoconjugates may be salvaged by its utility in delivering ^{177}Lu to bone.

7.3 Conclusions

The acyclic ligand H_6phospa and the bifunctional derivative *p*-SCN-Bn-H_6phospa have been synthesized using 2-nitrobenzenesulfonamide (nosyl) protection chemistry, conjugated to trastuzumab (3.3 ± 0.1 chelates per antibody), and evaluated via radiolabeling with ^{89}Zr, ^{111}In, and ^{177}Lu. Radiolabeling of the H_6phospa-trastuzumab immunoconjugate was achieved with ^{111}In in 70-90% yields at room temperature in 30 minutes (2.9 ± 0.7 mCi/mg), and with ^{177}Lu under the same conditions in yields of 40-80% (2.8 ± 0.8 mCi/mg). Human serum stability experiments revealed that the ^{111}In-phospa-trastuzumab immunoconjugate was 52.0 ± 5.3% intact after 5 days, and ^{177}Lu-phospa-trastuzumab was only 2.0 ± 0.3% intact. The room temperature radiolabeling conditions afforded by H_6phospa produced the ^{111}In-phospa-trastuzumab conjugate with high immunoreactivity (97.9 ± 2.6%, as indicated by cellular binding assays). Small animal SPECT/CT imaging

was performed using nude athymic mice bearing subcutaneous SKOV-3 xenografts, and it was found that ^{111}In-phospa-trastuzumab successfully identified and delineated small (~2 mm in diameter) tumours from surrounding tissues; however, some uptake was observed in the kidneys and bone due to moderate radiometal-chelate complex instability. The *in vivo* behaviour of the ^{177}Lu-phospa-trastuzumab immunoconjugate was likewise studied via SPECT/CT and, as expected from its poor *in vitro* stability in serum, it displayed no tumour uptake and high uptake in the bones and joints, suggesting complete radiometal dissociation. The weak binding of ^{177}Lu by H_6phospa-trastusumab and the rapid *in vivo* release of ^{177}Lu radiometal ions highlights a potential application of H_6phospa in transient lanthanide chelation for delivery of therapeutic doses to the bone. The radiolabeling efficiency of H_6phospa-trastuzumab was tested with ^{89}Zr, and while H_6phospa offered an improvement over H_4octapa-trastuzumab, the results were modest with 7-8% incorporation of ^{89}Zr after 1 hour at room temperature. DTPA was previously the best alternative ligand to DFO, providing ^{89}Zr-radiolabeling yields of < 0.1% after 1 hour at room temperature. To our knowledge, H_6phospa now provides the second highest ^{89}Zr radiolabeling yields reported to date, with only DFO being superior. It can be concluded from this chapter that H_6phospa is a less suitable ligand for use with ^{111}In and ^{177}Lu when compared to DOTA and H_4octapa, but an improvement for ^{89}Zr radiolabeling. Radiolabeling yields were inferior to the current "gold standard" desferrioxamine (DFO), but valuable insight was gained for the design of new ^{89}Zr ligands, with H_6phospa being an excellent starting point.

7.4 Experimental

7.4.1 Materials and methods

The general materials and methods used in this chapter were the same as those used in Chapter 3, with the following exceptions. All NMR spectra were internally referenced to residual solvent peaks except for ^{13}C NMR spectra in D_2O, which were externally referenced to a sample of CH_3OH/D_2O, and ^{31}P NMR spectra in D_2O, which were externally referenced to 85% phosphoric acid. ^{89}Zr was produced at Memorial Sloan-Kettering Cancer Center on an EBCO TR19/9 variable-beam energy cyclotron (Ebco Industries Inc., British Columbia, Canada) via the $^{89}Y(p,n)^{89}Zr$ reaction and purified in accordance with previously reported methods to yield ^{89}Zr with a specific activity of 5.28-13.43 mCi/μg (195-497 MBq/μg).[301]

7.4.2 *N,N′*-[6-(Methoxycarbonyl)pyridin-2-yl]methyl-1,2-diaminoethane (7.1)

Compound **7.1** was prepared in the same fashion as in Chapter 3, in 3 synthetic steps (70-75% cumulative yield).[87] ^1H NMR (300 MHz, MeOD, 25 °C) δ: 8.02 (d, J = 7.5 Hz, 2H), 7.94 (t, J = 7.6 Hz, 2H), 7.66 (d, J = 7.5 Hz, 2H), 3.96 (s, 6H), 2.79 (s, 4H). ^{13}C NMR (75 MHz, MeOD, 25 °C) δ: 167.0, 161.4, 148.5, 139.5, 127.6, 124.8, 54.9, 53.4, 50.0, 49.3. HR-ESI-MS calcd. for $[C_{18}H_{22}N_4O_4+H]^+$: 359.1719; found: 359.1720, $[M+H]^+$, PPM = 0.2.

7.4.3 H_6phospa, (7.2), *N,N′*-(Methylphosphonate)-*N,N′*-[6-(methoxycarbonyl)pyridin-2-yl]methyl]-1,2-diaminoethane

Compound **7.2** was prepared according to a modified literature procedure.[268,269] To a solution of **7.1** (74.0 mg, 0.207 mmol) in HCl (5 mL, 6 M) was added phosphorous acid (340 mg, 4.13 mmol), followed by paraformaldehyde in small portions (25.0 mg, 0.827 mmol).

The reaction mixture was heated to reflux overnight, and over a period of 48 hours another 8 equiv of paraformaldehyde was added (50.0 mg, 1.65 mmol). The reaction mixture was concentrated *in vacuo* to form the water-insoluble HCl salt, which was washed with cold HCl (3 M) *ad libitum* to yield H_6phospa **(7.2)** as a white solid (70%). ^{1}H NMR (300 MHz, D_2O, 25 °C) δ: 7.68 (m, 4H), 7.39-7.36 (m, 2H), 4.12 (s, 4H), 3.32 (s, 4H), 2.96 (d, J = 11.2 Hz, 4H). ^{13}C NMR (75 MHz, D_2O, 25 °C, externally referenced to MeOH in D_2O) δ: 172.1, 153.0, 152.8, 125.8, 123.4, 58.9, 58.8, 52.7, 50.9, 50.4, 50.3. ^{31}P[^{1}H] NMR (121.5 MHz, D_2O, 25 °C, externally referenced to 85% phosphoric acid) 16.0, 2.8. HR-ESI-MS calcd. for $[C_{18}H_{22}N_4O_{10}P_2+H]^+$: 517.0889; found: 517.0884, $[M+H]^+$, PPM = -1.0. IR (neat, ATR-IR): n = 1624 cm^{-1} (C=O), 1584 cm^{-1} (C=C py), 1430 cm^{-1} (P=O).

7.4.4 Na_3[Lu(phospa)] (7.3)

H_6phospa **(7.2)** metal complex synthesis was attempted, but not confirmed. H_6phospa **(7.2)** (14.1 mg, 0.027 mmol) was suspended in 0.1 M HCl (0.5 mL), and $LuCl_3$•$6H_2O$ (15 mg, 0.033 mmol) was added. The pH was adjusted to 4-5 using 0.1 M NaOH and then the solution was stirred at room temperature. After 1 hour, the reaction mixture was analysed by mass spectrometry, but no product could be identified. Evaporating the solvent gave a white solid that could not be dissolved in MeOD, D_2O, or DMSO-d_6, and thus characterization was not performed; metal complex formation could not be confirmed.

7.4.5 Na_3[In(phospa)] (7.4)

H_6phospa **(7.2)** metal complex synthesis was attempted, but not confirmed. H_6phospa **(7.2)** (16.1 mg, 0.031 mmol) was suspended in 0.1 M HCl (0.5 mL), and $In(ClO_4)_3$•$6H_2O$ (20

mg, 0.037 mmol) was added. The pH was adjusted to 4-5 using 0.1 M NaOH, and then the solution was stirred at room temperature. After 1 hour, analysis of the reaction mixture via low-resolution and high-resolution mass spectrometry confirmed the presence of a species consistent with the molecular formula proposed for the indium complex. As with the $[Lu(phospa)]^{3-}$ complex, after reducing to dryness *in vacuo*, the white solid could not be dissolved, and therefore further characterization was not obtained, and no crystals suitable for X-ray crystallography were obtained. HR-ESI-MS calcd. for $[C_{18}H_{21}InN_4O_{10}P_2 - H]^-$: 628.9693; found: 628.9700 $[M - H]^-$, PPM = 1.1.

7.4.6 1-(*p*-Nitrobenzyl)ethylenediamine (7.5)

Compound **7.5** was prepared according to a literature preparation,[342] and was purified with a modified procedure using column chromatography (CombiFlash R_f automated column system; 40 g HP silica;, A: 95% dichloromethane 5% ammonium hydroxide, B: 95% methanol 5% ammonium hydroxide, 100% A to 30% B gradient) to afford a **7.7** as brown/amber oil in a cumulative yield of 40% over 3 steps. ^{1}H NMR (300 MHz, $CDCl_3$, 25 °C) δ: 7.91 (d, J = 8.9 Hz, 2H), 7.18 (d, J = 8.5 Hz, 2H), 2.80-2.57 (m, 3H), 2.45-2.31 (m, 2H). ^{13}C NMR (75 MHz, $CDCl_3$, 25 °C) δ: 147.1, 147.7, 129.4, 122.8, 54.3, 47.5, 41.4. HR-ESI-MS calcd. for $[C_9H_{13}N_3O_2+H]^+$: 196.1086; found: 196.1084 [M + H], PPM = -1.0.

7.4.7 *N,N'*-(2-Nitrobenzenesulfonamide)-1-(*p*-nitrobenzyl)-1,2-diaminoethane (7.6)

Compound **7.6** was prepared as in Chapter 3.[87] ^{1}H NMR (300 MHz, acetone-d_6, 25 °C) δ: 8.18-8.15 (m, 1H), 7.99-7.94 (m, 2H), 7.79-7.57 (m, 5H), 7.33 (d, J = 8.5 Hz, 2H), 7.04-6.98 (m, 2H), 4.01 (br s, 1H), 3.41-3.38 (m, 2H), 3.26 (dd, J = 3.4, 13.7 Hz, 1H), 2.98

(m, 1H). ^{13}C NMR (75 MHz, acetone-d_6, 25 °C) δ: 206.3, 149.2, 148.1, 147.6, 146.7, 135.2, 134.8, 134.3, 133.9, 133.8, 133.6, 131.7, 131.4, 130.9, 126.0, 125.7, 123.9, 57.7, 49.4, 38.2. HR-ESI-MS calcd. for $[C_{21}H_{19}N_5O_{10}S_2+Na]^+$: 588.0471; found: 588.0465 $[M+Na]^+$, PPM = -1.0.

7.4.8 *N,N'*-(2-Nitrobenzenesulfonamide)-*N,N''*-[6-(methoxycarbonyl)pyridin-2-yl]methyl]-1-(*p*-nitrobenzyl)-1,2-diaminoethane (7.7)

To a solution of **7.6** (1.03 g, 1.82 mmol) in dimethylformamide (5 mL, dried over molecular sieves 4 Å) was added methyl-6-bromomethylpicolinate (921 mg, 4.01 mmol) and sodium carbonate (~2 g). The yellow reaction mixture was stirred at 60 °C for 48 h, filtered to remove sodium carbonate, and concentrated *in vacuo*. The crude product was purified by silica chromatography (CombiFlash R_f automated column system; 40 g HP silica; A: ethyl acetate, B: petroleum ether, 100% A to 100% B gradient) to yield **7.7** as white fluffy solid (Rf = 0.9 in DCM, 95%). ^{1}H NMR (300 MHz, $CDCl_3$, 25 °C) δ: 8.00-7.81 (m, 4H), 7.78-7.70 (m, 2H), 7.65-7.63 (m, 5H), 7.55-7.44 (m, 4H), 7.38-7.36 (m, 1H), 6.98 (d, J = 8.5 Hz, 2H), 4.96-4.65 (m, 4 H), 4.36 (m, 1H), 3.89 (s, 3H), 3.84 (s, 3H), 3.56-3.50 (m, 1H), 3.39-3.31 (m, 1H), 3.15-3.01 (m, 2H). ^{13}C NMR (75 MHz, $CDCl_3$, 25 °C) δ: 164.9, 164.9, 157.5, 155.9, 147.7, 147.2, 147.0, 147.0, 146.1, 144.6, 137.9, 137.8, 133.7, 133.5, 132.4, 131.8, 131.8, 131.1, 130.0, 129.5, 126.7, 125.6, 124.1, 123.9, 123.9, 122.9, 58.4, 53.4, 52.6, 52.5, 52.2, 49.7, 34.5. HR-ESI-MS calcd. for $[C_{37}H_{33}N_7O_{14}S_2+Na]^+$: 886.1425; found: 886.1447, $[M+Na]^+$, PPM = 2.5.

7.4.9 *N,N'*-[6-(Methoxycarbonyl)pyridin-2-yl]methyl]-*p*-nitrobenzyl)-1,2-diaminoethane (7.8)

To a solution of **7.7** (1.39 g, 1.62 mmol) in tetrahydrofuran (7 mL) was added thiophenol (364 mL, 3.55 mmol) and potassium carbonate (excess, ~1 g). The reaction mixture was stirred at ambient temperature for 72 hours, while a slow color change from colorless to dark yellow occurred. The reaction mixture was split into two 20 mL falcon tubes, diluted with additional tetrahydrofuran, centrifuged for 5 minutes at 4000 rpm, and then the solvent was decanted. The potassium carbonate, which remained in the centrifuge tubes after decanting, was rinsed with tetrahydrofuran and then centrifuged a total of 5 times, all decanted solvent was pooled, and then concentrated to dryness *in vacuo*. The resulting crude yellow oil was purified by alumina column chromatography (CombiFlash R_f automated column system; 24 g neutral alumina; A: dichloromethane, B: methanol, 100% A to 30% B gradient) to yield **7.8** as clear yellow oil (90%). ^{1}H NMR (300 MHz, $CDCl_3$, 25 °C) δ: 8.07-8.04 (m, 2H), 7.96-7.93 (m, 2H), 7.77-7.70 (m, 2H), 7.53-7.46 (m, 2H), 7.34-7.28 (m, 2H), 4.05-3.95 (m, 2H), 3.93-3.92 (s, 6H), 3.91-3.86 (m, 2H), 3.00-2.49 (m, 4H), 2.20 (br s, 2H). ^{13}C NMR (75 MHz, $CDCl_3$, 25 °C) δ: 165.6, 165.5, 160.5, 147.3, 147.2, 147.1, 146.3, 137.3, 130.0, 125.5, 123.4, 123.3, 58.3, 54.9, 52.7, 52.3, 51.7, 39.1. HR-ESI-MS calcd. for $[C_{25}H_{27}N_5O_6+H]^+$: 494.2040; found: 494.2039, $[M+H]^+$, PPM = -0.2.

7.4.10 *N,N'*-[Methylphosphonate]-*N,N'*-[(6-carboxylato)pyridin-2-yl)methyl]-1-(*p*-nitrobenzyl)-1,2-diaminoethane (7.9)

To a solution of **7.8** (96.0 mg, 0.194 mmol) in HCl (5 mL, 6 M) was added phosphorous acid (320 mg, 3.89 mmol), and the reaction mixture was brought to reflux.

Paraformaldehyde (48.0 mg, 1.56 mmol) was added in small portions over 8 hours, and the resulting suspension/solution was heated to reflux overnight. An additional 8 equiv of paraformaldehyde (48.0 mg, 1.65 mmol) and 20 equiv of phosphorous acid (320 mg, 3.89 mmol) were added over a period of 8 hours and heating was continued for an additional night (48 h total). The reaction mixture was concentrated *in vacuo,* and the resulting yellow oil was purified by RP-HPLC on a semi-preparative column (A: 0.1% TFA in deionized water, B: 0.1% TFA in CH_3CN, 5% B to 90% B gradient over 30 minutes) to yield **7.9** (R_t = 12 minutes) as a white solid (42%). ^{1}H NMR (300 MHz, MeOD, 25 °C) δ: 8.12-7.94 (m, 2H), 7.82-7.62 (m, 2H), 7.51-7.34 (m, 3H), 7.24-7.16 (m, 2H), 7.03 (br s, 1H), 4.02-3.46 (m, 3H), 3.15-3.12 (m, 3H), 2.95-1.94 (several m, 7H). ^{13}C NMR (75 MHz, MeOD, 25 °C) δ: 172.7, 172.3, 166.0, 158.2, 152.6, 152.2, 149.1, 145.8, 138.2, 137.7, 130.3, 125.8, 123.7, 123.5, 122.5, 122.3, 58.4, 55.8, 55.6, 54.2, 31.3. ^{31}P[^{1}H] NMR (121.5 MHz, D_2O, 25 °C, externally referenced to 85% phosphoric acid) 16.4, 15.9. HR-ESI-MS calcd. for $[C_{25}H_{29}N_5O_{12}P_2+H]^+$: 654.1366; found: 654.1359, $[M+H]^+$, PPM = -1.1.

7.4.11 *p*-SCN-Bn-H_6phospa, *N,N'*-(methylphosphonate)-*N,N'*-[(6-carboxylato)pyridin-2-yl)methyl]-1-(*p*-benzyl-isothiocyanato)-1,2-diaminoethane (7.10)

Compound **7.9** (52.0 mg, 0.080 mmol) was dissolved in glacial acetic acid (1.5 mL) with hydrochloric acid (1.5 mL, 3 M), palladium on carbon (~10 mg, 20 wt%) was added, and hydrogen gas (balloon) bubbled in under a rubber septum with a syringe. The reaction mixture was stirred vigorously at RT for 1 hour, then filtered to remove Pd/C and washed *ad libitum* with methanol and hydrochloric acid (3 M). The crude reaction mixture was concentrated *in vacuo*, and without purification, was dissolved in hydrochloric acid (1 mL, 3

M) and then mixed with thiophosgene in chloroform (91 mL, 1.20 mmol) to react overnight at ambient temperature with vigorous stirring. The reaction mixture was extracted with chloroform (5 x 1 mL) by vigorous biphasic stirring, followed by decanting and discarding of the organic phase with a pipette in the reaction vial to remove excess thiophosgene. The aqueous phase was diluted to a volume of 4.5 mL with deionized water, and injected directly onto a semi-prep RP-HPLC column for purification (A: 0.1% TFA in deionized water, B: 0.1% TFA in CH_3CN, 5% B to 70% B gradient over 30 minutes). Compound **7.10** eluted at R_t = 17.5 minutes, was lyophilized overnight, and was isolated as a fluffy off-white solid (14% over 2 steps from **7.9**). ^{1}H NMR (600 MHz, DMSO-d6, 25 °C) δ: 8.17-7.90 (m, 3H), 7.76-7.63 (m, 3H), 7.46-7.23 (m, *4*H), 54.54 (br s, 1H), 4.34-4.32 (m, 2H), 3.94-3.85 (m, 3H), 3.33-3.21 (m, 3H), 3.02-2.94 (m, 3H), 2.61 (s, 1H). ^{13}C NMR (150 MHz, MeOD, 25 °C) δ: 174.5, 169.3, 167.4, 167.2, 160.8, 149.1, 148.6, 140.0, 139.9, 139.0, 137.1, 131.8, 131.7, 131.1, 128.0, 127.0, 126.9, 126.1, 125.3, 125.1, 61.1, 61.1, 38.2, 35.2, 34.7, 34.7. HR-ESI-MS calcd. for $[C_{26}H_{29}N_5O_{10}P_2S+Na]^+$: 688.1008; found: 688.0998, $[M+H]^+$, PPM = -1.5. IR (neat, ATR-IR): n = 2075 cm^{-1} (-N=C=S), 1719 cm^{-1} (C=O), 1594 cm^{-1} (C=N py), 1348 cm^{-1} (P=O).

7.4.12 Trastuzumab bioconjugation

Trastuzumab (purchased commercially as Herceptin, Genentech, San Francisco, CA) was purified using centrifugal filter units with a 50,000 molecular weight cutoff (Amicon® ultra centrifuge filters, Ultracel®-50: regenerated cellulose, Millipore Corp., Billerica, MA) and phosphate buffered saline (PBS, pH 7.4) to remove α-α-trehalose dihydrate, L-histidine, and polysorbate 20 additives. After purification, the antibody was taken up in PBS pH 7.4.

Subsequently, 300 μL of antibody solution (150-250 μM) was combined with 100 μL PBS (pH 8.0) and 4 equiv of *p*-SCN-Bn-H_6phospa in 10 μL DMSO, and the pH was adjusted to 9. The reactions were heated at 37 °C for 1 h, followed by centrifugal filtration to purify the resultant antibody conjugate. The final modified antibody stock solutions were stored in PBS pH 7.4 at 4 °C.

7.4.13 ^{111}In-, ^{89}Zr-, and ^{177}Lu-phospa-trastuzumab radiolabeling

Aliquots of the H_6phospa-trastuzumab immunoconjugate were transferred to 2 mL microcentrifuge tubes and made up to 1 mL with ammonium acetate buffer (pH 5.5, 200 mM), and then aliquots of ^{177}Lu or ^{111}In were added (~1-3 mCi). The H_6phospa-trastuzumab mixtures were incubated at room temperature for 30-60 minutes at ambient temperature and then analyzed via iTLC with an eluent of 50 mM EDTA (pH 5). EDTA solution (30 μL, 50 mM, pH 5) was then added to the reaction mixtures to quench the reaction, and then the resulting radiolabeled immunoconjugates were purified using size-exclusion chromatography (Sephadex G-25 M, PD-10 column, 30 kDa, GE Healthcare; dead volume = 2.5 mL, eluted with 1 mL fractions of PBS, pH 7.4) and centrifugal column filtration (Amicon® ultra 50k). The radiochemical purity of the final radiolabeled bioconjugate was assayed by radio-iTLC. For ^{89}Zr radiolabeling experiments, the same procedure was followed as above, with phosphate buffered saline (PBS, pH 7.4) being used in place of ammonium acetate. ^{89}Zr radiolabeling was also attempted in ammonium acetate (200 mM, pH 5.5-6.5) and HEPES buffer (100-500 mM, pH 7-7.2), with PBS ultimately deemed the most suitable buffer. In the iTLC experiments, ^{111}In-, ^{89}Zr-, and ^{177}Lu-phospa-trastuzumab remained near the baseline,

while $^{177}Lu^{3+}/^{111}In^{3+}/^{89}Zr^{4+}$ ions were coordinated as [$^{177}Lu/^{111}In/^{89}Zr$]-EDTA and eluted with or near the solvent front. iTLC methods were followed from previous work.[30,56,87,285,301]

7.4.14 Chelate number – radiometric isotopic dilution assay

These experiments were performed with ^{111}In, ^{111}In-phospa-trastuzumab, and SKOV-3 ovarian cancer cells, in the same manner as in Chapter 3.[87]

7.4.15 *In vitro* immunoreactivity assay

The immunoreactivity of the $^{111}In/^{177}Lu$-phospa-trastuzumab bioconjugates was determined using radioactive cellular-binding assays following procedures derived from Lindmo et al., using the same procedure as in Chapter 3.[347,348]

7.4.16 ^{111}In- and ^{177}Lu-phospa-trastuzumab blood serum competition experiments

Frozen human blood serum was thawed for 30 minutes, and 300 μL aliquots were transferred to 2.0 mL Corning centrifuge vials. A portion of radiolabeled immunoconjugate (~300 mCi) was transferred to the blood serum (n = 3 for each ligand). Serum competition samples were then incubated at 37 ± 0.1 °C with gentle agitation (300 rpm) and analyzed via iTLC (Bioscan AR-2000) with an EDTA eluent (50 mM, pH 5.0) at time points 0, 24, 48, 72, 96, and 120 hours.

7.4.17 Cell culture

Human ovarian cancer cell line SKOV-3 was obtained from the American Tissue Culture Collection (ATCC, Bethesda, MD) and maintained in a 1:1 mixture of Dulbecco's

Modified Eagle medium: F-12 medium, supplemented with 10% heat- inactivated fetal calf serum (Omega Scientific, Tarzana, Ca), 2.0 mM glutamine, nonessential amino acids, 100 units/mL penicillin, and 100 units/mL streptomycin in a 37 °C environment containing 5% CO_2. Cell lines were harvested and passaged weekly using a formulation of 0.25% trypsin/0.53 mM EDTA in Hank's Buffered Salt Solution without calcium and magnesium.

7.4.18 SKOV-3 xenograft mouse models

All experiments were performed under an Institutional Animal Care and Use Committee-approved protocol at Memorial Sloan-Kettering Cancer Center, and the experiments followed institutional guidelines for the proper and humane use of animals in research. Six- to eight-week-old athymic nu/nu female mice (NCRNU-M) were obtained from Taconic Farms Incorporated (Hudson, NY). Animals were housed in ventilated cages, were given food and water *ad libitum*, and were allowed to acclimatize for approximately 1 week prior to treatment. After several days, SKOV-3 tumours were induced on the right shoulder by a subcutaneous injection of 1.0×10^6 cells in a 100 μL cell suspension of a 1:1 mixture of fresh media/BD Matrigel (BD Biosciences, Bedford, Ma).

7.4.19 ^{111}In- and ^{177}Lu-phospa-trastuzumab SPECT/CT imaging studies

Mice with SKOV-3 ovarian cancer xenografts (right shoulder, ~2 mm diameter) were imaged with ^{111}In (n = 2) and ^{177}Lu (n = 2) labeled immunoconjugates, using a four-headed NanoSPECT/CT®PLUS camera (Bioscan Inc., Washington DC, USA) with a multi-pinhole focused collimator and a temperature controlled animal bed unit (Minerve equipment veterinaire). Nine pinhole apertures with a diameter of 2.5 mm were used on each head, with

a field of view (FOV) of 24 mm. Settings of the ^{111}In energy peaks were 245 and 171 keV, and the ^{177}Lu peaks were 208, 112, and 56 keV. A CT at 45 kVp was acquired (180 projections, pitch of 1). Based on the helical CT topogram, SPECT images were obtained over a range of 85 mm. For H_6phospa-trastuzumab, mice were administered doses of ~800-810 μCi ^{111}In-labeled (specific activity ~3 mCi/mg, ~ 250 μg of immunoconjugate per mouse) and ~575 μCi of ^{177}Lu-labeled (~3 mCi/mg, ~ 190 μg) agents each in 200 μL of sterile saline (0.9% NaCl), via intravenous tail vein injection. Approximately 5 minutes prior to SPECT/CT image acquisition, mice were anesthetized via inhalation of 2% isoflurane/oxygen gas mixture (Baxter Healthcare, Deerfield, IL), placed on the scanner bed, and anesthesia was maintained during imaging using a reduced 1.5% isoflurane/oxygen mixture. Animals were imaged at 24, 72, and 120 h p.i. for ^{111}In, and 24 / 72 h p.i. for ^{177}Lu to determine the general ^{111}In/^{177}Lu-phospa-trastuzumab biodistribution and tumour uptake. ^{177}Lu-immunoconjugate mice were imaged for 1.5-2 hours each, and ^{111}In-immunoconjugate mice were imaged for 45-60 min each. Image collection was performed using Nucline software (V1.02 build 009), and images were processed and reconstructed using InVivoScope (2.00 patch3, 64 bit) and HiSPECT (v 1.4.3049) software.

7.4.20 Animal protocol

All animal experiments were performed according to a protocol approved by Memorial Sloan-Kettering Cancer Center's Institutional Animal Care and Use Committee (#08-07-013).

Chapter 8: H_2azapa: a click-based acyclic multifunctional ligand for $^{67/68}$Ga, ^{64}Cu, ^{111}In, and ^{177}Lu

This chapter is an adaptation of published work, and is reproduced in part, with permission from Bailey, G. A.*; Price, E. W.*; Zeglis, B. M.; Ferreira, C. L.; Boros, E.; Lacasse, M. J.; Patrick, B. O.; Lewis, J. S.; Adam, M. J.; Orvig, C., H_2azapa: a Versatile Acyclic Multifunctional Chelator for ^{67}Ga, ^{64}Cu, ^{111}In, and ^{177}Lu. *Inorg. Chem.* **2012**, *51* (22), 12575-12589, Copyright 2012 The American Chemical Society. (*These authors contribued equally to this work).

8.1 Introduction

There is currently strong interest in the development of new and efficient ligands that form stable complexes with the burgeoning variety of radiometal isotopes applicable for diagnostic imaging and targeted radiotherapy, such as $^{67/68}$Ga, ^{111}In, $^{64/67}$Cu, $^{86/90}$Y, ^{177}Lu, ^{225}Ac, ^{213}Bi, ^{212}Pb, and ^{89}Zr.[6,28] Radioisotopes that are readily available from commercial generators and/or small cyclotrons, such as the positron emission tomography (PET) isotopes ^{64}Cu, ^{68}Ga, and ^{89}Zr and the single photon emission computed tomography (SPECT) isotopes ^{111}In, ^{67}Ga, and ^{99m}Tc have practical value for widespread clinical use. In light of recent recurrent global shortages of ^{99}Mo, the parent isotope of the clinically important diagnostic nuclide ^{99m}Tc, proper utilization of these "non-standard" isotopes is of increasing importance.[362] Radiometals that emit particle radiation (β^-/α), have intermediate (12-240 h) half-lives suitable for targeted radiotherapy, or β^+ emissions for diagnostic imaging and

dosimetry calculations ("theranostic" isotopes) are of very high utility in cancer patients.[165,363-365] One isotope that fits into this class is ^{64}Cu ($t_{1/2}$ = 12.7 h; β^+: 656 KeV, 19%; β^-: 573 KeV, 40%), which is made especially attractive due to the existence of imaging and/or therapeutic surrogate isotopes with complementary half-lives and decay properties, which can be interchanged due to their identical chemical properties (e.g. ^{67}Cu: $t_{1/2}$ = 61.9 h, β^-: 395-577 KeV, 100%).[165,363-365]

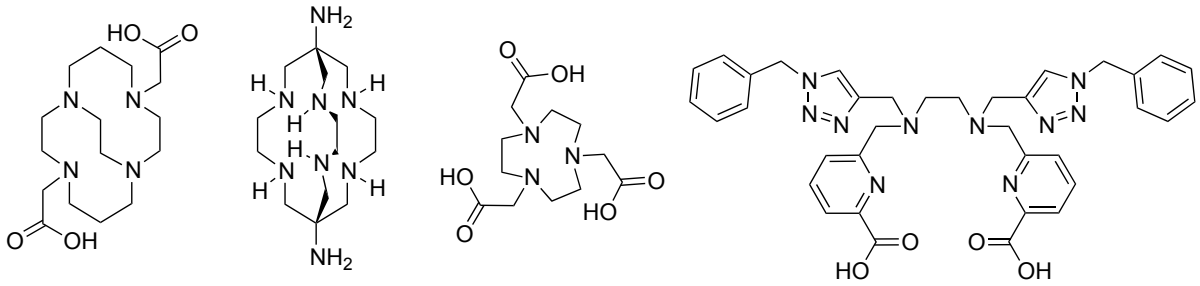

Figure 8.1 Structures of selected state-of-the-art "gold standard" ^{64}Cu ligands, and the new ligand H_2azapa.

Contemporary research in the field of receptor-based radiopharmaceutical targeting has focused almost exclusively on bifunctional chelators (BFCs) based on the tetraazamacrocyclic polycarboxylates and derivatives of the acyclic diethylenetriaminepentaacetic acid (DTPA) scaffold (Chapter 1). As discussed throughout this thesis, DOTA has historically been the most effective and commonly used ligand for a variety of radiometals, including isotopes of Cu(II), Ga(III), Y(III), In(III), and Lu(III), while 1,4,7-triazacyclononane-1,4,7-triacetic acid (NOTA) is the new benchmark ligand for Ga(III) and Cu(II). The quest for the ideal BFC for copper has been particularly challenging due to the facile ligand exchange kinetics and biologically accessible redox chemistry of Cu(II), but

the availability of a selection of copper radioisotopes ($^{60/61/62/64/67}$Cu) with useful properties for therapy and imaging diagnosis/dosimetry drives basic research and development. The cross-bridged macrocycle CB-TE2A (Figure 8.1) is a Cu(II) ligand with exceptional stability in acid decomplexation experiments[72] and unparalleled *in vivo* inertness,[173,366,367] but it requires unsuitably harsh conditions (1-2 h at 95 °C) for radiolabeling. Alternatively, the sarcophagine ligands (e.g. DiamSar), NOTA, and recently developed methylenephosphonate analogs of CB-TE2A (CB-TE1A1P and CB-TE2P) can be efficiently labeled at reduced temperatures.[174,368-370] While investigation of these ligands as bifunctional conjugates remains in its infancy, preliminary biodistribution studies have shown the unconjugated chelate-radiometal complexes to have slightly reduced stabilities compared to CB-TE2A, as demonstrated by their increased accumulation and slower clearance from the kidney, liver, and bone marrow over 24 hours.[174,368-370] A new Tyr^3-octreotide conjugate of CB-TE1A1P has shown promise, being radiolabeled with ^{64}Cu under mild conditions (40 °C in 1 hour) and offering similar *in vivo* performance to CB-TE2A conjugates.[371]

Through our work to build on these pyridinecarboxylate-based ligands we have required new and efficient ways of functionalizing the scaffold towards biomolecule (e.g. peptides and antibodies) conjugation. To this end, we were interested in a "click" approach towards functionalization through incorporation of 1,2,3-triazole rings that could be synthesized *via* the Huisgen 1,3-dipolar cycloaddition ("click" reaction) of alkynes and azides. The model ligand H_2azapa (Figure 8.1) was designed as an elaboration of the "click-to-chelate" approach pioneered by Mindt and coworkers for the construction and conjugation of a BFC in a single, easy step since the triazole rings would not only serve as convenient linkers between the ligand and biomolecules, but as chelating arms towards the coordination

sphere of large metal ions such as In(III), Y(III), and Lu(III).[372,373] For H_2azapa, benzyl groups are employed as placeholders for biological targeting vectors as a model ligand, in order to facilitate easy synthesis, characterization, and study of the metal complexes. Herein we report the synthesis and characterization of H_2azapa, a novel and bifunctional triazole-containing acyclic ligand with promising characteristics for copper radiopharmaceuticals. The metal ion coordination behaviour of H_2azapa with non-radioactive In(III), Ga(III), and Lu(III) was studied by NMR spectroscopy, and crystal structures of [In(azapa)(H_2O)][ClO_4] and [Cu(azapa)] are presented. Radiolabeling and serum stability experiments were performed with the radiometals ^{67}Ga, ^{111}In, ^{64}Cu, and ^{177}Lu, and biodistribution experiments and PET imaging studies were performed in healthy nude athymic mice with [^{64}Cu(azapa)].

8.2 Results and discussion

8.2.1 Synthesis of H_2azapa

The bifunctional chelator H_2azapa was synthesized with a new reaction scheme that was designed to improve on methods discussed in Chapter 2 to synthesize H_4octapa (Figure 8.1) and a number of other pyridinecarboxylate ligands in our current library.[89] The previous strategy to synthesize H_4octapa (Chapter 2) involved benzyl protection of the primary amines on ethylenediamine (en) using a simple reductive amination with benzaldehyde, followed by alkylation of the two secondary amines with two equivalents of *tert*-butyl bromoacetate, and then benzyl deprotection to facilitate subsequent amine-alkylation with methyl-6-(bromomethyl)picolinate.[89] The main disadvantage to this method is that the requisite hydrogenation reaction to remove the benzyl protecting groups is not satisfactory in the presence of olefin, alkyne, or picolinate substituents; here, the hydrogenation of *N,N'*-

dibenzyl-*N,N'*-bis[6-(methoxycarbonyl)pyridin-2-yl]methyl-1,2-diaminoethane resulted in non-selective cleavage of both benzyl and picolinate substituents from the 1,2-ethylenediamine amines, although various hydrogenation conditions (methanol or acetic acid as a solvent, varying catalyst loading, varying concentration) were attempted. It is important to note that the work presented in this chapter was performed prior to the work performed in Chapter 3 with nosyl-protection chemistry, which may indeed be superior to the boc protection used in this chapter.

Scheme 8.1 Synthesis of click-based ligand H_2azapa (**8.5**) [a]

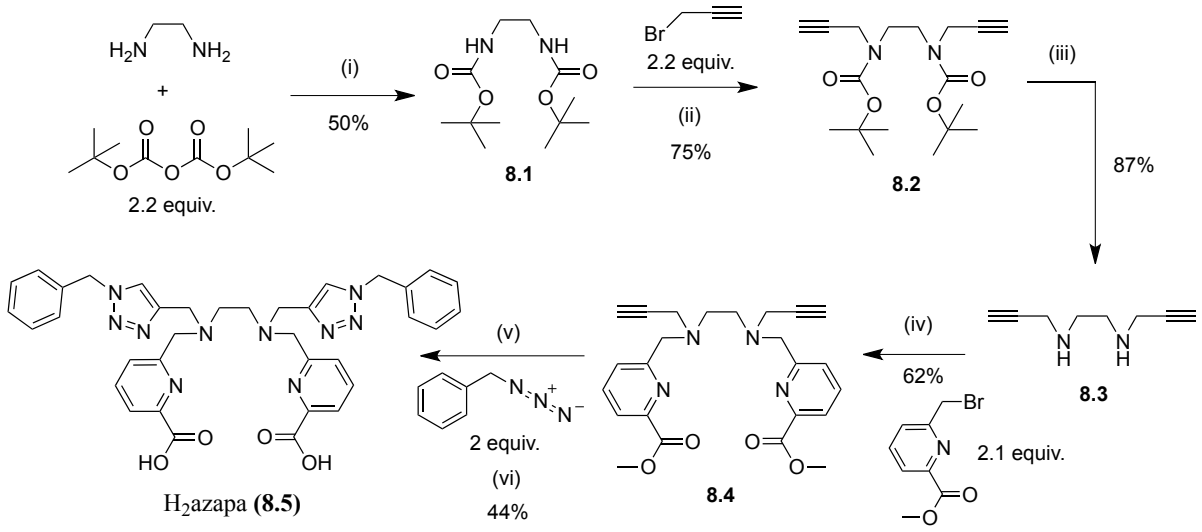

[a] (i) THF, RT, 3 h; (ii) NaO^{t}Bu, TBAI, MeCN, 0 °C – RT, 48 h; (iii) 2:1 DCM/TFA, RT, 1 h; (iv) Na_2CO_3, MeCN, RT, 48 h; (v) sodium ascorbate (0.2 equiv), $Cu(OAc)_2$ (2.1 equiv), 1:1 *t*-BuOH/H_2O, RT, 16 h; (vi) Na_2S, 1:1 THF/H_2O, 24 h.

Thinking ahead to potential challenges that could be encountered during scale-up and commercialization of a BFC, we pursued a protecting group strategy for the synthesis of H_2azapa that would be fast, versatile, and high yielding with maximal purity (Scheme 1). We

also desired a tunable system that could be used for the synthesis of a library of ligands bearing picolinate, acetate, triazole, and other arms on a selection of alkylamino backbones (e.g. en, pn, dien, TREN). To this end, a novel *N,N'-tert*-butoxycarbonyl (boc) protecting group strategy was employed (Scheme 8.1), which relied on a carbamate alkylation reaction of the boc-protected intermediate **8.1** with propargyl bromide, based on a similar but non-compatible carbamate alkylation described in the literature (no reaction occurred following literature protocols).[374]

This strategy led to the successful synthesis of the alkyne precursor to H_2azapa, (**8.4**), in four synthetic steps from commercially available ethylenediamine and methyl-6-(bromomethyl)picolinate, in 10% cumulative yield. This method is a slight improvement over the synthetically analogous (but non-compatible) previously used *N*-benzyl protection strategy (Chapter 2) towards the fully protected ligand precursor to H_4octapa.[89] For the carbamate alkylation, a non-trivial variant of a literature protocol was performed,[374] and it was found that working with an insoluble, non-nucleophilic base (NaO*t*Bu) in a polar enolizable solvent (acetonitrile) afforded principally product, whereas other conditions attempted *ad hoc* or from the literature (e.g. combinations of bases such as Cs_2CO_3/Na_2CO_3/K_2CO_3/KOtBu/NaOH and solvents such as DMF/THF/^{t}BuOH/MeOH) resulted in either uncontrolled carbamate alkylations and deprotections with no evidence of product formation, or no reaction. In the carbamate deprotection step, attempts to extract the free amine (**8.3**) from a saturated $NaHCO_3$ solution were exceptionally inefficient (25 x 1 mL extractions), although they eventually led to the isolation of product (**8.3**) in 87% yield.

During the synthesis of the H_2azapa alkyne precursor (**8.4**), it was found that the boc protecting group strategy was a slight improvement over the benzyl protection strategy used

for the synthesis of H_4octapa and related ligands, both in terms of the simplicity of the synthetic protocols, and the overall yield of the synthesis. A drawback was the time required for the synthesis (minimum 7 days), although this could conceivably be reduced through optimization. Unfortunately, attempts to react 1,2-di-*tert*-butylethane-1,2-dicarbamate (**8.1**) with *tert*-butylbromoacetate or methyl 6-(bromomethyl)picolinate did not result in the formation of product; instead the intact starting material was reisolated in quantitative yield, and it appears this reaction is only efficient with propargyl bromide as the electrophile. It is likely that the scope of the carbamate alkylation reaction is limited by the reactivity of the alkyl halides, where propargyl halide > acetyl halide > picolinyl alkyl halide. The nosyl protection strategy that was first discussed in Chapter 3 was devised after this work was completed, but could potentially replace the boc protection group and improve the yields and scope of this chemistry in the future.

The reaction of compound **8.4** with two equivalents of benzyl azide in the presence of Cu(I) (generated *in situ* by the reduction of $Cu(OAc)_2$ with catalytic sodium ascorbate) resulted in the formation of two 1-benzyl-1,2,3-triazole rings and, simultaneously, the quantitative deprotection of the picolinate methyl esters. The progress of the reaction could be followed by a gradual but distinct colour change from brown to blue-green over the course of 4 hours, after which a blue-green solid corresponding to the neutral and lipophilic [Cu(azapa)] complex could be observed to precipitate gradually out of solution. It was observed that super-stoichiometric rather than catalytic $Cu(OAc)_2$ was required to effect quantitative triazole formation and methyl ester deprotection, possibly due to the increased reactivity of Cu(II) when tightly bound to the six-coordinate picolinate core (N_4O_2) of H_2azapa and compound **8.4**. Because this ligand system is very effective at sequestering

copper, catalytic quantities of copper were insufficient to complete the click-reaction, and an excess of copper was required. Stoichiometric Cu(II) may effect the picolinate methyl ester deprotection of H_2azapa by binding to the picolinate and *N,N'*-en nitrogen atoms of the molecule and interacting with the lone pairs on nearby carbonyl oxygen atoms to weaken the double bonds, making them susceptible to nucleophilic attack by an incoming water molecule.[375] In addition, lowering the pK_a of aqua ligands bound to the *N,N'*-en-Cu(II) complex may facilitate the production of hydroxide species in close proximity to the methyl esters, resulting in ester cleavage.[375] After initial isolation of the copper-bound ligand [Cu(azapa)] by filtration, the free ligand was liberated by reaction of the complex with an excess of Na_2S, which sequestered any free or bound Cu(II) as black/brown insoluble CuS that could be removed by filtration.

8.2.2 NMR Characterization

For receptor-targeted radiopharmaceuticals, a BFC should ideally exhibit minimal static or fluxional isomerization in solution, since fluxional interconversion between different isomers is thought to affect *in vivo* stability, and the presence of multiple static isomers may in some circumstances lead to divergent biological properties, such as pharmacokinetics and biodistribution.[7,120,376,377] The simple and readily interpretable ^{1}H NMR spectrum of $[Ga(azapa)]^+$ is consistent with a single isomer being present in solution (Figure 8.2). The spectrum shows prominent diastereotopic splittings for the methylene hydrogen atoms associated with the picolinate and the triazole arms at 4.75/4.28 ppm (^{2}J = 18 Hz) and 4.00/3.92 ppm (^{2}J = 15 Hz), respectively. Methylene hydrogen atoms on the en bridge are observed to exhibit minimal diastereotopic splitting, and show in the ^{1}H NMR spectra as a

broad quartet, which is barely resolvable at 600 MHz, with a chemical shift of 3.10 ppm. The benzyl methylene hydrogen atoms behave similarly, and are resolved as a sharp quartet with a characteristic downfield shift centered at 5.64 ppm.

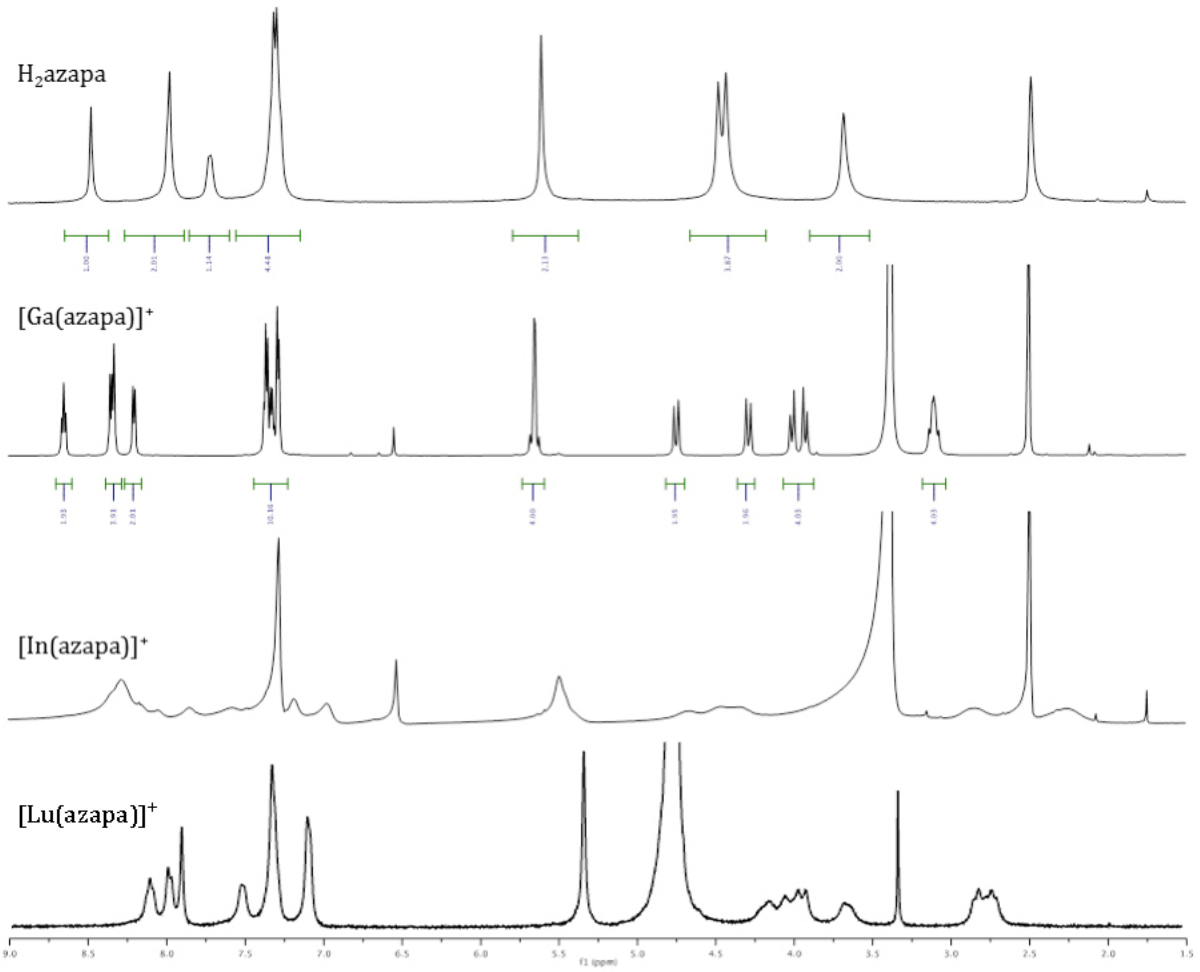

Figure 8.2 ^{1}H NMR spectra (DMSO-d_6, 25 °C) of (top) H_2azapa, 300 MHz; (middle) $[Ga(azapa)]^+$, 600 MHz; (middle) $[In(azapa)]^+$, 400 MHz; and (bottom, 300 MHz, D_2O) $[Lu(azapa)]^+$.

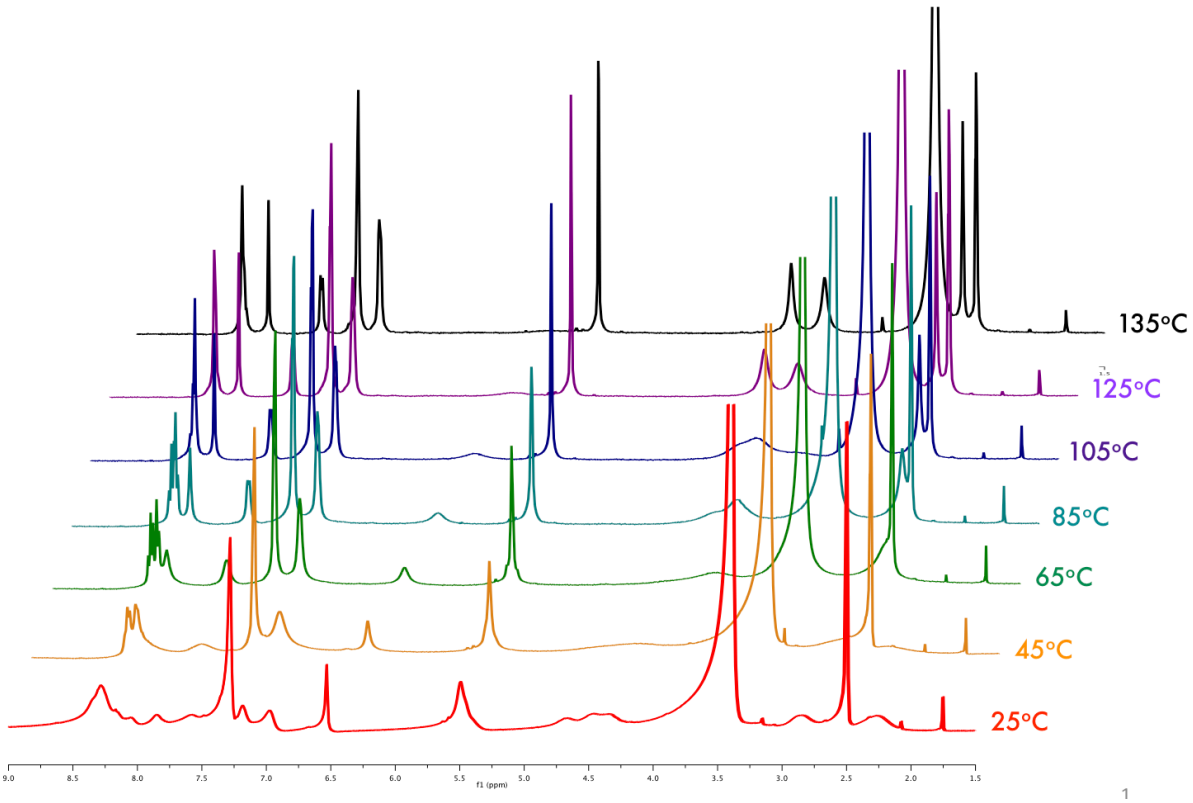

Figure 8.3 Variable temperature (VT) ^{1}H NMR spectra of $[In(azapa)]^{+}$ (400 MHz, DMSO-d_6) with the temperature increasing from 25 °C to 135 °C.

The less prominent diastereotopic splittings exhibited by the benzyl and en methylene hydrogen atoms can be explained by invoking partial flexibility in the en backbone and partial free rotation of the triazole arms, which are extending away from the coordination center as unbound (but potentially chelating) arms. This explanation is consistent with crystal structures of the Ga(III) complex of H_2dedpa[118] and its nitrogen *p*-NO_2-benzyl functionalized derivative, which showed highly symmetric octahedral geometries at the Ga(III) center with the six-coordinate picolinate core (N_4O_2) of the molecule bound in each case. Peak broadening for the en backbone methylene hydrogen atoms is also commonly observed in the ^{1}H NMR spectra of pyridinecarboxylate ligands coordinated to metals.[118] The highly symmetric $[Ga(azapa)]^{+}$ complex has approximately C_{2v} symmetry in solution as

confirmed by the ^{13}C NMR spectrum, which gives rise to only one signal per pair of equivalent carbon atoms on either half of the coordinated ligand.

In contrast to that of $[Ga(azapa)]^+$, the ^1H NMR spectrum of $[In(azapa)]^+$ at room temperature shows a series of broad signals consistent with solution fluxional behavior commonly observed for complexes of larger trivalent metals such as In(III), Y(III), and Lu(III) with ligands of high denticities (Figure 8.2).[120,376,377] Variable temperature (VT) ^1H NMR spectroscopy has been used to confirm the solution fluxional behavior of $[In(azapa)]^+$ (Figure 8.3); increasing the temperature of the solution stepwise from 25 °C to 135 °C resulted in the gradual sharpening and coalescing of peaks towards a series of singlets quite distinct from those observed for the free ligand (Figure 8.2). The kinetics of fluxional isomerization became more rapid with increasing temperature, resulting in an overall averaging effect. Coalescence of a pair of broad signals located at 2.25 and 2.81 ppm at 25 °C can be observed at 65-85 °C, which could suggest an asymmetric, seven-coordinate structure with one triazole arm bound in solution, resulting in non-equivalence of the two pairs of methylene hydrogen atoms on either end of the en bridge at 25 °C.

8.2.3 X-ray crystallography

The solid-state molecular structure of $[In(azapa)(H_2O)][ClO_4]$ was obtained by X-ray crystallographic analysis of a colourless rhombic plate crystal grown by slow evaporation of a saturated solution of 1:1 MeOH/DMSO (Figure 8.4, data in the appendix, Table A.2). The X-ray structure reveals an eight-coordinate complex in the solid-state featuring a highly distorted square antiprismatic geometry with the picolinate core, one triazole arm, and one aqua ligand bound to In(III). While six- and seven-coordinate binding modes for In(III) are

common,[6] very few empirical eight-coordinate structures are known,[120,378,379] and to our knowledge [In(azapa)(H_2O)][ClO_4] was the fourth such reported structure at publication. Of the reported structures, all display distorted square antiprismatic geometries, and all are fully saturated by chelating arms.[120,378,379] Given the propensity of In(III) towards seven-coordinate binding modes, an eight-coordinate structure featuring a heptadentate ligand with an additional aqua solvent ligand bound is unusual.

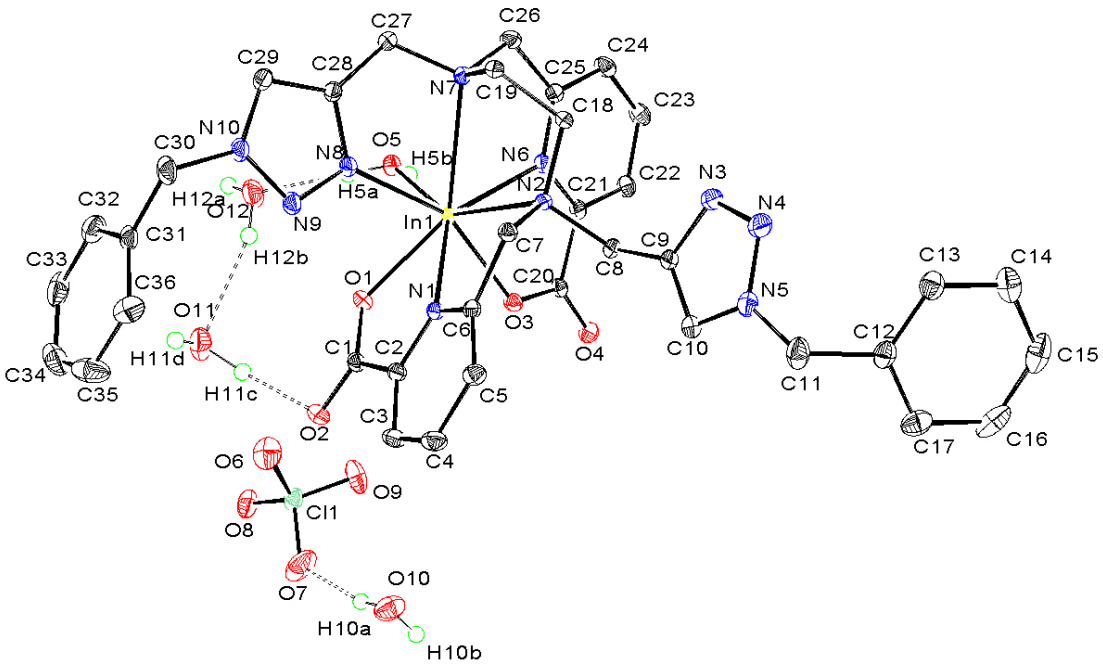

Figure 8.4 ORTEP drawing of the solid-state molecular structure of [In(azapa)(H_2O)][ClO_4] obtained by X-ray diffraction. Hydrogen atoms are omitted for clarity.

The metal-to-ligand oxygen bond lengths in [In(azapa)(H_2O)][ClO_4] vary between 2.216/2.320 Å for the indium-carboxylate bonds In-O(3)/O(1) and 2.219 Å for the indium-aqua ligand bond In-O(5). The indium-en backbone nitrogen bonds In-N(2)/N(7) are longer

at 2.461/2.561 Å, while the indium-triazole nitrogen bond In-N(8) is the shortest of the indium-nitrogen bonds at 2.292 Å (Table 8.1). The In-X bond lengths for equivalent donor atoms on either side of the ligand's ~C_2 symmetry axis are similar but not identical, as is to be expected for the asymmetric heptadentate binding mode with indium. The triazole arm is bound to indium at the *N3* position of the triazole ring (see Figure 8.1), which is consistent with previously reported crystal structures[373,380-382] and calculated structures[383] in which the triazole chelating arm is attached to the ligand at the *C4* position of the triazole ring.[381,384] The relatively short In-N(8) bond in [In(azapa)(H_2O)][ClO_4] is consistent with recent DFT calculations[372,385,386] which suggested that a greater concentration of electron density at the *N3* position of the triazole in 1,4-substituted triazoles (as used here) should result in relatively strong electron donating capability to a metal center.

Table 8.1 Selected bond angles and lengths in the X-ray crystal structure of [In(azapa)(H_2O)][ClO_4].

Bond	Length [Å]	Angle	Degree [°]
In-O(3)	2.216(1)	O(3)-In-O(6)	70.25(4)
In-O(5)	2.219(1)	N(6)-In-N(7)	68.10(4)
In-N(8)	2.292(1)	O(5)-In-N(6)	76.39(4)
In-O(1)	2.320(1)	O(1)-In-O(5)	74.03(4)
In-N(1)	2.303(1)	O(1)-In-N(8)	82.89(4)
In-N(6)	2.345(1)	N(2)-In-O(3)	91.69(4)
In-N(2)	2.461(1)	N(2)-In-N(8)	97.22(4)
In-N(7)	2.561(1)	O(3)-In-O(5)	102.51(4)

Since characterization using NMR spectroscopy was not feasible with the paramagnetic d^9 Cu(II) complex of H_2azapa, the bulk composition of C, N, and H in a RP-HPLC-purified batch of [Cu(azapa)] was confirmed by elemental analysis. A small, blue-green, cubic crystal of [Cu(azapa)] suitable for characterization using X-ray diffraction was

grown by slow evaporation of a saturated solution of purified complex in 50% acetonitrile in water. The solid-state molecular structure of [Cu(azapa)] features a distorted octahedral metal-ligand environment typical of six-coordinate complexes of Cu(II) (Figure 8.5, data in Table A.1).[6] The central binding of H_2azapa *via* the picolinate (N_4O_2) core is typical for crystal structures reported by our group thus far for Cu(II) and Ga(III) complexes of dedpa^{2-} and its bifunctional derivatives, corroborating the notion that the picolinate core of these ligands provides a versatile coordination pocket for a variety of metal ions.[118,273,274] A high degree of symmetry for these complexes, along with an approximately equally distributed set of metal-ligand bond lengths, is thought to correlate well with their high stability and favorable biological properties.[118,273] That [Cu(azapa)] is more symmetric and evenly distributed than [Cu(dedpa)],[273] and nearly as symmetric as [Ga(dedpa)][ClO_4][118] is belied only by the relatively long en-nitrogen Cu-N(2) bond distances (Table 8.2), which suggest that, as in [In(azapa)][ClO_4] and [Ga(dedpa)][ClO_4], the en-*N*,*N*' backbone may be somewhat loosely bound to the metal center. The relatively long and weak Cu-N(2) bonds could conceivably facilitate attack from a biological nucleophile *in vivo*; on the other hand, the chelating ability of the triazole arms, which are covalently fixed to the en-backbone and held in close proximity to the metal center could also play a role in fluxional solution behavior by transiently binding Cu(II) to improve stability and inertness. Alternatively, it is conceivable that the elongated Cu-N(2) distances could be a simple result of energetic contributions from packing in the solid-state.

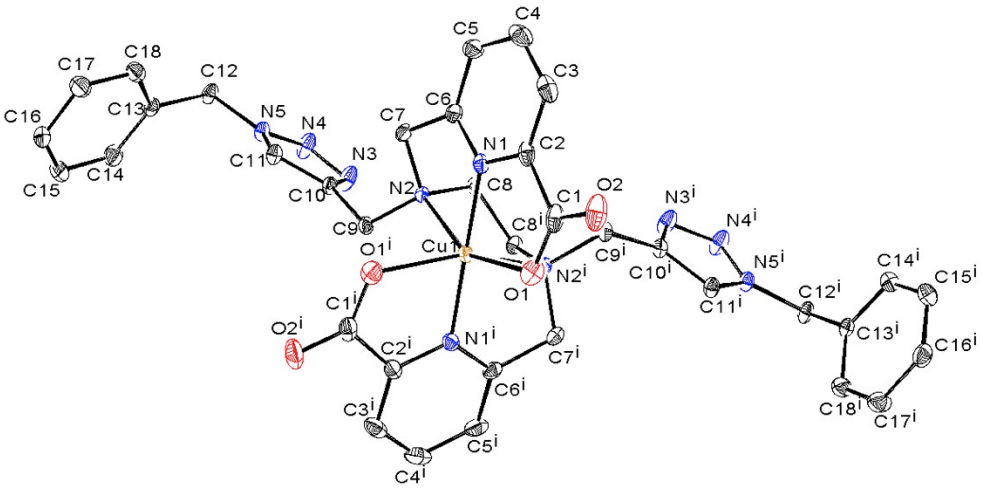

Figure 8.5 ORTEP drawing of the solid-state molecular structure of [Cu(azapa)]. Hydrogen atoms are omitted for clarity.

Table 8.2 Selected bond angles and lengths in the X-ray crystal structure of [Cu(azapa)]. Relevant bond angles are compared to the analogous bond angles in the previously reported X-ray crystal structure of $[Ga(dedpa)]^+$ and [Cu(dedpa)].[118,273]

Bond	Length [Å] Cu(azapa)	Length [Å] Cu(dedpa)[273]	Length [Å] Ga(dedpa)[118]	Angle	Degree [°]
Cu-N(1)	1.935(1)	1.9386(13)	1.987(2)	O(3)-In-O(6)	70.25(4)
Cu-N(1)^i	1.935(1)	2.0008(12)	1.990(2)	N(6)-In-N(7)	68.10(4)
Cu-O(1)	2.120(1)	2.3014(11)	1.971(1)	O(5)-In-N(6)	76.39(4)
Cu-O(1)^i	2.120(1)	2.0430(10)	1.983(1)	O(1)-In-O(5)	74.03(4)
Cu-N(2)	2.326(1)	2.1364(13)	2.112(2)	O(1)-In-N(8)	82.89(4)
Cu-N(2)^i	2.326(1)	2.3171(13)	2.113(1)	N(2)-In-O(3)	91.69(4)

Potentiometric titrations of H_2azapa with copper were attempted so that the binding affinity (log K_{ML}, pM) could be determined, but the insolubility of [Cu(azapa)] forestalled these experiments and aqueous cyclic voltammetry experiments. Synthesis of pegylated hydrophilic derivatives of H_2azapa is proposed, since clickable hydrophilic polyethylene glycol (PEG) moieties are commercially available and should be more amenable towards aqueous experiments than the lipophilic benzyl groups of H_2azapa. The modular synthetic

scheme for H_2azapa will allow for the "clickable" alkyne precursor **4** to be easily transformed into a variety of derivatives.

8.2.4 Radiolabeling experiments

Initial radiolabeling experiments have confirmed the efficiency of H_2azapa to rapidly form radioactive complexes of ^{67}Ga, ^{111}In, ^{64}Cu, and ^{177}Lu quantitatively at ambient temperature in aqueous buffer (pH 4-5, NaOAc, 10 min), as determined by integration of RP-HPLC radio-traces. In contrast, DOTA required 20 minutes at 80 °C in a microwave reactor for quantitative radiolabeling with ^{111}In, and 60 minutes at 90 °C for ^{64}Cu and ^{177}Lu.[89] The single, sharp peak in the HPLC radio-traces obtained for $[^{67}Ga(azapa)]^+$ (t_R = 12.8 min) and $[^{111}In(azapa)]^+$ (t_R = 11.4 min) is consistent with the NMR solution structural data for these complexes, which indicate a single, robust, highly symmetric coordination isomer for $[^{67}Ga(azapa)]^+$ and rapid fluxional interconversion between multiple isomers for $[^{111}In(azapa)]^+$ on the NMR/HPLC time scale. Single peaks were also observed in the HPLC radiotraces of $[^{177}Lu(azapa)]^+$ (t_R = 19.3 min) and $[^{64}Cu(azapa)]$ (t_R = 20.9 min) during subsequent radiolabeling experiments. RP-HPLC retention times for these radiometals indicated the increased lipophilicity of the M^{n+}(azapa) complexes compared to the M^{n+}(DOTA) and M^{n+}(DTPA) standards. For example, retention times for the ^{177}Lu/^{64}Cu complexes of H_2azapa were t_R = 19.3/20.9 min, and for the same complexes of DOTA they were t_R = 6.8/7.1 min. The absence of free radiometal (t_R ~ 0-4 min) in the radioactive trace was confirmed in all cases by the RP-HPLC radiotraces.

8.2.5 Blood serum stability studies

Table 8.3 Stability data collected in mouse blood serum at 25 °C for ^{67}Ga and ^{111}In, and in human blood serum with agitation (550 rpm) at 37 °C for ^{64}Cu and ^{177}Lu, with H_2azapa and selected ligand standards. The % stability shown is the percentage of ligand-bound radiometal, and the error is expressed as standard deviation (n = 3).

Complex[a]	a) Short-term stability[a] (%)	b) Medium-term stability (%)	c) Long-term stability (%)
$[^{67}Ga(azapa)]^+$	69 (±2)	48 (±2)	52 (±4)
$[^{67}Ga(dedpa)]^+$	>99	>99	>99
$[^{67}Ga(dp\text{-}N\text{-}NO_2)]^+$	88	69	51
$[^{67}Ga(dp\text{-}bb\text{-}NO_2)]^+$	98	97	97
$[^{111}In(azapa)]^+$	-	95.1 (±0.6)	65 (±4)
$[^{111}In(DTPA)]^{2-}$	-	87 (±2)	88 (±2)
$[^{111}In(DOTA)]^-$	-	90 (±2)	89 (±2)
$[^{64}Cu(azapa)]$	-	99.9 (±0.1)	98.3 (±0.2)
$[^{64}Cu(DOTA)]^{2-}$	-	77 (±6)	74 (±1)
$[^{177}Lu(azapa)]^+$	-	55 (±4)	46 (±1)
$[^{177}Lu(DOTA)]^-$	-	87.7 (±0.7)	87 (±2)
$[^{177}Lu(DTPA)]^{2-}$	-	77 (±1)	82 (±2)

a) Short-term stability data at 15 min for $[^{67}Ga(azapa)]^+$ and 10 min for all other complexes; b) medium-term stability data at 1 h, except for ^{177}Lu complexes which were at 1.5 h; c) long-term stability data at 2 h for ^{67}Ga complexes, 20 h for ^{64}Cu complexes, and 24 h for ^{111}In and ^{177}Lu complexes. [a]Relevant data for the ^{67}Ga complexes of H_2dedpa and the nitrogen and backbone *p*-NO_2-benzyl functionalized H_2dedpa derivatives H_2dp-*N*-NO_2 and H_2dp-bb-NO_2 are from previously reported *apo*-transferrin challenge experiments.[118]

The serum stability data for the complexes of H_2azapa with ^{67}Ga, ^{111}In, ^{64}Cu, and ^{177}Lu establish H_2azapa as a viable target for further investigation with ^{64}Cu (Table 8.3). $[^{64}Cu(azapa)]$ displays excellent stability over the 20 hour time period studied (37 °C), with less than 2% of ^{64}Cu transchelated to blood serum proteins at that time, compared to $[^{64}Cu(DOTA)]^{2-}$, which remained only 77% and 74% intact after 1 hour and 20 hours, respectively. These data also compare favorably to a recent report of a mouse serum competition experiment of H_2dedpa and a *N,N'*-*p*-NO_2-benzyl functionalized H_2dedpa derivative that were conjugated to a peptide (cRGDyk),[273] H_2RGD-2, where 23% of ^{64}Cu

from [^{64}Cu(dedpa)] and 12% of ^{64}Cu from [^{64}Cu(RGD2)] were each transchelated to serum proteins after 24 hours at ambient temperature,[273] suggesting that H_2azapa is a more stable/inert ligand for copper than are H_2dedpa and its *N,N'*-en-nitrogen functionalized derivatives.

Ligands that remain robust with isotopes of copper over a much longer time period (e.g. 24-72 hours) while efficiently radiolabeling at room temperature are highly sought to advance receptor-based targeting using antibodies and other sensitive biological vectors, for a combination of PET imaging with ^{64}Cu and therapy using ^{67}Cu.[44,387-390] Antibodies have long biological half-lives, sluggishly distribute to target tissues, and must be radiolabeled at reduced temperatures (20-37 °C) to avoid protein denaturation and retarded immunoreactivity and binding affinity.[388,389,391] PET using antibody targeting is typically optimized at ~24-72 hours post injection, which requires the chelate-radiometal complex to be stable over that entire time period.[392,393] Furthermore, tumour targeting for therapy using isotopes such as ^{67}Cu, ^{177}Lu, and ^{90}Y requires an even longer biological stability window, because the chelate-radiometal complex should be delivered to the targeted tumour tissue and then remain intact until the majority of the isotope has decayed (e.g. ^{67}Cu: $t_{1/2}$ = 61.9 h).[389,393] Kinetic inertness has been shown to be a more accurate predictor of the biological stability of chelate-radiometal complexes than thermodynamic stability,[6,77,367,394] and to date the most relevant assays for biological stability, besides *in vivo* experiments, are *in vitro* blood serum / *apo*-transferrin / superoxide dismutase competition challenges.

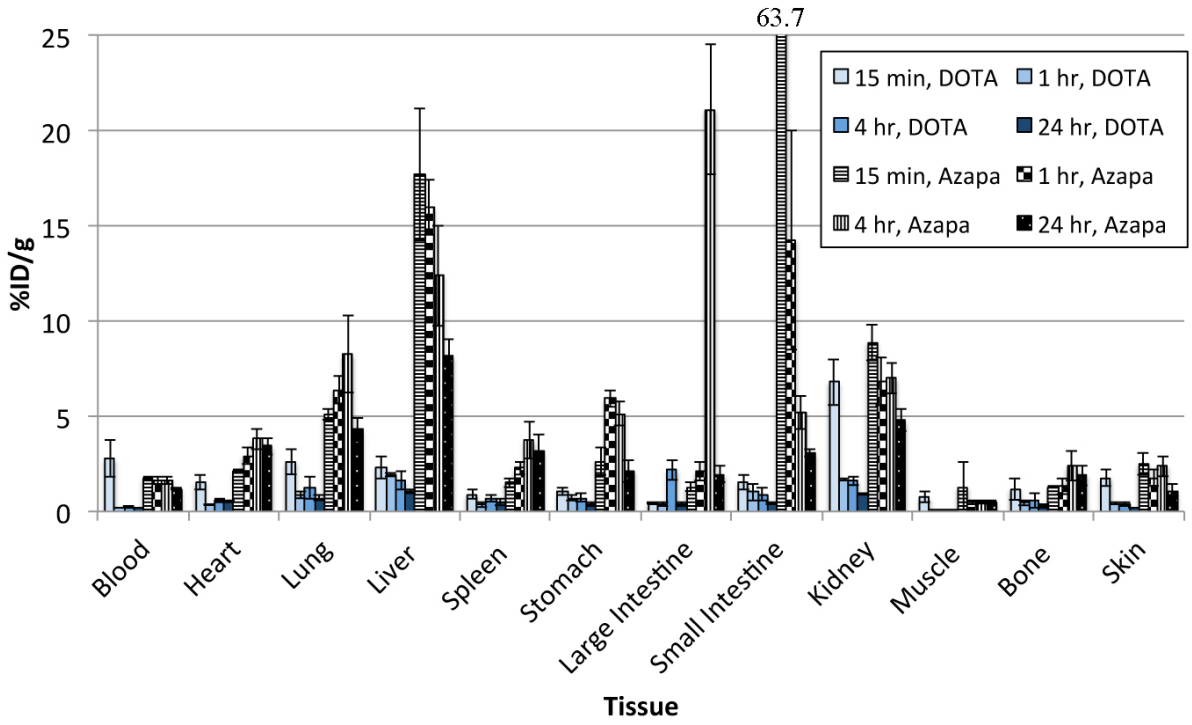

Figure 8.6 Biodistribution of [^{64}Cu(azapa)] and [^{64}Cu(DOTA)]$^{2-}$ showing organ and tissue uptake as percent injected dose per gram (% ID/g) obtained over 24 h in healthy athymic nude mice; Y-axis is normalized at 25% ID/g for clarity.

The blood serum stability data for selected ligands with ^{67}Ga, ^{111}In, and ^{177}Lu reveal the stability of H_2azapa with each of these radiometals (Table 8.3). The H_2azapa-bound ^{177}Lu and ^{111}In were 54% and 35% transchelated by serum proteins after 24 hours, compared with our leading candidate for these radiometals, H_4octapa, which was > 85% stable at 24 hours with both ^{177}Lu and ^{111}In (< 15% transchelated to serum proteins).[89] H_2azapa displays roughly comparable stability with ^{67}Ga to the similar nitrogen functionalized *p*-NO_2-benzyl H_2dedpa derivative H_2dp-*N*-NO_2, which was roughly 50% intact after 2 hours in a similar *apo*-transferrin challenge experiment.[118] Amongst the quintet of H_2azapa,[88] H_2dedpa,[118,272-274] H_4octapa,[87,89] H_5decapa,[89] and H_6phospa,[304] we have a large number of clinically relevant and high impact metal ions / isotopes well covered.

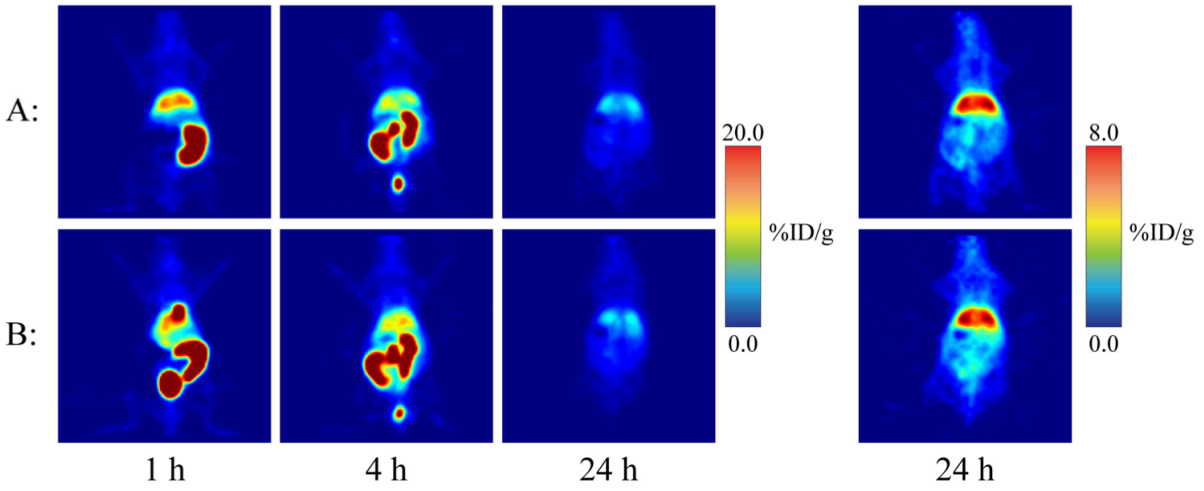

Figure 8.7 PET images of two (A and B) healthy female nude athymic mice injected with [^{64}Cu(azapa)] and imaged at 1, 4, and 24 h post injection, with the scales being different for the left images at 20 %ID/g and for the right images being 8 %ID/g.

8.2.6 Biodistribution and PET imaging studies

A much more demanding test of chelate-radiometal complexes, which probes biological stability and distrubtion, is biodistribution in animals. The ability of the complex to resist transchelation by native biological chelating proteins and enzymes such as superoxide dismutase (SOD), serum albumin, and transferrin is ultimately tested by its effective clearance through the kidneys (ideally) and low uptake in the liver, lung, spleen, kidneys, intestines, blood, and bone. The clearance and biological distribution pattern of a metal complex is dependent on the size, shape, charge, thermodynamic stability, kinetic inertness, and overall polarity of the complex, such that these same properties can be manipulated to modulate pharmacokinetics and promote effective uptake into, or away from, various organs.[7,274] It is sometimes difficult to discern whether a complex shows uptake in an organ due to its instability/transchelation to proteins within that organ (or blood), or whether the intact complex is being taken up and retained due to its physical properties (e.g. lipophilicity). Metabolism studies, which can help identify % authentic intact (% AI)

complex within a given organ vs "free" radiometal can be useful to this end.[366,367] For bifunctional chelate-based radiopharmaceuticals, the biodistribution profile is largely dominated by the properties of the attached biovector (e.g. antibody, peptide, nanoparticle), particularly in the case of large targeting vectors such as antibodies (MW~150 kDa) and antibody fragments.[118,173,174,272] For non-conjugated, "free" radiometal-chelate complexes, evaluation of stability *in vivo* can be obfuscated by rapid clearance/excretion or by abnormal organ uptake, which may not be observed when administered as a bioconjugate (e.g. peptide, antibody).

An evaluation of biodistribution data for [^{64}Cu(azapa)] shows elevated uptake in all organs compared to [^{64}Cu(DOTA)]$^{2-}$, particularly in the liver, lung, heart, spleen, stomach, intestines, and kidneys (Figure 8.6). [^{64}Cu(azapa)] can be observed to move through the digestive tract over a 24 hour time period, with activity levels peaking at 15 minutes post injection in the small intestines (going from 63.7 to 14.3 %ID/g from 15 min to 1 h), peaking in the large intestine at 4 hours (21.1 %ID/g), and finally being excreted through the feces, as imaged via PET (Figure 8.7), confirming elimination through the digestive system (Table 8.4). Elevated uptake in the stomach was also observed, with activity levels peaking at 1 hour post injection (p.i.) (5.6 %ID/g). Although metabolism and clearance appeared to be mostly through the hepatobiliary and digestive systems, there was also some kidney clearance observed, and the amount of activity decreased over 24 hours in both of these organs (liver: 17.7 down to 8.1 %ID/g; kidney: 8.9 down to 4.8 %ID/g, from 15 min to 24 h p.i.). While an increase in ^{64}Cu uptake in the liver and kidneys is often cited as being evidence for instability of the ^{64}Cu chelate-radiometal complex *in vivo*, the complex [^{64}Cu(azapa)] is accumulated in many other organs as well, suggesting distribution of the

intact lipophilic complex. DOTA in particular is known to display instability and transchelation of ^{64}Cu in mice when injected as vector-bioconjugates,[366,367,395,396] and the differences in the biodistribution of H_2azapa and DOTA, particularly the elevated uptake of [^{64}Cu(azapa)] in the stomach, intestines, heart, and lung, suggest that the mechanism of uptake in these organs is related to the physical characteristics (lipophilic) of the intact complex, as opposed to instability of [^{64}Cu(azapa)] and resultant transchelation to proteins in these organs.

Persistent uptake in the liver, lungs, heart, and digestive tract is expected for small lipophilic molecules, and elevated uptake in the blood and kidneys is also often observed.[397-399] The pressing issue with ^{64}Cu is that "free" or transchelated Cu(II) is known to accumulate in the liver, and highly lipophilic molecules (such as [Cu(azapa)]) are also known to accumulate in the liver, which makes the standard assessment of ^{64}Cu-chelate stability by monitoring the amount of ^{64}Cu accumulated in the liver problematic. Furthermore, with the high abundance of superoxide dismutase (SOD) in the liver, accumulation and retention of the intact and lipophilic [^{64}Cu(azapa)] complex in the liver could result in very harsh metabolic conditions and a very strict Cu(II) transchelation challenge with SOD.[400] This is in sharp contrast to the hydrophilic $[Cu(DOTA)]^{2-}$ complex, which cleared very quickly through the kidneys/bladder/urine, and since a majority of the injected activity was cleared within 15 minutes, the complex was not subject to the same harsh and transchelating environment (liver) as [^{64}Cu(azapa)] (Table 8.4).

Table 8.4 Biodistribution of [^{64}Cu(azapa)] and [^{64}Cu(DOTA)]$^{2-}$ in healthy nude athymic mice (n=4) showing organ uptake as % ID/g, with the error expressed as standard deviation (SD), at 15 min, 1 h, 4 h, and 24 h time points.

Organ	15 min (±SD)	1 h (±SD)	4 h (±SD)	24 h (±SD)
		[^{64}Cu(azapa)]		
Blood	1.72 (±0.12)	1.62 (±0.20)	1.62 (±0.20)	1.19 (±0.08)
Heart	2.12 (±0.12)	2.91 (±0.43)	3.81 (±0.55)	3.44 (±0.44)
Lung	5.10 (±0.28)	6.39 (±0.71)	8.24 (±2.03)	4.30 (±0.60)
Liver	17.71 (±3.48)	15.97 (±1.43)	12.39 (±2.64)	8.14 (±0.94)
Spleen	1.50 (±0.22)	2.27 (±0.33)	3.72 (±0.97)	3.13 (±0.96)
Stomach	2.64 (±0.75)	5.93 (±0.43)	5.11 (±0.62)	2.13 (±0.58)
Large Intestine	1.28 (±0.21)	2.11 (±0.50)	21.12 (±3.44)	1.93 (±0.44)
Small Intestine	63.73 (±26.06)	14.28 (±5.77)	5.18 (±0.85)	3.05 (±0.18)
Kidney	8.87 (±0.93)	6.84 (±1.28)	6.98 (±0.77)	4.80 (±0.60)
Muscle	1.27 (±1.31)	0.45 (±0.08)	0.47 (±0.06)	0.48 (±0.07)
Bone	1.27 (±0.06)	1.30 (±0.39)	2.38 (±0.78)	1.88 (±0.50)
Skin	2.52 (±0.59)	1.77 (±0.45)	2.38 (±0.54)	1.04 (±0.36)
		[^{64}Cu(DOTA)]$^{2-}$		
Blood	2.77 (±0.95)	0.21 (±0.02)	0.22 (±0.03)	0.16 (±0.01)
Heart	1.53 (±0.43)	0.37 (±0.04)	0.57 (±0.10)	0.52 (±0.07)
Lung	2.61 (±0.66)	0.89 (±0.20)	1.25 (±0.60)	0.71 (±0.12)
Liver	2.32 (±0.61)	1.91 (±0.07)	1.64 (±0.50)	1.04 (±0.10)
Spleen	0.90 (±0.23)	0.34 (±0.11)	0.69 (±0.18)	0.48 (±0.16)
Stomach	1.03 (±0.21)	0.70 (±0.17)	0.72 (±0.20)	0.35 (±0.10)
Large Intestine	0.42 (±0.03)	0.37 (±0.10)	2.19 (±0.53)	0.35 (±0.08)
Small Intestine	1.53 (±0.43)	1.01 (±0.47)	0.88 (±0.36)	0.44 (±0.08)
Kidney	6.81 (±1.22)	1.66 (±0.07)	1.59 (±0.20)	0.93 (±0.05)
Muscle	0.72 (±0.29)	0.09 (±0.02)	0.09 (±0.03)	0.09 (±0.03)
Bone	1.17 (±0.57)	0.45 (±0.13)	0.55 (±0.40)	0.27 (±0.07)
Skin	1.76 (±0.47)	0.40 (±0.04)	0.34 (±0.11)	0.17 (±0.03)

In order to observe a fair competition between these ligands, in the future bioconjugates (e.g. peptide) must be synthesized and compared *in vivo*. The rapid clearance of high amounts of ^{64}Cu through the digestive system, as well as the high uptake in the lungs and heart, suggest that [^{64}Cu(azapa)] remains largely intact. Recent investigation into a series of small, cationic, lipophilic derivatives of H_2dedpa bearing lipophilic methoxyphenyl substituents showed that with $^{67/68}$Ga, the complexes that were the most stable *in vitro* with ^{67}Ga, and were concurrently the most lipophilic by RP-HPLC, displayed greatly elevated uptake in the liver, intestine, heart, and lung. They were concluded to be stable as confirmed

by low bone uptake of "free" ^{67}Ga.[274] Uptake and clearance from the kidneys was also prominent in the biodistribution for each of these compounds, particularly those that were unstable *in vitro*. For comparison, Ando *et al.* injected $^{64}CuCl_2$ into Donryu rats with implanted sarcomas, and found that activity accumulation was highest for "free" metal in the liver and kidney,[93] while for ^{64}Cu complexes of DOTA, TETA, and cross-bridged cyclams known to be unstable *in vivo*,[366,396,400] abnormal accumulation in the blood and bone was also commonly observed.[366,396,400]

The reason for elevated uptake of [^{64}Cu(azapa)] in various organs is difficult to explain with the currently available data; however, the model ligand H_2azapa was never intended as a biologically relevant ligand, with its lipophilic benzyl "placeholders" used for studies with standard analytical techniques, but not intended for final radiopharmaceutical formulations *in vivo*. The elevated uptake of [^{64}Cu(azapa)] in the small intestine, large intestines, stomach, spleen, heart, and lungs suggests that the physical properties of the neutral, lipophilic complex facilitate uptake of the intact complex into these organs. This promising observation suggests that future elaborations of the H_2azapa scaffold as hydrophilic peptide bioconjugates will hopefully remain intact *in vivo*, and ultimately work well as ^{64}Cu PET imaging agents. Efforts are currently underway to synthesize hydrophilic PEG-3 and peptide conjugates of H_2azapa to modulate the pharmacokinetics away from the digestive tract, liver, and lungs, and optimize selective tumour uptake for imaging and therapy. It is anticipated that the propensity of [^{64}Cu(azapa)] towards persistent organ uptake is solely a result of its lipophilic character, and the modular and "clickable" H_2azapa scaffold should be a promising candidate for receptor-based targeting using larger, more sensitive

biological targeting vectors such as peptides and antibody fragments that require low temperature radiolabeling.

The ability of H_2azapa to radiolabel with ^{177}Lu, ^{111}In, ^{67}Ga, and ^{64}Cu quantitatively in 10 minutes at ambient temperature, albeit not with optimal stability for all isotopes, shows impressive flexibility and versatility. It is also of interest to note that high heart uptake was observed over 24 hours (uptake of 3.8 %ID/g at 4 h and 3.4 %ID/g at 24 h), with a heart/blood ratio of 1.9 at 1 hour and 2.9 at 24 hours, which is comparable to many of the H_2dedpa cardiac derivatives recently published,[274] and fortuitously suggests that a modified version of this neutrally charged Cu(II) ligand scaffold could be used for heart imaging. Further, the neutral and lipophilic physical properties of H_2azapa could lead to applications in tumour hypoxia imaging through decoration of the molecular scaffold with a nitroimidazole functionality. The modularity of the "clickable" precursor **8.4** (alkyne functionalized ligand) adds a large degree of versatility to this scaffold, as many different bifunctional derivatives can by synthesized from the same precursor (e.g. peptide, antibody, antibody fragment, nanoparticle, PEG chain, nitroimidazole), which will allow for facile and simple synthesis of these derivatives with little or no changes in synthetic methodology.

8.3 Conclusions

In this chapter we have presented the synthesis, characterization, metal complexation, and radiolabeling of H_2azapa, the first known example of a bifunctional triazole-containing acyclic ligand based on a "clickable" version of the pyridinecarboxylate scaffold. Besides investigating its metal complexation and stability properties with a selection of radiometals of current interest in nuclear medicine, we were interested to investigate the feasibility of an

alternative "click" approach towards biovector conjugation and derivatization of the scaffold towards potentially higher denticity systems with larger metals such as In(III), Y(III), and Lu(III). Our hypothesis was that the formation of robust, coordinatively saturated complexes in the solution phase would result in kinetically inert chelate-radiometal complexes *in vivo*. From the preliminary investigation presented in this chapter, H_2azapa appears to be a viable candidate as a "clickable" bifunctional chelator for copper radiopharmaceuticals, and a valuable addition to the "pa" family of ligands (H_2dedpa, H_4octapa, H_6phospa, and H_5decapa). This is demonstrated by the ability of H_2azapa to quantitatively radiolabel with ^{64}Cu in 10 minutes at ambient temperature in aqueous buffer (pH 4-5), and by its robust inertness in human blood serum, in which it shows only 2% transchelation by serum proteins after a 20 hour incubation period. This is in stark contrast to DOTA, which required elevated temperatures for radiolabeling and was only 74% intact after the 20-hour incubation period with human blood serum, further substantiating its non-optimal properties for both antibody and peptide radiolabeling with ^{64}Cu. The solid-state molecular structure of [Cu(azapa)] confirmed a coordinatively saturated six-coordinate structure with the picolinate (N_4O_2) core of the molecule bound and the triazole arms extending away from the metal center. Although the In(III) complex of H_2azapa was unstable in serum and was not further investigated *in vivo*, it formed a highly unusual and rare eight-coordinate complex with In(III) showing coordination to the picolinate core, one triazole arm, and one aqua ligand, one of only a handful of 8-coordinate In(III) complexes.

Despite the high *in vitro* stability of [^{64}Cu(azapa)] in the presence of biological serum proteins, *in vivo* uptake in a variety of organs, notably the liver, stomach, intestines, and kidneys was observed in nude athymic mice, most likely due to its neutrally charged and

highly lipophilic physical properties. [^{64}Cu(azapa)] cleared from the liver and passed through the intestines and digestive tract relatively rapidly in mice, with ~8% ID/g remaining in the liver after 24 hours; however, persistent uptake in the liver, lung, heart, and digestive tract is expected for small lipophilic molecules, and H_2azapa is merely a model ligand designed for preliminary study. Taken together, these results suggest potential for future elaboration of the H_2dedpa scaffold with hydrophilic peptide biovectors. The modular design of this "clickable" system will hopefully facilitate the fast and simple synthesis of a number of new derivatives. Further investigation into the biological stability of bifunctional bioconjugates of H_2azapa exploiting hydrophilic peptides and PEG groups may secure the potential of H_2azapa as a useful bifunctional ligand for copper.

8.4 Experimental section

8.4.1 Materials and Methods

General materials and methods used were the same as those in Chapters 2 and 3, with the following exceptions. Radiochemical experiments with ^{67}Ga and ^{111}In were performed at TRIUMF/Nordion in Vancouver, BC. ^{67}Ga and ^{111}In were cyclotron produced (Advanced Cyclotron Systems, Model TR30) by proton bombardment through the reactions ^{68}Zn(*p,2n*)^{67}Ga and ^{111}Cd(*p,n*)^{111}In and provided by Nordion as $^{67}GaCl_3$ and $^{111}InCl_3$ solutions in 0.05 M HCl. Analysis of radiolabeled compounds was performed using an analytical HPLC system consisting of a Waters xbridge BEH130 C18 reverse phase (150 x 6 mm) analytical column and a Waters Alliance HT 2795 separation module equipped with a Raytest Gabi Star NaI (Tl) detector (Raytest GmbH, Straubenhardt, Germany) and a Waters 996 photodiode array (PDA) detector. Blood serum competition experiments with ^{67}Ga/^{111}In

were performed using previously frozen mouse blood serum (Sigma, M5905-5 mL). Blood serum competition solutions were analyzed using GE Healthcare Life Sciences PD-10 desalting columns (GE Healthcare, United Kingdom, MW < 5000 Da filter) conditioned by elution of 20 mL phosphate-buffered saline (PBS) before use. Radioactivity counting for ^{67}Ga and ^{111}In was performed using a Capintec CRC 15R dose calibrator (Capintec, Ramsey, NJ).

Radiochemical experiments with ^{177}Lu and ^{64}Cu were performed at Memorial Sloan-Kettering Cancer Center (MSKCC) in New York and utilized the following materials and methods. ^{177}Lu was procured from Perkin Elmer (Perkin Elmer Life and Analytical Sciences, Wellesley, MA, effective specific activity of 29.27 Ci/mg) as $^{177}LuCl_3$ in 0.05 M HCl. ^{64}Cu was purchased from Washington University, St. Louis (Washington University School of Medicine Cyclotron, model CS-15, Cyclotron Corp., ^{64}Ni(p,n)^{64}Cu) and purified as previously described to yield [^{64}Cu]$CuCl_2$ with an effective specific activity of 200-400 mCi/μg (7.4-14.8 GBq/μg).[401] The HPLC used was a Shimadzu SPD-20A prominence UV/Vis, LC-20AB prominence LC, a Bioscan flow-count radiation detector, and a C18 reverse phase column (Phenomenex Luna Analytical 250 x 4.6 mm). Blood serum competition experiments with ^{64}Cu/^{177}Lu were performed using human blood serum (Sigma, Sera, human, aseptically filled, S7023-100 mL). Human blood serum competition solutions were agitated at 550 rpm and held at 37 °C using an Eppendorf Thermomixer and then analyzed using GE Healthcare Life Sciences PD-10 desalting columns as described above for ^{67}Ga and ^{111}In serum competition solutions. Radioactivity in samples was measured using a Capintec CRC-15R dose calibrator (Capintec, Ramsey, NJ), and for biodistribution studies a Perkin-Elmer (Waltham, MA) Automated Wizard Gamma Counter was used for counting

organ activities and creating calibration curves. PET imaging was performed using a micro-PET R4 rodent scanner (Concord Microsystems).

8.4.2 Di-*tert*-butyl ethane-1,2-dicarbamate (8.1)

To a solution of ethylenediamine (770 μL, 11.5 mmol) in THF (60 mL) was added dropwise a solution of di-*tert*-butyl dicarbonate (5.449 g, 25.0 mmol, 2.2 equiv) in THF (10 mL). A white solid precipitated immediately. The resulting white suspension was stirred under argon at ambient temperature and monitored by TLC and EI-MS. TLC showed the gradual disappearance of *tert*-butyl dicarbonate (R_f : 0.65, TLC in 25% EtOAc in hexanes/ $KMnO_4$ staining) in favour of product (R_f : 0.25). After 3 hours the reaction mixture was concentrated *in vacuo* to dryness and the resulting white solid was re-dissolved in dichloromethane (100 mL). The organic layer was washed with water (2 x 20 mL) and brine (1 x 20 mL). The combined aqueous layers were dried ($MgSO_4$), filtered, and concentrated *in vacuo* to dryness. The resulting colourless solid was dissolved in a minimum volume (~5 mL) of dichloromethane and purified by column chromatography (CombiFlash R_f automated column system; 40 g HP silica; eluted with a gradient of 0 - 100% EtOAc in hexanes) to afford the product **8.1** as a white solid (1.49 g, 50%, R_f : 0.25, TLC in 25% EtOAc in hexanes/ $KMnO_4$ staining). ^{1}H NMR (300 MHz, $CDCl_3$, 25 °C) δ: 5.08 (s, 2H), 3.18 (s, 4H), 1.40 (s, 18H). ^{13}C NMR (75 MHz, $CDCl_3$, 25 °C) δ: 156.3, 79.2, 40.7, 28.3. HR-ESI-MS calcd. for $[C_{12}H_{24}N_2O_4+Na]^+$: 261.1814; found: 261.1814.

8.4.3 *N,N'*-Propargyl-*N,N'*-*tert*-butoxycarbonyl-1,2-diaminoethane (8.2)

Compound **8.1** (500 mg, 1.92 mmol) was suspended in dry acetonitrile (20 mL, distilled over CaH_2 in house) and sodium *tert*-butoxide (462 mg, 4.80 mmol, 2.5 equiv) was added. The white suspension coloured immediately to yellow. The suspension was cooled (0 °C) and propargyl bromide (1242 μL, 0.5 mmol, 6 equiv) in dry acetonitrile (5 mL) was added dropwise over 5-10 minutes. The reaction mixture darkened to light orange during the addition. Tetrabutyl ammonium iodide (TBAI) (1.4 g, 2 equiv) was added and the reaction mixture was left to stir, warming to room temperature as the ice melted. TLC revealed the 100% consumption of starting material (R_f: 0.45, TLC in 40% EtOAc in hexanes) in favour of product (R_f: 0.65) after 48 hours. The reaction mixture was filtered to remove sodium *tert*-butoxide, rinsed well with acetonitrile, and the combined filtrate was concentrated *in vacuo* to dryness. The resulting orange oil was dissolved in dichloromethane (5 mL) and the mixture was filtered over a short silica plug, rinsing well with dichloromethane (50 mL) to elute the toxic propargyl bromide. The filtrate was set aside and the silica was washed with ethyl acetate (50 mL). The ethyl acetate eluent was concentrated *in vacuo* to dryness and the resulting yellow oil was purified by column chromatography (CombiFlash R_f automated column system; 24 g HP silica; eluted with a gradient of 0 - 50% EtOAc in hexanes) to afford the product **8.2** as a yellow solid (485 mg, 75%, R_f : 0.65, TLC in 40% EtOAc in hexanes/$KMnO_4$ staining). ^{1}H NMR (300 MHz, $CDCl_3$, 25 °C) δ: 4.02 (d, 4H), 3.44 (s, 4H), 2.18 (s, 2H), 1.42 (s, 18H). ^{13}C NMR (75 MHz, $CDCl_3$, 25 °C) δ: 154.5, 80.2, 79.2, 71.7, 43.9, 36.4, 28.1. HR-ESI-MS calcd. for $[C_{18}H_{28}N_2O_4+H]^+$: 337.2127; found: 337.2127, $[M+H]^+$.

8.4.4 *N,N'*-Propargyl-1,2-diaminoethane (8.3)

To a solution of **8.2** (134 mg, 0.40 mmol) in dichloromethane (2 mL) was added trifluoroacetic acid (TFA, 1 mL), and the yellow solution darkened to orange. The reaction mixture was stirred for 1 hour at ambient temperature and then concentrated *in vacuo* to dryness. The resulting brown oil was dissolved in saturated $NaHCO_3$ (2 mL) and the resulting aqueous layer was extracted using dichloromethane (25 x 1 mL) until the extractions stained only faintly by TLC with $KMnO_4$ staining. The combined organic layers were dried (Na_2SO_4), filtered, and concentrated *in vacuo* to dryness. The resulting orange oil **8.3** was carried onto the next step without further purification (47 mg, 87%). ^{1}H NMR (300 MHz, $CDCl_3$, 25 °C) δ: 3.45 (s, 4H), 2.85 (s, 4H), 2.22 (s, 2H), 1.77 (s, 2H). ^{13}C NMR (75 MHz, $CDCl_3$, 25 °C) δ: 82.1, 71.2, 47.5, 37.8. HR-ESI-MS calcd. for $[C_8H_{12}N_2+H]^+$: 137.1079; found: 137.1076, $[M+H]^+$.

8.4.5 *N,N'*-[6-(Methoxycarbonyl)pyridin-2-yl]methyl-*N,N'*-propargyl-1,2-diaminoethane (8.4)

To a solution of **8.3** (196 mg, 1.43 mmol) in dry acetonitrile (9 mL, distilled over CaH_2) was added methyl 6-(bromomethyl)picolinate[89] (695 mg, 3.02 mmol, 2.1 equiv) and sodium carbonate (320 mg, 3.02 mmol, 2.1 equiv). The reaction was stirred at ambient temperature. Reaction monitoring by TLC revealed the formation and consumption of a singly alkylated intermediate (R_f : 0.50, TLC in 10% MeOH in DCM/ UV activity) and formation of product (R_f : 0.55). After 48 hours, sodium carbonate was filtered out and the filtrate was concentrated *in vacuo* to dryness. The resulting brown oil was purified by column chromatography (CombiFlash R_f automated column system; 24 g HP silica; eluted

with a gradient of 0 - 10% MeOH in DCM) to afford the product **8.4** as a yellow solid (387 mg, 62%, R_f: 0.55, TLC in 10% MeOH in DCM/UV activity). ^{1}H NMR (300 MHz, $CDCl_3$, 25 °C) δ: 7.96 (d, 2H), 7.71 (m, 4H), 3.94 (s, 6H), 3.90 (s, 4H), 3.42 (s, 4H), 2.71 (s, 4H), 2.18 (s, 2H). ^{13}C NMR (75 MHz, $CDCl_3$, 25 °C) δ: 165.8, 160.1, 147.4, 137.3, 125.9, 123.6, 78.5, 73.3, 60.2, 52.8, 51.0, 42.8. HR-ESI-MS calcd. for $[C_{24}H_{26}N_4O_4+H]^+$: 435.2032; found: 435.2030, $[M+H]^+$.

8.4.6 *N,N'*-[1-Benzyl-1,2,3-triazole-4-yl]methyl-*N,N'*-[6-(carboxy)pyridin-2-yl]-1,2-diaminoethane (H_2azapa•2HCl•1.5H_2O) (8.5•2HCl•1.5H_2O)

Compound **8.4** (300 mg, 0.69 mmol, 1 equiv) was suspended in 1:1 *tert*-butanol/water and benzyl azide (172 μL, 1.38 mmol, 2 equiv) was carefully added using precautionary blast shield protection and a plastic-tipped auto-pipet to prevent a friction-induced explosion. Sodium ascorbate (27 mg, 0.14 mmol, 0.2 equiv) was added, followed by copper(II) acetate monohydrate (276 mg, 1.38 mmol, 2 equiv). The suspension turned dark brown on addition of copper(II) acetate but over 4 hours the solid gradually dissolved and the solution lightened to blue-green. The reaction mixture was stirred at ambient temperature overnight (16 hours) after which time a light blue-green precipitate was observed. The suspension was concentrated *in vacuo* to dryness. The resulting light blue-green solid was dissolved in 1:1 THF/water (50 mL) and sodium sulphide (829 mg, 3.5 mmol, 5 equiv) was added. A brown solid precipitated immediately, and the suspension was left to stir at ambient temperature for 24 hours. The brown solid was filtered out using a fine fritted filter and the colourless filtrate was concentrated *in vacuo* to dryness. The resulting colourless solid was dissolved in a minimum volume of water and pre-purified using a Waters C18 Sep-Pak® 6 cc Vac cartridge

(1 g sorbent, 55-100 μm particle size, gradient: 100% water to 50% MeOH/water to 100% MeOH) in 6-8 small portions. The cartridge was conditioned with methanol (2 x 2 mL) and water (2 x 2 mL) before each use. UV activity was confirmed in the 50% MeOH/water fractions by TLC before they were combined and concentrated *in vacuo* to dryness. The partially purified white solid was purified by semi-preparative HPLC (A: 0.1% TFA, B: 100% MeCN, 0 - 100% B over 25 minutes, t_R (broad) 15.7-18.0 minutes, 50 mg injections) to afford the product **8.5**•TFA as a white crystalline solid (272 mg, 44% based on 2 TFA per molecule). ^{1}H NMR (300 MHz, MeOD, 25 °C) δ: 8.18 (s, 2H), 7.87 (m, 4H), 7.49 (d, 2H), 7.24 (s, 10H), 5.49 (s, 4H), 4.39 (s, 8H), 3.56 (s, 4H). ^{13}C NMR (75 MHz, MeOD, 25 °C) δ: 167.30, 155.86, 148.58, 140.68, 139.99, 136.54, 130.17, 129.80, 129.39, 128.17, 127.66, 125.80, 58.24, 55.14, 50.98, 50.20. The synthesis was continued to form the HCl salt of H_2azapa. **8.5**•TFA (272 mg, 0.30 mmol) was dissolved in acetonitrile (3 mL). 0.1 M HCl (10 mL) was added and the resulting solution was concentrated *in vacuo* to dryness. This procedure was repeated 4-5 times to afford the white solid **8.5**•2HCl•1.5H_2O which was dried under high vacuum for several days before use (removal of TFA confirmed via ^{19}F NMR). NMR structural assignments were confirmed using two-dimensional NMR experiments (Figures A.13, A.14). ^{1}H NMR (600 MHz, D_2O, 25 °C) δ: 7.57 (d, 2H; *H*3), 7.53 (s, 2H; *H*5), 7.41 (t, 2H, *H*4), 6.90 (m, 12H; *H*11, Ph*H*), 5.13 (s, 4H: *H*12), 3.37 (s, 4H: *H*9), 3.34 (s, 4H, *H*7), 2.26 (s, 4H, *H*8). ^{13}C NMR (150 MHz, D_2O, 25 °C) δ: 172.7 (*C*1), 157.2 (*C*10), 153.1 (*C*4), 143.6 (*C*6), 138.1 (*C*2), 134.9 (*C*13), 128.9 (*C*15), 128.6 (*C*16), 128.0 (*C*14), 125.2 (*C*11), 124.8 (*C*5), 122.5 (*C*3), 59.7 (*C*9), 53.7 (*C*12), 50.4 (*C*8), 48.4 (*C*7). HR-ESI-MS calcd. for $[C_{36}H_{36}N_{10}O_4+H]^+$: 673.2999; found: 673.3000, $[M+H]^+$. Anal.

Calcd. (found) for $C_{36}H_{36}N_{10}O_4$•2HCl•1.5H_2O: C, 55.96 (56.06); H, 5.35 (5.23); N, 18.13 (18.11).

8.4.7 Metal complexation experiments: general procedure

H_2azapa•2HCl•1.5H_2O (~0.015 mmol) was suspended in 0.1 M HCl (1.5 mL) and the appropriate metal chloride or perchlorate (1.2 equiv) was added. The pH was adjusted to 4-5 using 0.1 M NaOH and then the solution was stirred at 60 °C. Any remaining solid dissolved upon heating. The reaction was stirred overnight (24 hours), maintaining the same temperature.

8.4.7.1 [Cu(azapa)]

H_2azapa•2HCl•1.5H_2O (**8.5)** (13.8 mg, 0.018 mmol) was mixed with copper(II) chloride dihydrate (3.7 mg, 0.0215 mmol, 1.2 equiv) to react. After 24 hours, a light blue precipitate was filtered out and purified by semi-preparative HPLC (gradient: A: water, B: MeCN, 0 - 100% B over 25 minutes, t_R (broad) 16.2-17.5 minutes) to afford the product [Cu(azapa)] as a green solid. HR-ESI-MS calcd. for $[C_{36}H_{34}{}^{63}CuN_{10}O_4+Na]^+$: 756.1958; found: 756.1951, $[M+Na]^+$. Anal. Calcd. (found) for $C_{36}H_{34}CuN_{10}O_4$•1.5H_2O: C, 56.80 (56.88); H, 4.90 (4.81); N, 18.40 (18.38).

8.4.7.2 [Ga(azapa)][ClO_4]

H_2azapa•2HCl•1.5H_2O (9.7 mg, 0.013 mmol) was mixed with gallium(III) perchlorate hexahydrate (7.2 mg, 0.015 mmol, 1.2 equiv) to react. After 24 hours, a white crystalline precipitate was filtered out to afford [Ga(azapa)][ClO_4]. NMR structural

assignments were confirmed using two-dimensional NMR experiments. ^{1}H NMR (600 MHz, DMSO-d_6, 25 °C) δ: 8.65 (t, 2H; *H*4), 8.34 (m, 4H; *H*3, *H*11), 8.20 (d, 2H; *H*5), 7.32 (m, 10H; Ph*H*), 5.65 (q, 4H; *H*12, *H*12'), 4.74 and 4.28 (2d, 4H; *H*7, *H*7', ^{2}J = 18 Hz), 4.00 and 3.92 (2d, 4H; *H*9, *H*9', ^{2}J = 15 Hz), 3.10 (m, 4H; *H*8, *H*8'). ^{13}C NMR (150 MHz, DMSO-d_6, 25 °C) δ: 162.3 (*C*1), 150.6 (*C*6), 146.5 (*C*4), 143.6 (*C*2), 137.7 (*C*10), 135.7 (*C*13), 128.8 (Ph*C*), 128.4 (*C*5), 128.2 (Ph*C*), 127.9 (Ph*C*), 127.1 (*C*11), 123.5 (*C*3), 56.3 (*C*7), 52.9 (*C*12), 47.8 (*C*8), 46.0 (*C*9). HR-ESI-MS calcd. for $[C_{36}H_{34}{}^{69}GaN_{10}O_4]^+$: 739.2020; found: 739.2014, $[M]^+$.

8.4.7.3 [In(azapa)(H_2O)][ClO_4]

H_2azapa•2HCl•1.5H_2O (9.8 mg, 0.013 mmol) was mixed with indium(III) perchlorate hexahydrate (8.5 mg, 0.015 mmol, 1.2 equiv) to react. After 24 hours, a white crystalline precipitate was filtered out to afford the product [In(azapa)(H_2O)][ClO_4]. ^{1}H NMR (400 MHz, DMSO-d_6, 25 °C) δ: 8.54-6.87 (br m, 18H), 5.49 (br s, 4H) 4.80-4.18 (m, 4H), 2.84 (s, 2H), 2.24 (s, 2H). ^{1}H NMR (400 MHz, DMSO-d_6, 135 °C) δ: 8.19 (m, 4H), 7.98 (s, 2H), 7.57 (s, 2H), 7.29 (m, 6H), 7.12 (m, 4H), 5.42 (s, 4H), 3.93 (s, 4H), 3.66 (s, 4H), 2.59 (s, 4H). HR-ESI-MS calcd. for $[C_{36}H_{34}{}^{115}InN_{10}O_4]^+$: 785.1803; found: 785.1806, $[M]^+$.

8.4.7.4 [Lu(azapa)][ClO_4]

H_2azapa•2HCl•1.5H_2O (9.8 mg, 0.013 mmol) was mixed with lutetium(III) chloride hexahydrate (6.1 mg, 0.015 mmol, 1.2 equiv) to react. After 4 hours the product was confirmed via mass spectrometry and the solvent was removed *en vacuo* to yield [Lu(azapa)][Cl]. ^{1}H NMR (300 MHz, D_2O, 25 °C) δ: 8.09 (br m, 2H), 7.98 (br m, 2H), 7.89

(s, 2H), 7.49 (br m, 2H), 7.31 (br m, 6H), 7.09 (br m, 4H), 5.32 (s, 4H) 4.14-3.91 (m, 6H), 3.65 (br m, 2H), 2.80-2.72 (m, 4H). ^{13}C NMR (400 MHz, D_2O, 25 °C) δ: 172.5, 157.8, 150.3, 142.9, 134.4, 129.2, 129.0, 128.4, 125.6, 125.5, 124.0, 59.7, 54.7, 54.4, 52.9, 49.1. HR-ESI-MS calcd. for $[C_{36}H_{34}{}^{175}LuN_{10}O_4]^+$: 845.2172; found: 845.2166 $[M]^+$.

8.4.8 X-Ray crystallography

A small blue prism crystal of [Cu(azapa)] having approximate dimensions 0.10 x 0.41 x 0.45 mm was grown by slow evaporation from a saturated solution in 1:1 MeCN/H_2O. A brown plate crystal of $[In(azapa)(H_2O)][ClO_4]\bullet 2.5H_2O$ having approximate dimensions of 0.10 x 0.22 x 0.27 mm was grown by slow evaporation of a saturated solution in 1:1 MeOH/DMSO. The crystals were mounted onto respective glass fibers, and measurements were made on a Bruker Apex DUO diffractometer at -183 °C with graphite-monochromated Mo-Kα radiation. All data were collected and integrated using the Bruker SAINT[402] software package. Data were corrected for adsorption effects, and Lorentz and polarization effects using the SADABS[403] program. The structures were solved by direct methods using the SIR97[404] software and refined using SHELXL-97[405] *via* the WinGX[406] interface. $[In(azapa)][ClO_4]$ crystallizes with 3 molecules of water in the crystal lattice. X-ray work was performed by Dr. Brian O. Patrick. A summary of crystallographic data is presented in Table 8.1 for $[In(azapa)(H_2O)][ClO_4]$ and in Table 8.2 for [Cu(azapa)]. Relevant bond lengths and angles are found in the appendix, Tables A.1 and A.2.

8.4.9 ^{67}Ga/^{111}In Radiolabeling

For ^{67}Ga radiolabeling experiments, a 1 mg/mL stock solution of H_2azapa was made by dissolving 1.8 mg in 1.8 mL NaOAc buffer (10 mM, pH 4) with mild heat and vortex-mixing. An aliquot of ligand stock (750 μL) was transferred to a 20 mL sterile vial, and $^{67}GaCl_3$ (10 μL, ~5 mCi) solution was added followed by NaOAc buffer (1.785 mL, 10 mM, pH 4) up to a total ligand concentration of 0.3 mg/mL. ^{111}In labeling was performed similarly, with $^{111}InCl_3$ (15 μL, ~6 mCi) and NaOAc buffer (1.240 mL, 10 mM, pH 5) being added to an aliquot of ligand stock solution (495 μL). The mixtures were agitated briefly and then allowed to react for 10 minutes at ambient temperature. The radiometal complex solutions were analyzed by analytical RP-HPLC (linear gradient A: 0.05% TFA, B: MeCN, 0 - 100% B over 20 minutes) to determine radiolabeling yields through peak integration: $[^{67}Ga(azapa)]^+$ t_R = 12.8 min, >99%; $[^{111}In(azapa)]^+$ t_R = 11.4 min, >99%. The retention times for the radioactive metal complexes determined by the Raytest NaI (Tl) detector were confirmed by analyzing the fully characterized non-radioactive metal complexes by RP-HPLC using the PDA detector: $[Ga(azapa)]^+$ t_R = 12.7 min; $[In(azapa)]^+$ t_R = 11.4 min.

8.4.10 ^{177}Lu/^{64}Cu Radiolabeling

For ^{177}Lu experiments, the ligands H_2azapa, DTPA, and DOTA were all dissolved up to 1 mg/mL in NaOAc buffer (10 mM, pH 5.0) as stock solutions. DTPA and H_2azapa required heating at 37 °C and frequent vortexing for 1-2 hours to dissolve. Aliquots of each ligand stock solution were transferred to Corning® 2.0 mL self-standing micro-centrifuge tubes containing ~1.2 mCi of ^{177}Lu to a concentration of ~182 μM, and made up to 1 mL with NaOAc buffer (10 mM, pH 5.0). H_2azapa and DTPA were allowed to radiolabel at

ambient temperature for 10 minutes and DOTA was radiolabeled for 1 hour at 90 °C. Radiometal complexes were then evaluated using radio-HPLC (linear gradient A: 0.1% TFA in H_2O, B: MeCN, 0 - 80% B over 30 minutes): $[^{177}Lu(azapa)]^+$ t_R = 19.3 min, >99%; $[^{177}Lu(DOTA)]^-$ t_R = 6.8 min, >99%, $[^{177}Lu(DTPA)]^{2-}$ t_R = 5.2 min, >99%. ^{64}Cu labeling was performed in a similar manner with H_2azapa and DOTA at the same ligand concentrations previously used for labeling with ^{177}Lu (182 μM) and with ~800-1000 μCi of ^{64}Cu. DOTA was radiolabeled at 90 °C for 60 minutes, and H_2azapa in 10 minutes at ambient temperature, and both were evaluated by RP-HPLC $[^{64}Cu(azapa)]$ t_R = 20.9 min, >99%; $[^{64}Cu(DOTA)]^{2-}$ t_R = 7.1 min, >99%.

8.4.11 $^{67}Ga/^{111}In$ Mouse serum competition experiments

Frozen mouse serum was allowed to thaw for 30 minutes, and 750 μL of $[^{67}Ga(azapa)]^+$ solution was added in triplicate to 20 mL sterile vials containing 1250 μL of thawed mouse serum and 500 μL of PBS. The solutions sat at ambient temperature, and 800 μL aliquots were removed from each vial at 15 minutes, 1 hour, and 2 hour time points and diluted to a final volume of 2.5 mL with PBS in sterile vials. A 500 μL aliquot of $[^{111}In(azapa)]^+$ was added in triplicate to 20 mL sterile vials containing 750 μL of thawed mouse serum and 250 μL of PBS. The solutions were allowed to sit at ambient temperature, and 750 μL aliquots were removed at 1 hour and 24 hour time points, and diluted to a final volume of 2.5 mL with PBS in sterile vials. The activities were counted, and the diluted mouse serum competitions were immediately loaded onto conditioned PD-10 size-exclusion columns. The 2.5 mL loading volumes were eluted and discarded into dedicated ^{111}In or ^{67}Ga radioactive waste containers, and the columns were then eluted with an additional 3.5

mL of PBS, which was collected into fresh 20 mL sterile vials. The activities of the eluents, which contained transchelated metal ions bound/associated with serum proteins were counted and compared with the activity values obtained exactly prior to column loading to determine the percent radiometal ions that had been retained on the column as chelate-bound activity.

8.4.12 ^{177}Lu/^{64}Cu Blood serum competition experiments

Frozen human blood serum thawed for 30 minutes, and 750 μL aliquots were transferred to 2.0 mL Corning centrifuge vials. 300 μL of each ^{177}Lu(chelate) was transferred to the blood serum, along with 450 μL of PBS to a total volume of 1.5 mL (in triplicate for each ligand). The final ^{177}Lu(chelate) concentration present in serum was ~36 μM. Serum competition samples were then incubated at 37 ± 0.1 °C with constant agitation (550 rpm) and analyzed via PD-10 size-exclusion column elution (filters MW < 5000 Da) at 1.5 hour and 24 hour time points and counted using a Capintec CRC-15R dose calibrator. 750 μL of each serum/^{177}Lu(chelate) competition solution (in triplicate) was removed from the competition vial, diluted to 2.5 mL with PBS, and counted. The diluted aliquot of serum competition mixture was loaded onto a conditioned PD-10 column. The loading volume (2.5 mL) was eluted into radioactive waste, and then an additional 3.5 mL of PBS was loaded, collected, and counted in the dose calibrator as the serum-bound ^{177}Lu (non-chelate bound). Percent stability was reported as a percentage of ^{177}Lu still chelate-bound and not associated with serum proteins (MW < 5000 Da). Human serum competitions with ^{64}Cu were performed in an identical fashion as described above for ^{177}Lu, but with time points of 1 hour and 20 hours.

8.4.13 ^{64}Cu Biodistribution studies

Biodistribution studies evaluated the basic stability and clearance of the ^{64}Cu complexes of the commonly used ligand DOTA, and the novel entrant H_2azapa. Although the ligand NOTA is also widely used with ^{64}Cu, and is known to be superior to DOTA in terms of *in vivo* stability and radiolabeling kinetics, DOTA was used as an initial first benchmark due to its wide availability and common use (currently used in 2 of 3 ^{64}Cu-based clinical trials), and its superior properties with the isotopes ^{111}In and ^{177}Lu used in this study.[232,367,368] DOTA and H_2azapa were radiolabeled with ^{64}Cu under the same conditions as described above, and prepared for biodistribution studies in healthy nude athymic mice (female, 6-8 weeks old). The ^{64}Cu(chelate) complexes were purified via RP-HPLC, concentrated *in vacuo* to dryness, and then suspended in 2:1 sterile saline 0.9% NaCl:PBS (pH 7) to a concentration and dose of ~30 μCi in 200 μL per mouse (specific activity ~ 10 mCi/mg, ~ 3 mg ^{64}Cu(chelate) per mouse). Each mouse was intravenously injected through the tail vein and sacrificed by CO_2 inhalation at time points of 15 minutes, 1 hour, 4 hours, and 24 hours (n = 4). Tissues collected after sacrifice included blood, heart, lungs, liver, spleen, kidneys, large intestine, small intestine, muscle, bone (femur), and skin. All organs were rinsed in water after removal and air-dried for 5 minutes. Tissues were weighed and counted (calibrated for ^{64}Cu), the counts were background- and decay-corrected from the time of injection and then converted to the percentage of injected dose (%ID) per gram of organ tissue (%ID/g). The ^{64}Cu counts measured in each organ were converted to activity using a calibration curve created from known standards of ^{64}Cu.

8.4.14 Small-animal ^{64}Cu-PET imaging

PET imaging was performed using a micro-PET R4 rodent scanner (Concord Microsystems) in order to visually confirm biodistribution results and monitor clearance of ^{64}Cu. Two healthy, nude athymic mice (female, 6-8 weeks old) were administered doses of ~300 μCi in 200 μL of 2:1 sterile saline (0.9% NaCl):PBS (pH 7) via intravenous tail vein injection (specific activity ~10 μCi/μg, ~30 μg of [^{64}Cu(azapa)] per mouse). Approximately 5 minutes prior to PET image acquisition, mice were anesthetized via inhalation of 2% isoflurane (Baxter Healthcare, Deerfield, IL)/oxygen gas mixture, placed on the scanner bed, and anesthesia was maintained during imaging using a reduced 1% isoflurane/oxygen mixture. Images were acquired at time points 1 h, 4 h, and 24 h, with PET data being recorded via static scans with a minimum of 10 million coincident events (30-60 minutes). An energy window of 350-700 keV and a coincidence timing window of 6 ns were used. Data were sorted into 2D histograms by Fourier rebinning, and transverse images were reconstructed by filtered back-projection (FBP) into a 128 x 128 x 63 (0.72 x 0.72 x 1.3 mm^3) matrix. The image data were normalized to correct for non-uniformity of response of the PET, dead-time count losses, positron branching ratio, and physical decay to the time of injection, but no attenuation, scatter, or partial-volume averaging correction was applied. The counting rates in the reconstructed images were converted to activity concentrations (percentage injected dose [%ID] per gram of tissue) by use of a system calibration factor derived from the imaging of a mouse-sized water-equivalent phantom containing ^{64}Cu. Images were analyzed using *ASIPro VM* software (Concorde Microsystems).

Chapter 9: Conclusions and future work

9.1.1 Overview and conclusions for "pa" family of picolinic acid-based ligands

Amongst the quintet of H_2azapa,[88] H_2dedpa,[118,272-274] H_4octapa,[87,89] H_5decapa,[89] and H_6phospa,[304] our group has a large number of clinically relevant and high impact metal ions / isotopes well covered. Of these five ligands, all but H_2dedpa were studied and discussed throughout this thesis. Although many promising ligands have been studied, each ligand requires further investigation at the time of writing this thesis.

Chapter 2 outlined the initial synthesis and study of the ligand H_4octapa, which was very promising for use with ^{111}In. In Chapter 3 a new synthetic route using nosyl-protection chemistry was devised for making H_4octapa and its bifunctional derivative *p*-SCN-Bn-H_4octapa, and they were studied *in vivo* with both ^{111}In and ^{177}Lu. It was found that when conjugated to trastusuzmab, H_4octapa was an excellent ligand for ^{111}In and ^{177}Lu, matching the industry "gold standard" ligand DOTA. The yttrium isotopes $^{86/90}$Y are commonly used in conjunction with ^{111}In and ^{177}Lu, and the ubiquitous ligand DOTA has been shown to be excellent for all three elements. Although Chapter 5 has discussed preliminary studies of H_4octapa with Y^{3+}, no radioactive work with $^{86/90}$Y has been performed to date; thus it should be completed and compared to DOTA in the future. Chapter 5 also outlines a new protection chemistry strategy for these picolinic acid-based ligands; it uses *tert*-butyl esters to protect the picolinic acid moieties, allowing for facile deprotection and incorporation into peptides synthesized on-resin. To date, the new *tert*-butyl ester protected ligands discussed in Chapter 5 have not been applied to any sensitive scaffolds, and so future work with *p*-SCN-Bn-(tBu)$_2$dedpa and peptides synthesized on-resin for ^{68}Ga PET imaging would be of interest.

Chapter 4 discussed the high-denticity ligands H_3nonapa and H_3trenpa (and derivatives), and it was found that these ligands were inferior to H_4octapa and other commonly used ligands with ^{111}In. These ligands were not tested with any other radiometals, but the similarities in aqueous chemistry between ^{111}In, ^{177}Lu, and $^{86/90}$Y bodes poorly for any future use of these ligands. If an application for these ligands were to present itself, they could be re-synthesized using the nosyl-based synthesis outlined in Chapter 3, instead of the old synthetic route used in Chapter 4.

Chapter 6 demonstrated a very important point of ligand-design (as discussed in Chapter 1), through the synthesis and study of the H_4octapa derivative H_4C3octapa. The ligand H_4C3octapa differed from H_4octapa by merely 1 carbon atom (a central propylene bridge vs ethylene bridge), yet the differences in solution chemistry, DFT calculated structures, radiolabeling properties, and complex stability were dramatic. The important lesson learned from this chapter was that 5-membered chelate rings should always be utilized, as their stability and geometry are far superior to those of 6-membered chelate rings. The ligand H_4C3octapa does not have any potential for use with the common radiometal ions discussed throughout this thesis, but an efficient synthetic protocol has been developed should it find a new purpose in the future.

Chapter 7 outlined the synthesis of the H_4octapa derivative, H_6phospa, which had the two acetate arms of H_4C3octapa replaced with methylenephosphonate arms, having the goal of improving radiolabeling performance with the extremely difficult radiometal ^{89}Zr. This goal was achieved, as H_6phospa was able radiolabel with higher efficiency than H_4octapa (~8% vs ~0% after 1 hour, rt); however, this increase was too modest to warrant *in vivo* experimentation and further work. The ligand H_6phospa is interesting because other than the

current "gold standard" ligand desferrioxamine, H_6phospa is the only ligand synthesized to date that can radiolabel with ^{89}Zr with any reasonable yield. Also, this work demonstrates that methylenephosphonate groups are preferred for ^{89}Zr radiolabeling over acetate groups, which was not previously known. Due to the difficulty in synthesizing H_6phospa, and the solubility problems encountered with HCl salts of H_6phospa, this ligand will probably not be studied in the future. It is also becoming apparent that ^{89}Zr ligands should be oxygen-rich, with O_8 donor sets being ideal.

Chapter 8 discussed the ligand H_2azapa, which utilized click-chemistry for the dual purposes of providing a bioconjugation linkage to a biovector (e.g. peptide) for cancer delivery, as well as a metal-coordinating group (triazole ring). This work revealed that H_2azapa was most promising with the copper isotope ^{64}Cu; however, the high lipophilicity of the model-ligand H_2azapa meant that *in vivo* behavior was non-optimal. As mentioned in Chapter 8, hydrophilic peptide conjugates must be synthesized so that H_2azapa can be properly evaluated *in vivo* and compared to existing ligands. Very early work towards this end, which was not discussed in this thesis, has been unsuccessful because the conditions required to remove copper from H_2azapa during synthesis (Na_2S) have proven incompatible with peptides. Although a very interesting ligand, it may be necessary to abandon future development, as the super-stoichiometric quantities of copper required for completion of the click-reaction cannot currently be removed without destruction of the attached peptides. This system would be compatible with copper-free click reactions, as discussed in Chapter 1; however, copper-free click conjugations would not introduce the metal-binding triazole rings used in H_2azapa, which was largely the purpose of this ligand.

9.1.2 General direction for future ligand design

Current directions in radiochemistry and nuclear medicine highlight the importance of PET imaging, and subsequently the significance of optimal utilization of a growing number of β^+ emitting radiometal ions. Promising new PET isotopes such as ^{44}Sc and ^{89}Zr currently have poorly elaborated chelate chemistry, and moving forward the development of fast-radiolabeling and exceptionally stable ligands for these isotopes will be important. ^{68}Ga is perhaps the most promising of all isotopes discussed here, primarily due to its highly portable and long-lived generator system. To properly utilize ^{68}Ga and translate it to the clinic, the wide-range of excellent ^{68}Ga ligands that are currently under investigation must be transformed into viable imaging agents to provide useful diagnostic tools to the medical community. α-Emitting isotopes are also currently of strong interest, as they are extremely effective, when targeted, at site-specifically delivering therapeutic doses of radioactivity to a variety of cancers. The caveat for α-emitters is their potentially fatal toxicity, and therefore robust chelate chemistry is of utmost importance for the development of therapeutic agents based on isotopes such as ^{225}Ac, $^{212/213}$Bi, and ^{212}Pb.

Further study of the large decadentate ligand H_5decepa (Chapter 2) with large radiometals such as ^{225}Ac, $^{212/213}$Bi, and ^{212}Pb is of interest. Additionally, a bifunctional derivative of H_5decapa should be synthesized so that the ligand can be conjugated to an antibody and properly evaluated with ^{225}Ac, $^{212/213}$Bi, and ^{212}Pb. Synthesis of ^{89}Zr ligands should focus on removal of nitrogen from the coordination sphere, and addition of oxygen-donor atoms with groups such as hydroxamates or catechols should be performed. The radiometal ^{44}Sc should be evaluated with H_4octapa, as DOTA is currently the best available ligand for ^{44}Sc, and H_4octapa has been shown to have excellent radiolabeling and stability

properties with many of the same radiometals as DOTA. ^{68}Ga work should be continued with H_2dedpa, with the *tert*-butyl picolinic acid protection chemistry studied in Chapter 5 potentially being of use. More *in vivo* proof-of-principle work should be performed with H_2dedpa, with the industry "gold standard" NOTA being used for direct comparison.

Bibliography

(1) Price, E. W.; Orvig, C. *Chem. Soc. Rev.* **2014**, *43*, 260-290.
(2) Ramogida, C. F.; Orvig, C. *Chem. Commun.* **2013**, *49*, 4720-4739.
(3) Zeglis, B. M.; Houghton, J. L.; Evans, M. J.; Viola-Villegas, N.; Lewis, J. S. *Inorg. Chem.* **2013**.
(4) Bartholomä, M. D. *Inorg. Chim. Acta* **2012**, *389*, 36-51.
(5) Cutler, C. S.; Hennkens, H. M.; Sisay, N.; Huclier-Markai, S.; Jurisson, S. S. *Chem. Rev.* **2012**, *113*, 858-883.
(6) Wadas, T. J.; Wong, E. H.; Weisman, G. R.; Anderson, C. J. *Chem. Rev.* **2010**, *110*, 2858-2902.
(7) Bartholomä, M. D.; Louie, A. S.; Valliant, J. F.; Zubieta, J. *Chem. Rev.* **2010**, *110*, 2903-2920.
(8) Vallabhajosula, S.; Springer Berlin Heidelberg: 2009, p 179-196.
(9) Anderson, C. J.; Welch, M. J. *Chem. Rev.* **1999**, *99*, 2219-2234.
(10) Pentlow, K. S.; Graham, M. C.; Lambrecht, R. M.; Cheung, N.-K. V.; Larson, S. M. *Med. Phys.* **1991**, *18*, 357-366.
(11) Williams, H.; Robinson, S.; Julyan, P.; Zweit, J.; Hastings, D. *Eur. J. Nucl. Med. Mol. Imaging* **2005**, *32*, 1473-1480.
(12) Robinson, S.; Julyan, P. J.; Hastings, D. L.; Zweit, J. *Phys. Med. Biol.* **2004**, *49*, 5505.
(13) Chu, S. Y. F.; Ekström, L. P.; Firestone, R. B. *WWW table of radioactive isotopes, database version 2/28/1999, from* http://nucleardata.nuclear.lu.se/nucleardata/toi/ **1999**.
(14) Lederer, C. M.; Shirley, V. S. *Table of Isotopes*; 7th ed.; John Wiley & Sons: New York, 1978.
(15) Holland, J. P.; Williamson, M. J.; Lewis, J. S. *Mol. Imaging* **2010**, *9*, 1-20.
(16) Qaim, S. M. *Q. J. Nucl. Med. Mol. Imaging* **2008**, *52*, 111-120.
(17) Połosak, M.; Piotrowska, A.; Krajewski, S.; Bilewicz, A. *J. Radioanal. Nucl. Chem.* **2013**, *295*, 1867-1872.
(18) Zeng, D.; Anderson, C. J. *Chem. Commun.* **2013**, *49*, 2697-2699.
(19) Nayak, T. K.; Garmestani, K.; Milenic, D. E.; Baidoo, K. E.; Brechbiel, M. W. *PLoS One* **2011**, *6*, e18198.
(20) Nayak, T. K.; Garmestani, K.; Baidoo, K. E.; Milenic, D. E.; Brechbiel, M. W. *Int. J. Cancer* **2010**, *128*, 920-926.
(21) Palm, S.; Enmon, R. M.; Matei, C.; Kolbert, K. S.; Xu, S.; Zanzonico, P. B.; Finn, R. L.; Koutcher, J. A.; Larson, S. M.; Sgouros, G. *J. Nucl. Med.* **2003**, *44*, 1148-1155.
(22) Gordon, L. I.; Witzig, T. E.; Wiseman, G. A.; Flinn, I. W.; Spies, S. S.; Silverman, D. H.; Emmanuolides, C.; Cripe, L.; Saleh, M.; Czuczman, M. S.; Olejnik, T.; White, C. A.; Grillo-López, A. J. *Semin. Oncol.* **2002**, *29*, 87-92.
(23) Giblin, M. F.; Veerendra, B.; Smith, C. J. *In Vivo* **2005**, *19*, 9-29.
(24) Herzog, H.; Rösch, F.; Stöcklin, G.; Lueders, C.; Qaim, S. M.; Feinendegen, L. E. *J. Nucl. Med.* **1993**, *34*, 2222-2226.
(25) Rösch, F.; Baum, R. P. *Dalton Trans.* **2011**, *40*, 6104-6111.
(26) Kelkar, S. S.; Reineke, T. M. *Bioconjugate Chem.* **2011**, *22*, 1879-1903.

(27) Walrand, S.; Flux, G.; Konijnenberg, M.; Valkema, R.; Krenning, E.; Lhommel, R.; Pauwels, S.; Jamar, F. *Eur. J. Nucl. Med. Mol. Imaging* **2011**, *38*, 57-68.
(28) Zeglis, B. M.; Lewis, J. S. *Dalton Trans.* **2011**, *40*, 6168-6195.
(29) Zeng, D.; Zeglis, B. M.; Lewis, J. S.; Anderson, C. J. *J. Nucl. Med.* **2013**, *54*, 829-832.
(30) Zeglis, B. M.; Sevak, K. K.; Reiner, T.; Mohindra, P.; Carlin, S. D.; Zanzonico, P.; Weissleder, R.; Lewis, J. S. *J. Nucl. Med.* **2013**, *54*, 1389-1396.
(31) Reiner, T.; Keliher, E. J.; Earley, S.; Marinelli, B.; Weissleder, R. *Angew. Chem., Int. Ed.* **2011**, *50*, 1922-1925.
(32) Karver, M. R.; Weissleder, R.; Hilderbrand, S. A. *Angew. Chem., Int. Ed.* **2012**, *51*, 920-922.
(33) Karver, M. R.; Weissleder, R.; Hilderbrand, S. A. *Bioconjugate Chem.* **2011**, *22*, 2263-2270.
(34) Reiner, T.; Lacy, J.; Keliher, E.; Yang, K. S.; Ullal, A.; Kohler, R. H.; Vinegoni, C.; Weissleder, R. *Neoplasia* **2012**, *14*, 169-177.
(35) Lin, M.; Welch, M.; Lapi, S. *Mol. Imaging Biol.* **2013**, *15*, 1-8.
(36) Deri, M. A.; Zeglis, B. M.; Francesconi, L. C.; Lewis, J. S. *Nucl. Med. Biol.* **2013**, *40*, 3-14.
(37) Breeman, W. A. P.; de Blois, E.; Sze Chan, H.; Konijnenberg, M.; Kwekkeboom, D. J.; Krenning, E. P. *Semin. Nucl. Med.* **2011**, *41*, 314-321.
(38) Rice, S. L.; Roney, C. A.; Daumar, P.; Lewis, J. S. *Semin. Nucl. Med.* **2011**, *41*, 265-282.
(39) Li, Z.; Conti, P. S. *Adv. Drug Delivery Rev.* **2010**, *62*, 1031-1051.
(40) Glaser, M.; Robins, E. G. *J. Label. Compd. Radiopharm.* **2009**, *52*, 407-414.
(41) Urch, D. S. *Annual Reports Section "A" (Inorganic Chemistry)* **2009**, *105*, 460-476.
(42) Liu, S. *Adv. Drug Delivery Rev.* **2008**, *60*, 1347-1370.
(43) Lewis, J. S.; Anderson, C. J. In *Peptide Characterization and Application Protocols*; Fields, G. B., Ed.; Humana Press, Inc.: New York, 2007; Vol. 386, p 227-240.
(44) Wadas, T. J.; Wong, E. H.; Weisman, G. R.; Anderson, C. J. *Curr. Pharm. Des.* **2007**, *13*, 3-16.
(45) Boswell, C. A.; Brechbiel, M. W. *Nucl. Med. Biol.* **2007**, *34*, 757-778.
(46) van Dongen, G. A. M. S.; Visser, G. W. M.; Lub-de Hooge, M. N.; de Vries, E. G.; Perk, L. R. *The Oncologist* **2007**, *12*, 1379-1389.
(47) Urch, D. S.; Welch, M. J. *Annual Reports Section "A" (Inorganic Chemistry)* **2006**, *102*, 542-563.
(48) Liu, S. *ChemInform* **2005**, *36*, 445-461.
(49) Liu, S.; Edwards, D. In *Contrast agents II: optical, ultrasound, x-ray and radiopharmaceutical imaging*; Krause, W., Ed.; Springer-Verlag, Berlin Heidelberg: 2002; Vol. 222, p 259-278.
(50) Koehler, L.; Gagnon, K.; McQuarrie, S.; Wuest, F. *Molecules* **2010**, *15*, 2686-2718.
(51) Brechbiel, M. W. *Q. J. Nucl. Med. Mol. Imaging* **2008**, *52*, 166-173.
(52) Pagani, M.; Stone-Elander, S.; Larsson, S. A. *Eur. J. Nucl. Med. Mol. Imaging* **1997**, *24*, 1301-1327.
(53) Fani, M.; André, J. P.; Maecke, H. R. *Contrast Media Mol. Imaging* **2008**, *3*, 53-63.
(54) Hassfjell, S.; Brechbiel, M. W. *Chem. Rev.* **2001**, *101*, 2019-2036.
(55) Correia, J. D. G.; Paulo, A.; Raposinho, P. D.; Santos, I. *Dalton Trans.* **2011**, *40*, 6144-6167.

(56) Zeglis, B. M.; Mohindra, P.; Weissmann, G. I.; Divilov, V.; Hilderbrand, S. A.; Weissleder, R.; Lewis, J. S. *Bioconjugate Chem.* **2011**, *22*, 2048-2059.
(57) Byegård, J.; Skarnemark, G.; Skålberg, M. *J. Radioanal. Nucl. Chem.* **1999**, *241*, 281-290.
(58) Stimmel, J. B.; Kull Jr, F. C. *Nucl. Med. Biol.* **1998**, *25*, 117-125.
(59) Stimmel, J. B.; Stockstill, M. E.; Kull, F. C. *Bioconjugate Chem.* **1995**, *6*, 219-225.
(60) Camera, L.; Kinuya, S.; Garmestani, K.; Wu, C.; Brechbiel, M. W.; Pai, L. H.; McMurry, T. J.; Gansow, O. A.; Pastan, I.; Paik, C. H.; Carrasquillo, J. A. *J. Nucl. Med.* **1994**, *35*, 882-889.
(61) Harrison, A.; Walker, C. A.; Parker, D.; Jankowski, K. J.; Cox, J. P. L.; Craig, A. S.; Sansom, J. M.; Beeley, N. R. A.; Boyce, R. A.; Chaplin, L.; Eaton, M. A. W.; Farnsworth, A. P. H.; Millar, K.; Millican, A. T.; Randall, A. M.; Rhind, S. K.; Secher, D. S.; Turner, A. *Int. J. Rad. Appl. Instrum. [B]* **1991**, *18*, 469-476.
(62) Hancock, R. D. *J. Chem. Educ.* **1992**, *69*, 615-621.
(63) Liu, S.; Edwards, D. S. *Bioconjugate Chem.* **2000**, *12*, 7-34.
(64) Kukis, D. L.; DeNardo, S. J.; DeNardo, G. L.; O'Donnell, R. T.; Meares, C. F. *J. Nucl. Med.* **1998**, *39*, 2105-2110.
(65) Jang, Y. H.; Blanco, M.; Dasgupta, S.; Keire, D. A.; Shively, J. E.; Goddard, W. A. *J. Am. Chem. Soc.* **1999**, *121*, 6142-6151.
(66) Martell, A. E.; Smith, R. M. *Critical Stability Constants, Vol. 3: Other Organic Ligands*; Plenum Press: New York, 1977.
(67) Smith, R. M.; Martell, A. E. *Sci. Total Environ.* **1987**, *64*, 125-147.
(68) Clarke, E. T.; Martell, A. E. *Inorg. Chim. Acta* **1991**, *190*, 37-46.
(69) Harris, W. R.; Pecoraro, V. L. *Biochemistry* **1983**, *22*, 292-299.
(70) Raymond, K. N.; Müller, G.; Matzanke, B. In *Top. Curr. Chem.*; Boschke, F. L., Ed.; Springer-Verlag, Berlin, Heidelberg: 1984; Vol. 123, p 49-102.
(71) Kappel, M. J.; Raymond, K. N. *Inorg. Chem.* **1982**, *21*, 3437-3442.
(72) Woodin, K. S.; Heroux, K. J.; Boswell, C. A.; Wong, E. H.; Weisman, G. R.; Niu, W.; Tomellini, S. A.; Anderson, C. J.; Zakharov, L. N.; Rheingold, A. L. *Eur. J. Inorg. Chem.* **2005**, *2005*, 4829-4833.
(73) Morfin, J.-F.; Tóth, É. *Inorg. Chem.* **2011**, *50*, 10371-10378.
(74) Broan, C. J.; Cox, J. P. L.; Craig, A. S.; Kataky, R.; Parker, D.; Harrison, A.; Randall, A. M.; Ferguson, G. *J. Chem. Soc., Perkin Trans. 2* **1991**, 87-99.
(75) Kubíček, V.; Havlíčková, J.; Kotek, J.; Tircsó, G.; Hermann, P.; Tóth, É.; Lukeš, I. *Inorg. Chem.* **2010**, *49*, 10960-10969.
(76) Sun, X.; Wuest, M.; Weisman, G. R.; Wong, E. H.; Reed, D. P.; Boswell, C. A.; Motekaitis, R.; Martell, A. E.; Welch, M. J.; Anderson, C. J. *J. Med. Chem.* **2001**, *45*, 469-477.
(77) Bass, L. A.; Wang, M.; Welch, M. J.; Anderson, C. J. *Bioconjugate Chem.* **2000**, *11*, 527-532.
(78) Rae, T. D.; Schmidt, P. J.; Pufahl, R. A.; Culotta, V. C.; V. O'Halloran, T. *Science* **1999**, *284*, 805-808.
(79) Harris, W. R.; Messori, L. *Coord. Chem. Rev.* **2002**, *228*, 237-262.
(80) Sun, H.; Li, H.; Sadler, P. J. *Chem. Rev.* **1999**, *99*, 2817-2842.
(81) Harris, W. In *Less Common Metals in Proteins and Nucleic Acid Probes*; Clarke, M. J., Ed.; Springer-Verlag, Berlin Heidelberg: 1998; Vol. 92, p 121-162.
(82) Šimeček, J.; Hermann, P.; Wester, H.-J.; Notni, J. *ChemMedChem* **2013**, *8*, 95-103.
(83) Notni, J.; Pohle, K.; Wester, H.-J. *EJNMMI Res* **2012**, *2*, 1-5.
(84) Notni, J.; Šimeček, J.; Hermann, P.; Wester, H.-J. *Chem. Eur. J.* **2011**, *17*, 14718-14722.

(85) Šimeček, J.; Schulz, M.; Notni, J.; Plutnar, J.; Kubíček, V.; Havlíčková, J.; Hermann, P. *Inorg. Chem.* **2011**, *51*, 577-590.
(86) Zeng, D.; Anderson, C. J. *Solvent Extr. Ion Exch.* **2013**, *31*, 337-344.
(87) Price, E. W.; Zeglis, B. M.; Cawthray, J. F.; Ramogida, C. F.; Ramos, N.; Lewis, J. S.; Adam, M. J.; Orvig, C. *J. Am. Chem. Soc.* **2013**, *135*, 12707-12721.
(88) Bailey, G. A.; Price, E. W.; Zeglis, B. M.; Ferreira, C. L.; Boros, E.; Lacasse, M. J.; Patrick, B. O.; Lewis, J. S.; Adam, M. J.; Orvig, C. *Inorg. Chem.* **2012**, *51*, 12575-12589.
(89) Price, E. W.; Cawthray, J. F.; Bailey, G. A.; Ferreira, C. L.; Boros, E.; Adam, M. J.; Orvig, C. *J. Am. Chem. Soc.* **2012**, *134*, 8670-8683.
(90) Ferreira, C. L.; Lamsa, E.; Woods, M.; Duan, Y.; Fernando, P.; Bensimon, C.; Kordos, M.; Guenther, K.; Jurek, P.; Kiefer, G. E. *Bioconjugate Chem.* **2010**, *21*, 531-536.
(91) Ferreira, C. L.; Yapp, D. T.; Lamsa, E.; Gleave, M.; Bensimon, C.; Jurek, P.; Kiefer, G. E. *Nucl. Med. Biol.* **2008**, *35*, 875-882.
(92) Li, W. P.; Ma, D. S.; Higginbotham, C.; Hoffman, T.; Ketring, A. R.; Cutler, C. S.; Jurisson, S. S. *Nucl. Med. Biol.* **2001**, *28*, 145-154.
(93) Ando, A.; Ando, I.; Hiraki, T.; Hisada, K. *Int. J. Rad. Appl. Instrum. [B]* **1989**, *16*, 57-80.
(94) Cooper, M. S.; Ma, M. T.; Sunassee, K.; Shaw, K. P.; Williams, J. D.; Paul, R. L.; Donnelly, P. S.; Blower, P. J. *Bioconjugate Chem.* **2012**, *23*, 1029-1039.
(95) Laitinen, I.; Notni, J.; Pohle, K.; Rudelius, M.; Farrell, E.; Nekolla, S.; Henriksen, G.; Neubauer, S.; Kessler, H.; Wester, H.-J. *EJNMMI Res* **2013**, *3*, 1-9.
(96) Hofmann, M. H.; Maecke, H. M.; Börner, A.; Weckesser, E. W.; Schöffski, P.; Oei, M. O.; Schumacher, J. S.; Henze, M. H.; Heppeler, A. H.; Meyer, G. M.; Knapp, W. K. *Eur. J. Nucl. Med. Mol. Imaging* **2001**, *28*, 1751-1757.
(97) Liu, S.; Pietryka, J.; Ellars, C. E.; Edwards, D. S. *Bioconjugate Chem.* **2002**, *13*, 902-913.
(98) Fichna, J.; Janecka, A. *Bioconjugate Chem.* **2003**, *14*, 3-17.
(99) Chappell, L. L.; Rogers, B. E.; Khazaeli, M. B.; Mayo, M. S.; Buchsbaum, D. J.; Brechbiel, M. W. *Bioorg. Med. Chem.* **1999**, *7*, 2313-2320.
(100) Eigner, S.; Vera, D. R. B.; Fellner, M.; Loktionova, N. S.; Piel, M.; Lebeda, O.; Rösch, F.; Roß, T. L.; Henke, K. E. *Mol. Imaging Biol.* **2013**, *15*, 79-86.
(101) Filosofov, D. V.; Loktionova, N. S.; Rösch, F. *Radiochim. Acta* **2010**, *98*, 149-156.
(102) Majkowska-Pilip, A.; Bilewicz, A. *J. Inorg. Biochem.* **2011**, *105*, 313-320.
(103) Chappell, L. L.; Deal, K. A.; Dadachova, E.; Brechbiel, M. W. *Bioconjugate Chem.* **2000**, *11*, 510-519.
(104) Chaves, S.; Delgado, R.; Da Silva, J. J. R. F. *Talanta* **1992**, *39*, 249-254.
(105) Delgado, R.; da Silva, J. J. R. F. *Talanta* **1982**, *29*, 815-822.
(106) Garrison, J. C.; Rold, T. L.; Sieckman, G. L.; Figueroa, S. D.; Volkert, W. A.; Jurisson, S. S.; Hoffman, T. J. *J. Nucl. Med.* **2007**, *48*, 1327-1337.
(107) McQuade, P.; Miao, Y.; Yoo, J.; Quinn, T. P.; Welch, M. J.; Lewis, J. S. *J. Med. Chem.* **2005**, *48*, 2985-2992.
(108) Hausner, S. H.; Kukis, D. L.; Gagnon, M. K. J.; Stanecki, C. E.; Ferdani, R.; Marshall, J. F.; Anderson, C. J.; Sutcliffe, J. L. *Mol. Imaging* **2009**, *8*, 111-121.
(109) Biddlecombe, G. B.; Rogers, B. E.; de Visser, M.; Parry, J. J.; de Jong, M.; Erion, J. L.; Lewis, J. S. *Bioconjugate Chem.* **2007**, *18*, 724-730.
(110) Martell, A. E.; Motekaitis, R. J.; Clarke, E. T.; Delgado, R.; Sun, Y.; Ma, R. *Supramol. Chem.* **1996**, *6*, 353-363.

(111) Velikyan, I.; Sundberg, Å. L.; Lindhe, Ö.; Höglund, A. U.; Eriksson, O.; Werner, E.; Carlsson, J.; Bergström, M.; Långström, B.; Tolmachev, V. *J. Nucl. Med.* **2005**, *46*, 1881-1888.
(112) Dimitrakopoulou-Strauss, A.; Hohenberger, P.; Haberkorn, U.; Mäcke, H. R.; Eisenhut, M.; Strauss, L. G. *J. Nucl. Med.* **2007**, *48*, 1245-1250.
(113) Kramer-Marek, G.; Shenoy, N.; Seidel, J.; Griffiths, G.; Choyke, P.; Capala, J. *Eur. J. Nucl. Med. Mol. Imaging* **2011**, *38*, 1967-1976.
(114) Decristoforo, C.; Hernandez Gonzalez, I.; Carlsen, J.; Rupprich, M.; Huisman, M.; Virgolini, I.; Wester, H.-J.; Haubner, R. *Eur. J. Nucl. Med. Mol. Imaging* **2008**, *35*, 1507-1515.
(115) Gabriel, M.; Decristoforo, C.; Kendler, D.; Dobrozemsky, G.; Heute, D.; Uprimny, C.; Kovacs, P.; Von Guggenberg, E.; Bale, R.; Virgolini, I. J. *J. Nucl. Med.* **2007**, *48*, 508-518.
(116) Wei, L.; Miao, Y.; Gallazzi, F.; Quinn, T. P.; Welch, M. J.; Vavere, A. L.; Lewis, J. S. *Nucl. Med. Biol.* **2007**, *34*, 945-953.
(117) Sun, Y.; Anderson, C. J.; Pajeau, T. S.; Reichert, D. E.; Hancock, R. D.; Motekaitis, R. J.; Martell, A. E.; Welch, M. J. *J. Med. Chem.* **1996**, *39*, 458-470.
(118) Boros, E.; Ferreira, C. L.; Cawthray, J. F.; Price, E. W.; Patrick, B. O.; Wester, D. W.; Adam, M. J.; Orvig, C. *J. Am. Chem. Soc.* **2010**, *132*, 15726-15733.
(119) Martell, A. E.; Smith, R. M. *Critical Stability Constants, Vol. 1-6*; Plenum Press: New York, 1974-1989.
(120) Liu, S.; He, Z.; Hsieh, W.-Y.; Fanwick, P. E. *Inorg. Chem.* **2003**, *42*, 8831-8837.
(121) Li, L.; Bading, J.; Yazaki, P. J.; Ahuja, A. H.; Crow, D.; Colcher, D.; Williams, L. E.; Wong, J. Y. C.; Raubitschek, A.; Shively, J. E. *Bioconjugate Chem.* **2007**, *19*, 89-96.
(122) Chakraborty, S.; Shi, J.; Kim, Y.-S.; Zhou, Y.; Jia, B.; Wang, F.; Liu, S. *Bioconjugate Chem.* **2010**, *21*, 969-978.
(123) Tatsi, A.; Maina, T.; Cescato, R.; Waser, B.; Krenning, E.; de Jong, M.; Cordopatis, P.; Reubi, J.; Nock, B. *EJNMMI Res* **2012**, *2*, 1-13.
(124) Breeman, W. A. P.; de Jong, M.; Visser, T. J.; Erion, J. L.; Krenning, E. P. *Eur. J. Nucl. Med. Mol. Imaging* **2003**, *30*, 917-920.
(125) Tóth, È.; Brücher, E. *Inorg. Chim. Acta* **1994**, *221*, 165-167.
(126) Hens, M.; Vaidyanathan, G.; Zhao, X.-G.; Bigner, D. D.; Zalutsky, M. R. *Nucl. Med. Biol.* **2010**, *37*, 741-750.
(127) Kang, C. S.; Sun, X.; Jia, F.; Song, H. A.; Chen, Y.; Lewis, M.; Chong, H.-S. *Bioconjugate Chem.* **2012**, *23*, 1775-1782.
(128) Milenic, D. E.; Garmestani, K.; Chappell, L. L.; Dadachova, E.; Yordanov, A.; Ma, D.; Schlom, J.; Brechbiel, M. W. *Nucl. Med. Biol.* **2002**, *29*, 431-442.
(129) Rasaneh, S.; Rajabi, H.; Babaei, M. H.; Johari Daha, F. *J. Label. Compd. Radiopharm.* **2010**, *53*, 575-579.
(130) Perk, L. R.; Visser, G. W. M.; Vosjan, M. J. W. D.; Stigter-van Walsum, M.; Tijink, B. M.; Leemans, C. R.; van Dongen, G. A. M. S. *J. Nucl. Med.* **2005**, *46*, 1898-1906.
(131) Kumar, K.; Chang, C. A.; Francesconi, L. C.; Dischino, D. D.; Malley, M. F.; Gougoutas, J. Z.; Tweedle, M. F. *Inorg. Chem.* **1994**, *33*, 3567-3575.
(132) Koudelková, M.; Vinšová, H.; Jedináková-Křížová, V. *J. Chromatogr. A* **2003**, *990*, 311-316.
(133) Norenberg, J. P.; Krenning, B. J.; Konings, I. R. H. M.; Kusewitt, D. F.; Nayak, T. K.; Anderson, T. L.; de Jong, M.; Garmestani, K.; Brechbiel, M. W.; Kvols, L. K. *Clin. Cancer Res.* **2006**, *12*, 897-903.

(134) Cordier, D.; Forrer, F.; Bruchertseifer, F.; Morgenstern, A.; Apostolidis, C.; Good, S.; Müller-Brand, J.; Mäcke, H.; Reubi, J. C.; Merlo, A. *Eur. J. Nucl. Med. Mol. Imaging* **2010**, *37*, 1335-1344.
(135) Wild, D.; Frischknecht, M.; Zhang, H.; Morgenstern, A.; Bruchertseifer, F.; Boisclair, J.; Provencher-Bolliger, A.; Reubi, J.-C.; Maecke, H. R. *Cancer Res.* **2011**, *71*, 1009-1018.
(136) Horak, E.; Hartmann, F.; Garmestani, K.; Wu, C.; Brechbiel, M.; Gansow, O. A.; Landolfi, N. F.; Waldmann, T. A. *J. Nucl. Med.* **1997**, *38*, 1944-1950.
(137) Ruble, G.; Wu, C.; Squire, R. A.; Gansow, O. A.; Strand, M. *Int. J. Radiat. Oncol., Biol., Phys.* **1996**, *34*, 609-616.
(138) Baidoo, K. E.; Milenic, D. E.; Brechbiel, M. W. *Nucl. Med. Biol.* **2013**, *40*, 592-599.
(139) McDevitt, M. R.; Ma, D.; Simon, J.; Frank, R. K.; Scheinberg, D. A. *Appl. Radiat. Isot.* **2002**, *57*, 841-847.
(140) Ballangrud, Å. M.; Yang, W.-H.; Palm, S.; Enmon, R.; Borchardt, P. E.; Pellegrini, V. A.; McDevitt, M. R.; Scheinberg, D. A.; Sgouros, G. *Clin. Cancer Res.* **2004**, *10*, 4489-4497.
(141) Mier, W.; Hoffend, J.; Krämer, S.; Schuhmacher, J.; Hull, W. E.; Eisenhut, M.; Haberkorn, U. *Bioconjugate Chem.* **2004**, *16*, 237-240.
(142) Chappell, L. L.; Ma, D.; Milenic, D. E.; Garmestani, K.; Venditto, V.; Beitzel, M. P.; Brechbiel, M. W. *Nucl. Med. Biol.* **2003**, *30*, 581-595.
(143) McMurry, T. J.; Brechbiel, M.; Kumar, K.; Gansow, O. A. *Bioconjugate Chem.* **1992**, *3*, 108-117.
(144) Eisenwiener, K.-P.; Powell, P.; Mäcke, H. R. *Bioorg. Med. Chem. Lett.* **2000**, *10*, 2133-2135.
(145) Bernhard, C.; Moreau, M.; Lhenry, D.; Goze, C.; Boschetti, F.; Rousselin, Y.; Brunotte, F.; Denat, F. *Chem. Eur. J.* **2012**, *18*, 7834-7841.
(146) Song, H.; Hobbs, R. F.; Vajravelu, R.; Huso, D. L.; Esaias, C.; Apostolidis, C.; Morgenstern, A.; Sgouros, G. *Cancer Res.* **2009**, *69*, 8941-8948.
(147) Miederer, M.; McDevitt, M. R.; Sgouros, G.; Kramer, K.; Cheung, N.-K. V.; Scheinberg, D. A. *J. Nucl. Med.* **2004**, *45*, 129-137.
(148) Boswell, C. A.; Sun, X.; Niu, W.; Weisman, G. R.; Wong, E. H.; Rheingold, A. L.; Anderson, C. J. *J. Med. Chem.* **2004**, *47*, 1465-1474.
(149) Niu, W.; Wong, E. H.; Weisman, G. R.; Peng, Y.; Anderson, C. J.; Zakharov, L. N.; Golen, J. A.; Rheingold, A. L. *Eur. J. Inorg. Chem.* **2006**, *2006*, 676-677.
(150) Carlton, L.; Hancock, R. D.; Maumela, H.; Wainwright, K. P. *J. Chem. Soc., Chem. Commun.* **1994**, *0*, 1007-1008.
(151) Yong, K. J.; Milenic, D. E.; Baidoo, K. E.; Brechbiel, M. W. *Br. J. Cancer* **2013**, *108*, 2013-2020.
(152) Yong, K. J.; Milenic, D. E.; Baidoo, K. E.; Brechbiel, M. W. *Int. J. Radiat. Oncol., Biol., Phys.* **2013**, *85*, 1119-1126.
(153) Chappell, L. L.; Dadachova, E.; Milenic, D. E.; Garmestani, K.; Wu, C.; Brechbiel, M. W. *Nucl. Med. Biol.* **2000**, *27*, 93-100.
(154) Maumela, H.; Hancock, R. D.; Carlton, L.; Reibenspies, J. H.; Wainwright, K. P. *J. Am. Chem. Soc.* **1995**, *117*, 6698-6707.
(155) Song, H. A.; Kang, C. S.; Baidoo, K. E.; Milenic, D. E.; Chen, Y.; Dai, A.; Brechbiel, M. W.; Chong, H.-S. *Bioconjugate Chem.* **2011**, *22*, 1128-1135.
(156) Ait-Mohand, S.; Fournier, P.; Dumulon-Perreault, V. r.; Kiefer, G. E.; Jurek, P.; Ferreira, C. L.; Bénard, F. o.; Guérin, B. *Bioconjugate Chem.* **2011**, *22*, 1729-1735.

(157) Yapp, D. T.; Ferreira, C. L.; Gill, R. K.; Boros, E.; Wong, M. Q.; Mandel, D.; Jurek, P.; Kiefer, G. E. *Mol. Imaging* **2013**, *12*, 263-272.
(158) Knetsch, P. A.; Petrik, M.; Rangger, C.; Seidel, G.; Pietzsch, H.-J.; Virgolini, I.; Decristoforo, C.; Haubner, R. *Nucl. Med. Biol.* **2013**, *40*, 65-72.
(159) Knetsch, P. A.; Petrik, M.; Rangger, C.; Seidel, G.; Pietzsch, H. J.; Virgolini, I.; Decristoforo, C.; Haubner, R. *Nucl. Med. Biol.* **2013**, *40*, 65-72.
(160) Bartoś, B.; Lyczko, K.; Kasperek, A.; Krajewski, S.; Bilewicz, A. *J. Radioanal. Nucl. Chem.* **2013**, *295*, 205-209.
(161) Chong, H.-S.; Milenic, D. E.; Garmestani, K.; Brady, E. D.; Arora, H.; Pfiester, C.; Brechbiel, M. W. *Nucl. Med. Biol.* **2006**, *33*, 459-467.
(162) Yong, K.; Brechbiel, M. W. *Dalton Trans.* **2011**, *40*, 6068-6076.
(163) Baes, C. F., Jr.; Mesmer, R. E. *The Hydrolysis of Cations*; Wiley-Interscience: New York, 1976.
(164) Anderson, C. J.; Dehdashti, F.; Cutler, P. D.; Schwarz, S. W.; Laforest, R.; Bass, L. A.; Lewis, J. S.; McCarthy, D. W. *J. Nucl. Med.* **2001**, *42*, 213-221.
(165) Blower, P. J.; Lewis, J. S.; Zweit, J. *Nucl. Med. Biol.* **1996**, *23*, 957-980.
(166) Pandya, D. N.; Kim, J. Y.; Park, J. C.; Lee, H.; Phapale, P. B.; Kwak, W.; Choi, T. H.; Cheon, G. J.; Yoon, Y.-R.; Yoo, J. *Chem. Commun.* **2010**, *46*, 3517-3519.
(167) Dale, A. V.; Pandya, D. N.; Kim, J. Y.; Lee, H.; Ha, Y. S.; Bhatt, N.; Kim, J.; Seo, J. J.; Lee, W.; Kim, S.; Yoon, Y.-R.; An, G. I.; Yoo, J. *ACS Med. Chem. Lett.* **2013**, *4*, 927-931.
(168) Clarke, E. T.; Martell, A. E. *Inorg. Chim. Acta* **1991**, *190*, 27-36.
(169) Kodama, M.; Koike, T.; Mahatma, A. B.; Kimura, E. *Inorg. Chem.* **1991**, *30*, 1270-1273.
(170) Lewis, M. R.; Boswell, C. A.; Laforest, R.; Buettner, T. L.; Ye, D.; Connett, J. M.; Anderson, C. J. *Cancer Biother. Radiopharm.* **2001**, *16*, 483-494.
(171) Maillet, M.; Kwok, C. S.; Noujaim, A. A.; Snieckus, V. *Tetrahedron Lett.* **1998**, *39*, 2659-2662.
(172) Deshpande, S. V.; DeNardo, S. J.; Meares, C. F.; McCall, M. J.; Adams, G. P.; Moi, M. K.; DeNardo, G. L. *J. Nucl. Med.* **1988**, *29*, 217-225.
(173) Wei, L.; Ye, Y.; Wadas, T. J.; Lewis, J. S.; Welch, M. J.; Achilefu, S.; Anderson, C. J. *Nucl. Med. Biol.* **2009**, *36*, 277-285.
(174) Ferdani, R.; Stigers, D. J.; Fiamengo, A. L.; Wei, L.; Li, B. T. Y.; Golen, J. A.; Rheingold, A. L.; Weisman, G. R.; Wong, E. H.; Anderson, C. J. *Dalton Trans.* **2012**, *41*, 1938-1950.
(175) Dumont, R. A.; Deininger, F.; Haubner, R.; Maecke, H. R.; Weber, W. A.; Fani, M. *J. Nucl. Med.* **2011**, *52*, 1276-1284.
(176) Fani, M.; Del Pozzo, L.; Abiraj, K.; Mansi, R.; Tamma, M. L.; Cescato, R.; Waser, B.; Weber, W. A.; Reubi, J. C.; Maecke, H. R. *J. Nucl. Med.* **2011**, *52*, 1110-1118.
(177) Sprague, J. E.; Peng, Y.; Fiamengo, A. L.; Woodin, K. S.; Southwick, E. A.; Weisman, G. R.; Wong, E. H.; Golen, J. A.; Rheingold, A. L.; Anderson, C. J. *J. Med. Chem.* **2007**, *50*, 2527-2535.
(178) Eiblmaier, M.; Andrews, R.; Laforest, R.; Rogers, B. E.; Anderson, C. J. *J. Nucl. Med.* **2007**, *48*, 1390-1396.
(179) Boswell, C. A.; Regino, C. A. S.; Baidoo, K. E.; Wong, K. J.; Bumb, A.; Xu, H.; Milenic, D. E.; Kelley, J. A.; Lai, C. C.; Brechbiel, M. W. *Bioconjugate Chem.* **2008**, *19*, 1476-1484.
(180) Stigers, D. J.; Ferdani, R.; Weisman, G. R.; Wong, E. H.; Anderson, C. J.; Golen, J. A.; Moore, C.; Rheingold, A. L. *Dalton Trans.* **2010**, *39*, 1699-1701.

(181) Suzuki, K.; Satake, M.; Suwada, J.; Oshikiri, S.; Ashino, H.; Dozono, H.; Hino, A.; Kasahara, H.; Minamizawa, T. *Nucl. Med. Biol.* **2011**, *38*, 1011-1018.
(182) Lears, K. A.; Ferdani, R.; Liang, K.; Zheleznyak, A.; Andrews, R.; Sherman, C. D.; Achilefu, S.; Anderson, C. J.; Rogers, B. E. *J. Nucl. Med.* **2011**, *52*, 470-477.
(183) Di Bartolo, N.; Sargeson, A. M.; Smith, S. V. *Org. Biomol. Chem.* **2006**, *4*, 3350-3357.
(184) Di Bartolo, N. M.; Sargeson, A. M.; Donlevy, T. M.; Smith, S. V. *Dalton Trans.* **2001**, *0*, 2303-2309.
(185) Liu, S.; Li, Z.; Yap, L.-P.; Huang, C.-W.; Park, R.; Conti, P. S. *Chem. Eur. J.* **2011**, *17*, 10222-10225.
(186) Mume, E.; Asad, A.; Di Bartolo, N. M.; Kong, L.; Smith, C.; Sargeson, A. M.; Price, R.; Smith, S. V. *Dalton Trans.* **2013**, 14402-14410.
(187) Velikyan, I.; Maecke, H.; Langstrom, B. *Bioconjugate Chem.* **2008**, *19*, 569-573.
(188) Clarke, E. T.; Martell, A. E. *Inorg. Chim. Acta* **1991**, *181*, 273-280.
(189) Lin, M.; Ranganathan, D.; Lapi, S.; Welch, M. *J NUCL MED MEETING ABSTRACTS* **2012**, *53*, 1457-.
(190) Shannon, R. *Acta Crystallogr.* **1976**, *A32*, 751-767.
(191) Zhang, Y.; Hong, H.; Engle, J. W.; Bean, J.; Yang, Y.; Leigh, B. R.; Barnhart, T. E.; Cai, W. *PLoS One* **2011**, *6*, e28005.
(192) Chang, A. J.; Sohn, R.; Lu, Z. H.; Arbeit, J. M.; Lapi, S. E. *PLoS One* **2013**, *8*, e58949.
(193) Bevilacqua, A.; Gelb, R. I.; Hebard, W. B.; Zompa, L. J. *Inorg. Chem.* **1987**, *26*, 2699-2706.
(194) Strand, J.; Honarvar, H.; Perols, A.; Orlova, A.; Selvaraju, R. K.; Karlström, A. E.; Tolmachev, V. *PLoS One* **2013**, *8*, e70028.
(195) Fuchs, A.; Greguric, I.; Roe, G. *Nucl. Med. Biol.* **2010**, *37*, 692.
(196) McMurry, T. J.; Brechbiel, M.; Wu, C.; Gansow, O. A. *Bioconjugate Chem.* **1993**, *4*, 236-245.
(197) Eisenwiener, K.-P.; Prata, M. I. M.; Buschmann, I.; Zhang, H.-W.; Santos, A. C.; Wenger, S.; Reubi, J. C.; Maecke, H. R. *Bioconjugate Chem.* **2002**, *13*, 530-541.
(198) Tolmachev, V.; Altai, M.; Sandström, M.; Perols, A.; Karlström, A. E.; Boschetti, F.; Orlova, A. *Bioconjugate Chem.* **2011**, *22*, 894-902.
(199) André, J. P.; Maecke, H. R.; Zehnder, M.; Macko, L.; Akyel, K. G. *Chem. Commun.* **1998**, 1301-1302.
(200) Chong, H.-S.; Song, H. A.; Birch, N.; Le, T.; Lim, S.; Ma, X. *Bioorg. Med. Chem. Lett.* **2008**, *18*, 3436-3439.
(201) Chong, H.-S.; Song, H. A.; Ma, X.; E. Milenic, D.; D. Brady, E.; Lim, S.; Lee, H.; Baidoo, K.; Cheng, D.; Brechbiel, M. W. *Bioconjugate Chem.* **2008**, *19*, 1439-1447.
(202) Chong, H.-s.; Garmestani, K.; Ma, D.; Milenic, D. E.; Overstreet, T.; Brechbiel, M. W. *J. Med. Chem.* **2002**, *45*, 3458-3464.
(203) Kang, C. S.; Song, H. A.; Milenic, D. E.; Baidoo, K. E.; Brechbiel, M. W.; Chong, H.-S. *Nucl. Med. Biol.* **2013**, *40*, 600-605.
(204) Chong, H.-S.; Song, H. A.; Kang, C. S.; Le, T.; Sun, X.; Dadwal, M.; Lee, H.; Lan, X.; Chen, Y.; Dai, A. *Chem. Commun.* **2011**, *47*, 5584-5586.
(205) Ma, R.; Welch, M. J.; Reibenspies, J.; Martell, A. E. *Inorg. Chim. Acta* **1995**, *236*, 75-82.
(206) Sun, Y.; Cutler, C. S.; Martell, A. E.; Welch, M. J. *Tetrahedron* **1999**, *55*, 5733-5740.
(207) Sun, Y.; Martell, A. E.; Motekaitis, R. J.; Welch, M. J. *Tetrahedron* **1998**, *54*, 4203-4210.

(208) Chong, H.-S.; Ma, X.; Lee, H.; Bui, P.; Song, H. A.; Birch, N. *J. Med. Chem.* **2008**, *51*, 2208-2215.
(209) Aschoff, P.; Öksüz, M.; Kemke, B.; Zhernosekov, K.; Jennewein, M.; Rösch, F.; Bihl, H. *Nuklearmedizin* **2005**, *44*, A58(V144).
(210) Aschoff, P.; Kemke, B.; Öksüz, M.; Zhernosekov, K.; Jennewein, M.; Rösch, F.; Bihl, H. *Nuklearmedizin* **2005**, *44*, A59(V146).
(211) Hohloch, K.; Zinzani, P. L.; Linkesch, W.; Jurczak, W.; Deptala, A.; Lorsbach, M.; Windemuth-Kiesselbach, C.; Wulf, G. G.; Truemper, L. H. *Bone Marrow. Transplant.* **2010**, *46*, 901-903.
(212) *clinicaltrials.gov*, Accessed July 29, **2013**
(213) Carrasquillo, J. A.; White, J. D.; Paik, C. H.; Raubitschek, A.; Le, N.; Rotman, M.; Brechbiel, M. W.; Gansow, O. A.; Top, L. E.; Perentesis, P.; Reynolds, J. C.; Nelson, D. L.; Waldmann, T. A. *J. Nucl. Med.* **1999**, *40*, 268-276.
(214) Sharkey, R. M.; Burton, J.; Goldenberg, D. M. *Expert Rev. Clin. Immunol.* **2005**, *1*, 47-62.
(215) Brechbiel, M. W.; Gansow, O. A.; Atcher, R. W.; Schlom, J.; Esteban, J.; Simpson, D.; Colcher, D. *Inorg. Chem.* **1986**, *25*, 2772-2781.
(216) Wu, C.; Kobayashi, H.; Sun, B.; Yoo, T. M.; Paik, C. H.; Gansow, O. A.; Carrasquillo, J. A.; Pastan, I.; Brechbiel, M. W. *Bioorg. Med. Chem.* **1997**, *5*, 1925-1934.
(217) Panizzi, P.; Nahrendorf, M.; Figueiredo, J.-L.; Panizzi, J.; Marinelli, B.; Iwamoto, Y.; Keliher, E.; Maddur, A. A.; Waterman, P.; Kroh, H. K.; Leuschner, F.; Aikawa, E.; Swirski, F. K.; Pittet, M. J.; Hackeng, T. M.; Fuentes-Prior, P.; Schneewind, O.; Bock, P. E.; Weissleder, R. *Nat. Med.* **2011**, *17*, 1142-1146.
(218) Kojima, S.; Jay, M. *Eur. J. Nucl. Med.* **1987**, *13*, 366-370.
(219) Bakker, W. H.; Albert, R.; Bruns, C.; Breeman, W. A. P.; Hofland, L. J.; Marbach, P.; Pless, J.; Pralet, D.; Stolz, B.; Koper, J. W.; Lamberts, S. W. J.; Visser, T. J.; Krenning, E. P. *Life Sci.* **1991**, *49*, 1583-1591.
(220) Lub-de Hooge, M. N.; Kosterink, J. G. W.; Perik, P. J.; Nijnuis, H.; Tran, L.; Bart, J.; Suurmeijer, A. J. H.; de Jong, S.; Jager, P. L.; de Vries, E. G. E. *Br. J. Pharmacol.* **2004**, *143*, 99-106.
(221) Liu, S.; Edwards, D. S. *Bioconjugate Chem.* **2001**, *12*, 630-634.
(222) Koppe, M. J.; Bleichrodt, R. P.; Soede, A. C.; Verhofstad, A. A.; Goldenberg, D. M.; Oyen, W. J. G.; Boerman, O. C. *J. Nucl. Med.* **2004**, *45*, 1224-1232.
(223) Perk, L. R.; Visser, O. J.; Stigter-van Walsum, M.; Vosjan, M. J. W. D.; Visser, G. W. M.; Zijlstra, J. M.; Huijgens, P. C.; Dongen, G. A. M. S. *Eur. J. Nucl. Med. Mol. Imaging* **2006**, *33*, 1337-1345.
(224) Kozak, R. W.; Waldmann, T. A.; Atcher, R. W.; Gansow, O. A. *Trends Biotechnol.* **1986**, *4*, 259-264.
(225) Milenic, D. E.; Roselli, M.; Mirzadeh, S.; Pippin, C. G.; Gansow, O. A.; Colcher, D.; Brechbiel, M. W.; Schlom., J. *Cancer Biother. Radiopharm.* **2001**, *16*, 133-146.
(226) Ruegg, C. L.; Anderson-Berg, W. T.; Brechbiel, M. W.; Mirzadeh, S.; Gansow, O. A.; Strand, M. *Cancer Res.* **1990**, *50*, 4221-4226.
(227) Brechbiel, M. W.; Gansow, O. A. *Bioconjugate Chem.* **1991**, *2*, 187-194.
(228) Camera, L.; Kinuya, S.; Garmestani, K.; Pai, L. H.; Brechbiel, M. W.; Gansow, O. A.; Paik, C. H.; Pastan, I.; Carrasquillo, J. A. *Nucl. Med. Biol.* **1993**, *20*, 955-962.

(229) Camera, L.; Kinuya, S.; Garmestani, K.; Brechbiel, M.; Wu, C.; Pai, L.; McMurry, T.; Gansow, O.; Pastan, I.; Paik, C.; Carrasquillo, J. *Eur. J. Nucl. Med.* **1994**, *21*, 640-646.
(230) Roselli, M.; Schlom, J.; Gansow, O. A.; Brechbiel, M. W.; Mirzadeh, S.; Pippin, C. G.; Milenic, D. E.; Colcher, D. *Int. J. Rad. Appl. Instrum. [B]* **1991**, *18*, 389-394.
(231) Wei, L.; Zhang, X.; Gallazzi, F.; Miao, Y.; Jin, X.; Brechbiel, M. W.; Xu, H.; Clifford, T.; Welch, M. J.; Lewis, J. S.; Quinn, T. P. *Nucl. Med. Biol.* **2009**, *36*, 345-354.
(232) Schneider, D. W.; Heitner, T.; Alicke, B.; Light, D. R.; McLean, K.; Satozawa, N.; Parry, G.; Yoo, J.; Lewis, J. S.; Parry, R. *J. Nucl. Med.* **2009**, *50*, 435-443.
(233) Blend, M. J.; Stastny, J. J.; Swanson, S. M.; Brechbiel., M. W. *Cancer Biother. Radiopharm.* **2003**, *18*, 355-363.
(234) Borgman, M. P.; Coleman, T.; Kolhatkar, R. B.; Geyser-Stoops, S.; Line, B. R.; Ghandehari, H. *J. Controlled Release* **2008**, *132*, 193-199.
(235) Malmberg, J.; Tolmachev, V.; Orlova, A. *Experimental and Therapeutic Medicine* **2011**, *2*, 523-528.
(236) Tolmachev, V.; Wållberg, H.; Andersson, K.; Wennborg, A.; Lundqvist, H.; Orlova, A. *Eur. J. Nucl. Med. Mol. Imaging* **2009**, *36*, 1460-1468.
(237) Hosseinimehr, S. J.; Orlova and, A.; Tolmachev, V. *Hum. Antib.* **2010**, *19*, 107-111.
(238) McMurry, T. J.; Pippin, C. G.; Wu, C.; Deal, K. A.; Brechbiel, M. W.; Mirzadeh, S.; Gansow, O. A. *J. Med. Chem.* **1998**, *41*, 3546-3549.
(239) Nayak, T. K.; Garmestani, K.; Baidoo, K. E.; Milenic, D. E.; Brechbiel, M. W. *Int. J. Cancer* **2011**, *128*, 920-926.
(240) Nayak, T. K.; Garmestani, K.; Baidoo, K. E.; Milenic, D. E.; Brechbiel, M. W. *J. Nucl. Med.* **2010**, *51*, 942-950.
(241) Nayak, T.; Regino, C.; Wong, K.; Milenic, D.; Garmestani, K.; Baidoo, K.; Szajek, L.; Brechbiel, M. *Eur. J. Nucl. Med. Mol. Imaging* **2010**, *37*, 1368-1376.
(242) Clifford, T.; Boswell, C. A.; Biddlecombe, G. B.; Lewis, J. S.; Brechbiel, M. W. *J. Med. Chem.* **2006**, *49*, 4297-4304.
(243) Lee, F. T.; Mountain, A. J.; Kelly, M. P.; Hall, C.; Rigopoulos, A.; Johns, T. G.; Smyth, F. E.; Brechbiel, M. W.; Nice, E. C.; Burgess, A. W.; Scott, A. M. *Clin. Cancer Res.* **2005**, *11*, 7080s-7086s.
(244) Brechbiel, M. W.; Gansow, O. A.; Pippin, C. G.; Rogers, R. D.; Planalp, R. P. *Inorg. Chem.* **1996**, *35*, 6343-6348.
(245) Nikula, T. K.; McDevitt, M. R.; Finn, R. D.; Wu, C.; Kozak, R. W.; Garmestani, K.; Brechbiel, M. W.; Curcio, M. J.; Pippin, C. G.; Tiffany-Jones, L.; Geerlings, M. W.; Apostolidis, C.; Molinet, R.; Gansow, O. A.; Scheinberg, D. A. *J. Nucl. Med.* **1999**, *40*, 166-176.
(246) McDevitt, M. R.; Finn, R. D.; Ma, D.; Larson, S. M.; Scheinberg, D. A. *J. Nucl. Med.* **1999**, *40*, 1722-1727.
(247) Brechbiel, M. W.; Gansow, O. A. *J. Chem. Soc., Perkin Trans. 1* **1992**, *0*, 1173-1178.
(248) Gansow, O. A. *Int. J. Rad. Appl. Instrum. [B]* **1991**, *18*, 369-381.
(249) Šimeček, J.; Hermann, P.; Havlíčková, J.; Herdtweck, E.; Kapp, T. G.; Engelbogen, N.; Kessler, H.; Wester, H.-J.; Notni, J. *Chem. Eur. J.* **2013**, *19*, 7748-7757.
(250) Notni, J.; Pohle, K.; Wester, H.-J. *Nucl. Med. Biol.* **2013**, *40*, 33-41.
(251) Notni, J.; Plutnar, J.; Wester, H.-J. *EJNMMI Res* **2012**, *2*, 1-4.
(252) Šimeček, J.; Zemek, O.; Hermann, P.; Wester, H.-J.; Notni, J. *ChemMedChem* **2012**, *7*, 1375-1378.

(253) Notni, J.; Hermann, P.; Havlíčková, J.; Kotek, J.; Kubíček, V.; Plutnar, J.; Loktionova, N.; Riss, P. J.; Rösch, F.; Lukeš, I. *Chem. Eur. J.* **2010**, *16*, 7174-7185.
(254) Simecek, J.; Wester, H.-J.; Notni, J. *Dalton Trans.* **2012**, *41*, 13803-13806.
(255) Baranyai, Z.; Uggeri, F.; Giovenzana, G. B.; Bényei, A.; Brücher, E.; Aime, S. *Chem. Eur. J.* **2009**, *15*, 1696-1705.
(256) Waldron, B. P.; Parker, D.; Burchardt, C.; Yufit, D. S.; Zimny, M.; Roesch, F. *Chem. Commun.* **2013**, *49*, 579-581.
(257) Parker, D.; Waldron, B. P. *Org. Biomol. Chem.* **2013**, *11*, 2827-2838.
(258) Parker, D.; Waldron, B. P.; Yufit, D. S. *Dalton Trans.* **2013**, *42*, 8001-8008.
(259) Kimura, R. H.; Cheng, Z.; Gambhir, S. S.; Cochran, J. R. *Cancer Res.* **2009**, *69*, 2435-2442.
(260) Haubner, R.; Wester, H.-J.; Burkhart, F.; Senekowitsch-Schmidtke, R.; Weber, W.; Goodman, S. L.; Kessler, H.; Schwaiger, M. *J. Nucl. Med.* **2001**, *42*, 326-336.
(261) Baum, R. P.; Kulkarni, H. R. *Theranostics* **2012**, *2*, 437-447.
(262) Ferreiros-Martinez, R.; Esteban-Gomez, D.; Platas-Iglesias, C.; de Blas, A.; Rodriguez-Blas, T. *Inorg. Chem.* **2009**, *48*, 10976-10987.
(263) Ferreiros-Martinez, R.; Esteban-Gomez, D.; de Blas, A.; Platas-Iglesias, C.; Rodriguez-Blas, T. *Inorg. Chem.* **2009**, *48*, 11821-11831.
(264) Roca-Sabio, A.; Mato-Iglesias, M.; Esteban-Gomez, D.; Toth, E.; Blas, A. d.; Platas-Iglesias, C.; Rodriguez-Blas, T. *J. Am. Chem. Soc.* **2009**, *131*, 3331-3341.
(265) Vaiana, L.; Esteban-Gómez, D.; Mato-Iglesias, M.; Platas-Iglesias, C.; de Blas, A.; Rodríguez-Blas, T. *Eur. J. Inorg. Chem.* **2009**, *2009*, 400-411.
(266) Ferreiros-Martinez, R.; Esteban-Gomez, D.; Platas-Iglesias, C.; Blas, A. d.; Rodriguez-Blas, T. *Dalton Trans.* **2008**, 5754-5765.
(267) Mato-Iglesias, M.; Roca-Sabio, A.; Palinkas, Z.; Esteban-Gomez, D.; Platas-Iglesias, C.; Toth, E.; de Blas, A.; Rodriguez-Blas, T. *Inorg. Chem.* **2008**, *47*, 7840-7851.
(268) Balogh, E.; Mato-Iglesias, M.; Platas-Iglesias, C.; Toth, E.; Djanashvili, K.; Peters, J. A.; de Blas, A.; Rodriguez-Blas, T. *Inorg. Chem.* **2006**, *45*, 8719-8728.
(269) Mato-Iglesias, M.; Balogh, E.; Platas-Iglesias, C.; Toth, E.; Blas, A. d.; Blas, T. R. *Dalton Trans.* **2006**, 5404-5415.
(270) Mato-Iglesias, M.; Platas-Iglesias, C.; Djanashvili, K.; Peters, J. A.; Toth, E.; Balogh, E.; Muller, R. N.; Elst, L. V.; Blas, A. d.; Rodriguez-Blas, T. *Chem. Commun. (Cambridge, U. K.)* **2005**, 4729-4731.
(271) Platas-Iglesias, C.; Mato-Iglesias, M.; Djanashvili, K.; Muller, R. N.; Elst, L. V.; Peters, J. A.; de Blas, A.; Rodríguez-Blas, T. *Chem. Eur. J.* **2004**, *10*, 3579-3590.
(272) Boros, E.; Ferreira, C. L.; Yapp, D. T. T.; Gill, R. K.; Price, E. W.; Adam, M. J.; Orvig, C. *Nucl. Med. Biol.* **2012**, *39*, 785-794.
(273) Boros, E.; Cawthray, J. F.; Ferreira, C. L.; Patrick, B. O.; Adam, M. J.; Orvig, C. *Inorg. Chem.* **2012**, *51*, 6279-6284.
(274) Boros, E.; Ferreira, C. L.; Patrick, B. O.; Adam, M. J.; Orvig, C. *Nucl. Med. Biol.* **2011**, *38*, 1165–1174.
(275) Struthers, H.; Spingler, B.; Mindt, T. L.; Schibli, R. *Chem. Eur. J.* **2008**, *14*, 6173-6183.
(276) Motekaitis, R. J.; Sun, Y.; Martell, A. E. *Inorg. Chim. Acta* **1989**, *159*, 29-39.
(277) Ma, R.; Motekaitis, R. J.; Martell, A. E. *Inorg. Chim. Acta* **1994**, *224*, 151-155.
(278) Eder, M.; Krivoshein, A. V.; Backer, M.; Backer, J. M.; Haberkorn, U.; Eisenhut, M. *Nucl. Med. Biol.* **2010**, *37*, 405-412.

(279) Eder, M.; Wängler, B.; Knackmuss, S.; LeGall, F.; Little, M.; Haberkorn, U.; Mier, W.; Eisenhut, M. *Eur. J. Nucl. Med. Mol. Imaging* **2008**, *35*, 1878-1886.
(280) Mathias, C. J.; Sun, Y.; Welch, M. J.; Green, M. A.; Thomas, J. A.; Wade, K. R.; Martell, A. E. *Int. J. Rad. Appl. Instrum. [B]* **1988**, *15*, 69-81.
(281) Schuhmacher, J.; Kaul, S.; Klivényi, G.; Junkermann, H.; Magener, A.; Henze, M.; Doll, J.; Haberkorn, U.; Amelung, F.; Bastert, G. *Cancer Res.* **2001**, *61*, 3712-3717.
(282) Brillouet, S.; Dorbes, S.; Courbon, F.; Picard, C.; Delord, J. P.; Benoist, E.; Poirot, M.; Mestre-Voegtlé, B.; Silvente-Poirot, S. *Bioorg. Med. Chem.* **2010**, *18*, 5400-5412.
(283) Havas, F.; Danel, M.; Galaup, C.; Tisnès, P.; Picard, C. *Tetrahedron Lett.* **2007**, *48*, 999-1002.
(284) Berry, D. J.; Ma, Y.; Ballinger, J. R.; Tavare, R.; Koers, A.; Sunassee, K.; Zhou, T.; Nawaz, S.; Mullen, G. E. D.; Hider, R. C.; Blower, P. J. *Chem. Commun. (Cambridge, U. K.)* **2011**, *47*, 7068-7070.
(285) Holland, J. P.; Divilov, V.; Bander, N. H.; Smith-Jones, P. M.; Larson, S. M.; Lewis, J. S. *J. Nucl. Med.* **2010**, *51*, 1293-1300.
(286) Meijs, W. E.; Herscheid, J. D. M.; Haisma, H. J.; Pinedo, H. M. *Int. J. Rad. Appl. Instrum. [A]* **1992**, *43*, 1443-1447.
(287) Börjesson, P. K. E.; Jauw, Y. W. S.; Boellaard, R.; de Bree, R.; Comans, E. F. I.; Roos, J. C.; Castelijns, J. A.; Vosjan, M. J. W. D.; Kummer, J. A.; Leemans, C. R.; Lammertsma, A. A.; van Dongen, G. A. M. S. *Clin. Cancer Res.* **2006**, *12*, 2133-2140.
(288) Nagengast, W. B.; de Vries, E. G.; Hospers, G. A.; Mulder, N. H.; de Jong, J. R.; Hollema, H.; Brouwers, A. H.; van Dongen, G. A.; Perk, L. R.; Lub-de Hooge, M. N. *J. Nucl. Med.* **2007**, *48*, 1313-1319.
(289) Hong, H.; Severin, G.; Yang, Y.; Engle, J.; Zhang, Y.; Barnhart, T.; Liu, G.; Leigh, B.; Nickles, R.; Cai, W. *Eur. J. Nucl. Med. Mol. Imaging* **2011**, *39*, 138-148.
(290) Holland, J. P.; Caldas-Lopes, E.; Divilov, V.; Longo, V. A.; Taldone, T.; Zatorska, D.; Chiosis, G.; Lewis, J. S. *PLoS One* **2010**, *5*, e8859.
(291) Chang, A. J.; DeSilva, R.; Jain, S.; Lears, K.; Rogers, B.; Lapi, S. *Pharmaceuticals* **2012**, *5*, 79-93.
(292) Kim, W. D.; Kiefer, G. E.; Maton, F.; McMillan, K.; Muller, R. N.; Sherry, A. D. *Inorg. Chem.* **1995**, *34*, 2233-2243.
(293) Tircsó, G.; Benyó, E. T.; Suh, E. H.; Jurek, P.; Kiefer, G. E.; Sherry, A. D.; Kovács, Z. *Bioconjugate Chem.* **2009**, *20*, 565-575.
(294) Ferreira, C. L.; Yapp, D. T. T.; Mandel, D.; Gill, R. K.; Boros, E.; Wong, M. Q.; Jurek, P.; Kiefer, G. E. *Bioconjugate Chem.* **2012**, *23*, 2239-2246.
(295) Evers, A.; Hancock, R. D.; Martell, A. E.; Motekaitis, R. J. *Inorg. Chem.* **1989**, *28*, 2189-2195.
(296) Verel, I.; Visser, G. W. M.; Boellaard, R.; Stigter-van Walsum, M.; Snow, G. B.; van Dongen, G. A. M. S. *J. Nucl. Med.* **2003**, *44*, 1271-1281.
(297) Vosjan, M. J. W. D.; Perk, L. R.; Visser, G. W. M.; Budde, M.; Jurek, P.; Kiefer, G. E.; van Dongen, G. A. M. S. *Nat. Protocols* **2010**, *5*, 739-743.
(298) Perk, L.; Vosjan, M.; Visser, G.; Budde, M.; Jurek, P.; Kiefer, G.; van Dongen, G. *Eur. J. Nucl. Med. Mol. Imaging* **2010**, *37*, 250-259.
(299) Tinianow, J. N.; Gill, H. S.; Ogasawara, A.; Flores, J. E.; Vanderbilt, A. N.; Luis, E.; Vandlen, R.; Darwish, M.; Junutula, J. R.; Williams, S. P.; Marik, J. *Nucl. Med. Biol.*, *37*, 289-297.

(300) Heneweer, C.; Holland, J. P.; Divilov, V.; Carlin, S.; Lewis, J. S. *J. Nucl. Med.* **2011**, *52*, 625-633.
(301) Holland, J. P.; Sheh, Y.; Lewis, J. S. *Nucl. Med. Biol.* **2009**, *36*, 729-739.
(302) Dijkers, E. C. F.; Kosterink, J. G. W.; Rademaker, A. P.; Perk, L. R.; van Dongen, G. A. M. S.; Bart, J.; de Jong, J. R.; de Vries, E. G. E.; Lub-de Hooge, M. N. *J. Nucl. Med.* **2009**, *50*, 974-981.
(303) Meijs, W. E.; Haisma, H. J.; Klok, R. P.; van Gog, F. B.; Kievit, E.; Pinedo, H. M.; Herscheid, J. D. M. *J. Nucl. Med.* **1997**, *38*, 112-118.
(304) Price, E. W.; Zeglis, B. M.; Lewis, J. S.; Adam, M. J.; Orvig, C. *Dalton Trans.* **2014**, *43*, 119-131.
(305) Pauwels, S.; Barone, R.; Walrand, S.; Borson-Chazot, F.; Valkema, R.; Kvols, L. K.; Krenning, E. P.; Jamar, F. *J. Nucl. Med.* **2005**, *46*, 92S-98S.
(306) Lubberink, M.; Tolmachev, V.; Widström, C.; Bruskin, A.; Lundqvist, H.; Westlin, J.-E. *J. Nucl. Med.* **2002**, *43*, 1391-1397.
(307) Rösch, F.; Qaim, S. M.; Novgorodov, A. F.; Ying-Ming, T. *Appl. Radiat. Isot.* **1997**, *48*, 19-26.
(308) Lamb, H.; Faulds, D. *Drugs Aging* **1998**, *12*, 293-304.
(309) Shi, W.; Johnston, C. F.; Buchanan, K. D.; Ferguson, W. R.; Laird, J. D.; Crothers, J. G.; McIlrath, E. M. *QJM* **1998**, *91*, 295-301.
(310) Cremonesi, M.; Ferrari, M.; Zoboli, S.; Chinol, M.; Stabin, M. G.; Orsi, F.; Maecke, H. R.; Jermann, E.; Robertson, C.; Fiorenza, M.; Tosi, G.; Paganelli, G. *Eur. J. Nucl. Med. Mol. Imaging* **1999**, *26*, 877-886.
(311) Thakur, M. L.; Segal, A. W.; Louis, L.; Welch, M. J.; Hopkins, J.; Peters, T. J. *J. Nucl. Med.* **1977**, *18*, 1022-1026.
(312) Förster, G. J.; Engelbach, M. J.; Brockmann, J. J.; Reber, H. J.; Buchholz, H. G.; Mäcke, H. R.; Rösch, F. R.; Herzog, H. R.; Bartenstein, P. R. *Eur. J. Nucl. Med.* **2001**, *28*, 1743-1750.
(313) Rösch, F.; Herzog, H.; Stolz, B.; Brockmann, J.; Köhle, M.; Mühlensiepen, H.; Marbach, P.; Müller-Gärtner, H.-W. *Eur. J. Nucl. Med. Mol. Imaging* **1999**, *26*, 358-366.
(314) Maecke, H. R.; Riesen, A.; Ritter, W. *J Nucl Med* **1989**, *30*, 1235-1239.
(315) Hsieh, W.-Y.; Liu, S. *Inorg. Chem.* **2004**, *43*, 6006-6014.
(316) Laverman, P.; de Vries, I. J. M.; Scharenborg, N. M.; de Boer, A.; Broekema, M.; Oyen, W. J. G.; Figdor, C. G.; Adema, G. J.; Boerman, O. C. *Nucl. Med. Biol.* **2006**, *33*, 453-458.
(317) Geraldes, C. F. G. C.; Delgado, R.; Urbano, A. M.; Costa, J.; Jasanada, F.; Nepveu, F. *J. Chem. Soc., Dalton Trans.* **1995**, 327-335.
(318) Harris, W. R.; Chen, Y.; Wein, K. *Inorg. Chem.* **1994**, *33*, 4991-4998.
(319) Brandt, K. D.; Johnson, D. K. *Bioconjugate Chem.* **1992**, *3*, 118-125.
(320) De Sousa, M.; Carroll, A. M.; Herman, P. G.; Kerr, S.; Boulton, J.; Zalutsky, M. R. *Int. J. Nucl. Med. Biol.* **1985**, *12*, 89-96.
(321) Beamish, M. R.; Brown, E. B. *Blood* **1974**, *43*, 693-701.
(322) Van Hulle, M.; De Cremer, K.; Cornelis, R.; Lameire, N. *J. Environ. Monit.* **2001**, *3*.
(323) Zeng, X.; Coquière, D.; Alenda, A.; Garrier, E.; Prangé, T.; Li, Y.; Reinaud, O.; Jabin, I. *Chemistry – A European Journal* **2006**, *12*, 6393-6402.
(324) Gran, G. *Analyst* **1952**, *77*, 661-671.
(325) Duckworth, P. *Private communication*.
(326) Gans, P.; Sabatini, A.; Vacca, A. *Talanta* **1996**, *43*, 1739-1753.

(327) M. J. Frisch, G. W. T., H. B. Schlegel, G. E. Scuseria, M. A. Robb, J. R. Cheeseman, G. Scalmani, V. Barone, B. Mennucci, G. A. Petersson, H. Nakatsuji, M. Caricato, X. Li, H. P. Hratchian, A. F. Izmaylov, J. Bloino, G. Zheng, J. L. Sonnenberg, M. Hada, M. Ehara, K. Toyota, R. Fukuda, J. Hasegawa, M. Ishida, T. Nakajima, Y. Honda, O. Kitao, H. Nakai, T. Vreven, J. A. Montgomery, Jr., J. E. Peralta, F. Ogliaro, M. Bearpark, J. J. Heyd, E. Brothers, K. N. Kudin, V. N. Staroverov, R. Kobayashi, J. Normand, K. Raghavachari, A. Rendell, J. C. Burant, S. S. Iyengar, J. Tomasi, M. Cossi, N. Rega, J. M. Millam, M. Klene, J. E. Knox, J. B. Cross, V. Bakken, C. Adamo, J. Jaramillo, R. Gomperts, R. E. Stratmann, O. Yazyev, A. J. Austin, R. Cammi, C. Pomelli, J. W. Ochterski, R. L. Martin, K. Morokuma, V. G. Zakrzewski, G. A. Voth, P. Salvador, J. J. Dannenberg, S. Dapprich, A. D. Daniels, Ö. Farkas, J. B. Foresman, J. V. Ortiz, J. Cioslowski, and D. J. Fox *Gaussian, Inc., Wallingford CT* **2010**, *Gaussian 09, Revision C.01*.

(328) Lee, C.; Yang, W.; Parr, R. G. *Phys. Rev. B.* **1988**, *37*, 785-789.

(329) Becke, A. D. *J. Chem. Phys.* **1993**, *98*, 5648-5652.

(330) Vermeer, A. W. P.; Norde, W. *Biophys. J.* **2000**, *78*, 394-404.

(331) Boros, E.; Lin, Y.-H. S.; Ferreira, C. L.; Patrick, B. O.; Hafeli, U. O.; Adam, M. J.; Orvig, C. *Dalton Trans.* **2011**, *40*, 6253-6259.

(332) Masuda, R.; Oishi, S.; Ohno, H.; Kimura, H.; Saji, H.; Fujii, N. *Bioorg. Med. Chem.* **2011**, *19*, 3216-3220.

(333) Dioury, F.; Guéné, E.; Scala-Roulleau, A. D.; Ferroud, C.; Guy, A.; Port, M. *Tetrahedron Lett.* **2005**, *46*, 611-613.

(334) Favre-Réguillon, A.; Segat-Dioury, F.; Nait-Bouda, L.; Cosma, C.; Siaugue, J.-M.; Foos, J.; Guy, A. *Synlett* **2000**, *2000*, 0868-0871.

(335) Fukuyama, T.; Jow, C.-K.; Cheung, M. *Tetrahedron Lett.* **1995**, *36*, 6373-6374.

(336) Salvatore, R. N.; Yoon, C. H.; Jung, K. W. *Tetrahedron* **2001**, *57*, 7785-7811.

(337) Viola, N. A.; Rarig Jr, R. S.; Ouellette, W.; Doyle, R. P. *Polyhedron* **2006**, *25*, 3457-3462.

(338) Cacheris, W. P.; Nickle, S. K.; Sherry, A. D. *Inorg. Chem.* **1987**, *26*, 958-960.

(339) Loncin, M. F.; Desreux, J. F.; Merciny, E. *Inorg. Chem.* **1986**, *25*, 2646-2648.

(340) Anderegg, G.; Arnaud-Neu, F.; Delgado, R.; Felcman, J.; Popov, K. *Pure Appl. Chem.* **2005**, *77*, 1445-1495.

(341) Thorek, D. L. J.; Abou, D. S.; Beattie, B. J.; Bartlett, R. M.; Huang, R.; Zanzonico, P. B.; Grimm, J. *J. Nucl. Med.* **2012**, *53*, 1438-1445.

(342) Kumar Mishra, A.; Panwar, P.; Chopra, M.; Kumar Sharma, R.; Chatal, J.-F. *New J. Chem.* **2003**, *27*, 1054-1058.

(343) Cao, X.; Dolg, M. *J. Chem. Phys.* **2001**, *115*, 7348-7355.

(344) Anderson, C. J.; Connett, J. M.; Schwarz, S. W.; Rocque, P. A.; Guo, L. W.; Philpott, G. W.; Zinn, K. R.; Meares, C. F.; Welch, M. J. *J. Nucl. Med.* **1992**, *33*, 1685-1691.

(345) Anderson, C. J.; Schwarz, S. W.; Connett, J. M.; Cutler, P. D.; Guo, L. W.; Germain, C. J.; Philpott, G. W.; Zinn, K. R.; Greiner, D. P.; Meares, C. F.; Welch, M. J. *J. Nucl. Med.* **1995**, *36*, 850-858.

(346) Smith-Jones, P. M.; Fridrich, R.; Kaden, T. A.; Novak-Hofer, I.; Siebold, K.; Tschudin, D.; Maecke, H. R. *Bioconjugate Chem.* **1991**, *2*, 415-421.

(347) Lindmo, T.; Boven, E.; Cuttitta, F.; Fedorko, J.; Bunn Jr, P. A. *J. Immunol. Methods* **1984**, *72*, 77-89.

(348) Lindmo, T.; Bunn Jr, P. A. *Methods Enzymol.* **1986**, *121*, 678-691.

(349) Weiner, R.; Thakur, M. *BioDrugs* **2005**, *19*, 145-163.
(350) Forrer, F.; Waldherr, C.; Maecke, H. R.; Mueller-Brand, J. *Anticancer Res.* **2006**, *26*, 703-707.
(351) Forrer, F.; Uusijärvi, H.; Storch, D.; Maecke, H. R.; Mueller-Brand, J. *J. Nucl. Med.* **2005**, *46*, 1310-1316.
(352) Armstrong, A.; Brackenridge, I.; Jackson, R. F. W.; Kirk, J. M. *Tetrahedron Lett.* **1988**, *29*, 2483-2486.
(353) Gultneh, Y.; Ahvazi, B.; Tesema, Y. T.; Yisgedu, T. B.; Butcher, R. J. *J. Coord. Chem.* **2006**, *59*, 1835-1846.
(354) Harris, W. R.; Yang, B.; Abdollahi, S.; Hamada, Y. *J. Inorg. Biochem.* **1999**, *76*, 231-242.
(355) Subramanian, R.; Colony, J.; Shaban, S.; Sidrak, H.; Haspel, M. V.; Pomato, N.; Hanna, M. G.; McCabe, R. P. *Bioconjugate Chem.* **1992**, *3*, 248-255.
(356) Ikotun, O. F.; Lapi, S. E. *Future Med Chem* **2011**, *3*, 599-621.
(357) Perk, L.; Visser, O.; Stigter-van Walsum, M.; Vosjan, M.; Visser, G.; Zijlstra, J.; Huijgens, P.; van Dongen, G. *Eur. J. Nucl. Med. Mol. Imaging* **2006**, *33*, 1337-1345.
(358) Wooten, A.; Madrid, E.; Schweitzer, G.; Lawrence, L.; Mebrahtu, E.; Lewis, B.; Lapi, S. *Appl. Sci.* **2013**, *3*, 593-613.
(359) Walther, M.; Gebhardt, P.; Grosse-Gehling, P.; Würbach, L.; Irmler, I.; Preusche, S.; Khalid, M.; Opfermann, T.; Kamradt, T.; Steinbach, J.; Saluz, H.-P. *Appl. Radiat. Isot.* **2011**, *69*, 852-857.
(360) Mawani, Y.; Cawthray, J. F.; Chang, S.; Sachs-Barrable, K.; Weekes, D. M.; Wasan, K. M.; Orvig, C. *Dalton Trans.* **2013**, *42*, 5999-6011.
(361) Barta, C. A.; Sachs-Barrable, K.; Jia, J.; Thompson, K. H.; Wasan, K. M.; Orvig, C. *Dalton Trans.* **2007**, 5019-5030.
(362) Jones-Wilson, T. M.; Motekaitis, R. J.; Sun, Y.; Anderson, C. J.; Martell, A. E.; Welch, M. J. *Nucl. Med. Biol.* **1995**, *22*, 859-868.
(363) Laforest, R.; Dehdashti, F.; Lewis, J. S.; Schwarz, S. W. *Eur. J. Nucl. Med. Mol. Imaging* **2005**, *32*, 764-770.
(364) Anderson, C. J.; Ferdani, R. *Cancer Biother. Radiopharm.* **2009**, *24*, 379-393.
(365) Novak-Hofer, I.; Schubiger, A. *Eur. J. Nucl. Med. Mol. Imaging* **2002**, *29*, 821-830.
(366) Sun, X.; Wuest, M.; Weisman, G. R.; Wong, E. H.; Reed, D. P.; Boswell, C. A.; Motekaitis, R.; Martell, A. E.; Welch, M. J.; Anderson, C. J. *J. Med. Chem.* **2002**, *45*, 469-477.
(367) Boswell, C. A.; Sun, X.; Niu, W.; Weisman, G. R.; Wong, E. H.; Rheingold, A. L.; Anderson, C. J. *J. Med. Chem.* **2004**, *47*, 1465-1474.
(368) Cooper, M. S.; Ma, M. T.; Sunassee, K.; Shaw, K. P.; Williams, J. D.; Paul, R. L.; Donnelly, P. S.; Blower, P. J. *Bioconjug. Chem.* **2012**, 10.1021/bc300037w.
(369) Stigers, D. J.; Ferdani, R.; Weisman, G. R.; Wong, E. H.; Anderson, C. J.; Golen, J. A.; Moore, C.; Rheingold, A. L. *Dalton Trans.* **2009**, *39*, 1699-1701.
(370) Kotek, J.; Lubal, P.; Hermann, P.; Cisarova, I.; Lukes, I.; Godula, T.; Svobodova, I.; Taborsky, P.; Havel, J. *Chem. Eur. J.* **2003**, *9*, 233-248.
(371) Nguyen, K.; Parry, J. J.; Rogers, B. E.; Anderson, C. J. *Nucl. Med. Biol.* **2012**, *39*, 187-197.
(372) Mindt, T. L.; Struthers, H.; Brans, L.; Anguelov, T.; Schweinsberg, C.; Maes, V.; Tourwé, D.; Schibli, R. *J. Am. Chem. Soc.* **2006**, *128*, 15096-15097.
(373) Struthers, H.; Spingler, B.; Mindt, T. L.; Schibli, R. *Chem.-Eur. J.* **2008**, *14*, 6173-6183.

(374) Salvatore, R. N.; Shin, S. I.; Flanders, V. L.; Jung, K. W. *Tetrahedron Lett.* **2001**, *42*, 1799-1801.
(375) Nakon, R.; Angelici, R. J. *J. Am. Chem. Soc.* **1973**, *95*, 3170-3174.
(376) Liu, S.; Pietryka, J.; Ellars, C. E.; Edwards, D. S. *Bioconjugate Chem.* **2002**, *13*, 902-913.
(377) Hsieh, W.-Y.; Liu, S. *Inorg. Chem.* **2004**, *43*, 6006-6014.
(378) Malyarick, M. A.; Ilyuhin, A. B.; Petrosyants, S. P. *Main Group Met. Chem.* **1994**, *17*, 707-718.
(379) Maecke, H. R.; Riesen, A.; Ritter, W. *J. Nucl. Med.* **1989**, *30*, 1235-1239.
(380) Mindt, T. L.; Schweinsberg, C.; Brans, L.; Hagenbach, A.; Abram, U.; Tourwé, D.; Garcia-Garayoa, E.; Schibli, R. *ChemMedChem* **2009**, *4*, 529-539.
(381) Struthers, H.; Mindt, T. L.; Schibli, R. *Dalton Trans.* **2010**, *39*, 675-696.
(382) Tamanini, E.; Rigby, S. E. J.; Motevalli, M.; Todd, M. H.; Watkinson, M. *Chem.-Eur. J.* **2009**, *15*, 3720-3728.
(383) Lebedev, A. Y.; Holland, J. P.; Lewis, J. S. *Chem. Commun.* **2010**, *46*, 1706-1708.
(384) Bratsos, I.; Urankar, D.; Zangrando, E.; Genova-Kalou, P.; Kosmrlj, J.; Alessio, E.; Turel, I. *Dalton Trans.* **2011**, *40*, 5188-5199.
(385) Maisonial, A.; Serafin, P.; Traikia, M.; Debiton, E.; Thery, V.; Aitken, D. J.; Lemoine, P.; Viossat, B.; Gautier, A. *Eur. J. Inorg. Chem.* **2008**, *2008*, 298-305.
(386) Bastero, A.; Font, D.; Pericas, M. A. *J. Org. Chem.* **2007**, *72*, 2460-2468.
(387) Mirick, G. R.; O'Donnell, R. T.; DeNardo, S. J.; Shen, S.; Meares, C. F.; DeNardo, G. L. *Nucl. Med. Biol.* **1999**, *26*, 841-845.
(388) Connett, J. M.; Anderson, C. J.; Guo, L.-W.; Schwarz, S. W.; Zinn, K. R.; Rogers, B. E.; Siegel, B. A.; Philpott, G. W.; Welch, M. J. *Proc. Natl. Acad. Sci. USA* **1996**, *93*, 6814-6818.
(389) DeNardo, G. L.; Kukis, D. L.; Shen, S.; DeNardo, D. A.; Meares, C. F.; DeNardo, S. J. *Clin. Cancer Res.* **1999**, *5*, 533-541.
(390) Ferreira, C. L.; Yapp, D. T. T.; Crisp, S.; Sutherland, B. W.; Ng, S. S. W.; Gleave, M.; Bensimon, C.; Jurek, P.; Kiefer, G. E. *Eur. J. Nucl. Med. Mol. Imaging* **2010**, *37*, 2117-2126.
(391) Rogers, B. E.; Anderson, C. J.; Connett, J. M.; Guo, L. W.; Edwards, B.; Sherman, E. L. C.; Zinn, K. R.; Welch, M. J. *Bioconjugate Chem.* **1996**, *7*, 511-522.
(392) Anderson, C. J.; Connett, J. M.; Schwarz, S. W.; Rocque, P. A.; Guo, L. W.; Philpott, G. W.; Zinn, K. R.; Meares, C. F.; Welch, M. J. *J. Nucl. Med.* **1992**, *33*, 1685-1691.
(393) Zimmermann, K.; Grünberg, J.; Honer, M.; Ametamey, S.; August Schubiger, P.; Novak-Hofer, I. *Nucl. Med. Biol.* **2003**, *30*, 417-427.
(394) Cole, W. C.; DeNardo, S. J.; Meares, C. F.; McCall, M. J.; DeNardo, G. L.; Epstein, A. L.; O'Brien, H. A.; Moi, M. K. *Int. J. Rad. Appl. Instrum. [B]* **1986**, *13*, 363-368.
(395) McQuade, P.; Miao, Y.; Yoo, Y.; Quinn, T. P.; Welch, M. J.; Lewis, J. S. *J. Med. Chem.* **2005**, *48*, 2985-2992.
(396) Sprague, J. E.; Peng, Y.; Sun, X.; Weisman, G. R.; Wong, E. H.; Achilefu, S.; Anderson, C. J. *Clin. Cancer. Res.* **2004**, *10*, 8674-8682.
(397) Packard, A. B.; Kronauge, J. F.; Barbarics, E.; Kiani, S.; Treves, S. T. *Nucl. Med. Biol.* **2002**, *29*, 289-294.
(398) John, E. K.; Green, M. A. *J. Med. Chem.* **1990**, *33*, 1764-1770.
(399) Kelly, J. D.; Forster, A. M.; Higley, B.; Archer, C. M.; Booker, F. S.; Canning, L. R.; Chiu, K. W.; edwards, B.; Gill, H. K.; McPartlin, M.; Nagle, K.; Latham, I.; Pickett, R.; Storey, A.; Webbon, P. *J. Nucl. Med.* **1993**, *34*, 222-227.

(400) Bass, L. A.; Wang, M.; Welch, M. J.; Anderson, C. J. *Bioconjugate Chem.* **2000**, *11*, 527-532.
(401) McCarthy, D. W.; Shefer, R. E.; Klinkowstein, R. E.; Bass, L. A.; Margeneau, W. H.; Cutler, C. S.; Anderson, C. J.; Welch, M. J. *Nucl. Med. Biol.* **1997**, *24*, 35-43.
(402) *SAINT*, Version 7.68A, Bruker AXS Inc.: Madison, WI, **1997-2010.**
(403) Riss, P. J.; Kroll, C.; Nagel, V.; Rösch, F. *Bioorg. Med. Chem. Lett.* **2008**, *18*, 5364-5367.
(404) Altomare, A.; Burla, M. C.; Camalli, M.; Cascarano, G. L.; Giacovazzo, C.; Guagliardi, A.; Moliterni, A. G. G.; Polidori, G.; Spagna, R. SIR97. *J. Appl. Cryst.* Published Online: 1999.
(405) *SHELXTL*, Version 2008/4, Bruker AXS Inc.: Madison, WI, **2008.**
(406) Farrugia, L. J. *J. Appl. Cryst.* **1999**, *32*, 837-838.

Appendix

Appendix A Supplementary figures and data

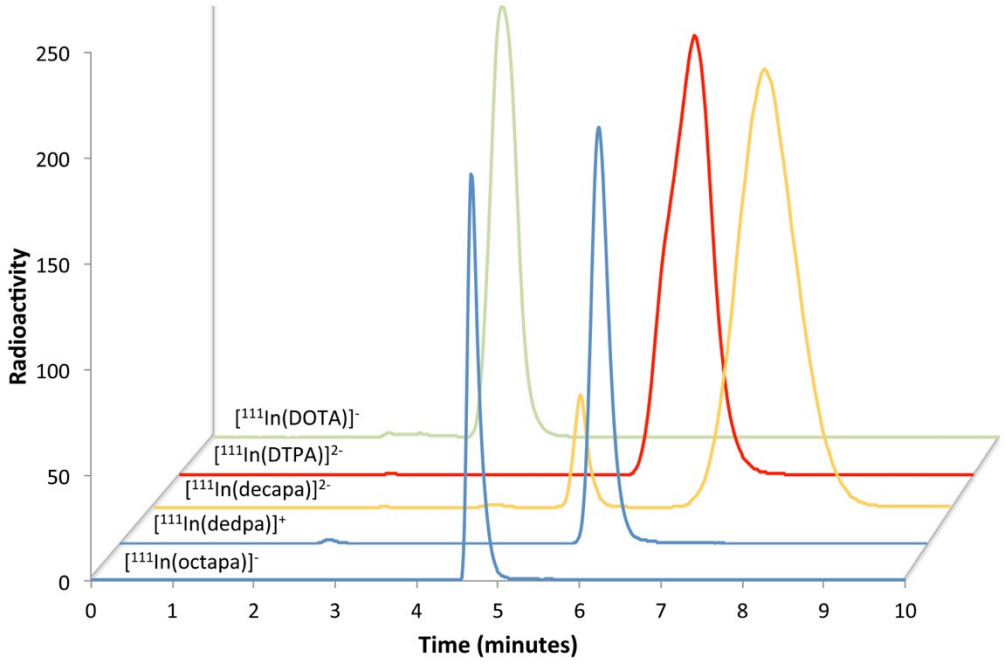

Figure A.1 HPLC radiotrace overlay, with all ^{111}In radiolabeling performed at ambient temperature except for **[^{111}In(DOTA)]$^{-}$** at 80°C via μW reactor (gradient for **[^{111}In(dedpa)]$^{+}$**: A: 10 mM NaOAc buffer pH 4.5, B: CH_3CN. 0-5% B linear gradient 20 min; gradient for all other complexes: A: 10 mM NaOAc buffer pH 4.5, B: CH_3CN. 0-100% B linear gradient 20 min); all compounds labeled in >99% radiochemical yields, **[^{111}In(dedpa)]$^{+}$** (t_R = 5.9 min), **[^{111}In(octapa)]$^{-}$** (t_R = 4.7 min), **[^{111}In(decapa)]$^{2-}$** (t_R = 5.4 min (5%), 7.7 min (95%)). **[^{111}In(DTPA)]$^{2-}$** (t_R = 6.5 min), **[^{111}In(DOTA)]$^{-}$** (t_R = 3.5 min).

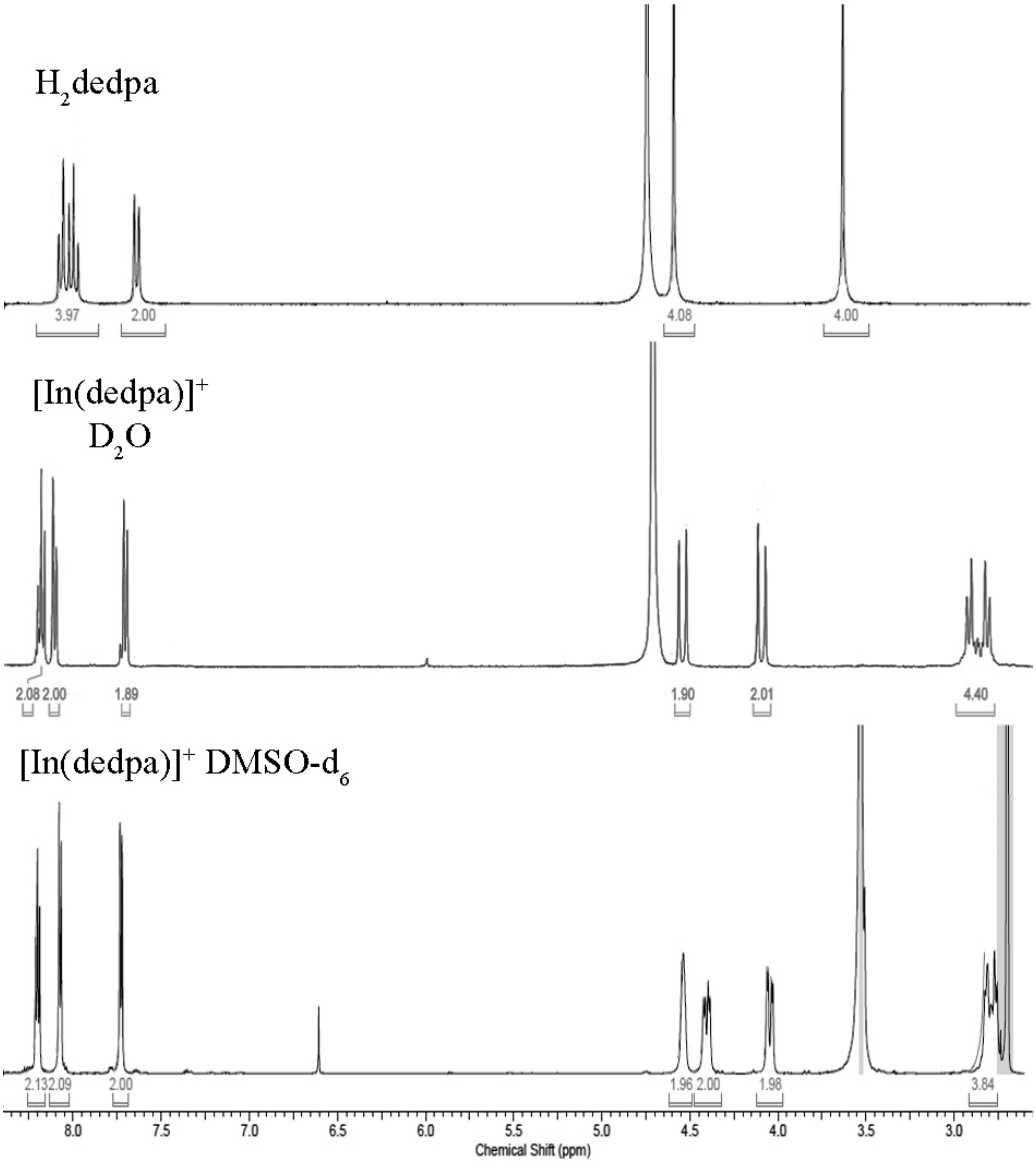

Figure A.2 ^{1}H NMR spectra of **H_2dedpa** in D_2O (top), and **[In(dedpa)]$^{+}$** in D_2O (middle) and DMSO-d_6 (bottom) at ambient temperature (300 MHz, RT).

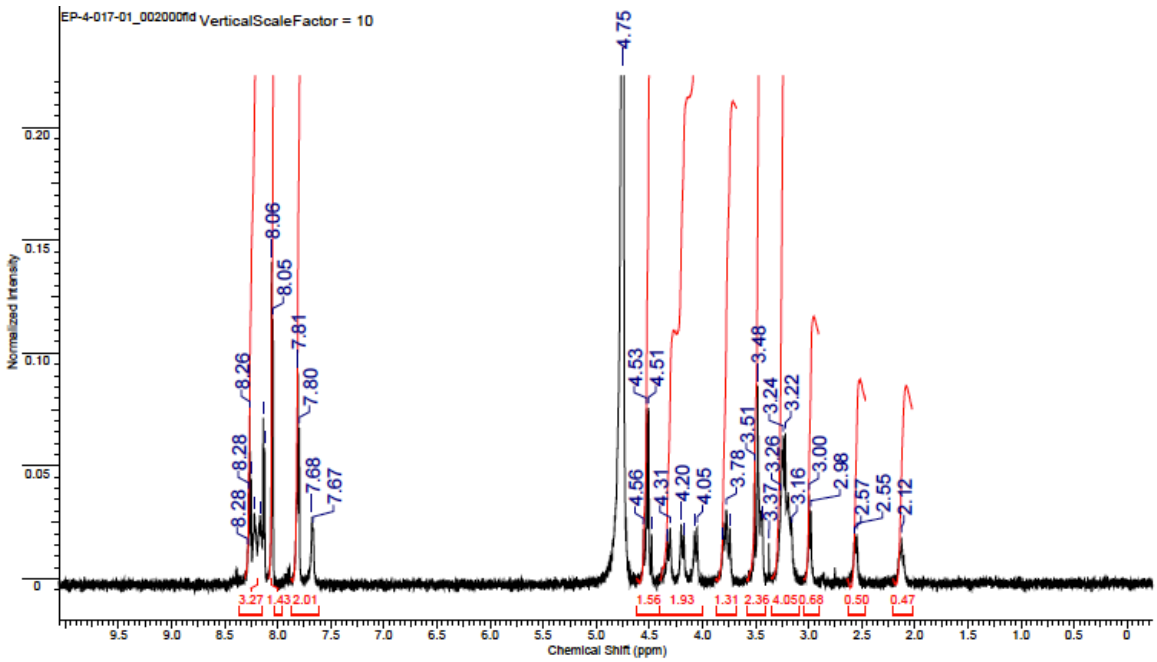

Figure A.3 ^{1}H NMR spectrum (600 MHz, D_2O, RT) of [**Lu(octapa)**]$^{-}$.

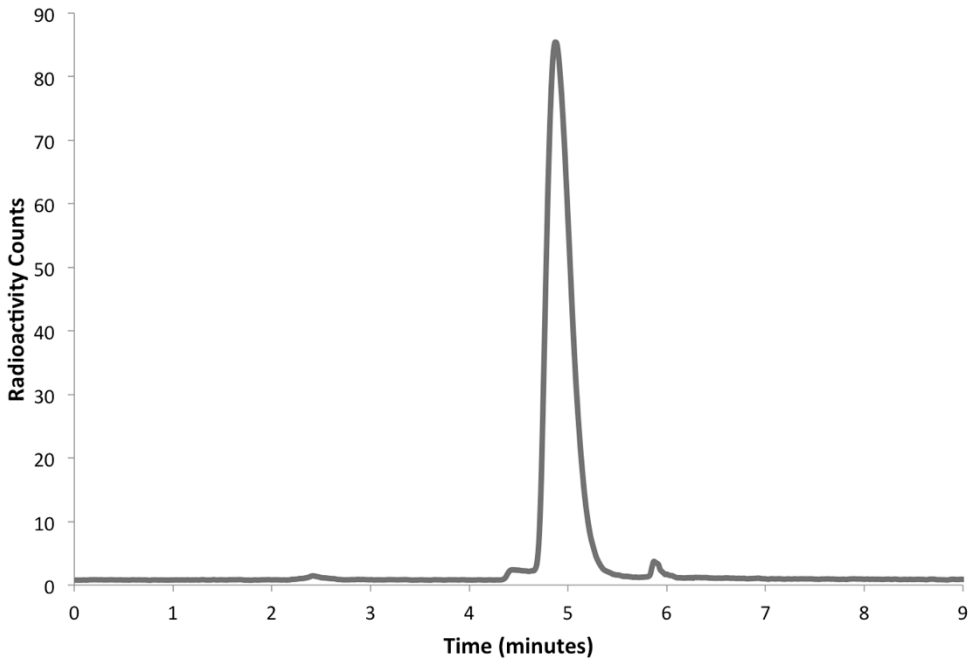

Figure A.4 HPLC radiotrace of ^{111}In(nonapa) (t_R = 5.0 min, 97% RCY), showing small impurities.

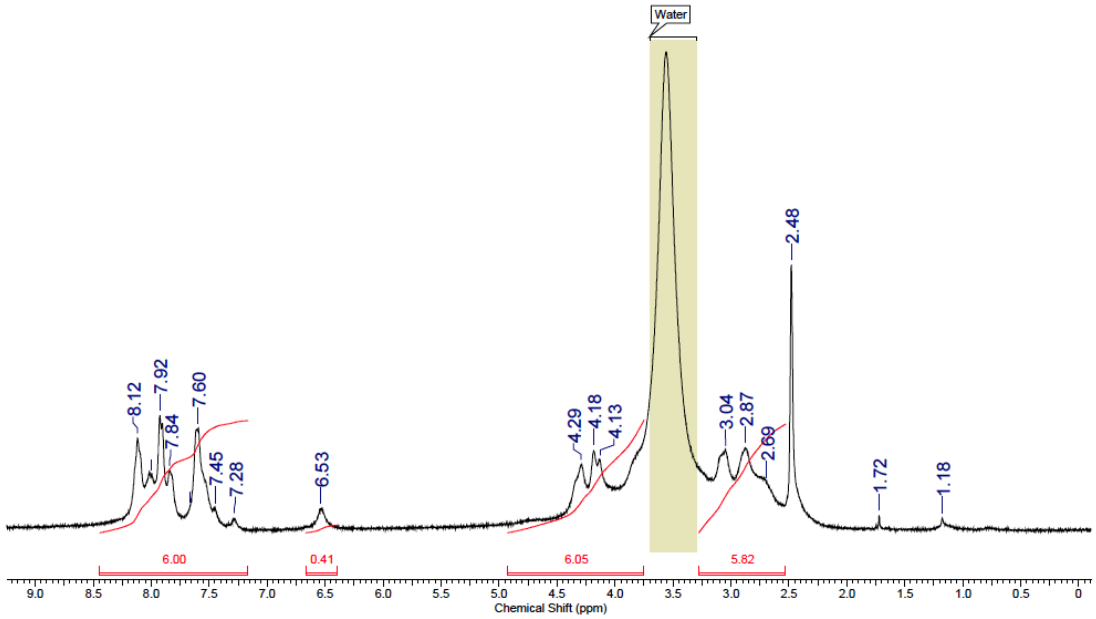

Figure A.5 ^{1}H NMR spectrum (300 MHz, DMSO-d_6, RT) of [Y(octapa)]$^{-}$ (9).

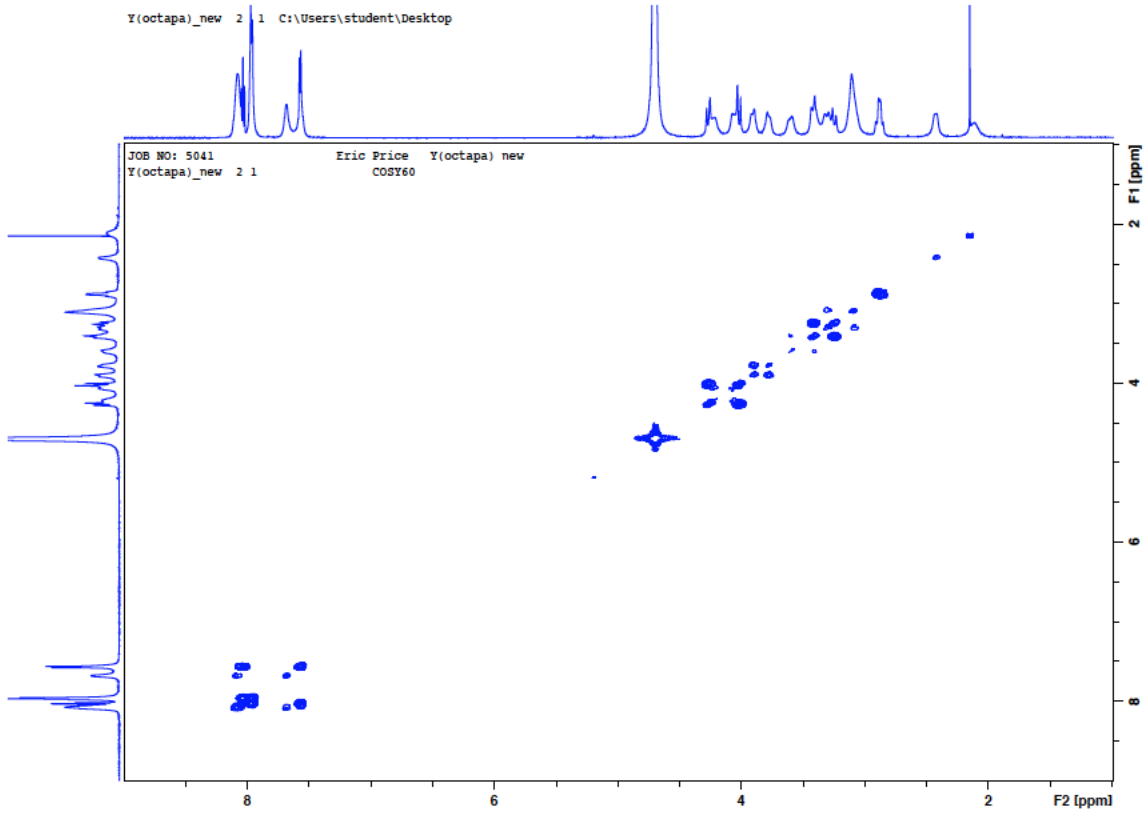

Figure A.6 ^{1}H-^{1}H COSY NMR full spectrum of [Y(octapa)]$^{-}$ (600 MHz, D_2O, RT).

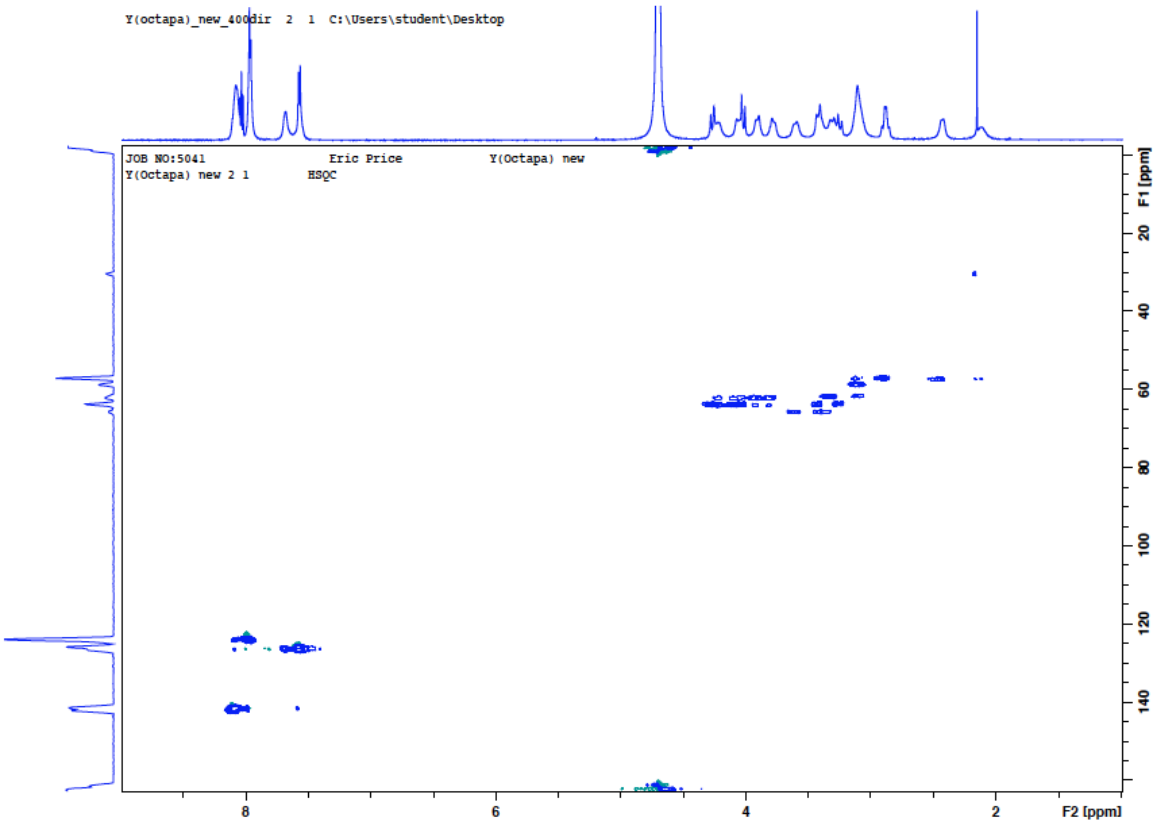

Figure A.7 ^{1}H-^{13}C HSQC NMR full spectrum of $[Y(octapa)]^-$ (400 MHz, 100 MHz, D_2O, RT).

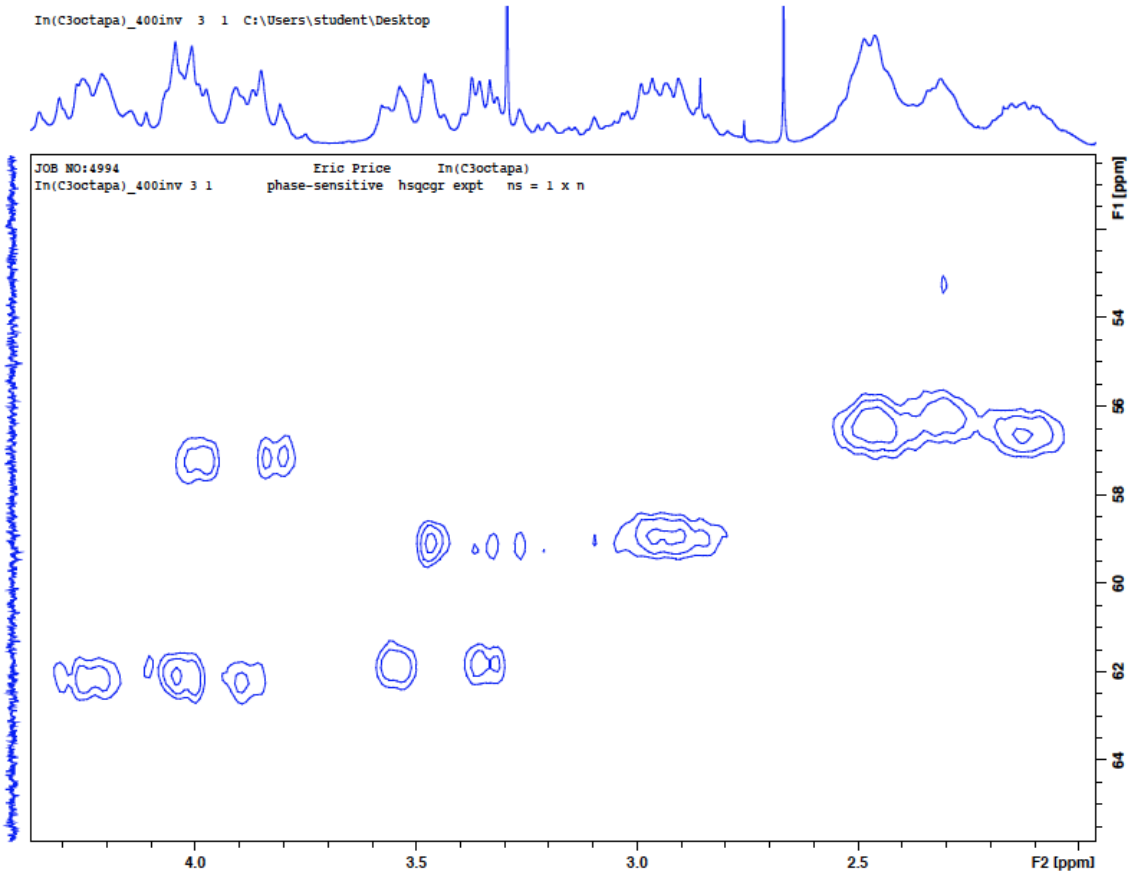

Figure A.8 ^{1}H-^{13}C HSQC NMR alkyl-region expansion of $[In(C3octapa)]^-$ (400 MHz, 100 MHz, D_2O, RT).

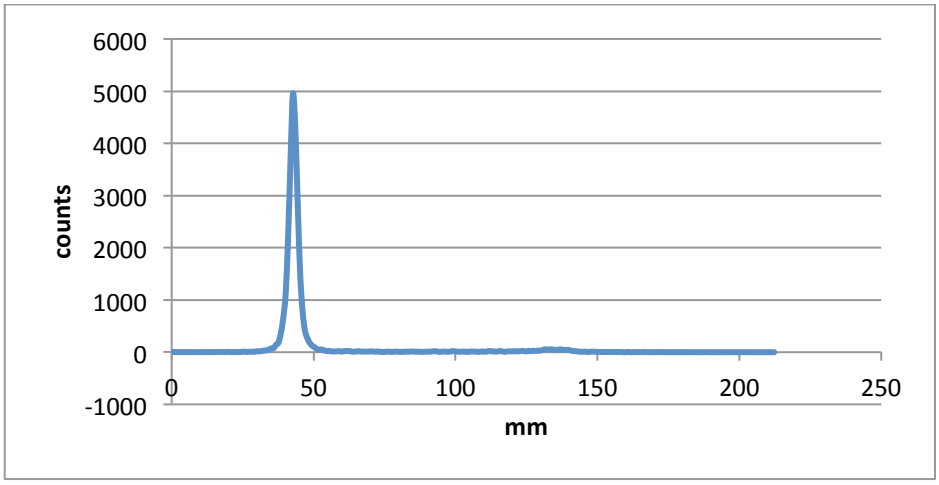

Figure A.9 iTLC radiochromatograph of **^{111}In-octapa-trastuzumab** (radiolabeled in NH_4Ac buffer pH 5.5 100 mM, 30 min, RT and eluted with a mobile phase of 50 mM EDTA, pH 5) purified by size-exclusion centrifugation and PD-10 column elution, showing pure radiolabeled immunoconjugate at ~ 40 mm. "Free" ^{111}In(EDTA) elutes near the solvent front ~150-200 mm.

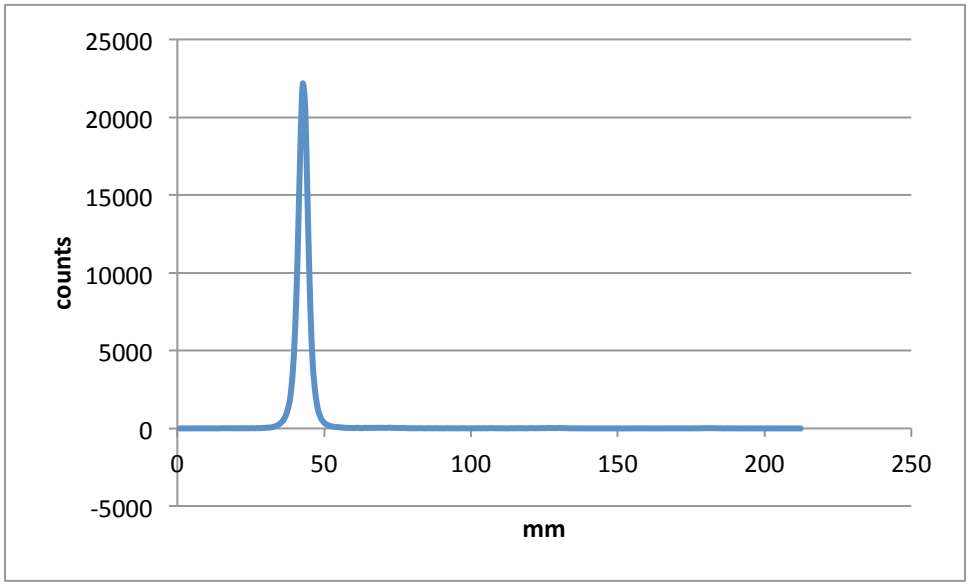

Figure A.10 iTLC radiochromatograph of **^{177}Lu-octapa-trastuzumab** (radiolabeled in NH_4Ac buffer pH 5.5 100 mM, 30 min, RT and eluted with a mobile phase of 50 mM EDTA, pH 5) purified by size-exclusion centrifugation and PD-10 column elution, showing pure radiolabeled immunoconjugate at ~ 40 mm. "Free" ^{77}Lu(EDTA) elutes near the solvent front ~150-200 mm.

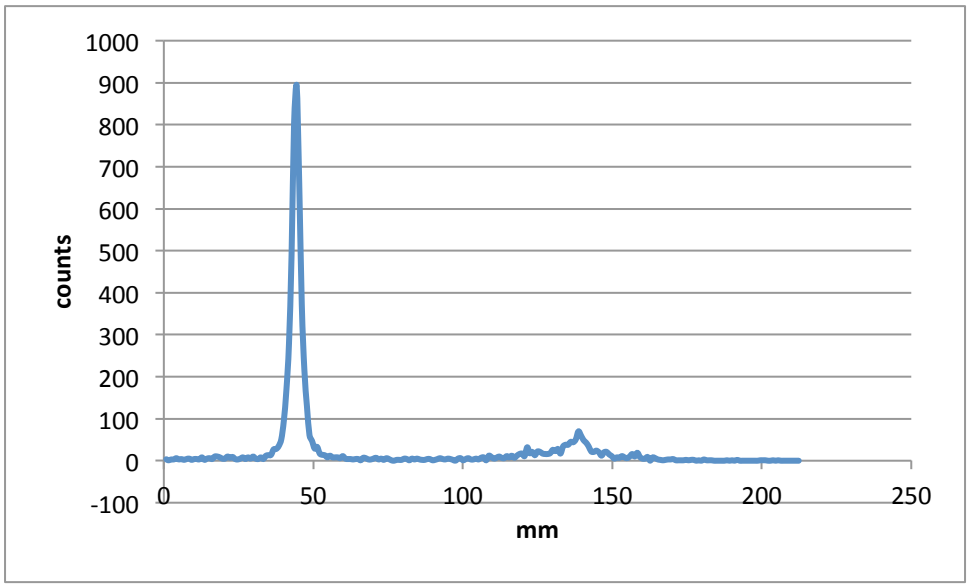

Figure A.11 iTLC radiochromatograph of **^{111}In-C3octapa-trastuzumab** (radiolabeled in NH_4Ac buffer pH 5.5 100 mM, 60 min, RT and eluted with a mobile phase of 50 mM EDTA, pH 5) purified by size-exclusion centrifugation and PD-10 column elution, showing pure radiolabeled immunoconjugate at ~ 40 mm, and a small amount of "free" ^{111}In(EDTA) eluting near the solvent front ~150 mm, suggesting some transchelation by EDTA mobile phase.

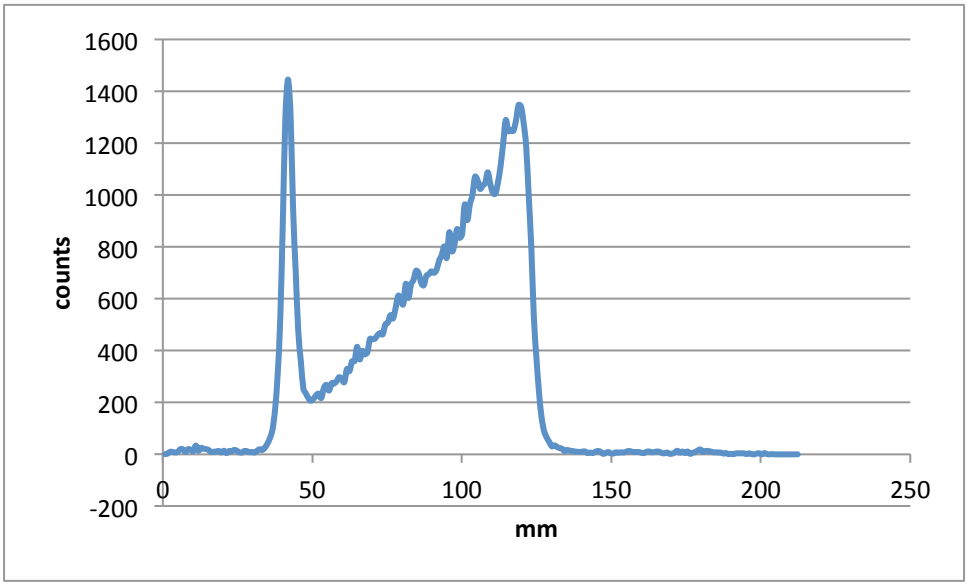

Figure A.12 iTLC radiochromatograph of **^{177}Lu-C3octapa-trastuzumab** (radiolabeled in NH_4Ac buffer pH 5.5 100 mM, 60 min, RT and eluted with a mobile phase of 50 mM EDTA, pH 5) purified by size-exclusion centrifugation and PD-10 column elution, showing pure radiolabeled immunoconjugate at ~ 40 mm, and a large quantity of "free" ^{177}Lu(EDTA) eluting with the solvent front from ~50-150 mm, showing significant leaching and transchelation of ^{177}Lu by EDTA mobile phase, suggesting severe instability of the $[Lu(C3octapa)]^-$ complex.

Table A.1 X-ray structural data for [Cu(azapa)]

Empirical Formula	$C_{36}H_{34}N_{10}CuO_4$
Formula Weight	734.27
Crystal Colour, Habit	blue, prism
Crystal Dimensions	0.10 x 0.41 x 0.45 mm
Crystal System	orthorhombic
Lattice Type	Primitive
Lattice Parameters	a = 10.8066(3) Å b = 10.6179(3) Å c = 27.9331(7) Å a = 90° b = 90° g = 90° V = 3205.1(2) Å^3
Space Group	*P bcn* (#60)
Z value	4
D_{calc}	1.522 g/cm^3
F_{000}	1524.00
m(Mo-Ka)	7.41 cm^{-1}

Bond lengths [Å] and angles [deg] for [Cu(azapa)]

Bond	Length (Å)
C(1)-O(2)	1.2339(17)
C(1)-O(1)	1.2712(18)
C(1)-C(2)	1.523(2)
C(2)-N(1)	1.3419(16)
C(2)-C(3)	1.3827(19)
C(3)-C(4)	1.388(2)
C(3)-H(3)	0.9500
C(4)-C(5)	1.387(2)
C(4)-H(4)	0.9500
C(5)-C(6)	1.3895(18)
C(5)-H(5)	0.9500
C(6)-N(1)	1.3410(16)
C(6)-C(7)	1.5052(18)
C(7)-N(2)	1.4770(16)
C(7)-H(7A)	0.9900
C(7)-H(7B)	0.9900
C(8)-N(2)	1.4807(15)
C(8)-C(8)#1	1.526(2)
C(8)-H(8A)	0.9900
C(8)-H(8B)	0.9900
C(9)-N(2)	1.4872(15)
C(9)-C(10)	1.4973(16)
C(9)-H(9A)	0.9900
C(9)-H(9B)	0.9900
C(10)-N(3)	1.3590(16)
C(10)-C(11)	1.3732(17)
N(3)-N(4)	1.3179(16)
N(4)-N(5)	1.3412(15)
C(11)-N(5)	1.3455(15)
C(11)-H(11)	0.9500
C(12)-N(5)	1.4713(15)
C(12)-C(13)	1.5047(18)
C(12)-H(12A)	0.9900
C(12)-H(12B)	0.9900
C(13)-C(18)	1.3910(19)
C(13)-C(14)	1.3947(18)
C(14)-C(15)	1.386(2)
C(14)-H(14)	0.9500
C(15)-C(16)	1.384(2)
C(15)-H(15)	0.9500
C(16)-C(17)	1.3875(19)
C(16)-H(16)	0.9500
C(17)-C(18)	1.392(2)
C(17)-H(17)	0.9500
C(18)-H(18)	0.9500
N(1)-Cu(1)	1.9355(11)
N(2)-Cu(1)	2.3259(10)
O(1)-Cu(1)	2.1199(10)
Cu(1)-N(1)#1	1.9355(11)
Cu(1)-O(1)#1	2.1199(10)
Cu(1)-N(2)#1	2.3259(10)

Bonds	Angle
O(2)-C(1)-O(1)	127.75(15)
O(2)-C(1)-C(2)	117.33(13)
O(1)-C(1)-C(2)	114.92(11)
N(1)-C(2)-C(3)	120.73(13)
N(1)-C(2)-C(1)	114.77(12)
C(3)-C(2)-C(1)	124.48(12)
C(2)-C(3)-C(4)	118.90(13)
C(2)-C(3)-H(3)	120.6
C(4)-C(3)-H(3)	120.6
C(5)-C(4)-C(3)	119.53(13)
C(5)-C(4)-H(4)	120.2
C(3)-C(4)-H(4)	120.2
C(4)-C(5)-C(6)	119.17(14)
C(4)-C(5)-H(5)	120.4
C(6)-C(5)-H(5)	120.4
N(1)-C(6)-C(5)	120.15(12)
N(1)-C(6)-C(7)	115.19(11)
C(5)-C(6)-C(7)	124.66(12)
N(2)-C(7)-C(6)	109.25(10)
N(2)-C(7)-H(7A)	109.8
C(6)-C(7)-H(7A)	109.8
N(2)-C(7)-H(7B)	109.8
C(6)-C(7)-H(7B)	109.8
H(7A)-C(7)-H(7B)	108.3
N(2)-C(8)-C(8)#1	112.01(8)
N(2)-C(8)-H(8A)	109.2
C(8)#1-C(8)-H(8A)	109.2
N(2)-C(8)-H(8B)	109.2
C(8)#1-C(8)-H(8B)	109.2
H(8A)-C(8)-H(8B)	107.9
N(2)-C(9)-C(10)	116.06(10)
N(2)-C(9)-H(9A)	108.3
C(10)-C(9)-H(9A)	108.3
N(2)-C(9)-H(9B)	108.3
C(10)-C(9)-H(9B)	108.3
H(9A)-C(9)-H(9B)	107.4
N(3)-C(10)-C(11)	108.10(11)
N(3)-C(10)-C(9)	122.75(11)
C(11)-C(10)-C(9)	129.05(11)
N(4)-N(3)-C(10)	108.81(11)
N(3)-N(4)-N(5)	107.36(10)
N(5)-C(11)-C(10)	104.95(11)
N(5)-C(11)-H(11)	127.5
C(10)-C(11)-H(11)	127.5
N(5)-C(12)-C(13)	110.90(10)
N(5)-C(12)-H(12A)	109.5
C(13)-C(12)-H(12A)	109.5
N(5)-C(12)-H(12B)	109.5
C(13)-C(12)-H(12B)	109.5
H(12A)-C(12)-H(12B)	108.0
C(18)-C(13)-C(14)	119.04(12)
C(18)-C(13)-C(12)	120.11(12)

Bonds	Angle	Bonds	Angle
C(14)-C(13)-C(12)	120.83(12)	C(7)-N(2)-Cu(1)	103.07(7)
C(15)-C(14)-C(13)	120.79(13)	C(8)-N(2)-Cu(1)	105.79(7)
C(15)-C(14)-H(14)	119.6	C(9)-N(2)-Cu(1)	113.07(7)
C(13)-C(14)-H(14)	119.6	N(4)-N(5)-C(11)	110.78(10)
C(16)-C(15)-C(14)	119.87(13)	N(4)-N(5)-C(12)	119.55(10)
C(16)-C(15)-H(15)	120.1	C(11)-N(5)-C(12)	129.65(11)
C(14)-C(15)-H(15)	120.1	C(1)-O(1)-Cu(1)	113.11(9)
C(15)-C(16)-C(17)	119.91(13)	N(1)#1-Cu(1)-N(1)	178.49(6)
C(15)-C(16)-H(16)	120.0	N(1)#1-Cu(1)-O(1)#1	80.46(4)
C(17)-C(16)-H(16)	120.0	N(1)-Cu(1)-O(1)#1	100.51(4)
C(16)-C(17)-C(18)	120.27(13)	N(1)#1-Cu(1)-O(1)	100.51(4)
C(16)-C(17)-H(17)	119.9	N(1)-Cu(1)-O(1)	80.46(4)
C(18)-C(17)-H(17)	119.9	O(1)#1-Cu(1)-O(1)	101.39(6)
C(13)-C(18)-C(17)	120.11(13)	N(1)#1-Cu(1)-N(2)	101.35(4)
C(13)-C(18)-H(18)	119.9	N(1)-Cu(1)-N(2)	77.47(4)
C(17)-C(18)-H(18)	119.9	O(1)#1-Cu(1)-N(2)	93.94(4)
C(6)-N(1)-C(2)	121.46(12)	O(1)-Cu(1)-N(2)	155.06(4)
C(6)-N(1)-Cu(1)	121.73(9)	N(1)#1-Cu(1)-N(2)#1	77.47(4)
C(2)-N(1)-Cu(1)	116.45(9)	N(1)-Cu(1)-N(2)#1	101.35(4)
C(7)-N(2)-C(8)	110.75(9)	O(1)#1-Cu(1)-N(2)#1	155.06(4)
C(7)-N(2)-C(9)	110.54(9)	O(1)-Cu(1)-N(2)#1	93.94(4)
C(8)-N(2)-C(9)	113.09(10)	N(2)-Cu(1)-N(2)#1	79.30(5)

Table A.2 X-ray structural data for [In(azapa)(H_2O)][ClO_4]

Empirical Formula	$C_{36}H_{41}N_{10}O_{11.5}InCl$
Formula Weight	948.06
Crystal Colour, Habit	brown, plate
Crystal Dimensions	0.10 x 0.22 x 0.27 mm
Crystal System	monoclinic
Lattice Type	primitive
Lattice Parameters	a = 11.565(1) Å b = 12.575(1) Å c = 14.794(2) Å a = 95.694(2)^o b = 107.281(2)^o g = 102.783(2)^o V = 1971.9(4) Å^3
Space Group	*P* -1 (#2)
Z value	2
D_{calc}	1.597 g/cm^3
F_{000}	970.00
m(Mo-Ka)	7.32 cm^{-1}

Bond lengths [Å] and angles [deg] for [In(azapa)][ClO_4].

Bond	Length (Å)	Bond	Length (Å)
C(1)-O(2)	1.2521(17)	C(2)-N(1)	1.3386(17)
C(1)-O(1)	1.2631(17)	C(2)-C(3)	1.387(2)
C(1)-C(2)	1.515(2)	C(3)-C(4)	1.390(2)

Bond	Length (Å)
C(3)-H(3)	0.9500
C(4)-C(5)	1.390(2)
C(4)-H(4)	0.9500
C(5)-C(6)	1.3896(19)
C(5)-H(5)	0.9500
C(6)-N(1)	1.3347(18)
C(6)-C(7)	1.5011(19)
C(7)-N(2)	1.4848(17)
C(7)-H(7A)	0.9900
C(7)-H(7B)	0.9900
C(8)-C(9)	1.4970(19)
C(8)-N(2)	1.4990(17)
C(8)-H(8A)	0.9900
C(8)-H(8B)	0.9900
C(9)-N(3)	1.3624(18)
C(9)-C(10)	1.377(2)
C(10)-N(5)	1.3480(19)
C(10)-H(10)	0.9500
C(11)-N(5)	1.475(2)
C(11)-C(12)	1.515(2)
C(11)-H(11A)	0.9900
C(11)-H(11B)	0.9900
C(12)-C(13)	1.391(2)
C(12)-C(17)	1.395(2)
C(13)-C(14)	1.389(2)
C(13)-H(13)	0.9500
C(14)-C(15)	1.387(3)
C(14)-H(14)	0.9500
C(15)-C(16)	1.379(3)
C(15)-H(15)	0.9500
C(16)-C(17)	1.399(3)
C(16)-H(16)	0.9500
C(17)-H(17)	0.9500
C(18)-N(2)	1.4885(17)
C(18)-C(19)	1.5167(19)
C(18)-H(18A)	0.9900
C(18)-H(18B)	0.9900
C(19)-N(7)	1.4877(18)
C(19)-H(19A)	0.9900
C(19)-H(19B)	0.9900
C(20)-O(4)	1.2429(17)
C(20)-O(3)	1.2727(16)
C(20)-C(21)	1.5120(19)
C(21)-N(6)	1.3470(18)
C(21)-C(22)	1.3816(19)
C(22)-C(23)	1.396(2)
C(22)-H(22)	0.9500
C(23)-C(24)	1.380(2)
C(23)-H(23)	0.9500
C(24)-C(25)	1.3997(19)
C(24)-H(24)	0.9500
C(25)-N(6)	1.3314(18)
C(25)-C(26)	1.508(2)
C(26)-N(7)	1.4777(18)
C(26)-H(26A)	0.9900
C(26)-H(26B)	0.9900
C(27)-N(7)	1.4799(17)
C(27)-C(28)	1.4908(19)
C(27)-H(27A)	0.9900
C(27)-H(27B)	0.9900
C(28)-N(8)	1.3563(18)
C(28)-C(29)	1.3712(19)
C(29)-N(10)	1.3535(19)
C(29)-H(29)	0.9500
C(30)-N(10)	1.4719(18)
C(30)-C(31)	1.504(2)
C(30)-H(30A)	0.9900
C(30)-H(30B)	0.9900
C(31)-C(36)	1.382(2)
C(31)-C(32)	1.392(2)
C(32)-C(33)	1.390(3)
C(32)-H(32)	0.9500
C(33)-C(34)	1.388(3)
C(33)-H(33)	0.9500
C(34)-C(35)	1.389(3)
C(34)-H(34)	0.9500
C(35)-C(36)	1.384(3)
C(35)-H(35)	0.9500
C(36)-H(36)	0.9500
N(1)-In(1)	2.3028(12)
N(2)-In(1)	2.4614(12)
N(3)-N(4)	1.3165(19)
N(4)-N(5)	1.3462(19)
N(6)-In(1)	2.3447(12)
N(7)-In(1)	2.5609(12)
N(8)-N(9)	1.3225(16)
N(8)-In(1)	2.2921(12)
N(9)-N(10)	1.3339(17)
O(1)-In(1)	2.3200(10)
O(3)-In(1)	2.2165(10)
O(5)-In(1)	2.2190(10)
O(5)-H(5A)	0.83(3)
O(5)-H(5B)	0.79(3)
O(6)-Cl(1)	1.4366(13)
O(7)-Cl(1)	1.4447(14)
O(8)-Cl(1)	1.4474(13)
O(9)-Cl(1)	1.4369(12)
O(10)-H(10A)	0.81(7)
O(10)-H(10B)	0.77(8)
O(11)-H(11C)	0.96(3)
O(11)-H(11D)	0.83(4)
O(12)-H(12A)	0.80(3)
O(12)-H(12B)	0.79(3)

Bonds	Angle
O(2)-C(1)-O(1)	125.89(13)
O(2)-C(1)-C(2)	118.05(13)
O(1)-C(1)-C(2)	116.02(12)
N(1)-C(2)-C(3)	121.47(13)
N(1)-C(2)-C(1)	114.15(12)

Bonds	Angle
C(3)-C(2)-C(1)	124.32(13)
C(2)-C(3)-C(4)	118.68(13)
C(2)-C(3)-H(3)	120.7
C(4)-C(3)-H(3)	120.7
C(3)-C(4)-C(5)	119.29(13)
C(3)-C(4)-H(4)	120.4
C(5)-C(4)-H(4)	120.4
C(6)-C(5)-C(4)	118.75(13)
C(6)-C(5)-H(5)	120.6
C(4)-C(5)-H(5)	120.6
N(1)-C(6)-C(5)	121.34(13)
N(1)-C(6)-C(7)	114.31(12)
C(5)-C(6)-C(7)	124.31(13)
N(2)-C(7)-C(6)	109.32(11)
N(2)-C(7)-H(7A)	109.8
C(6)-C(7)-H(7A)	109.8
N(2)-C(7)-H(7B)	109.8
C(6)-C(7)-H(7B)	109.8
H(7A)-C(7)-H(7B)	108.3
C(9)-C(8)-N(2)	114.79(11)
C(9)-C(8)-H(8A)	108.6
N(2)-C(8)-H(8A)	108.6
C(9)-C(8)-H(8B)	108.6
N(2)-C(8)-H(8B)	108.6
H(8A)-C(8)-H(8B)	107.5
N(3)-C(9)-C(10)	108.29(13)
N(3)-C(9)-C(8)	121.81(13)
C(10)-C(9)-C(8)	129.90(13)
N(5)-C(10)-C(9)	104.57(13)
N(5)-C(10)-H(10)	127.7
C(9)-C(10)-H(10)	127.7
N(5)-C(11)-C(12)	111.20(13)
N(5)-C(11)-H(11A)	109.4
C(12)-C(11)-H(11A)	109.4
N(5)-C(11)-H(11B)	109.4
C(12)-C(11)-H(11B)	109.4
H(11A)-C(11)-H(11B)	108.0
C(13)-C(12)-C(17)	119.14(15)
C(13)-C(12)-C(11)	120.04(14)
C(17)-C(12)-C(11)	120.78(15)
C(14)-C(13)-C(12)	120.75(16)
C(14)-C(13)-H(13)	119.6
C(12)-C(13)-H(13)	119.6
C(15)-C(14)-C(13)	119.72(17)
C(15)-C(14)-H(14)	120.1
C(13)-C(14)-H(14)	120.1
C(16)-C(15)-C(14)	120.28(16)
C(16)-C(15)-H(15)	119.9
C(14)-C(15)-H(15)	119.9
C(15)-C(16)-C(17)	120.15(16)
C(15)-C(16)-H(16)	119.9
C(17)-C(16)-H(16)	119.9
C(12)-C(17)-C(16)	119.95(17)
C(12)-C(17)-H(17)	120.0
C(16)-C(17)-H(17)	120.0

Bonds	Angle
N(2)-C(18)-C(19)	111.34(11)
N(2)-C(18)-H(18A)	109.4
C(19)-C(18)-H(18A)	109.4
N(2)-C(18)-H(18B)	109.4
C(19)-C(18)-H(18B)	109.4
H(18A)-C(18)-H(18B)	108.0
N(7)-C(19)-C(18)	111.74(11)
N(7)-C(19)-H(19A)	109.3
C(18)-C(19)-H(19A)	109.3
N(7)-C(19)-H(19B)	109.3
C(18)-C(19)-H(19B)	109.3
H(19A)-C(19)-H(19B)	107.9
O(4)-C(20)-O(3)	124.61(13)
O(4)-C(20)-C(21)	119.54(12)
O(3)-C(20)-C(21)	115.85(12)
N(6)-C(21)-C(22)	122.36(13)
N(6)-C(21)-C(20)	114.48(12)
C(22)-C(21)-C(20)	123.16(12)
C(21)-C(22)-C(23)	118.21(13)
C(21)-C(22)-H(22)	120.9
C(23)-C(22)-H(22)	120.9
C(24)-C(23)-C(22)	119.34(13)
C(24)-C(23)-H(23)	120.3
C(22)-C(23)-H(23)	120.3
C(23)-C(24)-C(25)	119.10(13)
C(23)-C(24)-H(24)	120.4
C(25)-C(24)-H(24)	120.4
N(6)-C(25)-C(24)	121.31(13)
N(6)-C(25)-C(26)	118.72(12)
C(24)-C(25)-C(26)	119.95(13)
N(7)-C(26)-C(25)	113.68(11)
N(7)-C(26)-H(26A)	108.8
C(25)-C(26)-H(26A)	108.8
N(7)-C(26)-H(26B)	108.8
C(25)-C(26)-H(26B)	108.8
H(26A)-C(26)-H(26B)	107.7
N(7)-C(27)-C(28)	108.44(11)
N(7)-C(27)-H(27A)	110.0
C(28)-C(27)-H(27A)	110.0
N(7)-C(27)-H(27B)	110.0
C(28)-C(27)-H(27B)	110.0
H(27A)-C(27)-H(27B)	108.4
N(8)-C(28)-C(29)	107.43(13)
N(8)-C(28)-C(27)	119.76(12)
C(29)-C(28)-C(27)	132.80(13)
N(10)-C(29)-C(28)	104.23(12)
N(10)-C(29)-H(29)	127.9
C(28)-C(29)-H(29)	127.9
N(10)-C(30)-C(31)	112.15(12)
N(10)-C(30)-H(30A)	109.2
C(31)-C(30)-H(30A)	109.2
N(10)-C(30)-H(30B)	109.2
C(31)-C(30)-H(30B)	109.2
H(30A)-C(30)-H(30B)	107.9
C(36)-C(31)-C(32)	119.86(15)

Bonds	Angle
C(36)-C(31)-C(30)	119.38(15)
C(32)-C(31)-C(30)	120.74(15)
C(33)-C(32)-C(31)	119.72(16)
C(33)-C(32)-H(32)	120.1
C(31)-C(32)-H(32)	120.1
C(34)-C(33)-C(32)	120.27(18)
C(34)-C(33)-H(33)	119.9
C(32)-C(33)-H(33)	119.9
C(33)-C(34)-C(35)	119.64(17)
C(33)-C(34)-H(34)	120.2
C(35)-C(34)-H(34)	120.2
C(36)-C(35)-C(34)	120.06(18)
C(36)-C(35)-H(35)	120.0
C(34)-C(35)-H(35)	120.0
C(31)-C(36)-C(35)	120.40(17)
C(31)-C(36)-H(36)	119.8
C(35)-C(36)-H(36)	119.8
C(6)-N(1)-C(2)	120.37(12)
C(6)-N(1)-In(1)	120.52(9)
C(2)-N(1)-In(1)	118.81(9)
C(7)-N(2)-C(18)	109.80(10)
C(7)-N(2)-C(8)	109.36(10)
C(18)-N(2)-C(8)	111.20(10)
C(7)-N(2)-In(1)	105.71(8)
C(18)-N(2)-In(1)	110.47(8)
C(8)-N(2)-In(1)	110.15(8)
N(4)-N(3)-C(9)	108.87(13)
N(3)-N(4)-N(5)	107.21(12)
N(4)-N(5)-C(10)	111.05(13)
N(4)-N(5)-C(11)	119.38(13)
C(10)-N(5)-C(11)	129.50(14)
C(25)-N(6)-C(21)	119.65(12)
C(25)-N(6)-In(1)	124.14(9)
C(21)-N(6)-In(1)	115.91(9)
C(26)-N(7)-C(27)	109.82(11)
C(26)-N(7)-C(19)	111.05(11)
C(27)-N(7)-C(19)	109.68(11)
C(26)-N(7)-In(1)	113.54(8)
C(27)-N(7)-In(1)	108.61(8)
C(19)-N(7)-In(1)	103.96(8)
N(9)-N(8)-C(28)	110.65(12)
N(9)-N(8)-In(1)	128.08(9)
C(28)-N(8)-In(1)	120.72(9)
N(8)-N(9)-N(10)	105.19(12)

Bonds	Angle
N(9)-N(10)-C(29)	112.50(12)
N(9)-N(10)-C(30)	120.32(13)
C(29)-N(10)-C(30)	127.12(13)
C(1)-O(1)-In(1)	120.07(9)
C(20)-O(3)-In(1)	122.47(9)
In(1)-O(5)-H(5A)	115.7(17)
In(1)-O(5)-H(5B)	114.0(18)
H(5A)-O(5)-H(5B)	107(2)
H(10A)-O(10)-H(10B)	108(6)
H(11C)-O(11)-H(11D)	105(3)
H(12A)-O(12)-H(12B)	104(3)
O(6)-Cl(1)-O(9)	110.97(9)
O(6)-Cl(1)-O(7)	109.90(10)
O(9)-Cl(1)-O(7)	109.47(9)
O(6)-Cl(1)-O(8)	109.21(8)
O(9)-Cl(1)-O(8)	109.29(8)
O(7)-Cl(1)-O(8)	107.95(10)
O(3)-In(1)-O(5)	102.51(4)
O(3)-In(1)-N(8)	155.47(4)
O(5)-In(1)-N(8)	81.74(4)
O(3)-In(1)-N(1)	79.84(4)
O(5)-In(1)-N(1)	141.05(4)
N(8)-In(1)-N(1)	81.97(4)
O(3)-In(1)-O(1)	75.31(4)
O(5)-In(1)-O(1)	74.03(4)
N(8)-In(1)-O(1)	82.89(4)
N(1)-In(1)-O(1)	69.00(4)
O(3)-In(1)-N(6)	70.25(4)
O(5)-In(1)-N(6)	76.39(4)
N(8)-In(1)-N(6)	133.60(4)
N(1)-In(1)-N(6)	137.48(4)
O(1)-In(1)-N(6)	127.66(4)
O(3)-In(1)-N(2)	91.69(4)
O(5)-In(1)-N(2)	147.78(4)
N(8)-In(1)-N(2)	97.22(4)
N(1)-In(1)-N(2)	69.49(4)
O(1)-In(1)-N(2)	138.05(4)
N(6)-In(1)-N(2)	81.64(4)
O(3)-In(1)-N(7)	137.19(4)
O(5)-In(1)-N(7)	76.98(4)
N(8)-In(1)-N(7)	67.33(4)
N(1)-In(1)-N(7)	127.29(4)
O(1)-In(1)-N(7)	140.88(4)
N(6)-In(1)-N(7)	68.10(4)
N(2)-In(1)-N(7)	73.07(4)

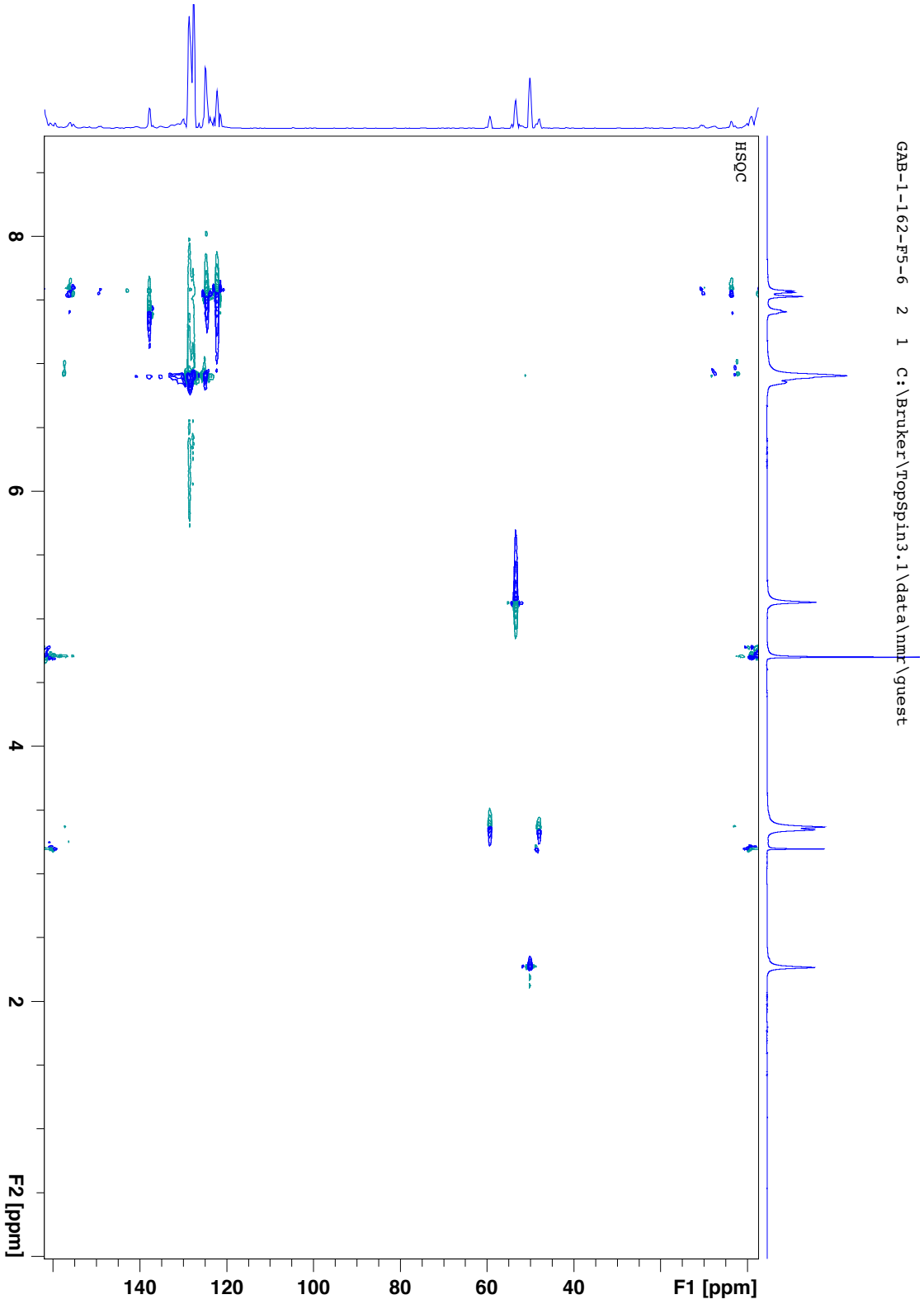

Figure A.13 HSQC 2D NMR spectrum (600 MHz, D_2O, RT) of **H_2azapa•2HCl**.

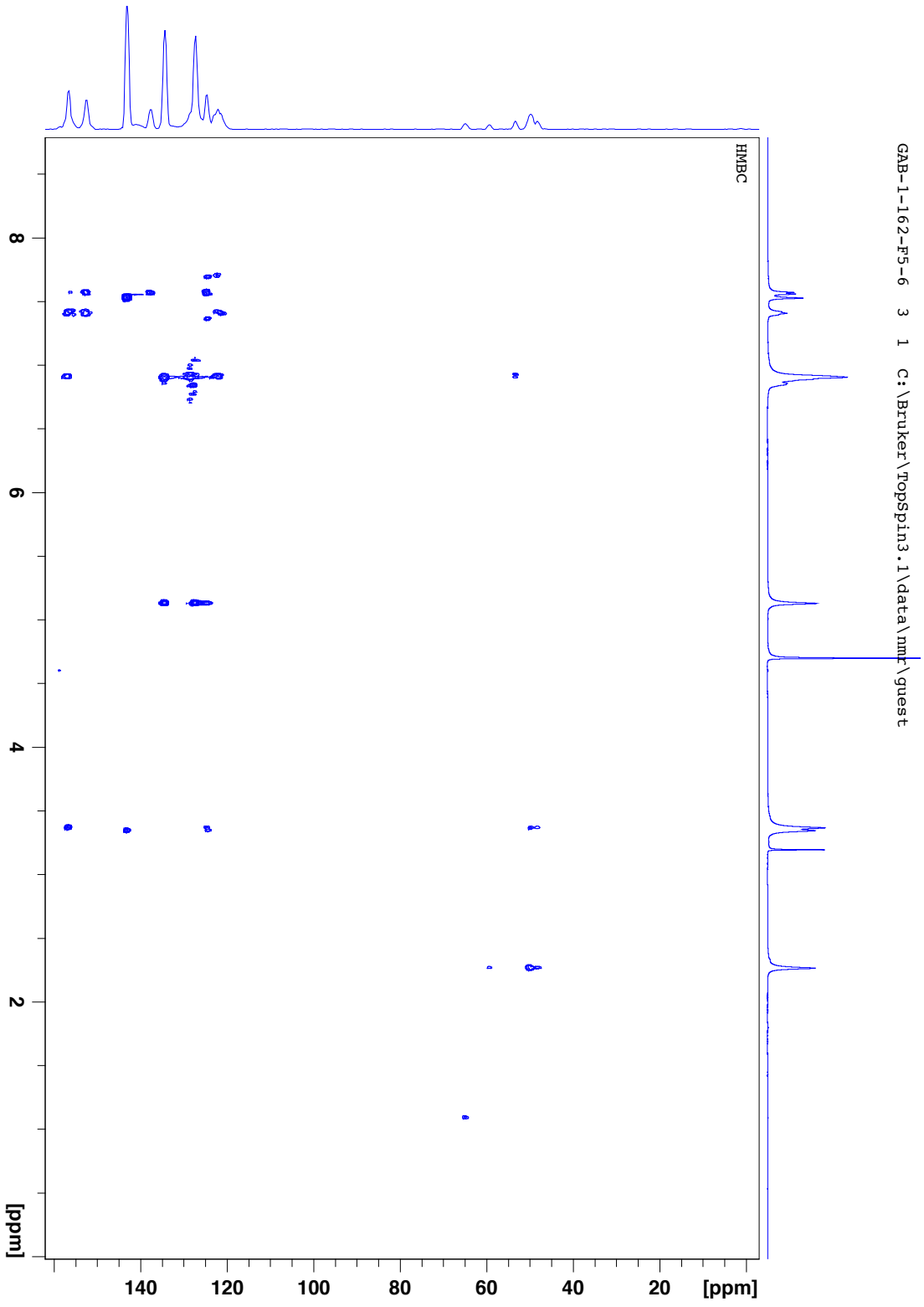

Figure A.14 HMBC 2D NMR spectrum (600 MHz, D_2O, RT) of **H_2azapa•2HCl**.